



energies

Special Issue Reprint

Advanced Energy Systems in Zero/Positive Energy Buildings, Communities and Districts

Edited by
Ala Hasan and Hassam Ur Rehman

mdpi.com/journal/energies



Advanced Energy Systems in Zero/Positive Energy Buildings, Communities and Districts

Advanced Energy Systems in Zero/Positive Energy Buildings, Communities and Districts

Editors

Ala Hasan

Hassam Ur Rehman



Basel • Beijing • Wuhan • Barcelona • Belgrade • Novi Sad • Cluj • Manchester

Editors

Ala Hasan
VTT Technical Research Centre of Finland
Espoo
Finland

Hassam Ur Rehman
VTT Technical Research Centre of Finland
Espoo
Finland

Editorial Office

MDPI
St. Alban-Anlage 66
4052 Basel, Switzerland

This is a reprint of articles from the Special Issue published online in the open access journal *Energies* (ISSN 1996-1073) (available at: https://www.mdpi.com/journal/energies/special_issues/zero_positive_building_communities).

For citation purposes, cite each article independently as indicated on the article page online and as indicated below:

Lastname, A.A.; Lastname, B.B. Article Title. <i>Journal Name</i> Year , <i>Volume Number</i> , Page Range.
--

ISBN 978-3-7258-0705-5 (Hbk)

ISBN 978-3-7258-0706-2 (PDF)

doi.org/10.3390/books978-3-7258-0706-2

© 2024 by the authors. Articles in this book are Open Access and distributed under the Creative Commons Attribution (CC BY) license. The book as a whole is distributed by MDPI under the terms and conditions of the Creative Commons Attribution-NonCommercial-NoDerivs (CC BY-NC-ND) license.

Contents

About the Editors	vii
Preface	ix
Hassam ur Rehman and Ala Hasan Energy Flexibility and towards Resilience in New and Old Residential Houses in Cold Climates: A Techno-Economic Analysis Reprinted from: <i>Energies</i> 2023 , <i>16</i> , 5506, doi:10.3390/en16145506	1
Federica Leone, Francesco Reda, Ala Hasan, Hassam ur Rehman, Fausto Carmelo Nigrelli, Francesco Nocera and Vincenzo Costanzo Lessons Learned from Positive Energy District (PED) Projects: Cataloguing and Analysing Technology Solutions in Different Geographical Areas in Europe Reprinted from: <i>Energies</i> 2023 , <i>16</i> , 356, doi:10.3390/en16010356	31
Jahangir Hossain, Aida. F. A. Kadir, Ainain. N. Hanafi, Hussain Shareef, Tamer Khatib, Kyairul. A. Baharin and Mohamad. F. Sulaima A Review on Optimal Energy Management in Commercial Buildings Reprinted from: <i>Energies</i> 2023 , <i>16</i> , 1609, doi:10.3390/en16041609	59
Pedro Fernández de Córdoba, Frank Florez Montes, Miguel E. Iglesias Martínez, Jose Guerra Carmenate, Romeo Selvas and John Taborda Design of an Algorithm for Modeling Multiple Thermal Zones Using a Lumped-Parameter Model Reprinted from: <i>Energies</i> 2023 , <i>16</i> , 2247, doi:10.3390/en16052247	99
Francesca Ceglia, Elisa Marrasso, Chiara Martone, Giovanna Pallotta, Carlo Roselli and Maurizio Sasso Towards the Decarbonization of Industrial Districts through Renewable Energy Communities: Techno-Economic Feasibility of an Italian Case Study Reprinted from: <i>Energies</i> 2023 , <i>16</i> , 2722, doi:10.3390/en16062722	121
Muhammad Mubashir Ajmal, Asad Ullah Qazi, Ali Ahmed, Ubaid Ahmad Mughal, Safeer Abbas, Syed Minhaj Saleem Kazmi and Muhammad Junaid Munir Structural Performance of Energy Efficient Geopolymer Concrete Confined Masonry: An Approach towards Decarbonization Reprinted from: <i>Energies</i> 2023 , <i>16</i> , 3579, doi:10.3390/en16083579	144
Gonçalo Roque Araújo, Ricardo Gomes, Maria Glória Gomes, Manuel Correia Guedes and Paulo Ferrão Surrogate Models for Efficient Multi-Objective Optimization of Building Performance Reprinted from: <i>Energies</i> 2023 , <i>16</i> , 4030, doi:10.3390/en16104030	171
Han Vandevyvere, Dirk Ahlers and Annemie Wyckmans The Sense and Non-Sense of PEDs—Feeding Back Practical Experiences of Positive Energy District Demonstrators into the European PED Framework Definition Development Process Reprinted from: <i>Energies</i> 2022 , <i>15</i> , 4491, doi:10.3390/en15124491	184
Gabriele Battista, Emanuele de Lieto Vollaro, Andrea Vallati and Roberto de Lieto Vollaro Technical–Financial Feasibility Study of a Micro-Cogeneration System in the Buildings in Italy Reprinted from: <i>Energies</i> 2023 , <i>16</i> , 5512, doi:10.3390/en16145512	200

Joscha Reber, Xenia Kirschstein and Nadja Bishara Evaluation of Building Mass Characterization for Energy Flexibility through Rule- and Schedule-Based Control: A Statistical Approach Reprinted from: <i>Energies</i> 2023 , <i>16</i> , 6878, doi:10.3390/en16196878	215
João Faria, Carlos Marques, José Pombo, Sílvio Mariano and Maria do Rosário Calado Optimal Sizing of Renewable Energy Communities: A Multiple Swarms Multi-Objective Particle Swarm Optimization Approach Reprinted from: <i>Energies</i> 2023 , <i>16</i> , 7227, doi:10.3390/en16217227	232
Charalampos Rafail Lazaridis, Iakovos Michailidis, Georgios Karatzinis, Panagiotis Michailidis and Elias Kosmatopoulos Evaluating Reinforcement Learning Algorithms in Residential Energy Saving and Comfort Management Reprinted from: <i>Energies</i> 2024 , <i>17</i> , 581, doi:10.3390/en17030581	265

About the Editors

Ala Hasan

Ala Hasan is a Principal Scientist in the Smart Energy and Built Environment Research Area at VTT, the Technical Research Centre of Finland. He has been working in the field of energy in buildings since 1982. He joined VTT in 2013. Prior to this, he has worked at the Helsinki University of Technology and Aalto University since 1998. He held the position of Research Fellow at the Academy of Finland, and was also the PI of several Academy of Finland research projects. He was evaluated as a Full University Professor in 2015. Dr. Hasan has an excellent portfolio of research, scientific publications, earning research funding, as well as offering services to the international scientific community. He has more than 120 publications in international scientific journals, conferences, book chapters, and reports. He was listed within the top 2% most cited scientists in the world in his field as published by Elsevier BV and Stanford University in the years 2020 and 2021. He is a member of the Editorial Board of the MDPI *Buildings* journal in Switzerland, and is a member of the Editorial Board of the *International Journal of Low Carbon Technologies*–Oxford Journals, UK. He has acted as an advisor and examiner of several PhD and Licentiate degree students in Finland, Sweden, and Denmark. He was elected in 2021 as a Fellow of IBPSA (The International Building Performance Simulation Association). He initiated IBPSA-Nordic as the first president. He was a member of the IBPSA-World Board of Directors for several years. He was a member of the Executive Committee of the International Energy Agency (IEA), Energy in Buildings and Communities (EBC)

Hassam Ur Rehman

Hassam Ur Rehman (D.Sc.) has completed a Ph.D. in the field of Energy Engineering from Aalto University, Finland. Presently, he is working as a senior scientist at the VTT Technical Research center of Finland. He is also a Postdoctoral researcher fellow at the Research Council of Finland (Suomen Akatemia) and a PI. To these roles, he brings the experience in building energy simulation, energy system design for buildings, community-sized energy systems, energy storage, electric vehicle, and multi-objective optimization for the planning of a stable and carbon-neutral society. Currently, he is involved in developing positive energy building concepts and energy resilience at the national and European level, along with technical, social, and business-related studies. He is representing Finland in the International Energy Agency (IEA), Energy in Buildings and Communities (EBC) as an Executive Committee member, leading the Annex on Energy resilience (operating agent), and coordinating IEA EBC Annex83.

Preface

The building sector is vital for Climate Action efforts in cities around the world to reduce their greenhouse gas emissions. Therefore, energy levels in buildings, communities, and districts must be considered in our attempt to mitigate emissions, ensuring a sustainable, self-sufficient, and safe future. This Special Issue aims to provide and collect high quality research on the concept of net-zero/positive energy buildings and districts that have emerged in recent years, with the ultimate goal of shaping cities into carbon-neutral communities in the near future. These buildings and districts are also vital in reaching self-sufficiency, engaging users, and providing energy resiliency during outages. Moreover, the important economic, environmental, and social aspects in buildings and districts are discussed, along with technical aspects.

This Special Issue presents innovative research in the domain of buildings, districts, and built environments, while providing pathways for future challenging research avenues. A large number of research topics covered highlight the diversity of this evolving field. We hope that the research results will contribute to the future development and research of the field of built environments.

As the Guest Editor of this Special Issue, we would like to thank the authors and coauthors who published their articles. We are also grateful for the wonderful reviewers whose valuable time, comments, and suggestions have helped in improving the quality of the articles, as well as the MDPI editorial staff who helped us throughout the entire process of producing this Special Issue.

The Special Issue was supported by the Research Council of Finland (Suomen Akatemia), under the following project names: Research Council of Finland project “Energy Resilience in Buildings in Extreme Cold Weather Conditions in Finland 2022–2025 (FinERB) [Grant number: 348060]”, Research Council of Finland project “Integration of Building Flexibility into Future Energy Systems 2020–2024 (FlexiB) [Decision number: 333364]”, ‘EXCESS (FlexiBle user-Centric Energy positive houseS)’, from the [European Union’s Horizon 2020 research and innovation programme H2020-LC-EEB-03-2019] [Euratom research and training programme 2014–2018], under grant agreement No [870157] and SPARCS from the European Union’s Horizon 2020 research and innovation programme, under Grant Agreement No. 864242. The authors also gratefully acknowledge IEA EBC Annex 83 Positive Energy Districts.

Ala Hasan and Hassam Ur Rehman

Editors

Article

Energy Flexibility and towards Resilience in New and Old Residential Houses in Cold Climates: A Techno-Economic Analysis

Hassam ur Rehman * and Ala Hasan

VTT Technical Research Centre of Finland Ltd., P.O. Box 1000, FI-02044 Espoo, Finland; ala.hasan@vtt.fi
* Correspondence: hassam.rehman@vtt.fi; Tel.: +358-40-621-5917

Abstract: One of the main sectors that contribute to climate change is the buildings sector. While nearly zero-energy buildings are becoming a new norm in many countries in the world, research is advancing towards energy flexibility and resilience to reach energy efficiency and sustainability goals. Combining the energy flexibility and energy resilience concept is rare. In this article, we aim to investigate the effect of energy efficiency in a new single-family building on the energy flexibility potential and resilience characteristics and compare these with those for an old building in the cold climate of Finland. These two objectives are dependent on the buildings' respective thermal mass. The heat demands of the two buildings are compared. Their technical and economic performance are calculated to compare their flexibility and resilience characteristics. Dynamic simulation software is used to model the buildings. The results show that the old building has better flexibility and higher energy cost savings when including the energy conservation activation strategy. In the old building, savings can be around EUR 400 and flexibility factor can be around 24–52% depending on the activation duration and strategy. The new building, due to higher efficiency, may not provide higher energy cost savings, and the energy conservation activation strategy is better. In the new building, savings can be around EUR 70 and the flexibility factor reaches around 7–14% depending on the activation duration and strategy. The shifting efficiency of the new house is better compared to that of the old house due to its higher storage capacity. For energy resilience, the new building is shown to be better during power outages. The new building can be habitable for 17 h, while the old building can provide the same conditions for 3 h only. Therefore, it is essential to consider both energy flexibility and resilience as this can impact performance during the energy crisis.

Keywords: energy flexibility; energy resilience; thermal energy; energy crisis; energy pricing; Nordic climate

Citation: Rehman, H.u.; Hasan, A. Energy Flexibility and towards Resilience in New and Old Residential Houses in Cold Climates: A Techno-Economic Analysis. *Energies* **2023**, *16*, 5506. <https://doi.org/10.3390/en16145506>

Academic Editor: Ludovico Danza

Received: 26 June 2023
Revised: 16 July 2023
Accepted: 18 July 2023
Published: 20 July 2023



Copyright: © 2023 by the authors. Licensee MDPI, Basel, Switzerland. This article is an open access article distributed under the terms and conditions of the Creative Commons Attribution (CC BY) license (<https://creativecommons.org/licenses/by/4.0/>).

1. Introduction

Climate change is one of the biggest challenges that is being faced. The transition towards a sustainable society requires buildings to be flexible and resilient to reduce climate change, emissions and energy crises. Therefore, the European Union (EU) plans to include renewable energy sources in an amount of 40% until 2030 in the energy mix and increase it further until 2050 compared to 1990 levels towards carbon neutrality [1,2]. Building accounts for almost 40% of the total CO₂ emissions and, therefore, buildings can play a major role in CO₂ emission reduction [3]; the Directive on Energy Performance of Buildings (EPBD) has been introduced to decarbonize the building stock by 2050 [4]. The reduction in emissions, integration of renewables and reduction in peak loads can be carried out by including energy flexibility in a building. Another challenge faced now is the energy crisis, which is causing prolonged power outages to buildings. Due to an increase in ambient temperature and climate change, multiple climate-related extreme events such as forest fires, extreme temperatures, storms and heavy rain occur in different regions resulting in grid loss and blackouts [5]. These events are becoming more visible in recent times, and

include floods in Germany and the United States of America and forest fires in Greece, Italy and Turkey. With rapid urbanization and the eminent threat of climate change, these events can have an impact on a building's energy infrastructure and its occupants due to grid loss [6]. Other factors of the energy crisis include human-made factors such as political issues between Russia and Ukraine that are causing energy and power shortages globally due to supply chain issues. Therefore, buildings have to be energy-resilient to address periods of power outage and flexible to reduce energy consumption and save costs.

1.1. Energy Flexibility

Energy flexibility can assist in reducing CO₂ as it addresses the effective implementation of renewable energy generation, reduces peak load, balances energy use in the grid and helps in reducing the price for the end user. The energy consumption of a building can be increased when the prices are low or it can be reduced when the prices are high [7], e.g., increasing the indoor temperature when the prices are low or decreasing the temperature when the prices are high while keeping thermal comfort [8]. This modulation or activation is also known as a demand response, i.e., shifting the energy use based on signals such as weather and price.

The importance of the demand response or energy flexibility is increasing with the increase in energy prices [9,10]. The financial aspect and benefits have to be identified. Various studies have been carried out to show the benefits of energy flexibility [11,12]. It has been found that the operation of a ground-source heat pump based on price signals can save up to 15% of the energy costs [13] in the cold climate. Another study showed that controlling the heating and cooling of a building can save up to 11% of the energy cost in warm climatic conditions [14]. Similarly, it has been found that 14% of the energy demand and cost can be reduced in commercial buildings by implementing energy flexibility for heating and cooling [15]. An experimental study shows that the energy flexibility action can reduce the energy cost by 4% depending on the flexibility options available [16]. Integrating solar energy and energy storage such as phase change materials [17], batteries or tanks [16] can also be used for better flexibility. All the studies show that further analysis is needed to identify the benefits of energy flexibility in terms of cost and flexibility. Moreover, the benefit of such a modulation in cold climatic regions has been further analyzed especially for different ages of buildings. Another important factor is the control strategies for the activation. Usually, set point temperatures of indoor air are used for energy flexibility; this may cause uncomfortable indoor conditions. Studies showed that energy saving can be up to 20% in Mediterranean climatic conditions through varying the indoor air's set point temperature and heat pump operation [18]. However, there is a challenge of deteriorating thermal comfort depending on weather conditions. Another study showed that in Danish climatic conditions, there is a potential to use thermal mass to reduce the energy demand and cost; however, there is a possibility of overheating [8] in new buildings. In Finland, about 43% of the buildings were built before the 1980s and renovating them will take time. Therefore, the energy flexibility potential and control strategies both in the old and new buildings in terms of heating have to be identified and can help in reducing the energy costs and energy demand, and improve the flexibility factor in cold climatic conditions. The flexibility factor is defined as a factor that is used to show the ability of a building envelope to shift the heating demand from high- to low-price hours or to shift the peak hours' heating demand to that of low peak hours (based on weather conditions). This shifting is mainly carried out based on the activation of the thermal mass of the building using price or weather signals to control the heating system [8].

1.2. Energy Resilience

It is also vital that the transition towards a sustainable solution involves an adequate consideration of climate change, especially the occurrence of extreme events, to ensure the reliable minimum performance of a building's energy systems in the long run to support the building occupants' comfort and habitability. Methods to assess the impacts of extreme

events produced by climate change and uncertainties in the design and performance of a residential building's envelope need to be thoroughly investigated under Finnish climatic conditions. On the international level, research has been ongoing at the urban scale [19] and few studies are carried out on the building level for mild climatic conditions [19–22]. No research has been carried out at the building level for Finnish conditions [20]. In Finland, winters are extremely cold and the design temperature of outdoor air for the buildings' systems is $-26\text{ }^{\circ}\text{C}$ in southern Finland and $-38\text{ }^{\circ}\text{C}$ in northern Finland [23]; therefore, occupants' thermal comfort and habitability can be a big challenge. Therefore, the building has to be energy-resilient to maintain thermal comfort and habitability conditions. Research has been focused on 'habitability' as part of energy-resilient buildings [24] either for mild climates [25] or for overheating conditions under grid loss [21,22]. The concept of 'habitability' focuses on the indoor thermal conditions and comfort and it refers to the length the building can remain in habitable thermal conditions after power loss through a reduction in heat transfer, natural ventilation and natural light [26].

Energy-resilient buildings is an emerging concept that is increasingly used to represent the performance of buildings during grid power loss caused in extreme climatic events such as fires, extreme temperature storms, heavy rain, etc. [27]. Energy resilience in buildings is defined as the ability of a building to provide and maintain the minimum level of thermal comfort and habitability, and also to provide essential services, such as domestic hot water, ventilation and basic electrical power within the building, during grid power loss which challenges the normal operation of a building [28,29]. Energy-resilient residential buildings are important to be studied because 87% of the time is spent indoors by occupants in many developed countries [30] and occupants' thermal comfort is an essential service that a building must provide. However, the energy-resilient building concept has not yet been adequately explored in the cold climate of Finland, as its definition has not been clearly articulated and assessment is mostly carried out at the urban scale [31]. For this reason, habitability thresholds, boundary conditions and methods are needed to be defined, which requires extensive research on the extreme cold winters of Finland. Additionally, research where the aim is to evaluate both energy flexibility and resilience together is scarce. Therefore, a holistic study is needed that can not only address the energy flexibility issues but also consider and presents the energy resilience issues in cold climatic conditions.

This article contributes to analyzing the interaction between the energy flexibility and resilience of a building and addresses the research gap that exists in these connections. The novelty of the study is the close comparison between the energy performance of the old and new building (detached house) and highlighting the important link between the energy flexibility and resilience of the buildings. The technical and economic analyses of the buildings are carried out as case studies, that aim to achieve energy flexibility and resilience in Finland as an illustration of the Nordic climate. As no regulations or guidelines exist for the link between energy resilience and flexibility in cold climates, this article addresses this key interlink and gap. The objective of the article is to develop and combine the methods that can improve the energy flexibility of old and new buildings based on price signals and also to present the impact of thermal mass activation durations on building energy performance. Furthermore, a technical framework of energy-resilient buildings and their application in the Finnish environment is introduced. The focus of the study is on the heating energy and demand of the simulated buildings and neither renewable energy sources nor auxiliary energy storage (electrical or heat) is considered. This article is useful not only for cold climatic regions, such as the Nordics, Scandinavia, Canada, China, and the United States of America, but it is useful for the international perspective as well, as similar approaches and methods can be used in various climatic zones such as arid, tropical, Mediterranean, etc., to control and to estimate the performance of a building in terms of energy flexibility and energy resilience. The present study scope is limited to the modeling, computational and simulation activity and no experimental work is carried out. Moreover, no real or pilot building exists in the Finnish climatic conditions that integrate energy flexibility and resilience together. The buildings are modeled and simulated using

the TRNSYS (Transient System Simulation Tool) [32] dynamic simulation software, which is widely used in research and technical projects. The TRNSYS 17 software is used and validated in various energy projects such as in Finland, [33] Carlsheim, Germany [34], and in Drake Landing Solar Community, Canada [35]. The modeled buildings in the article are typical archetype buildings based on the Finnish buildings' regulations [23] and compared against the typical building parameters in Finland [33,36]. Simulations for energy flexibility and resilience are required in the context of residential buildings in the Nordic region that can be used to provide basic knowledge and a computational model for future experiments. These buildings can soften the impact of high energy costs and provide flexibility. Moreover, they can provide resilience against the energy crisis that is now evident.

This method can further be applied to other types of buildings in the Nordics and in the global level. The paper structure is as follows. Section 2 defines the method used in the article. The residential building design and parameters are mentioned in Section 3. The energy flexibility operation, control and component description are discussed in Section 4. The energy flexibility and cost calculation methods are mentioned in Section 5. The results and detailed discussion about energy flexibility are mentioned in Section 6. Section 7 analyzes and describes the energy resilience of the same old and new buildings in the cold climate. Finally, the conclusions are mentioned in Section 8.

2. Method

Dynamic simulation is used to design and analyze the energy flexibility and resilience performance of the old and new buildings. The simulation method, input specifications, control operations of the building system, and technical and economical calculation methods are defined in detail in the following sections.

3. Simulation Specification

The input parameters for the buildings are described in detail in Section 3.1.

3.1. Input Values for Building Simulation

Figure 1 shows the typical building model that was built and simulated in the TRNSYS simulation software. The building (living space) is considered a single zone and the attic is not considered for calculations. The building's heating system is assumed to be an ideal heater connected to the grid.

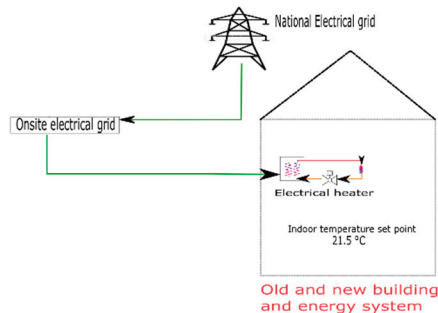


Figure 1. Case studies; old and new building zone in Finland. Green line shows the electricity flow, red line shows the supply water (hot) flow and orange line shows the return water (warm) flow.

3.1.1. Old Building

The building follows the Finnish buildings' regulation of the 1970s [23]. The parameters of the building are shown in Table 1.

Table 1. The parameters of the old building under study [36,37].

Parameters	Value	Material and Properties
Floor area	140 m ²	
Internal height	2.7 m	
Walls (U value)	0.5 W/m ² K	Gypsum (0.013 m, 700 kg/m ³), polyamide film (0.001 m, 1150 kg/m ³), mineral wool (0.063 m, 50 kg/m ³), wood fiber (0.012 m, 250 kg/m ³), air (0.022 m, 1.2 kg/m ³), and wood (0.020 m, 500 kg/m ³)
Roof (U value)	0.27 W/m ² K	Bitumen (0.010 m, 1100 kg/m ³), air (0.1 m, 1.2 kg/m ³), mineral wool (0.149 m, 50 kg/m ³), polyamide film (0.001 m, 1150 kg/m ³), air (0.022 m, 1.2 kg/m ³), and gypsum (0.013 m, 700 kg/m ³)
Floor (U value)	0.38 W/m ² K	Gypsum (0.03 m, 700 kg/m ³), air (0.022 m, 1.2 kg/m ³), polyamide film (0.001 m, 1150 kg/m ³), mineral wool (0.099 m, 50 kg/m ³), and wood (0.005 m, 250 kg/m ³)
Windows (U value)	2.5 W/m ² K	The glazing area is 12% of the total wall area, located on the north, south, and east
Gains (Person, equipment)	2.7 W, 2.3 W	
Ventilation	0.55 1/h	
Tightness q ₅₀	6 m ³ /h m ²	

3.1.2. New Building

The building follows the Finnish regulation [23]. The parameters of the building are shown in Table 2.

Table 2. The parameters of the new building under study [36,37].

Parameters	Value	Material and Properties
Floor area	140 m ²	
Internal height	2.7 m	
Walls (U value)	0.17 W/m ² K	Lime mortar (0.01 m, 1800 kg/m ³), concrete (0.1 m, 2400 kg/m ³), mineral wool (0.252 m, 50 kg/m ³), concrete (0.1 m, 2400 kg/m ³), and lime mortar (0.01 m, 1800 kg/m ³)
Roof (U value)	0.09 W/m ² K	Concrete cream (0.01 m, 1100 kg/m ³), mineral wool (0.486 m, 50 kg/m ³), concrete (0.150 m, 2400 kg/m ³), and lime mortar (0.01 m, 1800 kg/m ³)
Floor (U value)	0.16 W/m ² K	Light floor concrete (0.02 m, 500 kg/m ³), concrete (0.2 m, 2400 kg/m ³), and EPS (0.237 m, 20 kg/m ³)
Windows (U value)	1 W/m ² K	The glazing area is 12% of the total wall area, located on the north, south, east
Gains (Person, equipment)	2.7 W, 2.3 W	
Ventilation	0.55 1/h, 60%	
Tightness q ₅₀	2 m ³ /h m ²	

3.2. Simulation Software: TRNSYS

An energy simulation software known as TRNSYS 17 [32,34] was used to model and perform a dynamic simulation of the energy systems. This simulation software is

widely used by the scientific community, for instance in [38,39], and validated by the Drake Landing Community, in Canada [35]. In TRNSYS, the modules used were as follows: building (TYPE 56), control of indoor air set point temperature (TYPE 2b, 14 h), temperature control (TYPE 1233), and weather data (TYPE 15). TRNSYS is used for modeling buildings and their control systems as it provides flexibility [40].

4. Building Thermal Energy System Operation

In this article, the energy conservation and storage potential of the building's thermal mass is estimated. The reference indoor air set point temperature for the space heating of the zone is set at 21.5 ± 0.5 °C. This space heating temperature corresponds to the recommendation of the Finnish Society of Indoor Air Quality and Climate [41] and to the Finnish building regulations [23]. In this article, two activation methods are simulated for the typical heating period and also for the whole year. This is carried out to estimate the performance and behavior of the different types of buildings in detail under various situations of activation. Activation is carried out for different starting times and duration between 1 h–18 h. A duration of more than 18 h is not considered as occupants may not accept long changes in comfort [8] and uncertainties are higher in terms of energy cost and weather prediction. Activation is carried out by varying the indoor air set point temperature of the zone to evaluate the different performances of the two types of buildings in Finnish conditions. The two activation methods that are applied are discussed in Section 4.1. Space cooling and domestic hot water are not considered in the calculation.

4.1. Controls of the Thermal Energy System

The two activation methods that are applied for energy flexibility are heat energy conservation and heat energy storage. The heating system is assumed to be ideal and the building is heated using the heaters inside the zone.

In the method of heat energy conservation for energy flexibility, the indoor air set point temperature of the space heating is decreased by 1.5 °C depending on the price signal. This is selected as it is an acceptable range for the variation in the space heating temperature inside the building and for comfort [41].

In the method of heat energy storage for energy flexibility, instead of reducing the indoor air set point temperature of space heating, it is increased by 1.5 °C depending on the price signal. This is c to keep the change in the space heating temperature reasonable and for comfort [41].

5. Energy and Cost Calculations for Flexibility Assessment

5.1. Energy Flexibility Cases

Two types of energy flexibility cases are discussed in the article to analyze the performance of the old and new buildings. Weather-based and cost-based energy flexibility are considered. Weather-based analysis is performed to study the behavior while cost based flexibility is carried out to identify the cost saving potential and flexibility factor.

The building is heated during the heating period at the indoor air set point temperature to reach a steady period, and activation is carried out during the average heating period. The results of energy storage and energy conservation activations are evaluated separately, as they have different characteristics.

Some indicators are extracted from the simulations [8]:

$$Q_{\text{heat}} = Q_{\text{heat}} (\text{activation}) - Q_{\text{heat}} (\text{reference}) \quad (1)$$

$$Q_{\text{heat charge}} = \sum Q_{\text{heat}}, \text{ when } Q_{\text{heat}} > 0 \quad (2)$$

$$Q_{\text{heat discharge}} = \sum Q_{\text{heat}}, \text{ when } Q_{\text{heat}} < 0 \quad (3)$$

$$\text{Shifting efficiency} = -Q_{\text{heat discharge}}/Q_{\text{heat charge}} \quad (4)$$

$$\text{Flexibility factor} = \frac{\sum_{\text{low price}} Q_{\text{heat}} - \sum_{\text{high price}} Q_{\text{heat}}}{\sum_{\text{low price}} Q_{\text{heat}} + \sum_{\text{high price}} Q_{\text{heat}}} \quad (5)$$

Equation (1) shows the difference between the heat demand in the reference and the activation cases. In some scenarios, during the activation of the thermal mass, the energy consumption increases compared to that of the reference case (the reference indoor air set point temperature scenario). In this scenario, the amount of energy used is called charge heat ($Q_{\text{heat charge}}$) as shown in Equation (2). Similarly, energy consumption decreases compared to that of the reference case (the reference indoor air set point temperature scenario). In this scenario, the amount of energy used is called discharge heat ($Q_{\text{heat discharge}}$) as shown in Equation (3). The ratio of these two factors is called shifting efficiency (as shown in Equation (4)). On the other hand, in the case of conservation, this ratio is greater than 1 as energy consumption decreases. Equation (5) shows the flexibility factor; in other words, it shows the energy flexibility performance of the building. It shows the ability of the building to shift the energy use from certain hours to other hours based on the control strategies (such as shifting from high-price to low-price hours or using weather signals). It considers the energy charged and discharged based on the hourly energy price signals that vary at each time step. The energy price signal used for calculation is explained in Section 5.3. The energy flexibility potential of the building is better if the flexibility factor is high. Compared to the reference case, when additional energy is charged in the building to increase the indoor temperature based on the price signal, the heating energy is higher than the reference heating power and it is called a low-price Q_{heat} in Equation (5). Similarly, compared to the reference case, when the energy is discharged or removed from the building to decrease the indoor temperature based on the price signal, the heating energy is lower than the reference heating energy and it is called a high-price Q_{heat} in Equation (5). These energy flows are included in Equation (5) to calculate the flexibility factor. According to Equation (5) if no heat is charged or discharged and the heating use is the same in low- and high-price periods, then the factor is 0. The limitation of this flexibility factor is that it can lead to different values when it is used for other signals such as grid and climatic conditions [8].

5.2. Weather

In this paper, the weather data used are from the Helsinki Vantaa airport for the year 2016 [42]. The hourly ambient temperature and the duration curve of the ambient temperature are shown in Figure 2.

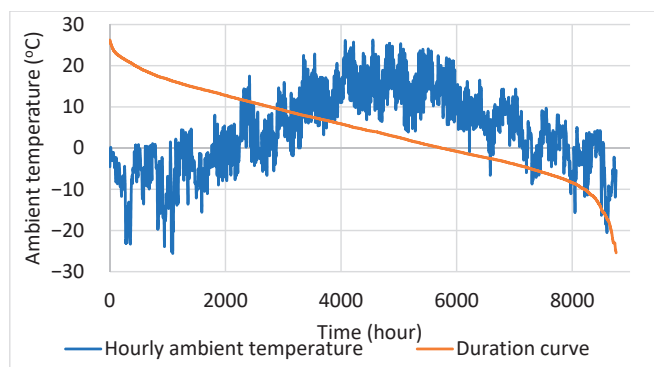


Figure 2. Hourly weather profile and duration curve of Helsinki, Finland.

5.3. Energy Cost Calculation

The hourly electricity price for the year 2016 is used for the energy cost calculation. The cost data are used from Nordpool and provide the real-time electricity price for each hour; see Figure 3. The cost includes the distribution and taxes [9]. This study is about the operational cost of the energy in the building. Figure 3 shows the duration curve of the electricity price and the price range is between 15 cents/kWh and 10 cents/kWh during most of the hours.

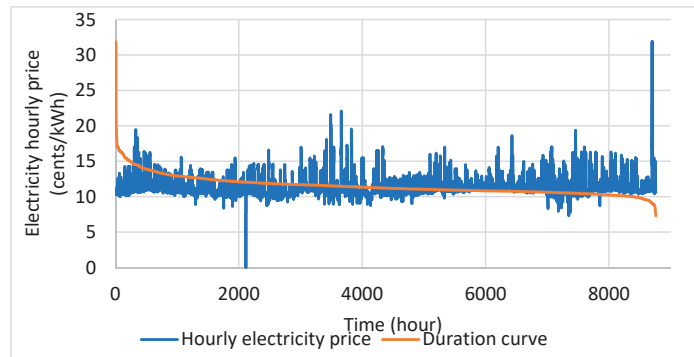


Figure 3. The hourly electricity price and duration curve in Finland year 2016 [9].

6. Results and Discussion

The result is divided into two main sections. Section 6.1 analyzes and describes the energy flexibility and activation behavior of the old and new buildings under heat energy conservation and storage activation using ambient temperature as a control signal only, and energy cost is not considered. For this study, a short duration (i.e., winter week) is considered to analyze the activation, temperature and heating behavior in detail as heating energy is essential in cold regions. This is carried out to analyze the energy flexibility potential and behavior of the old and new building structure with respect to the ambient temperature in detail. These initial findings are afterward extended for the whole year in Section 6.2, to study the impact of activation based on the findings in Section 6.1. Finally, Section 6.2 analyses and describes the energy flexibility and activation of the old and new buildings considering the electricity price for the whole year. This is carried out to analyze the energy flexibility potential of the old and new building structure based on energy price signals.

6.1. Weather Based Activation of the Building Mass

Section 6.1.1 presents the old building's heat energy storage and the conservation activation of the building mass. Section 6.1.2 presents the new building's heat energy storage and the conservation activation of the building mass.

6.1.1. Old Building

Heat Energy Storage

It is assumed that during heat energy storage activation, the indoor air set point temperature of the zone is increased by 1.5 °C. This is carried out to heat the thermal mass of the building and store heat, so it can be released when the indoor air set point temperature is back to the reference point of 21.5 ± 0.5 °C. Different activation durations are considered such as 2 h, 6 h and 18 h and compared against the reference case (without activation). Different duration hours are simulated to analyze the behavior under the short and long durations of activation. The change in the indoor air set point temperature is shown in Figure 4. The hours selected for analysis are from 615 to 687 h and the activation hour is 638 h. This duration is selected when the ambient temperature is cold at around

−10 °C—15 °C, which is the typical average temperature in winters in Southern Finland. The same time window is selected in the following new building case. It can be observed that when 2 h is selected for the activation duration, the building’s indoor temperature cannot reach the indoor air set point temperature of 23 °C. However, when 6 and 18 h are selected for the activation, the building’s indoor temperature reaches the indoor air set point temperature of 23 °C.

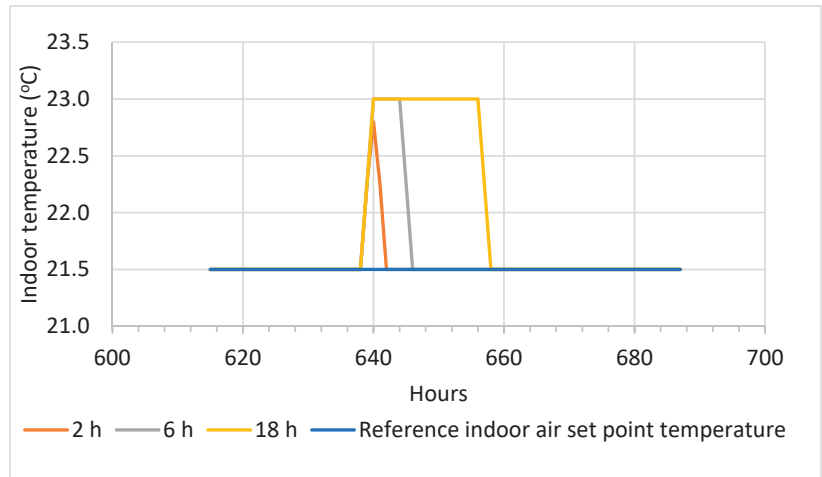


Figure 4. Indoor air temperature during heat energy storage activation in the old building.

Figure 5 shows the heat power demand for the reference case and for the activation hours of 2 h, 6 h and 18 h. In all the activation durations, when the indoor air set point temperature increases to 23 °C the heating power increases. As soon as the indoor air set point temperature is returned to the reference indoor air set point temperature of 21.5 °C, the heating power reduces and goes below the reference scenario’s heat power (blue line) for a few hours until it returns to the reference heating line.

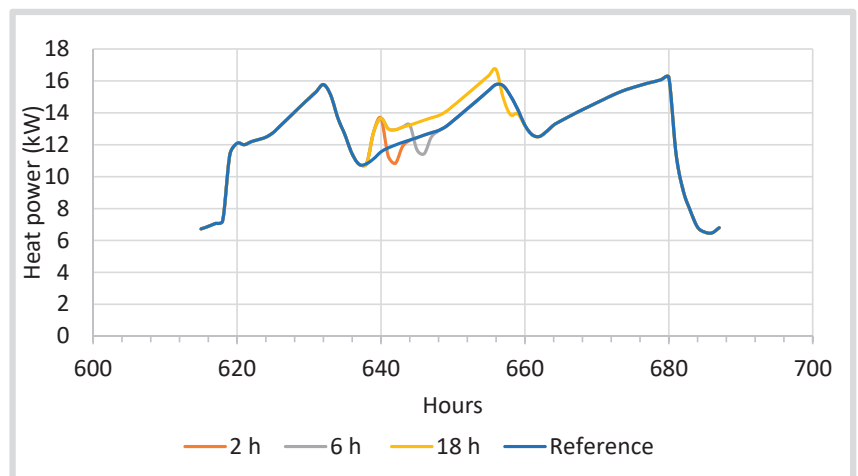


Figure 5. Heating power activation during heat energy storage in the old building.

Figure 6 shows the energy charged (blue bar) and discharged (orange bar) to reach the indoor air set point temperature of 23 °C for the activation of energy storage compared to the reference scenario's indoor air set point temperature of 21.5 °C. It can be observed that the amount of the energy charged and discharged varies depending on the activation duration. Generally, the energy charged and that discharged increase with the increase in the activation duration. The energy charge increases from 3.8 kWh (for 2 h) to 19 kWh (for 18 h). Similarly, the energy discharge increases from 1.9 kWh (2 h) to 2.41 kWh (for 18 h) as the energy stored in the structure is released back to the zone and this reduces the heating power to heat the zone compared to that of the reference scenario.

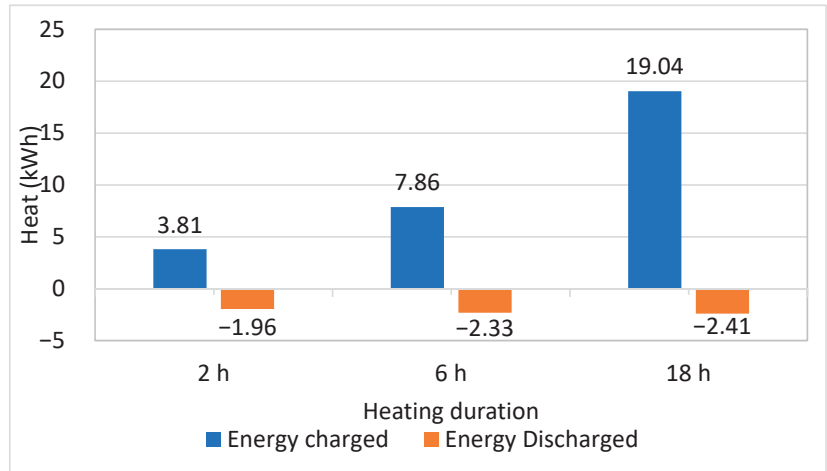


Figure 6. Energy charged and discharged during heat energy storage in the old building in Finland.

Figure 7 shows that in the case of storage activation, the shifting efficiency is less than one. The shifting efficiency reduces when the activation duration increases. This is because the longer the charging hour, the higher the losses to the ambient surroundings, and the energy discharge to the zone is less. The energy is mainly lost in the ambient surroundings due to the cold ambient temperature, and the envelope of the old building is inefficient (low U-value) in storing heat, resulting in higher losses. Similar behavior is observed in [8].

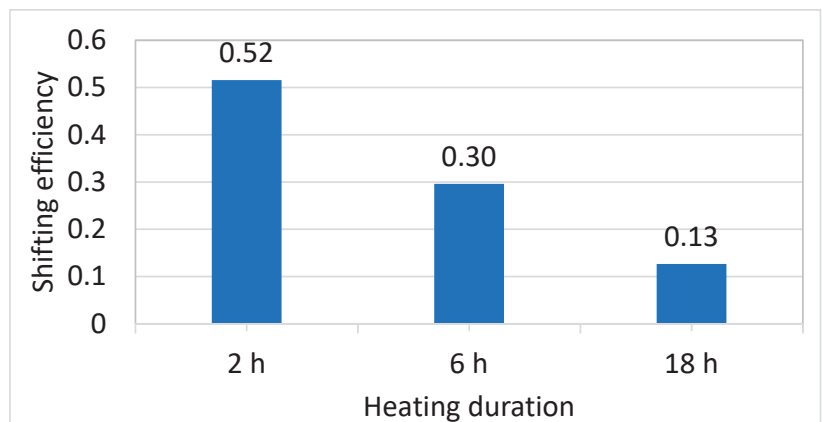


Figure 7. Shifting efficiency during heat energy storage in the old building.

Figure 8 shows the energy flexibility factor of the old building under the three activation durations. Equation (5) [8] is used for the flexibility factor calculation. Compared to the reference case, when additional energy is charged in the building to increase the indoor temperature to 23 °C, the heating energy (2 h, 6 h, 18 h) is higher than the reference heating power and it is called $Q_{\text{heat charged}}$. Similarly, compared to the reference case, when the energy is discharged from the building to decrease the indoor temperature to 21.5 °C, the heating energy is lower than the reference heating energy and it is called $Q_{\text{heat discharged}}$.

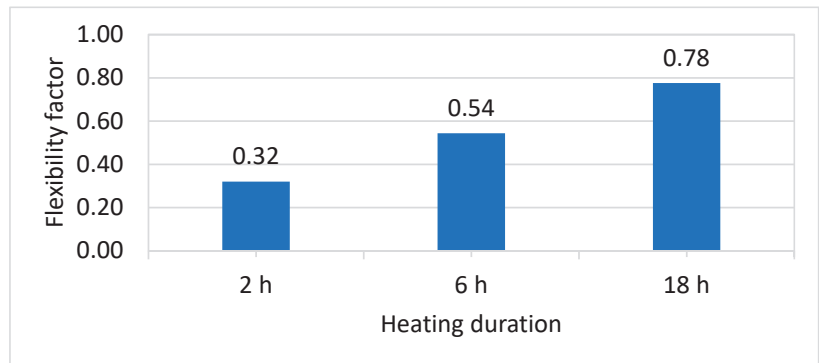


Figure 8. Flexibility factor during heat energy storage in the old building.

It can be observed that the energy flexibility factor increases as the activation duration increases. This is due to an increase in the difference between the energy charged and discharged as the activation duration increases. With higher activation durations, the amount of energy storage (energy charged) is larger while the energy discharge is lower resulting in higher flexibility as shown in Figure 8.

Heat Energy Conservation

It is assumed that depending on the weather, the indoor air set point temperature of the zone is decreased by 1.5 °C to 20 °C. This is carried to save energy for a time and after this, the set point is returned to the reference point of 21.5 °C. In the heat energy conservation strategy for old and new buildings, energy discharge occurs when the temperature drops from 21.5 °C to 20 °C, due to a decrease in the set point temperature, and energy charge refers to when the temperature increases from 20 °C to 21.5 °C (the reference set point). The hours selected for analysis are from 615 to 687 h and the activation hour is 638 h. The change in the indoor air set point temperature is shown in Figure 9. It can be observed that when energy conservation is carried out, the temperature drops to 20 °C in all the activation hours (2 h, 6 h and 18 h). Compared to the energy storage (Figure 4), the temperature drop is fast in all activation cases. This shows that the losses from the envelope are high.

Figure 10 shows the heat power demand for the reference case and the activation hours of 2 h, 6 h and 18 h. In all the activation durations, when the indoor air set point temperature decreases to 20 °C the heating power decreases. As soon as the indoor air set point temperature is returned to the reference indoor air set point temperature of 21.5 °C, the heating power increases (orange, grey and yellow line) and goes above the reference scenario heat power (blue line) for a few hours and then returns to the reference, and this is due to the rebound effect.

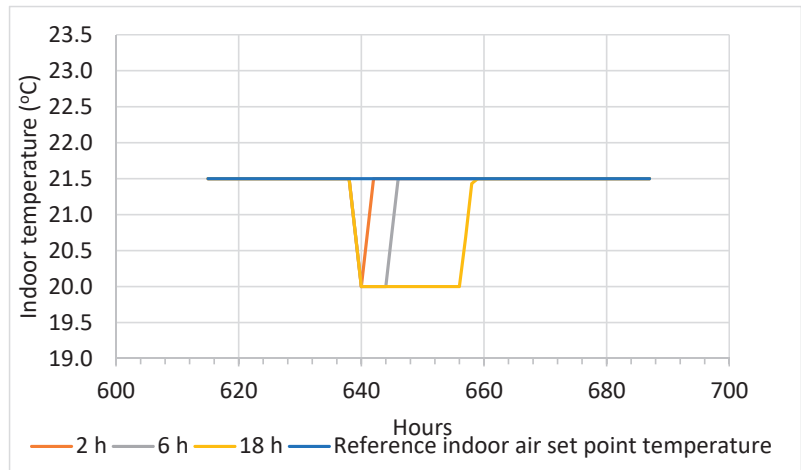


Figure 9. Indoor air temperature activation during heat energy conservation in the old building.

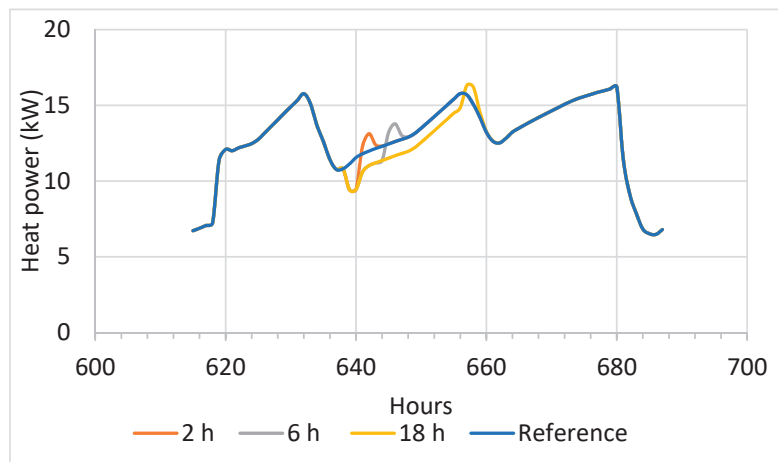


Figure 10. Heating activation during heat energy conservation in the old building.

Figure 11 also shows the energy discharged (orange bar) when the indoor air set point temperature is modulated; the activation of energy conservation occurs and the indoor air set point temperature is reduced to 20 °C. Figure 11 shows the energy charged (blue bar) to reach the reference indoor air set point temperature of 21.5 °C after activation. It can be observed that the energy charge and energy discharged vary depending on the activation duration. Generally, the energy discharge and charge increase with the activation duration. The energy discharged increases from 2 h to 18 h. The energy charge increases from 2 h to 18 h as a greater amount of energy is needed to return back to the reference indoor air set point temperature.

Figure 12 shows that in the case of conservation activation, the shifting efficiency is higher than one. The increase in efficiency is higher as the duration of activation increases. This is because the amount of energy needed to recharge increases as activation increases and also the losses are higher. Similar behavior is observed in [8].

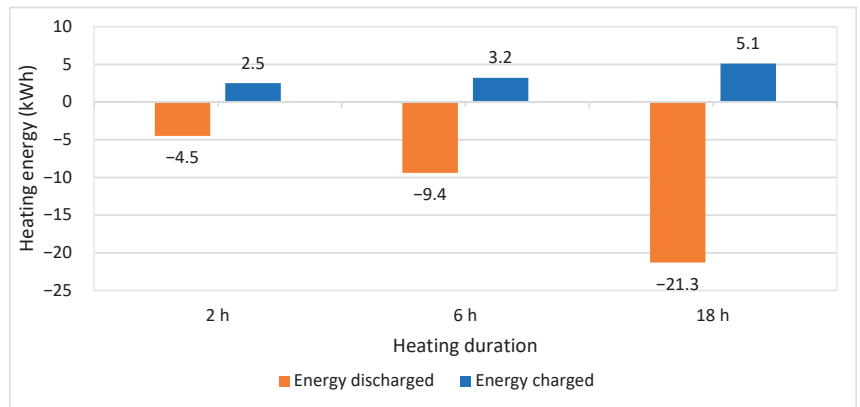


Figure 11. Energy charged and discharged during heat energy conservation in the old building.

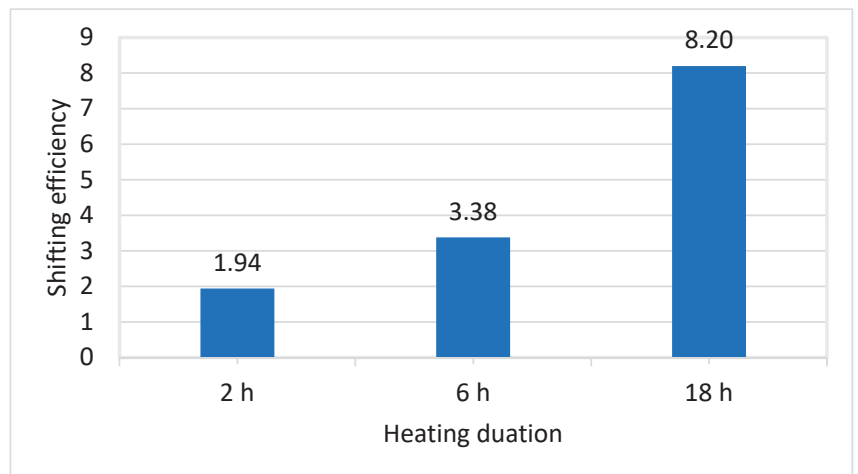


Figure 12. Shifting efficiency during heat energy conservation in the old building.

Figure 13 shows the energy flexibility of the old building under various activation durations for energy conservation. Compared to the reference case, when energy is discharged from the building to lower the indoor temperature to 20 °C, the heating energy (2 h, 6 h, 18 h) is lower than the reference heating power and it is called $Q_{\text{heat discharged}}$. Compared to the reference case, when the energy is charged in the building to increase the indoor temperature to 21.5 °C, the heating energy is higher than the reference heating energy and this energy flow is called $Q_{\text{heat charged}}$. The same approach is used in Section 6.1.2.

Similar behavior is observed as in the case of heat energy storage case. As the activation hour increases, the difference between the energy charged and discharged increases. With higher activation hours, the energy charged is larger while the energy discharge is lower compared to that charged, resulting in higher flexibility as shown in Figure 13.

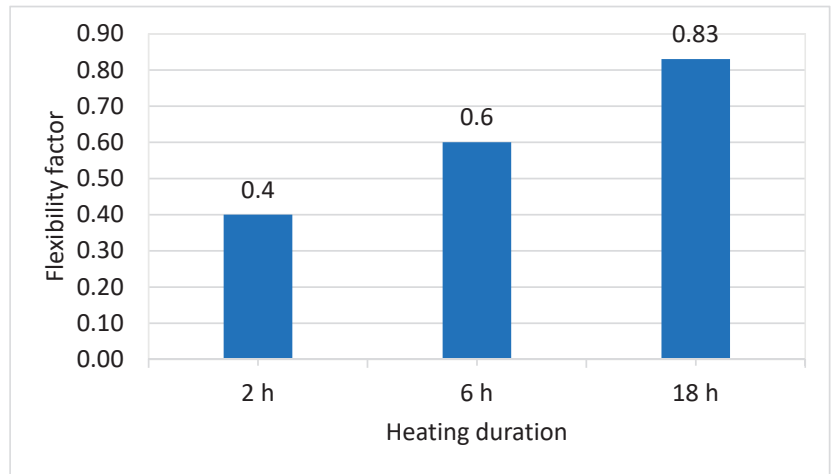


Figure 13. Flexibility factor during heat energy conservation in the old building.

6.1.2. New Building Heat Energy Storage

A similar activation method is used for energy storage activation in the new building. The indoor air set point temperature of the zone is increased by 1.5 °C. The hours selected for analysis are from 615–687 h and the activation hour is 638 h as shown in Figure 14. Similar behavior can be observed in terms of energy storage activation of the old building (Figure 4). However, it can be observed that when 2 h is selected for activation in the new building, it can reach the indoor air set point temperature of 23 °C (Figure 14), whereas in the old building, the indoor temperature is not able to reach the indoor air set point temperature of 23 °C. This is due to poor insulation level in the old building’s envelope.

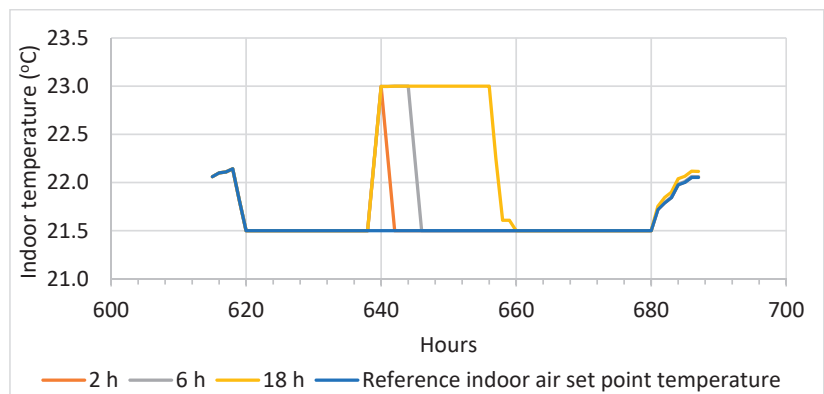


Figure 14. Temperature activation during heat energy storage in the new building.

Figure 15 shows the heat power demand for the reference scenario and also for the activation hours of 2 h, 6 h and 18 h. It can be observed that compared to the energy storage scenario of the old building (Figure 5), the maximum peak heating power is lower for the new building (8 kW), as the new building envelope is efficient, whereas for the old building the maximum heat power is 15.7 kW. There are a few instances when the heating power reaches near zero in the new building case (Figure 15) at 658 h, whereas in the old building case, the heating power Figure 5 does not go close to zero. This is due to the energy-efficient

envelope of the building and the thermal mass activation of the new building that releases the heat which is stored during activation.

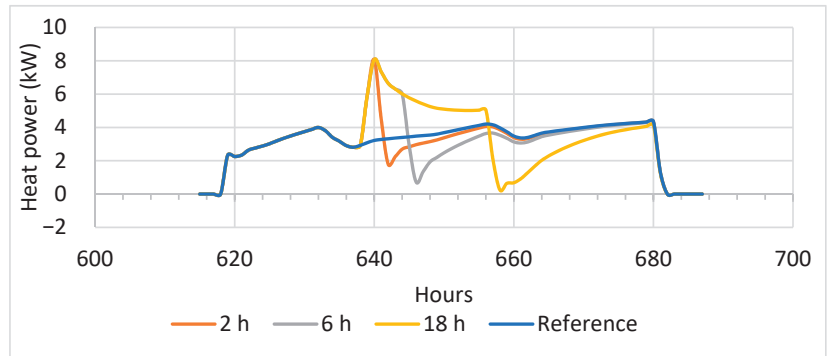


Figure 15. Heating activation during heat energy storage in the new building.

Figure 16 shows the energy charged (blue bar) and discharged (orange bar) to reach the indoor air set point temperature of 23 °C for the activation of energy storage compared to the reference scenario's indoor air set point temperature of 21.5 °C. It can be observed that the energy charge and energy discharge vary depending on the activation duration. In the energy storage case for the old building (Figure 6), the difference between the energy charged and discharged is large in each activation duration hour. In the new building, the difference between the energy charged and discharged is smaller in each activation duration hour. This again shows that new building is better at storing and using heat energy.

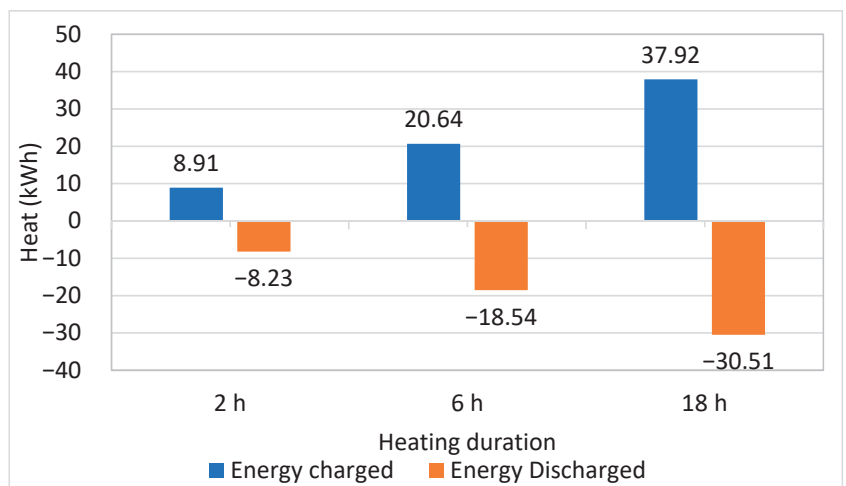


Figure 16. Energy charged and discharged during heat energy storage in the new building.

Figure 17 shows that in the case of storage activation, the shifting efficiency is less than one. The shifting efficiency reduces when the activation hour increases and similar behavior can be observed in Figure 7 in the old building. However, the shifting efficiency of the new building in Figure 17 is better compared (92% maximum) to that of the old building in Figure 7 (a maximum of 52%). This is because the loss in the new building is smaller compared to that in the old building; therefore, the efficiency is better. Similar behavior is observed in [8].

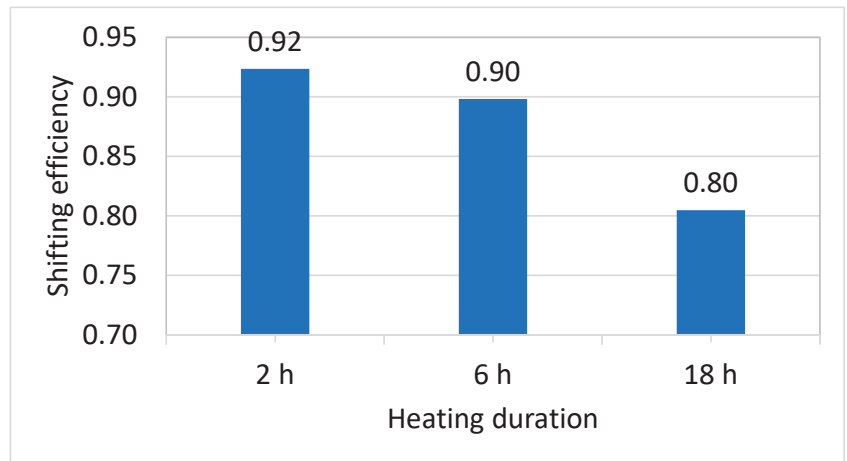


Figure 17. Shifting efficiency during heat energy storage in the new building.

Figure 18 shows the energy flexibility of the new building under various activation hours. It can be observed that the energy flexibility increases as the activation hour increases. This is due to an increase in the difference between the energy charged and discharged as the activation hour increases. Compared to the energy flexibility in Figure 8 of the old building, the flexibility of the new building in Figure 18 is much lower (an 11% maximum). This is due to smaller amount of energy saving potential in terms of the absolute heating demand in the new building that results in lower energy flexibility in the old building.

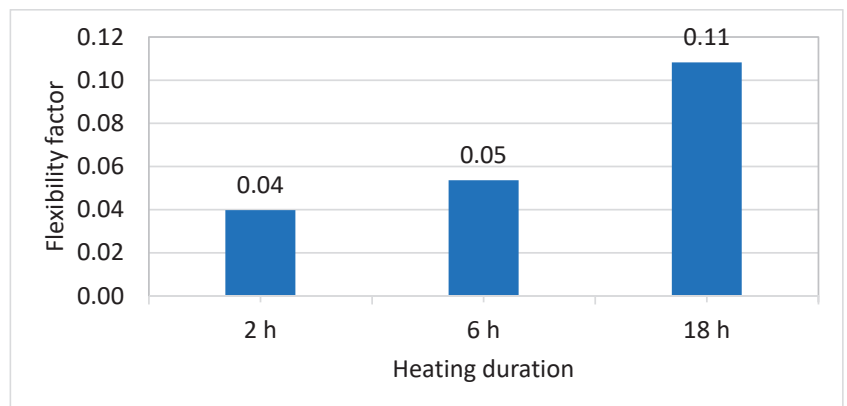


Figure 18. Flexibility factor during heat energy storage in the new building.

Heat Energy Conservation

It is assumed that depending on the weather, the indoor air set point temperature of the zone is decreased by 1.5 °C. Different activation duration hours are considered. The change in the indoor air set point temperature is shown in Figure 19. However, in the new building (Figure 19), the zone temperature drops to 20.6 °C under activation for 2 h and also the temperature drop is slower compared to that of the old building (Figure 9). For the two other activation durations of 6 h and 18 h, the temperature drops to 20 °C. This shows that the losses from the envelope are lower in the new building compared to those in the old building. Hence, the former can maintain a high temperature and comfort for a longer duration compared to the old building.

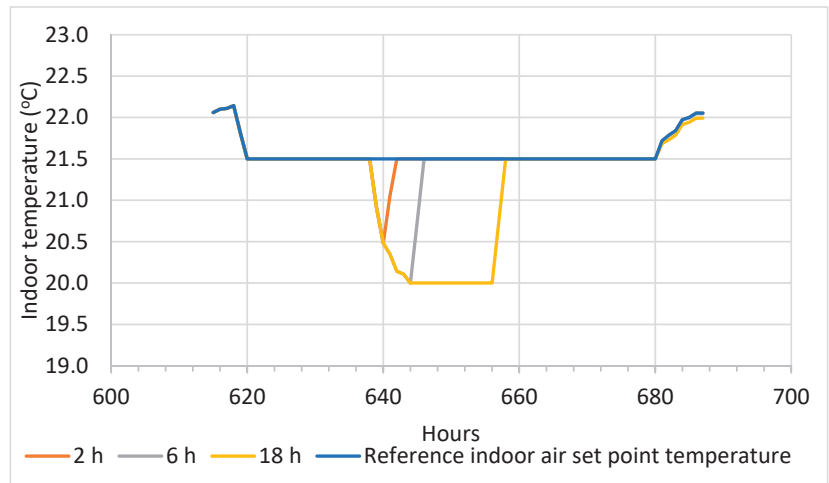


Figure 19. Temperature activation during heat energy conservation in the new building.

Figure 20 shows the heat power demand for the reference scenario and also for the activation hours of 2 h, 6 h and 18 h for the new building. It can be observed that compared to the energy conservation scenario of the old building (Figure 10), the minimum heating power is lower for the new building, as the new building envelope is efficient. There are few instances when the heating power reaches zero for a total of 3 h (from 640 h to 643 h) in the new building case, see Figure 20, whereas in the old building case, the heating power, see Figure 10, does not reach zero. This is due to the energy-efficient envelope of the building and the thermal mass activation of the new building that releases the heat which is stored during activation.

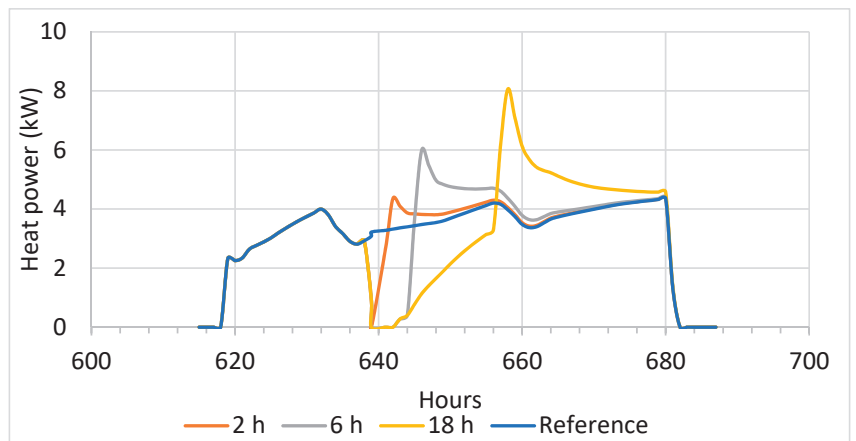


Figure 20. Heating activation during heat energy conservation in the new building.

Figure 21 also shows the energy discharged (orange bar) and energy charged (blue bar) to reach the reference indoor air set point temperature of 21.5 °C. Similar behavior is observed in Figure 16; however, this occurs in the opposite direction of the energy flows.

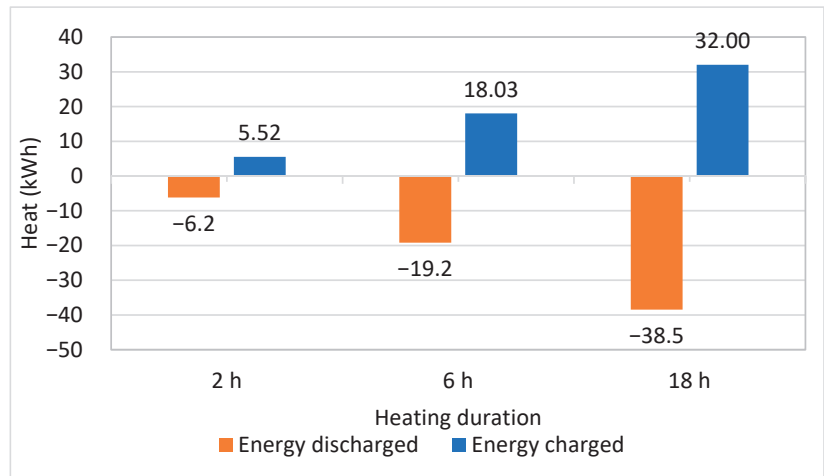


Figure 21. Energy charged and discharged during heat energy conservation in the new building.

Figure 22 shows that in the case of conservation activation, the shifting efficiency is higher than one. The shifting efficiency of the new building in Figure 22 is better compared to that of the old building in Figure 12 as it is closer to one. This is because the losses in the new building are smaller. The losses increase as the activation hour increases. Similar behavior is observed in [8]. The amounts of heat energy discharged and charged are close to each other in the new building compared to those of the old building. In the old building, the energy discharged is higher compared to the charged energy. This shows that the new building can store energy efficiently compared to the old building as the losses are less. It is also observed that the shifting efficiency is close to one in the new building and it is higher than one in the old building. This again shows that the discharged energy, i.e., the energy loss to the ambient surroundings is higher in the old building compared to that in the new building. This is the reason why the new building takes a longer time to reach the set point of 20 °C and it allows it to maintain the indoor temperature effectively in the heat conservation case as it can better store the heat energy.

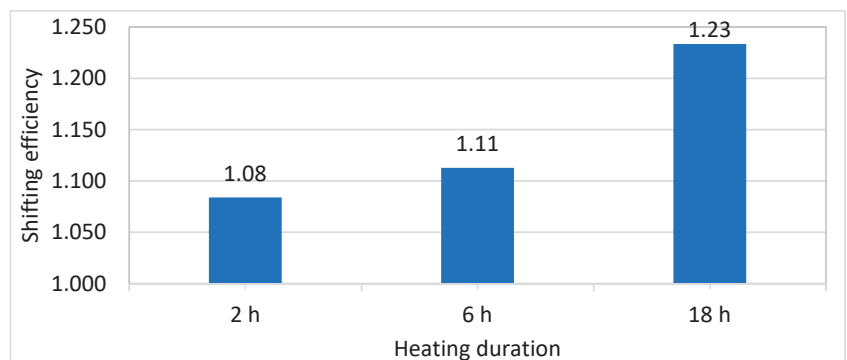


Figure 22. Shifting efficiency during heat energy conservation in the new building.

Figure 23 shows the energy flexibility of the new building under various activation durations. Compared to the energy flexibility (Figure 13) of the old building, the flexibility of the new building (Figure 23) is much smaller. This is due to the large amount of savings in terms of absolute heating energy in the old building that results in higher energy flexibility

in the old building. Therefore, the new building has a lower flexibility factor compared to the old building.

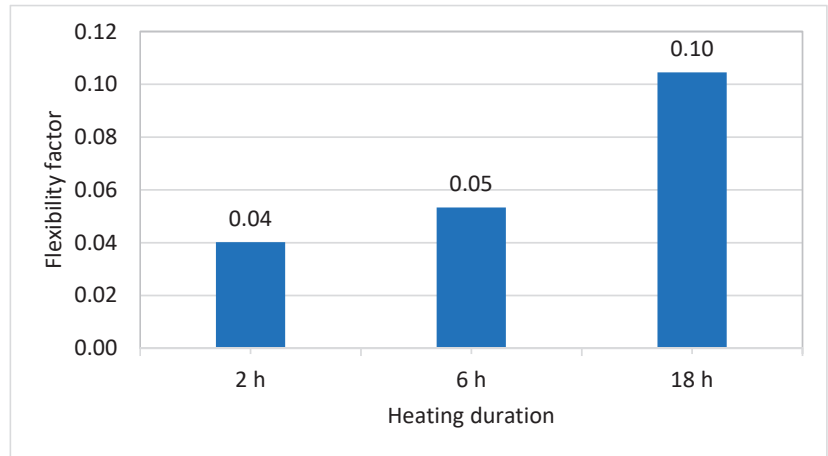


Figure 23. Flexibility factor during heat energy conservation in the new building.

6.2. Flexibility Based on Electricity Price

This section aims to present the energy flexibility potential in the old and new buildings, using the price signals (as shown in Figure 3) [9]. The study is carried out to show the effect of energy conservation and storage activation on thermal mass activation, to save energy costs. For the electricity price signal, the Nordpool price is used (Figure 3). The price signals are divided based on the percentile. The price above the 80% percentile is assumed to be a high price and the price below 20% is assumed to be a low price. The window for the price signal that is analyzed to be marked as a high price or low price is 12 h (at each present time step of 1 h). This 12 h time window moves with the following time step. The rest of the price signals are normal prices. A similar approach is proposed by the authors of [16,43]. Using the price signals and percentiles, different activation cases are generated to identify the flexibility actions to be taken in the old and new buildings. Section 6.2.1 shows the results of the old building and Section 6.2.2 shows the results of the new building.

6.2.1. Old Building

Heat Energy Storage

In this situation, the indoor air set point temperature of the zone is increased by 1.5 °C to 23 °C. Four activation durations are considered, which are 1 h, 2 h, 4 h and 6 h, and compared against the reference case (without activation). A long activation duration is not considered as it is found in Section 6.1, that losses are high, the window for the activation duration is long as price varies and short activation durations are better in terms of shifting efficiency. The impact on the annual total energy cost and flexibility factor due to the activation duration can be observed in Figure 24.

It can be observed that when 1 to 2 h is selected for activation, the building's energy cost reduces from EUR 6001 (reference case) to EUR 5767 (for 1 h activation) and EUR 5935 (for 2 h activation), and it can benefit from storage control activation. In all the other activation durations, it increases to EUR 6039 (4 h activation) and EUR 6085 (6 h activation). This shows that for short activation durations, the building can save energy costs by storing excess heat and releasing it. However, for the longer activation durations, the losses through the envelope and windows are high and the building is not able to benefit from the increased energy storage by reducing the energy cost. Another source of heat loss is the exhaust air leaving the building which is lost to the ambient surroundings

at higher temperatures. Due to these losses at higher temperatures, the building needs to be heated even though the price may be higher.

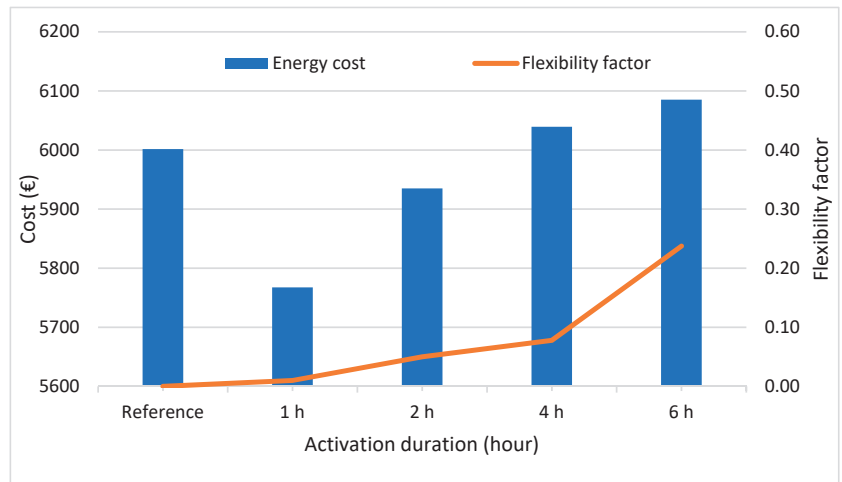


Figure 24. Yearly energy cost and flexibility factor during heat energy storage in the old building.

On the other hand, the energy flexibility factor is higher with longer activation durations, which is due to the higher variation in the energy charged and discharged under long activation durations. Hence, the energy flexibility increases with longer activation durations; however, the energy cost also increases.

Heat Energy Conservation

In this case, the indoor air set point temperature of the zone is decreased by 1.5 °C to 20 °C. Different activation durations are considered. The impact on the cost and flexibility factor due to the activation duration can be observed in Figure 25.

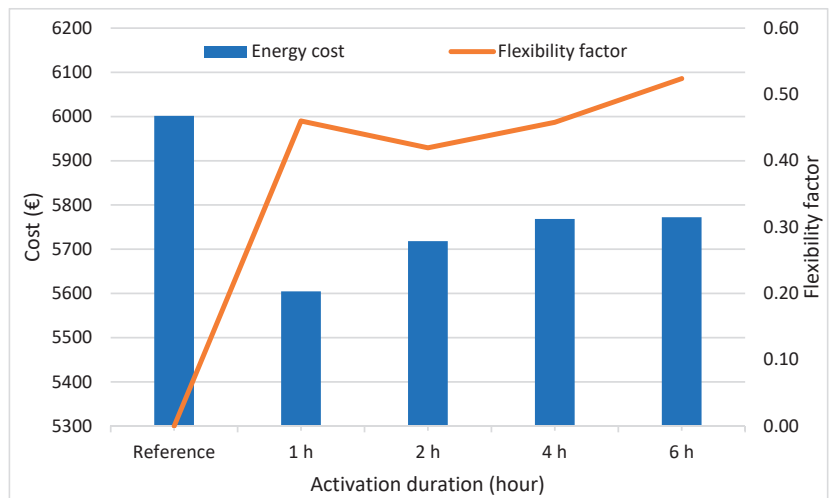


Figure 25. Yearly energy cost and flexibility factor during heat energy conservation in the old building.

It can be observed that when 1 h, 2 h, 4 h and 6 h are selected for activation, the building's energy cost reduces from EUR 6001 to EUR 5604 (for 1 h activation) and EUR

5772 (for 6 h activation). This shows that for short activation durations, the building is able to save significant amount of the energy cost (around EUR 400). However, the energy cost increases as the activation duration increases. This is because when the indoor air set point temperature is reduced for a longer duration to 20 °C, a larger amount of heat is needed to return to the reference indoor air set point temperature of 21.5 °C, resulting in an instantaneous increase in heat energy input as discussed in Section 6.1.1.

On the other hand, the energy flexibility factor is higher with longer activation durations, and this is due to higher variation in the energy charged and discharged under long activation durations. Hence, the energy flexibility may increase with longer activation durations, and the energy price may also increase.

6.2.2. New Building

Heat Energy Storage

In this situation, the indoor air set point temperature of the zone is increased by 1.5 °C to 23 °C. This is carried out to heat the thermal mass of the building and store heat, so it can be released when the indoor air set point temperature is back to the reference point of 21.5 °C. The impact on the cost and flexibility factor due to the activation duration can be observed in Figure 26.

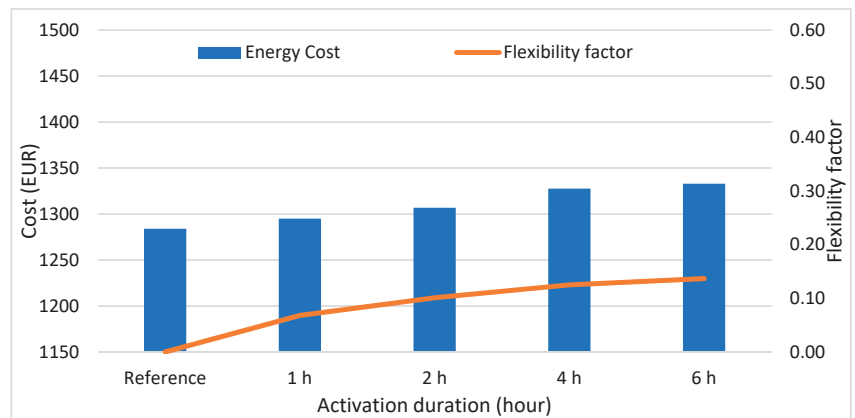


Figure 26. Yearly energy cost and flexibility factor during heat energy storage in the new building.

It can be observed that the building's energy price increases from EUR 1283 to EUR 1332 as the activation duration increases. This is because, due to the higher temperature, it results in higher losses in the new building. Similar behavior is observed; that is, higher energy costs in the old building (Figure 24). The losses through the envelope and windows are high and the building is not able to benefit from the increased energy storage. Another source of heat loss is the exhaust air leaving the building which is lost to the ambient surroundings at higher temperatures. Only for the short activation durations (1 h or 2 h), the old building (Figure 24) is able to reduce the energy cost as the heating demand is high in an old building and the use of energy storage is effective for short activation durations.

On the other hand, the energy flexibility factor is higher with longer activation durations, and this is due to the higher variation in the energy charged and discharged under long activation durations. Hence, the energy flexibility may increase with longer activation durations, and the energy price may also increase. However, compared to the energy flexibility (Figure 24) of the old building, it is around 50% for 6 h of activation, whereas the flexibility of the new building (Figure 26) is less at around 15% for 6 h of activation. This is due to a large amount of savings in terms of the absolute heating demand in the old building that results in higher energy flexibility in the old building.

Heat Energy Conservation

In this case, the indoor air set point temperature of the zone is decreased by 1.5 °C to 20 °C. The impact on the cost and flexibility factor due to the activation duration can be observed in Figure 27.

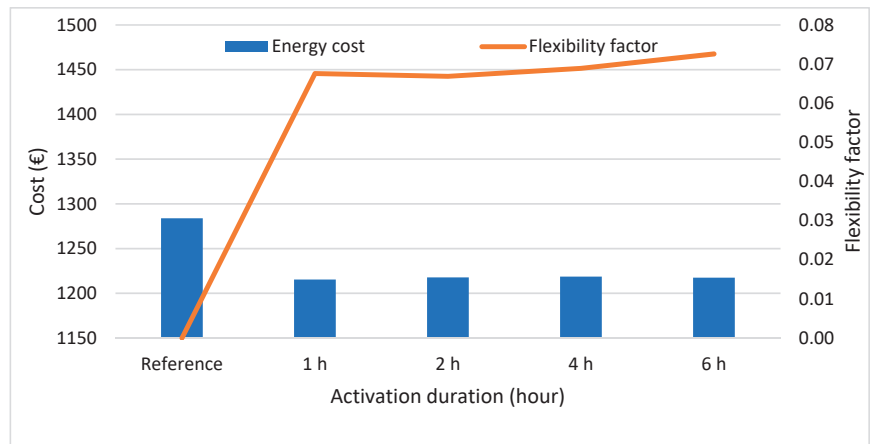


Figure 27. Yearly energy cost and flexibility factor during heat energy conservation in the new building.

The building's energy price reduces from EUR 1283 to EUR 1217 as the activation duration increases. This shows that for short activation hours, the building is able to save more in terms of costs compared to under large activation duration. However, the energy cost increases as the activation duration increases, although it remains lower than the reference energy cost. Compared to the energy storage scenario (Figure 26), the energy cost remains lower in the energy conservation scenario (Figure 27).

The energy flexibility factor is higher with longer activation durations, and this is due to the higher variation in the energy charged and discharged under long activation durations (Figure 27). Hence, energy flexibility may increase with longer activation durations, and the energy price may also increase. Compared to that in the new building's energy storage scenario (Figure 26), the energy flexibility factor remains lower in the energy conservation scenario (Figure 27). Overall, the energy flexibility factor of the new building is smaller compared to that of the old building for both energy storage and conservation activation scenarios.

7. Energy Resilience of the New and Old Building

As discussed in the introduction, human-related activity is significantly driving climate crises according to the Intergovernmental Panel on Climate Change (IPCC) [44]. It is expected that in 20 years, human activities can cause global temperatures to rise above 1.5 °C from those in 1850–1900. As a result, disasters such as huge storms, fires and, heavy rains are very frequent and are becoming more visible in recent times. Therefore, the globe is expected to face increased extreme events of heat waves [45], longer warm seasons and extreme cold events, which can last for several days and be accompanied by power outages of electricity and heat. In addition to the climate-driven reasons, there are nowadays increased serious threats of power outages due to political conflicts, wars or accidents.

When a power outage takes place in times of very cold weather in winter, the challenge is whether or not buildings are still able to keep minimum habitable temperatures and provide minimum basic levels of services to its occupants. Although the probability of the occurrence of such events is low, it is increasing nowadays and is expected to be higher in the future. However, if the events take place, the impact will be very extensive on the health and life of people in buildings and on building systems and infrastructures [44].

Energy flexibility focuses on the energy saving and cost saving aspects of the building. However, during the activation of a thermal mass and indoor air set point temperature variation, there is a risk to the thermal comfort and habitable temperature inside the building. This risk becomes severe when a power outage occurs during cold weather conditions in Nordics. There is a risk of indoor room temperature decay especially when energy conservation activation continues and a power outage occurs. In this condition, the energy resilience of the building becomes important. This interaction and connection has not been studied under Nordic conditions and the regulations are not clear for this. Therefore, another novel aspect that this article discusses, and presents is a study on the performance of old and new residential buildings in the Finnish climate to find their thermal behavior in winter during a short-period power outage and their resilience characteristics. In a short-period outage (1–2 days), which can be either a controlled action, due to a shortage in power generation, or an uncontrolled one, due to unforeseen reasons, the question is about the occupant's thermal comfort and the robustness duration that shows the energy resilience of the building. Controlled short-period outages of power to buildings in Finland can take place more often next winter due to challenges in supplying sufficient power.

The robustness period (RP) presents the duration for which the building's indoor temperature can be maintained after a power outage [46]. The building is highly prepared for facing an outage if the the robustness period of the particular building is higher.

The reference indoor air set point temperature is 21.5 ± 0.5 °C which is required in any normal condition, whereas the robustness threshold is the point above which the performance (i.e., zone temperature) can be considered robust performance. If the zone temperature is below this point, the performance is not robust. The World Health Organization [47] recommends that for general health, well-being and safety, a minimum temperature of 18 °C is recommended in the cold seasons in cold climatic conditions. Therefore, 18 °C has been used as the minimum robustness threshold for old and new buildings. Moreover, 15 °C is chosen as the habitability threshold based on the study of old and new buildings. Below this point, it can be assumed that the building is not able to provide the minimum comfort conditions for its occupants and the building is not thermally resilient anymore.

The robustness period for the old and new buildings is presented in Sections 7.1 and 7.2 respectively.

7.1. Old Building

The hours selected for the study are from hour 615 to hour 687 when the ambient temperature is around -10 °C– -15 °C (cold conditions; it is assumed that the power outage occurs at hour 637). The same time slot is assumed for further analysis. It can be observed that when the indoor air set temperature is 21 ± 0.5 °C, it drops to 18 °C (robustness threshold) in 3 h in an old building, when a power outage occurs and heating stops as shown in Figure 28 (orange line), and it drops to 15 °C in the next 5 h. On the other hand, when the indoor air set temperature is 18 °C, it drops to 14 °C in 3 h, when a power outage occurs at this point as shown in Figure 28 (blue line). When the minimum indoor temperature is 18 °C (as recommended by the WHO [47]), the building may not be able to provide thermal comfort as the robustness period is zero and the building may become inhabitable (less than 15 °C) as soon as a power outage occurs for a short duration. Therefore, depending on the indoor air set point temperature, ambient temperature, and the time when a power outage occurs, the robustness duration of the old building will also be affected which can impact the energy resilience of the building. It is essential to plan and manage the minimum indoor air set point temperature in the old building while keeping the energy crisis and resilience aspect in present times in mind. It is also found in Figure 28 (orange line) that when the electricity is restored in the building, it takes around 14 h to recover and reach the indoor air set temperature of 21.5 ± 0.5 °C.

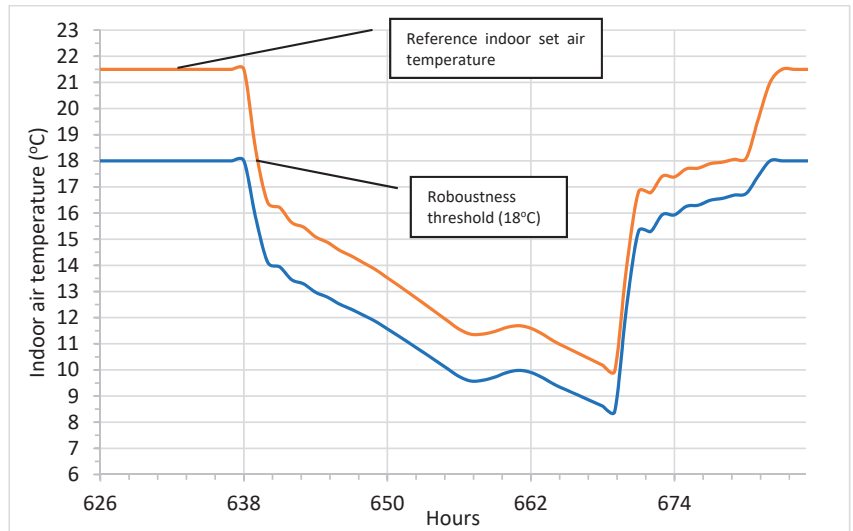


Figure 28. Energy resilience of the old building and robustness period in cold climates under a power outage.

The Finnish building code [23] indicates 21.5 ± 0.5 °C as the design indoor air temperature during the heating season, and the decree of the Finnish Ministry of Social Affairs and Health [48] indicates 18 °C as the lowest room air temperature during the heating season. Therefore, for a short power outage in such old buildings, under the coldest weather, thermal comfort could be difficult to maintain for a longer duration. The effect of a loss of heating for several hours on people's thermal comfort should be thoroughly studied, especially in context of old detached houses since the energy conservation measures in those houses are normally poor due to the low quality of the building envelope's insulation, windows and air tightness.

7.2. New Building

It can be observed that when the indoor air set temperature is 21 ± 0.5 °C, it drops to 18 °C (robustness threshold) in 17 h in the new building when a power outage occurs and heating stops as shown in Figure 29 (orange line). On the other hand, when the indoor air set temperature is 18 °C, it drops to 15.5 °C in 17 h, when a power outage occurs at this point as shown in Figure 29 (blue line). When the operating temperature is 18 °C the new building will provide thermal comfort for a few hours as the robustness period is very short. However, the building may be habitable (above 15 °C) for 17–18 h after a power outage occurs for a short duration. Therefore, depending on the indoor air set point temperature of the indoor temperature, ambient temperature and time when a power outage occurs, the robustness duration of the old building will also be affected which can impact the energy resilience of the building.

It is essential to plan and manage the minimum indoor air set point temperatures in new buildings while considering the energy crisis and the resilience aspects in the present situation.

It is also found in Figure 29 (orange line) that when the electricity is restored in the building, it takes around 4 h–5 h to recover and reach the indoor air set temperature of 21.5 ± 0.5 °C. Compared to the old building (Figure 28), the new building (Figure 29) can recover earlier and faster. Therefore, new buildings are better prepared to address the power shortage and energy crises and are resilient compared to the old buildings.

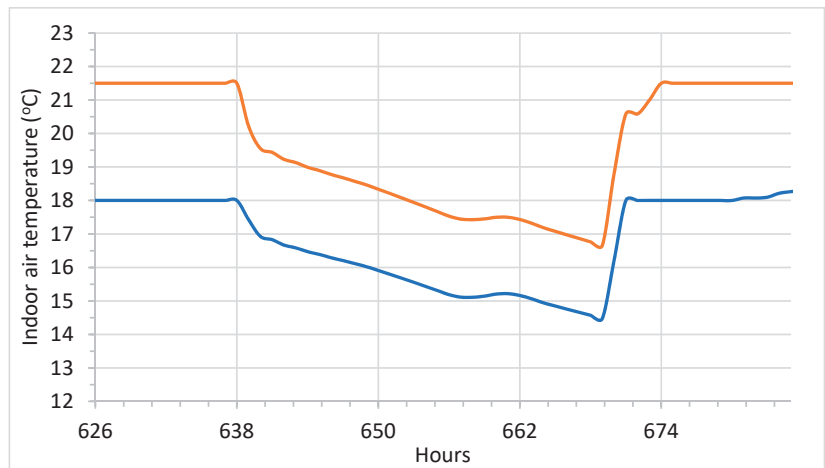


Figure 29. Energy resilience of the new building and robustness period in cold climates under a power outage.

Overall, during a short power outage in cold weather conditions, such new buildings would maintain better thermal comfort for a longer duration (Figure 29) compared to old buildings (Figure 28). The effect of the loss of heating for several hours on people’s thermal comfort in new buildings is better. However, the thermal comfort in new buildings should be thoroughly studied for longer durations of power outages.

With the current and near-future political circumstances for energy supply and the global warming implications on weather conditions, there is an urgent need to conduct a comprehensive systematic study on different types and ages of residential buildings in the Finnish building stock. Their thermal characteristics in winter during short-period power outages and their resilience in terms of habitability and survivability during long-period power outages are required to be found. This will assist in classifying buildings’ readiness to withstand power outages. This article briefly introduces the challenge and performance of buildings in the cold climatic conditions of Finland. Future studies are needed for the technical power solutions to be applied in different types of buildings to avoid critical health and safety effects on the health and life of the residents, which should be economically feasible as well. New ways to improve the resilience of buildings have to be further studied such as by integrating renewable energy sources and energy storages. For instance, solar energy and the use of energy storage (such as phase change materials [17], batteries, tanks, etc.) can assist in improving the resilience as well as the flexibility of the building stock. Moreover, required changes in the codes and regulations should be identified with the aim of developing a robust energy resilience strategy for buildings in Finland.

8. Conclusions

Cities and districts are setting ambitious targets to make buildings carbon-neutral and flexible in an economical manner. Energy flexibility is important in managing and reducing energy costs via the activation of zone temperatures and activation of the thermal mass of buildings. On the other hand, energy resilience in buildings has a crucial impact on the health and life of a building’s occupants during total power outages. Therefore, the challenge is how to achieve the two objectives of flexibility and resilience. The article presents the quantitative analysis and management of the operation of the two old and new buildings to reach the two different objectives of energy flexibility and energy resilience together since both are competing for the same available sources i.e. thermal mass. This includes proposing control strategies for activating buildings’ thermal mass

(through energy conservation and energy storage strategies). The focus of the analysis lies in the energy flexibility improvement potential, cost reduction potential, and energy resilience improvement potential of the two buildings. These concepts and the control of the heating system of the house are presented. The following are the key findings on the energy flexibility:

- The dynamic behavior of the old building during heat energy storage shows that when a short duration (2 h) is selected for activation, the building's indoor areas are not able to reach the provided indoor air set point temperature of 23 °C. However, when 6 and 18 h are selected for activation, the building indoor temperature reaches the indoor air set point temperature of 23 °C. Generally, energy charge and discharge increase with the increase in the activation duration. The shifting efficiency reduces when the activation duration increases due to high losses as the duration increases. It is observed that the energy flexibility increases as the activation duration increases. Heat energy conservation shows that for all activation durations, the building indoor temperature drops quickly to 20 °C. In the case of conservation activation, the shifting efficiency is higher than one. It is observed that the energy flexibility increases as the activation duration increases, though it is slightly less than that in the energy storage case.
- The dynamic behavior of the new building during heat energy storage shows that compared to the old building's energy storage scenario, the building's indoor temperature is able to reach the provided indoor air set point temperature of 23 °C in 2 h of activation. The shifting efficiency of the new building is better compared to that of the old building. Moreover, the flexibility of the new building is lower compared to the energy flexibility of the old building. Heat energy conservation shows that the zone temperature drops to 20.6 °C under activation for 2 h and the temperature drop is slower compared to that of the old building for all activation durations. In addition, there are a few instances when the heating power reaches zero in the new building case whereas in the old building case, the heating power does not reach zero.
- This study analyzed the energy storage activation of the thermal mass based on the price signals for the old and new buildings. The overall energy cost is higher in the old building compared to that in the new building due to the higher heating demand. Generally, in the energy storage case, the energy cost increases due to an increase in the indoor air set point temperature and activation caused by the losses in the old and new buildings. Only for the short activation duration (1 h or 2 h), the old building is able to reduce the energy cost as the heating demand is high in an old building and the implementation of energy storage is effective for short activation durations. Moreover, the energy flexibility increases with higher activation durations. The energy flexibility of the old building is around 50% for a 6 h activation duration, whereas the flexibility of the new building is lower at around 15% for 6 h of activation. This shows that the flexibility factor and potential are higher in old buildings due to the higher heating demand and saving potential.
- For energy conservation activation based on the price signals, the overall energy cost is lower in the new building compared to that in the old building due to the lower heating demand in the new building. Generally, the energy cost reduces due to a reduction in the indoor air set point temperature and activation duration. This is carried out to save energy for some time and after this the indoor air set point temperature is returned to the reference point of 21.5 °C. It is found that for short activation durations, the old and new buildings can save a large amount of the energy cost. However, the energy cost increases as the activation duration increases, although it remains lower than the reference energy cost. For both buildings, the energy flexibility factor is higher with a higher activation duration, and this is due to the higher variation in the energy charged and discharged under a high activation duration. The energy flexibility may increase with a higher activation duration; on the contrary, the energy price may also increase.

The energy resilience of buildings is essential along with energy flexibility. It is assumed that when a power outage takes place during winter, the challenge is whether or not the old and new buildings can keep minimum habitable temperatures and thermal comfort while ensuring energy flexibility. The robustness period is estimated for both the new and old buildings that are at different indoor air set temperatures (due to energy flexibility activation). The result presents the duration for which a building's indoor temperature can be maintained after a power outage [46]. A building is highly prepared for facing the outage if the robustness period of the particular building is higher. Some of the main findings are as follows:

- Overall, in cold weather conditions, new buildings would maintain better thermal comfort for a longer duration compared to old buildings. The reduction in thermal comfort is smaller in new buildings compared to that in old buildings during power outage.
- For an old building, when a power outage occurs (heating stops), the indoor air set temperature drops to 18 °C from 21.5 ± 0.5 °C and the robustness threshold is 3 h. On the other hand, when the indoor air set temperature is 18 °C, it drops to 14 °C in 3 h. This shows that when the operating temperature is 21.5 °C, the building may provide 3 h of thermal comfort (due to the robustness period) and when the operating temperature is 18 °C (due to flexibility) the building may not be able to provide thermal comfort as the robustness period is zero. Therefore, it is essential to plan and manage the minimum indoor air set point temperature in an old building while keeping the energy crisis and resilience aspect in mind.
- For a new building, when a power outage occurs (heating stops), the indoor air set temperature drops to 18 °C from 21.5 ± 0.5 °C and the robustness threshold is 17 h. On the other hand, when the indoor air set temperature is 18 °C, it drops to 15.5 °C in 17 h. A new building may provide thermal comfort when the operating temperature is 18 °C a few hours as the robustness period is very short. However, the new building may be habitable (above 15 °C) for 17–18 h when the power outage is short.

This research focuses on cold climatic conditions. With the increase in the energy prices and the expected forthcoming energy crises, this research provides solutions to address the challenges. These challenges are faced not only in cold climatic regions but also internationally. This research is beneficial not only for cold climatic regions such as the Nordics but it is useful for the international perspective. To address these challenges, buildings and their energy systems have to be smart and flexible. The energy flexibility and activation of building mass based on price and weather signals show the energy saving potential. These solutions will support in addressing energy pricing concerns. Moreover, they will support the energy efficiency and carbon neutrality policy of Europe in general as the energy storage and conservation activation control strategies help in reducing carbon emissions and energy consumption as well. These control strategies can also support the better integration of renewable energy sources within the energy network and provide flexibility to the grid from the building side. Further research is needed to estimate the energy flexibility factor for different types of construction, users and weather. It can be assumed that activation can occur during unoccupied hours along with the price signals and control strategies can be built for it. Another future evaluation that can be carried out is the use of onsite renewable energy generation and storage in the buildings. The use of innovative technology and energy storage such as phase change materials [17], batteries [26] and tanks can be integrated into the building's mass which can improve both energy flexibility and the energy resilience of the building, for example. These methods and control strategies would also impact the energy grid and support smart grids. However, further analysis is needed to analyze the benefits of implementing renewable energy generation and energy storage at the building, grid and district levels.

Finally, energy-resilient buildings are key elements for the future sustainability of society in Europe and in other parts of the world. It is, therefore, essential to plan for resilient buildings. Improved policy and research are needed at the European and national levels that will provide guidelines to society, businesses and end users to build energy-

resilient buildings. Therefore, another aspect that needs further analysis is the definition of energy resilience and a framework to estimate the performance of a building under a power outage. This is essential due to the eminent energy crises that are faced by many countries. This study can be extended for different types of buildings and end users especially in cold climatic conditions. This study will ultimately support the further improvement of building regulations and directives so they can integrate energy efficiency, energy resilience and flexibility. As energy flexibility and resilience are competing for the same resources in a building, further studies are needed to balance and optimize resource utilization. The present study is limited to the simulation activity so the scope of the work can be further extended into an experimental phase in future work. This can help in analyzing and comparing the energy flexibility and resilience performance of buildings in the real environment, validate the findings of the simulation and provide a platform on which various technologies such as solar energy and energy storage [17] can be tested.

Author Contributions: Conceptualization, H.u.R. and A.H.; methodology, H.u.R.; software, H.u.R.; validation, H.u.R. and A.H.; formal analysis, H.u.R.; investigation, H.u.R. and A.H.; resources, H.u.R. and A.H.; data curation, H.u.R.; writing—original draft preparation, H.u.R.; writing—review and editing, H.u.R. and A.H.; visualization, H.u.R.; supervision, H.u.R. and A.H.; project administration, H.u.R. and A.H.; funding acquisition, H.u.R. and A.H. All authors have read and agreed to the published version of the manuscript.

Funding: This research was funded by Academy of Finland, project “Energy Resilience in Buildings in Extreme Cold Weather Conditions in Finland 2022–2025 (FinERB), Grant number: 348060” and Academy of Finland project “Integration of Building Flexibility into Future Energy Systems 2020–2024 (FlexiB), Grant number: 333364”.

Data Availability Statement: The data presented in this study are available on request from the corresponding author.

Acknowledgments: The authors would like to acknowledge IEA EBC Annex 83 on Positive Energy Districts.

Conflicts of Interest: The authors declare no conflict of interest. The funders had no role in the design of the study; in the collection, analyses, or interpretation of data; in the writing of the manuscript; or in the decision to publish the results.

Nomenclature

CO ₂	Carbon dioxide
°C	Centigrade
EPBD	Energy performance of building directives
EPS	Expanded polystyrene insulation
EU	European Union
h	Hour
IPCC	Intergovernmental Panel on Climate Change
K	Kelvin
kg	Kilogram
m	Mass
PCM	Phase change material
Q _{heat}	Heat transfer
q ₅₀	Air infiltration
RP	Robustness period
TRNSYS	Transient System Simulation Tool
U value	Thermal transmittance
W	Watt
WHO	World Health Organization
EUR	Euro

References

- European Commission. 2050 Long-Term Strategy Climate Action. Available online: https://ec.europa.eu/clima/policies/strategies/2050_en (accessed on 4 November 2019).
- European Commission. “Fit for 55”: Council Adopts Key Pieces of Legislation Delivering on 2030 Climate Targets—Consilium. Available online: <https://www.consilium.europa.eu/en/press/press-releases/2023/04/25/fit-for-55-council-adopts-key-pieces-of-legislation-delivering-on-2030-climate-targets/> (accessed on 13 May 2023).
- European Commission. Clean Energy for All Europeans. *Euroheat Power (Engl. Ed.)* **2019**, *14*, 3. [CrossRef]
- The European Parliament and the Council of the European Union Directive (EU). Directive 2018/844 of the European Parliament and of the Council of 30 May 2018 Amending Directive 2010/31/EU on the Energy Performance of Buildings and Directive 2012/27/EU on Energy Efficiency. *Off. J. Eur. Union* **2018**, *L 156/75*. Available online: <http://data.europa.eu/eli/dir/2018/844/oj> (accessed on 22 November 2020).
- Attia, S.; Levinson, R.; Ndongo, E.; Holzer, P.; Berk Kazanci, O.; Homaei, S.; Zhang, C.; Olesen, B.W.; Qi, D.; Hamdy, M.; et al. Resilient Cooling of Buildings to Protect against Heat Waves and Power Outages: Key Concepts and Definition. *Energy Build.* **2021**, *239*, 110869. [CrossRef]
- Flores-Larsen, S.; Filippin, C. Energy Efficiency, Thermal Resilience, and Health during Extreme Heat Events in Low-Income Housing in Argentina. *Energy Build.* **2021**, *231*, 110576. [CrossRef]
- Al Assaad, D.; Sengupta, A.; Breesch, H. Demand-Controlled Ventilation in Educational Buildings: Energy Efficient but Is It Resilient? *Build. Environ.* **2022**, *226*, 109778. [CrossRef]
- Le Dréau, J.; Heiselberg, P. Energy Flexibility of Residential Buildings Using Short Term Heat Storage in the Thermal Mass. *Energy* **2016**, *111*, 991–1002. [CrossRef]
- Nord Pool as Historical Market Data (Finland). Available online: <https://www.nordpoolgroup.com/en/Market-data1/Dayahead/Area-Prices/FI/Hourly/?dd=FI&view=table> (accessed on 22 November 2020).
- Li, H.; Hong, T. A Semantic Ontology for Representing and Quantifying Energy Flexibility of Buildings. *Adv. Appl. Energy* **2022**, *8*, 100113. [CrossRef]
- Ren, H.; Sun, Y.; Albdoor, A.K.; Tyagi, V.V.; Pandey, A.K.; Ma, Z. Improving Energy Flexibility of a Net-Zero Energy House Using a Solar-Assisted Air Conditioning System with Thermal Energy Storage and Demand-Side Management. *Appl. Energy* **2021**, *285*, 116433. [CrossRef]
- Arteconi, A.; Mugnini, A.; Polonara, F. Energy Flexible Buildings: A Methodology for Rating the Flexibility Performance of Buildings with Electric Heating and Cooling Systems. *Appl. Energy* **2019**, *251*, 113387. [CrossRef]
- Alimohammadisagvand, B.; Jokisalo, J.; Sirén, K. Comparison of Four Rule-Based Demand Response Control Algorithms in an Electrically and Heat Pump-Heated Residential Building. *Appl. Energy* **2018**, *209*, 167–179. [CrossRef]
- Yoon, J.H.; Bladick, R.; Novoselac, A. Demand Response for Residential Buildings Based on Dynamic Price of Electricity. *Energy Build.* **2014**, *80*, 531–541. [CrossRef]
- Christantoni, D.; Oxizidis, S.; Flynn, D.; Finn, D.P. Implementation of Demand Response Strategies in a Multi-Purpose Commercial Building Using a Whole-Building Simulation Model Approach. *Energy Build.* **2016**, *131*, 76–86. [CrossRef]
- Delgado, B.M.; Ruusu, R.; Hasan, A.; Kilpeläinen, S.; Cao, S.; Sirén, K. Energetic, Cost, and Comfort Performance of a Nearly-Zero Energy Building Including Rule-Based Control of Four Sources of Energy Flexibility. *Buildings* **2018**, *8*, 172. [CrossRef]
- Du, Z.; Liu, G.; Huang, X.; Xiao, T.; Yang, X.; He, Y.L. Numerical Studies on a Fin-Foam Composite Structure towards Improving Melting Phase Change. *Int. J. Heat Mass Transf.* **2023**, *208*, 124076. [CrossRef]
- Péan, T.Q.; Ortiz, J.; Salom, J. Impact of Demand-Side Management on Thermal Comfort and Energy Costs in a Residential NZEB. *Buildings* **2017**, *7*, 37. [CrossRef]
- Nik, V.M.; Perera, A.T.D.; Chen, D. Towards Climate Resilient Urban Energy Systems: A Review. *Natl. Sci. Rev.* **2021**, *8*, 2021. [CrossRef]
- Kopányi, A.; Poczobutt, K.; Pallagi, L.Á. Resilient Cooling—Case Study of a Residential Building in Ry (Denmark). Master’s Thesis, Aalborg University, Aalborg, Denmark, 2020.
- Breesch, H.; Janssens, A. Performance Evaluation of Passive Cooling in Office Buildings Based on Uncertainty and Sensitivity Analysis. *Sol. Energy* **2010**, *84*, 1453–1467. [CrossRef]
- Enright, P. *Passive Cooling Measures for Multi-Unit Residential Buildings*; Morrison Hershfield: Vancouver, BC, Canada, 2017.
- Ministry of the Environment. The National Building Code of Finland—Ympäristöministeriö. Available online: <https://ym.fi/en/the-national-building-code-of-finland> (accessed on 22 February 2021).
- Wilson, A. Passive Survivability. Available online: <https://www.buildinggreen.com/op-ed/passive-survivability> (accessed on 22 August 2021).
- Sengupta, A.; Al Assaad, D.; Bastero, J.B.; Steeman, M.; Breesch, H. Impact of Heatwaves and System Shocks on a Nearly Zero Energy Educational Building: Is It Resilient to Overheating? *Build. Environ.* **2023**, *234*, 110152. [CrossRef]
- Homaei, S.; Hamdy, M. Quantification of Energy Flexibility and Survivability of All-Electric Buildings with Cost-Effective Battery Size: Methodology and Indexes. *Energies* **2021**, *14*, 2787. [CrossRef]
- Oberg, B.K.; Urban, A.; Leffel, E.; Goebel, J.; Perry, M.; Vas, D.; Broderson, D.; Liesen, R.; Zhivov, A. Thermal Energy System Resilience: Temperature Decay in Cold/Arctic Climates—Part I. Available online: <https://annex73.iea-ebc.org/Data/Sites/4/media/papers/vc-21a-002.pdf> (accessed on 30 April 2023).

28. Sovacool, B.K. Evaluating Energy Security in the Asia Pacific: Towards a More Comprehensive Approach. *Energy Policy* **2011**, *39*, 7472–7479. [CrossRef]
29. Liu, J.; Jian, L.; Wang, W.; Qiu, Z.; Zhang, J.; Dastbaz, P. The Role of Energy Storage Systems in Resilience Enhancement of Health Care Centers with Critical Loads. *J. Energy Storage* **2021**, *33*, 102086. [CrossRef]
30. Nguyen, A.T.; Reiter, S.; Rigo, P. A Review on Simulation-Based Optimization Methods Applied to Building Performance Analysis. *Appl. Energy* **2014**, *113*, 1043–1058. [CrossRef]
31. Charani Shandiz, S.; Foliente, G.; Rismanchi, B.; Wachtel, A.; Jeffers, R.F. Resilience Framework and Metrics for Energy Master Planning of Communities. *Energy* **2020**, *203*, 117856. [CrossRef]
32. University of Wisconsin. TRNSYS A TRAnsient SYStems Simulation Program. Available online: <https://sel.me.wisc.edu/trnsys/> (accessed on 5 September 2020).
33. ur Rehman, H.; Hasan, A.; Reda, F. Challenges in Reaching Positive Energy Building Level in Apartment Buildings in the Nordic Climate: A Techno-Economic Analysis. *Energy Build.* **2022**, *262*, 111991. [CrossRef]
34. Bauer, D.; Marx, R.; Nußbicker-Lux, J.; Ochs, F.; Heidemann, W.; Müller-Steinhagen, H. German Central Solar Heating Plants with Seasonal Heat Storage. *Sol. Energy* **2010**, *84*, 612–623. [CrossRef]
35. Sibbitt, B.; McClenahan, D.; Djebbar, R.; Thornton, J.; Wong, B.; Carriere, J.; Kokko, J. The Performance of a High Solar Fraction Seasonal Storage District Heating System—Five Years of Operation. *Energy Procedia* **2012**, *30*, 856–865. [CrossRef]
36. Saari, A.; Airaksinen, M.; Sirén, K.; Jokisalo, J.; Hasan, A.; Nissinen, K.; Vainio, T.; Möttönen, V.-J.; Pulakka, S.; Heljo, J.; et al. *Energiatehokkuutta Koskevien Vähimmäisvaatimusten Kustannusoptimaalisten Tasojen Laskenta: Suomi*; Balint, G., Antala, B., Carty, C., Mabieme, J.-M.A., Amar, I.B., Kaplanova, A., Eds.; Uniwersytet Śląski. Wydział Matematyki, Fizyki i Chemii: Helsinki, Finland, 2013; Volume 7.
37. European Union Commission. EXCESS—Horizon 2020. Available online: <https://positive-energy-buildings.eu/> (accessed on 24 September 2020).
38. ur Rehman, H.; Hirvonen, J.; Kosonen, R.; Sirén, K. Computational Comparison of a Novel Decentralized Photovoltaic District Heating System against Three Optimized Solar District Systems. *Energy Convers. Manag.* **2019**, *191*, 39–54. [CrossRef]
39. Cao, S.; Hasan, A.; Sirén, K. On-Site Energy Matching Indices for Buildings with Energy Conversion, Storage and Hybrid Grid Connections. *Energy Build.* **2013**, *64*, 423–438. [CrossRef]
40. ur Rehman, H. Techno-Economic Performance of Community Sized Solar Heating Systems in Nordic Conditions. Available online: <https://aaltodoc.aalto.fi/handle/123456789/34808> (accessed on 4 November 2019).
41. Ahola, M.; Säteri, J.; Sariola, L. Revised Finnish Classification of Indoor Climate 2018. *E3S Web Conf.* **2019**, *111*, 02017. [CrossRef]
42. ur Rehman, H.; Hirvonen, J.; Jokisalo, J.; Kosonen, R.; Sirén, K. EU Emission Targets of 2050: Costs and CO₂ Emissions Comparison of Three Different Solar and Heat Pump-Based Community-Level District Heating Systems in Nordic Conditions. *Energies* **2020**, *13*, 4167. [CrossRef]
43. Johra, H.; Heiselberg, P.; Dréau, J. Le Influence of Envelope, Structural Thermal Mass and Indoor Content on the Building Heating Energy Flexibility. *Energy Build.* **2019**, *183*, 325–339. [CrossRef]
44. Intergovernmental Panel on Climate Change (IPCC). Climate Change Widespread, Rapid, and Intensifying—IPCC. Available online: <https://www.ipcc.ch/2021/08/09/ar6-wg1-20210809-pr/> (accessed on 16 August 2021).
45. Machard, A.; Inard, C.; Alessandrini, J.M.; Pelé, C.; Ribéron, J. A Methodology for Assembling Future Weather Files Including Heatwaves for Building Thermal Simulations from the European Coordinated Regional Downscaling Experiment (EURO-CORDEX) Climate Data. *Energies* **2020**, *13*, 3424. [CrossRef]
46. Homaei, S.; Hamdy, M. Thermal Resilient Buildings: How to Be Quantified? A Novel Benchmarking Framework and Labelling Metric. *Build. Environ.* **2021**, *201*, 108022. [CrossRef]
47. World Health Organization (WHO). WHO Housing and Health Guidelines. Recommendations to Promote Healthy Housing for a Sustainable and Equitable Future. Available online: <https://www.who.int/publications/i/item/9789241550376> (accessed on 6 November 2022).
48. Ministry of Social Affairs and Health. Sosiaali—Ja Terveysministeriön Asetus Asunnon Ja Muun Oleskelutilan Terveystieteistä Olosuhteista Sekä Ulkopuolisten Asiantuntijoiden Pätevyysvaatimuksista. Available online: <https://www.finlex.fi/fi/laki/alkup/2015/20150545#Pidm45237817260688> (accessed on 26 September 2022).

Disclaimer/Publisher’s Note: The statements, opinions and data contained in all publications are solely those of the individual author(s) and contributor(s) and not of MDPI and/or the editor(s). MDPI and/or the editor(s) disclaim responsibility for any injury to people or property resulting from any ideas, methods, instructions or products referred to in the content.

Review

Lessons Learned from Positive Energy District (PED) Projects: Cataloguing and Analysing Technology Solutions in Different Geographical Areas in Europe

Federica Leone ^{1,*}, Francesco Reda ², Ala Hasan ², Hassam ur Rehman ², Fausto Carmelo Nigrelli ¹, Francesco Nocera ¹ and Vincenzo Costanzo ¹

¹ Department of Civil Engineering and Architecture, University of Catania, 95100 Catania, Italy

² VTT Technical Research Centre of Finland Ltd., P.O. Box 1000, FI-02044 Espoo, Finland

* Correspondence: federica.leone@phd.unict.it; Tel.: +39-392-227-5652

Abstract: A Positive Energy District (PED) is a portion of urban area with defined boundaries that can produce energy in excess of its own consumption. The aim of this study is to analyse design variations among the six projects (12 case studies) of PED belonging to the European Smart Cities and Communities programme. Thus, it will be possible to identify the reasons behind the energy choices related to generation, storage and distribution that appear in the different geographical areas. To achieve this, different data were collected by consulting official documents and creating questionnaires that were communicated with the project representatives. Thus, the result of this study is a catalogue of the energy system solutions adopted in the studied PEDs with a critical analysis of the different motivations behind them in order to outline general trends in the geographical areas with similar characteristics. In conclusion, this study defined which technological choices are the most common in territories with similar profiles and how divergent those with different profiles are. Furthermore, applied to a large catalogue of PED, the methodology identified would make it possible to create different operating models for different territorial types and urban settlements.

Citation: Leone, F.; Reda, F.; Hasan, A.; Rehman, H.u.; Nigrelli, F.C.; Nocera, F.; Costanzo, V. Lessons Learned from Positive Energy District (PED) Projects: Cataloguing and Analysing Technology Solutions in Different Geographical Areas in Europe. *Energies* **2023**, *16*, 356. <https://doi.org/10.3390/en16010356>

Academic Editor: Krushna Mahapatra

Received: 15 November 2022

Revised: 18 December 2022

Accepted: 22 December 2022

Published: 28 December 2022



Copyright: © 2022 by the authors. Licensee MDPI, Basel, Switzerland. This article is an open access article distributed under the terms and conditions of the Creative Commons Attribution (CC BY) license (<https://creativecommons.org/licenses/by/4.0/>).

Keywords: positive energy district; PED; PED model; PED technologies; energy communities; smart cities; sustainable urban development

1. Introduction

In recent decades, climate change and the resulting climate crisis, caused mainly by carbon dioxide emissions, have led states to implement plans, agreements and mitigation methods to counter the consequences of this crisis [1–5]. One of the methods of counteracting these consequences is the commitment made by states through the 2015 Paris Agreement (during COP 21) to achieve a transition towards carbon neutrality [6–11].

The term ‘towards carbon neutrality’ refers to the commitment to undertake a profound and systematic change in our urban, industrial, infrastructural and energy realities in order to reach a state of net-zero carbon dioxide emissions within a short period of time [11–15].

In largely anthropised territories, such as Europe, it was necessary to think about readjustment and modification of existing urban areas [16–19]. For this reason, research organisations have sprung up to promote punctual retrofits and modifications initially at the building scale, with the development of projects such as nearly-Zero Energy Buildings (n-ZEB) [20], Net-Zero Energy Buildings (NZEB) [21], Zero Energy Buildings (ZEB) [21] and Positive Energy Buildings (PEB) [22]. Then, development moved to the district scale with the Retrofitted Energy District (RED) [23,24], the Net-Zero Energy District (NZED) [25], and up to the most innovative solution currently being implemented, the Positive Energy District (PED) [26,27].

The PED is developed as an evolution of the Positive Energy Buildings (PEB) and Neighbourhood (PEN) [28] themes and is part of the green conversion of urban areas [24].

A PED is an urban area with defined boundaries that generates more energy from renewable sources in a year than it consumes [23,24]. There are different types of PEDs (autonomous, dynamic and virtual) which, while maintaining common principles, have different operating characteristics [23]. Actually, each of these typologies has a different level of dialogue with the energy network outside their borders [23].

As the state of the art of district-scale energy communities, the concept is still under development. Given its derivation from previous concepts, there was no linear development of the concept, but a parallel study of many projects funded by EU grants or municipalities [29].

Actually, to facilitate the development of these realities and their related technologies, the European Union has promoted various research programmes. The idea is to promote different solutions that implement research and innovation concepts that accelerate this transition period [30–39]. These programmes include the JPI Urban Europe programme, the SCC1-H2020 programme [40], Annex83 (IEA-EBC PED analysis and investigation group) [27] and many independent projects. Therefore, different solutions and different PED prototypes were developed. However, application and design methodologies are still being developed and, to date, the authors of this study are aware of the existence of archetypal models for different geographical/climatic areas or urban contexts. In order to contribute to the development of this area of investigation, this study aims to create an initial catalogue of technological and design solutions with a small sample of comparable case studies. Specifically, it intends to analyse the design variations between the PEDs, as they are in different geographical areas and provide a methodology to expand the model catalogue in the future. To achieve this, it was decided to use as a sample for analysis the experiences of PED present in the EU Smart Cities and Communities SCC1-H2020 programme [41].

The programme Smart Cities and Communities SCC1-H2020, referred to in this study, is ascribed to this contest of stimulating research into the modification of urban centres in the direction of a move Towards Carbon Neutrality [42–44]. This programme was created with the aim of proposing innovative development solutions and urban models that are best suited to the needs of today's current reality. Although not all the projects within it are related to PEDs, (as the main focus is on smart cities), there are six projects with this definition. Of these, many case studies (within these six projects) also share membership of the JPI Urban Europe programme. This is the reason why SCC1-H2020 programme was selected. Projects that did not have a declared PED membership were discarded in order to make the data easily comparable. Furthermore, in the projects analysed, a distinction was made between projects that were implemented or are in the process of being implemented (lighthouse cities) that serve as a model for other urban centres interested in this type of transition and that replicate the experience proposed by the lighthouse cities (fellow cities). This study took into account only the lighthouse cities of the PED programmes within SCC1-H2020, as projects are customisable on them, many are in the implementation phase and consequently have more data available.

To sum up, among the programmes that have addressed the PED topic, SCC1-H2020 was selected and only the six projects defined as PEDs were selected. Having selected only the lighthouse cities of the six projects, 12 case studies (two per project) were identified. Each of them had a variable number of districts within it, so in the end, 25 different district were analysed, thus providing a sufficiently large catalogue to study the results and obtain representative models to refer to [41].

Thus, this study presents a novelty in this field as it opens up a whole strand of research on the characterisation of PEDs under varying climatic, geographic and urban layout conditions.

2. Literature Review

As already mentioned in the previous chapter, PEDs are part of the larger process of changing territories to enable progressive decarbonisation and counter the climate crisis and its consequences. An updated and newly created form, PEDs derive from antecedent types of energy communities such as PEB and PEN [24]. The concept of a PED has recently gained ground as the most energy-efficient and effective district-scale area if properly planned [45]. A PED is an urban area with defined boundaries that generates more energy (electricity, heat and cooling) within their borders from renewable sources in a year than it consumes [46].

The PED concept is mainly located in Europe, as the European Community has financed many projects and programmes to follow the development of this concept. These include the Strategic Energy Technology Information System (SETIS-SET Plan) [47] and the Cooperation in Science and Technology (COST Action/CA19126) [48], which cooperate with various programmes to ensure the development of the DPE concept and foster networking among researchers working in this field. In addition to the SET Plan and COST Action, there is the ANNEX83 building and community energy technology collaboration programme [27]. Among the objectives of these plans is to promote the development of at least 100 PEDs on European soil by 2025 (in which the JPI Urban Europe and SCC1-H2020 programmes fit in).

For the successful operation of PED, various aspects such as technological, environmental, economic, social and spatial must be taken into account [49]. In addition, besides the correct energy balance, other objectives are also considered during the planning of these districts. These are not mandatory for the proper functioning of PEDs, but pursuing them brings long-term improvements to the district [49]. It is precisely the non-compulsory nature of these objectives that has led to projects pursuing one or more objectives with different compositions. These objectives include zero emissions, energy efficient, carbon free and many others [49].

For the proper functioning of PEDs, the technologies required include all those capable of generating or storing electricity or heat from renewable energy sources. This can be done by integrating them at the building scale, at the district scale or even by decentralising their production and storage of electricity outside the district boundaries [50]. In addition to these technologies, there are also those related to modifying the transport infrastructure using E-mobility [50]. However, an electrification of transport expands the demand for electricity accordingly [51]. Therefore, the main sources of energy demand, which the PED will have to provide for, will be buildings within the district boundaries and e-mobility [26]. The choice of which technologies to use, and whether to centralise them within the district boundaries or relocate them, depends on various factors, such as climate, availability of infrastructure, the type of district in which the intervention is to take place, any historical, cultural or landscape constraints, the urban fabric, the presence of previous programmes or interventions involving the city or region, the spatial conformation and the availability of various energy supplies [46]. According to the set of choices and to the autonomy or connection with the rest of the territory and infrastructures, three different models of PED are mentioned: autonomous, dynamic and virtual PED [23]. A PED is defined as a portion of an urban area that has defined boundaries where its own energy production from renewable energy sources is higher than its own energy demand on an annual basis. In the following figures, electricity and heat generation and storage solutions are identified as ‘solutions’. Whereas, e-mobility has been included as ‘demand’ (along with buildings), due to its energy-consuming nature.

Figure 1 presents an autonomous or self-sufficient PED: in this type of PED, energy export is foreseen. However, no type of import from an external energy grid or district heating/gas network takes place [23], which is the reason why the connection to the electricity grid is absent from the picture (to conceptualise the complete autonomy of the district).

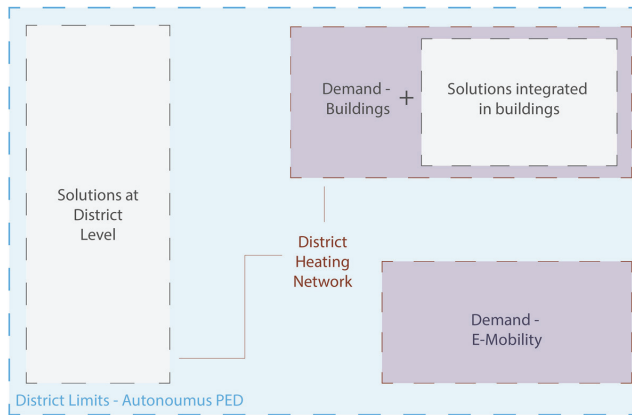


Figure 1. Autonomous PED.

Figure 2 presents a dynamic PED. In this type of PED, both energy import and export are foreseen, communicating with external energy grids or district heating/gas networks and other PEDs [23].

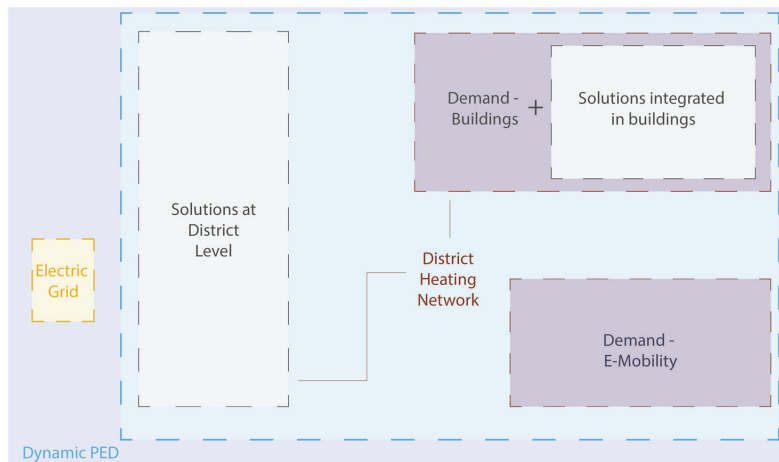


Figure 2. Dynamic PED.

Figure 3 presents a virtual PED: In this type of PED, the energy generation and storage is within its physical boundary and beyond [23].

From a technological point of view, for the production of electricity, solar, wind, hydro, geothermal and biomass technologies can be used (the latter two are very often used for the direct production of heat). For the production and distribution of heat and cooling, the most frequent technologies are the district heating network (DHN), waste heat, bio-combined heat and power (Bio-CHP), heat [ump (both district and building integrated) and those using hydrogen fuel. The storage of heat and electricity (both feasible at district scale and building-integrated, only the electrical storage can be developed outside the district borders) and E-Mobility for both public and private vehicles [52–54] must be added to these technologies.

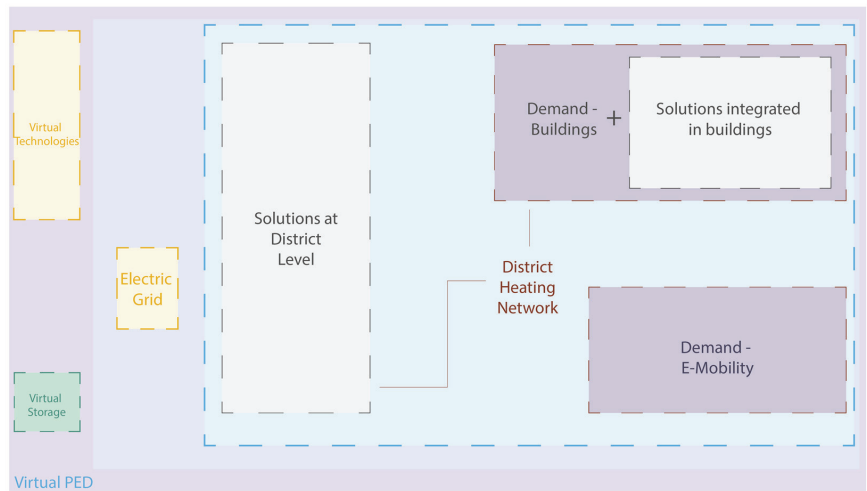


Figure 3. Virtual PED.

During the design and implementation phases of PEDs, analyses and tests are required to prove the effectiveness and efficiency of the identified solutions [55]. For this reason, many simulations are carried out. These simulations can be energy, mobility, indoor and/or outdoor comfort simulations. Different simulation tools can be used [55]. Due to the great contribution that simulations make to the correct development of PEDs, various projects soon started to implement Digital Twins [55]. Digital Twins refers to the creation of a digital model, in this case a recreation of the district on which it is to operate, with the intention of monitoring, modelling and optimising a complex, multidisciplinary system based on a real-time large dataset [55–57]. The use of this method would make it possible to create a better, more liveable environment for the population and better manageable. However, for the proper functioning of the Digital Twins, different tools and the joint use of machine and artificial intelligence are required [55].

Additionally, due to a fragmentary and parallel development and the recent development of this type of energy community, the development of this concept often changes as the project varies, since there are no guidelines to follow for their design. This leads to different models and different combinations of technology and intentions that often differ even in similar contexts. This study is framed precisely in this context, trying to begin to define models of functioning in different climatic and geographical contexts.

3. Materials and Methods

This study was designed to define similarities and dissonances in design and technology choices in PEDs located in different contexts. In order to carry out the research, a step study was carried out, as shown in Figure 4. First, a literature review study on PEDs, Towards-PED, Energy Communities and renewable energy sources with all the related technologies (generation, storage, distribution and mobility) was carried out. This step, preliminary and preparatory for the subsequent steps, is necessary to develop sufficient knowledge of the topic to support further decisions and analyses. At the same time, a sample of case studies on which to carry out the analysis was selected. First, the Smart Cities and Communities SCC1-H2020 Programme was selected both for its relevance to the theme of urban transformation and for the focus of some projects on the theme of energy communities. Among the various projects, a selection was made, choosing only those that defined themselves as PEDs. In fact, the focus of the SCC1-H2020 programme is smart cities and not specifically PEDs, so only a few projects fit into the criteria selected. Six projects were identified with a varying number of case studies divided between lighthouse and

fellow cities. The lighthouse cities of the PEDs participating in SCC1-H2020 were chosen to be analysed, as they are the most representative case studies of the projects. Each of these cities (12 in total) had several districts, so 25 different districts were catalogued.

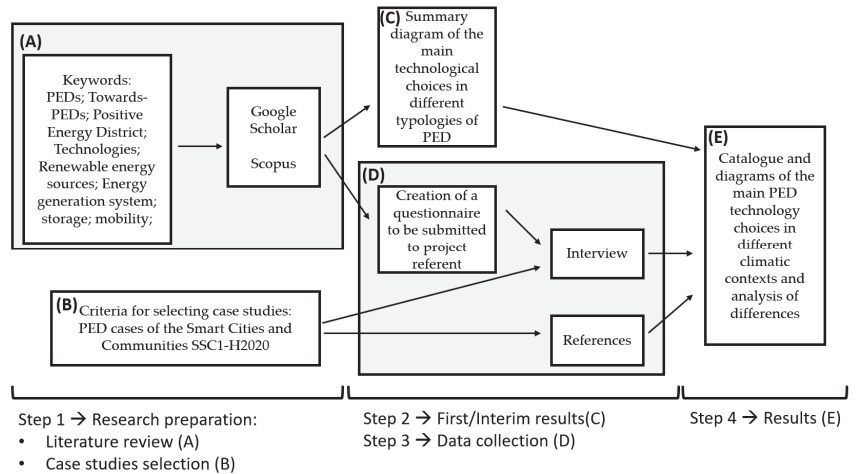


Figure 4. Implemented method in this study.

Once the research preparation phase was completed, the first results were obtained. Using the knowledge obtained from studying the literature review, it was possible to create a summary diagram of the main technological choices in different typologies of PEDs. This step is important as this diagram will serve as a basis for the analysis of the next steps. The next step was the data collection. Starting from literature review and the experience gained from the authors' participation in Annex83, a questionnaire was created to provide a full description of the technological operation of various types of PEDs. Data were collected on the following: the scale of intervention, the number of districts for lighthouse cities, the area involved in metres square, type of settlement, spatial features, information on the population involved in the project and settled in general in the city and the territory, information on energy generation system, storage, mobility and renewable energy sources. The questionnaire was filled in either by using the literature review sources as references and by submitting it to the project representatives and conducting interviews with them to validate the information already identified in order to collect data on the capacity of the single technologies used and to understand the difference between the design and monitoring phases. This step is important as made it possible to understand the functioning of the individual districts.

The last step concerns the production of results and their analysis. Starting from the data collected from the questionnaires, the information was reorganised to create a catalogue of the technological choices and objectives pursued by the various case studies. Finally, the same data were reformulated graphically, based on the summary diagram created in the second step. The end result is three diagrams representing the technological choices in different climatic contexts. Following this method, therefore, made a critical analysis of the different approaches in the design of PEDs possible and made it possible to draw a preliminary trend on the development of different models under varying geographical and urban conditions.

Materials

The Smart Cities and Communities SCC1-H2020 Programme, linked to the Paris Agreement of 2015 from COP 21 (which among other objectives aims to limit global warming to well below two, preferably to one point five degrees Celsius, compared to pre-industrial levels), was developed to promote the development and transition to Smart

Cities (involving aspects of urban planning, energy, facilities, social, economic and market) across Europe [10,11]. The aim of this programme is to propose models of development and modification of cities as an alternative to the current urban area model [29]. With the idea of promoting the development of Smart Cities, the issue of PEDs was not always addressed by the programmes involved, while wishing to analyse in this study the data obtained from lighthouse cities with declared ambitions towards the implementation of PEDs, only the latter will be taken into account [41]. Figure 5 shows the geographical location of the PEDs that are part of the SCC1-H2020 [4].

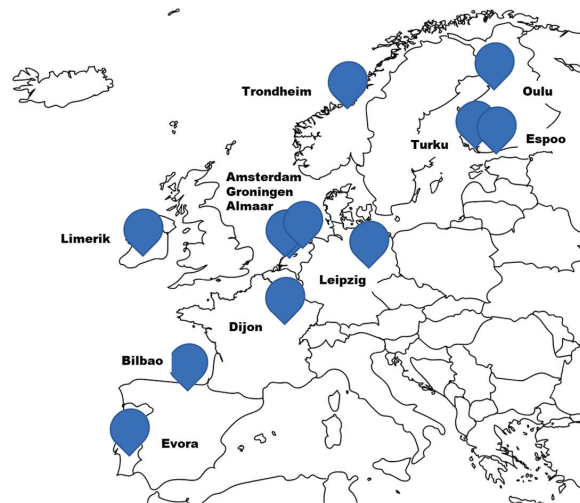


Figure 5. Geographical location of the analysed PEDs.

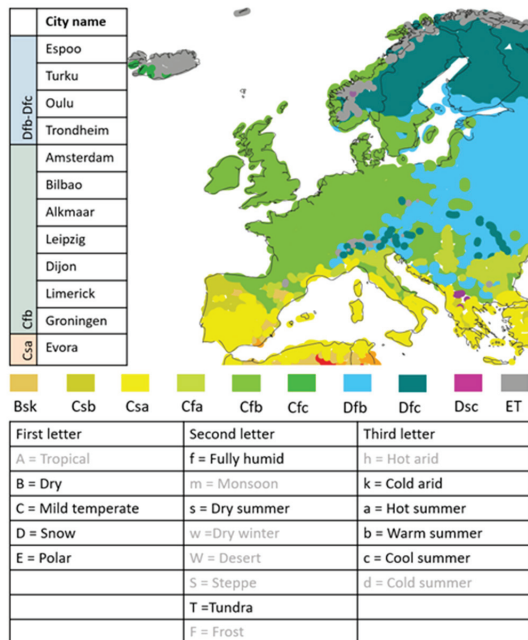
A total of six declared PED programmes (Sparcs, RESPONSE, Atelier, MAKING-CITYMAKING-CITY, +CityxChange and POCITYF) were identified within which each contains two case studies selected to be lighthouse cities [41,46]. The distribution of lighthouse cities per country is as follows: three lighthouse cities are located in Finland, one in Norway, one in Ireland, three in The Netherlands, one in Germany, one in France, one in Spain and one in Portugal.

Each city has a variable number of districts within it (from one to six). Therefore, 12 case studies with a total of 25 districts as lighthouse districts were identified. Each district differs in its location and design choices. Table 1 shows the distribution of the lighthouse cities in each project.

General data on climatic, spatial, urban, infrastructural and renewable energy characteristics were collected and compared with the information obtained from the individual districts through bibliographic sources and by submitting specially created questionnaires to representatives of the individual projects, and the results were grouped under the Lighthouse Cities to which they belonged. The information obtained was then organised according to the climate category of the Köppen Climate Classification to which they pertained [105–107]. This systemisation of information according to the climatic class is due to the different requirements that urban centres face as a result of their climatic situation. Four climate classes were identified: Dfb—warm summer humid continental climate, Dfc—subarctic climate, Cfb—temperate oceanic climate and Csa—hot summer Mediterranean climate. Due to the few case studies analysed and the similarities between Dfb and Dfc, it was decided to take into account the macroclasses: continental climate, oceanic climate and Mediterranean climate [105–107]. Figure 6 shows the Köppen climate classification map and the class of the cities examined.

Table 1. Case studies examined.

Project Name	City	Website	References
Sparcs	Espoo (FI)	ESPOO Sparcs	[58–61]
Sparcs	Leipzig (DE)	LEIPZIG Sparcs	[62–64]
RESPONSE	Turku (FI)	Lighthouse Cities—RESPONSE (h2020RESPONSE.eu)	[65–70]
RESPONSE	Dijon (FR)	Lighthouse Cities—RESPONSE (h2020RESPONSE.eu)	[65–70]
Atelier	Amsterdam (NL)	General Information—ATELIER (smartcity-atelier.eu)	[71–80]
Atelier	Bilbao (ES)	Bilbao—ATELIER (smartcity-atelier.eu)	[72,73,75–80]
MAKING-CITYMAKING-CITY	Groningen (NL)	GRONINGEN—MAKING-CITY	[81–85]
MAKING-CITYMAKING-CITY	Oulu (FI)	OULU—MAKING-CITY	[81–85]
+CityxChange	Limerik (IR)	Our Cities—+CityxChange	[86–91]
+CityxChange	Trondheim (NO)	Our Cities—+CityxChange	[89,90,92–96]
POCITYF	Evora (PT)	Évora—POCITYF—POCITYF	[97–104]
POCITYF	Alkmaar (NO)	Alkmaar—POCITYF—POCITYF	[97–104]

**Figure 6.** Köppen climate classification map and the class of the examined cities [105–107].

Each city has made different technological, social and spatial planning choices according to its characteristics, needs and implemented policies. Espoo (the only case study without a defined historical centre) chose one in an existing area, and one in a new built-up area, such as lighthouse districts, with the aim of turning them into mobility, social and economic nerve centres of the city [108,109]. Turku developed a student village (thus paying particular attention to social and economic aspects) in a partially built-up area [110]. Oulu has placed the district in a partially built-up area [85]. Trondheim's is near the city centre in a very important city snood [84,92]. Amsterdam has decided to place several districts

across the city [71,97]. Bilbao (the only one that chose to implement an autonomous PED) has designed its district within an island inside the city [71]. Alkmaar chose to implement two prototypes, one in an almost totally built-up area close to the historic centre, the other in a peripheral expansion area [97]. Leipzig placed its district in a densely built-up area outside the historic centre in an expansion area [62,108]. Dijon has placed its district in a wide, partially built-up area away from the city centre [65]. Limerick has chosen as its PED its city centre and a peripheral area [86]. Groningen's, on the other hand, is in an almost totally built-up area, making a distinction between Groningen south and Groningen north [85]. Evora has chosen to implement three different districts in three totally different contexts: the city centre, an industrial area in a city expansion zone and a neighbouring village that we could define as the inner-city area of Evora [97].

4. Results

Starting from the literature review, the data provided by the JPI Urban Europe catalogue and the experience gained within Annex83, one of the first results of this study was the creation of a model summarising the functioning of the three PED models from a technological point of view. This model was useful both to get a general picture of how PEDs work, but also to have a catalogue of the technologies used and usable in the different areas (production, storage, distribution and mobility) and their scope of application. Figure 7 shows the diagram of the main technological choices of a PED in the three variants: autonomous, dynamic and virtual. The model was created by taking into account the functioning of the three types of PEDs and maintaining the distinction between energy supply and energy demand. For energy supply, the production and storage of electricity and heat in a virtual, district and building-integrated manner was considered. There is also a connection to the electric grid and the district heating network. For energy demand, buildings within the district and mobility were considered.

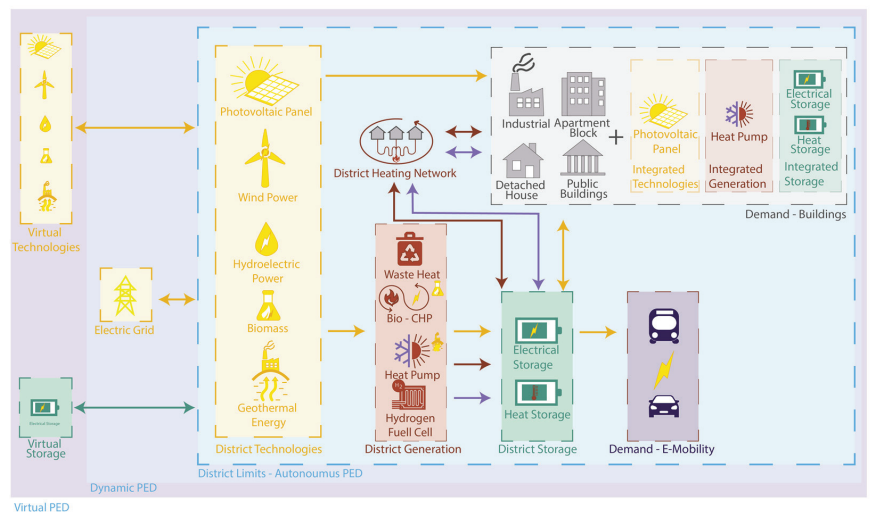


Figure 7. Summary diagram of the main technological choices in different typologies of PED.

Once the functioning of the various models had been described and the technology catalogue created, the next step was to create a questionnaire (Appendix A). This was created on the basis of the lessons learnt during the creation of the summary diagram and the literature study. The aim was to be able to describe in as much detail as possible the needs and technological choices identified as solutions by the individual districts. Once completed, 12 questionnaires (one for each case study) were filled in both using the literature review and by conducting interviews with the project representatives.

Starting from these premises, the choices made by the individual cities were analysed and grouped into technical choices and objectives pursued so that the overall picture of their design choices and objectives could be compared. In addition, the cities were grouped by climate class (based on the Köppen climate classification), so as to be more evident as to the presence (or absence) of a leitmotif in the choices as the climate changes. Figure 8 shows the results obtained from the collection of these data.

		Dfb - Dfc				Cfb						Csa	
		Esposo (FI) Virtual	Turku (FI) Dynamic	Oulu (FI) Dynamic	Trondheim (NO) Dynamic	Amsterdam (NL) Virtual	Bilbao (ES) Autonomous	Alkmaar (NL) Dynamic	Leipzig (DE) Virtual	Dijon (FR) Dynamic	Limerick (IE) Dynamic	Groningen (NL) Dynamic	Evora (PT) Dynamic
Technical choices	Wind Speed W/m2	311	345	370	307	325	396	508	250	250	561	459	277
	Solar	●	●	●	●	●	●	●	●	●	●	●	●
	Wind	●	-	-	-	-	-	-	-	-	-	-	-
	Hydrogen	-	-	-	-	-	-	●	-	-	-	-	-
	Geothermal	●	●	●	●	●	●	●	-	-	-	●	-
	Bioenergy	●	●	-	-	●	-	●	●	-	-	●	-
	Waste Heat	●	●	●	●	-	-	●	●	-	●	-	-
	Electrical Storage	●	●	●	-	●	●	●	●	-	●	-	-
	Heat Storage	-	●	●	●	●	●	-	●	-	●	-	-
	E-Mobility	●	-	●	●	●	●	●	●	●	●	●	●
	Heat Pumps	●	●	●	●	●	●	●	-	-	-	●	-
	District Heating Network	●	●	●	●	●	-	●	●	●	●	●	-
	Combined Heat & Power	●	-	●	-	-	-	-	●	-	●	-	-
Objective pursued	Positive Energy	●	●	●	●	●	●	●	●	●	●	●	●
	Zero Emission	●	-	●	-	●	●	-	●	-	-	●	-
	Energy Efficient	●	●	●	-	●	-	-	●	●	-	-	●
	Carbon Free	●	-	●	-	-	●	-	●	●	-	-	-

Figure 8. Data collection and systemisation of information of the analysed case studies. “●” means that the technological solution was carried out, “-” means that the technology was not selected. Wind

speed information was obtained with the Global Wind Atlas developed by the Technical University of Denmark [111].

Please refer to the “Discussion” section for a detailed analysis of this figure. To better analyse the technological choices and understand which ones were the most recurrent, the data obtained were reorganised and a diagram was created to show the order of preference of the various technologies. Referring to Figure 9, the number of technology selections in the case studies, with reference to the total number of 12, selections are as follows: solar 12, wind 1, hydrogen 1, geothermal 8, bioenergy 6, waste heat 7, electrical storage 8, heat storage 7, e-mobility 11, heat pumps 8, district heating network 10, combined heat and power 4 and hydroelectrical 0. Thus, this table made it clear which technologies are the most used and at the same time which are the least used or even discarded.

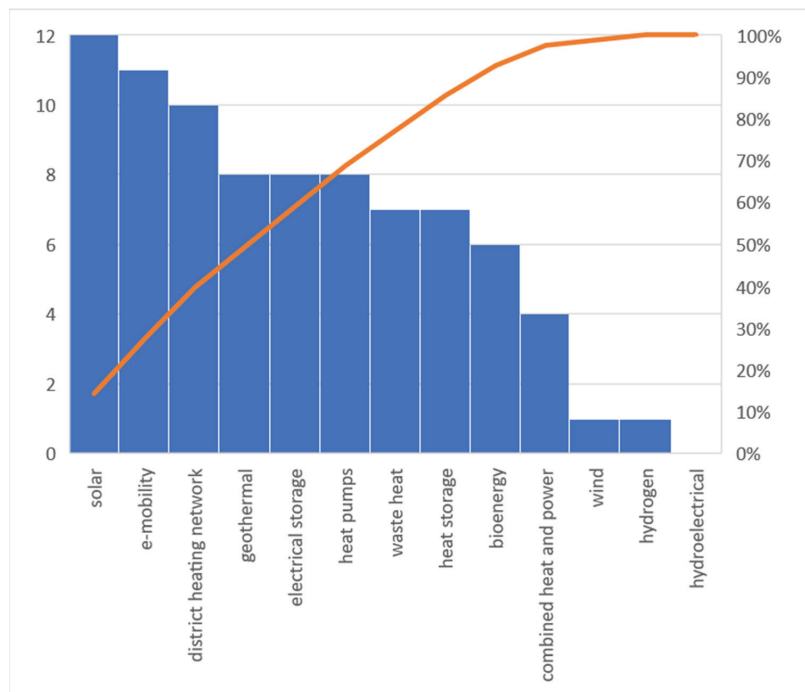


Figure 9. Number of technology selections with reference to the total number of case studies.

Having collected all the necessary data, it was then possible to take the summary diagram of the main technological choices (Figure 5) in order to create three different models describing the different climate zones identified. It would be logical to conclude with a scheme summarising the main technological choices made by districts in different parts of Europe. Following the cataloguing and systemisation of the case studies examined, three schemes were derived from the identified climate macro-classes that describe the main technological choices in different climates, as it is one of the factors that most influences energy needs and renewable energy source availability.

Starting from the diagram of the main technological choices, Figure 10 shows the summary diagram of the most frequently used technological choices in Continental climates. A dynamic PED model was selected. For heat production, waste heat, bio-combined heat and power (only at the district scale), the district heating network and heat pumps (also in building integrated form) were selected. For electricity production, bioenergy (which will be used to provide electricity for heat production) and photovoltaic panels (both at the

district scale and integrated in buildings) were selected. These other solutions are planned: electricity and heat storage (at the district scale and integrated in buildings) and E-mobility.

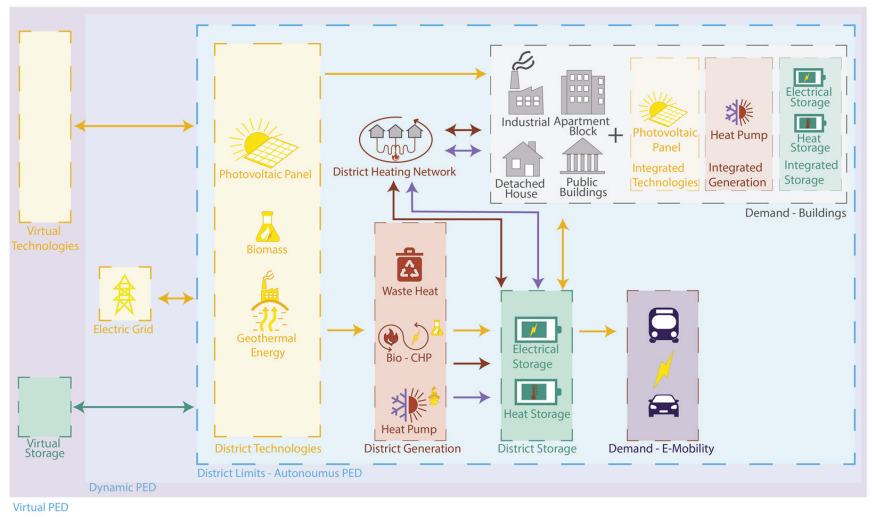


Figure 10. Summary diagrams of the most frequently used technological choices in continental climate Dfb/Dfc.

Figure 11 shows the summary diagram of the most frequently used technological choices in continental climates. A dynamic PED model was selected. For heat production, the district heating network, heat pumps (at district scale and in building integrated form) and geothermal energy were selected. For electricity production, photovoltaic panels (at the district scale) were selected. These other solutions are planned: electricity and heat storage (at the district scale), E-mobility.

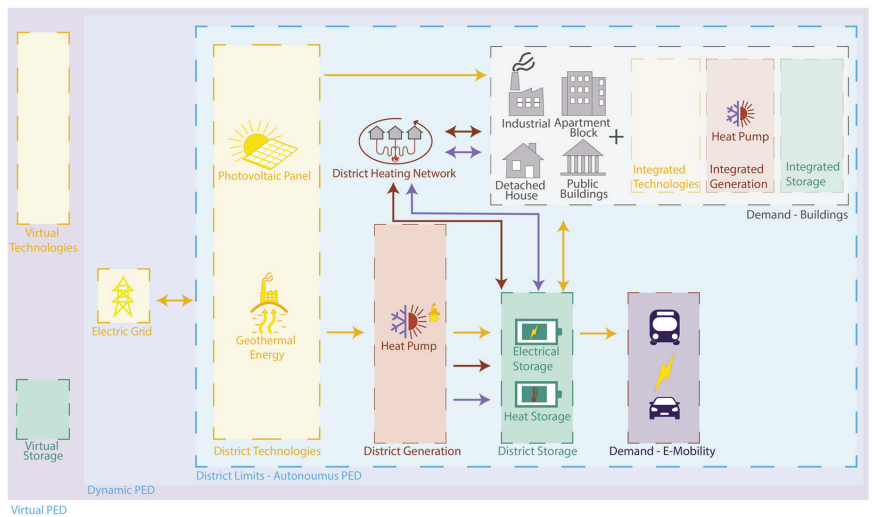


Figure 11. Summary diagrams of the most frequently used technological choices in oceanic climate Cfb.

Figure 12 shows the summary diagram of the most frequently used technological choices in Mediterranean climates. A dynamic PED model was selected. For heat produc-

tion, heat pumps were inserted only at the scale of the building. For electricity production photovoltaic panels (both at the district scale and integrated in buildings) were selected. These other solutions are planned: electricity (at the district scale) and E-mobility. There is no district heating network.

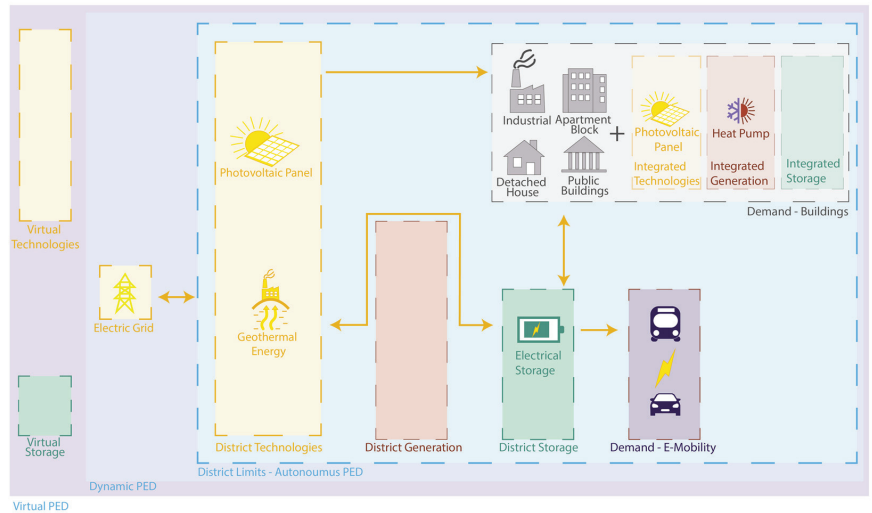


Figure 12. Summary diagrams of the most frequently used technological choices in Mediterranean climate Csa.

These models, therefore, make it clear, even graphically, what the similarities and differences in technological solutions are in geographical areas with different climatic requirements.

5. Discussion

Project choices were influenced by geographical, political and economic reasons. An example of this is the city of Espoo, which (in addition to the Smart Otaniemi programme) joined the Sparcs programme following the city's adhesion to the Covenant of Mayors and chose to buy renewable certified electricity [108]. It means that the city buys electricity from renewable sources (in this case mainly wind), as they are not implemented or implementable in inhabited areas. This is why Espoo is referred to as a virtual PED [108]. Leipzig, which has a history as an energy metropolis, decided to use solar thermal, as it already had a programme to implement this technology in the city [112]. This is a similar situation to Alkmaar, which integrated hydrogen technologies, as the city and region had previous development programmes [65]. The opposite choice is made by Groningen, which despite having a programme for the development of hydrogen technologies decided not to integrate them into the design of the PEDs.

An example of design choices made on the basis of particular geographical conditions is Bilbao, which, having chosen to develop its districts within the Zorrotzaurre Island, has opted for the development of autonomous PEDs [26].

From a geographical analysis of the lighthouse cities, these are mainly located in northern and central Europe. This distribution may be due to the fact that northern cities are better prepared (in optimisation, optimised planning process, design process, digitisations of city infrastructure and co-creation project) for the realisation of such projects. In addition, many municipalities in these areas already have sustainable energy planning offices, which are able to implement this type of project by connecting the various actors (technology producers, energy utilities and building developers) in the area. Another factor that would influence this distribution could be the greater number of start-ups and companies that

already exist in the area and can guarantee a rapid design and realisation of the installations and companies that are able to guarantee the maintenance of the infrastructure over time.

Most of the districts opted for a dynamic PED, thus influencing the model forms used. Espoo, Amsterdam and Leipzig adopted a virtual PED, while Bilbao (having developed its district on an island) was the only one to design an autonomous PED. All the case studies analysed chose to use solar technologies, both at the district scale and integrated in buildings. Other frequent choices were E-mobility, heat pumps and the district heating network. The least used technologies are wind energy, hydrogen and hydroelectrical. In general, common and shared technological choices were observed. Deviations from the canonical choices were noted when the city examined already had development programmes for different technologies: for instance, Leipzig (Sparcs) chose to use solar thermal, because the city had a solar thermal implementation plan with a state subsidy, and Alkmaar (POCITYF) chose to use hydrogen fuel cell and hydrogen from biogas, because both the city and the region have a hydrogen programme [65,112].

Thus, when analysing the data from this study, it appears that there are significant differences between northern and southern Europe, both in terms of the distribution of case studies, that is decreasing moving from north to south, and in terms of the choices and objectives set. Moreover, it appears that solar energy generation mismatch also influences the choices on the type of the PED settlement system, as in cold climates, in order to overcome this problem and reach the thresholds necessary for the proper functioning of a PED, the virtual PED typology of settlement is more common in northern Europe [108,113]. This could be one of the reasons why there are more virtual solutions as the climate gets colder. However, this option can be effective, as the ultimate intention is to promote and foster a transition to renewable energy sources. Therefore, buying green electricity, instead of producing it independently, is a valid option for the functioning of the districts. When analysing all the examined case studies, it appears that there is no coordinated plan to manage the development of PEDs, but they are designed individually, adapting to the needs of the individual district being examined. However, to ensure their development on a large scale, in our opinion, it is necessary to promote the development of high-level planning and the creation of a prototype.

Critical Reflection on Technological Choices

As shown graphically in Figure 5 (and consequently in Figures 10–12) a first distinction must be made between electricity and heat when discussing the technologies required for PEDs, and then a second, more detailed distinction must be made with technologies related to production, storage, distribution (of heat and/or cooling) and E-mobility. Taking into account, at first, only technologies for the production, storage and distribution of heat (and cooling), it can be said that these solutions are found more in the north than in the south of Europe. Heat pumps are preferred, either district or on a building level. This technology, in most cases, uses geothermal energy, especially if it is on a district scale. Other very frequent technologies are district heating networks, present in all cases surveyed except Evora. This could be due to the fact that, in Southern Europe, not all areas have developed infrastructural systems for heat distribution as a result of their lesser need for heat given their geographical and climatic location, and specifically, in Evora, where either gas by means of cylinders or heat pumps are used in most cases [114–120]. A very common technology for obtaining heat is waste heat, probably due to the wide availability industries and machinery that, as a result, produce heat [113–115]. In fact, many case studies study, apply or use it at district scale, such as Espoo, Leipzig, Alkmaar and Dijon. Less common, but still used technologies are combined heat and power (CHP), used by the case studies of Dijon, Espoo and Leipzig [119–121]. Finally, in the presence of active policies or programmes, previously uncommon technologies for PED were used in other realities, such as hydrogen fuel cell in Alkmaar and solar thermal in Leipzig [99,108]. For hydrogen this is probably because hydrogen was not convenient for the energy market at the time the study was conducted [122–125]. With the energy crisis and gas issues, the

situation could change. If the focus on hydrogen, with the consequent implementation of the technologies necessary for its production and storage, increases and the price of equipment decreases, it could be a viable solution to replace gas, otherwise not. As far as solar thermal is concerned, however, this could be because, for many cities, this solution is not economically feasible or due to the absence in or near the cities themselves of companies that would easily allow installation and maintenance [126]. This would suggest that in order to implement this technology, it would first be necessary to promote the large-scale development of companies capable of guaranteeing this service.

With regard to the production of electricity from renewable energy sources, the most widely used is solar photovoltaic (PV), both on a district scale or integrated into the building, with Leipzig being the only exception that uses this source outside the district boundaries [108].

Although solar energy gives many gaps in its production, especially in the Nordic countries (not only at night but also in winter), this was the most adopted solution [127–130]. The reason for this trend could be either because this technology is the cheapest for energy production, or the easiest to install both in the ground and integrated in buildings and different companies are widely present to guarantee long-term maintenance [131]. Therefore, for economic and feasibility reasons, it makes sense to select this technology in all urban and climatic conditions.

Despite being the most convenient source of renewable energy, wind energy was the least selected. This may be due to the difficulty of installation in urban contexts, landscape deterrents, social resistance that this form of energy production encounters and for the high cost of their installation and maintenance [132,133]. In addition to largely altering the appearance of the land on which they are installed, wind turbines emit noise and vibrations, so society does not tend to accept the installation of these technologies near built-up areas [132,133]. From the experience of Espoo (Finland), however, the adoption of virtual wind energy was a satisfactory choice [113]. This city, however, was one of the few to have chosen the virtual form precisely in order to be able to integrate wind energy into its districts [108]. This would suggest that the use of virtual PEDs would offer more opportunities as it would develop technologies in the region and not only in the punctual area of the district.

Regarding energy storage systems, this is divided into electricity and heat storage and can be installed either on a district scale or by integrating them into buildings, while only electricity can also be stored virtually [134,135]. These technologies are highly expensive but reliable, so that more district-scale and less building-integrated solutions were developed [134,135]. In fact, for electricity, all the case studies adopted district-scale solutions, with Turku, Groningen and Oulu also having building-integrated solutions. With regard to the technological solutions adopted for heat storage, Leipzig, Turku, Dijon, Alkmaar, Groningen, Trondheim and Oulu use district-scale heat storage technologies. While Espoo has a pilot project on how the thermal energy capacity of the building and its structures can be used in a similar way as a heating storage. Of these, Alkmaar, Amsterdam and one of the Groningen districts use the aquifer thermal energy storage.

All the districts surveyed have a mobility plan, which implies the siting of electric vehicles in public transport and encouraging the choice and use of private electric vehicles through the installation of charging stations throughout the districts [53]. Alkmaar and Turku use vehicle to grid.

Regarding the results obtained through the creation of summary diagrams of the main technological choices in different climatic context (Figures 10–12), it was a challenge to succeed in creating models that are representative of all the examined climatic realities due to the disproportionate distribution of the case studies in the European continent. On the one hand, the case studies in continental or oceanic climates are sufficient to outline a general trend in the technological choices and solutions adopted. On the other hand, in the Mediterranean climate, the only case study present made it possible to create a model that represents a reality in a that climate, but it is not sufficient to outline a common trend, as

it is descriptive of that specific district. This disproportion is probably attributable to the problems presented in the previous chapter (the absence of realities capable of enabling the simple creation and maintenance of infrastructures, the absence of administrative agencies designed to foster environmental protection, etc.).

If the trend present in this study were to be confirmed in other districts, in the Mediterranean area, the main focus would be on electricity and almost none on heating. Whereas in the continental climate, although district heating networks are widely used, there is still a great deal of focus on building-integrated heating. It would, therefore, be desirable, in our judgement, to consider promoting the development and large-scale installation of this type of heat distribution, both to ensure greater safety for the population and to protect environmental aspects (less wasteful use of materials). In addition to the increased development of district heating networks, it would seem that the promotion and development of new solutions such as seasonal energy storage, hydrogen and district heating and cooling networks would be of great help in the development of PEDs throughout Europe.

Furthermore, in addition to the already existing electrification of transport with e-mobility, there would seem to be a process of electrification in heat generation that would lead to an increase in the demand for electricity. This trend can be seen through the extensive use of heat generation with heat pumps focused on electricity. In our opinion, this increase in demand for electricity could be met by a large-scale increase in wind energy due to its high performance. Another alternative could be the use of small nuclear reactors, assuming that it is not up to us to discuss the nature of nuclear power and whether it belongs to sustainable technologies. The energy resulting from nuclear power could also be a viable solution for powering DHN.

It appears that gas would be totally replaced by heat production due to its polluting particles, unless CO₂ could be captured out of it. However, the remaining particulate matter, a consequence of gas combustion, would remain a problem to be solved in order not to disuse this energy source.

Finally, it would also be necessary from a technological point of view to develop high-level planning to ensure optimum energy efficiency.

6. Conclusions

This study collected, catalogued and analysed the data from 25 PEDs of 12 different case studies from the European Smart Cities and Communities SCC1-H2020 projects. The districts are distributed in different parts of the European continent, with case studies located in different proportions in northern, central and southern Europe. The data collected from these case studies through literature research and questionnaires submitted by interviewing project leaders were organised and critically analysed in order to create summary models of the technologies used under different conditions. As a result, information on the objectives and technological choices was systematised, making it possible to outline the trend of PED development in those areas. Specifically, this study arrived at the following considerations:

- A general trend in the establishment of PEDs in Northern and Central Europe was noted, to the disadvantage of the south, which could be due to a potentially lower institutional and start-up presence in the south;
- The most frequently used type of PED is the dynamic PED, which would seem to be the most effective and adaptable form of PED for current urban conditions. However, the virtual PED could offer more effective solutions especially in Northern Europe to counter the energy mismatch;
- Recurring choices were noted in the selection of technologies for the proper functioning of PEDs, declined from time to time in different ways to suit the needs of the area. When technological choices differed, the reason was the presence of previous regional or city programmes that aimed at promoting the development and use of a specific technology. Some examples are the choices made by Alkmaar, with the use of hydrogen fuel cell, and Leipzig, with solar thermal;

- Among the most widely used technologies is solar PV energy technologies, which could be due to its lower price, ease of installation and the large presence of companies capable of guaranteeing proper maintenance. In addition, the district heating network is also more common, which could be due to the high effectiveness and efficiency of this technology and their greater safety. Moreover, E-mobility has a large presence;
- Despite being one of the most energy-efficient renewable energy sources, wind energy was found to have lower use. Actually, only the Espoo case study (Sparcs) has adopted it in a virtual way, as it is among the green certified electricity solutions. The reasons behind its low use could be the difficulty of installation in the urban context, the high cost of installation and maintenance, landscape deterrents and social resistance;
- A progressive focus on solutions related to the production, storage and distribution of heat was noted in the progression towards Northern Europe, probably due to the geographical and climatic typical needs of those territories;
- There was an acceleration in the electrification process of PEDs regarding e-mobility and heat generation technologies (especially large heat pumps in district networks). One of the possible solutions to this increased demand for electricity could, in our opinion, be found in a greater exploitation of wind energy sources and through the utilisation of electricity produced by nuclear reactors on a regional or national scale;
- Technological solutions at the district scale were often preferred to building-integrated solutions, this is probably due to higher efficiency with larger units, better control and management and distribution of energy in the territory. However, one disadvantage is the higher energy losses associated with long distribution lines;
- In order to promote the development of PED on a large scale, it would be desirable to develop a high level of planning that considers the entire territory and systematises the development of PED on a regional scale. This way, a network of PEDs and greater efficiency could be achieved. For this reason, a good solution, in our opinion, could be the use of the new territorial acupuncture methodology.

The delimitation of the study, as far as it was possible to carry out an initial analysis and note the variations in different geographical areas, was the challenge to obtain all the necessary data and to create summary diagrams of all the climatic realities analysed. This is probably due to the fact that the sample of case studies analysed at this stage is limited (there were no other PEDs within the European Smart Cities and Communities SCC1-H2020 project). Indeed, the small number of case studies provides a partial view of the proposed diagrams. For this reason, it would be interesting in the future to extend the range of case studies examined and repeat the analyses carried out in this study to see whether the conclusions reached are confirmed. Another future development of this study would be to apply it to an adequate number of case studies in order to define archetypal forms descriptive of different climatic conditions and/or different urban fabrics.

Author Contributions: Conceptualisation, F.L., F.R., A.H. and H.u.R.; methodology, F.L., F.R., A.H. and H.u.R.; formal analysis, F.L., F.R., A.H. and H.u.R.; investigation, F.L., F.R., A.H. and H.u.R.; resources, F.L., H.u.R., F.R. and A.H.; data curation, F.L., F.R., A.H. and H.u.R.; writing—original draft preparation, F.L.; writing—review and editing, F.L., F.R., A.H., H.u.R., F.C.N., F.N. and V.C.; visualisation, F.L., F.R., A.H. and H.u.R.; supervision, F.R., A.H., H.u.R., F.C.N., F.N. and V.C.; funding acquisition, F.R. and F.N. All authors have read and agreed to the published version of the manuscript.

Funding: This research was funded by the Sparcs project (grant number 864242) and the University of Catania. The Sparcs project has received funding from the European Union’s Horizon 2020 research and innovation programme under Grant Agreement No. 864242. The sole responsibility for the content of this publication lies with the authors. It does not necessarily reflect the opinion of the European Communities. The European Commission is not responsible for any use that may be made of the information contained therein. The funding bodies had no such involvement in preparing the manuscript, methods and results, etc., and this manuscript reflects only the authors’ views and does not necessarily reflect their opinion. The financing bodies cannot be held responsible for any use that may be made of the information contained herein.

Institutional Review Board Statement: Not applicable.

Informed Consent Statement: Not applicable.

Data Availability Statement: The data presented in this study are available on request from the corresponding author.

Acknowledgments: The authors would like to acknowledge Mari Hukkalainen, Zarrin Fatima and Krzysztof Klobut (Sparcs), Beril Alpagut (MAKING-CITYMAKING-CITY), Mikko Virtanen (RESPONSE), Júlia Oliveira Pereira (POCITYF), and the IEA Energy in Buildings and Communities (EBC) Annex 83 PEDs, for cooperation. The funding bodies had no such involvement in preparing the manuscript, methods and results, etc., and this manuscript reflects only the authors' views and does not necessarily reflect the opinion of the European Commission. Neither the EU nor any of its institutions or agencies can be held responsible for any use that may be made of the information contained herein.

Conflicts of Interest: The authors declare no conflict of interest. The funders had no role in the design of the study; in the collection, analyses, or interpretation of data; in the writing of the manuscript, or in the decision to publish the results.

Appendix A

In this appendix, a copy of the questionnaire created in this study and submitted to the representatives of the projects is proposed. The questionnaire consists of eight pages and five parts.



1 (8)

Questionnaire on Positive Energy Districts (PEDs)

This questionnaire aims to collect data on Positive Energy Districts. The document is structured in five parts: General information, Information on district, Energy information, Project Data and Other Information. In each part you will be required to either enter values and/or tick boxes describing the district.

Part.1 General information

In this section we will collect general information about the project and the case study. Please fill in the missing information or correct the present data if necessary:

City:	
State:	
Project name:	
Status:	
year:	
total area involved:	
Scale:	
number of district:	
Lighthouse/fellow cities:	
Type of PED:	
Population involved:	

Part.2 Information on districts

In this section we will collect general information about the district; in particular, we will focus on information regarding the location of the district in relation to the rest of the urban fabric and the project area involved.

Please fill in the missing information and tick the box with an 'X' that best describes the location of the project area in relation to the urban contest, and, when required, write the type of building involved.

1. Project area

Name of district	Residential buildings useful area m2	Office buildings useful area m2	Commercial buildings useful area m2	(Other) buildings useful area m2 (school, hotel, etc.)	Total useful area involved m2

beyond the obvious

Figure A1. Copy of the first page of the questionnaire produced to conduct this study.



2. Location in relation to the urban context

Name of District	In the city centre	totally/fully built-up area	partially built-up area	New construction area

Part.3 Energy information

In this session we will collect various data on the technologies used in the project; in particular we will focus on information regarding energy generation system, renewable energy sources, energy storage and mobility.

Please tick the box with an 'Yes' or 'No' if the technology has been adopted and, if the data is available, enter the capacity in MW (optional)

1. Energy generation system:

District name	DHN - District Heating Network (Yes/No, MW)	DH&CN – District Heating & Cooling Network (Yes/No, MW)	HP – Heat Pump (Yes/No, MW)	EL - Efficient External Lighting (Yes/No, MW)

District name	HFC – Hydrogen Fuel Cell (Yes/No, MW)	CHP COAL (Yes/No, MW)	CHP BIOMASS (Yes/No, MW)	OTHER (Specify the name, MW)

2. Renewable energy sources:

District Name	ST - Solar Thermal Collectors (Yes/No, MW)	PV - Photovoltaic Modules (Yes/No, MW)	PVT - Hybrid Collectors (Yes/No, MW)	BIPV - Building Integrated Photovoltaics (Yes/No, MW)	W - Wind Power (>30kW) (Yes/No, MW)	MW - Micro Wind Power (<30kW) (Yes/No, MW)

beyond the obvious

Figure A2. Copy of the second page of the questionnaire produced to conduct this study.



District Name	BE – Bioenergy (Yes/No, MW)	WP - Tide, Wave, Ocean Power (Yes/No, MW)	HEP - Hydroelectric Power (Yes/No, MW)	RMW - Renewable Municipal Waste (Yes/No, MW)	WH - Waste Heat (Yes/No, MW)

District Name	GDN - Geothermal District Network (Yes/No, MW)	GB - Geothermal Boreholes (Yes/No, MW)	GE - Geothermal Energy (Yes/No, MW)	ATES - Aquifer Thermal Energy Storage (Yes/No, MW)

3. Other informations:

District name	Storage		Mobility		PH – Passive House (Yes/No)
	ES - Electric Storage (Yes/No, MW - MWh)	STES - Seasonal Thermal Energy Storage (Yes/No, MW - MWh)	EM - Electric Mobility (Yes/No, # Number)	V2G - Vehicle to Grid (Yes/No, # Number)	

Part.4 Project Data

In this section we will collect the project data; in particular, we will focus on total final energy (heat and electricity) generation, consumption and import and on CO2 saved per each district.

Please fill in the boxes with the required information.

District name:

Building load, design				
Building typology <small>(Write the Building typology, e.g. residential, office, school, etc.)</small>	Heating energy (MWh/year)	Electrical energy (MWh/year)	Cooling energy (MWh/year)	Total energy (MWh/year)

beyond the obvious

Figure A3. Copy of the third page of the questionnaire produced to conduct this study.



Building load, monitoring				
Building typology <small>(Write the Building typology, e.g. residential, office, school, etc.)</small>	Heating energy (MWh/year)	Electrical energy (MWh/year)	Cooling energy (MWh/year)	Total energy (MWh/year)

GENERATION, design						
Technology <small>(Write the technology, e.g. PV, CHP-biomass, etc.)</small>	Heating energy (MWh/year)	Electrical energy (MWh/year) <small>(Specify if in the electrical load is included lighting and appliances)</small>	Cooling energy (MWh/year)	Other type of energy (MWh/year)	Total energy (MWh/year)	Type of energy used in positivity calculation <small>(site energy, primary energy, etc.)</small>

GENERATION, monitoring						
Technology <small>(Write the technology, e.g. PV, CHP-biomass, etc.)</small>	Heating energy (MWh/year)	Electrical energy (MWh/year) <small>(Specify if in the electrical load is included lighting and appliances)</small>	Cooling energy (MWh/year)	Other type of energy (MWh/year)	Total energy (MWh/year)	Type of energy used in positivity calculation <small>(site energy, primary energy, etc.)</small>

beyond the obvious

Figure A4. Copy of the fourth page of the questionnaire produced to conduct this study.



Import, design						
Technology (Write the technology, e.g. Grid, District heating, PV, CHP, biomass, etc.)	Heating energy (MWh/year)	Electrical energy (MWh/year) (Specify if in the electrical load is included lighting and appliances)	Cooling energy (MWh/year)	Other type of energy (MWh/year)	Total energy (MWh/year)	Type of energy used in positivity calculation (site energy, primary energy, etc.)

Import, monitoring						
Technology (Write the technology, e.g. Grid, District heating, PV, CHP, biomass, etc.)	Heating energy (MWh/year)	Electrical energy (MWh/year) (Specify if in the electrical load is included lighting and appliances)	Cooling energy (MWh/year)	Other type of energy (MWh/year)	Total energy (MWh/year)	Type of energy used in positivity calculation (site energy, primary energy, etc.)

CO2 savings designed (KgCO2eq/a)	CO2 savings monitoring (KgCO2eq/a)

beyond the obvious

Figure A5. Copy of the fifth page of the questionnaire produced to conduct this study.

References

1. Godfray, H.C.J.; Beddington, J.R.; Crute, I.R.; Haddad, L.; Lawrence, D.; Muir, J.F.; Pretty, J.; Robinson, S.; Thomas, S.M.; Toulmin, C. Food Security: The Challenge of Feeding 9 Billion People. *Science* **2010**, *327*, 812–818. [CrossRef] [PubMed]
2. Walther, G.-R.; Post, E.; Convey, P.; Menzel, A.; Parmesan, C.; Beebee, T.J.C.; Fromentin, J.-M.; Hoegh-Guldberg, O.; Bairlein, F. Ecological responses to recent climate change. *Nature* **2002**, *416*, 389–395. [CrossRef] [PubMed]
3. Rayner, N.A.; Parker, D.E.; Horton, E.B.; Folland, C.K.; Alexander, L.V.; Rowell, D.P.; Kent, E.C.; Kaplan, A. Global analyses of sea surface temperature, sea ice, and night marine air temperature since the late nineteenth century. *J. Geophys. Res.* **2003**, *108*, 4407. [CrossRef]

4. Parmesan, C.; Yohe, G. A globally coherent fingerprint of climate change impacts across natural systems. *Nature* **2003**, *421*, 37–42. [CrossRef]
5. Foley, J.A.; DeFries, R.; Asner, G.P.; Barford, C.; Bonan, G.; Carpenter, S.R.; Chapin, F.S.; Coe, M.T.; Daily, G.C.; Gibbs, H.K.; et al. Global consequences of land use. *Science* **2005**, *309*, 570–574. [CrossRef]
6. United Nations. Paris Agreement—Status of Ratification. In Proceedings of the 21st Paris Climate Change Conference, Paris, France, 30 November–11 December 2015.
7. Mitchell, D.; Allen, M.R.; Hall, J.W.; Muller, B.; Rajamani, L.; Le Quéré, C. The myriad challenges of the Paris Agreement. *Philos. Trans. R. Soc. A Math. Phys. Eng. Sci.* **2018**, *376*, 20180066. [CrossRef]
8. United Nations. *What Is the Paris Agreement?* *United Nations Climate Change*; UNFCCC: Rio de Janeiro, Brazil; New York, NY, USA, 2015.
9. United Nations. Adoption of the Paris Agreement. In Proceedings of the 2015 United Nations Climate Change Conference, Paris, France, 30 November–12 December 2015; p. 21932.
10. United Nations. *Summary of the Paris Agreement*; United Nations Framework Convention on Climate Change: Rio de Janeiro, Brazil; New York, NY, USA, 2015.
11. United Nations. Paris Agreement COP21. In Proceedings of the 2015 United Nations Climate Change Conference, Paris, France, 30 November–12 December 2015.
12. Zhao, X.; Ma, X.; Chen, B.; Shang, Y.; Song, M. Challenges toward carbon neutrality in China: Strategies and countermeasures. *Resour. Conserv. Recycl.* **2022**, *176*, 105959. [CrossRef]
13. Zou, C.; Xue, H.; Xiong, B.; Zhang, G.; Pan, S.; Jia, C.; Wang, Y.; Ma, F.; Sun, Q.; Guan, C.; et al. Connotation, innovation and vision of “carbon neutrality”. *Nat. Gas Ind. B* **2021**, *8*, 523–537. [CrossRef]
14. Wang, F.; Harindintwali, J.D.; Yuan, Z.; Wang, M.; Li, S.; Yin, Z.; Huang, L.; Fu, Y.; Li, L.; Chang, S.X.; et al. Technologies and perspectives for achieving carbon neutrality. *Innovation* **2021**, *2*, 100180. [CrossRef]
15. Pulselli, R.M.; Broersma, S.; Martin, C.L.; Keeffe, G.; Bastianoni, S.; van den Dobbelaere, A. Future city visions. The energy transition towards carbon-neutrality: Lessons learned from the case of Roeselare, Belgium. *Renew. Sustain. Energy Rev.* **2021**, *137*, 110612. [CrossRef]
16. Bonoli, A.; Zanni, S.; Serrano-Bernardo, F. Sustainability in Building and Construction within the Framework of Circular Cities and European New Green Deal. The Contribution of Concrete Recycling. *Sustainability* **2021**, *13*, 2139. [CrossRef]
17. Špaček, R.; Legény, J.; Gregor, P. Challenge and response at all levels in sustainable architecture education. *World Trans. Eng. Technol. Educ.* **2020**, *18*, 18–23.
18. Wolf, S.; Teitge, J.; Mielke, J.; Schütze, F.; Jaeger, C. The European Green Deal—More Than Climate Neutrality. *Intereconomics* **2021**, *56*, 99–107. [CrossRef]
19. Salvia, M.; Reckien, D.; Pietrapertosa, F.; Eckersley, P.; Spyridaki, N.-A.; Krook-Riekkola, A.; Olazabal, M.; De Gregorio Hurtado, S.; Simoes, S.G.; Geneletti, D.; et al. Will climate mitigation ambitions lead to carbon neutrality? An analysis of the local-level plans of 327 cities in the EU. *Renew. Sustain. Energy Rev.* **2021**, *135*, 110253. [CrossRef]
20. Magrini, A.; Lentini, G.; Cuman, S.; Bodrato, A.; Marengo, L. From nearly zero energy buildings (NZEB) to positive energy buildings (PEB): The next challenge—The most recent European trends with some notes on the energy analysis of a forerunner PEB example. *Dev. Built Environ.* **2020**, *3*, 100019. [CrossRef]
21. Kolokotsa, D.; Rovas, D.; Kosmatopoulos, E.; Kalaitzakis, K. A roadmap towards intelligent net zero- and positive-energy buildings. *Sol. Energy* **2011**, *85*, 3067–3084. [CrossRef]
22. Ala-Juusela, M.; Rehman, H.U.; Hukkalainen, M.; Reda, F. Positive Energy Building Definition with the Framework, Elements and Challenges of the Concept. *Energies* **2021**, *14*, 6260. [CrossRef]
23. Lindholm, O.; Rehman, H.U.; Reda, F. Positioning Positive Energy Districts in European Cities. *Buildings* **2021**, *11*, 19. [CrossRef]
24. Marotta, I.; Guarino, F.; Longo, S.; Cellura, M. Environmental Sustainability Approaches and Positive Energy Districts: A Literature Review. *Sustainability* **2021**, *13*, 13063. [CrossRef]
25. Becchio, C.; Bottero, M.C.; Corgnati, S.P.; Dell’Anna, F. Decision making for sustainable urban energy planning: An integrated evaluation framework of alternative solutions for a NZED (Net Zero-Energy District) in Turin. *Land Use Policy* **2018**, *78*, 803–817. [CrossRef]
26. Vandevyvere, H.; Ahlers, D.; Alpagut, B.; Cerna, V.; Cimini, V.; Haxhija, S.; Hukkalainen, M.; Kuzmic, M.; Livik, K.; Padilla, M.; et al. *Positive Energy Districts Solution Booklet*; European Union: Brussels, Belgium, 2020.
27. Hedman, Å.; Rehman, H.U.; Gabaldón, A.; Bisello, A.; Albert-Seifried, V.; Zhang, X.; Guarino, F.; Grynning, S.; Eicker, U.; Neumann, H.-M.; et al. IEA EBC Annex83 positive energy districts. *Buildings* **2021**, *11*, 130. [CrossRef]
28. Ala-Juusela, M.; Crosbie, T.; Hukkalainen, M. Defining and operationalising the concept of an energy positive neighbourhood. *Energy Convers. Manag.* **2016**, *125*, 133–140. [CrossRef]
29. Zhang, X.; Penaka, S.R.; Giriraj, S.; Sánchez, M.N.; Civiero, P.; Vandevyvere, H. Characterizing Positive Energy District (PED) through a Preliminary Review of 60 Existing Projects in Europe. *Buildings* **2021**, *11*, 318. [CrossRef]
30. Lorenzoni, I.; Pidgeon, N.F. Public Views on Climate Change: European and USA Perspectives. *Clim. Chang.* **2006**, *77*, 73–95. [CrossRef]
31. Stoate, C.; Báldi, A.; Beja, P.; Boatman, N.; Herzon, I.; van Doorn, A.; de Snoo, G.; Rakosy, L.; Ramwell, C. Ecological impacts of early 21st century agricultural change in Europe—A review. *J. Environ. Manag.* **2009**, *91*, 22–46. [CrossRef] [PubMed]

32. Olesen, J.E.; Bindi, M. Consequences of climate change for European agricultural productivity, land use and policy. *Eur. J. Agron.* **2002**, *16*, 239–262. [CrossRef]
33. Davis, S.J.; Caldeira, K. Consumption-based accounting of CO₂ emissions. *Proc. Natl. Acad. Sci. USA* **2010**, *107*, 5687–5692. [CrossRef]
34. Lindner, M.; Maroschek, M.; Netherer, S.; Kremer, A.; Barbati, A.; Garcia-Gonzalo, J.; Seidl, R.; Delzon, S.; Corona, P.; Kolström, M.; et al. Climate change impacts, adaptive capacity, and vulnerability of European forest ecosystems. *For. Ecol. Manag.* **2010**, *259*, 698–709. [CrossRef]
35. Wawrzyniak, D. CO₂ Emissions in the Visegrad Group Countries and the European Union Climate Policy. *Comp. Econ. Res. Central East. Eur.* **2020**, *23*, 73–91. [CrossRef]
36. Billson, M.; Pourkashanian, M. The Evolution of European CCS Policy. *Energy Procedia* **2017**, *114*, 5659–5662. [CrossRef]
37. Montanarella, L.; Panagos, P. The relevance of sustainable soil management within the European Green Deal. *Land Use Policy* **2021**, *100*, 104950. [CrossRef]
38. Claeys, G.; Tagliapietra, S.; Zachmann, G. *How to Make the European Green Deal Work*; Bruegel: Brussels, Belgium, 2019.
39. Boeri, A.; Longo, D.; Palma, M. Climate-neutral limate-neutral and smart cities: A European polices' overview. *WIT Trans. Ecol. Environ.* **2021**, *253*, 3–14. [CrossRef]
40. Bossi, S.; Gollner, C.; Theierling, S. Towards 100 Positive Energy Districts in Europe: Preliminary Data Analysis of 61 European Cases. *Energies* **2020**, *13*, 6083. [CrossRef]
41. Bartholmes, J. *Smart Cities and Communities SCC1-2020*; European Commission: Brussels, Belgium, 2020.
42. Bilotta, S.; Nesi, P.; Paoli, I. Real-time System for Short- and Long-Term Prediction of Vehicle Flow. In Proceedings of the 2020 IEEE International Conference on Smart Data Services, SMDS, Virtual, 18–24 October 2020; pp. 97–104. [CrossRef]
43. Haarstad, H.; Wathne, M.W. Are smart city projects catalyzing urban energy sustainability? *Energy Policy* **2019**, *129*, 918–925. [CrossRef]
44. Calzada, I. Replicating Smart Cities: The City-to-City Learning Programme in the Replicate EC-H2020-SCC Project. *Smart Cities* **2020**, *3*, 978–1003. [CrossRef]
45. Gouveia, J.P.; Seixas, J.; Palma, P.; Duarte, H.; Luz, H.; Cavadini, G.B. Positive Energy District: A Model for Historic Districts to Address Energy Poverty. *Front. Sustain. Cities* **2021**, *3*, 648473. [CrossRef]
46. Maestosi, P.C. Smart Cities and Positive Energy Districts: Urban Perspectives in 2020. *Energies* **2021**, *14*, 2351. [CrossRef]
47. Soriano, F.H.; Mulatero, F. EU Research and Innovation (R&I) in renewable energies: The role of the Strategic Energy Technology Plan (SET-Plan). *Energy Policy* **2011**, *39*, 3582–3590. [CrossRef]
48. Turci, G.; Alpagut, B.; Civiero, P.; Kuzmic, M.; Pagliula, S.; Massa, G.; Albert-Seifried, V.; Seco, O.; Soutullo, S. A Comprehensive PED-Database for Mapping and Comparing Positive Energy Districts Experiences at European Level. *Sustainability* **2021**, *14*, 427. [CrossRef]
49. Derkenbaeva, E.; Vega, S.H.; Hofstede, G.J.; van Leeuwen, E. Positive energy districts: Mainstreaming energy transition in urban areas. *Renew. Sustain. Energy Rev.* **2022**, *153*, 111782. [CrossRef]
50. Krangsås, S.G.; Steemers, K.; Konstantinou, T.; Soutullo, S.; Liu, M.; Giancola, E.; Prebreza, B.; Ashrafian, T.; Murauskaitė, L.; Maas, N. Positive Energy Districts: Identifying Challenges and Interdependencies. *Sustainability* **2021**, *13*, 10551. [CrossRef]
51. Castillo-Calzadilla, T.; Alonso-Vicario, A.; Borges, C.E.; Martin, C. E-Mobility in Positive Energy Districts. *Buildings* **2022**, *12*, 264. [CrossRef]
52. Moreno, A.G.; Vélez, F.; Alpagut, B.; Hernández, P.; Montalvillo, C.S. How to Achieve Positive Energy Districts for Sustainable Cities: A Proposed Calculation Methodology. *Sustainability* **2021**, *13*, 710. [CrossRef]
53. Frolova, M.; Centeri, C.; Benediktsson, K.; Hunziker, M.; Kabai, R.; Scognamiglio, A.; Martinopoulos, G.; Sismani, G.; Brito, P.; Muñoz-Cerón, E.; et al. Effects of renewable energy on landscape in Europe: Comparison of hydro, wind, solar, bio-, geothermal and infrastructure energy landscapes. *Hung. Geogr. Bull.* **2019**, *68*, 317–339. [CrossRef]
54. Miskolczi, M.; Földes, D.; Munkácsy, A.; Jászberényi, M. Urban mobility scenarios until the 2030s. *Sustain. Cities Soc.* **2021**, *72*, 103029. [CrossRef]
55. Zhang, X.; Shen, J.; Saini, P.K.; Lovati, M.; Han, M.; Huang, P.; Huang, Z. Digital Twin for Accelerating Sustainability in Positive Energy District: A Review of Simulation Tools and Applications. *Front. Sustain. Cities* **2021**, *3*, 663269. [CrossRef]
56. Shahat, E.; Hyun, C.; Yeom, C. City Digital Twin Potentials: A Review and Research Agenda. *Sustainability* **2021**, *13*, 3386. [CrossRef]
57. Jones, D.; Snider, C.; Nassehi, A.; Yon, J.; Hicks, B. Characterising the Digital Twin: A systematic literature review. *CIRP J. Manuf. Sci. Technol.* **2020**, *29*, 36–52. [CrossRef]
58. Ranta, M.; Hajduk, P.; Tartia, J.; Santala, S.; Tukka, T.; Juhmen, J.; Boldt, D.; Häsä, S.; Töyräs, J.; Ekelund, E.; et al. D3.5 EV Mobility Integration and Its Impacts in Espoo. 2022. Available online: <https://www.sparcs.info/about/deliverables/d305-ev-mobility-integration-and-its-impacts-espoo> (accessed on 18 December 2022).
59. Klobut, K.; Piira, K.; Abdurafikov, R.; Laitinen, A.; Juslin, A.; Juhmen, J.; Saari, M.; Soinio, T.; Laakso, S.; Tukka, T.; et al. D3.4 Interoperability of Holistic Energy Systems in Espoo. 2022. Available online: <https://www.sparcs.info/about/deliverables/d304-interoperability-holistic-energy-systems-espoo> (accessed on 18 December 2022).

60. Fatima, Z. D3.6 Optimizing People Flow and User Experience for Energy Positive Districts. 2022. Available online: <https://www.sparcs.info/about/deliverables/d306-optimizing-people-flow-and-user-experience-energy-positive-districts> (accessed on 17 December 2022).
61. Wanne, E.; Tartia, J.; Juslin, A.; Mäkinen, J.; Hukkalainen, M.; Fatima, Z.; Klobut, K.; Piira, K.; Ranta, M.; Hajduk, p.; et al. D3.3 Implemented Demonstrations of Solutions for Energy Positive Blocks in Espoo. 2022. Available online: <https://www.sparcs.info/about/deliverables/d303-implemented-demonstrations-solutions-energy-positive-blocks-espoo> (accessed on 28 November 2022).
62. Lei, L. D4.2 Midterm Report on the Implemented Solutions for Energy Positive Blocks in Leipzig. 2021. Available online: <https://www.sparcs.info/about/deliverables/d402-midterm-report-implemented-solutions-energy-positive-blocks-leipzig> (accessed on 18 December 2022).
63. Riedel, N.; Müller, I.; Albrecht, S.; Jelinek, E.; Kühne, J.M.; Schutt, T.; Vöhl, A.; Kondziella, H.; Baumet, S.; Bolognesi, P.; et al. D4.3 Implemented Demonstrations of Solutions for Energy Positive Blocks in Leipzig. 2022, pp. 1–125. Available online: <https://www.sparcs.info/about/deliverables/d403-implemented-demonstrations-solutions-energy-positive-blocks-leipzig> (accessed on 18 December 2022).
64. City of Leipzig. D4.01 Detailed Plan of the Leipzig Smart City Lighthouse Demonstrations. 2020. Available online: <https://www.sparcs.info/about/deliverables/d401-detailed-plan-leipzig-smart-city-lighthouse-demonstrations> (accessed on 28 November 2022).
65. Martinopoulos, G.; Nikolopoulos, N.; Tsompanidou, E.; Matsoukas, S.; Angelakoglou, K.; Paraskevi Gkiourka, K.K. D 4.6 Planning and Management of Open Innovation Challenges in Dijon and Turku—V1. 2022. Available online: <https://h2020response.eu/wp-content/uploads/2022/05/D4.6-Planning-and-management-of-Open-Innovation-Challenges-in-Dijon-Turku-%E2%80%93V1.pdf> (accessed on 14 December 2022).
66. Lanna, M.; Py, E. Response Data Governance and CIP Operational Framework. 2022. Available online: <https://h2020response.eu/wp-content/uploads/2022/05/D3.2-RESPONSE-Data-Governance-and-CIP-Operational-Framework.pdf> (accessed on 15 December 2022).
67. Rouchette, H. D1.1 Elicitation of Citizens and Stakeholder Requirements, Risk Perception and User Acceptance Determinants. 2021. Available online: <https://h2020response.eu/wp-content/uploads/2022/05/D1.1-Elicitation-of-citizens-and-stakeholder-requirements-risk-perception-and-user-acceptance-determinants.pdf> (accessed on 28 November 2022).
68. Evens, C. D1.5 Master City Plans for TA#3 Sustainable Energy Storage. 2021. Available online: <https://h2020response.eu/wp-content/uploads/2022/05/D1.5-Master-City-Plans-for-TA3-Sustainable-Energy-Storage.pdf> (accessed on 28 November 2022).
69. Shemeikka, J. D1.3 Master City Plans for TA#1 Positive Energy Building Systems. 2021. Available online: <https://h2020response.eu/wp-content/uploads/2022/05/D1.3-Master-City-Plans-for-TA1-Positive-Energy-Building-Systems.pdf> (accessed on 13 December 2022).
70. Néstor Rodríguez Pérez, R.C.A. D1.2 Assessment of Smart Cities Regulatory and Legal Environment—V1. 2021. Available online: <https://h2020response.eu/wp-content/uploads/2022/05/D1.2-Assessment-of-Smart-Cities-Regulatory-and-Legal-Environment-V1.pdf> (accessed on 13 November 2022).
71. Kallenbach, M. Matthijs Janssen Paul Roßteutscher Thomas van de Voort, ir Determining Critical Factors in the Atelier Positive Energy District Pilot in Buiksloterham Mark van Wees. 2021. Available online: https://smartcity-atelier.eu/app/uploads/ATELIER-Critical_learning_factors-report.pdf (accessed on 28 November 2022).
72. García, C.; Urrutia, K.; Muñoz, I.; López, A.; Vallejo, E.; Rodríguez, C.; Verspeek, F.; Nathalia, K.; Andonegui, C.; Molinete, B. Deliverable 2.3: Common Methodological Framework for Vision Development. 2021. Available online: <https://smartcity-atelier.eu/outcomes/deliverables/d2-3/> (accessed on 13 December 2022).
73. DEUSTO, Version, D.; Level, D. Deliverable 1.7: Open Access Research Data. 2020. Available online: <https://smartcity-atelier.eu/outcomes/deliverables/d1-7/> (accessed on 28 November 2022).
74. Van Doornink, M. *Amsterdam Climate Office New Amsterdam Climate*.; City of Amsterdam: Amsterdam, The Netherlands, 2016, pp. 1–6. Available online: <https://smartcity-atelier.eu/app/uploads/RoadmapAmsterdam-Climate-Neutral-2050-full-version-ENG.pdf> (accessed on 17 December 2022).
75. Remmele, B. *Dissemination & Communication Strategy Plan*.; Atelier: Amsterdam, The Netherlands, 2020, pp. 1–50. Available online: <https://smartcity-atelier.eu/outcomes/deliverables/d10-8/> (accessed on 23 November 2022).
76. University of Deusto, Amsterdam University of Applied Science, Paul Scherrer Institute, Atelier Monitoring and Evaluation Framework deliverable 9.1: Repository of Definitions of Terms, Key Characteristics Archetypes, and a Set of KPIs WP9, Task 9.1. Repository of Definitions of Terms, Key Characteristics Archetypes, and a Set of KPIs. 2020. Available online: <https://smartcity-atelier.eu/outcomes/deliverables/d9-1/> (accessed on 15 November 2022).
77. Waag Deu Auas D7.1: Citizen and Stakeholder Engagement Plans. 2021. 2021. Available online: <https://smartcity-atelier.eu/outcomes/deliverables/d7-1/> (accessed on 23 November 2022).
78. DEUSTO. Deliverable 1.3: Data Management Plan. 2021. 2020. Available online: <https://smartcity-atelier.eu/outcomes/deliverables/d1-3/> (accessed on 15 November 2022).
79. Rev, T. Deliverable 3.1: The PED Innovation Atelier Organisation Document. 2021, pp. 1–55. Available online: <https://smartcity-atelier.eu/outcomes/deliverables/d3-1/> (accessed on 15 November 2022).

80. Remmele, B. The ATELIER Project. Citizen-Driven Positive Energy Districts in Amsterdam, Bilbao and beyond Smart City, Smart Mobility, Horizon 2020, Lighthouse Cities. 2020, pp. 50–52. Available online: <https://smartcity-atelier.eu/news/international-strategies-article-introducing-atelier/> (accessed on 28 November 2022).
81. Arrizabalaga, E.; García-Gusano, D.; Hermoso, N.; Muñoz, L.; Fernandez, N.; Alpagut, B.; Olivadese, R.; Dourlens, S.; Action, I. D1.3-Tools for Modelling Energy Demand, Supply Side, Simulation of Scenarios and Estimation of Impacts WP1, Task 1.3 November 2020 [M24]. 2020, pp. 1–147. Available online: https://makingcity.eu/wp-content/uploads/2021/12/MakingCity_D1_3_Tools_for_modelling_Final.pdf (accessed on 27 November 2022).
82. De Torre, C.; Rodriguez, C.; Vasallo, A. Making City. D1.2—City Diagnosis: Analysis of Existing City Plans. 2020, pp. 1–395. Available online: https://makingcity.eu/wp-content/uploads/2020/09/MakingCity_D1_2_City_Diagnosis_analysis_of_existing_city_plans_Final_V1-2.pdf (accessed on 27 November 2022).
83. Rankinen, J.-A.; Lakkala, S.; Haapasalo, H.; Hirvonen-Kantola, S. Stakeholder management in PED projects: Challenges and management model. *Int. J. Sustain. Energy Plan. Manag.* **2022**, *34*, 91–106. [CrossRef]
84. Schouten, C.; Brezet, H. The Urban Financial Metabolism Model: Quantifying the Societal Impact of Residential Energy Poverty in Groningen, the Netherlands. 2020. Available online: https://makingcity.eu/wp-content/uploads/2021/02/Schouten_395366_Research-Project-Report-edition-for-MAKING-CITY-website.pdf (accessed on 28 November 2022).
85. Montalvillo, C.S.; Frey, J.; Jaramillo, V.; Cartif, F.; Belver, A.V.; Rankinen, J.A.; Lakkala, S.; Haapasalo, H.; Hirvonen-Kantola, S.; Name, F.; et al. VI Congreso Edificios Energía Casi Nula Proyecto Making-City: Tres Distritos De Energía Positiva En Dos Ciudades Faro (Goningen Y Oulu). *Int. J. Sustain. Energy Plan. Manag.* **2020**, *34*, 1–147.
86. Kerrigan, R.; Purshouse, N.; De Donatis, L.; Neu, O. D4.1: Limerick DST (Integrated Modelling and Decision Support Tool) Including Training Manuals/Videos +CityxChange Project Title Positive City Exchange. 2020. Available online: <https://cityxchange.eu/knowledge-base/d4-1-limerick-dst-integrated-modelling-and-decision-support-tool-including-training-manuals-videos/> (accessed on 13 December 2022).
87. Package, C.W.; Lccc, J.T.; Ul, H.F.; Lccc, R.W.; Lccc, T.C. D4.8: Limerick Citizen Observatory. 2022. Available online: <https://cityxchange.eu/knowledge-base/d4-8-limerick-citizen-observatory/> (accessed on 14 December 2022).
88. Walsh, G.; Fitzgerald, H.; Lyes, M.; Mee, A. +CityxChange D4.10: Limerick Innovation Lab Solutions Catalogue 2. 2022, pp. 1–60. Available online: <https://cityxchange.eu/knowledge-base/d4-10-limerick-innovation-lab-solutions-catalogue-2/> (accessed on 22 December 2022).
89. Sørum, A.B.; Ove Berthelsen, B.; Skoglund, T.R.; Bratseth, E.A.; Nørbech, T.; Lauvland, M.; Jensen, T.; Riedesel, K.; Gulbrandsøy, E.; Ahlers, D.; et al. D5.13: +Trondheim eMaaS Demonstration. Available online: <https://cityxchange.eu/knowledge-base/d5-13-trondheim-emaas-demonstration/> (accessed on 28 November 2022).
90. Introduction to Cityxchange. Available online: https://view.officeapps.live.com/op/view.aspx?src=https%3A%2F%2Fcityxchange.eu%2Fwp-content%2Fuploads%2F2019%2F10%2FIntroduction_CxC-3.pptx&wdOrigin=BROWSELINK (accessed on 28 November 2022).
91. Antolic, M.; Wright, S. D4.4: Limerick DPBE Implementation Guide 1. 2021. Available online: <https://cityxchange.eu/knowledge-base/d4-4-limerick-dpbe-implementation-guide-1/> (accessed on 13 December 2022).
92. Purshouse, N.; De Donatis, L.; Neu, O.; Kerrigan, R.; Berthelsen, B.O. D5.2: +Trondheim DST Including Training Manuals/Videos +CityxChange Project Title Positive City Exchange. 2021. Available online: <https://cityxchange.eu/knowledge-base/d5-2-trondheim-dst-including-training-manuals-videos/> (accessed on 28 November 2022).
93. Urban, S.; Package, C.W. D5.7: + Trondheim 2050 Bold City Vision and Guidelines. 2022. Available online: <https://cityxchange.eu/knowledge-base/d5-7-trondheim-2050-bold-city-vision-and-guidelines-vision-for-sustainable-urban-transition/> (accessed on 22 December 2022).
94. Grabinsky, C.; Riedesel, K.; Haugslett, A. D5.10: Trondheim Innovation Lab Solutions Catalogue (+ Trondheim Implementation of Innovation Playground). 2021. Available online: <https://cityxchange.eu/knowledge-base/d5-10-trondheim-innovation-lab-solutions-catalogue/> (accessed on 13 December 2022).
95. Package, C.W.; Tk, K.R.; Grabinsky, C.M.; Rk, M.M.; Mansilla, W.A.; Ntnu, D.A. D5.8: + Trondheim Citizen Observatory. 2021. Available online: <https://cityxchange.eu/knowledge-base/d5-8-trondheim-citizen-observatory/> (accessed on 17 November 2022).
96. Walsh, G.; Mee, A. D4.3: Limerick Innovation Lab Catalogue 1.2020. Available online: <https://cityxchange.eu/knowledge-base/d4-3-limerick-innovation-lab-solutions-catalogue-1/> (accessed on 28 November 2022).
97. Gonçalves, J. Project Management Roadmap Technical References Project Acronym Pocityf Project Title a Positive Energy City Transformation Framework. 2021. Available online: https://pocityf.eu/wp-content/uploads/2022/06/POCITYF-864400_D11.2_Project-Management-Roadmap-version-2.pdf (accessed on 26 October 2022).
98. Gonçalves, J. D11.4 Quality Assessment, Risk Assessment and Contingency Plans. 2020. Available online: https://pocityf.eu/wp-content/uploads/2022/06/POCITYF-864400_D11.4_Quality-Assessment-Risk-Assessment-and-Contingency-Plans.pdf (accessed on 28 November 2022).
99. Serra, L.; Leitão, D.; Michi, C.; Schmid, E.; Bilo, N. Pocityf, D9.1: Pocityf Clustering Action Plan. Pocityf. 2020. Available online: https://pocityf.eu/wp-content/uploads/2020/09/POCITYF-864400_D9.1_Clustering-Action-Plan.pdf (accessed on 28 October 2022).

100. Kort, J.; Klösters, M.; de Koning, N. Becoming Sustainable Together with Residents. Participation and Communication Manual for Housing Corporations. Pocityf and Tno. 2022. Available online: <https://pocityf.eu/news/becoming-sustainable-together-with-residents-participation-and-communication-manual-for-housing-corporations/> (accessed on 28 November 2022).
101. Michi, C.; Material, M.D. D10.5 Multi Dissemination Material Version 2. Pocityf. 2020. Available online: https://pocityf.eu/wp-content/uploads/2020/09/POCITYF-864400_D10.5_Multi-Dissemination-material-version-2.pdf/ (accessed on 13 December 2022).
102. Gonçalves, L.; Patrício, L.; Teixeira, J.; Bănică, B.; Pocityf, D. 4.1: Engagement, C. Pocityf Citizen Engagement Plan. Pocityf. 2020. Available online: https://pocityf.eu/wp-content/uploads/2022/06/POCITYF-864400_D4.1_POCITYF-Citizen-Engagement-Plan.pdf (accessed on 25 October 2022).
103. Prokscha, S. D11.8 The Data Management Plan. In *Practical Guide to Clinical Data Management*, 3rd ed.; CRC Press: Boca Raton, FL, USA, 2020; pp. 25–30. [CrossRef]
104. Kourtzanidis, K.; Angelakoglou, K.; Giourka, P.; Tsarchopoulos, P.; Nikolopoulos, N.; Ioannidis, D.; Kantorovitch, J.; Formiga, J.; Verbeek, K.; de Vries, M.; et al. Technical and Innovation Management Plans. Pocityf. 2020. Available online: https://pocityf.eu/wp-content/uploads/2022/06/POCITYF-864400_D11.7_Technical-and-Innovation-Management-Plans.pdf (accessed on 28 November 2022).
105. Kottek, M.; Grieser, J.; Beck, C.; Rudolf, B.; Rubel, F. World map of the Köppen-Geiger climate classification updated. *Meteorol. Z.* **2006**, *15*, 259–263. [CrossRef] [PubMed]
106. Beck, H.E.; Zimmermann, N.E.; McVicar, T.R.; Vergopolan, N.; Berg, A.; Wood, E.F. Present and future Köppen-Geiger climate classification maps at 1-km resolution. *Sci. Data* **2018**, *5*, 180214. [CrossRef] [PubMed]
107. Chen, D.; Chen, H.W. Using the Köppen classification to quantify climate variation and change: An example for 1901–2010. *Environ. Dev.* **2013**, *6*, 69–79. [CrossRef]
108. Fatima, Z.; Pollmer, U.; Santala, S.-S.; Kontu, K.; Ticklen, M. Citizens and Positive Energy Districts: Are Espoo and Leipzig Ready for PEDs? *Buildings* **2021**, *11*, 102. [CrossRef]
109. Hukkalainen, M.; Fatima, Z.; Klobut, K.; Piira, K.; Ranta, M.; Hajduk, P.; Vainio-Kaila, T.; Wanne, E.; Tartia, J.; Bartel, A.; et al. D3.2 Midterm Report on the Implemented Demonstrations of Solutions for Energy Positive Blocks in Espoo. 2021. Available online: <https://www.sparcs.info/about/deliverables/d302-midterm-report-implemented-demonstrations-solutions-energy-positive-blocks> (accessed on 13 December 2022).
110. Martinopoulos, G.; Nikolopoulou, N.; Angelakoglou, K.; Giourka, P. RESPONSE D2.1 KPI Framework. 2021. Available online: <https://h2020response.eu/wp-content/uploads/2022/05/D2.1-RESPONSE-KPI-Framework.pdf> (accessed on 13 December 2022).
111. Technical University of Denmark; Global Wind Atlas. Global Wind Atlas 30. 2021. Available online: <https://globalwindatlas.info/en> (accessed on 14 November 2022).
112. Hukkalainen, M.; Zarrin, F.; Klobut, K.; Lindholm, O.; Ranta, M.; Vainio-Kaila, T.; Wanne, E.; Tartia, J.; Horn, H.; Kontu, K.; et al. D3.1 Detailed Plan of the Espoo Smart City Lighthouse Demonstrations; Sparcs: Espoo, Finland, 2020.
113. Li, H.; Svendsen, S. District Heating Network Design and Configuration Optimization with Genetic Algorithm. *J. Sustain. Dev. Energy Water Environ. Syst.* **2013**, *1*, 291–303. [CrossRef]
114. Krug, R.; Mehrmann, V.; Schmidt, M. Nonlinear optimization of district heating networks. *Optim. Eng.* **2021**, *22*, 783–819. [CrossRef]
115. Delange, A.; Lambert, R.S.C.; Shah, N.; Acha, S.; Markides, C.N. Modelling and optimising the marginal expansion of an existing district heating network. *Energy* **2017**, *140*, 209–223. [CrossRef]
116. Zhang, S.; Gu, W.; Qiu, H.; Yao, S.; Pan, G.; Chen, X. State estimation models of district heating networks for integrated energy system considering incomplete measurements. *Appl. Energy* **2021**, *282*, 116105. [CrossRef]
117. Sartor, K.; Thomas, D.; Dewallef, P. A comparative study for simulating heat transport in large district heating networks. *Int. J. Heat Technol.* **2018**, *36*, 301–308. [CrossRef]
118. Forman, C.; Muritala, I.K.; Pardemann, R.; Meyer, B. Estimating the global waste heat potential. *Renew. Sustain. Energy Rev.* **2016**, *57*, 1568–1579. [CrossRef]
119. Wahlroos, M.; Pärssinen, M.; Rinne, S.; Syri, S.; Manner, J. Future views on waste heat utilization—Case of data centers in Northern Europe. *Renew. Sustain. Energy Rev.* **2018**, *82*, 1749–1764. [CrossRef]
120. Papapetrou, M.; Kosmadakis, G.; Cipollina, A.; La Commare, U.; Micale, G. Industrial waste heat: Estimation of the technically available resource in the EU per industrial sector, temperature level and country. *Appl. Therm. Eng.* **2018**, *138*, 207–216. [CrossRef]
121. Chien, F.; Kamran, H.W.; Albashar, G.; Iqbal, W. Dynamic planning, conversion, and management strategy of different renewable energy sources: A Sustainable Solution for Severe Energy Crises in Emerging Economies. *Int. J. Hydrogen Energy* **2021**, *46*, 7745–7758. [CrossRef]
122. Haseli, Y. Maximum conversion efficiency of hydrogen fuel cells. *Int. J. Hydrogen Energy* **2018**, *43*, 9015–9021. [CrossRef]
123. Manoharan, Y.; Hosseini, S.E.; Butler, B.; Alzahrani, H.; Senior, B.T.F.; Ashuri, T.; Krohn, J. Hydrogen Fuel Cell Vehicles; Current Status and Future Prospect. *Appl. Sci.* **2019**, *9*, 2296. [CrossRef]
124. Khan, U.; Yamamoto, T.; Sato, H. An insight into potential early adopters of hydrogen fuel-cell vehicles in Japan. *Int. J. Hydrogen Energy* **2021**, *46*, 10589–10607. [CrossRef]
125. Ardente, F.; Beccali, G.; Cellura, M.; Brano, V.L. Life cycle assessment of a solar thermal collector. *Renew. Energy* **2005**, *30*, 1031–1054. [CrossRef]

126. Hirst, L.C.; Ekins-Daukes, N.J. Fundamental losses in solar cells. *Prog. Photovolt. Res. Appl.* **2010**, *19*, 286–293. [CrossRef]
127. van der Ende, B.M.; Aarts, L.; Meijerink, A. Lanthanide ions as spectral converters for solar cells. *Phys. Chem. Chem. Phys.* **2009**, *11*, 11081–11095. [CrossRef]
128. Huang, X.; Han, S.; Huang, W.; Liu, X. Enhancing solar cell efficiency: The search for luminescent materials as spectral converters. *Chem. Soc. Rev.* **2012**, *42*, 173–201. [CrossRef]
129. Jurasz, J.; Canales, F.A.; Kies, A.; Guezgouz, M.; Beluco, A. A review on the complementarity of renewable energy sources: Concept, metrics, application and future research directions. *Sol. Energy* **2020**, *195*, 703–724. [CrossRef]
130. Liu, X.; Wang, Y.; Xie, F.; Yang, X.; Han, L. Improving the Performance of Inverted Formamidinium Tin Iodide Perovskite Solar Cells by Reducing the Energy-Level Mismatch. *ACS Energy Lett.* **2018**, *3*, 1116–1121. [CrossRef]
131. Westerlund, M. Social Acceptance of Wind Energy in Urban Landscapes. *Technol. Innov. Manag. Rev.* **2020**, *10*, 49–62. [CrossRef]
132. Leiren, M.D.; Aakre, S.; Linnerud, K.; Julsrud, T.E.; Di Nucci, M.-R.; Krug, M. Community Acceptance of Wind Energy Developments: Experience from Wind Energy Scarce Regions in Europe. *Sustainability* **2020**, *12*, 1754. [CrossRef]
133. Chen, H.; Cong, T.N.; Yang, W.; Tan, C.; Li, Y.; Ding, Y. Progress in electrical energy storage system: A critical review. *Prog. Nat. Sci.* **2009**, *19*, 291–312. [CrossRef]
134. AL Shaqsi, A.Z.; Sopian, K.; Al-Hinai, A. Review of energy storage services, applications, limitations, and benefits. *Energy Rep.* **2020**, *6*, 288–306. [CrossRef]
135. Olabi, A.G.; Onumaegbu, C.; Wilberforce, T.; Ramadan, M.; Abdelkareem, M.A.; Alami, A.H.A. Critical review of energy storage systems. *Energy* **2021**, *214*, 118987. [CrossRef]

Disclaimer/Publisher’s Note: The statements, opinions and data contained in all publications are solely those of the individual author(s) and contributor(s) and not of MDPI and/or the editor(s). MDPI and/or the editor(s) disclaim responsibility for any injury to people or property resulting from any ideas, methods, instructions or products referred to in the content.

Review

A Review on Optimal Energy Management in Commercial Buildings

Jahangir Hossain ¹, Aida. F. A. Kadir ^{1,*}, Ainain. N. Hanafi ¹, Hussain Shareef ², Tamer Khatib ^{3,*},
Kyairul. A. Baharin ¹ and Mohamad. F. Sulaima ¹

¹ Faculty of Electrical Engineering, Universiti Teknikal Malaysia Melaka, Melaka 76100, Malaysia

² Department of Electrical Engineering, United Arab Emirates University, Al-Ain 15258, United Arab Emirates

³ Department of Energy Engineering, An-Najah National University, Nablus 97300, Palestine

* Correspondence: fazliana@utem.edu.my (A.F.A.K.); t.khatib@najah.edu (T.K.)

Abstract: The rising cost and demand for energy have prompted the need to devise innovative methods for energy monitoring, control, and conservation. In addition, statistics show that 20% of energy losses are due to the mismanagement of energy. Therefore, the utilization of energy management can make a substantial contribution to reducing the unnecessary usage of energy consumption. In line with that, the intelligent control and optimization of energy management systems integrated with renewable energy resources and energy storage systems are required to increase building energy efficiency while considering the reduction in the cost of energy bills, dependability of the grid, and mitigating carbon emissions. Even though a variety of optimization and control tactics are being utilized to reduce energy consumption in buildings nowadays, several issues remain unsolved. Therefore, this paper presents a critical review of energy management in commercial buildings and a comparative discussion to improve building energy efficiency using both active and passive solutions, which could lead to net-zero energy buildings. This work also explores different optimum energy management controller objectives and constraints concerning user comfort, energy policy, data privacy, and security. In addition, the review depicts prospective future trends and issues for developing an effective building energy management system, which may play an unavoidable part in fulfilling the United Nations Sustainable Development Goals.

Keywords: energy management system; intelligent energy management system; net-zero energy management system; demand side management; sustainable development goals

Citation: Hossain, J.; Kadir, A.F.A.; Hanafi, A.N.; Shareef, H.; Khatib, T.; Baharin, K.A.; Sulaima, M.F. A Review on Optimal Energy Management in Commercial Buildings. *Energies* **2023**, *16*, 1609. <https://doi.org/10.3390/en16041609>

Academic Editors: Ala Hasan and Hassam Ur Rehman

Received: 20 December 2022

Revised: 30 January 2023

Accepted: 1 February 2023

Published: 6 February 2023



Copyright: © 2023 by the authors. Licensee MDPI, Basel, Switzerland. This article is an open access article distributed under the terms and conditions of the Creative Commons Attribution (CC BY) license (<https://creativecommons.org/licenses/by/4.0/>).

1. Introduction

Global economic growth is booming with the increasing population. This will lead to higher electricity demands in the future. Statistics indicate that 44% of global energy comes from fossil fuels [1]. Moreover, building energy consumption is deemed the primary energy consumer compared with other sectors, with a high percentage of energy wastage due to poor management and the ineffective implementation of strategies. Currently, the rate of increase in global energy consumption is at 2.9%, and it is forecasted to rapidly increase in the upcoming years. Notably, the Asian regions are now consuming more electricity than the United States of America because of the trends in developing countries' economic growth. Buildings account for 40% of global energy consumption [2], and release one third of all greenhouse gas emissions while incurring energy losses ranging from 2% to 20% due to irresponsible consumer behavior and inefficient appliances [3]. Buildings in Malaysia consume 14.3% of the total energy generated [4], with 80% to 90% of the population spending most of their time inside buildings [3,4], with the majority of the energy being consumed by cooling and lighting loads. More than 94% of generated electricity resources come from the combustion of fossil fuels. As a result, carbon dioxide emissions have increased by 221%, placing Malaysia at 26th among the world's top 30 greenhouse gas emitters [3].

In the US, buildings consume approximately 40% of the entire country's energy consumption [5,6], and almost 40% of energy is used in residential and commercial buildings in Europe [7]. Buildings consumed 284 TWh of electricity in 2007, accounting for 65% of the total electricity usage in France (434 TWh). A total of 404 million tons of CO₂ were emitted, which was 22.6% of the total emissions [8]. As a result of global warming trends and rising atmospheric temperatures, the heating demand for global residential buildings will decrease by 34% in the year 2100, while cooling demands will increase by 72% [9].

Due to rising energy demands, the industrial revolution has brought with it a slew of new issues. This phenomenon fosters the development of more resource-efficient control approaches. The building sector has a huge potential to mitigate energy demand using intelligent energy management systems (IEMS) [10] and the concept of the internet of energy (IoE). The IoE combines features of a smart grid and the internet of things (IoT). The IoT refers to internet-based architecture in two ways: communication allows the system to be monitored and controlled in real time via cloud computing or another internet service [9–11]. It is proven that the potential of IoE-based building energy management system BEMS will enhance the performance of future building energy utilization [9].

The key idea of BEMS is monitoring and controlling the energy consumption in buildings with the aim of reducing emissions. The design of BEMS has taken into account factors such as efficiency, scalability, robustness, flexibility, and an ability to sense the environment and make decisions autonomously [12]. A structure of an IEMS is shown in Figure 1. The IEMS consists of an optimization controller that acts like a center controller and interfaces with the operating browser via communication protocols. In practice, the user interface allows interaction seamlessly with connected devices using the same operating browser. Weather information is also taken into account for forecasting energy consumption and generation for the day ahead. Moreover, renewable energy resources (RER), energy storage, and a standby generator for emergency purposes are also considered to reduce the dependency on the grid and compensate for the peak hour and optimal load scheduling. At present, electric vehicles (EVs) are also included, and an IEMS ensures the optimal charging and discharging of vehicle-to-grid (V2G) and G2V during peak and off-peak hours. Furthermore, by educating consumers about the concept of being prosumers, excess RER generation can be sold to the grid with both the utility provider's and the consumer's consent.

Several significant articles have been published on BEMS. Aguilar [13] and Alanne [14] discussed artificial intelligence (AI) in demand-side management to compromise energy cost and occupant comfort. However, the authors did not provide a pro and con outline of controllers and optimizations. Gong [15] focused on the consideration of human comforts and intelligent controls, whereas the authors did not discuss the objectives and constraints related to all air-indexed parameters. Parvin [16] overviewed the optimization control in building heating, ventilation and air condition HVAC systems to demand-side management (DSM) and also focused on occupants' comfort. However, the authors did not discuss reducing heating and cooling load demand to increase energy efficiency using both passive and active methods. Zhou [17] demonstrated building energy efficiency by regulating optimal loads while improving the building envelope in existing buildings. The authors, however, did not provide an outline of strategies for the energy-efficient retrofitting of both existing and new buildings, which could lead to zero energy building (ZEB). Kanakadhurga [18] presented energy management concerning the minimization of energy cost with the utilization of RER, but the authors did not overview the load's categorization as it is required for optimal scheduling. Hannan et al. [9] discussed the internet of energy for DSM and smart grids, which lead to smart cities, but the authors did not emphasize end-user data privacy and security as well as the risk management for national security. Hern [19] surveyed the literature on BEMS, considering building energy efficiency using control management strategies. However, the implementation of the energy policy for DSM was not covered in detail. The work in [20,21] discussed the rage of BEMS with respect to the UN's sustainability goals.

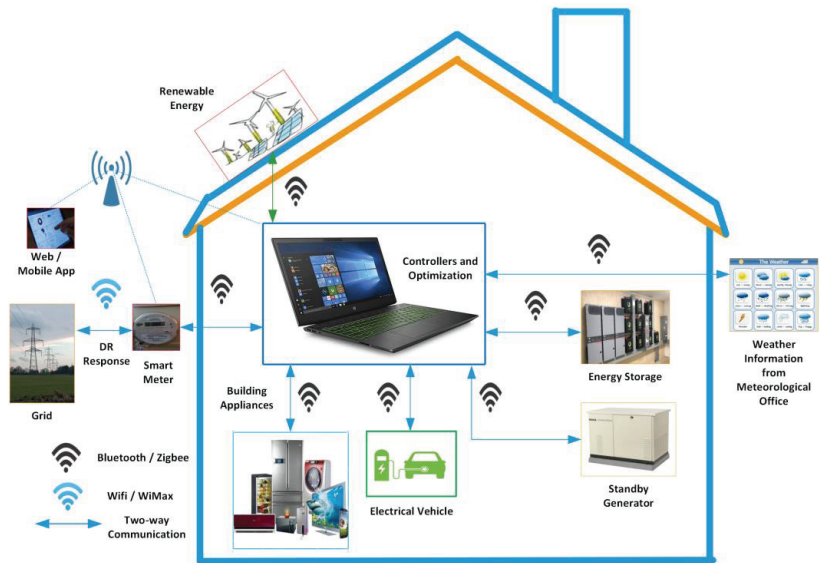


Figure 1. The structure of an intelligent energy management system in a building.

To address the gaps, this study presents a full investigation of the controllers and optimization for BEMS in terms of SDGs. The main contributions of this review are listed as follows:

- This work summarizes optimizing algorithms and various control strategies in achieving energy reduction, together with their benefits and drawbacks.
- This paper also presents the importance of commercial building load classification and categorization, energy policy, data privacy, and security to DSM.
- The subject of passive and active design solutions for energy efficient retrofitting to ZEB is highlighted.
- The study implies the development of an efficient BEMS that connects to the UN SDGs for achieving future sustainability through low carbon emissions, sustainable cities, green jobs, cost-effective energy supplies, and healthier living.

The rest of the paper is organized as follows. In Section 2, a summary of load classification in commercial buildings is described. Conventional BEMS techniques are discussed in Section 3. A thorough discussion of current and advanced methods in BEMS is included in Section 4. Furthermore, optimization control strategies in BEMS are described in Section 5. A summary of future trends and issues is presented in Section 6. Finally, a discussion and conclusions are drawn in Section 7.

2. Load Classification in Commercial Buildings

In the US, small and medium-sized building loads, specifically HVAC systems, dominate energy consumption, followed by lighting and plug loads [5]. Lighting and cooling are the most common electrical loads in commercial buildings, accounting for more than half of total electricity use, as shown in Figure 2 [22], and they are also responsible for the majority of commercial electricity costs.

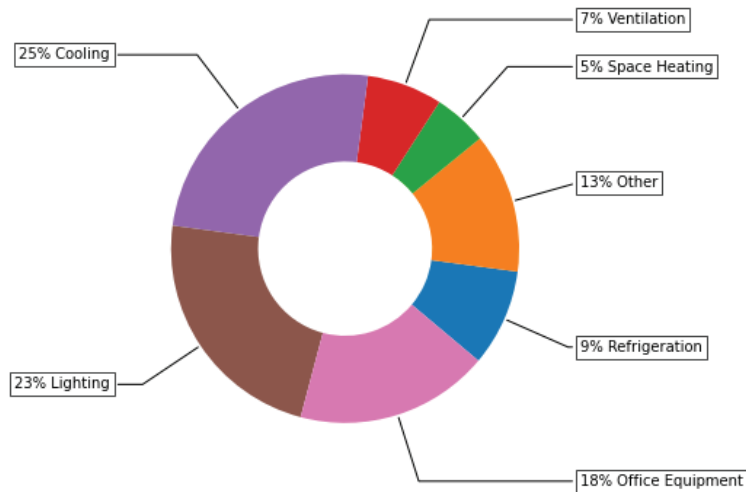


Figure 2. Energy usage data of commercial buildings in the US [22].

2.1. HVAC Loads

Heating, ventilation, and air-conditioning (HVAC) systems are utilized to regulate the temperature, moisture content, circulation, and purity of the air within a place to achieve the intended effects on the occupants of the space or the manufactured items and equipment stored there. They are used in commercial buildings all year. A typical HVAC system is shown in Figure 3. An HVAC system also refers to central air-conditioning [23]. High-capacity central systems are primarily used in large buildings. The main A/C unit is usually placed in a mechanical room, generally at a distance from the conditioned spaces. The air is then conditioned, according to the operating mode (cooling or heating) of the system. For cooling purposes, the air is cooled and, if necessary, it is also dehumidified. Similarly, for heating purposes, the air is pre-heated by passing it through a system supplied with steam, hot water, or an electric heating element. If necessary, water vapor is also added by passing it through a humidifier, and finally, the air is heated again by using steam, hot water, or an electric heating element. The central unit is connected to the air handling unit (AHU) through a duct/piping system. Then, the air is transported with fans through a duct system to individual units which are installed usually at ceiling height, floor level, or near windows, in order to ensure the best possible air circulation in each air-conditioned space. The outdoor air is introduced into the main unit and is mixed with a certain amount of recirculated air. The mixture then passes through air filters to remove any dust or other foreign particles [24,25]. In addition, a fan coil unit (FCU) is used in commercial buildings to heat or cool a room without connecting the ductwork. To condition a specific space of a room, an FCU circulates hot or cold water through a coil. The FCU draws hot or cold water from a central plant to make a human-occupied zone comfortable, with all the air-indexed properties under consideration, using a mechanical HVAC system. That results in a significant amount of energy consumption, which is associated with three factors that lead to excess electricity consumption, such as an HVAC sizing capacity that does not meet consumer needs accordingly, unnecessary usage, and lack of best practices in installation. In European countries, space cooling constitutes 40% to 60% of total building energy use. In the US, HVAC systems contribute to 50% of the energy use in buildings which is about 20% of their total energy consumption [26]. Cooling systems in the Middle East utilize more than 70% of all building energy [27]. Fan and supply air cooling account for 60% of HVAC energy use in Singapore and it is predicted to reach 70% [28]. Inefficiencies such as unneeded HVAC activity and exaggerated temperature settings waste a total of 10–40% of this electrical energy [29]. Without a doubt, due to economic growth and rising occupant

comfort demands, the global energy demand for buildings will continue to climb in the foreseeable future.

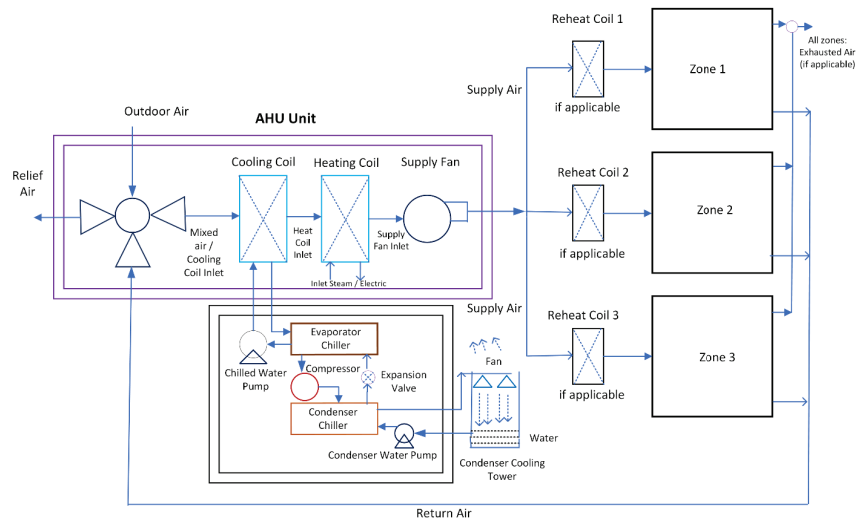


Figure 3. A typical view of a HVAC system.

2.2. Lighting Loads

When it comes to energy use, commercial buildings are crucial and utilize over one-third of the total primary energy needs of the US [30]. Undoubtedly, artificial lighting is one of the most common sources of power in commercial buildings, accounting for around 17% of overall energy usage [31]. In [32], office buildings were analyzed separately and lighting energy demand accounted for 25–35% of total energy usage. As a result, reducing the lighting load in commercial buildings can have a significant impact on lowering power demands, which in turn helps to reduce the carbon footprint [33], and is currently a major emphasis for energy engineers. Various countries, international, and regional organizations advocate specific energy-saving criteria for lighting systems [34]. Manual lighting controls are mostly based on human behavior, occupancy patterns, and general energy conservation awareness [35]. Different types of switching systems can be used to control lighting at the user level. In addition, a large number of investigations show how to improve lighting efficiency from control schemes, which involve maintaining optimal lighting conditions while using as little energy as possible [36].

2.3. Plug Loads

Water heaters, refrigerators, freezers, and clothes dryers are important energy consumers, accounting for roughly 18% of total building energy consumption. Around 36% of building energy demand is spread across a variety of systems, the bulk of which are electric. For example, computers, televisions, imaging equipment (e.g., printers and multifunction devices), audio/video equipment, telephone devices, kitchen, and household appliances, as well as kitchen ventilation are all included in commercial building plug loads [37].

2.4. Plumbing and Sanitation

Multi-story buildings are constructions having more than one story, but in the context of plumbing, a multi-story building is one that can't be fed entirely and effectively by the municipal water supply due to inadequate pressure [38]. A normal two-story building can be supplied by water main pressures of 8–12 m (25–40 feet), while higher buildings may require pressure booster systems. Multi-story structures also necessitate drainage, sewage, and ventilation systems that can accommodate a large number of people living in a vertical

layout. Drains from plumbing fixtures are connected to vertical drain stacks in a multi-story building's drainage system, which transport waste and sewage to below the building's lowest floor. All plumbing fittings below ground level should be pumped into the sewer or a drainage system that leads to the sewer [39]. Tianjin Tiejian Tower consumes energy in terms of plumbing and sanitation which is 0.6% of all its energy consumption [40].

2.5. Fire Protection

Electrical fires in commercial and industrial facilities can result in significant losses in terms of business continuity, opportunity costs, assets, and output loss. Electrical fire risks from overcurrent, overvoltage, and the overheating of electrical appliances can be decreased if an electrical design adheres to requirements, including International Electrotechnical Commissions (IEC) standards and national regulations, and uses compliant equipment. Electrical installations, on the other hand, can deteriorate with time owing to environmental conditions such as heat and humidity. It is critical to comprehend the operation of fire alarm systems. Different systems work in different ways, but they all have the same goal: to detect a fire and protect the structure, its residents, and valuables [41]. As reported in [40], the energy consumption of Tianjin Tiejian Tower for fire protection equipment is 2.8%, which ensures that consumption growth will increase in the upcoming years.

2.6. Data Networks

Network access has become practically ubiquitous, and the energy consumption of the equipment necessary to provide it is increasing. Edge devices such as PCs, servers, and other sources and sinks of Internet Protocol (IP) traffic are notably excluded from this category, which comprises devices that primarily switch and route IP packets from a source to a destination. A case study was conducted on networks on a campus, in a medium-sized commercial building, and in a typical residence. It was estimated that network equipment in the US consumed 18 TWh in 2008, or about 1% of total building power, and that consumption would rise at a rate of roughly 6% per year to 23 TWh in 2012; global usage in 2008 was 51 TWh. Furthermore, network switches in office buildings and residential equipment are the two most energy-intensive groupings, accounting for 40% and 30% of total energy consumption, respectively [42].

2.7. Transportation

The transportation and building sectors are two important areas for electrification. Light-duty electric vehicle (EVs) adoption for consumer ownership dominates transportation electrification. Light-duty EVs for personal use are driving transportation electrification and are frequently classified into plug-in hybrid electric vehicles (PHEVs) and battery electric vehicles (BEVs). In 2018, about 1 million EVs (around 0.5% of all vehicles) were registered in the US. By 2021, another 1 million EVs were estimated to be registered [43]. EV sales currently account for 1–2% of the light-duty market, and they are predicted to grow consecutively [44]. EV sales projections vary widely, but realistic estimates include 7–12% adoption by 2030 and 11–48% adoption by 2050 [45]. The 0.58 million EVs sold in the US utilized around 1 TWh of electricity in 2017. By 2025, electricity consumption is expected to reach 33 TWh per year, rising to 551 TWh by 2040 [43]. In the near future, transportation, in particular, is predicted to have the greatest impact on power usage. Uncontrolled EV charging is a huge barrier to grid operations, but control solutions offer a way to boost efficiency [46].

2.8. Miscellaneous

Lifts and escalators are also included in commercial buildings, which consume 3.3% of the entire building consumption [47]. There is potential to conserve energy by using automation based on occupancy presence along with a variable voltage variable frequency drive (VVVFD) as an induction motor. A power factor improvement will be required to minimize the operating costs. In addition, people are encouraged to use the stairs if the

lift and escalator are less conveniently located, which may help meet the LBC's "Health" petal [48]. In addition, street lighting, garden lighting, safety, and security (e.g., CCTV and RFID) equipment are also responsible for consuming electricity in commercial buildings.

3. Conventional BEMS Techniques

Building control systems are critical components in achieving energy efficiency and long-term sustainability in buildings. A few traditional control systems for load monitoring, such as (i) thermostats, (ii) proportional–integral (PI), and (iii) proportional–integral–derivative (PID), have been extensively used in conventional BEMS. These control systems have also been used in a variety of applications and disrupted environmental situations, and they have consistently performed poorly and do not provide an optimal control approach [49].

3.1. Thermostat

ON/OFF is one of the most basic and often-used control modes. This mode can be used in building HVAC, lighting, and shading systems [50]. A thermostat is a device that regulates the temperature within a user-defined range [51]. When the temperature falls below the set point, the thermostat turns off the power, and then restores it when the temperature rises above the set point [52]. A typical structure of a thermostat is shown in Figure 4. Thermostats can be found in water heaters, ovens, refrigerators, and HVAC systems and are often used for heating or cooling to a fixed-point temperature. In BEMS, the thermostat is used to minimize power fluctuations [53], lower cooling electricity costs [54], control space heating [55], improve thermal comfort [56], and increase energy efficiency [57]. Although this approach offers the simplest ON/OFF control operations which occur frequently in the system, when the controlled device is turned on, it constantly operates at maximum or default capacity, consuming a large amount of power in each action [58]. Furthermore, the ON/OFF action may cause oscillations in the controlled temperature, resulting in energy waste. In some complicated energy systems, ON/OFF-based controllers are ineffective to achieve control variables and objectives with merely discrete ON or OFF values [59].

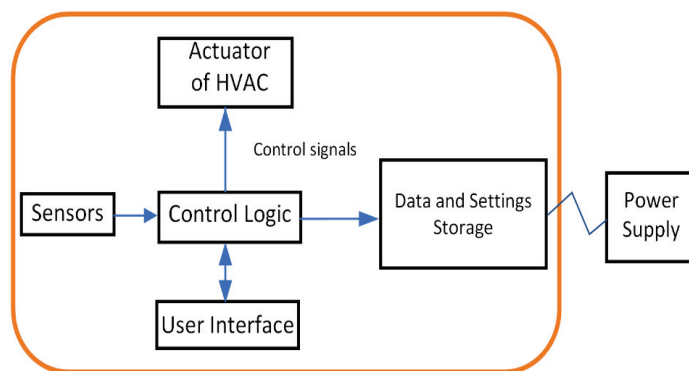


Figure 4. A typical structure of a thermostat.

3.2. PID Control

All three types (proportional, integral, and derivative) of action are utilized in most digital controllers to incorporate advantages such as removing offset and speeding up the response of the control function. In a nutshell, the integral control function tends to destabilize the system, whereas the derivative control function tends to reinforce it. The integral function is frequently used to reduce or eliminate the offset of proportional control and to provide more precise control. A typical structure of a PID controller is shown in Figure 5 [60]. The time domain function of PID control is shown in Equation (1).

$$u(t) = K_p \left[e(t) + \frac{1}{T_i} \int_0^t e(\tau) d\tau + T_d \frac{de(t)}{dt} \right] \quad (1)$$

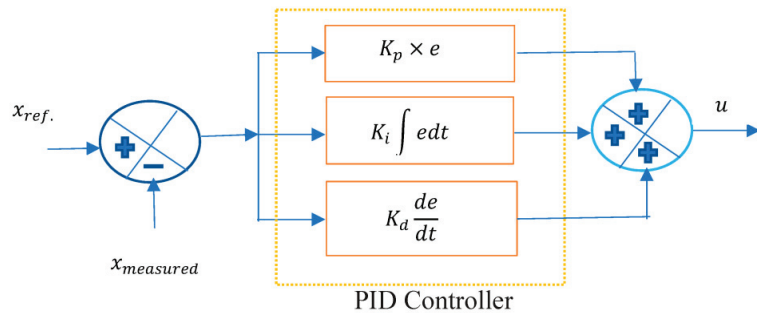


Figure 5. A structure of PID controller [49].

The transfer function of PID control can be written in “Ideal form” and “parallel form”, respectively, as shown in following Equations (2) and (3).

$$PID(s) = K_p \left(1 + \frac{1}{T_i s} + T_d s \right) \quad (2)$$

$$u(t) = K_p e(t) + \frac{1}{K_i} \int_0^t e(\tau) d\tau + K_d \frac{de(\tau)}{d\tau} \quad (3)$$

where, K_p , K_i , and K_d denote proportional gain, integral gain, and derivative gain, respectively. T_i and T_d are integral and derivative time constants, respectively. Since P, PI, and PID controllers are closed loop/feedback controls that have constant parameters and do not have a direct knowledge of the system to be regulated. When utilized alone, they give poor control performance for noisy and non-linear processes with long-time delays [61]. In general, the PID controller has been effectively used in a variety of building sections, including lighting management [62], tracking performance improvement [63], and energy consumption reduction. There is no doubt that PID performance is more efficient than thermostat [64]; however, there is still a demanding task of choosing the suitable settings of K_p , T_i , and T_d , respectively. In addition, when integral functions are introduced to eliminate the offset of proportional control to obtain a more accurate control of variables and objectives, their effect might cause the system to oscillate and deteriorate control [49]. To tackle these issues of PID controllers, optimization control strategies in BEMS are explained in Section 5.

3.3. Energy Efficiency

In the context of global initiatives for sustainable development, a commitment to energy-efficiency improvement is becoming increasingly crucial, and buildings have a lot of potential in this area. Energy efficiency allows you to use less energy while maintaining the same level of service. To permanently minimize demand during peak and off-peak periods, energy efficiency measures are implemented as part of normal operations. Energy efficiency in buildings is often achieved through efficient building designs, energy-efficient equipment, and efficient building operations. Since efficiency measures are a long-term feature of normal operations, they are usually distinguished from demand response (DR), which involves only short-term changes to normal operations [65]. The following two types of energy efficiency measures, such as passive and active strategies, are used in buildings.

3.3.1. Passive Methods

The use of energy in many buildings can be greatly decreased by implementing passive techniques. These methods may not necessitate additional financial resources. For example, an integrated building rehabilitation approach that incorporates passive approaches can reduce a building's energy usage while also compensating for the higher cost of new technologies [66]. Passive energy conservation strategies aim to reduce energy demand by maximizing the use of natural heating, cooling, and lighting resources, as well as limiting energy losses through the building envelope [67].

Traditional buildings used to be built with climatic conditions in mind and incorporated passive cooling and heating methods for both summer and winter, respectively. Most buildings nowadays have mechanical or active heating, cooling, and lighting systems, which consume a lot of energy [66]. Passive methods, such as the use of solar energy or creative architectural design, can greatly reduce total energy usage in a building. Passive solar energy is becoming increasingly popular. In 1974, a large south-facing window was used as the first passive solar heating system in New Mexico [68]. Using direct or indirect passive solar energy to alleviate heating, increase cooling capacities, and reduce a building's energy consumption is a basic approach, taking advantage of free solar energy [69]. In the winter, solar energy is used to warm the indoor atmosphere to a comfortable temperature. Solar radiation is absorbed directly through the transparent parts of the building exterior, particularly those facing south. This radiation is converted to heat, which elevates the temperature within the house. Solar radiation can also be employed as a source of natural illumination. Indirectly, solar radiation can be utilized in the winter. Multi- or double-skin façades, Trombe walls, and linked sunspaces are all popular methods for indirect solar advantages [67]. The effect of different insulating materials, construction systems based on sustainable materials, the incorporation of thermal energy storage (TES), phase-change materials (PCM) in building envelopes, and green infrastructures such as green roofs and walls are among the research fields of passive technologies [70]. By lowering the energy demand in buildings, passive energy techniques could reduce reliance on fossil fuels and capital-intensive renewable energy technologies. However, understanding building science ideas and energy control principles is essential for the effective implementation of these strategies.

3.3.2. Active Methods

Active energy-saving technology has also been widely employed to lower the energy consumption of buildings. Active measures include enhancing HVAC systems, energy-efficient appliances, lighting systems, and the use of renewable energy, as well as distributing energy as efficiently as possible while ensuring occupant comfort [67]. The active systems were also designed to take advantage of various renewable energy sources, such as solar thermal, free cooling with night air, or geothermal heat, by utilizing thermal energy storage systems to shift heating and cooling loads [71].

To improve a building's energy efficiency, a variety of active approaches have been adopted. Heat pumps and boilers, for example, are active tactics in traditional air-conditioning. Furthermore, advancements in compressor technology and hybrid systems help to increase heat pump efficiency [72]. Active techniques, on the other hand, have some insurmountable restrictions. A heat pump's coefficient of performance (COP) is rarely greater than six, whereas a boiler's combustion efficiency is far less than 100%. Heat pumps and boilers are used in HVAC systems to overcome a significant temperature difference between indoor and outside temperatures (e.g., 10C in summer and 20C in winter). Inevitably, this would result in the system's overall energy efficiency being low [73].

Substantial energy savings can also be achieved in existing mechanical HVAC systems. Air conditioners that are properly maintained can reduce peak demand, conserve energy, and save running expenses. Correcting low air-flow rates, rectifying refrigerant overcharging and undercharging, and addressing duct leaks are just a few examples of individual repair techniques. Heat pumps and other high-efficiency mechanical systems can be used

to replace older technology equipment in applications where air-conditioning is required, resulting in significant energy savings [24].

After HVAC systems, lighting uses a significant amount of electrical energy in buildings. Lighting efficiency is the most cost-effective active technique, and air conditioning efficiency was the second [74]. A well-designed lighting system can conserve energy while also providing the maximum visual comfort to building occupants [75]. Standard groups such as the European Committee for Standardization have developed standards to guide and provide specifications and requirements for technological systems in order to achieve lighting system energy efficiency in buildings. The European Standard EN12464-1 (i.e., for interior design) [76], the European Standard EN12464-2 (i.e., for external design) [77], and the European Standard EN15193 (i.e., for lighting system) [78], and the European Standard EN15193 (i.e., for performance evaluation) [79]. LED is a prominent energy-efficient lamp, used in lieu of conventional lamps, with a greater photometric performance (e.g., luminous flux, color rendering index, and luminous efficiency) and easier to regulate when compared to other lamps [75]. The regulation of a lighting system is the most important factor to increase energy savings in buildings, and it has received a lot of attention from researchers in the previous decade. Lastly, it is recommended that traditional appliances should be replaced with five-star energy-efficient appliances [80]. Many other energy-saving strategies are also employed in a low-energy-consumption structure. Included are energy-saving air conditioning designs, equipment energy-saving, behavior energy-saving, and energy-saving by operation adjustment, among other things.

In summary, active and passive techniques each have their own set of benefits and drawbacks, and neither can be considered a replacement for the other [81]. To take advantage of the benefits of both tactics, a growing number of passive strategies are being coupled with active strategies or used actively. As a result, a combination of passive and active technology is both promising for energy savings and good interior environment assurance.

4. Current and Advanced Methods in BEMS

Intelligent automated control systems are introduced in current and advanced methods of BEMS, and are capable of minimizing energy usage while respecting the comfort and actions of building occupants [82]. The control of energy-related smart devices and appliances in a building is referred to as smart energy building control. It is based on a predetermined strategy and policy, as well as user choice if desired. These control systems are centralized, integrated hardware and software networks that monitor and regulate the indoor climatic conditions in buildings. These control systems are typically used to safeguard buildings' operational performances as well as the safety and comfort of their residents [83]. Finding the optimal trade-off between occupant comfort and total energy usage is a fundamental challenge for building control. Several building control systems and methods for building energy and comfort management have been presented [84], both in the research and commercial fields, with the goal of attaining energy savings through intelligent control.

4.1. Automation

Energy management is a fundamental function of building automation systems. Building automation concepts and applications are not new, having been introduced by Warren S. Johnson in 1985 [85]. The term "Building Automation System" (BAS) also known as "Building Management System" (BMS) refers to a collection of systems that control the operation of a structure. Notably, a BAS is one of the most important intelligent building systems [49]. The system is also referred to as an Energy Management and Control System (EMCS) or a BEMS, rather than a BAS or BMS, if the main reason for installing it is to save energy [86]. As a result, an EMCS or BEMS is typically included in a BAS or BMS. EMCS or BEMS can be implemented as the monitoring and control systems for building service (HVAC systems, electrical systems, lighting systems, fire systems, security systems, and lift systems are all examples of building services) systems that have a substantial impact

on building energy usage [49]. Figure 6 illustrates the hierarchy of building automation systems. Meanwhile Figure 7 shows the steps of BAS development steps [78–88].

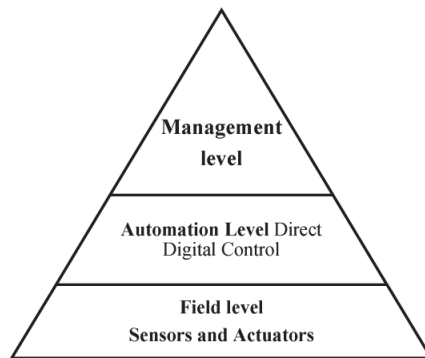


Figure 6. Hierarchy of building automation systems.

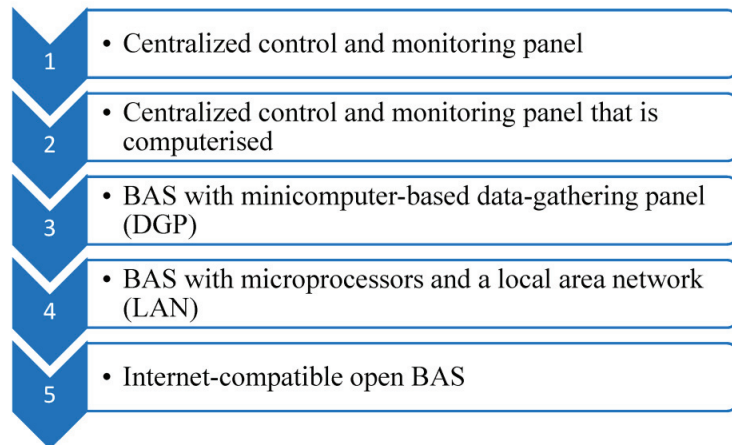


Figure 7. The steps of the BAS development process.

BAS systems are mostly processor-based [89]. A communication network is built into the BAS and extends across the building or set of buildings. In the event of smoke, fire, intrusion, or other events that could potentially harm equipment, this same communication system can be used to send alarms to an operator or security agency. In addition, this is accomplished through strategies such as load duty-cycling to save energy, peak load management to control total power consumption during peak hours, the scheduled start/stop of building HVAC systems at the start and end of each day, and the real-time control of building systems in response to occupancy detection, all of which are possible with BAS. Moreover, a BAS has made it possible for buildings to respond dynamically to current weather conditions, room occupancy, time of day, and other inputs, resulting in significant energy savings. To increase energy economy and occupant comfort, a BAS allows the centralized administration of climate control, lighting, and security systems [90]. These solutions help to cut down on energy waste and expenditures while also increasing occupant productivity.

4.2. Intelligent Devices

Intelligent devices are referred to by a variety of names, including intelligent instruments, intelligent sensors, smart sensors, and smart transmitters. However, because there

are no universal definitions for these terms, devices with similar characteristics but from different manufacturers may be called by different names [91]. The objective of intelligent buildings is to integrate intelligence directly into manufactured building equipment and components, allowing them to transmit information via standard protocols for intelligent system operations (control, maintenance, and service) [92]. Most building components, including individual lights, sensors, compressors, valves, heat exchangers, pumps, freezers, and dishwashers, could eventually be connected with embedded intelligence. Remote diagnostics and pricing estimates for appliance repairs could be provided by service providers. Reduced downtime, service costs, and utility expenses are the most important advantages of automated fault detection and diagnostic systems for heating, ventilation, and air conditioning and refrigeration (HVAC&R) equipment. Even though major commercial buildings use computer control and monitoring systems, they do not currently have many diagnostic capabilities [93]. In addition, appliances could be built to be grid friendly, responding to utility management or pricing signals and coordinating themselves to reduce electrical usage during peak demand hours.

Consumers are increasingly profiting from technological advancements, and intelligent devices such as the smart controlling of light, HVAC systems, smart plugs/sockets, and other intelligent devices which provide more convenient and efficient services. To improve maintenance efficiency, most intelligent devices are now connected to the central server of their relevant carriers via network optical fibers [94]. In order to achieve intelligent D2D (device-to-device) communication, devices will require intelligent routing protocols [95].

4.2.1. Advanced Metering Infrastructure (AMI)

Smart meters, communications networks, and data management systems are all part of the AMI, which allows utilities and customers to communicate in real time. The system can automatically and remotely assess electricity usage, connect and deactivate service, detect tampering and theft, identify faults and outages, and monitor voltage, among other features that were previously unavailable or required manual intervention [96,97].

4.2.2. Smart Thermostat

HVAC&R smart controlling management has become a major concern for both residential and commercial buildings. A smart thermostat is a device that learns user temperature preferences and is utilized in thermostatically regulated loads. It also makes things easier for customers by allowing remote access and communication with AMI based on price indications [98]. The smart features of programmable thermostats include sensing, machine learning, and a network connection. These thermostats are equipped with proximity and motion sensors, and their learning algorithm adapts to the user's past preferences at various times of the day. Various strategies have been investigated to sense the real-time occupancy/vacancy of HVAC zones in order to save energy without affecting occupant comforts, such as Radio Frequency Identification (RFID) [99], IR motion sensors [100], and programable thermostats [101]. However, the accuracy of detecting the occupant in a conditioned space is being questioned using a smart controller. To avoid this issue, the study in [29] describes a new wireless device platform and prototype development that combines an infrared (IR) and an optical (OP) camera to enable collaborative intelligence with minimal power consumption and improved accuracy. The system saves up to 26% of HVAC energy when compared to a programmed thermostat and schedule-based HVAC control.

Furthermore, the availability of embedded intelligence in HVAC&R equipment might significantly reduce the cost of applying intelligent control systems, allowing for a much broader applicability. A cooling tower fan controller, for example, may have access to embedded performance data from each tower fan and chiller on the local network. Likewise, a chiller sequencing controller may obtain part-load information from individual chillers [88]. In addition, a compressor might have an embedded chip with a performance map and sensor inputs for suction and discharge conditions, allowing the map to be used to calculate refrigerant mass flow rate and compressor power consumption. Similarly, a condenser

might contain a chip with a model, state variable readings, and a virtual refrigerant mass flow measurement to offer a virtual sensor for condenser airflow. The airflow through the condenser might therefore be used as a diagnostic signal for fouling or fan issues [93]. In addition, the spread of low-cost information for monitoring, diagnostics, and greater control can be enabled through embedded intelligence.

4.2.3. Smart Lighting

For intelligent lighting control, the study in [102] presents a low-cost, wireless, simple-to-install, adaptive, and smart LED lighting system that adjusts the light intensity automatically to save energy while retaining consumer pleasure. The system uses Zigbee connectivity to combine motion and light sensors in a low-power wireless solution. To conduct a daylight adaptive closed-loop control, researchers suggested a smart lighting control approach that incorporated linear optimization and neural networks (NN). The proposed method used a NN to learn the impact of each luminary on the zone's maintained illuminance and modify the luminary dimming levels to achieve the desired illuminance [103]. Implementing intelligent lighting control systems, such as the integration of sensor technologies (occupancy and light sensors), advanced architectures (wireless and network-based architectures), and intelligent control techniques (artificial intelligence and optimization), has a significant potential to reduce energy consumption. Furthermore, an intelligent control system can improve occupants' visual comfort while lowering electricity use [104].

4.2.4. Smart Plugs

A smart plug is an electric device that transforms regular household equipment into smart devices. In addition, a smart plug is able to determine the type of connected home appliance based on the appliance's energy consumption profile. It can connect to a wireless home network using inbuilt wireless communication protocols so that a user can measure energy usage and control the electronic device which is plugged into the smart plug over the internet [105]. A remotely controlled intelligent power outlet system that is specifically designed to detect electrical events in low-current loads. The power outlet of the proposed system comprises a microcontroller, a ZigBee interface, an RFID reader, a relay, and a current sensor. The system's main functions include the remote management of the power outlet, real-time monitoring of current consumption, customization and programming of the power supply time schedule, automated vampire current cut-off, and protection of certain types of electrical fires and electrocutions [106]. Smart plugs can be used to manage legacy devices such as water heaters, pool pumps, and lighting fixtures that do not have inbuilt controllers or communication capabilities. Smart plugs are smart power outlets that have measuring and communication capabilities, allowing for device energy monitoring and remote device shutdown.

4.2.5. Smart Appliances

Inbuilt controllers or communication abilities in smart appliances use IoT technology to communicate with smart devices such as smartphones and tablets, giving the homeowner remote access [107]. These appliances can also communicate with the smart meter wirelessly and help to reduce energy use by automatically adjusting to changes in power availability and dynamic tariffs. The advantages of smart appliances include the ability to run in energy-saving modes or defer operation until prices fall below a certain threshold when electricity prices are high. Smart dishwashers, for example, may receive DR signals and postpone wash cycles until off-peak periods; microwave ovens might automatically cut power levels during peak periods; and refrigerators might delay defrosting operations until off-peak periods [108].

4.3. Uses of IoT in BEMS

Any device that can be controlled and monitored over the internet is referred to as an IoT-based load, and it can be implemented in BEMS to monitor and control loads, thereby

saving energy that is purposefully wasted by human behaviors [109]. Achieving smarter buildings by deploying IoT devices is called home automation. In [6], the open-source software known as building energy management open-source software (BEMOSS) was introduced, which can run on a single board computer such as Odroid to control and monitor IoT devices in buildings. BEMOSS allows the user to access the supported IoT devices remotely via the web or an app to seamlessly control and monitor them in real-time [5,6]. Building and implementing a smart home using Long Range (LoRa) can be one of the most effective solutions in the IoT. The system works for both short-range and long-range, utilizing multiple communication technologies: LoRaWAN, a server-based LoRa gateway, and Bluetooth connectivity. The adopted system can communicate without a Wi-Fi connection or internet network as it uses LoRa RYRL400 to control the appliances in the home, which is dependent on radio frequency [110].

Reducing energy losses and unnecessary electrical consumption allows the identification and tracking of multiple users by internal Wi-Fi handover using a smartphone. Furthermore, innovative outlets (IO) and the IoT concerning NFC (near-field communication) identification can be used to extract accurate data about consumption, electric current, and voltage along with the identification of electric household appliances. Thus, the objective of this architecture is to identify the user location and persons in the room, and what appliances they are using and consuming with an interoperable middleware solution that provides the option to help the consumer optimize their consumption [111]. The emerging usages of the IoT in real life ease the quality of life and lead to cities being more sustainably developed without impacts on the environment, by addressing the production of devices and interfaces with hardware, energy efficiency, cyber security, e-waste, and cost-effectiveness. Not only is the usage of IoT devices required but also a focus on device recycling, as harmful materials are involved, alongside having a low consumption rate with a better life span. Moreover, to monitor and control the smart grid (SG) and DSM, the data needs to be processed in real time as the purpose of implementation is to reduce the desired electricity consumption [112].

4.4. Demand Response (DR)

DR is a set of actions that reduce or shift electricity to improve electric grid dependability, manage electricity costs, and provide systems that incentivize load shifting or shedding when the grid is near capacity or electricity prices are high. The development of DR has been highlighted as a critical national goal for improving electricity markets and system dependability [113]. The purpose of DR solutions is to reach the electric shed savings targets while minimizing any negative consequences for building occupants or processes [114]. Direct load control (DLC) and indirect load control (ILC) are the two main categories of DR approaches (ILC). DLC is a program in which utility companies reward customers for having direct control over their chosen loads. The ILC technique, on the other hand, allows AMI to participate in the optimization process. With distributed decision makers, the utility grid shares either the day-ahead load profile projection, the dynamic energy retail price, or both. All consumers have access to this information, and by using it, they might strive to enhance their benefit (i.e., lower their consumption cost) cooperatively or competitively [115,116].

Home appliances can be classified into three categories based on their potential to participate in DR: baseline loads (lighting, cooking stove, etc.), burst loads (clothes dryer, dishwasher, etc.), and regular loads (HVAC system, refrigerator, etc.), with implemented numeric and logistic algorithms that are solved based on the finite state machine (FSM) and spring algorithm [117]. To obtain the desired goal, a unique technique of arrangement of those household loads is divided into NINSLs (non-interruptible and non-schedulable loads), INSLs (interruptible non-schedulable loads), and SLs (schedulable loads), and solved with a genetic algorithm [118]. The proposed model has shown three categories of loads: fixed, flexible, and uninterruptible, which are optimally scheduled under the

time of use (TOU) tariffs based on mixed-integer linear programming (MILP) to minimize consumption and cost [119].

Moreover, DR is currently a viable approach for dealing with the problem of growing peak demand on the grid. In order to reduce peak energy consumption or demand, the scheduling of residential or industrial energy use in each appliance is optimized [120]. In [121], an interactive control unit approach was demonstrated that uses peak clipping techniques to reduce peak demand with a day-ahead scheduling mechanism that uses load shifting strategies to optimize the load. A new heuristic demand response technique has been developed for appliance consumption scheduling in order to decline the peak-to-average ratio (PAR) of power demand [116]. Peak demand can also be reduced through load shifting from on-peak to off-peak or enhancing TOU tariffs [122–124]. If the consumer is not interested in rescheduling the loads for off-peak hours, they may increase the temperature of the HVAC system. As a result, consumers could feel somewhat uncomfortable for a while, but be able to decrease the temperature setting during off-peak hours [125]. In the same way, lighting intensity can be reduced and increased during on-peak and off-peak hours, respectively. A smart plug can be utilized to prevent phantom power. If the priority of comfort is determined by consumer needs over time, the time gap must be filled with either renewable energy (RE) or energy storage systems (ESS). The presence of PV and EES can help to maintain the indoor temperature by using inverter-based AC, with ESS compensating for peak-hour demand and when there is less RE generation [119]. Coordinating the operation of electric vehicles (EVs), PV units, and BESS with an improved decision-tree-based algorithm can be used to reduce peak demand in residential distribution networks [126]. The peak reduction in power and prediction of long-term load forecasting for over 300 homes were studied, focusing on peak shaving and load shifting with intelligent devices [15]. The idea was to minimize the total energy usage and peak demand by regulating HVAC systems, water heaters, and batteries so that both utility authorities and consumers could benefit. There are significant opportunities to reduce energy consumption by optimizing the loads on different chillers or heat pumps, such that their (variable with the load) COP is maximized. Futuristic, intelligent homes might integrate information technology and provide the opportunity to incorporate other innovative technologies such as PV, intelligent devices, and energy storage.

5. Optimization Control Strategies in Bems

The majority of commercial BEMS on the market today are reactive rule-based. This indicates that when an event occurs, an action is triggered. As a result, these systems are unable to forecast future situations or anticipate events in order to optimize building operations [127]. To overcome these issues, users can manage their energy use at home more efficiently by optimizing their use of resources and assets. The process of identifying the circumstances that provide the highest benefit or the lowest cost of a process is known as optimization. The fundamental goal of optimization in published studies is to reduce the PAR in load demand and customer electricity costs while maintaining comfort [105]. The various optimization control strategies utilized in prior works are reviewed in this section.

5.1. Uses of Intelligent Controls in BEMS

Several research works have been carried out on different intelligent methods for BEMS, and the most used are categorized as: (i) learning based methods of the AI domain, including a support vector machine (SVM) [128,129], K-nearest neighbor (K-NN) [128], artificial neural network (ANN) [130], reinforce learning (RL) [131], etc.; and (ii) model-based methods, such as the model predictive control (MPC) technique [132].

A learning-based control model where self-scheduling loads and the ESS of the building ensure the maximum usage of PV power, curtailment load profiles, and a reduced energy cost. The optimization algorithm optimizes the building cost and minimizes the fluctuation between PV generation and energy consumption, relying on predicted control information using a machine-learning algorithm [11]. In addition, it demonstrates

the benefit of combining model-based and learning-based control methods into a single management framework for controlling multiple aspects of building performance [11,133].

The predictive algorithm model of energy consumption in smart buildings with a Microsoft Azure cloud-based machine learning platform wherein three methodologies namely SVM, K-NN, and ANN have been adopted for comparison to find the most accurate prediction model as compared to actual demand. Notably, the collected data is partitioned between 70% training data and 30% testing data. Though it took the most time to train, SVM was able to predict more accurately than the other two. The K-NN approach, on the other hand, was faster at completing the training, and ANN was faster than SVM, but it took many hours. However, a high training time is required for the SVM model to achieve a higher performance [134]. Most researchers focus on maintaining the indoor comfort of the buildings by implementing complexity prediction algorithms with higher cost and computational time, and power consumption. The model is carried out and investigated on five standard supervised machine learning models: polynomial regression (PR), support vector regression (SVR), random forest (RF), extreme gradient boost (XGB), and neural network (NN). In contrast, the best result output is shown for the SVR model with a tiny prediction error. A trustworthy NN model needs extensive data training set input and more processing time, while the amount of data is relatively small in the proposed system application, so it is rational to avoid the NN [135].

A novel deep neural-network-based algorithm for the day-ahead hourly energy consumption profile prediction of residential and commercial buildings in terms of occupancy rate and seasonality was investigated. A survey was conducted by a business manager, an electrical engineer, and a data scientist about all machine learning techniques, in which deep ANN achieved the highest score (multi-criteria analysis = 189) with a high accuracy prediction rate of about 98%. Firstly, training data was generated using synthetic load generation, where 100,000 data set points (load profiles) were produced for each occupancy rate type. The proposed forecasting model introduced these data to train an eight-layer deep neural network-based model and made decisions based on a limited number of inputs, evaluated using root mean square error (RMSE) and the coefficient of determination metrics [136].

Q-learning-based peak load reduction (QL-PLR) uses RL to present the optimal residential energy management (REM), which can decline only peak load demand and is associated with the dissatisfaction of consumers [137]. The designation of a dueling deep Q network (DDQN) captures the real-time state of the grid, demand-side strategy for interruptible loads (IL), along with the safe limit of regulating the system voltage and a reduction in peak demand loads, and the operation cost of distribution system operators (DSO). It is noteworthy that deep reinforcement learning (DRL) is adopted with DDQNs to optimize the DR management of IL under the TOU tariff and variable patterns of electricity consumption. To obtain the long-term profit for the DR management problem of IL, the Markov decision process (MDP) was formulated and solved using a DDQN-based DRL algorithm [133]. In addition, in comparison to a rule-based control (RBC) policy, DRL may also be utilized to control thermal storage in commercial buildings and can lower system operating costs by more than 50% [133].

MPC has a high level of efficiency in a building's energy management. On the other hand, finding a good control-oriented model for MPC is a difficult task. To address this issue, data-driven models are applied to MPC tasks that have universal approximation capabilities [138]. To improve a building's performance and take advantage of the TES's operating flexibility, an MPC technique was devised. The findings revealed that having a TES in a commercial building allows for more flexibility in participating in DR programs, resulting in lower energy costs and demand charges while maintaining occupants' comfort [139]. In the presence of an ESS, MPC was utilized to control the functioning of a commercial building in DR programs for bi-directional power flow with the main grid. The results of this study demonstrated that by exploiting the flexibility of the HVAC system,

MPC resulted in a reduction in building running costs as well as an improvement in power grid performance [140].

5.2. Uses of Optimization Algorithms in BEMS

In designing low-energy buildings, mathematical optimization can be used as a powerful tool to minimize the consumption of energy, while continuous and discrete issues are the two primary types of optimization challenges [141,142]. These problems can be formulated as binary, integer, or mixed integer optimization problems. Optimization algorithms are applied to solve these types of problems in various engineering fields [143].

A brief summary of the most selected optimization algorithms applied to BEMS problems is as follows:

5.2.1. Ant Colony Optimization (ACO)

ACO was motivated by observations of ant behavior [144]. This approach was originally created to handle discrete optimization problems before being expanded to include continuous variables. ACO for the continuous domain is the name of the extension (ACOR). ACOR showed better performance in finding the best solution as compared to other benchmark algorithms: particle swarm optimization with inertia weight (PSO-IW), hybrid particle swarm optimization and Hooke–Jeeves (PSO-HJ), and the Nelder–Mead (NM) algorithm [142]. An ACO load scheduling strategy for a smart home was proposed. The goal was to achieve the best possible use of integrated renewable energy sources. This is accomplished by concentrating on the total electricity bill, TOU, and the overall improved quality of life (QoL) [145].

5.2.2. Artificial Bee Colony (ABC)

ABC is an optimization algorithm based on honey bee foraging behavior [146]. In [147], a HEMS for household appliances was proposed by implementing DR schemes for residential consumers with facilitating renewable energy integration. This framework was solved based on an improved ABC algorithm. In [148], the authors proposed a new approach of ABC with Knowledge Base (ABC-KB) for the management of power and the occupant's preferred environment inside a residential building. ABC-KB uses less power than GA and PSO.

5.2.3. Particle Swarm Optimization (PSO)

PSO is an optimization technique based on the social behavior of bird flocking or fish schooling [149]. The conventional continuous PSO algorithm was modified to binary spaces, while BPSO is a binary variant of PSO. It is a bird-inspired optimization technique based on flocks of birds looking for food. Birds move in certain locations and velocities when foraging for food [150]. In [151], they adopted and developed cooperative particle swarm optimization (CPSO) to optimize user comfort and the electricity bills of individual homes as well as avoiding peak loads and peak rebounds on the grid. In [152], they provided a regularized PSO algorithm for optimally controlling battery energy in a grid-connected microgrid, lowering power costs.

5.2.4. Genetic Algorithm (GA)

GA is an iterative optimization technique inspired by live creatures' genetic processes. New genes are created that inherit the characteristics of their parents [153]. Chromosome representation and algorithmic flows are the two main components of a GA. An algorithmic flow is an iterative technique for generating and evolutionarily selecting chromosomes to obtain high-quality solutions, while a chromosomal representation is a scheme for modeling a solution [154]. GA was used to optimize the scheduling of ESS and plug-in electric vehicle (PEV) operations in a home energy management strategy in order to reduce daily electrical energy expenditure for the user [155]. Residential load management solutions may necessitate appliance scheduling to achieve specific goals such as load factor reduction, a PAR ratio reduction, or energy cost reduction. This problem is solved using GA [156].

5.2.5. Other Optimization Algorithms

In [157], the proposed hybrid algorithms have better performance and faster convergence compared to a single-based algorithm. The hybrid-based algorithms such as bacterial foraging optimization (BFO), gray wolf optimization (GWO), wind-driven optimization (WDO), enhanced differential evolution (EDE), and the harmonic search (HS) algorithm can solve the DSM optimization problems in SG. A detailed summary of other optimization algorithms is illustrated in Table 1.

Table 1. Summary of others optimization approaches in BEMS.

Optimization Techniques	Objectives	Contributions	Ref.
HEDE based on EDE and HSA	Cost, PAR, and user comfort optimization.	EDE performance is better than HSA in terms of cost reduction and HSA is better in terms of PAR as compared to EDE.	[158]
Dijkstra algorithm (DA)	Consumption cost, curtailed loads, grid imbalances, and used energy mixes optimization.	DA reduced 51.72% of the cost when attaching RER and 10.22% of PAR.	[159]
Satin bowerbird optimization (SBO) algorithm	To optimize the scheduling of appliances within a discrete comfort window (DCW).	Reduced the electricity cost from ₹29.14/day to ₹22.84/day, and reduction of PAR is 10.28%.	[160]
Cuckoo search optimization (CSO) algorithm	Reduction in electricity cost, PAR, and minimum user waiting time.	CSOA is superior in terms of cost and PAR compared to CSA and GA.	[161]
Hybrid genetic particle swarm optimization (HGPO) algorithm	Optimization of electricity bills, carbon emissions, user comfort, PAR.	Reduction of electricity cost by 25.55%, PAR by 36.98, and carbon emissions by 24.02%, respectively.	[162]
Genetic BPSO (GBPSO) algorithm	Electricity bills and PAR optimization.	GBPSO is better in terms of both cost reduction and curtailment of PAR compared to GA, BPSO, WDO, and BFOA.	[163]
Binary backtracking search (BBS) algorithm	Reducing and scheduling energy usage.	BBSA provides better performance compared to BPSO, in terms of reducing energy consumption, total electricity bills, and saving the energy of certain loads at peak hours.	[164]
Harmony search gray wolf optimization (HSGWO) algorithm.	Efficient scheduling	HSGWO performs better than HSA and GWO in terms of cost and user comfort.	[165]

5.2.6. Neighborhood Energy Optimization Algorithms for a Set of Commercial Buildings

A single subject owns a number of the neighborhood's buildings in the single-owner scenario. The architecture for energy optimization is centralized in design. The neighborhood buildings are owned by various subjects in the multi-owner scenario, each of whom seeks to reduce their individual energy costs. The building owners additionally consent to provide flexibility to the entire neighborhood and run their own local generation and storage units in a coordinated manner to achieve neighborhood-level goals. The architecture for energy optimization is hierarchical. A centralized optimization for a single-owner neighborhood with a high level of transparency and a hierarchical two-level optimization for a neighborhood with multiple owners and a reduced level of transparency are two separate optimization algorithms. Additionally, in order to lower the neighborhood net load as viewed from the grid side and maintain the neighborhood pollution emissions below a predetermined threshold, the neighborhood energy optimization algorithms schedule the generation and storage equipment based on energy prices. It has been demonstrated that the use of flexible resources, such as thermal storage (related to thermal comfort levels) or electrical storage, enables one to pursue an economic goal while utilizing the flexibility of the local energy supply.

5.3. The Impact of Dual Optimization Techniques in BEMS for a Commercial Building

Building optimization problems are considered MILP problems that have been solved using MPC [117]. Intelligent controlling has been used to manage loads efficiently and an ANN strategy has been adopted to maintain a comfort zone in the building for the occupant, with an MILP scheduling technique to decay the peak demand of consumer [166]. An energy management agent (EMA) consists of an ANN and MPC for the modeling and optimization of building flexibility. The Monte Carlo Tree search-based planning and control was used to find the optimal policies with an ANN. The system can predict the demand for a day ahead and has a tiny prediction error [167]. The proposed system consisted of an ANN and MPC. In contrast, an ANN was used for renewable energy (i.e., solar and wind) forecasting and ensured the optimized usages of generated energy, and MPC is adopted for intelligent home control [168].

The ANN is used to accurately predict power consumption and indoor temperature selection by given weather, occupancy, and temperature setpoints as input. At the same time, a GA has been taken to adapt to the ANN to minimize energy consumption, and an optimization control strategy was assessed in case of the day ahead and MPC [169].

The uncertainty of environmental variables and users' preferences has been tackled using a data-driven machine-learning approach. Furthermore, a lifelong multitask framework was adopted to exploit structural similarities in control policies as there were different room sizes in buildings. Kernel-based learning was pursued as well to mitigate the non-linearity policy. Finally, a dual decomposition method was employed to cope with DR constraints across the spaces, transforming the overall problem into a series of unconstrained stochastic optimization problems for individual rooms. The method was verified via numerical experimental based on semi-real data sets [170].

Three artificial intelligence techniques were used to solve the problem of energy demand planning in smart homes. First, the modification of the elitist none-dominated sorting genetic algorithm II to demand-side management was applied and accounted for electricity fluctuations over time, priority in the use of equipment, operating cycles, and a battery bank. Second, the forecast of demand-side consumers, distribution generation, renewable energies, and weather for a day ahead from the nearest meteorology office was considered for demand-side management by employing the SVR technique. Third, the k determined user comfort levels through the cluster technique [171]. Table 2 shows a full explanation of each optimization control technique, along with its benefits and drawbacks.

5.4. The Impact of Dual Optimization Techniques in BEMS for a Set of Commercial Buildings

Neighborhoods or districts are not frequently included in the application of optimum control ideas to achieve energy efficiency in buildings and the optimal exploitation of regional resources. In [171], they consider a neighborhood with several buildings that have agreed to coordinate how they use their energy loads and resources in order to achieve some overall objectives, while still allowing for the pursuit of individual optimization goals. When this occurs, a building's local resources should work together with a top-level optimization engine to balance the accomplishment of local optimization goals with neighborhood-level goals. A hierarchical optimization algorithm was introduced to divide the optimization at the building level and the neighborhood level in such a way that the bottom level managed the individual building objectives and the top level addressed the neighborhood-level objective, in order to address the most general case of multiple ownership neighborhoods. In particular, the building-level energy management would give the top-level optimizer flexibility and provide recommendations on control measures to implement to move the neighborhood closer to achieving its objectives [172]. The optimistic assumption in bilevel optimization (i.e., the two layers of optimization tasks are nested one inside the other) states that the consumers choose the best option that benefits the retailer the most. The pessimistic variant, on the other hand, deals with the scenario in which the consumers give the retailer their least preferred optimal response, protecting against potential losses brought on by an unexpected choice. However, the work in [173] shows

the formal properties of the best solutions to a bilevel tariff optimization issue for both the computationally challenging general case with an arbitrary number of consumers and the particular case with an easily tractable single consumer. The key relevance of these findings is that by perturbing the issue data and the optimal price vector, the pessimistic variant may be reduced to the optimistic one, which also yields the first effective solution technique for the pessimistic version. On the other hand, a numerical case study was offered to show that, if consumers do not select their optimal solution as expected, addressing the optimistic problem could directly result in a significant loss of profit for the retailer. In [174], they emphasize the distinction between the optimistic and pessimistic versions of the bilevel optimization problem with regard to energy management.

Table 2. A comparison of the most commonly used optimization methods in BEMS.

Ref.	Control Techniques	Benefits	Drawbacks	Observations
[9]	Internet of Energy (IoE)	Maximizing energy efficiency by minimizing losses and environmental impact using IoE.	The requirement of big data processing and large storage.	21% of energy loads can be deducted with significant cost reduction and energy saving.
[111]	Combination of machine-learning and model-based control approach.	Considered all physical characteristics of the building and human comfort compared to other researchers.	There is no real implementation and performance of the proposed system, which is only comparable to theoretical ideas.	Reduces the consumption of energy by 8–18%.
[117]	DDQN	An aggregation controller has been used which aggregates all IEs in the system and remotely reads and interrupts the IEs.	There is less consideration of user preferences and comfort satisfaction.	Decreases the operating cost by 16.9% in a day.
[118]	ANN and MILP	Smart controlling to manage the loads efficiently.	Longer computation time.	Reduction of up to 12.5% of energy consumption and 10% improvement in peak demand.
[119]	MILP with PV and ESS	During 90% of the peak tariff, consumers can sell electricity to the grid.	If all consumers were motivated to buy in the same period, the demand may have increased dramatically.	Reducing the flexible loads by 40% while saving 30% of overall costs.
[124]	Rule-based algorithm	Strong control reliability and system reduces significant power.	The number of people detected in the room and consumption rate are not considered.	Savings of 23.5 kWh and USD 2.898 in total daily energy consumption.
[137]	DANN	Synthetic load profile generator is a robust and adaptable solution.	Slow convergence and longer computational time.	Achieved an average RMSE value of 111W and coefficient of determination is 97.5%.
[138]	QL-PLR using RL	Higher convergence rate.	Consumer preference was not prioritized.	The system can reduce peak load demand by 9.28%.
[167]	ANN and MPC	The next-day electricity price is provided to EMA to optimize the energy cost by controlling the heat pump.	There is a variation that may introduce the disturbance of human comfort.	Reduces energy costs by 14.8%, when only heat pumps are used.
[168]	ANN and MPC	Provides good forecasting results compared to real assumptions with fewer error percentages.	The system will be required to investigate variable loads.	The system can sell energy to the grid for EGP 3.2 (Egyptian pound) within one day.
[169]	GA, ANN, and MPC	When loads are shifted within TOU, the results of energy savings increase by 27%.	The authors have considered 100% accurate forecasting which is not possible in a real scenario.	A total of 25% energy savings.
[171]	Flexibility envelop concept and MPC	The MPC-based schemes increase the self-sufficiency of buildings.	No consideration of any forecasting error which is impossible in real cases.	16% cost savings and 10% emission savings in the winter season, whereas in the summer, they were 26% and 29%, respectively.
[172]	MILP and MPC	Attempt to maintain energy consumption below the expected consumption for purpose of balancing.	HVAC model was out of the present work.	Saves approximately 125 KWh of net energy.
[173]	MG-EMS	Scalability, reliability, and extensibility.	It is implemented for residential use as one room at a time able to connect with solar energy.	The main power grid's peak energy demand is reduced by 30.6%.
[174]	EMS-in-Bs	Each function is critically synthesized by sub-function.	There is no clear direction in which methods might be preferable for BEMS.	"Control-optimize" achieves the highest energy saving rates of around 30% compared to "estimate-predict" with 10%.

6. Future Trends and Issues

Most high-rise buildings are constructed in city/urban areas rather than rural areas where there is an increased density of buildings and no outer space to use the solar energy. The following are future trends and issues which may have the potential to increase the building energy efficiency for both existing and new buildings.

6.1. Building Integrated Photovoltaics (BIPVs)

The current global power demand is roughly 15 Tera Watt (15×10^4 W), or 10^4 times less than solar power incidents on the earth. The solar energy received in less than an hour is thought to be enough to cover a year's worth of the global energy budget [175]. Therefore, photovoltaic (PV) technology is one of the most attractive options for making efficient use of solar energy. BIPVs are photovoltaic modules that are incorporated into the building envelope, therefore replacing the traditional components of the building envelope. PV modules are used as roofs, facades, and skylights in this application. In comparison to non-integrated systems, BIPVs have a significant benefit because land allocation and stand-alone PV systems are not required [176]. Photovoltaic foils, photovoltaic tiles, photovoltaic modules, and solar cell glazing are some of the different types of BIPV buildings, as shown in Figures 8 and 9, respectively, that use BIPV technology to become energy producers rather than consumers.

The advancement of BIPV technology and its incorporation into the building envelope provides aesthetic, economic, and technical benefits [175]. BIPV systems can be a powerful and versatile tool to meet the increasing demand for zero energy and zero emission buildings in the near future [177]. BIPVs are capable of delivering electricity at less than the cost of grid-connected electricity to end users at certain peak demand, which may lead to peak shaving without compromising human comfort [178].

Weather protection, thermal insulation, noise reduction, heating and cooling load reduction, and other benefits are all provided by the BIPV [179,180]. Utilizing a BIPV semi-transparent arrangement, some of the sunlight can be used for day illumination inside the building [181]. Due to the scarcity of ground area and the abundance of underutilized roof space, rooftop solar PV systems are gaining popularity, resulting in the prediction that the BIPV industry will increase rapidly soon [182]. In addition, feed-in tariffs (FiTs) and other government-sponsored solar energy programs have gained widespread acceptability around the world. Sanyo, Schott Solar, Sharp, and Sun-tech are among the firms developing innovative BIPV technologies for façades, skylights, and windows. FiT implementation, public acceptance, government economic support in the form of subsidies, and technical elements such as power losses and architectural concerns are the most significant impediments to BIPV system adoption [183]. However, a BIPV system's power-generating efficiency is lower than that of stand-alone and BIPV/T systems, but it eliminates the need for an additional power-generation space [184]. Overall, due to its functional qualities, this technology has a promising future in the coming years.

6.2. Net Zero Energy Building Concepts

The primary enabler of a future smart building is the energy performance of buildings, which leads to energy flexibility, generation, and interaction between users. Energy retrofitting for net-zero energy buildings (NZEBs), in conjunction with passive control strategies, energy-efficient technologies, and RER integration, creates a balance between demand and generation while also taking grid integration into account. Smart home energy retrofitting strategies are adapted for the improvement of existing buildings along with key performance indicators for measuring the performance and success of acquiring sustainability in intelligent buildings [188]. A ZEB or NZEB implies the integration of renewable resources if weighted supply and weighted demand are equal to zero, focusing on energy storage systems and materials, energy routers, renewable resources, and plug-and-play interfaces [9,11]. In addition, an NZEB is a preferred sustainable building style since it can meet its own energy needs while also producing surplus energy to feed into the grid.

However, NZEBs are involved in more energy-related systems and grid linkages, and their energy systems are more intricate than in conventional buildings [189].



Figure 8. Available BIPV systems on the market [185].



Figure 9. (a) BIPV façades powered by electricity to assist natural ventilation [186]; (b) an entrance with a PV skylight [187].

In [188], the EU adopted long-term goals to reduce 80–95% of carbon by 2050, where existing buildings will require a renovation rate greater than 3% per year in 2050 to achieve decarbonization. In addition, the occupant's behavior variation may lead to a 40% change in energy usage [11]. The UK was the first country to mandate NZEBs on a large scale in 2016 and France followed in 2020. The EU announced plans to initiate NZEBs in January 2021, and the US Department of Energy (DOE) targeted marketable zero-energy homes in 2020, followed by commercial zero-energy buildings in 2025. Other than that, ASHRAE (American Society of Heating, Refrigeration and Air-conditioning Engineers) plans to customize NZEBs in 2030, as shown in Figure 10. Moreover, Denmark has shown 100% renewable energy usage for heating and cooling systems [190].

In new and existing buildings, for example, it is possible to achieve total energy savings of 20%. Significant energy savings for cooling can be achieved by reducing external loads with proper building façade shading, reducing internal loads from lighting with

energy-efficient fluorescent lamps, and using natural cooling techniques such as ground, evaporative, and radiative cooling, as well as night ventilation [24].

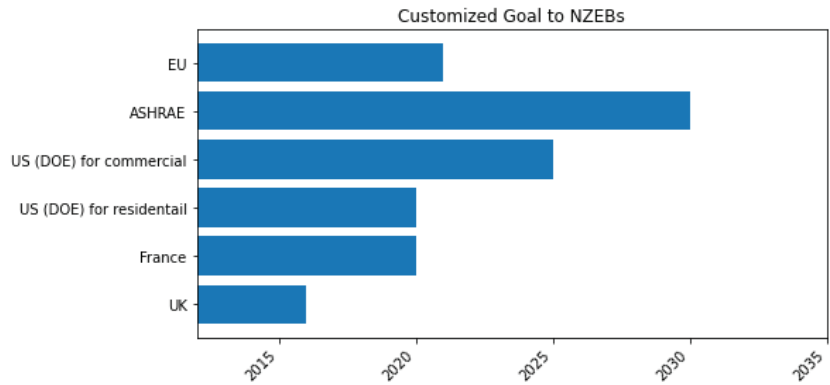


Figure 10. The aim of countries is to customize NZEBs over the years.

In [191], the authors presented a unique yet viable and cost-effective method for advancing the state-of-the-art of smart energy buildings and achieving the real meaning of net-zero energy buildings. The proposed solution consisted of new trigeneration solar collectors without a battery, a highly creative form of heat pump integration that needed minimal size and expense, and the two-way interaction of a building with local energy networks. A zero-energy building is self-sufficient in terms of energy use, producing as much as it consumes. In ZEBs, both passive and active design methods were used to minimize energy consumption, with renewable energy strategies (mostly solar panels) used to meet demand following the reduction [192].

A study was conducted to investigate ZEBs in Southeast Asia, which was adapted from an existing structure and used a variety of passive and active design solutions appropriate for a tropical climate. According to the research findings, active and passive measures should be incorporated into building design to improve energy efficiency. Passive design, in particular, must be used on a broad scale in order to achieve significant energy savings [74]. The combination of active and passive design solutions toward ZEBs are shown in Table 3.

Table 3. Strategies of energy efficient retrofitting for ZEB.

Domain Area	Achieving Strategies of Energy Efficiency Using Retrofitting	Ref.
Passive design solution	<ul style="list-style-type: none"> Conduction heat gains through the walls and roofs can be reduced by implementing insulation or both sides of the walls and roofs can be polished or coated using colors. Those materials that have higher thermal resistivity can be selected. Solar radiation through window glasses can be minimized up to 75%, by having two or more layers, and inside, between them, will be dead air. Using localized treatment can make an outstanding contribution to reducing heat gains, such as shading, modification lighting, removal of machines from conditioned space, etc. Pre-heating and pre-cooling can be adopted before occupying the conditioned area. Green roofs and green walls are highly efficient in managing cooling loads. 	[23,25,48,193–195]
	<ul style="list-style-type: none"> Natural ventilation with solar assistance. 	[74,196]
	<ul style="list-style-type: none"> Mirror ducts Lights shelves Light pipes Skylights 	[74,197]

Table 3. Cont.

Domain Area	Achieving Strategies of Energy Efficiency Using Retrofitting	Ref.	
Active design solutions	1. Correct system design	• The design should take into account the operational circumstances that occur over the majority of the running hours. Optimization under these conditions will be more beneficial than calculation at a single extreme design point.	[23,25,198]
	2. Control philosophy	• To guarantee low condensing temperatures are available during the part load operation, avoid fixed set head pressure control.	
		• Auxiliaries pump with set speeds can be avoided if possible, and fan power should be lowered at low loads.	
	3. Optimize components	• Ensure that defrosting is only used when absolutely necessary and that it is completed as effectively as possible.	
		• Compressor and condensing units should be selected at normal running conditions.	
		• Evaporator unit and temperature selection can be appointed based on human activities.	
	4. Proper installation	• Temperature differences must be considered for the choice of heat exchangers.	
		• Choose the appropriate refrigerant for application. If all other design parameters are optimized, the refrigerant's impact on efficiency is expected to be less than 5%.	
		• Following the guidance of the manufacturers for installation, such as maintaining the distance between indoor and outdoor units, leveling between them, and providing adequate space for air circulation to heat reject and absorb.	
5. Operation and maintenance	• It is required to have an accurate amount of gas charge that ensures no over- and undercharging.		
	• Correct adjustment of the expansion valve.		
	• No secondary flow problem.		
6. Energy efficiency lighting	• Ensure the cleanliness of filters, coils, and other components.		
	• If all installed systems are operating correctly, it can be estimated that an average of 10% energy savings can be achieved, reducing running costs.		
	• LED		
	• Task lights	[102,199–201]	
7. Intelligent BEMS	• Dimmers		
	• Sensors		
7. Intelligent BEMS	Building energy management System	[86,118,202]	
8. BESS	Battery energy storage system	[203–205]	
9. Renewable energy integration	Solar panels and wind turbines	[74,118,206]	

6.3. Demand Control Ventilation (DCV)

Commercial building ventilation is required to remove the airborne contaminants generated by occupants' and other living organisms' biological functions, occupant tasks and operations, equipment, supplies and furnishings, building materials, and the products of chemical reactions between contaminants from both indoor and outdoor sources [207]. Fisk [208] estimated that improving interior environmental conditions in commercial buildings might save USD tens of billions per year in the US. One of the few important elements required for these improvements was adequate ventilation. In nearly all U.S. climates, building HVAC systems require a large amount of energy to condition the external air utilized for ventilation. Natural ventilation, mechanical ventilation, or a combination of the two, referred to as hybrid ventilation, are examples of different types of ventilation systems [209]. In addition, there are also two types of ventilation airflow that can be supplied to the room by using constant air volume (CAV) or variable air volume (VAV). In industrial, commercial, educational, and office buildings, the VAV system is already widely used [210].

Several researchers have examined the effects of outdoor air supply rates (i.e., ventilation rates) on human health, comfort, and performance in commercial buildings. Lower rates of sick leave and the incidence of common respiratory disorders are linked to higher ventilation rates. Lower ventilation rates have been associated with building-related sickness (BRI), sometimes referred to as sick building syndrome (SBS). By adapting the ventilation air conditioning load to the actual occupancy, DCV can save energy. During this time, a variety of occupancy measurements were considered, including carbon dioxide (CO₂), volatile organic compound (VOC), and humidity concentrations [211].

It is important to have adequate ventilation since it protects our health as well as our buildings. However, the ventilation and energy needed for optimal indoor air quality (IAQ) may conflict [212]. Therefore, one of the most energy-efficient ways to obtain the best IAQ is to use DCV. As shown in Figure 11 [213], DCV is a typical concept in HVAC systems that uses signals from inside sensors to continuously match the ventilation airflow rate with the actual demand. Likewise, DCV refers to the control of mechanically supplied rates of external air intake into buildings based on occupant demand. A HVAC system is typically built and operated to keep the ideal environmental conditions in place in order to maintain acceptable thermal comfort and IAQ. In a recently constructed Swedish building, the effects of VAV ventilation on IAQ and the potential for energy savings were investigated. The VAV system can more efficiently satisfy thermal comfort requirements while using less energy than a CAV system. A VAV system combined with the DCV approach has become one of the most energy-efficient ways to ensure both optimal IAQ and thermal comfort as the DCV idea has evolved [214].

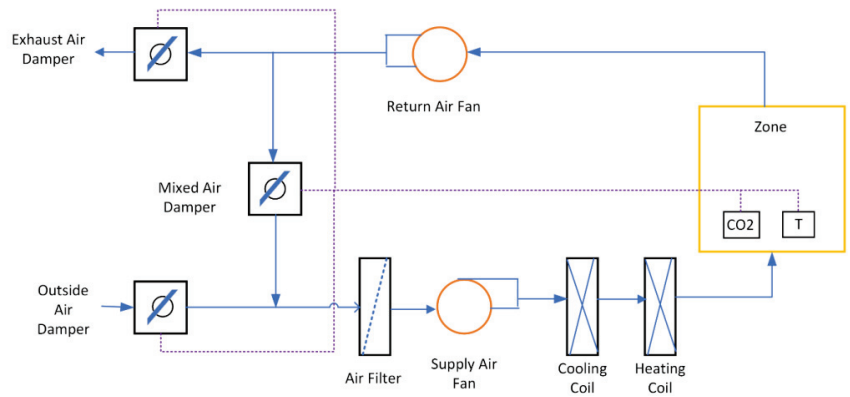


Figure 11. A typical view of demand control ventilation (DCV) [213].

In [212], research on a multi-residential complex examines the energy-saving possibilities of a ventilation system with an air-cleaning unit and demand control. This method is based on the need to save energy in ventilation by limiting the supply of outdoor air while maintaining the desired air quality by using air cleaning. As a result, in this study, the ventilation system's operation mode detects indoor CO₂ and formaldehyde (HCHO) concentrations in accordance with the IAQ standards for Korean dwellings. IAQ has recently gained prominence as a means of addressing specific occupant health and safety concerns.

To overcome the multi-zone demand-controlled ventilation system's over-ventilation and under-ventilation concerns, an air balancing method was developed. Increased energy efficiency has become a primary priority for the future accomplishment of zero usage in buildings. A mechanical ventilation system, which operates on a 12-month basis, is one of the most energy-intensive systems in HVAC. This suggests that lowering the airflow rates can save a lot of energy by reducing the fan's energy consumption and heating/cooling the supplied air [28]. As a result, it is suggested to investigate a building's ventilation system's energy-saving possibilities.

In [215], they proposed the integration of a two-level distributed method with an upper and lower-level control, where the upper level calculates zone mass flow rates to keep zone thermal comfort (TC) at a low cost of energy, and the bottom level strategically manages zone mass flow rates and ventilation rates to accomplish IAQ in conjunction with retaining higher levels of near-energy-saving performance. The results of certain studies have shown that the DCV technique has the potential to conserve energy, particularly in buildings with a high occupancy density [216,217].

6.4. Integrating SDG Goals

The UN presented 17 SDGs in 2015, with the goal of providing a common vision in terms of good living and a peaceful environment for this world and its people [218]. We investigated several studies to see if there was a link between BEMS and the SDG targets. We have found the importance of an IEMS's capability to achieve the UN SDGs. It shows that the improvement of a building's energy efficiency, by using the greater control and optimization of energy management with renewable energy resources, is thereby able to acquire three aspects of sustainability: social, economic, and environmental, all of which have a strong association with 7 out of the 17 SDGs [219], as shown in Table 4.

Table 4. BEMS helping to achieve the SDGs.







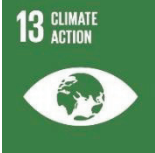
Domain	Goal	BEMS in the Pursuit of the SDGs	Ref.
Social	 <p>3 GOOD HEALTH AND WELL-BEING Ensure healthy lives for all ages and promote well-being.</p>	<ul style="list-style-type: none"> A smart building with the integration of an optimization controller which provides features such as thermal, humidity, and visual temperature comfort, alongside being able to reduce a significant amount of energy consumption, also results in less air pollution and emissions which creates healthy lives and well-being for inhabitants of a city. 	[134,135,220]
	 <p>7 AFFORDABLE AND CLEAN ENERGY Ensure that everyone has access to inexpensive, modern energy.</p>	<ul style="list-style-type: none"> To achieve affordable and modern energy using BEMS with the inclusion of optimization control strategies, RER, and ESS to become more cost-effective than fossil fuel alternatives. 	[220–222]
	 <p>11 SUSTAINABLE CITIES AND COMMUNITIES Ensures that cities and human settlements are inclusive, safe, resilient, and long-lasting.</p>	<ul style="list-style-type: none"> BEMS' concept, design, and technology can be used to create sustainable metropolitan cities and communities by reducing energy usage. 	[105,220]
Economic	 <p>8 DECENT WORK AND ECONOMIC GROWTH Foster inclusive, long-term economic growth, full and productive employment, and decent work for all.</p>	<ul style="list-style-type: none"> The demand for smart buildings is growing, and as a result, the manufacturing of diverse BEMS components demands a large workforce, creating opportunities for green jobs that lead to long-term economic growth. 	[220,223]
	 <p>9 INDUSTRY, INNOVATION AND INFRASTRUCTURE Build more resilient infrastructure, encourage inclusive and sustainable industrialization, and cheer on innovation.</p>	<ul style="list-style-type: none"> BEMS' optimization and control make building infrastructure more sustainable, resilient, and adaptable to changing global climate circumstances, allowing for economic success. 	[220,224,225]
	 <p>12 RESPONSIBLE CONSUMPTION AND PRODUCTION Ensure that consumption and production trends are long-term.</p>	<ul style="list-style-type: none"> In the form of microgrids, distributed power generation, smart grids, and virtual power plants, energy management in a smart building with proper controllers and optimization ensures a proper supply-load trade-off. 	[220,226]

Table 4. Cont.

Domain	Goal	BEMS in the Pursuit of the SDGs	Ref.
Environment	 <p>Take immediate action to address climate change and its effects.</p>	<ul style="list-style-type: none"> Using various RER combined with intelligent controllers in BEMS, the impact of carbon emissions on climate change can be reduced. 	[220,227]

6.5. Data Privacy and Security

For communication between appliances and the end-user in a smart house, various wireless communication technologies have been introduced. Smart building appliances are connected to a wireless control network such as ZigBee, Bluetooth, or Wi-Fi to receive and send commands remotely or automatically. The IEEE 802.11 (Wi-Fi), IEEE 802.16 (WiMAX), IEEE 802.15.1 (Bluetooth), and IEEE 802.15.4 (Zigbee) standards are the most widely used wireless technologies in smart homes [228]. Two types of communication protocols are usually used in IoT-enabled smart infrastructure: Zigbee for device-to-device communication and Wi-Fi for device-to-AMI connectivity [105]. A brief comparison of wireless communication protocols used in HEMS is presented in Table 5.

Table 5. Comparison of different wireless communication technologies for the smart home.

Technology	Spectrum	Data Rate	Coverage Range	Applications	Limitations	Power Consumption
Wi-Fi	2.4–5 GHz	Up to 300 Mbps	100–300 m	Monitoring and controlling	Interference and security	Very High
Bluetooth	2.4 GHz	1 Mbps	10 m	Device to device	Low data speed, short range, poor data security	Low
Zigbee	2.4 GHz	250 Kbps	30–40 m	Device to device	Low data speed and short range	Very low
WiMAX	2–11 GHz	Up to 70 Mbps	8–50 Km	AMI, Demand response	Lack of quality and interference	Much higher
5G	1–6 GHz	Up to 10 Gbps	About 1000 ft	AMI, Demand response	Privacy and security	Very much higher

The emergence of intelligent cities in the world is encountered chiefly to preserve the privacy and security of data involving big data analytics. Without the authorization of the owner's privacy, accessing data generated in smart cities will not be legal. In this case, personal data acquisition can be encouraged to motivate data owners by promoting incentives via an intelligent contract that provides privacy. Estonia introduced the world's first "data embassy" which can be operated from data centers outside of Estonia for reliable operation and to restrict potential cyber-attacks [229].

On top of this, the unveiling of the new innovative technology called blockchain is now the key to the data-driven world. The usage of blockchains is booming rapidly, with a market size of USD 3 billion to 39.7 billion by 2025 [1]. The integration of the constrained application protocol (CoAP) for the sending and receiving of data in IoT systems minimizes the power consumption of IoT devices with datagram transport layer protection (DTLS) security and the usage of CoAP in the intelligent building. However, that is less than the message queuing telemetry transport case (MQTT). The aim is to integrate the DTLS protocol with the secure hash algorithm (SHA-256) using optimization to improve security [230].

The essential features of blockchain are seamless authentication, privacy, security, effortless deployment, and maintenance. Smart cities are required to modernize

their buildings by implementing home automation with decarbonization and improved consumer security and privacy. The demonstration focuses on future energy management research by highlighting the key emerging areas, namely context-aware energy management, energy management for smart homes and grids, and the role of privacy preservation in IEMS. One paper addressed the technical challenges and possible solutions for their implementation in IEMS and also summarized the future perspectives to make the system more reliable, robust, and customized [231]. The problems in the centralized architecture of intelligent building energy management systems (IBEMS) are, namely, the difficulty of networking between end devices, the lack of flexibility, and the limited sharing of underlying information. The analysis of the formulation of a wireless sensor network (WSN) for the power supply, distribution management system, and design of a network model of the IBEMS can overcome these problems. For the security purposes of the IBEMS, a blockchain-based dynamic key management strategy was proposed, and experimental results show the reduction of data storage time and the space of sensors, which optimizes the control of the IBEMS. Moreover, research results assist in promoting blockchain technology in the scenario of Ubiquitous Power Internet of Things (UPIoT) [232]. To make a smart city where the whole area has to be digitalized by placing sensors everywhere, namely transport, e-health, agriculture, and so on, care must be taken with data privacy and security [112].

6.6. Emerging Energy Policies

At present, increasing the concentration on imposing energy policies to maximize efficiency with the minimization of generation costs alongside occupant comfort is necessary. Ensuring the proper utilization of energy requires an energy audit to analyze and compare them. The energy policy of the DSM must have objectives for emission reduction, energy security, affordability, and encompass energy efficiency, demand response, one-site backup generation, and storage [233,234].

Moreover, the energy policy in peninsular Malaysia, by proposing the enhanced time of use (ETOU), has a subsection of the time-based program by including TOU (enlarged to ETOU), off-peak tariff rider (OPTR), and Sunday tariff rider (STR). The authors illustrated that electricity bills are about 0.5% to 12% higher due to improper implementation of load management (LM) and DSM during ETOU tariff shafting [235]. The proposed strategy formulation has been demonstrated to DSM in order for valley filling, load clapping, and load shifting to be implemented. The major commercial and industrial consumers must be persuaded to use approximately 20–50% of LM based on a price-based program (PBP) [235]. DSM strategies motivate consumers to shift their loads to optimize energy usage—the motivation is based on two DR classifications, namely incentive and price-based. Whereas three control techniques have been proposed, namely passive, active, and transactive, only transactive controllers have bidirectional communication, allowing end-user loads to bid on their demand. The price is set based on the buyers' and sellers' bids [236].

According to the report [117], the guidance of energy traders to design cost-effective and efficient IEMS and system architecture consists of an admission controller (AC), a load balancer (LB), and a third layer composed of a demand response manager (DRM) and load forecaster (LF). Two-way demand response manager communication receives the critical peak pricing (CCP), TOU, and real-time pricing with predicted demand from load forecaster. Afterward, the available capacity is found by the admission controller and then allowed to appliances, otherwise rejecting again to LB, and that is the way to create a balance between the reduction of the valley falling and load shafting, and make the load consumption shape stable. A detailed summary of the energy policy is shown in Table 6.

Table 6. Energy policy to demand side management.

Ref.	Country	Programs	Challenges	Remarks
[235]	Malaysia	<ul style="list-style-type: none"> Mid peak time has been implanted in time zone segmentation that consists of 10 h while peak time segmentation is reduced to 4 h. If anyone is registering under the Sunday tariff rider, the charge for maximum demand (MD) rate by TNB is not considered. Some specific categories of domestic and commercial consumers receive a discount up to 10%, and domestic consumers whose electricity demands are under 300 kWh will also be eligible for an exemption of 6% service tax. 	<ul style="list-style-type: none"> Motivating consumers requires a significant amount of effort. 	<ul style="list-style-type: none"> Consumers and power plants are correlated. Therefore, energy implementation policies must also address consumers' comfort.
[237–239]	UK, EU	<ul style="list-style-type: none"> To stimulate the development of energy labeling, product standards, and certification of appliances and equipment through the EU's energy labeling framework and the eco-design directive. Balance mechanism during peak time by usage of backup generation, cross-border interconnection, storage, and DSM. 	<ul style="list-style-type: none"> It requires consensus between utility authorities and consumers or neighboring countries for cross-border inter-connection. 	<ul style="list-style-type: none"> Inspiring consumers through incentive-based load scheduling along with the adoption of smart control and monitoring.
[240]		<ul style="list-style-type: none"> DSM has been categorized into energy efficiency (EE), TOU, market DR, physical DR, spinning reserve (SR), and these are correlated with smart energy control policy. 	<ul style="list-style-type: none"> It necessitates an incentive for agreement between utility providers and consumers. 	<ul style="list-style-type: none"> It can also encourage the adoption of RER and ESS.
[241]		<ul style="list-style-type: none"> The policies of ESS are proposed to manage renewable energy integration and grid stability. ESS can also be used for power backup and energy arbitrage. 	<ul style="list-style-type: none"> It will have a larger investment and maintenance cost. 	<ul style="list-style-type: none"> ESS is being adopted in developed countries rather than developing countries, as they have the ability to afford it and the expertise.
[242]	Bangladesh	<ul style="list-style-type: none"> Efficiency improvement of home appliances and energy saving behavior in the residential sector would reduce consumption by about 50.7%, as shown in the Energy Efficiency and Conservation Master Plan (EECMP) of Bangladesh. 	<ul style="list-style-type: none"> It has the limitations of the existing technology in the developing world. 	<ul style="list-style-type: none"> Inspiring best practices of energy-saving behavior using print media and social networking.
[243]	Singapore	<ul style="list-style-type: none"> The three main DSM strategies in Singapore are the TOU price, real-time price, and direct DR program. 	<ul style="list-style-type: none"> There is no linearity that might affect the consumer. 	<ul style="list-style-type: none"> Rooftop solar, ESS, and real-time load control can be implemented for DSM.
[244]	USA	<ul style="list-style-type: none"> Using a battery is a promising solution to mitigate peak demand under a real-life tariff model in New York City. 	<ul style="list-style-type: none"> A longer payback period can create barriers for a wide scale of adaption. 	<ul style="list-style-type: none"> It can be developed based on a battery's life cycle cost assessment and degradation cost of the battery.
[245]	Kuwait	<ul style="list-style-type: none"> Incentive-based demand response programs can be considered in Kuwait. 	<ul style="list-style-type: none"> It is dependent on the consumer consensus. Existing electric grid requires upgrading to a smart grid. 	<ul style="list-style-type: none"> Solar energy and batteries can be emerging solutions to DSM in Kuwait.
[246,247]	China	<ul style="list-style-type: none"> In 2015, the central government of China provided 100 CNY/kWh for temporary peak load reduction using incentive-based DR in Beijing, Jiangsu, and Foshan provinces. 	<ul style="list-style-type: none"> Incentives are not enough to recover the cost of shifting and reducing loads. 	<ul style="list-style-type: none"> The power sector of China can be reformed by increasing the integration of renewable energy on both the generation and demand sides.

Table 6. Cont.

Ref.	Country	Programs	Challenges	Remarks
[248]	India	<ul style="list-style-type: none"> Highly concentrated on peak reduction in DSM programs in India, whereas agriculture and small-scale industries are heavily subsidized. National electricity policy also emphasizes periodic energy audits, labeling, and standardization of appliances for voluntary and self-regulatory initiatives. 	<ul style="list-style-type: none"> Several obstacles are impeding the implementation of DSM programs, and these obstacles must be identified and overcome for India's DSM potential to be fully realized. 	<ul style="list-style-type: none"> However, such rules must be updated, and regulatory mechanisms must be developed to encourage utility companies to implement DSM programs on a greater scale.
[249]	South Africa	<ul style="list-style-type: none"> The adoption of dynamic pricing for 100% household participation saves roughly ZAR 3,115,047 per day compared to TOU pricing in South Africa. DSM has been found to alleviate poverty by lowering household power expenses by 1.2%, 1.5%, and 2.9% on a monthly basis for households with 100%, 50%, and 30% involvement, respectively. 	<ul style="list-style-type: none"> The fact that pseudo-peaks could be formed during periods of lower electricity rates, which could disrupt grid operation if demand exceeds supply capacity, is a disadvantage of using the TOU pricing structure. 	<ul style="list-style-type: none"> In South Africa, there is a potential opportunity for solar energy on both the supply and demand sides.
[250]	Brazil	<ul style="list-style-type: none"> To encourage peak load reduction in Brazil, a set of levies was created for large consumers. To do so, consumers were divided into two categories: consumers with high voltage access and low-voltage-access consumers. Both tariffs are intended to reduce peak load consumption by moving load to off-peak hours or replacing generation. 	<ul style="list-style-type: none"> The main problem with these schemes for large consumers is that they may have inflexible loads during peak periods which encourage the consumers to have self-generation using fossil fuels. 	<ul style="list-style-type: none"> DSM treatments may create some consumer dissatisfaction, necessitating habit modifications in people who are affected.
[251]	Australia	<ul style="list-style-type: none"> Australia promotes demand-side opportunities by focusing on improving energy efficiency, the substitution of energy sources, load shifting, and peak shaving. 	<ul style="list-style-type: none"> To overcome the lack of consumer acceptance, awareness, and technical barriers to DSM. 	<ul style="list-style-type: none"> The consumer's preference must be prioritized.
[252,253]	Thailand	<ul style="list-style-type: none"> In Thailand, from 2003–2017, the use of energy efficiency programs and efficient power generation technologies would reduce CO₂ by 8.4%. 	<ul style="list-style-type: none"> High investment costs. 	<ul style="list-style-type: none"> Price- or incentive-based tariffs can be adopted.
[254]	Indonesia	<ul style="list-style-type: none"> Indonesia will reduce electricity demand by 5.2% in 2025 using lighting efficiency improvements in Java–Madura–Bali (Jamali) Islands. 	<ul style="list-style-type: none"> Less public awareness, financial limitations. 	<ul style="list-style-type: none"> It might be achieved if it receives support from the Indonesian government and the people.

7. Discussion and Conclusions

Following existing main issues in current research on BEMS, the corresponding suggestions are given, which can stimulate further research.

- Finding the best location for PV installation in terms of building density may not be optimal for mutual occlusion, reflecting the congestion of buildings in urban areas. Hence, BIPV technology can be implemented in buildings. In addition, it is required to focus on monitoring and controlling loads in real-time to save the significant energy consumption deliberately wasted by human behavior, along with an increasing awareness of energy utilization.
- Many researchers discussed the application of the IoE to BEMS but did not mention the assessment of cyber-attacks with an increasing threat to national security. Therefore, further studies can be conducted for multi-storied buildings because there will be many sub-controllers based on the central controller, handling large amounts of data to preserve privacy and security.
- An in-depth investigation is required to optimize the IEMS according to occupant comfort, considering all indoor air comfort index parameters such as thermal, visual, acoustic, and air quality properties.
- Many authors provided an overview of artificial intelligence (AI) and deep learning techniques, whereas they did not provide the outline of the best configuration in terms

of computational time and error in BEMS. More research is required to profoundly improve the performance of optimization algorithms with less computation time and error that might respond accordingly to consumer needs over time.

- Passive design solutions are undeniably important for reducing energy use and improving human comfort. Many green architects use passive design as part of their sustainable design strategy. However, because of temperature and density, passive design should be cautiously applied in existing building retrofits in hot–humid climates with crowded urban environments, taking into account cost and effectiveness [74].
- As renewable energies are intermittent, more emphasis should be given to finding the optimum sizing of RER and battery storage to minimize the initial and maintenance costs, which is the key way to approaching consumers for the encouragement of adopting BEMS.

This review paper has comprehensively extracted the contribution of BEMS to curtail load profile with optimization control, by introducing energy policies. As a result, significant energy savings may lead to sustained initiative, and the installation of new power plants, as an emerging technology that can perform decarbonization in an intelligent building with the optimization of self-generation and self-scheduling, and introduction of the prosumer. However, the impact of optimizing building energy management on SDGs must also be assessed as SDGs address global concerns. Building energy-saving strategies can save a significant amount of energy, which is beneficial to reducing a building's negative environmental effects and enhancing its sustainability. Therefore, the primary data, findings, analysis, and recommendations gleaned from this evaluation could be quite useful in building and implementing an optimum controller in the case of BEMS to design energy-efficient buildings.

Funding: The authors would like to thank the Ministry of Higher Education Malaysia for the financial support. The project is funded under the Fundamental Research Grant Support, No: FRGS/1/2020/TK0/UTEM/02/66.

Data Availability Statement: The data that supports the findings of this study are available within the article.

Acknowledgments: The authors also want to thank Universiti Teknikal Malaysia Melaka for all the support.

Conflicts of Interest: The authors declare no conflict of interest.

References

1. Aliero, M.S.; Qureshi, K.N.; Pasha, M.F.; Jeon, G. Smart Home Energy Management Systems in Internet of Things networks for green cities demands and services. *Environ. Technol. Innov.* **2021**, *22*, 101443. [CrossRef]
2. Yelisetti, S.; Kumar, R.; Gupta, V.; Saxena, A.; Lamba, R. Modelling and Analysis of Home Energy Management System Using Intelligent Algorithms. In Proceedings of the ICPECTS 2020—IEEE 2nd International Conference on Power, Energy, Control and Transmission Systems, Chennai, India, 10–11 December 2020. [CrossRef]
3. Hassan, J.S.; Zin, R.M.; Majid, M.Z.A.; Balubaid, S.; Hainin, M.R. Building energy consumption in Malaysia: An overview. *J. Teknol.* **2014**, *70*, 33–38. [CrossRef]
4. Shaikh, P.H.; Nor, N.B.M.; Sahito, A.A.; Nallagownden, P.; Elamvazuthi, I.; Shaikh, M.S. Building energy for sustainable development in Malaysia: A review. *Renew. Sustain. Energy Rev.* **2017**, *75*, 1392–1403. [CrossRef]
5. Pipattanasomporn, M.; Kuzlu, M.; Khamphanchai, W.; Saha, A.; Rathinavel, K.; Rahman, S. BEMOSS: An agent platform to facilitate grid-interactive building operation with IoT devices. In Proceedings of the 2015 IEEE Innovative Smart Grid Technologies-Asia (ISGT ASIA), Bangkok, Thailand, 3–6 November 2015; pp. 1–6. [CrossRef]
6. Khamphanchai, W.; Saha, A.; Rathinavel, K.; Kuzlu, M.; Pipattanasomporn, M.; Rahman, S.; Akyol, B.; Haack, J. Conceptual architecture of building energy management open source software (BEMOSS). In Proceedings of the IEEE PES Innovative Smart Grid Technologies, Europe, Istanbul, Turkey, 12–15 October 2014; Volume 2015, pp. 1–6. [CrossRef]
7. Balaras, C.A.; Grossman, G.; Henning, H.-M.; Ferreira, C.A.I.; Podesser, E.; Wang, L.; Wiemken, E. Solar air conditioning in Europe—An overview. *Renew. Sustain. Energy Rev.* **2007**, *11*, 299–314. [CrossRef]
8. Nguyen, N.-H.; Tran, Q.-T.; Leger, J.-M.; Vuong, T.-P. A real-time control using wireless sensor network for intelligent energy management system in buildings. In Proceedings of the 2010 IEEE Workshop on Environmental Energy and Structural Monitoring Systems, Taranto, Italy, 9 September 2010; pp. 87–92.

9. Hannan, M.A.; Faisal, M.; Ker, P.J.; Mun, L.H.; Parvin, K.; Mahlia, T.M.I.; Blaabjerg, F. A review of internet of energy based building energy management systems: Issues and recommendations. *IEEE Access* **2018**, *6*, 38997–39014. [CrossRef]
10. Al-Ali, A.-R.; Zualkernan, I.A.; Rashid, M.; Gupta, R.; AliKarar, M. A smart home energy management system using IoT and big data analytics approach. *IEEE Trans. Consum. Electron.* **2017**, *63*, 426–434. [CrossRef]
11. Eini, R.; Linkous, L.; Zohrabi, N.; Abdelwahed, S. Smart building management system: Performance specifications and design requirements. *J. Build. Eng.* **2021**, *39*, 102222. [CrossRef]
12. Khamphanchai, W.; Pipattanasomporn, M.; Kuzlu, M.; Rahman, S. An agent-based open source platform for building energy management. In Proceedings of the 2015 IEEE Innovative Smart Grid Technologies-Asia (ISGT ASIA), Bangkok, Thailand, 3–6 November 2015. [CrossRef]
13. Aguilar, J.; Garcés-jimenez, A.; R-moreno, M.D.; García, R. A systematic literature review on the use of artificial intelligence in energy self-management in smart buildings. *Renew. Sustain. Energy Rev.* **2021**, *151*, 111530. [CrossRef]
14. Alanne, K.; Sierla, S. An overview of machine learning applications for smart buildings. *Sustain. Cities Soc.* **2022**, *76*, 103445. [CrossRef]
15. Gong, H.; Rallabandi, V.; McIntyre, M.L.; Hossain, E.; Ionel, D.M. Peak reduction and long term load forecasting for large residential communities including smart homes with energy storage. *IEEE Access* **2021**, *9*, 19345–19355. [CrossRef]
16. Yao, Y.; Shekhar, D.K. State of the art review on model predictive control (MPC) in Heating Ventilation and Air-conditioning (HVAC) field. *Build. Environ.* **2021**, *200*, 107952. [CrossRef]
17. Zhou, Z.; Zhang, S.; Wang, C.; Zuo, J.; He, Q.; Rameezdeen, R. Achieving energy efficient buildings via retrofitting of existing buildings: A case study. *J. Clean. Prod.* **2016**, *112*, 3605–3615. [CrossRef]
18. Kanakadhurga, D.; Prabaharan, N. Demand side management in microgrid: A critical review of key issues and recent trends. *Renew. Sustain. Energy Rev.* **2022**, *156*, 111915. [CrossRef]
19. Mariano-Hernández, D.; Hernández-Callejo, L.; Zorita-Lamadrid, A.; Duque-Pérez, O.; García, F.S. A review of strategies for building energy management system: Model predictive control, demand side management, optimization, and fault detect & diagnosis. *J. Build. Eng.* **2021**, *33*, 101692. [CrossRef]
20. de Oliveira, K.B.; dos Santos, E.F.; Neto, A.F.; Santos, V.H.D.M.; de Oliveira, O.J. Guidelines for efficient and sustainable energy management in hospital buildings. *J. Clean. Prod.* **2021**, *329*, 129644. [CrossRef]
21. Alawneh, R.; Ghazali, F.; Ali, H.; Sadullah, A.F. A Novel framework for integrating United Nations Sustainable Development Goals into sustainable non-residential building assessment and management in Jordan. *Sustain. Cities Soc.* **2019**, *49*, 101612. [CrossRef]
22. Bushby, S.T.; Butler, J.F. BACnet[®] for Utilities and Metering. *Ashrae J.* **2008**, *50*, 22.
23. Hundy, G.F.; Trott, A.R.; Welch, T.C. *Refrigeration and Air-Conditioning*; Elsevier Science: Amsterdam, The Netherlands, 2008. Available online: <https://books.google.com.my/books?id=BuWLTqjv4kwC> (accessed on 1 January 2020).
24. Asimakopoulos, D.; Santamouris, M. *Passive Cooling of Buildings*; Routledge: Abingdon-on-Thames, UK, 2013.
25. ASHRAE. *ASHRAE Fundamental Handbook*; ASHRAE: Atlanta, GA, USA, 2001; p. 30.
26. Pérez-Lombard, L.; Ortiz, J.; Pout, C. A review on buildings energy consumption information. *Energy Build.* **2008**, *40*, 394–398. [CrossRef]
27. Vakiloroya, V.; Samali, B.; Fakhar, A.; Pishghadam, K. A review of different strategies for HVAC energy saving. *Energy Convers. Manag.* **2014**, *77*, 738–754. [CrossRef]
28. Jing, G.; Cai, W.; Zhang, X.; Cui, C.; Yin, X.; Xian, H. An energy-saving oriented air balancing strategy for multi-zone demand-controlled ventilation system. *Energy* **2019**, *172*, 1053–1065. [CrossRef]
29. Cao, N.; Ting, J.; Sen, S.; Raychowdhury, A. Smart sensing for HVAC control: Collaborative intelligence in optical and IR cameras. *IEEE Trans. Ind. Electron.* **2018**, *65*, 9785–9794. [CrossRef]
30. Li, D.H.W.; Cheung, K.L.; Wong, S.L.; Lam, T.N.T. An analysis of energy-efficient light fittings and lighting controls. *Appl. Energy* **2010**, *87*, 558–567. [CrossRef]
31. U.S. Energy Information Administration. *Commercial Buildings Energy Consumption Survey*; U.S. Energy Information Administration: Washington, DC, USA, 2012.
32. Pandharipande, A.; Caicedo, D. Daylight integrated illumination control of LED systems based on enhanced presence sensing. *Energy Build.* **2011**, *43*, 944–950. [CrossRef]
33. Altan, H. Energy efficiency interventions in UK higher education institutions. *Energy Policy* **2010**, *38*, 7722–7731. [CrossRef]
34. Burman, E.; Mumovic, D.; Kimpian, J. Towards measurement and verification of energy performance under the framework of the European directive for energy performance of buildings. *Energy* **2014**, *77*, 153–163. [CrossRef]
35. Yun, G.Y.; Kim, H.; Kim, J.T. Effects of occupancy and lighting use patterns on lighting energy consumption. *Energy Build.* **2012**, *46*, 152–158. [CrossRef]
36. Haq, M.A.U.; Hassan, M.Y.; Abdullah, H.; Rahman, H.A.; Abdullah, P.; Hussin, F.; Said, D.M. A review on lighting control technologies in commercial buildings, their performance and affecting factors. *Renew. Sustain. Energy Rev.* **2014**, *33*, 268–279. [CrossRef]
37. Doe, U. *An Assessment of Energy Technologies and Research Opportunities*; Quadrennial Technology Review; United States Department of Energy: Washington, DC, USA, 2015; pp. 12–19.

38. Ryu, Y.; Kwag, S.; Ju, B.S. Fragility assessments of multi-story piping systems within a seismically isolated low-rise building. *Sustainability* **2018**, *10*, 3775. [CrossRef]
39. World Health Organization. Design of Plumbing Systems for Multi-storey Buildings. 2015. Available online: http://www.who.int/water_sanitation_health/hygiene/plumbing14.pdf (accessed on 1 January 2022).
40. Ma, J.J.; Du, G.; Xie, B.C.; She, Z.Y.; Jiao, W. Energy Consumption Analysis on a Typical Office Building: Case Study of the Tiejian Tower, Tianjin. *Energy Procedia* **2015**, *75*, 2745–2750. [CrossRef]
41. Rodrigues, E.E.C.; Rodrigues, J.P.C.; da Silva Filho, L.C.P. Comparative study of building fire safety regulations in different Brazilian states. *J. Build. Eng.* **2017**, *10*, 102–108. [CrossRef]
42. Lanzisera, S.; Nordman, B.; Brown, R.E. Data network equipment energy use and savings potential in buildings. *Energy Effic.* **2012**, *5*, 149–162. [CrossRef]
43. Cooper, A.; Schefter, K. Electric Vehicle Sales Forecast and the Charging Infrastructure Required through 2030. 2018, Volume 1. Available online: <https://www.edisonfoundation.net/iei/publications/Documents/IEI%20Forecast%20Report%20Nov2018.pdf> (accessed on 1 August 2022).
44. Weiss, J.; Hagerty, J.M.; Castañer, M. The Coming Electrification of the North American Economy: Why We Need a Robust Transmission Grid. WIRES Group. March 2019. Available online: <https://wiresgroup.com/new/wpcontent/uploads/2019/03/Electrification%20BrattleReport%20WIRE%20FINAL%2003062019.Pdf> (accessed on 1 January 2020).
45. Bauer, G.; Hsu, C.-W.; Nicholas, M.; Lutsey, N. *Charging Up America: Assessing the Growing Need for US Charging Infrastructure through 2030*; White Paper ICCT; The International Council on Clean Transportation: Washington, DC, USA, 2021; Volume 28.
46. Blonsky, M.; Nagarajan, A.; Ghosh, S.; McKenna, K.; Veda, S.; Kroposki, B. Potential impacts of transportation and building electrification on the grid: A review of electrification projections and their effects on grid infrastructure, operation, and planning. *Curr. Sustain. Energy Rep.* **2019**, *6*, 169–176. [CrossRef]
47. Lam, J.C.; Chan, R.Y.C.; Tsang, C.L.; Li, D.H.W. Electricity use characteristics of purpose-built office buildings in subtropical climates. *Energy Convers. Manag.* **2004**, *45*, 829–844. [CrossRef]
48. Reeder, L. *Net Zero Energy Buildings: Case Studies and Lessons Learned*; Routledge: Abingdon-on-Thames, UK, 2016.
49. Wang, S. *Intelligent Buildings and Building Automation*; Routledge: Abingdon-on-Thames, UK, 2009.
50. Aste, N.; Manfren, M.; Marenzi, G. Building Automation and Control Systems and performance optimization: A framework for analysis. *Renew. Sustain. Energy Rev.* **2017**, *75*, 313–330. [CrossRef]
51. Duman, A.C.; Erden, H.S.; Gönül, Ö.; Güler, Ö. A home energy management system with an integrated smart thermostat for demand response in smart grids. *Sustain. Cities Soc.* **2021**, *65*, 102639. [CrossRef]
52. Wang, C.; Pattawi, K.; Lee, H. Energy saving impact of occupancy-driven thermostat for residential buildings. *Energy Build.* **2020**, *211*, 109791. [CrossRef]
53. Xia, M.; Song, Y.; Chen, Q. Hierarchical control of thermostatically controlled loads oriented smart buildings. *Appl. Energy* **2019**, *254*, 113493. [CrossRef]
54. Tabares-Velasco, P.C.; Speake, A.; Harris, M.; Newman, A.; Vincent, T.; Lanahan, M. A modeling framework for optimization-based control of a residential building thermostat for time-of-use pricing. *Appl. Energy* **2019**, *242*, 1346–1357. [CrossRef]
55. Bruce-Konuah, A.; Jones, R.V.; Fuertes, A.; Messi, L.; Giretti, A. The role of thermostatic radiator valves for the control of space heating in UK social-rented households. *Energy Build.* **2018**, *173*, 206–220. [CrossRef]
56. Tian, W.; Han, X.; Zuo, W.; Wang, Q.; Fu, Y.; Jin, M. An optimization platform based on coupled indoor environment and HVAC simulation and its application in optimal thermostat placement. *Energy Build.* **2019**, *199*, 342–351. [CrossRef]
57. Kazmi, H.; Suykens, J.; Balint, A.; Driesen, J. Multi-agent reinforcement learning for modeling and control of thermostatically controlled loads. *Appl. Energy* **2019**, *238*, 1022–1035. [CrossRef]
58. Fratean, A.; Dobra, P. Control strategies for decreasing energy costs and increasing self-consumption in nearly zero-energy buildings. *Sustain. Cities Soc.* **2018**, *39*, 459–475. [CrossRef]
59. Sangi, R.; Kümpel, A.; Müller, D. Real-life implementation of a linear model predictive control in a building energy system. *J. Build. Eng.* **2019**, *22*, 451–463. [CrossRef]
60. Hannan, M.A.; Lipu, M.S.H.; Ker, P.J.; Begum, R.A.; Agelidis, V.G.; Blaabjerg, F. Power electronics contribution to renewable energy conversion addressing emission reduction: Applications, issues, and recommendations. *Appl. Energy* **2019**, *251*, 113404. [CrossRef]
61. Li, Y.; Ang, K.H.; Chong, G.C.Y. PID control system analysis and design. *IEEE Control Syst. Mag.* **2006**, *26*, 32–41.
62. Copot, C.; Mac Thi, T.; Ionescu, C. PID based particle swarm optimization in offices light control. *IFAC-PapersOnLine* **2018**, *51*, 382–387. [CrossRef]
63. Zhao, B.Y.; Zhao, Z.G.; Li, Y.; Wang, R.Z.; Taylor, R.A. An adaptive PID control method to improve the power tracking performance of solar photovoltaic air-conditioning systems. *Renew. Sustain. Energy Rev.* **2019**, *113*, 109250. [CrossRef]
64. Ulpiani, G.; Borgognoni, M.; Romagnoli, A.; Di Perna, C. Comparing the performance of on/off, PID and fuzzy controllers applied to the heating system of an energy-efficient building. *Energy Build.* **2016**, *116*, 1–17. [CrossRef]
65. Watson, D.S.; Kilicote, S.; Motegi, N.; Piette, M.A. Strategies for demand response in commercial buildings. In Proceedings of the 2006 ACEEE Summer Study on Energy Efficiency in Buildings, Pacific Grove, CA, 13–18 August 2006.

66. Amirifard, F.; Sharif, S.A.; Nasiri, F. Application of passive measures for energy conservation in buildings—a review. *Adv. Build. Energy Res.* **2019**, *13*, 282–315. [CrossRef]
67. Konstantinou, T. *Facade Refurbishment Toolbox: Supporting the Design of Residential Energy Upgrades*; TU Delft: Delft, The Netherlands, 2014.
68. Bataineh, K.M.; Fayez, N. Analysis of thermal performance of building attached sunspace. *Energy Build.* **2011**, *43*, 1863–1868. [CrossRef]
69. Šadauskienė, J.; Banionis, K.; Paukštys, V. Air permeability tests of masonry structures. *J. Sustain. Archit. Civ. Eng.* **2014**, *9*, 74–82. [CrossRef]
70. de Gracia, A.; Navarro, L.; Coma, J.; Serrano, S.; Romani, J.; Pérez, G.; Cabeza, L.F. Experimental set-up for testing active and passive systems for energy savings in buildings—Lessons learnt. *Renew. Sustain. Energy Rev.* **2018**, *82*, 1014–1026. [CrossRef]
71. Ma, H.; Zhou, W.; Lu, X.; Ding, Z.; Cao, Y. Application of low cost active and passive energy saving technologies in an ultra-low energy consumption building. *Energy Procedia* **2016**, *88*, 807–813. [CrossRef]
72. Chua, K.J.; Chou, S.K.; Yang, W.M. Advances in heat pump systems: A review. *Appl. Energy* **2010**, *87*, 3611–3624. [CrossRef]
73. Rhee, K.-N.; Kim, K.W. A 50 year review of basic and applied research in radiant heating and cooling systems for the built environment. *Build. Environ.* **2015**, *91*, 166–190. [CrossRef]
74. Sun, X.; Gou, Z.; Lau, S.S.Y. Cost-effectiveness of active and passive design strategies for existing building retrofits in tropical climate: Case study of a zero energy building. *J. Clean. Prod.* **2018**, *183*, 35–45. [CrossRef]
75. Aman, M.M.; Jasmon, G.B.; Mokhlis, H.; Bakar, A.H.A. Analysis of the performance of domestic lighting lamps. *Energy Policy* **2013**, *52*, 482–500. [CrossRef]
76. ISO. *Light and Lighting—Lighting of Work Places—Part 1: Indoor Work Places*; ISO: Geneva, Switzerland, 2011.
77. Sawicki, D.; Wolska, A. UGR for exterior working environment? Why not. In Proceedings of the 28th Session of the CIE, Manchester, UK, 28 June–4 July 2015; Volume 1, pp. 1617–1622.
78. Fumagalli, S.; Blaso, L.; Testa, A.; Ruggieri, G.; Ransen, O. EN 15193, Lighting Energy Numeric Indicator: LENICALC calculations in a retirement home case study. In Proceedings of the 2021 International Conference on Engineering and Emerging Technologies (ICEET), Istanbul, Turkey, 27–28 October 2021; pp. 1–6.
79. European Committee for Standardization. *15193-Energy Performance of Buildings—Energy Requirements for Lighting*; European Committee for Standardization: Brussels, Belgium, 2007.
80. Abdul Mujeebu, M.; Bano, F. Energy-saving potential and cost-effectiveness of active energy-efficiency measures for residential building in Warm-humid climate. *Energy Sustain. Dev.* **2022**, *67*, 163–176. [CrossRef]
81. Li, X.; Shen, C.; Yu, C.W.F. Building energy efficiency: Passive technology or active technology? *Indoor Built Environ.* **2017**, *26*, 729–732. [CrossRef]
82. Kastner, W.; Neugschwandtner, G.; Soucek, S.; Newman, H.M. Communication systems for building automation and control. *Proc. IEEE* **2005**, *93*, 1178–1203. [CrossRef]
83. Shaikh, P.H.; Nor, N.B.M.; Nallagownden, P.; Elamvazuthi, I.; Ibrahim, T. A review on optimized control systems for building energy and comfort management of smart sustainable buildings. *Renew. Sustain. Energy Rev.* **2014**, *34*, 409–429. [CrossRef]
84. Tsolakis, A.C.; Moschos, I.; Zerzelidis, A.; Tropios, P.; Zikos, S.; Tryferidis, A.; Krinidis, S.; Ioannidis, D.; Tzovaras, D. Occupancy-based decision support system for building management: From automation to end-user persuasion. *Int. J. Energy Res.* **2019**, *43*, 2261–2280. [CrossRef]
85. Martirano, L.; Mitolo, M. Guest Editorial: Energy Efficiency, Building Automation, Metering, and Microgrids in Industrial and Commercial Power Systems. *IEEE Trans. Ind. Appl.* **2019**, *55*, 6997–6998.
86. Harris, D. *A Guide to Energy Management in Buildings*; Routledge: Abingdon-on-Thames, UK, 2016.
87. Iwayemi, A.; Wan, W.; Zhou, C. Energy management for intelligent buildings. *Energy Manag. Syst.* **2011**. [CrossRef]
88. Edwards, R. Intelligent Buildings and Building Automation. *Constr. Manag. Econ.* **2011**, *29*, 216–217. [CrossRef]
89. Levermore, J.; Chong, W.B. Performance lines and energy signatures: Review and analysis. *Build. Serv. Eng. Res. Technol.* **1989**, *10*, 105–114. [CrossRef]
90. Merz, H.; Hansemann, T.; Hübner, C. *Building Automation: Communication Systems with EIB/KNX, LON and BACnet*, 2009; Springer: Berlin/Heidelberg, Germany, 2009.
91. Morris, A.S.; Langari, R. Chapter 10—Intelligent Devices. In *Measurement and Instrumentation (Second Edition)*; Academic Press: Boston, MA, USA, 2016; pp. 289–314. [CrossRef]
92. Manic, M.; Wijayasekara, D.; Amarasinghe, K.; Rodriguez-Andina, J.J. Building energy management systems: The age of intelligent and adaptive buildings. *IEEE Ind. Electron. Mag.* **2016**, *10*, 25–39. [CrossRef]
93. Braun, J.E. Intelligent building systems—Past, present, and future. In Proceedings of the 2007 American Control Conference, New York, NY, USA, 9–13 July 2007; pp. 4374–4381. [CrossRef]
94. Yu, S.; Lv, K.; Shao, Z.; Guo, Y.; Zou, J.; Zhang, B. A High Performance Blockchain Platform for Intelligent Devices. In Proceedings of the 2018 1st IEEE International Conference on Hot Information-Centric Networking (HotICN), Shenzhen, China, 15–17 August 2018; pp. 260–261. [CrossRef]
95. Bello, O.; Zeadally, S. Intelligent Device-to-Device Communication in the Internet of Things. *IEEE Syst. J.* **2016**, *10*, 1172–1182. [CrossRef]
96. Mohammad, R. AMI Smart Meter Big Data Analytics for Time Series of Electricity Consumption. In Proceedings of the 2018 17th IEEE International Conference on Trust, Security and Privacy in Computing and Communications/ 12th IEEE International

- Conference on Big Data Science and Engineering (TrustCom/BigDataSE), New York, NY, USA, 1–3 August 2018; pp. 1771–1776. [CrossRef]
97. Wang, Y.; Chen, Q.; Hong, T.; Kang, C. Review of Smart Meter Data Analytics: Applications, Methodologies, and Challenges. *IEEE Trans. Smart Grid* **2019**, *10*, 3125–3148. [CrossRef]
 98. Liang, Y.; Levine, D.I.; Shen, Z.-J.M. Thermostats for the smart grid: Models, benchmarks, and insights. *Energy J.* **2012**, *33*, 61–95. [CrossRef]
 99. Li, N.; Calis, G.; Becerik-Gerber, B. Measuring and monitoring occupancy with an RFID based system for demand-driven HVAC operations. *Autom. Constr.* **2012**, *24*, 89–99. [CrossRef]
 100. Agarwal, Y.; Balaji, B.; Gupta, R.; Lyles, J.; Wei, M.; Weng, T. Occupancy-driven energy management for smart building automation. In Proceedings of the 2nd ACM Workshop on Embedded Sensing Systems for Energy-Efficiency in Building, Zurich, Switzerland, 2 November 2010; pp. 1–6.
 101. Yang, R.; Newman, M.W. Living with an intelligent thermostat: Advanced control for heating and cooling systems. In Proceedings of the 2012 ACM Conference on Ubiquitous Computing, Pittsburgh, PA, USA, 5–8 September 2012; pp. 1102–1107.
 102. Magno, M.; Polonelli, T.; Benini, L.; Popovici, E. A low cost, highly scalable wireless sensor network solution to achieve smart LED light control for green buildings. *IEEE Sens. J.* **2014**, *15*, 2963–2973. [CrossRef]
 103. Seyedolhosseini, A.; Masoumi, N.; Modarressi, M.; Karimian, N. Daylight adaptive smart indoor lighting control method using artificial neural networks. *J. Build. Eng.* **2020**, *29*, 101141. [CrossRef]
 104. Wagiman, K.R.; Abdullah, M.N.; Hassan, M.Y.; Mohammad Radzi, N.H.; Abu Bakar, A.H.; Kwang, T.C. Lighting system control techniques in commercial buildings: Current trends and future directions. *J. Build. Eng.* **2020**, *31*, 101342. [CrossRef]
 105. Sharda, S.; Singh, M.; Sharma, K. Demand side management through load shifting in IoT based HEMS: Overview, challenges and opportunities. *Sustain. Cities Soc.* **2021**, *65*, 102517. [CrossRef]
 106. Fernández-Caramés, T.M. An intelligent power outlet system for the smart home of the internet of things. *Int. J. Distrib. Sens. Netw.* **2015**, *2015*, 214805. [CrossRef]
 107. Aheleroff, S.; Xu, X.; Lu, Y.; Aristizabal, M.; Velásquez, J.P.; Joa, B.; Valencia, Y. IoT-enabled smart appliances under industry 4.0: A case study. *Adv. Eng. Inform.* **2020**, *43*, 101043. [CrossRef]
 108. Piette, M.A.; Ghatikar, G.; Kiliccote, S.; Watson, D.; Koch, E.; Hennage, D. Design and operation of an open, interoperable automated demand response infrastructure for commercial buildings. *J. Comput. Inf. Sci. Eng.* **2009**, *9*, 1–9. [CrossRef]
 109. Franco, P.; Martinez, J.M.; Kim, Y.C.; Ahmed, M.A. IoT Based Approach for Load Monitoring and Activity Recognition in Smart Homes. *IEEE Access* **2021**, *9*, 45325–45339. [CrossRef]
 110. Islam, R.; Rahman, M.W.; Rubaiat, R.; Hasan, M.M.; Reza, M.M.; Rahman, M.M. LoRa and server-based home automation using the internet of things (IoT). *J. King Saud Univ. -Comput. Inf. Sci.* **2021**, *34*, 3703–3712. [CrossRef]
 111. Andrade, S.H.M.; Contente, G.O.; Rodrigues, L.B.; Lima, L.X.; Vijaykumar, N.L.; Frances, C.R.L. A Smart Home Architecture for Smart Energy Consumption in a Residence with Multiple Users. *IEEE Access* **2021**, *9*, 16807–16824. [CrossRef]
 112. Nižetić, S.; Šolić, P.; López-de-Ipiña González-de-Artaza, D.; Patrono, L. Internet of Things (IoT): Opportunities, issues and challenges towards a smart and sustainable future. *J. Clean. Prod.* **2020**, *274*, 122877. [CrossRef]
 113. Wells, J.; Haas, D. *Electricity Markets: Consumers Could Benefit from Demand Programs, But Challenges Remain*; DIANE Publishing: Collingdale, PA, USA, 2004.
 114. Alstone, P.; Potter, J.; Piette, M.A.; Schwartz, P.; Berger, M.A.; Dunn, L.N.; Smith, S.J.; Sohn, M.D.; Aghajanzadeh, A.; Stensson, S.; et al. *2025 California Demand Response Potential Study—Charting California’s Demand Response Future. Final Report on Phase 2 Results*; Lawrence Berkeley National Lab: Berkeley, CA, USA, 2017.
 115. Deng, R.; Yang, Z.; Chow, M.-Y.; Chen, J. A survey on demand response in smart grids: Mathematical models and approaches. *IEEE Trans. Ind. Inform.* **2015**, *11*, 570–582. [CrossRef]
 116. Parizy, E.S.; Bahrami, H.R.; Choi, S. A Low Complexity and Secure Demand Response Technique for Peak Load Reduction. *IEEE Trans. Smart Grid* **2019**, *10*, 3259–3268. [CrossRef]
 117. Costanzo, G.T.; Zhu, G.; Anjos, M.F.; Savard, G. A system architecture for autonomous demand side load management in smart buildings. *IEEE Trans. Smart Grid* **2012**, *3*, 2157–2165. [CrossRef]
 118. Arun, S.L.; Selvan, M.P. Intelligent Residential Energy Management System for Dynamic Demand Response in Smart Buildings. *IEEE Syst. J.* **2018**, *12*, 1329–1340. [CrossRef]
 119. Esmael Nezhad, A.; Rahimnejad, A.; Gadsden, S.A. Home energy management system for smart buildings with inverter-based air conditioning system. *Int. J. Electr. Power Energy Syst.* **2021**, *133*, 107230. [CrossRef]
 120. Tang, S.; Huang, Q.; Li, X.Y.; Wu, D. Smoothing the energy consumption: Peak demand reduction in smart grid. In Proceedings of the 2013 Proceedings IEEE INFOCOM, Turin, Italy, 14–19 April 2013; pp. 1133–1141. [CrossRef]
 121. Mehr Nezhad, M.; Moghaddam, M.H.Y.; Asadi, M. Joint Peak Clipping and Load Scheduling Based on User Behavior Monitoring in an IoT Platform. *IEEE Syst. J.* **2021**, *15*, 1202–1213. [CrossRef]
 122. Wang, P.; Liu, Z.; Zhang, L. Sustainability of compact cities: A review of Inter-Building Effect on building energy and solar energy use. *Sustain. Cities Soc.* **2021**, *72*, 103035. [CrossRef]
 123. Ren, H.; Sun, Y.; Alldoor, A.K.; Tyagi, V.V.; Pandey, A.K.; Ma, Z. Improving energy flexibility of a net-zero energy house using a solar-assisted air conditioning system with thermal energy storage and demand-side management. *Appl. Energy* **2021**, *285*, 116433. [CrossRef]

124. Shareef, H.; Al-Hassan, E.; Sirjani, R. Wireless home energy management system with smart rule-based controller. *Appl. Sci.* **2020**, *10*, 4533. [CrossRef]
125. Zhang, X.; Adhikari, R.; Pipattanasomporn, M.; Kuzlu, M.; Bradley, S.R. Deploying IoT devices to make buildings smart: Performance evaluation and deployment experience. In Proceedings of the 2016 IEEE 3rd World Forum Internet Things, WF-IoT 2016, Reston, VA, USA, 12–14 December 2016; pp. 530–535. [CrossRef]
126. Mahmud, K.; Hossain, M.J.; Town, G.E. Peak-Load Reduction by Coordinated Response of Photovoltaics, Battery Storage, and Electric Vehicles. *IEEE Access* **2018**, *6*, 29353–29365. [CrossRef]
127. Macarulla, M.; Casals, M.; Forcada, N.; Gangoells, M. Implementation of predictive control in a commercial building energy management system using neural networks. *Energy Build.* **2017**, *151*, 511–519. [CrossRef]
128. Krishna Prakash, N.; Prasanna Vadana, D. Machine Learning Based Residential Energy Management System. In Proceedings of the 2017 IEEE International Conference on Computational Intelligence and Computing Research (ICIC), Coimbatore, India, 14–16 December 2017. [CrossRef]
129. Moradzadeh, A.; Mohammadi-Ivatloo, B.; Abapour, M.; Anvari-Moghaddam, A.; Roy, S.S. Heating and Cooling Loads Forecasting for Residential Buildings Based on Hybrid Machine Learning Applications: A Comprehensive Review and Comparative Analysis. *IEEE Access* **2022**, *10*, 2196–2215. [CrossRef]
130. Hafeez, G.; Alimgeer, K.S.; Wadud, Z.; Khan, I.; Usman, M.; Qazi, A.B.; Khan, F.A. An innovative optimization strategy for efficient energy management with day-ahead demand response signal and energy consumption forecasting in smart grid using artificial neural network. *IEEE Access* **2020**, *8*, 84415–84433. [CrossRef]
131. Dong, C.; Sun, J.; Wu, F.; Jia, H. Probability-Based Energy Reinforced Management of Electric Vehicle Aggregation in the Electrical Grid Frequency Regulation. *IEEE Access* **2020**, *8*, 110598–110610. [CrossRef]
132. Sturzenegger, D.; Gyalistras, D.; Morari, M.; Smith, R.S. Model predictive climate control of a swiss office building: Implementation, results, and cost-benefit analysis. *IEEE Trans. Control Syst. Technol.* **2015**, *24*, 1–12. [CrossRef]
133. Wang, B.; Li, Y.; Ming, W.; Wang, S. Deep Reinforcement Learning Method for Demand Response Management of Interruptible Load. *IEEE Trans. Smart Grid* **2020**, *11*, 3146–3155. [CrossRef]
134. Shapi, M.K.M.; Ramli, N.A.; Awalin, L.J. Energy consumption prediction by using machine learning for smart building: Case study in Malaysia. *Dev. Built Environ.* **2021**, *5*, 100037. [CrossRef]
135. Zhang, X.; Pipattanasomporn, M.; Chen, T.; Rahman, S. An IoT-Based Thermal Model Learning Framework for Smart Buildings. *IEEE Internet Things J.* **2020**, *7*, 518–527. [CrossRef]
136. Truong, L.H.M.; Chow, K.H.K.; Luevisadpaibul, R.; Thirunavukkarasu, G.S.; Seyedmahmoudian, M.; Horan, B.; Mekhilef, S.; Stojcevski, A. Accurate prediction of hourly energy consumption in a residential building based on the occupancy rate using machine learning approaches. *Appl. Sci.* **2021**, *11*, 2229. [CrossRef]
137. Kumari, A.; Tanwar, S. AI-based Peak Load Reduction Approach for Residential Buildings using Reinforcement Learning. In Proceedings of the 2021 International Conference on Computing, Communication, and Intelligent Systems (ICCCIS), Greater Noida, India, 19–20 February 2021; pp. 972–977.
138. Cao, Y.; Du, J.; Soleymanzadeh, E. Model predictive control of commercial buildings in demand response programs in the presence of thermal storage. *J. Clean. Prod.* **2019**, *218*, 315–327. [CrossRef]
139. Wang, J.; Li, S.; Chen, H.; Yuan, Y.; Huang, Y. Data-driven model predictive control for building climate control: Three case studies on different buildings. *Build. Environ.* **2019**, *160*, 106204. [CrossRef]
140. Razmara, M.; Bharati, G.R.; Hanover, D.; Shahbakhti, M.; Paudyal, S.; Robinett, R.D., III. Building-to-grid predictive power flow control for demand response and demand flexibility programs. *Appl. Energy* **2017**, *203*, 128–141. [CrossRef]
141. Si, B.; Tian, Z.; Jin, X.; Zhou, X.; Tang, P.; Shi, X. Performance indices and evaluation of algorithms in building energy efficient design optimization. *Energy* **2016**, *114*, 100–112. [CrossRef]
142. Bamdad, K.; Cholette, M.E.; Guan, L.; Bell, J. Ant colony algorithm for building energy optimisation problems and comparison with benchmark algorithms. *Energy Build.* **2017**, *154*, 404–414. [CrossRef]
143. Akay, B.; Karaboga, D.; Gorkemli, B.; Kaya, E. A survey on the Artificial Bee Colony algorithm variants for binary, integer and mixed integer programming problems. *Appl. Soft Comput.* **2021**, *106*, 107351. [CrossRef]
144. Dorigo, M.; Stützle, T. Ant colony optimization: Overview and recent advances. In *Handbook of Metaheuristics*; Springer: Berlin/Heidelberg, Germany, 2019; pp. 311–351.
145. Okonta, C.I.; Kemp, A.H.; Edopkia, R.O.; Monyei, G.C.; Okelue, E.D. A heuristic based ant colony optimization algorithm for energy efficient smart homes. In Proceedings of the 5th International Conference & Exhibition on Clean Energy, Montreal, QC, Canada, 22–24 August 2016; pp. 1–12.
146. Zhou, G.; Moayedi, H.; Bahiraei, M.; Lyu, Z. Employing artificial bee colony and particle swarm techniques for optimizing a neural network in prediction of heating and cooling loads of residential buildings. *J. Clean. Prod.* **2020**, *254*, 120082. [CrossRef]
147. Zhang, Y.; Zeng, P.; Zang, C. Optimization algorithm for home energy management system based on artificial bee colony in smart grid. In Proceedings of the 2015 IEEE International Conference on Cyber Technology in Automation, Control, and Intelligent Systems (CYBER), Shenyang, China, 8–12 June 2015; pp. 734–740.
148. Wahid, F.; Ghazali, R.; Ismail, L.H. An Enhanced Approach of Artificial Bee Colony for Energy Management in Energy Efficient Residential Building. *Wirel. Pers. Commun.* **2019**, *104*, 235–257. [CrossRef]

149. Niazi, G.; Lalwani, M. PSO based optimal distributed generation placement and sizing in power distribution networks: A comprehensive review. In Proceedings of the 2017 International Conference on Computer, Communications and Electronics (Comptelix), Jaipur, India, 1–2 July 2017; pp. 305–311.
150. Naseem, M.; Abid, S.; Khalid, R.; Hafeez, G.; Mahboob, S. Towards Heuristic Algorithms: GA, WDO, BPSO, and BFOA for Home Energy Management in Smart Grid. In *Advances on Broad-Band Wireless Computing, Communication and Applications*; Springer: Berlin/Heidelberg, Germany, 2018; pp. 267–278. [CrossRef]
151. Zhu, J.; Lauri, F.; Koukam, A.; Hilaire, V. Scheduling optimization of smart homes based on demand response. In Proceedings of the IFIP International Conference on Artificial Intelligence Applications and Innovations, Bayonne, France, 14–17 September 2015; pp. 223–236.
152. Hossain, M.A.; Pota, H.R.; Squartini, S.; Abdou, A.F. Modified PSO algorithm for real-time energy management in grid-connected microgrids. *Renew. Energy* **2019**, *136*, 746–757. [CrossRef]
153. Mirjalili, S. Genetic algorithm. In *Evolutionary Algorithms and Neural Networks*; Springer: Berlin/Heidelberg, Germany, 2019; pp. 43–55.
154. Lin, C.-S.; Lee, I.-L.; Wu, M.-C. Merits of using chromosome representations and shadow chromosomes in genetic algorithms for solving scheduling problems. *Robot. Comput. Integr. Manuf.* **2019**, *58*, 196–207. [CrossRef]
155. Liemthong, R.; Srithapon, C.; Ghosh, P.K.; Chatthaworn, R. Home Energy Management Strategy-Based Meta-Heuristic Optimization for Electrical Energy Cost Minimization Considering TOU Tariffs. *Energies* **2022**, *15*, 537. [CrossRef]
156. Liemthong, R.; Srithapon, C.; Ghosh, P.K.; Chatthaworn, R. Home Energy Management Strategy-Based Meta-Heuristic Optimization for Electrical Energy Cost Minimization Considering TOU Tariffs. *Energies* **2022**, *15*, 537S. [CrossRef]
157. Sarker, E.; Halder, P.; Seyedmahmoudian, M.; Jamei, E.; Horan, B.; Mekhilef, S.; Stojcevski, A. Progress on the demand side management in smart grid and optimization approaches. *Int. J. Energy Res.* **2021**, *45*, 36–64. [CrossRef]
158. Khan, Z.A.; Zafar, A.; Javaid, S.; Aslam, S.; Rahim, M.H.; Javaid, N. Hybrid meta-heuristic optimization based home energy management system in smart grid. *J. Ambient Intell. Humaniz. Comput.* **2019**, *10*, 4837–4853. [CrossRef]
159. Ullah, I.; Rasheed, M.B.; Alquthami, T.; Tayyaba, S. A Residential Load Scheduling with the Integration of On-Site PV and Energy Storage Systems in Micro-Grid. *Sustainability* **2020**, *12*, 184. [CrossRef]
160. Chellamani, G.K.; Chandramani, P.V. An optimized methodical energy management system for residential consumers considering price-driven demand response using satin bowerbird optimization. *J. Electr. Eng. Technol.* **2020**, *15*, 955–967. [CrossRef]
161. Aslam, S.; Iqbal, Z.; Javaid, N.; Khan, Z.A.; Aurangzeb, K.; Haider, S.I. Towards efficient energy management of smart buildings exploiting heuristic optimization with real time and critical peak pricing schemes. *Energies* **2017**, *10*, 2065. [CrossRef]
162. Imran, A.; Hafeez, G.; Khan, I.; Usman, M.; Shafiq, Z.; Qazi, A.B.; Khalid, A.; Thoben, K.-D. Heuristic-based programmable controller for efficient energy management under renewable energy sources and energy storage system in smart grid. *IEEE Access* **2020**, *8*, 139587–139608. [CrossRef]
163. Javaid, N.; Naseem, M.; Rasheed, M.B.; Mahmood, D.; Khan, S.A.; Alrajeh, N.; Iqbal, Z. A new heuristically optimized Home Energy Management controller for smart grid. *Sustain. Cities Soc.* **2017**, *34*, 211–227. [CrossRef]
164. Ahmed, M.S.; Mohamed, A.; Khatib, T.; Shareef, H.; Homod, R.Z.; Abd Ali, J. Real time optimal schedule controller for home energy management system using new binary backtracking search algorithm. *Energy Build.* **2017**, *138*, 215–227. [CrossRef]
165. Nazeer, O.; Javaid, N.; Rafique, A.A.; Kiani, S.; Javaid, Y.; Khurshid, Z. Home energy management using hybrid meta-heuristic optimization technique. In *Innovative Mobile and Internet Services in Ubiquitous Computing*; Springer: Berlin/Heidelberg, Germany, 2018; pp. 599–609.
166. Latifah, A.; Supangkat, S.H.; Ramelan, A. Smart Building: A Literature Review. In Proceedings of the 7th International Conference on ICT for Smart Society (ICISS), Bandung, Indonesia, 19–20 November 2020. [CrossRef]
167. Kiljander, J.; Sarala, R.; Rehu, J.; Pakkala, D.; Paakkonen, P.; Takalo-Mattila, J.; Kansala, K. Intelligent Consumer Flexibility Management with Neural Network-Based Planning and Control. *IEEE Access* **2021**, *9*, 40755–40767. [CrossRef]
168. Megahed, T.F.; Abdelkader, S.M.; Zakaria, A. Energy Management in Zero-Energy Building Using Neural Network Predictive Control. *IEEE Internet Things J.* **2019**, *6*, 5336–5344. [CrossRef]
169. Reynolds, J.; Rezgui, Y.; Kwan, A.; Piriou, S. A zone-level, building energy optimisation combining an artificial neural network, a genetic algorithm, and model predictive control. *Energy* **2018**, *151*, 729–739. [CrossRef]
170. Kim, S.; Mowakea, R.; Kim, S.J.; Lim, H. Building energy management for demand response using kernel lifelong learning. *IEEE Access* **2020**, *8*, 82131–82141. [CrossRef]
171. Rocha, H.R.O.; Honorato, I.H.; Fiorotti, R.; Celeste, W.C.; Silvestre, L.J.; Silva, J.A.L. An Artificial Intelligence based scheduling algorithm for demand-side energy management in Smart Homes. *Appl. Energy* **2021**, *282*, 116145. [CrossRef]
172. Nagpal, H.; Avramidis, I.I.; Capitanescu, F.; Heiselberg, P. Optimal energy management in smart sustainable buildings—A chance-constrained model predictive control approach. *Energy Build.* **2021**, *248*, 111163. [CrossRef]
173. Zhang, C.; Wu, W.; Huang, H.; Yu, H. Fair energy resource allocation by minority game algorithm for smart buildings. In Proceedings of the 2012 Design, Automation & Test in Europe Conference & Exhibition (DATE), Dresden, Germany, 12–16 March 2012; pp. 63–68. [CrossRef]
174. Al-Ghaili, A.M.; Kasim, H.; Al-Hada, N.M.; Jorgensen, B.N.; Othman, M.; Jihua, W. Energy Management Systems and Strategies in Buildings Sector: A Scoping Review. *IEEE Access* **2021**, *9*, 63790–63813. [CrossRef]

175. Tripathy, M.; Sadhu, P.K.; Panda, S.K. A critical review on building integrated photovoltaic products and their applications. *Renew. Sustain. Energy Rev.* **2016**, *61*, 451–465. [CrossRef]
176. Pillai, D.S.; Shabunko, V.; Krishna, A. A comprehensive review on building integrated photovoltaic systems: Emphasis to technological advancements, outdoor testing, and predictive maintenance. *Renew. Sustain. Energy Rev.* **2022**, *156*, 111946. [CrossRef]
177. Jelle, B.P.; Breivik, C. State-of-the-art building integrated photovoltaics. *Energy Procedia* **2012**, *20*, 68–77. [CrossRef]
178. Norton, B.; Eames, P.C.; Mallick, T.K.; Huang, M.J.; McCormack, S.J.; Mondol, J.D.; Yohanis, Y.G. Enhancing the performance of building integrated photovoltaics. *Sol. Energy* **2011**, *85*, 1629–1664. [CrossRef]
179. Benemann, J.; Chehab, O.; Schaar-Gabriel, E. Building-integrated PV modules. *Sol. Energy Mater. Sol. Cells* **2001**, *67*, 345–354. [CrossRef]
180. Heinstejn, P.; Ballif, C.; Perret-Aebi, L.-E. Building integrated photovoltaics (BIPV): Review, potentials, barriers and myths. *Green* **2013**, *3*, 125–156. [CrossRef]
181. Zhang, X.; Lau, S.-K.; Lau, S.S.Y.; Zhao, Y. Photovoltaic integrated shading devices (PVSDs): A review. *Sol. Energy* **2018**, *170*, 947–968. [CrossRef]
182. Jelle, B.P.; Breivik, C.; Drolsum Røkenes, H. Building integrated photovoltaic products: A state-of-the-art review and future research opportunities. *Sol. Energy Mater. Sol. Cells* **2012**, *100*, 69–96. [CrossRef]
183. Agathokleous, R.A.; Kalogirou, S.A. Status, barriers and perspectives of building integrated photovoltaic systems. *Energy* **2020**, *191*, 116471. [CrossRef]
184. Shukla, A.K.; Sudhakar, K.; Baredar, P. A comprehensive review on design of building integrated photovoltaic system. *Energy Build.* **2016**, *128*, 99–110. [CrossRef]
185. Gholami, H.; Nils Røstvik, H.; Steemers, K. The Contribution of Building-Integrated Photovoltaics (BIPV) to the Concept of Nearly Zero-Energy Cities in Europe: Potential and Challenges Ahead. *Energies* **2021**, *14*, 6015. [CrossRef]
186. Tominaga, M. Opportunities for Thin Film Photovoltaics in Building Integrated Photovoltaics (BIPV) with a Focus on Australia. Doctoral Dissertation, Murdoch University, Perth, Australia, 2009.
187. Strong, S. Building integrated photovoltaics. *Sol. Des. Assoc.* **2005**, *11*.
188. Al Dakheel, J.; Del Pero, C.; Aste, N.; Leonforte, F. Smart buildings features and key performance indicators: A review. *Sustain. Cities Soc.* **2020**, *61*, 102328. [CrossRef]
189. Tumminia, G.; Guarino, F.; Longo, S.; Aloisio, D.; Cellura, S.; Sergi, F.; Brunaccini, G.; Antonucci, V.; Ferraro, M. Grid interaction and environmental impact of a net zero energy building. *Energy Convers. Manag.* **2020**, *203*, 112228. [CrossRef]
190. Wei, W.; Skye, H.M. Residential net-zero energy buildings: Review and perspective. *Renew. Sustain. Energy Rev.* **2021**, *142*, 110859. [CrossRef]
191. Arabkoohsar, A.; Behzadi, A.; Nord, N. A highly innovative yet cost-effective multi-generation energy system for net-zero energy buildings. *Energy Convers. Manag.* **2021**, *237*, 114120. [CrossRef]
192. U.S. Department of Energy by the National Institute of Building Science. *A Common Definition for Zero Energy Buildings*; U.S. Department of Energy by the National Institute of Building Science: Washington, DC, USA, 2015.
193. Azis, S.S.A. Improving present-day energy savings among green building sector in Malaysia using benefit transfer approach: Cooling and lighting loads. *Renew. Sustain. Energy Rev.* **2021**, *137*, 110570. [CrossRef]
194. Chartered Institution of Building Services Engineers. *Energy Efficiency in Buildings*; Chartered Institution of Building Services Engineers: London, UK, 2004.
195. Miller, W.; Crompton, G.; Bell, J. Analysis of Cool Roof Coatings for Residential Demand Side Management in Tropical Australia. *Energies* **2015**, *8*, 5303–5318. [CrossRef]
196. Sun, B.; Luh, P.B.; Jia, Q.-S.; Jiang, Z.; Wang, F.; Song, C. Building energy management: Integrated control of active and passive heating, cooling, lighting, shading, and ventilation systems. *IEEE Trans. Autom. Sci. Eng.* **2012**, *10*, 588–602.
197. Han, H.J.; Mehmood, M.U.; Ahmed, R.; Kim, Y.; Dutton, S.; Lim, S.H.; Chun, W. An advanced lighting system combining solar and an artificial light source for constant illumination and energy saving in buildings. *Energy Build.* **2019**, *203*, 109404. [CrossRef]
198. Jones, W.P. *Air Conditioning Engineering*; Routledge: Abingdon-on-Thames, UK, 2007.
199. Liu, J.; Zhang, W.; Liu, Y. Primary frequency response from the control of LED lighting loads in commercial buildings. *IEEE Trans. Smart Grid* **2016**, *8*, 2880–2889. [CrossRef]
200. Pellegrino, A.; Lo Verso, V.R.M.; Blaso, L.; Acquaviva, A.; Patti, E.; Osello, A. Lighting control and monitoring for energy efficiency: A case study focused on the interoperability of building management systems. *IEEE Trans. Ind. Appl.* **2016**, *52*, 2627–2637. [CrossRef]
201. Williams, A.; Atkinson, B.; Garbesi, K.; Page, E.; Rubinstein, F. Lighting controls in commercial buildings. *Leukos* **2012**, *8*, 161–180. [CrossRef]
202. Levermore, G.J. *Building Energy Management System: Applications to Low-Energy HVAC and Natural Ventilation Control*; E & FN Spon: London, UK, 2000.
203. Mariaud, A.; Acha, S.; Ekins-Daukes, N.; Shah, N.; Markides, C.N. Integrated optimisation of photovoltaic and battery storage systems for UK commercial buildings. *Appl. Energy* **2017**, *199*, 466–478. [CrossRef]
204. Hesse, H.C.; Martins, R.; Musilek, P.; Naumann, M.; Truong, C.N.; Jossen, A. Economic optimization of component sizing for residential battery storage systems. *Energies* **2017**, *10*, 835. [CrossRef]

205. Long, M.; Simpkins, T.; Cutler, D.; Anderson, K. A statistical analysis of the economic drivers of battery energy storage in commercial buildings. In Proceedings of the 48th North American Power Symposium (NAPS), Denver, CO, USA, 18–20 September 2016. [CrossRef]
206. Zhang, Y.; Zhang, X.; Huang, P.; Sun, Y. Global sensitivity analysis for key parameters identification of net-zero energy buildings for grid interaction optimization. *Appl. Energy* **2020**, *279*, 115820. [CrossRef]
207. Apte, M.G. *A Review of Demand Control Ventilation*; LBNL-60170 Report; Lawrence Berkeley National Laboratory: Berkeley, CA, USA, 2006; Volume 4, pp. 371–376.
208. Fisk, W.J.; Faulkner, D.; Sullivan, D.P. Measuring outdoor airflow into HVAC systems. *ASHRAE J.* **2005**, *48*, LBNL-58753.
209. Aktacir, M.A.; Büyükalaca, O.; Yilmaz, T. Life-cycle cost analysis for constant-air-volume and variable-air-volume air-conditioning systems. *Appl. Energy* **2006**, *83*, 606–627. [CrossRef]
210. Hesaraki, A.; Huda, N. A comparative review on the application of radiant low-temperature heating and high-temperature cooling for energy, thermal comfort, indoor air quality, design and control. *Sustain. Energy Technol. Assess.* **2021**, *49*, 101661. [CrossRef]
211. Emmerich, S.J.; Persily, A.K. *State-of-the-Art Review of CO2 Demand Controlled Ventilation Technology and Application*, NISTIR 6729; US National Institute of Standards and Technology: Gaithersburg, MD, USA, 2001.
212. Cho, W.; Song, D.; Hwang, S.; Yun, S. Energy-efficient ventilation with air-cleaning mode and demand control in a multi-residential building. *Energy Build.* **2015**, *90*, 6–14. [CrossRef]
213. Bhatia, A. *HVAC—Guide to Demand Control Ventilation*; Continuing Education and Development, Inc.: Woodcliff Lake, NJ, USA, 2014; ISBN 978-1502485656.
214. Zhang, B.; Li, Y.; Lau, J.; Liu, M. Demand control ventilation: Influence of terminal box minimum airflow setting on system energy use. *Energy Build.* **2014**, *79*, 173–183. [CrossRef]
215. Yang, Y.; Srinivasan, S.; Hu, G.; Spanos, C.J. Distributed Control of Multizone HVAC Systems Considering Indoor Air Quality. *IEEE Trans. Control Syst. Technol.* **2021**, *29*, 2586–2597. [CrossRef]
216. Hesaraki, A.; Holmberg, S. Demand-controlled ventilation in new residential buildings: Consequences on indoor air quality and energy savings. *Indoor Built Environ.* **2015**, *24*, 162–173. [CrossRef]
217. Liu, G.; Dasu, A.R.; Zhang, J. *Review of Literature on Terminal Box Control, Occupancy Sensing Technology and Multi-Zone Demand Control Ventilation (DCV)*; Pacific Northwest National Laboratory: Washington, DC, USA, 2012.
218. Moyer, J.D.; Hedden, S. Are we on the right path to achieve the sustainable development goals? *World Dev.* **2020**, *127*, 104749. [CrossRef]
219. Parvin, K.; Lipu, M.S.H.; Hannan, M.A.; Abdullah, M.A.; Jern, K.P.; Begum, R.A.; Mansur, M.; Muttaqi, K.M.; Mahlia, T.M.I.; Dong, Z.Y. Intelligent Controllers and Optimization Algorithms for Building Energy Management Towards Achieving Sustainable Development: Challenges and Prospects. *IEEE Access* **2021**, *9*, 41577–41600. [CrossRef]
220. ONU. Sustainable Development Goals: Guidelines for the Use of the SDG Logo. *United Nations Department of Global Communications*. May 2020, pp. 1–68. Available online: <https://www.un.org/sustainabledevelopment/news/communications-material/> (accessed on 3 October 2021).
221. Liu, Y.; Wang, Y.; Luo, X. Design and operation optimization of distributed solar energy system based on dynamic operation strategy. *Energies* **2021**, *14*, 69. [CrossRef]
222. Somu, N.; Gauthama Raman, M.R.; Ramamritham, K. A hybrid model for building energy consumption forecasting using long short term memory networks. *Appl. Energy* **2020**, *261*, 114131. [CrossRef]
223. Benefits of Green Buildings. Available online: https://www.worldgbc.org/bene_ts-green-buildings (accessed on 21 January 2020).
224. Pisacane, O.; Severini, M.; Fagiani, M.; Squartini, S. Collaborative energy management in a micro-grid by multi-objective mathematical programming. *Energy Build.* **2019**, *203*, 109432. [CrossRef]
225. Copiello, S. Economic parameters in the evaluation studies focusing on building energy efficiency: A review of the underlying rationale, data sources, and assumptions. *Energy Procedia* **2019**, *157*, 180–192. [CrossRef]
226. Tang, R.; Wang, S.; Li, H. Game theory based interactive demand side management responding to dynamic pricing in price-based demand response of smart grids. *Appl. Energy* **2019**, *250*, 118–130. [CrossRef]
227. Balaras, C.; Gaglia, A.G.; Sarafidis, Y. Evaluating the need for economic support policies in promoting greenhouse gas emission reduction measures in the building sector: The case of Greece. *Energy Policy* **2006**, *34*, 2012–2031. [CrossRef]
228. Shareef, H.; Ahmed, M.S.; Mohamed, A.; Al Hassan, E. Review on home energy management system considering demand responses, smart technologies, and intelligent controllers. *IEEE Access* **2018**, *6*, 24498–24509. [CrossRef]
229. Majeed, U.; Khan, L.U.; Yaqoob, I.; Kazmi, S.M.A.; Salah, K.; Hong, C.S. Blockchain for IoT-based smart cities: Recent advances, requirements, and future challenges. *J. Netw. Comput. Appl.* **2021**, *181*, 103007. [CrossRef]
230. Kumar, A.; Sharma, S.; Goyal, N.; Singh, A.; Cheng, X.; Singh, P. Secure and energy-efficient smart building architecture with emerging technology IoT. *Comput. Commun.* **2021**, *176*, 207–217. [CrossRef]
231. Ali, M.; Prakash, K.; Hossain, M.A.; Pota, H.R. Intelligent energy management: Evolving developments, current challenges, and research directions for sustainable future. *J. Clean. Prod.* **2021**, *314*, 127904. [CrossRef]
232. Jia, C.; Ding, H.; Zhang, C.; Zhang, X. Design of a dynamic key management plan for intelligent building energy management system based on wireless sensor network and blockchain technology. *Alex. Eng. J.* **2021**, *60*, 337–346. [CrossRef]

233. Iqbal, S.; Sarfraz, M.; Ayyub, M.; Tariq, M.; Chakraborty, R.; Ryan, M.; Alamri, B. A Comprehensive Review on Residential Demand Side Management Strategies in Smart Grid Environment. *Sustainability* **2021**, *13*, 7170. [CrossRef]
234. Haley, B.; Gaede, J.; Winfield, M.; Love, P. From utility demand side management to low-carbon transitions: Opportunities and challenges for energy efficiency governance in a new era. *Energy Res. Soc. Sci.* **2020**, *59*, 101312. [CrossRef]
235. Sulaima, M.F.; Dahlan, N.Y.; Yasin, Z.M.; Rosli, M.M.; Omar, Z.; Hassan, M.Y. A review of electricity pricing in peninsular Malaysia: Empirical investigation about the appropriateness of Enhanced Time of Use (ETOU) electricity tariff. *Renew. Sustain. Energy Rev.* **2019**, *110*, 348–367. [CrossRef]
236. Vidyamani, T.; Swarup, K.S. Analysis of Active and Transactive Demand Response Strategies for Smart Residential Buildings. In Proceedings of the 2018 20th National Power Systems Conference (NPSC), Tiruchirappalli, India, 14–16 December 2018; pp. 3–7. [CrossRef]
237. Warren, P. A review of demand-side management policy in the UK. *Renew. Sustain. Energy Rev.* **2014**, *29*, 941–951. [CrossRef]
238. Warren, P. The use of systematic reviews to analyse demand-side management policy. *Energy Effic.* **2014**, *7*, 417–427. [CrossRef]
239. Bergaentzle, C.; Clastres, C.; Khalfallah, H. Demand-side management and European environmental and energy goals: An optimal complementary approach. *Energy Policy* **2014**, *67*, 858–869. [CrossRef]
240. Palensky, P.; Dietrich, D. Demand side management: Demand response, intelligent energy systems, and smart loads. *IEEE Trans. Ind. Inform.* **2011**, *7*, 381–388. [CrossRef]
241. Sani, S.B.; Celvakumaran, P.; Ramachandaramurthy, V.K.; Walker, S.; Alrazi, B.; Ying, Y.J.; Dahlan, N.Y.; Rahman, M.H.A. Energy storage system policies: Way forward and opportunities for emerging economies. *J. Energy Storage* **2020**, *32*, 101902. [CrossRef]
242. Khan, I. Energy-saving behaviour as a demand-side management strategy in the developing world: The case of Bangladesh. *Int. J. Energy Environ. Eng.* **2019**, *10*, 493–510. [CrossRef]
243. Bai, X.; Thong, G.; Alvina, P. Demand Side Management Solutions Study in Singapore Market. In Proceedings of the 2018 Asian Conference on Energy, Power and Transportation Electrification (ACEPT), Singapore, 30 October–2 November 2018; pp. 1–6.
244. Wang, Y.; Song, Z.; De Angelis, V.; Srivastava, S. Battery life-cycle optimization and runtime control for commercial buildings Demand side management: A New York City case study. *Energy* **2018**, *165*, 782–791. [CrossRef]
245. Alasser, R.; Tripathi, A.; Joji Rao, T.; Sreekanth, K.J. A review on implementation strategies for demand side management (DSM) in Kuwait through incentive-based demand response programs. *Renew. Sustain. Energy Rev.* **2017**, *77*, 617–635. [CrossRef]
246. Zhang, S.; Jiao, Y.; Chen, W. Demand-side management (DSM) in the context of China’s on-going power sector reform. *Energy Policy* **2017**, *100*, 1–8. [CrossRef]
247. Zhao, Z.; Yu, C.; Yew, M.; Liu, M. Demand side management: A green way to power Beijing. *J. Renew. Sustain. Energy* **2015**, *7*, 41505. [CrossRef]
248. Harish, V.S.K.V.; Kumar, A. Demand side management in India: Action plan, policies and regulations. *Renew. Sustain. Energy Rev.* **2014**, *33*, 613–624. [CrossRef]
249. Monyei, C.G.; Adewumi, A.O. Demand Side Management potentials for mitigating energy poverty in South Africa. *Energy Policy* **2017**, *111*, 298–311. [CrossRef]
250. Zurn, H.H.; Tenfen, D.; Rolim, J.G.; Richter, A.; Hauer, I. Electrical energy demand efficiency efforts in Brazil, past, lessons learned, present and future: A critical review. *Renew. Sustain. Energy Rev.* **2017**, *67*, 1081–1086. [CrossRef]
251. E. and R. Australian Government, Department of Industry, Science. Available online: <https://www.energy.gov.au/business/energy-management-business/large-energy-users/energy-procurement/demand-side-opportunities> (accessed on 25 January 2020).
252. Tanatvanit, S.; Limmeechokchai, B.; Shrestha, R.M. CO2 mitigation and power generation implications of clean supply-side and demand-side technologies in Thailand. *Energy Policy* **2004**, *32*, 83–90. [CrossRef]
253. Khalid, H.; Amin, F.R.; Chen, C. Comparing the status and challenges of demand-side management (DSM) implementation in Asia-Pacific region: A case study of China’s power sector. *Energy Procedia* **2018**, *152*, 101–108. [CrossRef]
254. Wijaya, M.E.; Limmeechokchai, B. Demand side management options in the household sector through lighting efficiency improvement for Java-Madura-Bali Islands in Indonesia. *J. Sustain. Energy Environ.* **2010**, *1*, 111–115.

Disclaimer/Publisher’s Note: The statements, opinions and data contained in all publications are solely those of the individual author(s) and contributor(s) and not of MDPI and/or the editor(s). MDPI and/or the editor(s) disclaim responsibility for any injury to people or property resulting from any ideas, methods, instructions or products referred to in the content.

Article

Design of an Algorithm for Modeling Multiple Thermal Zones Using a Lumped-Parameter Model

Pedro Fernández de Córdoba ¹, Frank Florez Montes ^{2,*}, Miguel E. Iglesias Martínez ¹, Jose Guerra Carmenate ¹, Romeo Selvas ³ and John Taborda ⁴

¹ Instituto Universitario de Matemática Pura y Aplicada, Universitat Politècnica de València, Camino de Vera s/n, 46022 Valencia, Spain

² Faculty of Engineering, Universidad Autónoma de Manizales, Manizales 170003, Colombia

³ Facultad de Ciencias Físico-Matemáticas, Universidad Autónoma de Nuevo León, FCFM Av. Universidad S/N, Cd. Universitaria, San Nicolas de los Garza 66455, Nuevo León, Mexico

⁴ Faculty of Engineering, Universidad del Magdalena, Santa Marta 470003, Colombia

* Correspondence: frankflorezm@autonoma.edu.co

Abstract: The generation of mathematical models for the analysis of buildings with multiple thermal zones is a large and complex task. Furthermore, the order and complexity of the dynamical model are increased by the number of included thermal zones. To overcome this problem, this paper presents an algorithm to define the mathematical model automatically, using the geometric and physics parameters as inputs. Additionally, the spatial position of each thermal zone must be recorded in an arrangement called a contact matrix. The algorithm for modeling systems with multiple thermal zones is the main contribution of this work. This algorithm is presented in pseudocode format and as an annex, an implementation in MATLAB software. One of the advantages of this methodology is that it allows us to work with parallelepipeds and not necessarily cubic thermal zones. The algorithm allows us to generate mathematical models with symbolic variables, starting from the knowledge of how many thermal zones compose the system and its geometric organization. This information must be organized in a matrix arrangement called a contact matrix. Different arrays of thermal zones were constructed with wooden boxes to verify the functionality of the models generated with the algorithm. Each case provided information that allowed us to adjust the mathematical models and their simulations, obtaining a range of errors between experimental and simulated temperatures from 2.08 to 5.6, depending on the number of thermal zones studied.

Keywords: buildings; lumped parameters; algorithm; mathematical model; experimental tests; reduced-scale models

Citation: Fernández de Córdoba, P.; Montes, F.F.; Martínez, M.E.I.; Carmenate, J.G.; Selvas, R.; Taborda, J. Design of an Algorithm for Modeling Multiple Thermal Zones Using a Lumped-Parameter Model. *Energies* **2023**, *16*, 2247. <https://doi.org/10.3390/en16052247>

Academic Editors: Ala Hasan and Hassam Ur Rehman

Received: 28 January 2023

Revised: 18 February 2023

Accepted: 25 February 2023

Published: 26 February 2023



Copyright: © 2023 by the authors. Licensee MDPI, Basel, Switzerland. This article is an open access article distributed under the terms and conditions of the Creative Commons Attribution (CC BY) license (<https://creativecommons.org/licenses/by/4.0/>).

1. Introduction

Building modeling is an increasingly important field of research. In the last decade, several papers have been published in this field [1–4]. This increase has been driven in part by international agreements for environmental protection, such as the Kyoto Protocol [5] and the Paris Agreement [6]. Countries participating in this agreement have committed to formalizing various policies to reduce energy consumption and CO₂ emissions, especially in cities and buildings, which, according to additional research, can consume up to 40% of the annual energy production. [7–9].

The energy consumption in buildings depends on different factors, such as occupant activity [9] and heating, ventilation and air conditioning (HVAC) systems [10], among others. However, to understand the causes of energy consumption, buildings must be studied individually, taking into account the minimum spaces and energy requirements to ensure occupant comfort [11,12]. In this sense, mathematical models and simulators play an essential role, allowing researchers to analyze different configurations and situations in buildings, including huge interior spaces in buildings [13] or green roofs [14].

Regarding tools and strategies to generate and study the mathematical models of buildings, several works have been carried out [15–18]. Many works use specific simulators such as Energy Plus [19], Contam [20] and Trnsys [21] to understand and model problems such as choosing the best cooling system, airflow and energy savings [4,10,11]. These issues are considerably more complex if the building has multiple thermal zones. Papers such as in [22,23] mention the use of machine learning strategies to tackle these problems.

In different investigations, the lumped-parameter technique (LPM) is used to analyze thermal zones [7,13]. This technique allows a deeper numerical understanding of the thermal behavior in a closed enclosure, as it allows the user to generate a clear mathematical model, where each term can be explained and studied individually. These models are known as gray-box models and are the equivalent of the black-box models used by academic simulators that do not clearly show the mathematical model used for the simulation [24–26].

The LPM makes it possible to generate an equivalent electrical circuit to analyze a thermal zone and, using Kirchhoff's laws, to define a mathematical model [27–30]. The order of the model depends on the number of resistors and capacitors used for each wall. However, the size and model requirements increase with the number of thermal zones studied. The need to consider multiple interacting thermal zones arises when studying more realistic buildings, such as residential houses or apartments. [31–34].

Figure 1 shows different combinations of thermal zones, providing a complex heat- and air-transfer modeling problem. In this paper, an algorithm for modeling multiple thermal zones is presented. The algorithm can be extended to consider as many zones as necessary, requiring only the geometrical and physical parameters and information about the spatial position of each zone. The proposed methodology is not limited to thermal zones having a square geometry. This is a problem presented in similar algorithms [35]. In addition, the algorithm presented in [32] showed a statistical model for multiple thermal zones, but that type of algorithm uses a complex nomenclature and may be more difficult to use than the proposed methodology. Other works presented algorithms for modeling but were limited by the geometry, excessive information requirements and mathematical complexity [15,36,37].

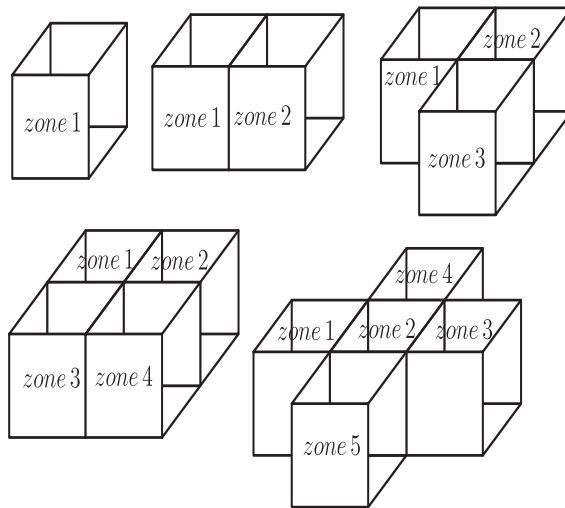


Figure 1. Multiple thermal zones located next to each other.

The paper is organized as follows: Section 2 is devoted to describing the different organizations of the thermal zones, classified into cases. The description of the algorithm is

given in Section 3. An experimental verification of the different mathematical models is presented in Section 4. Finally, conclusions and future work are presented in Section 6.

2. Mathematical Model

The lumped-parameter technique (LPM) represents the thermal zones with an RC circuit and defines a mathematical model using circuit analysis strategies. The size of the mathematical model can change depending on the structure used. The structure presented in Figure 2 was used in previous work, showing a good behavior and adaptability, and thus was used as equivalent for each thermal zone studied in this work [37–39].

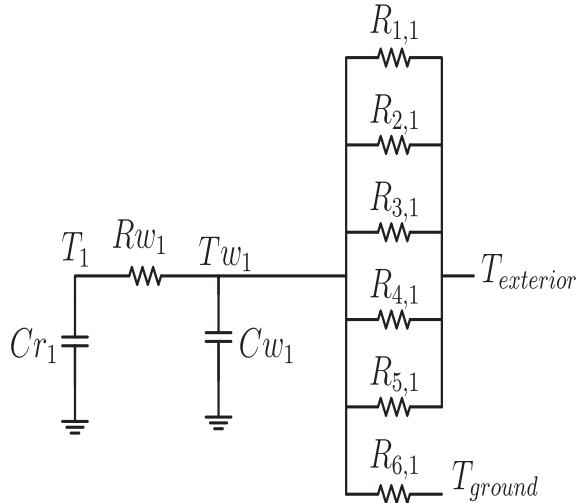


Figure 2. Circuit for a single thermal zone.

The resistance and capacitors are calculated as a function of the geometric and physical parameters of the thermal zones, such as wall dimensions (L for thickness and A for surface area), density (ρ), thermal conductivity (kt) and specific heat (Ce). Equations (1)–(6) show the relationships for each surface. The subscripts i and j have a key function: i represents each wall in the thermal zone. Because of that, $i = 1, 2, \dots, 6$ in all the cases. Furthermore, the subscript j represents the number of analyzed thermal zones (m), so $j = 1, 2, \dots, m$.

$$R_{i,j} = \frac{L_{i,j}}{2kt_{i,j}A_{i,j}} \tag{1}$$

$$R_{in_j} = \frac{1}{hi_jA_{i,j}} \tag{2}$$

$$R_{ex_j} = \frac{1}{he_jA_{i,j}} \tag{3}$$

$$Rw_j = \frac{\prod_{k=1}^6 (R_{k,j} + R_{in_j})}{\sum_{i=1}^6 \prod_{k=1}^6 \frac{R_{k,j} + R_{in_j}}{R_{i,j} + R_{in_j}}} \tag{4}$$

$$Cw_j = \sum_{i=1}^6 \rho_i Ce_i A_i L_i \tag{5}$$

$$Cr_j = \rho_a Ce_a V_a \tag{6}$$

The resistance $R_{i,j}$ represents the thermal resistance of the exterior half-wall and can be extended to include heat transfer to the surroundings by adding Equation (2) for cases where the surface is exposed to outside air. The resistance R_{w_j} corresponds to the parallel reduction of the resistances of the inner half-walls. The constants h_i and h_e are the heat transfer coefficients between the walls and the indoor and outdoor air, respectively. These values must be adjusted to each specific environmental situation [40,41]. Finally, C_{w_j} and C_{r_j} are used to represent the thermal capacity of the walls and internal air, respectively.

Traditionally, the process of developing a mathematical model using LPM consists of three stages:

1. The identification of geometrical and physical parameters of the thermal zones, including internal loads.
2. RC circuit construction and the calculation of resistors and capacitors
3. Define the equations of the dynamic system, using the theory of energy flow transfer.

These three steps can be arduous if the system includes several thermal zones. In addition, this section represents the final two steps of the analysis of a thermal zone with different spaces.

2.1. Case 1: A Single Thermal Zone ($m = 1$)

To facilitate understanding of the notation, the same wall numbering is always used in the remainder of this paper. Figure 3 shows the chosen assignment, taking the front and back faces as walls one and two, the right and left walls are denoted by walls three and four. Meanwhile, surfaces five and six are the top and bottom surfaces, respectively.

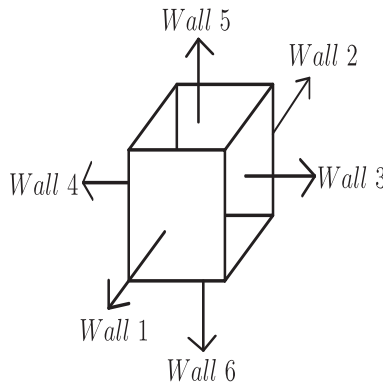


Figure 3. Numbering of the walls in a thermal zone.

The circuit for the single thermal zone case is presented in Figure 2. Using classical electrical circuit analysis strategies, Equations (7) and (8) were defined, where T_w and T represent the wall and indoor-air temperature, respectively.

$$C_{w_1} \dot{T}_{w_1} = \frac{T_1}{R_{w_1}} - T_{w_1} \left(\frac{1}{R_{1,1}} + \frac{1}{R_{2,1}} + \frac{1}{R_{3,1}} + \frac{1}{R_{4,1}} + \frac{1}{R_{5,1}} + \frac{1}{R_{6,1}} + \frac{1}{R_{w_1}} \right) + \left(\frac{1}{R_{1,1}} + \frac{1}{R_{2,1}} + \frac{1}{R_{3,1}} + \frac{1}{R_{4,1}} + \frac{1}{R_{5,1}} \right) T_{exterior} + \frac{T_{ground}}{R_{6,1}} \quad (7)$$

$$C_{r_1} \dot{T}_1 = -\frac{T_1}{R_{w_1}} + \frac{T_{w_1}}{R_{w_1}} \quad (8)$$

The state variable for this case can be shortened to $X = [T_{w_1} \quad T_1]^T$, the inputs to the system are the ambient temperature denoted by $T_{exterior}$ and the ground temperature denoted by T_{ground} ; for the specific situation where the thermal zone is separated from the ground, the ground temperature must be substituted for the environmental temperature. In addition,

Equation (8) can be extended to include thermal loads by adding the term $\pm Q$, taking Q as the power of the load, positive when the load is a heating load, and negative when the load is a cooling system. This case was studied in previous works and was not analyzed in depth in this paper [40,42].

2.2. Case 2: Two Thermal Zones ($m=2$)

Figure 4 shows the spatial location of the thermal zones. In this configuration, surface 3 of zone 1 is in contact with surface 4 of zone 2, according to the numbering presented in Figure 3.

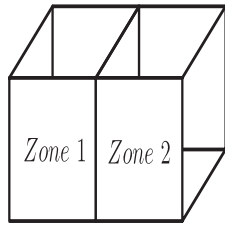


Figure 4. Two thermal zones.

For the case with two thermal zones, the circuit presented in Figure 2 must be extended to include the second thermal zone; Figure 5 shows the new circuit, taking T_{w2} and T_2 as the temperatures for the second zone. Using the circuit for two thermal zones it is possible to derive Equations (9) to (12).

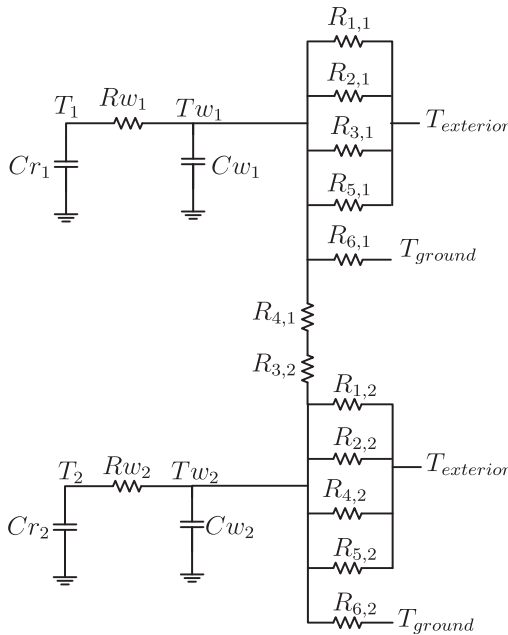


Figure 5. Circuit for a thermal zone with two places.

$$Cw_1\dot{T}w_1 = \frac{T_1}{Rw_1} - \left(\frac{1}{Rw_1} + \frac{1}{R_{1,1}} + \frac{1}{R_{2,1}} + \frac{1}{R_{4,1}} + \frac{1}{R_{5,1}} + \frac{1}{R_{6,1}} + \frac{1}{R_{3,1} + R_{4,2}} \right) Tw_1 + \frac{Tw_2}{R_{3,1} + R_{4,2}} + \left(\frac{1}{R_{1,1}} + \frac{1}{R_{2,1}} + \frac{1}{R_{4,1}} + \frac{1}{R_{5,1}} \right) T_{exterior} + \frac{T_{ground}}{R_{6,1}} \quad (9)$$

$$Cr_1\dot{T}_1 = -\frac{T_1}{Rw_1} + \frac{Tw_1}{Rw_1} \quad (10)$$

$$Cw_2\dot{T}w_2 = \frac{T_2}{Rw_2} - \left(\frac{1}{Rw_2} + \frac{1}{R_{1,2}} + \frac{1}{R_{2,2}} + \frac{1}{R_{3,2}} + \frac{1}{R_{5,2}} + \frac{1}{R_{6,2}} + \frac{1}{R_{4,2} + R_{3,1}} \right) Tw_2 + \frac{Tw_1}{R_{4,2} + R_{3,1}} + \left(\frac{1}{R_{1,2}} + \frac{1}{R_{2,2}} + \frac{1}{R_{3,2}} + \frac{1}{R_{5,2}} \right) T_{exterior} + \frac{T_{ground}}{R_{6,2}} \quad (11)$$

$$Cr_2\dot{T}_2 = -\frac{T_2}{Rw_2} + \frac{Tw_2}{Rw_2} \quad (12)$$

For this case, the state variables are $X = [Tw_1 \ T_1 \ Tw_2 \ T_2]^T$ and the system inputs are the same as in case 1. Analyzing this mathematical model, it is easy to deduce the relationship between the size of the mathematical model (N) and the number of thermal zones. Using the relation $N = 2m$, the size of the dynamic system can be known in future cases.

2.3. Case 3: Three Thermal Zones ($m = 3$)

The organization of three thermal zones is presented in Figure 6. In this case, thermal zone 1 is next to two independent zones, zone 2 on the left and zone 3 on the right.

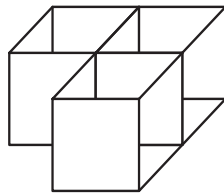


Figure 6. Three thermal zones.

Following the same process described in the two previous cases, the circuit designed for this configuration is presented in Figure 7. Resistors three and four in zone 1 are dedicated to linking the first thermal zone to the adjacent zones. Six differential equations ($N = 6$) are required to model this circuit, which are derived and presented in the following set of equations:

$$Cw_3\dot{T}w_3 = \frac{T_3}{Rw_3} - \left(\frac{1}{Rw_3} + \frac{1}{R_{1,3}} + \frac{1}{R_{2,3}} + \frac{1}{R_{3,3}} + \frac{1}{R_{4,3} + R_{3,1}} + \frac{1}{R_{5,3}} + \frac{1}{R_{6,3}} \right) Tw_3 + \frac{Tw_1}{R_{4,3} + R_{3,1}} + \left(\frac{1}{R_{1,3}} + \frac{1}{R_{2,3}} + \frac{1}{R_{3,3}} + \frac{1}{R_{5,3}} \right) T_{exterior} + \frac{T_{ground}}{R_{6,3}} \quad (13)$$

$$Cr_3\dot{T}_3 = -\frac{T_3}{Rw_3} + \frac{Tw_3}{Rw_3} \quad (14)$$

$$Cw_2\dot{T}w_2 = \frac{T_2}{Rw_2} - \left(\frac{1}{Rw_2} + \frac{1}{R_{1,2}} + \frac{1}{R_{2,2}} + \frac{1}{R_{3,2} + R_{4,1}} + \frac{1}{R_{4,2}} + \frac{1}{R_{5,2}} + \frac{1}{R_{6,2}} \right) Tw_2 + \frac{Tw_1}{R_{3,2} + R_{4,1}} + \left(\frac{1}{R_{1,2}} + \frac{1}{R_{2,2}} + \frac{1}{R_{4,2}} + \frac{1}{R_{5,2}} \right) T_{exterior} + \frac{T_{ground}}{R_{6,2}} \quad (15)$$

$$Cr_2\dot{T}_2 = -\frac{T_2}{Rw_2} + \frac{Tw_2}{Rw_2} \quad (16)$$

$$Cw_1\dot{T}w_1 = \frac{T_1}{Rw_1} + \frac{Tw_2}{R_{4,1} + R_{3,2}} + \frac{Tw_3}{R_{3,1} + R_{4,3}} + \left(\frac{1}{R_{1,1}} + \frac{1}{R_{2,1}} + \frac{1}{R_{5,1}} \right) T_{exterior} - \left(\frac{1}{Rw_1} + \frac{1}{R_{1,1}} + \frac{1}{R_{2,1}} + \frac{1}{R_{3,1} + R_{4,3}} + \frac{1}{R_{4,1} + R_{3,2}} + \frac{1}{R_{5,1}} + \frac{1}{R_{6,1}} \right) Tw_1 + \frac{T_{ground}}{R_{6,1}} \quad (17)$$

$$Cr_1\dot{T}_1 = -\frac{T_1}{Rw_1} + \frac{Tw_1}{Rw_1} \quad (18)$$

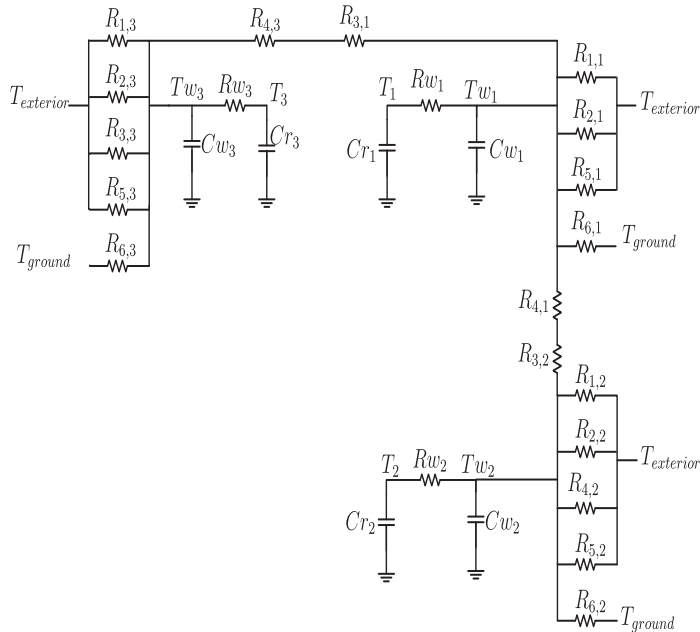


Figure 7. Circuit for a thermal zone with three places.

For this case, Tw_3 and T_3 correspond to the temperatures of the third thermal zone. In this model, the central thermal zone is influenced by the adjacent zones. This means that each zone can be affected by a maximum number of 6 thermal zones in the current configuration.

2.4. Case 4: Four Thermal Zones ($m = 4$)

The last case study is present in Figure 8; in this configuration, thermal zone 1 is influenced by the three adjacent thermal zones, using surfaces 1, 3 and 4 as contact areas and reducing the ambient temperature over the central zone.

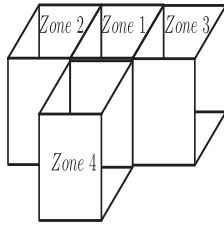


Figure 8. Four thermal zones.

The equivalent circuit for this configuration is shown in Figure 9. In this structure, it is evident that zones 2, 3 and 4 have no effect on each other. The only relationship is an indirect one, using zone 1 as a conductance.

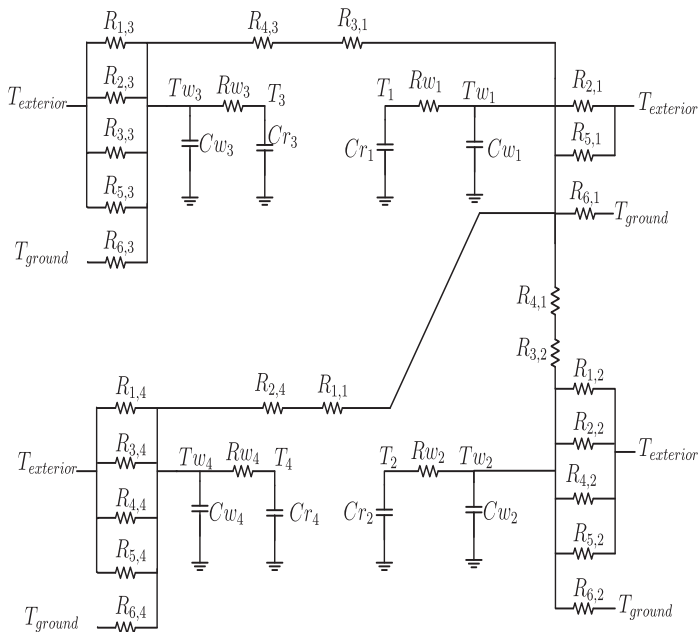


Figure 9. Circuit for a thermal zone with four places.

The mathematical model established for this case is present in Equations (19)–(26); it should be noted that only Equation (25) includes the wall temperature of all zones, allowing this zone to be a driver of the indirect relationship between adjacent zones.

$$Cw_4 \dot{T}w_4 = \frac{T_4}{Rw_4} - \left(\frac{1}{Rw_4} + \frac{1}{R_{1,4}} + \frac{1}{R_{2,4} + R_{1,1}} + \frac{1}{R_{3,4}} + \frac{1}{R_{4,4}} + \frac{1}{R_{5,4}} + \frac{1}{R_{6,4}} \right) Tw_4 + \frac{Tw_1}{R_{2,4} + R_{1,1}} + \left(\frac{1}{R_{1,4}} + \frac{1}{R_{3,4}} + \frac{1}{R_{4,4}} + \frac{1}{R_{5,4}} \right) T_{exterior} + \frac{T_{ground}}{R_{6,4}} \quad (19)$$

$$Cr_4 \dot{T}_4 = -\frac{T_4}{Rw_4} + \frac{Tw_4}{Rw_4} \quad (20)$$

$$Cw_3T\dot{w}_3 = \frac{T_3}{Rw_3} - \left(\frac{1}{Rw_3} + \frac{1}{R_{1,3}} + \frac{1}{R_{2,3}} + \frac{1}{R_{3,3}} + \frac{1}{R_{4,3} + R_{3,1}} + \frac{1}{R_{5,3}} + \frac{1}{R_{6,3}} \right) Tw_3 + \frac{Tw_1}{R_{4,3} + R_{3,1}} + \left(\frac{1}{R_{1,3}} + \frac{1}{R_{2,3}} + \frac{1}{R_{3,3}} + \frac{1}{R_{5,3}} \right) T_{exterior} + \frac{T_{ground}}{R_{6,3}} \quad (21)$$

$$Cr_3\dot{T}_3 = -\frac{T_3}{Rw_3} + \frac{Tw_3}{Rw_3} \quad (22)$$

$$Cw_2T\dot{w}_2 = \frac{T_2}{Rw_2} - \left(\frac{1}{Rw_2} + \frac{1}{R_{1,2}} + \frac{1}{R_{2,2}} + \frac{1}{R_{3,2} + R_{4,1}} + \frac{1}{R_{4,2}} + \frac{1}{R_{5,2}} + \frac{1}{R_{6,2}} \right) Tw_2 + \frac{Tw_1}{R_{3,2} + R_{4,1}} + \left(\frac{1}{R_{1,2}} + \frac{1}{R_{2,2}} + \frac{1}{R_{4,2}} + \frac{1}{R_{5,2}} \right) T_{exterior} + \frac{T_{ground}}{R_{6,2}} \quad (23)$$

$$Cr_2\dot{T}_2 = -\frac{T_2}{Rw_2} + \frac{Tw_2}{Rw_2} \quad (24)$$

$$Cw_1T\dot{w}_1 = \frac{T_1}{Rw_1} + \frac{Tw_2}{R_{3,2} + R_{4,1}} + \frac{Tw_3}{R_{3,1} + R_{4,3}} + \frac{Tw_4}{R_{1,1} + R_{2,4}} + \left(\frac{1}{R_{2,1}} + \frac{1}{R_{5,1}} \right) T_{exterior} - \left(\frac{1}{Rw_1} + \frac{1}{R_{1,1} + R_{2,4}} + \frac{1}{R_{2,1}} + \frac{1}{R_{3,1} + R_{4,3}} + \frac{1}{R_{4,1} + R_{3,2}} + \frac{1}{R_{5,1}} + \frac{1}{R_{6,1}} \right) Tw_1 + \frac{T_{ground}}{R_{6,2}} \quad (25)$$

$$Cr_1\dot{T}_1 = -\frac{T_1}{Rw_1} + \frac{Tw_1}{Rw_1} \quad (26)$$

The process described in this section is traditionally used to analyze single and multiple thermal zones [26,40]. In all cases, the model must be adjusted to reproduce the experimental measurements, which can be a complex task depending on the size of the model and the number of parameters considered. In this section, different numbers of thermal zones were presented, starting with a single $m = 1$ zone up to $m = 4$, moving from a 2×2 to an 8×8 system, increasing the tuning complexity and allowing for a more significant percentage error with respect to the experimental data.

3. Algorithm Design

The mathematical models presented in Section 2 and constructed manually require time and effort, but in the case of changes in the position of the thermal zones, steps 2 and 3 must be repeated.

A mathematical modeling algorithm was developed to avoid this problem, using the evidenced pattern. A pair of differential equations was added to the system for each thermal zone in all cases. The structure of these equations is presented in Equations (27) and (28). In this structure, the coefficients α , β and ϕ , which correspond to the impact of adjacent zones, the environment and the ground temperature in each zone, must be calculated.

$$Cw_jT\dot{w}_j = \frac{T_j}{Rw_j} + \sum_{z=1}^m \alpha_z Tw_z + \beta T_{exterior} + \phi T_{ground} \quad (27)$$

$$Cr_j\dot{T}_j = -\frac{T_j}{Rw_j} + \frac{Tw_j}{Rw_j} \quad (28)$$

To capture the spatial organization of the thermal zones, a matrix called a contact matrix was used. This matrix had the dimensions $m \times 6$; each row recorded the information of a different zone, thus the first row had information about zone 1, the second row about the second thermal zone, continuing up to the last thermal zone in row m .

The columns in the contact matrix maintained the surface numbering described in Figure 3, using column 1 to indicate whether there was a thermal zone adjacent to the front surface, column 2 to record the existence of a thermal zone on the rear surface and continuing this assignment for all six surfaces; in case there was no adjacent thermal zone, the elements in the column for these directions were replaced by zero.

$$u = \begin{bmatrix} u_{1,1} & u_{1,2} & u_{1,3} & \cdots & u_{1,6} \\ u_{2,1} & u_{2,2} & u_{2,3} & \cdots & u_{2,6} \\ \vdots & & \vdots & \ddots & \vdots \\ u_{m,1} & u_{m,2} & u_{m,3} & \cdots & u_{m,6} \end{bmatrix} \quad (29)$$

Equation (29) illustrates the structure of the contact matrix. Using the thermal zone configurations presented in Section 2, the contact matrices were built:

$$u_{m=1} = [0 \ 0 \ 0 \ 0 \ 0 \ 0] \quad (30)$$

$$u_{m=2} = \begin{bmatrix} 0 & 0 & 0 & 2 & 0 & 0 \\ 0 & 0 & 1 & 0 & 0 & 0 \end{bmatrix} \quad (31)$$

$$u_{m=3} = \begin{bmatrix} 0 & 0 & 3 & 2 & 0 & 0 \\ 0 & 0 & 1 & 0 & 0 & 0 \\ 0 & 0 & 0 & 1 & 0 & 0 \end{bmatrix} \quad (32)$$

$$u_{m=4} = \begin{bmatrix} 4 & 0 & 3 & 2 & 0 & 0 \\ 0 & 0 & 1 & 0 & 0 & 0 \\ 0 & 0 & 0 & 1 & 0 & 0 \\ 0 & 1 & 0 & 0 & 0 & 0 \end{bmatrix} \quad (33)$$

We had zone 4 adjacent to wall 1, so element $u(1,1)$ was 4; zone 3 was adjacent to the right surface in zone 1 and for this reason, $u(1,3)$ was 3; and applying the same logic, zone 2 was adjacent to the left surface in zone 1, so $u(1,4) = 2$. The zeros represented the surfaces not connected to the thermal zones in the contact matrix. Rows 2, 3 and 4 contained information about zones 2, 3 and 4. In these cases, the only adjacent zone was zone 1; for this reason, most of the spaces were filled with zeros, and the position of zone 1 indicated the position of the first thermal zone with respect to the current zone.

Using the number of thermal zones m , the contact matrix u , the resistances $R_{i,j}$ and the geometrical and physical parameters as inputs, Algorithm 1 was used to determine the differential equations for modeling the multiple-thermal-zone system.

The objective of the algorithm was to generate a pair of equations for each thermal zone, so the β , ϕ and α coefficients had to be determined for each pair of equations. However, they were initially assumed to be zero, and using the information from the contact matrix, they were recalculated.

The coefficient β represented all surfaces in contact with the outside air and contained the sum of the corresponding resistances. The coefficient ϕ was exclusively dedicated to regulate the heat transfer with the ground. Finally, the coefficients α summarized the influence of adjacent thermal zones on the current zone. However, there was a special case, the condition for $i = j$, where this coefficient summarized the impact of the thermal walls on the interior temperature. In case of walls without connection with other thermal zones, only their own resistance was considered; for this purpose, the δ function was used, using the following behavior:

$$\delta(x) = \begin{cases} 1 & \mapsto x = 0 \\ 0 & \mapsto \forall x \neq 0 \end{cases} \quad (34)$$

The constant k_1 grouped resistors for the walls with no connection to other zones, while the constant k_2 grouped resistors with adjacent zones.

Algorithm 1 Algorithm to design differential equation systems for multiple thermal zones

inputs: Contact matrix (u); number of thermal zones (m); Resistances ($R_{i,j}$); Geometric and physic parameters

for $i = 1 : m$ **do**

 initialization $\beta_i = 0$; $\phi_i = 0$; $\alpha_{1-6,i} = 0$

$$Rw_i = \frac{\prod_{k=1}^6 R_{k,i}}{\sum_{j=1}^6 \prod_{k=1}^6 R_{k,i}}$$

$$Cw_i = \rho_i C_{e_i} A_i L_i$$

$$Cr_i = \rho_a C_{e_a} V_i$$

for $s = 1 : 5$ **do**

if $u(i, s) == 0$ **then**

$$\quad \quad \beta_i = \beta_i + \frac{1}{R_{s,i}}$$

end

end

if $u(i, 6) == 0$ **then**

$$\quad \quad \phi_i = \frac{1}{R_{6,i}}$$

end

for $q = 1 : 6$ **do**

if $u(i, q) > 0$ **then**

if $\text{mod}(q) == 0$ **then**

$$\quad \quad \quad \alpha_{u(i,q),i} = \frac{1}{R_{q,i} + R_{q-1,u(i,q)}}$$

else

$$\quad \quad \quad \alpha_{u(i,q),i} = \frac{1}{R_{q,i} + R_{q+1,u(i,q)}}$$

end

end

end

$$k_1 = \frac{1}{Rw_i} + \frac{\delta(u(i,1))}{R_{1,i}} + \frac{\delta(u(i,2))}{R_{2,i}} + \frac{\delta(u(i,3))}{R_{3,i}} + \frac{\delta(u(i,4))}{R_{4,i}} + \frac{\delta(u(i,5))}{R_{5,i}} + \frac{\delta(u(i,6))}{R_{6,i}}$$

$$k_2 = \frac{1-\delta(u(i,1))}{R_{1,i}+R_{2,u(i,1)}} + \frac{1-\delta(u(i,2))}{R_{2,i}+R_{1,u(i,1)}} + \frac{1-\delta(u(i,3))}{R_{3,i}+R_{4,u(i,3)}} + \frac{1-\delta(u(i,4))}{R_{4,i}+R_{3,u(i,3)}} + \frac{1-\delta(u(i,5))}{R_{5,i}+R_{6,u(i,5)}} + \frac{1-\delta(u(i,6))}{R_{6,i}+R_{5,u(i,5)}}$$

$$\alpha_{i,j} = -(k_1 + k_2)$$

$$\text{Result: } \begin{cases} Cw_i \dot{T}w_i = \frac{T_i}{Rw_i} + \sum_{z=1}^m \alpha_{z,i} T w_z + \beta_i T_{\text{exterior}} + \phi_i T_{\text{ground}} \\ Cr_i \dot{T}_i = -\frac{T_i}{Rw_i} + \frac{T w_i}{Rw_i} \end{cases}$$

end

4. Experimental Development

To evaluate the behavior of the algorithm, a set of experimental tests was executed. Each test was designed to verify the different cases modeled in section two. These models were corroborated by the algorithm presented. The algorithm was programmed in MATLAB software and its results are presented in Appendix A.

The case study selected to evaluate the mathematical models was that of multiple thermal zones made with balsa wood. The physical and geometrical parameters are shown in Table 1.

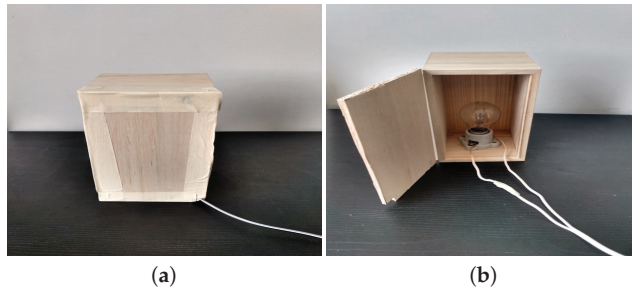
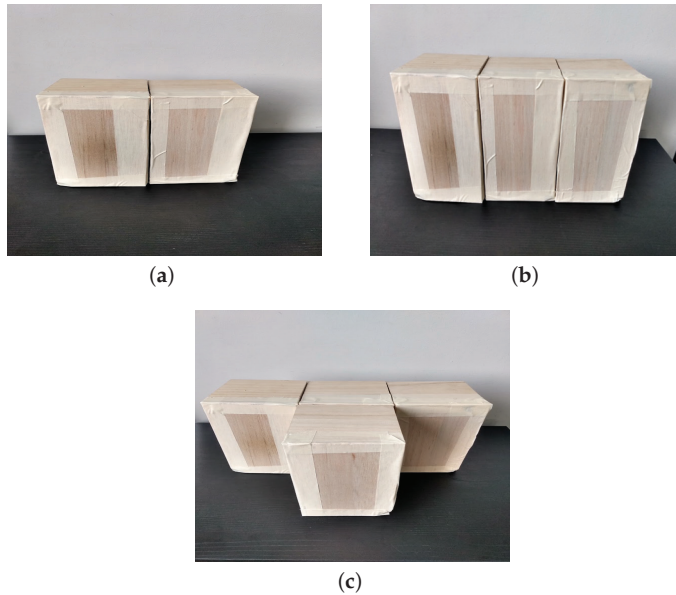
We used x , y and z as the horizontal length, depth and height of the thermal zone. L_d and L_w represented the door and wall thickness, respectively. The physical parameters were the density (ρ), specific heat (Ce) and thermal conductivity (kt) [43].

The experiment was run in various stages, increasing the number of thermal zones according to the case studies. In all cases, thermal zone 1 was equipped with an internal heating load. Figure 10 shows a 100 W incandescent bulb as the heat source.

Figure 11 shows the construction of multiple thermal zones according to cases 2, 3 and 4. In addition, each thermal zone had a DHT11 temperature sensor to record the internal temperature, and an additional sensor was dedicated to recording the ambient temperature.

Table 1. Physical and geometrical parameters.

Geometrical Parameters				
x	y	z	L_d	L_w
0.111 m	0.111 m	0.2 m	0.005 m	0.008 m
Physical Parameters				
ρ	C_e		kt	
150.7485 $\frac{\text{kg}}{\text{m}^3}$	3.0512 $\frac{\text{kJ}}{\text{kg}\cdot^\circ\text{C}}$		0.1882 $\frac{\text{kJ}}{\text{m}\cdot\text{h}\cdot^\circ\text{C}}$	

**Figure 10.** Thermal zone 1 with internal heating load. (a) Single thermal zone. (b) Single thermal zone with internal load.**Figure 11.** Thermal zones for cases 2, 3 and 4 with internal heating load. (a) Case 1. (b) Case 2. (c) Case 3.

The tests were conducted between 22 and 25 March 2021. Four databases were constructed, one for each case, in which charging processes were carried out with the internal heat source activated for 5 min then turned off and the thermal zones allowed to discharge, releasing the heat to the environment for 30 min.

Tuning Process

In order for the mathematical model to represent the phenomenon under study, a tuning process was carried out. The tuning process had two parts, the first one consisted of calculating fixed values, such as conduction resistances and thermal capacities. These parameters depended on fixed characteristics, such as geometrical and physical characteristics. The second part was dedicated to tuning the variable parameters, i.e., the heat transfer coefficients h_e and h_i . Each surface could calculate these coefficients, but in this work, it was assumed that all surfaces in a single thermal zone had the same coefficients h_e and h_i .

The pattern search algorithm was used to adjust the heat transfer coefficients, taking as objective function the error between the experimental data and the simulated results. The fitting process was performed for the loading and unloading phases independently, allowing a different set of coefficients for each phase and thermal zone.

Using the experimental database, the model was fitted for case 1. The results are presented in Figure 12, using a red line to represent the experimental data. The blue line represents the simulated results and finally, the green line is used to represent the ambient temperature. In that case, the error rate between experimental data and simulations was 2.0896% over 3 h of processing.

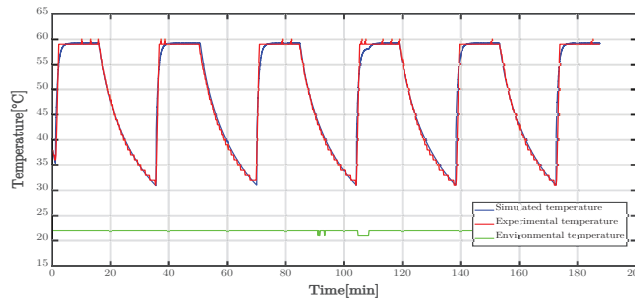


Figure 12. Experimental and simulated results for a single thermal zone.

Figure 13 shows the internal temperatures for two thermal zones, case 2. The blue and red lines represent the experimental and simulated temperature for zone 1. In addition, the green and black lines denote the experimental and simulated internal temperature in zone 2. In this case, the objective function used for the tuning process was the sum of the experimental and simulated results for each zone, i.e., $F_{objective} = e_1 + e_2$, using e_1 as the percentage error for zone 1 and e_2 the error for zone 2. The errors obtained were 2.94% and 2.97% for zone 1 and zone 2, respectively.

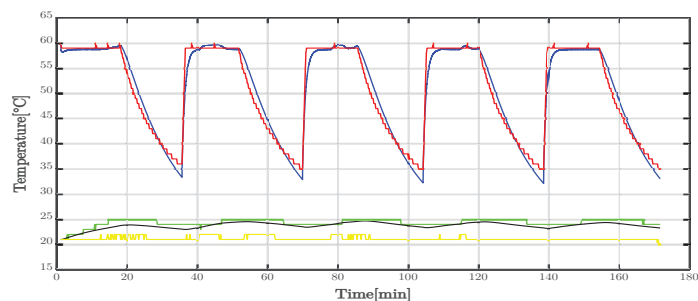


Figure 13. Experimental and simulated results for a double thermal zone.

The results of the study on case 3 are presented in Figure 14. In that graph, the first row represents the internal temperature for zone 1, using the blue line for the simulation

and the red line for the experiment, and the green line illustrates the environmental temperature. Similarly, the second and third rows represent the simulated and experimental temperatures for zones 2 and 3, respectively. For the case $m = 3$, the objective function used was $F_{objective} = \sum_{i=1}^m e_i$, considering the error rate simultaneously for the three zones and obtaining $e_1 = 3.97\%$, $e_2 = 3.7\%$ and $e_3 = 4.88\%$ for each thermal zone.

The last case studied ($m = 4$) is presented in Figure 15. In that figure, the first row shows the temperature for thermal zone 1, the second, third and fourth rows are dedicated to thermal zones 2, 3 and 4, respectively. The blue line corresponds to the simulation and the red line to the experimental results. The green lines represent the ambient temperature. The errors between the experimental and simulated temperature were $e_1 = 4.37\%$, $e_2 = 5.6\%$, $e_3 = 4.86\%$ and $e_4 = 4.9\%$.

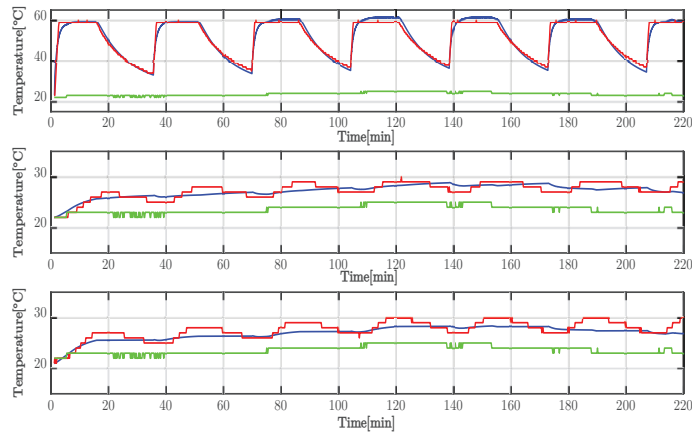


Figure 14. Experimental and simulated results for three thermal zones.

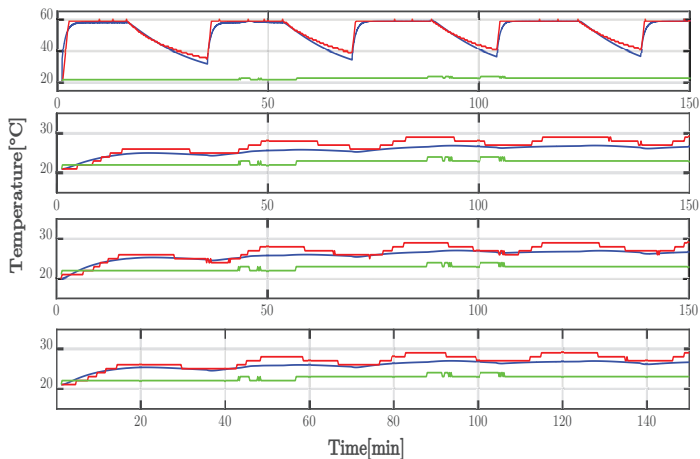


Figure 15. Experimental and simulated results for four thermal zones.

The mathematical model was tuned for the charging and discharging process. Table 2 shows the coefficients for the charging phase, explaining the coefficients used in each case. Similarly, Table 3 shows the heat transfer coefficients for the discharge process.

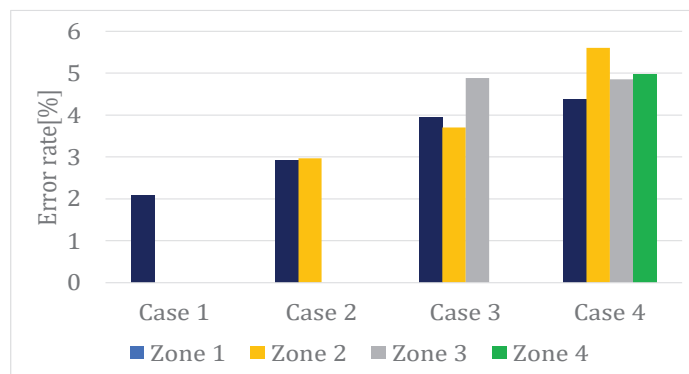
Table 2. Heat transmission coefficients for the charging process.

Zone	$hi \left(\frac{\text{kJ}}{\text{h}\cdot\text{m}\cdot\text{K}} \right)$				$he \left(\frac{\text{kJ}}{\text{h}\cdot\text{m}\cdot\text{K}} \right)$			
	1	2	3	4	1	2	3	4
Case 1	86.9	0	0	0	12.36	0	0	0
Case 2	34.88	0.0022	0	0	12.29	58.77	0	0
Case 3	179.54	0.0047	0	0	2.75	199.9	179.99	0
Case 4	37.44	0.0037	0.0047	0.0047	0.0001	60.95	61.70	103.14

Table 3. Heat transmission coefficients for the discharging process.

Zone	$hi \left(\frac{\text{kJ}}{\text{h}\cdot\text{m}\cdot\text{K}} \right)$				$he \left(\frac{\text{kJ}}{\text{h}\cdot\text{m}\cdot\text{K}} \right)$			
	1	2	3	4	1	2	3	4
Case 1	0.6576	0	0	0	0.0145	0	0	0
Case 2	0.0025	0.001	0	0	3.39	21.45	0	0
Case 3	0.0027	0.0018	0.00027	0	18.65	0.0008	0.8387	0
Case 4	0.0027	0.0008	0.0008	0.0008	0.0008	4.08	1.89	4.67

Figure 16 shows the comparison between the different errors calculated for each case. In all cases, the chosen objective function ($F_{objective} = \sum_{i=1}^m e_i$) allowed us to simultaneously tune the multiple heat transfer coefficients seeking to reduce the error between simulation and experimental results in each case.

**Figure 16.** Error rate for each zone and case studied.

Considering all error percentages equally valuable implied that all errors were minimized without emphasizing any one. On the other hand, the error obtained, for example in thermal zone 1, which was reused in all cases, showed a higher error percentage. This problem could be solved by implementing a function for the fitting process.

5. Discussion

In real applications, most offices and houses are composed of multiple thermal zones connected by walls, windows or doors. This situation drives research to formulate and use multiple-thermal-zone models. This paper described an algorithm to generate mathematical models for systems with equal geometry and materials.

The model used to evaluate the mathematical model was an arrangement of wooden boxes in a laboratory space with limited sources of error. However, in real applications, the

system can contain multiple heat sources with fixed and variable power, such as windows, doors and occupants. In these cases, heat sources can function as new sources of error that reduce the accuracy of the model and hinder the fitting process. In addition, in residential or larger buildings, the internal air temperature can vary due to internal and external phenomena. For example, the stratification produced by the natural organization of indoor air according to its temperature is especially evident in areas with a high roof. External conditions can produce a high-convection process on a single wall, resulting in a temperature imbalance in the thermal zone. This situation can be corrected by using IR systems or specific ventilation systems that regulate the thermal energy between the different thermal zones.

6. Conclusions

The study of buildings with multiple thermal zones involves the generation of large mathematical models. In this work, an algorithm for the automatic generation of mathematical models was proposed. Initially, a manual process of model generation was presented, considering four cases.

The paper presented the modeling of four systems with multiple thermal zones used as case studies. In each case the organization of the thermal zones, the equivalent electrical circuit and the set of differential equations that represented them were described. The calculation process for all elements of the equivalent electrical circuit was described, including fixed physical parameters such as density, conductivity and specific heat. Additionally, variable physical parameters such as convection coefficients were included, which depended on the conditions under which the experiment was recorded and therefore had to be adjusted for each case. The objective of this process was to demonstrate the complexity of analyzing systems with multiple thermal zones and then compare it with the use of the proposed algorithm.

The proposed algorithm was designed to use the growth pattern in the previously calculated differential equations and allowed us to directly formulate the set of differential equations without drawing the equivalent circuit and circuit analysis. The main input of the algorithm was the contact matrix, an array containing the geometric position of all individual zones according to the nomenclature defined in this article.

A set of experimental tests was used to calibrate the mathematical model generated by the proposed algorithm. These experiments were based on thermal zones with balsa wood for the walls and an internal heat source to ensure energy transfer between the different thermal zones and the environment. The experiments were conducted indoors to reduce the environmental impact. The four systems with multiple thermal zones studied previously were experimentally represented. In each case, the individual zones were equipped with temperature sensors.

The tuning process for the heat transfer coefficient of all thermal zones was carried out using the error temperature, considering the difference between the simulation and experimental data. The best error results was about 2.08% for a single thermal zone. Meanwhile, the maximal error was 5.6% obtained in the case of four thermal zones. That error increase can be a problem with a bigger number of zones but can be solved using a better objective function in the tuning process. It is expected to be possible to improve the tuning process in future works and obtain small errors even if large numbers of thermal zones are used.

The internal and external convection coefficient were adjusted in each case. The experiment with a single thermal zone obtained the best error rate between the experimental data and the simulations, obtaining a 2.0896% error. The second experiment with two thermal zones yielded an average error of 2.95%. The third experiment showed errors in each thermal zone of 3.97%, 3.7% and 4.88%. Finally, the experiment with four zones showed larger errors in each individual zone, reaching an error of 5.6%.

With the appropriate fitting process, the mathematical models generated with the proposed algorithm can represent any combination of thermal zones, providing the information

is in the format of contact matrices. For the case of systems consisting of parallelepipeds, the proposed algorithm can be a useful tool.

Author Contributions: Conceptualization and methodology, P.F.d.C. and J.T.; experimental development and data collection, R.S. and J.T.; data analysis and simulations F.F.M.; writing—original draft preparation, R.S. and F.F.M.; funding acquisition, P.F.d.C. and R.S.; Writing and editing, M.E.I.M. and J.G.C. The authors consider that all of them contributed equally to this work. All authors have read and agreed to the published version of the manuscript.

Funding: This research received no external funding.

Informed Consent Statement: Not applicable.

Data Availability Statement: Not applicable.

Acknowledgments: Miguel E. Iglesias Martínez’s acknowledges the postdoctoral research scholarship “Ayudas para la recualificación del sistema universitario español 2021–2023. Modalidad: Margarita Salas”, UPV, Ministerio de Universidades, Plan de Recuperación, Transformación y Resiliencia, Spain. Funded by the European Union-Next Generation EU. Pedro Fernández de Córdoba acknowledges the grant PID2021-128676OB-I00 funded by FEDER/MCIN.

Conflicts of Interest: The authors declare no conflict of interest.

Abbreviations

The following abbreviations are used in this manuscript:

HVAC	Heat, ventilation and air conditioning	
LPM	Lumped-parameter model	
RC	Resistor and capacitor circuit	
Nomenclature		
A	Superficial area	m^2
C_e	Specific heat	$\frac{kJ}{kg \cdot K}$
C_r	Air thermal capacity	$\frac{kJ}{K}$
C_w	Walls’ thermal capacity	$\frac{kJ}{K}$
e	Error rate	%
$F_{objective}$	Objective function	
h_i	Internal heat convection	$\frac{kJ}{h \cdot m^2 \cdot K}$
h_e	External heat convection	$\frac{kJ}{h \cdot m^2 \cdot K}$
kt	Thermal conductivity	$\frac{kJ}{h \cdot m^2 \cdot K}$
L	Thickness	m
m	Thermal zones number	
N	Number of equations	
R	Conduction thermal resistance	$\frac{h \cdot K}{kJ}$
R_{in}	Internal convection resistance	$\frac{h \cdot K}{kJ}$
R_{ex}	External convection resistance	$\frac{h \cdot K}{kJ}$
R_w	Inner envelope walls	$\frac{h \cdot K}{kJ}$
u	Contact matrix	
T	Internal temperature	$^{\circ}C$
T_w	Walls’ temperature	$^{\circ}C$
$T_{exterior}$	Environmental temperature	$^{\circ}C$
T_{ground}	Ground temperature	$^{\circ}C$
α	Heat transfer coefficient between zones	$\frac{kJ}{h \cdot K}$
β	Heat transfer coefficient with environmental conditions	$\frac{kJ}{h \cdot K}$
ϕ	Heat transfer coefficient with ground	$\frac{kJ}{h \cdot K}$
ρ	Density	$\frac{kg}{m^3}$

Appendix A

The algorithm to generate the mathematical models was coded in a Matlab file. Figures A1 and A2 show the code used for each specific case with different thermal zones and contact matrices. The algorithm results for each study case are presented in Figures A3–A6. In all cases, the contact matrix is presented before the mathematical model. These differential equations are string arrays used for building the mathematical model. For the simulation process, the resistances and capacitors must be adjusted to real values.

```

clc
clear all
m=1; % Number of Thermal zones
u=[0,0,0,0,0,0]; %case 1
%u=[0,0,0,2,0,0;0,0,0,1,0,0,0];%case 2
%u=[0,0,3,2,0,0;0,0,0,1,0,0,0;0,0,0,1,0,0,0];%case 3
%u=[4,0,3,2,0,0;0,0,0,1,0,0,0;0,0,0,1,0,0,0;0,1,0,0,0,0]; %case 4
%u=[0,0,2,0,0,0;0,0,0,3,1,0,0;0,0,0,4,2,0,0;0,0,5,3,0,0;0,0,0,4,0,0];%case 5
disp(u)% show the contact matrix
%Resistances and capacitors
Rw="Rw"; R="R"; Cw='Cw'; Cr='Cr';
%temperatures
T="T"; Tw="Tw"; Te="Te"; Tg="Tg";
%Mathematical operators and symbols
Ci="("; Cd=")"; ig="="; ma="+"; me="-"; sl="/"; uno="1"; De="D";
%Subscripts
sub1=["1","2","3","4","5","6"];
sub2=1:m;
sub2=string(sub2);
%String arrays for alpha, beta and phi coefficients
alfa=string(zeros(m,m));
beta=string(zeros(m,1));
fi=string(zeros(1,m));
kl=string();
SD=string(); %Dynamic system output
for i=1:m
    for s=1:5
        if u(i,s)==0
            Rbeta=strcat(uno,sl,R,sub1(s),sub2(i)); %calculation of beta
coefficients
            if beta(i,1)=='0'
                beta(i,1)=(Rbeta);%index first beta value
            else
                beta(i,1)=strcat(beta(i,1),ma,Rbeta);%index other beta value
            end
        end
    end
    if u(i,6)==0
        fi(i)=strcat(uno,sl,R,sub1(6),sub2(i)); %calculation of phi coefficients
    end
    for q=1:6
        if u(i,q)>0
            if mod(q,2)==0 %Calculation of alpha coefficients
                alfa(i,u(i,q))=strcat(uno,sl,Ci,R,sub1(q),sub2(i),ma,R,sub1(q-1),
sub2(u(i,q)),Cd);
            else
                alfa(i,u(i,q))=strcat(uno,sl,Ci,R,sub1(q),sub2(i),ma,R,sub1(q+1),
sub2(u(i,q)),Cd);
            end
        end
    end
end
for w=1:6% Calculate the alpha coefficient for equal subscripts
    if u(i,w)==0

```

Figure A1. Code to generate mathematical models (part a).

```

        km=strcat(uno,s1,R,sub1(w),sub2(i));
    else
        if mod(w,2)==0
            km=strcat(uno,s1,Ci,R,sub1(w),sub2(i),ma,R,sub1(w-1),sub2(u(i,w)),
Cd);
        else
            km=strcat(uno,s1,Ci,R,sub1(w),sub2(i),ma,R,sub1(w+1),sub2(u(i,w)),
Cd);
        end
    end
    k1= strcat(k1,ma,km);
end

alfa(i,i)=strcat(uno,s1,Rw,sub1(i),k1);
k1=string();
Tc=strcat(Cw,sub1(i),De,Tw,sub1(i),ig,T,sub1(i),s1,Rw,sub1(i));
for x=1:m %Dynamic system organization
    if alfa(i,x)~='0'
        if i==x
            Tc=strcat(Tc,me,Tw,sub2(x),Ci,alfa(i,x),Cd);
        else
            Tc=strcat(Tc,ma,Tw,sub2(x),Ci,alfa(i,x),Cd);
        end
    end
end
if beta(i,1)~='0'
    Tc=strcat(Tc,ma,Te,Ci,beta(i,1),Cd);
end
if fi(1,i)~='0'
    Tc=strcat(Tc,ma,Tg,Ci,fi(1,i),Cd);
end
Tc2=strcat(Cr,sub1(i),De,T,sub1(i),ig,me,T,sub1(i),s1,Rw,sub1(i),ma,Tw,sub1
(i),s1,Rw,sub1(i));
SD=[SD;Tc;Tc2];
end
SD=SD(2:end)%final dynamic system

```

Figure A2. Code to generate mathematical models (part b).

```

0    0    0    0    0    0

SD =

2x1 string array

"Cr1DTw1=T1/Rw1-Tw1(1/Rw1+1/R11+1/R21+1/R31+1/R41+1/R51+1/R61)+Te
(1/R11+1/R21+1/R31+1/R41+1/R51)+Tg(1/R61)"
"Cr1DT1=-T1/Rw1+Tw1/Rw1"

```

Figure A3. Case 1: Mathematical model for a single thermal zone.


```

0      0      0      2      0      0
0      0      1      0      0      0

SD =

4×1 string array

"Cw1DTw1=T1/Rw1-Tw1 (1/Rw1+1/R11+1/R21+1/R31+1/ (R41+R32) +1/R51+1/R61) +Tw2 (1/ (R41+R32) ) +Te (1/R11+1/R21+1/R31+1/R51) +Tg (1/R61) "
"Cr1DT1=-T1/Rw1+Tw1/Rw1"
"Cw2DTw2=T2/Rw2+Tw1 (1/ (R32+R41) ) -Tw2 (1/Rw2+1/R12+1/R22+1/ (R32+R41) ) +1/R42+1/R52+1/R62) +Te (1/R12+1/R22+1/R42+1/R52) +Tg (1/R62) "
"Cr2DT2=-T2/Rw2+Tw2/Rw2"

```

Figure A4. Case 2: Mathematical model for a double thermal zone.

```

0      0      3      2      0      0
0      0      1      0      0      0
0      0      0      1      0      0

SD =

6×1 string array

"Cw1DTw1=T1/Rw1-Tw1 (1/Rw1+1/R11+1/R21+1/ (R31+R43) +1/ (R41+R32) +1/R51+1/R61) +Tw2 (1/ (R41+R32) ) +Tw3 (1/ (R31+R43) ) +Te (1/R11+1/R21+1/R51) +Tg (1/R61) "
"Cr1DT1=-T1/Rw1+Tw1/Rw1"
"Cw2DTw2=T2/Rw2+Tw1 (1/ (R32+R41) ) -Tw2 (1/Rw2+1/R12+1/R22+1/ (R32+R41) ) +1/R42+1/R52+1/R62) +Te (1/R12+1/R22+1/R42+1/R52) +Tg (1/R62) "
"Cr2DT2=-T2/Rw2+Tw2/Rw2"
"Cw3DTw3=T3/Rw3+Tw1 (1/ (R43+R31) ) -Tw3 (1/Rw3+1/R13+1/R23+1/R33+1/ (R43+R31) ) +1/R53+1/R63) +Te (1/R13+1/R23+1/R33+1/R53) +Tg (1/R63) "
"Cr3DT3=-T3/Rw3+Tw3/Rw3"

```

Figure A5. Case 3: Mathematical model for three thermal zones.

```

4      0      3      2      0      0
0      0      1      0      0      0
0      0      0      1      0      0
0      1      0      0      0      0

SD =

8×1 string array

"Cw1DTw1=T1/Rw1-Tw1 (1/Rw1+1/ (R11+R24) +1/R21+1/ (R31+R43) +1/ (R41+R32) +1/R51+1/R61) +Tw2 (1/ (R41+R32) ) +Tw3 (1/ (R31+R43) ) +Tw4 (1/ (R11+R24) ) +Te (1/R21+1/R51) +Tg (1/R61) "
"Cr1DT1=-T1/Rw1+Tw1/Rw1"
"Cw2DTw2=T2/Rw2+Tw1 (1/ (R32+R41) ) -Tw2 (1/Rw2+1/R12+1/R22+1/ (R32+R41) ) +1/R42+1/R52+1/R62) +Te (1/R12+1/R22+1/R42+1/R52) +Tg (1/R62) "
"Cr2DT2=-T2/Rw2+Tw2/Rw2"
"Cw3DTw3=T3/Rw3+Tw1 (1/ (R43+R31) ) -Tw3 (1/Rw3+1/R13+1/R23+1/R33+1/ (R43+R31) ) +1/R53+1/R63) +Te (1/R13+1/R23+1/R33+1/R53) +Tg (1/R63) "
"Cr3DT3=-T3/Rw3+Tw3/Rw3"
"Cw4DTw4=T4/Rw4+Tw1 (1/ (R24+R11) ) -Tw4 (1/Rw4+1/R14+1/ (R24+R11) ) +1/R34+1/R44+1/R54+1/R64) +Te (1/R14+1/R34+1/R44+1/R54) +Tg (1/R64) "
"Cr4DT4=-T4/Rw4+Tw4/Rw4"

```

Figure A6. Case 4: Mathematical model for four thermal zones.

References

1. Czerniawski, T.; Leite, F. Automated digital modeling of existing buildings: A review of visual object recognition methods. *Autom. Constr.* **2020**, *113*, 103131. [CrossRef]
2. Deb, C.; Schlueter, A. Review of data-driven energy modelling techniques for building retrofit. *Renew. Sustain. Energy Rev.* **2021**, *144*, 110990. [CrossRef]
3. Hou, D.; Hassan, I.G.; Wang, L. Review on building energy model calibration by Bayesian inference. *Renew. Sustain. Energy Rev.* **2021**, *143*, 110930. [CrossRef]
4. Lu, D.B.; Warsinger, D.M. Energy savings of retrofitting residential buildings with variable air volume systems across different climates. *J. Build. Eng.* **2020**, *30*, 101223. [CrossRef]
5. United Nations. *The 2030 Agenda for Sustainable Development*; United Nations: New York, NY, USA, 2016. [CrossRef]
6. United Nations. *The Paris Agreement*; ONU: New York, NY, USA, 2016; pp. 78–79.
7. Li, W.; Wang, S.; Koo, C. A real-time optimal control strategy for multi-zone VAV air-conditioning systems adopting a multi-agent based distributed optimization method. *Appl. Energy* **2021**, *287*, 116605. [CrossRef]
8. Biyik, E.; Kahraman, A. A predictive control strategy for optimal management of peak load, thermal comfort, energy storage and renewables in multi-zone buildings. *J. Build. Eng.* **2019**, *25*, 100826. [CrossRef]
9. Harputlugil, T.; de Wilde, P. The interaction between humans and buildings for energy efficiency: A critical review. *Energy Res. Soc. Sci.* **2021**, *71*, 101828. [CrossRef]
10. Li, Z.; Zhang, J. Study on the distributed model predictive control for multi-zone buildings in personalized heating. *Energy Build.* **2021**, *231*, 110627. [CrossRef]
11. Cockroft, J.; Cowie, A.; Samuel, A.; Strachan, P. Potential energy savings achievable by zoned control of individual rooms in UK housing compared to standard central heating controls. *Energy Build.* **2017**, *136*, 1–11. [CrossRef]
12. Florez Montes, F. Análisis Dinámico del Confort en Edificios: Estrategias de Control Adaptativo en Modos Deslizantes. Ph.D. Thesis, Universidad Nacional de Colombia and Universitat Politècnica de València, Valencia, Spain, 2020.
13. Gunay, H.B.; Shi, Z.; Newsham, G.; Moromisato, R. Detection of zone sensor and actuator faults through inverse greybox modelling. *Build. Environ.* **2020**, *171*, 106659. [CrossRef]
14. Alwisy, A.; BuHamdan, S.; Gül, M. Evidence-based ranking of green building design factors according to leading energy modelling tools. *Sustain. Cities Soc.* **2019**, *47*, 101491. [CrossRef]
15. Gao, X.W.; Liu, H.Y.; Ruan, B. Discontinuous zone free element method with variable condensation and applications in thermal-stress analysis of functionally graded material structures with cracks. *Comput. Struct.* **2021**, *243*, 106411. [CrossRef]
16. Tian, W.; Sevilla, T.A.; Zuo, W.; Sohn, M.D. Coupling fast fluid dynamics and multizone airflow models in Modelica Buildings library to simulate the dynamics of HVAC systems. *Build. Environ.* **2017**, *122*, 269–286. [CrossRef]
17. Amin, U.; Hossain, M.J.; Fernandez, E. Optimal price based control of HVAC systems in multizone office buildings for demand response. *J. Clean. Prod.* **2020**, *270*, 122059. [CrossRef]
18. Berger, J.; Guernouti, S.; Woloszyn, M.; Chinesta, F. Proper Generalised Decomposition for heat and moisture multizone. *Energy Build.* **2015**, *105*, 334–351. [CrossRef]
19. Ng, L.C.; Musser, A.; Persily, A.K.; Emmerich, S.J. Multizone airflow models for calculating infiltration rates in commercial reference buildings. *Energy Build.* **2013**, *58*, 11–18. [CrossRef]
20. Garnier, A.; Eynard, J.; Caussanel, M.; Grieu, S. Predictive control of multizone HVAC systems in non-residential buildings. *IFAC Proc. Vol. IFAC-PapersOnline* **2014**, *19*, 12080–12085. [CrossRef]
21. Żabnieńska-Góra, A.; Khordehghah, N.; Jouhara, H. Annual performance analysis of the PV/T system for the heat demand of a low-energy single-family building. *Renew. Energy* **2021**, *163*, 1923–1931. [CrossRef]
22. Gao, Y.; Li, S.; Fu, X.; Dong, W.; Lu, B.; Li, Z. Energy management and demand response with intelligent learning for multi-thermal-zone buildings. *Energy* **2020**, *210*, 118411. [CrossRef]
23. Wang, Z.; Liu, J.; Zhang, Y.; Yuan, H.; Zhang, R.; Srinivasan, R.S. Practical issues in implementing machine-learning models for building energy efficiency: Moving beyond obstacles. *Renew. Sustain. Energy Rev.* **2021**, *143*, 110929. [CrossRef]
24. Killian, M.; Mayer, B.; Kozek, M. Effective fuzzy black-box modeling for building heating dynamics. *Energy Build.* **2015**, *96*, 175–186. [CrossRef]
25. Li, Y.; O'Neill, Z.; Zhang, L.; Chen, J.; Im, P.; DeGraw, J. Grey-box modeling and application for building energy simulations—A critical review. *Renew. Sustain. Energy Rev.* **2021**, *146*, 111174. [CrossRef]
26. Yu, X.; Georges, L.; Inslund, L. Data pre-processing and optimization techniques for stochastic and deterministic low-order grey-box models of residential buildings. *Energy Build.* **2021**, *236*, 110775. [CrossRef]
27. Abokersh, M.H.; Spiekman, M.; Vijlbrief, O.; van Goch, T.A.; Vallès, M.; Boer, D. A real-time diagnostic tool for evaluating the thermal performance of nearly zero energy buildings. *Appl. Energy* **2021**, *281*, 116091. [CrossRef]
28. Brastein, O.M.; Ghaderi, A.; Pfeiffer, C.F.; Skeie, N.O. Analysing uncertainty in parameter estimation and prediction for grey-box building thermal behaviour models. *Energy Build.* **2020**, *224*, 110236. [CrossRef]
29. Vivian, J.; Zarrella, A.; Emmi, G.; De Carli, M. An evaluation of the suitability of lumped-capacitance models in calculating energy needs and thermal behaviour of buildings. *Energy Build.* **2017**, *150*, 447–465. [CrossRef]
30. Underwood, C.P. An improved lumped parameter method for building thermal modelling. *Energy Build.* **2014**, *79*, 191–201. [CrossRef]

31. Parker, S.T.; Williamson, S. Visual assessment of contaminant impacts in multizone buildings. *Build. Environ.* **2016**, *102*, 39–53. [CrossRef]
32. Tagade, P.M.; Jeong, B.M.; Choi, H.L. A Gaussian process emulator approach for rapid contaminant characterization with an integrated multizone-CFD model. *Build. Environ.* **2013**, *70*, 232–244. [CrossRef]
33. Nguyen, D.H.; Funabashi, T. Decentralized Control Design for User Comfort and Energy Saving in Multi-zone Buildings. *Energy Procedia* **2019**, *156*, 172–176. [CrossRef]
34. Subramaniam, M.; Jain, T.; Yame, J. J. Bilinear model-based diagnosis of lock-in-place failures of variable-air-volume HVAC systems of multizone buildings. *J. Build. Eng.* **2020**, *28*, 101023. [CrossRef]
35. Ghiaus, C.; Ahmad, N. Thermal circuits assembling and state-space extraction for modelling heat transfer in buildings. *Energy* **2020**, *195*, 117019. [CrossRef]
36. Chegari, B.; Tabaa, M.; Simeu, E.; Moutaouakkil, F.; Medromi, H. Multi-objective optimization of building energy performance and indoor thermal comfort by combining artificial neural networks and metaheuristic algorithms. *Energy Build.* **2021**, *239*, 110839. [CrossRef]
37. Andrade-Cabrera, C.; Burke, D.; Turner, W.J.; Finn, D.P. Ensemble Calibration of lumped parameter retrofit building models using Particle Swarm Optimization. *Energy Build.* **2017**, *155*, 513–532. [CrossRef]
38. Rouchier, S.; Jiménez, M.J.; Castaño, S. Sequential Monte Carlo for on-line parameter estimation of a lumped building energy model. *Energy Build.* **2019**, *187*, 86–94. [CrossRef]
39. Dimitriou, V.; Firth, S.K.; Hassan, T.M.; Kane, T. The applicability of Lumped Parameter modelling in houses using in-situ measurements. *Energy Build.* **2020**, *223*, 110068. [CrossRef]
40. Lin, Y.; Middelkoop, T.; Barooah, P. Identification of control-oriented thermal models of rooms in multi-room buildings. In Proceedings of the 2012 IEEE 51st Annual Conference on Decision and Control (CDC), Maui, HI, USA, 10–13 December 2013; pp. 1–27.
41. Florez, F.; de Cordoba, P.F.; Tabora, J.; Polo, M.; Castro-Palacio, J.C.; Pérez-Quiles, M.J. Sliding modes control for heat transfer in geodesic domes. *Mathematics* **2020**, *8*, 902. [CrossRef]
42. Florez, F.; Córdoba, P.F.D.; Higón, J.L.; Olivar, G.; Tabora, J. Modeling, Simulation, and Temperature Control of a Thermal Zone with Sliding Modes Strategy. *Mathematics* **2019**, *7*, 503. [CrossRef]
43. Cengel, Y. *Heat and Mass Transfer*; John Wiley and Sons: Hoboken, NJ, USA, 2015.

Disclaimer/Publisher’s Note: The statements, opinions and data contained in all publications are solely those of the individual author(s) and contributor(s) and not of MDPI and/or the editor(s). MDPI and/or the editor(s) disclaim responsibility for any injury to people or property resulting from any ideas, methods, instructions or products referred to in the content.

Article

Towards the Decarbonization of Industrial Districts through Renewable Energy Communities: Techno-Economic Feasibility of an Italian Case Study

Francesca Ceglia, Elisa Marrasso, Chiara Martone, Giovanna Pallotta *, Carlo Roselli and Maurizio Sasso

Department of Engineering, University of Sannio, 82100 Benevento, Italy; fceglia@unisannio.it (F.C.); marrasso@unisannio.it (E.M.); c.martone4@studenti.unisannio.it (C.M.); croselli@unisannio.it (C.R.); sasso@unisannio.it (M.S.)

* Correspondence: giopallotta@unisannio.it

Abstract: In Europe, the recast of Directive 2018/2001 defined Renewable Energy Communities as innovative configurations for renewable energy sharing between different end user types. In this regard, this work aims to assess the benefits following the constitution of a Renewable Energy Community in the industrial area of Benevento (South of Italy), involving a mixed-use building and an industrial wastewater treatment plant. The alternative single end users' configuration has been also examined, and both solutions have been compared with the current state where the users' electric energy requests are fully met by the power grid. The users have been equipped with a 466 kW_p photovoltaic plant, modelled in HOMER Pro[®], providing in input experimental meteorological data (global solar radiation and air temperature) collected by one of the weather control units in Benevento. Real data about users' electric energy demand have been gathered from their electricity bills, and when unavailable their electric load profiles on an hourly basis have been reconstructed based on the aggregated monthly data. Energy sharing has been proven to increase energy self-consumption and the users' self-sufficiency. Annually, the primary energy demand is reduced by 577 MWh (1.2 MWh/kW_p), carbon dioxide emissions by 84 tCO₂ and operative costs by 101 kEUR.

Keywords: Renewable Energy Community; industrial districts; dynamic simulation; energy self-sufficiency; energy sharing; experimental data

Citation: Ceglia, F.; Marrasso, E.; Martone, C.; Pallotta, G.; Roselli, C.; Sasso, M. Towards the Decarbonization of Industrial Districts through Renewable Energy Communities: Techno-Economic Feasibility of an Italian Case Study. *Energies* **2023**, *16*, 2722. <https://doi.org/10.3390/en16062722>

Academic Editors: Ala Hasan and Hassam Ur Rehman

Received: 23 February 2023

Revised: 9 March 2023

Accepted: 13 March 2023

Published: 14 March 2023



Copyright: © 2023 by the authors. Licensee MDPI, Basel, Switzerland. This article is an open access article distributed under the terms and conditions of the Creative Commons Attribution (CC BY) license (<https://creativecommons.org/licenses/by/4.0/>).

1. Introduction

The recent European “Green Deal Industrial Plan” [1] reaffirms the commitment of the European Union towards the 55% reduction of carbon dioxide (CO₂) emissions compared to the 1990 levels by 2030 [2] and carbon neutrality by 2050 [3] by supporting the roll out of renewable energy sources (RESs) in the industrial sector. Yet, in 2021, the industrial sector’s global CO₂ emissions amounted to 9.4 GtCO₂ and represented one-quarter of the total (except for indirect emissions due to electricity production for industrial processes) [4]. As such, the industry is nowadays not on track to achieve either the Net Zero Emissions goal by 2050, or the objectives introduced by the Paris Agreement of the United Nations Framework Convention on Climate Change [5]. Albeit the increasing investments of industrial companies, the improvements in energy efficiency, the uptake of low-carbon technologies and the deployment of RES-based plants are advancing more slowly than needed [6,7]. Hence, they would require additional support and incentivization by single countries’ policies [8]. Techno-economic issues especially discourage single small and medium-sized enterprises from investing in energy efficiency and RESs, thus hindering the potentialities of these interventions. For instance, the valorization of large unused surfaces often available in industrial areas through RES-based plants would open up the opportunity to reinforce the provision of renewable energy in urban centers [9]. In turn, this solution would increase the social acceptability of industrial parks [10].

The Clean Energy for All European Package [11] may address these shortcomings. In 2018, the recast of the Renewable Energy Directive (REDII) introduced Renewable Energy Communities (RECs) [12], just before the Internal Electricity Market Directive [13] was launched in 2019 defining Citizen Energy Communities. Both directives promote energy sharing by identifying the novel central and active role of the consumer in the electricity market and support the spreading of RES-based plants by means of collective energy initiatives [14,15]. RECs, in particular, can involve different end user types. Indeed, they are open to voluntary participation, not only of natural persons and local authorities, including municipalities but also micro, small or medium-sized enterprises. The co-participation of different user types is beneficial to the performance of RECs [16], since it provides positive outcomes from the energy, economic and environmental point of view, as already stated before the definition of RECs in studies assessing the profitability of the load sharing approach [17]. Broadly speaking, the combination of different load curves increases the generation plants' operating hours [18] and results in a smoother aggregated load profile, which typically lowers the mismatch between energy demand and supply from RES-based plants. In this regard, a REC involving residential consumers and a winery in the city of Reguengos de Monsaraz (South of Portugal) has been examined [19], showing that the centralization of a photovoltaic (PV) plant improves the cost-effectiveness of the investment, but increases the usage of the electricity distribution grid. The optimal combination of different types of prosumers in Citizen Energy Communities and RECs has been assessed from the economic standpoint in [20] being complementarity of loads relevant to the optimal exploitation of dispatchable and non-dispatchable RESs. In particular, costs may be reduced up to 15–20% when coupling two prosumers, one belonging to the residential sector and equipped with a PV plant, and the other belonging to the industrial, agricultural or tertiary sector and served by an internal combustion engine. The heterogeneity of user types characterizing an Italian case study has been recognized as having the potential to highly enhance the flexibility and self-sufficiency of RECs also in [21], where the Schoonschip neighborhood in Amsterdam (The Netherlands) and the Marsciano Community in Marsciano (Central Italy) have been compared. The former involves only residential users, whereas the latter includes a dairy, an engineering studio, a medical center and a household.

As regards industrial areas, they can take advantage of the complementarity of loads as well, being characterized by energy requests relating to different end-use types, such as the activation of production processes, service facilities, safety and transportation systems, as well as the lighting, heating and cooling of office buildings [22]. Hence, the implementation of RECs in industrial areas may combine the potentialities offered by the growing integration of RES-based plants with the opportunities relating to the aggregation of complementary loads. The deployment of such configurations within the industrial sector constitutes a field of research still quite new, although the adoption of collective energy strategies aimed at supporting the implementation of projects involving multiple firms for reducing the reliance on fossil energy resources has been widely discussed in the literature [23,24]. Most scientific works provide insights about industrial and urban-industrial symbiosis [25,26]. In this framework, the concepts of energy industrial parks, zero-carbon industrial parks and positive energy industrial parks have been introduced [27,28]. In [29], the development of a zero-carbon emission industrial park in China has been assessed. The availability of RESs to fully decarbonize the provision of electric energy represents one of the main barriers to its development, as well as the production of waste and the indispensability of fossil materials for some processes, which require the use of carbon capture technologies. In addition to technical issues, insufficient funds may represent a significant financial obstacle and discourage enterprises from pursuing the realization of zero-carbon projects. In [30], the optimal configuration involving different RES-based plants serving a centralized water facility in a Malaysian industrial park has been defined by using mixed-integer non-linear programming techniques. The optimal solution obtained could reduce greenhouse gas emissions up to 70%. With regards to an Italian industrial district, the enhancing exploitation of RESs has been investigated in [31]. Based on the main

findings, an increased economic support would make the adoption of RES-based plants more attractive from the economic point of view. The development of community energy systems in industrial clusters has been examined in [32] by focusing on a case study in Arak (Iran). Again, this solution has been proven to be affected by economic and institutional barriers, despite the technical feasibility of RES-based plants meeting the electric energy demand of the firms joining the collective intervention. Renewable Energy Cooperatives as clusters of both enterprises and local stakeholders have been analyzed in [33], where they have been recognized as strategic configurations to manage the inherent uncertainty of investments for RES-based plants.

Ultimately, most scientific works dealing with collective actions aiming at supporting the deployment of RES-based plants in the industrial sector do not address the opportunities of constituting RECs. The majority of works focusing on the implementation of RECs refers to residential and tertiary sectors and most of them are based on PV plants because of its technology's readiness. For example, Cirone et al. [34] investigated the implementation of a REC in Soveria Mannelli (South of Italy), composed of four public buildings. Ancona et al. [35] analyzed the application potential of the REC concept with district heating networks, maximizing internal energy sharing through PV systems and heat pumps for self-consumption, self-sufficiency and efficient investments. Results show that the proposed design achieves a significant reduction in energy demand, emissions and costs. Ceglia et al. [36] analyzed a PV-based REC in Southern Italy, demonstrating its potential to significantly reduce the energy poverty index from 9.84% to 5.25% regarding a typical residential user. Among all others, these few examples demonstrate the potential of PV technology to provide clean and sustainable energy to communities in a cost-effective manner. However, according to Directive REDII, there is a need to support the uptake of renewable-based plants by citizens as well as small, medium and micro-enterprises by simplifying the notification procedures for the connection of small-size and decentralized renewable-based plants to the grid and clarifying the time-limits for authorization issues and administrative permit granting processes [12]. As regards industrial RECs, these actions are advocated considering their significant potential in terms of carbon emission reduction at the national level, which depends on the specific context, policies and regulations put in place to support their development. The International Energy Agency estimated the potential global carbon emission reduction achievable by 2050 through the implementation of RECs in the industrial sector as equal to 40% [37]. For this purpose, industrial RECs may take advantage of the collaboration between small and medium-sized enterprises, characterized by a high sense of community, social responsibility and openness to technological innovation. As additional benefits, the analysis and demonstration of social, economic and environmental benefits of a PV-based REC in an industrial district may provide to policy makers valuable information about the design and implementation of policies supporting the growth of sustainable communities, enhance the understanding of factors fostering community engagement and cooperation and identify potential barriers to their implementation and constitution. Yet, to the best of authors' knowledge, the literature lacks studies focused on industrial RECs. The exclusion of large companies from participation in such configurations may be a reason for the lack of interest in their constitution at the European level [38]. However, their potential is usually disregarded not only in the pathways towards the full decarbonization of the European industry [39] but also in studies focusing on the reduction of energy requests and carbon emissions of small- and medium-sized enterprises [40].

Therefore, this study aims at bridging this gap and investigates the constitution of a REC in the industrial area of Benevento (Italy). The REC under examination involves two different kinds of user, namely a mixed-use building and the consortium wastewater treatment plant (WWTP). Their choice is expected to take advantage of the diversity of users' load profiles due to electric energy demand linked to different end uses in a real case study. The ultimate goal is to demonstrate the feasibility of RECs in industrial areas without restraining the scope of interest to the boundaries of the industrial site being analyzed, but

rather to stimulate the replication of the analysis performed in this study within the literature in order to foster real applications. The users under examination have been equipped with a PV plant. Within the REC boundaries, energy sharing has been implemented according to the Italian regulation, that is, under the virtual self-consumption scheme. In addition to this proposed scenario, the alternative single end users' configuration where energy sharing has been neglected has been investigated too. In this case, the PV plant has been divided into two portions, each owned by one user. Accordingly, each portion of the PV plant has been assumed to supply electric energy only to its owner, and the potential surplus to be fed to the grid. Both examined scenarios have been compared with the current status, where the users' electric energy demand is covered by the power grid (PG), as detailed in Section 2, along with the users' load profiles, design and model adopted to simulate the PV plant. The results obtained from the comparison of both scenarios with the baseline case are introduced and discussed in Section 3, whereas in Section 4, the conclusions have been drawn.

2. Materials and Methods

In this section, the steps followed for developing the analysis carried-out in this work are detailed, starting from the characterization of investigated users' electric energy requests (Section 2.1) and then focusing on the design of the PV plant serving them (Section 2.2). Lastly, the models adopted for performing the dynamic simulation and the energy, environmental and economic analysis under two different scenarios are described (Section 2.3).

2.1. Users' Electric Energy Requests Characterization

The industrial area of Benevento covers a surface of 3,179,357 m². It is divided into seven zones and includes several micro, small, medium, as well as internationally renowned enterprises. The collective services center (CSC) building and the consortium WWTP have been considered as users in this study (*Us#1* and *Us#2*, respectively). Their location is shown in the satellite view obtained from Google Earth [41] in Figure 1. The CSC building is the setting of the Consortium Centre for Management, which is responsible for the management of the industrial area and common services, and four companies operating in the services sector. The WWTP is deputed to the treatment of the wastewater produced from the office building, the enterprises located in the area and urban wastewater produced in one of the districts of a municipality nearby.



Figure 1. Aerial view of users' location.

The data about users' electric energy demand in 2021 have been gathered from their electricity bills. They are referred to nine points of delivery (PODs), seven serving *Us#1* and two serving *Us#2*. In the case of two PODs (one serving *Us#1* and one serving *Us#2*), the 2021 electric load curves with a quarter-hour time step have been made available by the Italian electricity distributor [42]. For the remaining seven PODs, the load curves on a quarter-hourly basis have been constructed, manipulating the aggregated monthly data known from the bills. Namely, the monthly electric energy demand has been split

into hours, depending on the day of the week and distinguishing between peak hours (belonging to the F1 band), intermediate hours (belonging to the F2 band) and evening and weekend hours (belonging to the F3 band) [43], as detailed in Table 1.

Table 1. Time bands for electric energy purchase.

Time Band	Days	Time
F1: Peak hours	From Monday to Friday, excluding public holidays	From 8:00 a.m. to 7:00 p.m.
F2: Intermediate hours	From Monday to Friday, excluding public holidays	From 7:00 a.m. to 8:00 a.m. and from 7:00 p.m. to 11:00 p.m.
	Saturday, excluding public holidays	From 7:00 a.m. to 11:00 p.m.
F3: Evening and weekend hours	From Monday to Saturday	From 11:00 p.m. to 7:00 a.m.
	Sunday and public holidays	All-day

The users' total load profiles on a quarter-hourly basis are shown in Figure 2 with reference to 2021. The graphs have been constructed by varying the color of indicators depending on the time in order to emphasize the distribution of the electric load during the day. In the case of *Us#1*, the electric load is clearly higher during morning hours, and minimum load values are detected in the evening. By contrast, in the case of *Us#2*, the distinction between morning and evening loads is not straightforward. As it can be seen, the loads of the two users are characterized by different orders of magnitude. Indeed, the load of *Us#1* is at most equal to 46.5 kW in January. By contrast, *Us#2* has significantly higher requests, and its maximum load amounts to 186.0 kW in July. Moreover, the two load profiles are differently distributed throughout the year. In 2021, starting from January, the maximum electric energy requests of *Us#1* decrease during spring until June. In June, a rising trend can be found, which stops in July, and restarts from August onwards. Conversely, the electric energy requests of *Us#2* are characterized by a rising trend in the spring months until the end of June, when the maximum load is found. From July onwards, maximum load values start decreasing.

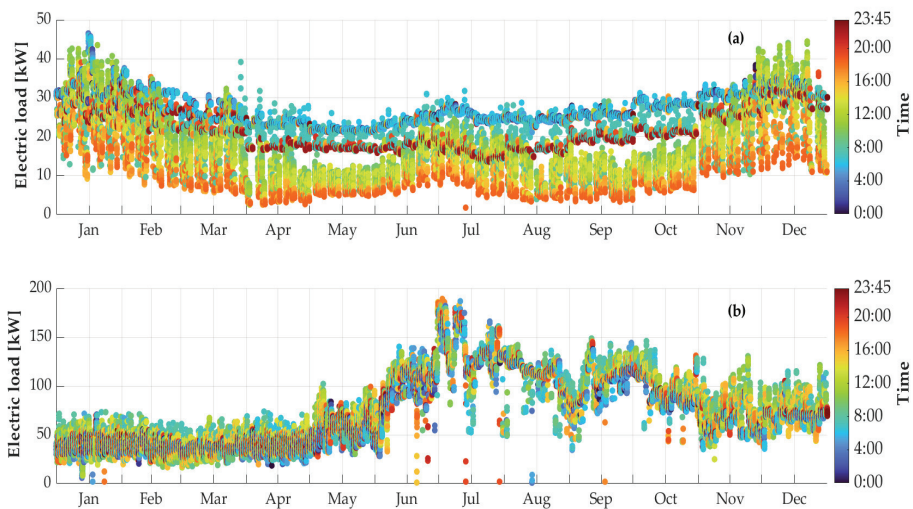


Figure 2. Electric load profile on a quarter-hourly basis of *Us#1* (a) and *Us#2* (b) in 2021.

The two users' electric energy demand (E_{el}^{Us}) is quantified on a monthly basis in Table 2, along with the relating average unitary purchase cost (c_{el}^{Us}) incurred by the users for electricity purchase (VAT included). First, the distinction between $Us\#1$ and $Us\#2$ has been made; then, their loads have been considered as a whole. In the latter case, the average unitary purchase cost of electricity (c_{el}^{REC}) has been evaluated as the ratio between the monthly grand total of users' expenses for electric energy purchase (that is, the sum of the costs monthly incurred by $Us\#1$ and $Us\#2$) and the total monthly electric load (that is, the sum of $E_{el}^{Us\#1}$ and $E_{el}^{Us\#2}$). As it can be seen, in all months of 2021 $E_{el}^{Us\#2}$ is higher than $E_{el}^{Us\#1}$, especially in summer and autumn months. Overall, in 2021, the electric energy demand of $Us\#1$ is equal to 190 MWh/y, whereas it amounts to 655 MWh/y regarding $Us\#2$. Hence, on a yearly basis, the two users require in total 846 MWh/y. c_{el}^{Us} ranges between 0.20 and 0.49 EUR/kWh. This maximum value is detected in December as regards $Us\#1$, whereas the maximum $c_{el}^{Us\#2}$, found again in December, is equal to 0.45 EUR/kWh. The maximum c_{el}^{REC} is intermediate compared to the maximum $c_{el}^{Us\#1}$ and $c_{el}^{Us\#2}$, being equal to 0.46 EUR/kWh in December.

Table 2. Users' monthly electric energy demand and relating average unitary purchase price of electricity in 2021.

Month	Electric Energy Demand [MWh]			Electricity Average Unitary Purchase Price [EUR/kWh]		
	$Us\#1$	$Us\#2$	Total	$c_{el}^{Us\#1}$	$c_{el}^{Us\#2}$	c_{el}^{REC}
January	21.6	29.9	51.5	0.22	0.20	0.21
February	17.0	25.9	42.9	0.23	0.20	0.21
March	15.7	26.9	42.6	0.24	0.21	0.22
April	12.4	28.1	40.6	0.23	0.22	0.22
May	12.2	42.0	54.2	0.23	0.22	0.22
June	13.3	71.0	84.4	0.23	0.23	0.23
July	14.5	100.2	114.7	0.23	0.22	0.22
August	13.3	83.6	96.9	0.28	0.23	0.24
September	13.4	74.7	88.2	0.33	0.29	0.30
October	15.8	71.6	87.4	0.38	0.37	0.37
November	19.0	47.9	66.9	0.41	0.39	0.39
December	22.1	53.5	75.5	0.49	0.45	0.46
Total	190	655	846	0.30	0.28	0.28

2.2. Photovoltaic Plant Design

The surfaces selected for installing the PV panels have been highlighted in Figure 3. Specifically, the PV panels belonging to $Us\#1$ have been assumed to be placed on the rooftop of the CSC building, on unused land nearby, and on PV canopies in the parking area, whereas those belonging to $Us\#2$ on the horizontal rooftop of seven establishments. Monocrystalline cell PV panels with 327 W of peak power have been chosen for installation [44]. Their main features are listed in Table 3.

The area of each surface has been measured by excluding the portions subjected to shading phenomena and considering a 15% reduction in order to ensure enough service spaces. Concerning PV canopies, the area of each parking spot has been estimated as equal to 12.5 m², being the minimum length and the minimum width of each equal to 5 m and 2.5 m, respectively [45]. Optimal installation conditions for the PV panels have been chosen in order to maximize the PV plant producibility by maximizing the solar radiation captured by each module and by avoiding shading phenomena between consecutive rows of panels [46]. In this regard, the minimum spacing distance D between adjacent panel rows needed to avoid shading phenomena has been determined using Equation (1),

$$D = L \cos \beta \left(1 + \frac{\tan \beta}{\tan \alpha} \right), \quad (1)$$

where the term L represents the height of each panel, α the sun elevation angle and β the tilt angle. Concerning the type of panel chosen, L is equal to 1.6 m. Both α and β depend on the latitude of the installation site, which is equal to 41° in the case of Benevento. For determining D , α has been evaluated on December 21st at noon. Hence, the resulting α is equal to 25.5° at the latitude of the installation site being analyzed. As regards β , in Italy its optimal value is equal to the difference between the latitude angle itself and 10° [46]. As a result, being β equal to 31° and α equal to 25.5° , D is equal to 3.0 m. The gross area of each panel, equal to 1.6 m^2 , has been increased by 1.5 m^2 , resulting in 3.1 m^2 . For estimating the number of panels installed on the tilted sector of the rooftop of the CSC building, the panels' gross area has not been increased since they are supposed to be directly integrated into the roof. Instead, as regards the parking area, four panels are supposed to be installed in each spot for a total of 63 spots. Overall, the total number of PV panels installable is equal to 1424, and the PV plant peak power is equal to 466 kW, of which 431 and 35 kW are installed in sites pertaining to $Us\#1$ and to $Us\#2$, respectively. The results obtained are detailed in Table 4. For each installation site, the type of surface (horizontal or tilted), the exposure, the area, the number of panels and the peak power are reported. The only tilted surface available is the semicircular sector representing the central portion of the rooftop of the CSC building. In particular, it is tilted about 5° and measures 170 m^2 . Since the gross area of each panel is equal to 1.6 m^2 , 104 panels have been assumed to be installed on this surface. The remaining surfaces are all horizontal and have an overall extension of 4163 m^2 . In particular, the horizontal portion of the rooftop of the CSC building measures 486 m^2 , the unused land 2550 m^2 and the rooftops of WWTP 340 m^2 in total. Considering the panels' gross area increased by the space needed to avoid the shading phenomena, 154, 807 and 107 panels have been assumed to be installed on each surface, respectively. In accordance with the assumptions of the dynamic simulation software and when not prevented by the installation site, the azimuth angle of panels installed on horizontal surfaces has been set as equal to 0° in order to have south-facing panels in compliance with optimal installation conditions in Italy.

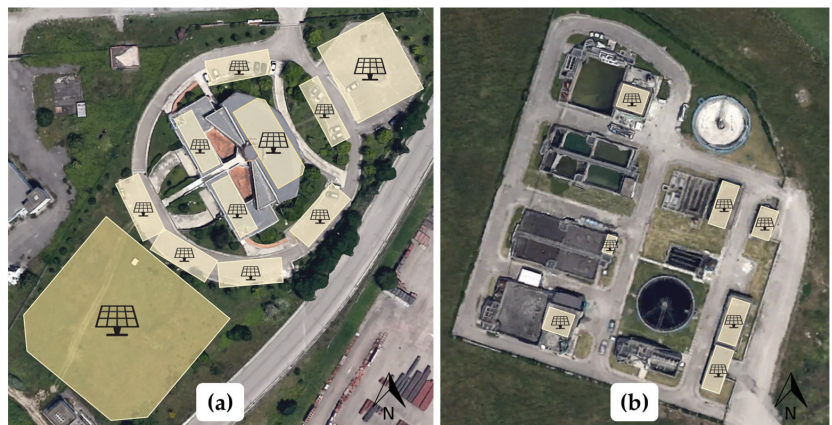


Figure 3. Aerial view of the surfaces selected for installing the PV plant, belonging to $Us\#1$ (a) and $Us\#2$ (b).

Table 3. PV panels' technical parameters [44].

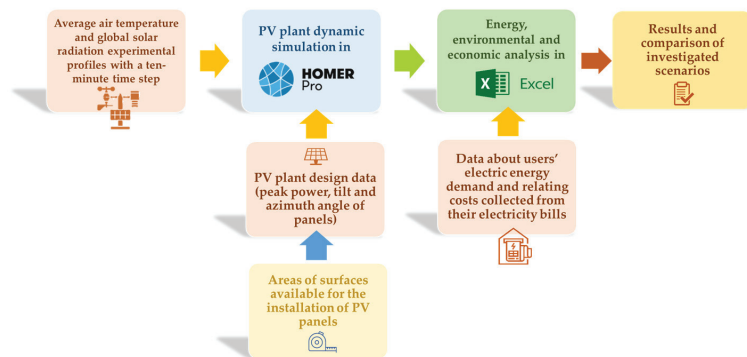
Parameter	Value
Peak power [W]	327
Efficiency [%]	20.1
Maximum power voltage [V]	54.7
Maximum power current [A]	6.0
Open circuit voltage [V]	64.9
Short circuit current [A]	6.5
Temperature coefficient of power [%/°C]	−0.4
Temperature coefficient of voltage [mV/°C]	−176.6
Temperature coefficient of current [mA/°C]	2.6
Gross area [m ²]	1.6

Table 4. Characterization of surfaces available for the installation of the PV panels.

User	Installation Site	Type of Surface	Exposure	Area [m ²]	Number of Panels	Peak Power [kW]
Us#1	CSC building's rooftop	Horizontal	South	486	154	50
	CSC building's rooftop	Tilted	South-West	170	104	34
			South	200	64	21
	Parking area	Horizontal	South-West	475	152	50
			South-East	112	36	12
Unused land	Horizontal	South	2550	807	264	
Us#2	Buildings' rooftop	Horizontal	South	340	107	35
Total	-	-	-	4333	1424	466

2.3. Model Description

A schematic overview of the methodology adopted in this work is shown in Figure 4. The electric energy production profile of each portion of the PV plant, distinguished based on the installation site and the exposure, has been evaluated on a quarter-hourly basis by using the software HOMER Pro[®] [47]. The dynamic simulation has been carried out over one year. Hourly meteorological data about global solar radiation and air temperature, evaluated as hourly average values of the data collected by one of the weather control units in Benevento during 2021 with a ten-minute time step, have been provided as input to the software.

**Figure 4.** Methodology.

The PV generation curves resulting from the simulation carried out in HOMER Pro[®] have been post-processed in Microsoft Excel [48] for evaluating with a one-hour time step (θ), the electric energy consumed on-site by the users ($E_{el}^{OSC}(\theta)$), the surplus fed into the grid ($E_{el}^{TG}(\theta)$) and the residual electric load drawn from the grid ($E_{el}^{PG}(\theta)$). Namely, $E_{el}^{OSC}(\theta)$ has been evaluated using Equation (2),

$$E_{el}^{OSC}(\theta) = \min\left(E_{el}^{PV}(\theta), E_{el}^{Us}(\theta)\right). \tag{2}$$

where the term $E_{el}^{PV}(\theta)$ represents the electric energy hourly supplied by the PV plant, evaluated starting from the quarter-hour data resulting from the dynamic simulation, and $E_{el}^{Us}(\theta)$ the users' hourly electric energy demand. $E_{el}^{PG}(\theta)$ and $E_{el}^{TG}(\theta)$ have been easily determined once estimated $E_{el}^{OSC}(\theta)$.

The profitability of the PV plant has been investigated under two different scenarios, shown in Figure 5, along with the reference baseline case (BC), where the users' electric energy demand is fully met by the PG. The two alternative solutions have been outlined as follows:

- in the single end users' scenario (hereinafter recalled as noREC scenario), the PV plant has been divided into two portions, each owned by one user, and the sharing of electric energy has been neglected. Thus, the PV panels installed in the sites pertaining to Us#1 (the rooftop of the CSC building, the parking area and the unused land) have been assumed to supply renewable electricity only to Us#1 itself. Likewise, those installed on the rooftop of the WWTP buildings only to Us#2. Hence, each user has the opportunity to self-consume the renewable electricity supplied by his own plant and inject into the PG the potential surplus;
- in the REC scenario, the PV plant has been treated as a whole and supplies electricity both to Us#1 and Us#2, which are involved in the REC. Electricity sharing has been implemented in compliance with the Italian regulation about RECs, that is, according to the virtual self-consumption scheme for users under the same primary electric substation. On the one hand, all the electric energy supplied by the PV plant is injected into the primary substation; on the other, the users draw electric energy from the primary substation to meet their requests since no physical self-consumption takes place. Electric energy virtual self-consumption is realized when the absorption from and injection to the primary substation occur simultaneously. The energy balance on the primary substation is evaluated on an hourly basis [49].

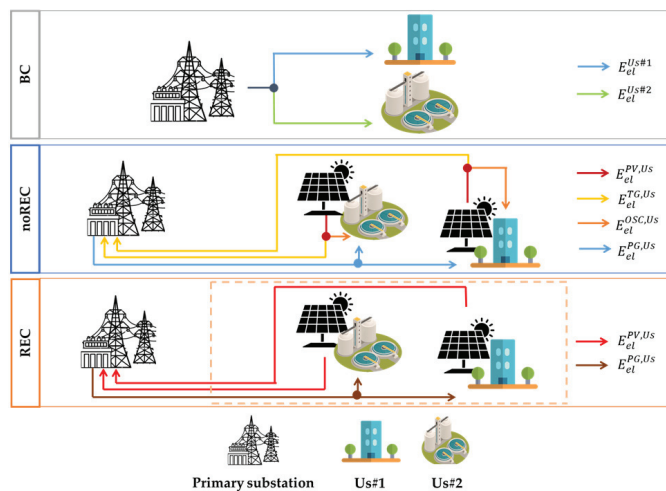


Figure 5. Layout of investigated scenarios.

No-REC and REC scenarios have been compared with the BC case from the energy, environmental and economic points of view. As for the energy analysis, the self-consumption d_i and self-sufficiency s_i indexes have been evaluated on a monthly basis. Namely, the subscript i accounts for the months in 2021 and thus ranges between January and December. In the no-REC scenario Equations (3) and (4) have been used, respectively. $E_{el,i}^{PV}$ and $E_{el,i}^{OSC}$ have been evaluated as stated in Equations (5) and (6), respectively, where the subscript k accounts for the hour of the i -th month in 2021, thus ranging between 1 and the total number of hours in the same month (NH_i). Two values of d_i^{Us} and s_i^{Us} have been determined, relating to $Us\#1$ ($d_i^{Us\#1}$ and $s_i^{Us\#1}$, respectively) and $Us\#2$ ($d_i^{Us\#2}$ and $s_i^{Us\#2}$, respectively). In particular, $d_i^{Us\#1}$ and $s_i^{Us\#1}$ have been evaluated by using the electric energy supplied on a monthly basis by the portion of the PV plant serving $Us\#1$ ($E_{el,i}^{PV,Us\#1}$), its monthly on-site electric energy consumption ($E_{el,i}^{OSC,Us\#1}$) and its monthly electric load ($E_{el,i}^{Us\#1}$), known from the bills. Likewise, $d_i^{Us\#2}$ and $s_i^{Us\#2}$ have been estimated by using the same variables but referred to as $Us\#2$ ($E_{el,i}^{PV,Us\#2}$, $E_{el,i}^{OSC,Us\#2}$ and $E_{el,i}^{Us\#2}$).

$$d_i^{Us} = \frac{E_{el,i}^{OSC,Us}}{E_{el,i}^{PV,Us}} \tag{3}$$

$$s_i^{Us} = \frac{E_{el,i}^{OSC,Us}}{E_{el,i}^{Us}} \tag{4}$$

$$E_{el,i}^{PV,Us} = \sum_{k=1}^{NH_i} E_{el}^{PV}(\theta_{k,i}) \tag{5}$$

$$E_{el,i}^{OSC,Us} = \sum_{k=1}^{NH_i} E_{el}^{OSC,Us}(\theta_{k,i}) \tag{6}$$

Conversely, in the REC scenario, d_i^{REC} and s_i^{REC} have been evaluated, as stated in Equations (7) and (8), respectively. In each month, $E_{el,i}^{PV,REC}$ has been evaluated as the sum of $E_{el,i}^{PV,Us\#1}$ and $E_{el,i}^{PV,Us\#2}$. Accordingly, $E_{el,i}^{REC}$ has been evaluated as the sum of $E_{el,i}^{Us\#1}$ and $E_{el,i}^{Us\#2}$. Instead, $E_{el,i}^{OSC,REC}$ has been determined according to Equation (9), where the sum of $E_{el,i}^{PV,Us\#1}(\theta_{k,i})$ and $E_{el,i}^{PV,Us\#2}(\theta_{k,i})$ amounts to $E_{el,i}^{PV,REC}(\theta_{k,i})$ and the sum of $E_{el,i}^{Us\#1}(\theta_{k,i})$ and $E_{el,i}^{Us\#2}(\theta_{k,i})$ amounts to $E_{el,i}^{REC}(\theta_{k,i})$. $E_{el,i}^{TG,REC}(\theta_{k,i})$ and $E_{el,i}^{PG,REC}(\theta_{k,i})$ have been determined as in the single end users' configuration once evaluated $E_{el,i}^{PV,REC}(\theta_{k,i})$ and $E_{el,i}^{REC}(\theta_{k,i})$.

$$d_i^{REC} = \frac{E_{el,i}^{OSC,REC}}{E_{el,i}^{PV,REC}} \tag{7}$$

$$s_i^{REC} = \frac{E_{el,i}^{OSC,REC}}{E_{el,i}^{REC}} \tag{8}$$

$$E_{el,i}^{OSC,REC} = \sum_{k=1}^{NH_i} \min\left(E_{el,i}^{PV,Us\#1}(\theta_{k,i}) + E_{el,i}^{PV,Us\#2}(\theta_{k,i}), E_{el,i}^{Us\#1}(\theta_{k,i}) + E_{el,i}^{Us\#2}(\theta_{k,i})\right) \tag{9}$$

Still referring to the energy analysis, the primary energy saving ($\Delta E_{p,i}$) compared to the BC has been evaluated on a monthly basis according to Equation (10) in the no-REC scenario and according to Equation (11) in the REC scenario. In both Equations, the term η_{el}^{PG} represents the average Italian power grid efficiency, equal to 0.509 in 2020 (the year for which the most recent data are available) [50]. $E_{el,i}^{PG,Us}$ and $E_{el,i}^{TG,Us}$ have been estimated on a monthly basis as the sum across the number of hours of the i -th month of $E_{el,i}^{PG,Us}(\theta_{k,i})$ and $E_{el,i}^{TG,Us}(\theta_{k,i})$,

respectively. $E_{el,i}^{PG,REC}$ and $E_{el,i}^{TG,REC}$ have been estimated on a monthly basis as the sum across the number of hours of the i -th month of $E_{el}^{PG,REC}(\theta_{k,i})$ and $E_{el}^{TG,REC}(\theta_{k,i})$, accordingly.

$$\Delta E_{p,i}^{noREC} = \frac{E_{el,i}^{Us\#1} + E_{el,i}^{Us\#2} - E_{el,i}^{PG,Us\#1} - E_{el,i}^{PG,Us\#2}}{\eta_{el}^{PG}} \quad (10)$$

$$\Delta E_{p,i}^{REC} = \frac{E_{el,i}^{REC} - E_{el,i}^{PG,REC}}{\eta_{el}^{PG}} \quad (11)$$

With regards to the environmental analysis, the CO₂ emissions reduction $\Delta CO_{2,i}$ owing to the installation of the PV plant, has been evaluated on a monthly basis. To this purpose, Equation (12) has been adopted in the noREC and Equation (13) in the REC scenario. In both Equations, the term α_{CO_2} represents the 2020 Italian power grid CO₂ emission factor, equal to 286.55 gCO₂/kWh_{el} [50].

$$\Delta CO_{2,i}^{noREC} = \left(E_{el,i}^{Us\#1} + E_{el,i}^{Us\#2} - E_{el,i}^{PG,Us\#1} - E_{el,i}^{PG,Us\#2} \right) \cdot \alpha_{CO_2} \quad (12)$$

$$\Delta CO_2^{REC} = \left(E_{el,i}^{REC} - E_{el,i}^{PG,REC} \right) \cdot \alpha_{CO_2} \quad (13)$$

Finally, as for the economic analysis, the variation in operating costs ΔOC in the noREC and REC scenario compared to the BC has been evaluated on a monthly basis. The monthly operative costs in the BC ($OC_i^{BC,Us\#1}$ and $OC_i^{BC,Us\#2}$) are known from the users' electricity bills. Instead, in the proposed scenarios, they have been evaluated as follows:

- in the noREC scenario, the electricity purchase price has been considered equal to the monthly average value paid in 2021 by each user in the BC, as stated in Table 2 (that is, equal to $c_{el}^{Us\#1}$ and $c_{el}^{Us\#2}$ regarding $Us\#1$ and $Us\#2$, respectively). The surplus electric energy injected into the grid has been supposed to be sold to the Italian "Gestore dei Servizi Energetici" (GSE) according to the Dedicated Withdrawn scheme [51]. In this framework, the hourly electricity selling price ($p_{el}(\theta_{k,i})$) has been assumed to be equal to the 2021 hourly zonal price of electricity in the Central-South bidding zone of the Italian day-ahead electricity market distinguished per month and time-band. As a result, Equation (14) has been used for estimating both $OC_i^{noREC,Us\#1}$ and $OC_i^{noREC,Us\#2}$,

$$OC_i^{noREC,Us} = \left(E_{el,i}^{PG,Us} \cdot c_{el,i}^{Us} + MC_i \right) - \sum_{k=1}^{NH_i} \left(E_{el}^{TG,Us}(\theta_{k,i}) \cdot p_{el}(\theta_{k,i}) \right) \quad (14)$$

In Equation (14), the subscript i keeps the same meaning as above, as well as NH_i . The term MC_i represents the costs due to the maintenance of the PV plant, which have been assumed to be constant and evaluated starting from an annual specific value equal to 10 EUR/kW_p [52]. Finally, ΔOC^{noREC} has been evaluated on a yearly basis as stated in Equation (15). Hereinafter, the sum of $OC_i^{noREC,Us\#1}$ and $OC_i^{noREC,Us\#2}$ will be recalled as OC_i^{noREC} .

$$\Delta OC^{noREC} = \sum_{i=Jan}^{Dec} \left(OC^{BC,Us\#1} + OC^{BC,Us\#2} - OC_i^{noREC,Us\#1} - OC_i^{noREC,Us\#2} \right) \quad (15)$$

- in the REC scenario, the monthly average electricity purchase price $c_{el,i}^{REC}$ has been evaluated as stated in Equation (16). The values obtained are reported in the last column of Table 2. Regarding the users' revenues, a distinction has been made between the electric energy shared within the REC boundaries ($E_{el}^{OSC,REC}(\theta)$) and sold to the grid ($E_{el}^{TG,REC}(\theta)$) on an hourly basis. Indeed, in Italy, article 42-bis of the Decree Law n.162/2019 [53] states that the sharing of electric energy hourly virtually self-consumed by the REC members is eligible for a network charge restoration due to avoided transit

on the PG, which accounts in total for 8.6 EUR/MWh in 2021 [54,55]. This contribute combines with the 110.0 EUR/MWh incentive recognized to the REC members by the Italian GSE [56], resulting in a total incentive (I_{el}^{REC}) equal to 118.6 EUR/MWh. Conversely, the share of surplus electric energy has been assumed to be sold to the Italian GSE in the same way as in the no-REC scenario. This additional revenue has been neglected with respect to $E_{el}^{OSC,REC}(\theta)$, in part because of the lack of clarity of the Italian legislation, which is still being defined, and in part to compensate the management costs of the REC, which have not been explicitly taken into account. The monthly values of OC_i^{REC} have been evaluated according to Equation (17). Instead, ΔOC^{REC} has been evaluated on a yearly basis as stated in Equation (18).

$$c_{el,i}^{REC} = \frac{E_{el,i}^{Us\#1} + E_{el,i}^{Us\#2}}{OC_i^{BC,Us\#1} + OC_i^{BC,Us\#2}} \quad (16)$$

$$OC_i^{REC} = \left(E_{el,i}^{PG,REC} \cdot c_{el,i}^{REC} + MC_i \right) - \sum_{k=1}^{NH_i} \left(E_{el}^{TG,Us}(\theta_{k,i}) \cdot p_{el}(\theta_{k,i}) + E_{el,i}^{OSC,REC}(\theta_{k,i}) \cdot I_{el}^{REC} \right) \quad (17)$$

$$\Delta OC^{REC} = \sum_{i=Jan}^{Dec} \left(OC_i^{BC,Us\#1} + OC_i^{BC,Us\#2} - OC_i^{REC} \right) \quad (18)$$

In the end, two economic performance indicators have been determined to estimate the profitability of the investment in the PV plant in the two scenarios: the discounted pay-back time (*PBT*) and the net present value (*NPV*). To this purpose, Equations (19) and (20) have been used, respectively. The former amounts to the number of years required to balance the investment cost (*IC*) by considering the yearly cashflows (F_j) throughout the investment horizon (N), equal to 20 y. During the investment horizon, which has been supposed to start in 2021, the values of F_j have been evaluated by assuming the electricity purchase and selling prices constant and equal to the values available in 2021. After the first year, the producibility of the PV plant has been assumed to be affected by reduced performance, according to the information reported in the panels' technical datasheet [44]. The discount rate (a) has been assumed to be equal to 1%. The *IC* has been estimated by using a specific price of 1000 EUR/kW_p [52].

$$PBT = \frac{IC}{\sum_{j=1}^N \frac{F_j}{(1+a)^j}} \quad (19)$$

$$NPV = \sum_{j=1}^N \frac{F_j}{(1+a)^j} - IC \quad (20)$$

3. Results

In this section, the results obtained from the energy (Section 3.1), environmental (Section 3.2) and economic (Section 3.3) analysis will be introduced.

3.1. Energy Analysis

In the next Figures, the results obtained in the noREC scenario are reported by distinguishing between *Us#1* and *Us#2*. The stacked bars in Figure 6 amount to $E_{el,i}^{PV,Us\#1}$. The green bars are equal to $E_{el,i}^{OSC,Us\#1}$, whereas the orange bars are equal to the share of $E_{el,i}^{PV,Us\#1}$ fed to the grid, that is $E_{el,i}^{TG,Us\#1}$. As shown by the azure line, which plots the trend of $d_i^{Us\#1}$ in 2021 with respect to the secondary axis, *Us#1* self-consumes at most 34.8% of $E_{el,i}^{PV,Us\#1}$ in December, being $E_{el,Dec}^{PV,Us\#1}$ equal to 11.8 MWh and $E_{el,Dec}^{OSC,Us\#1}$ equal to 4.1 MWh. In the months of highest producibility, such as May and July, when $E_{el,i}^{PV,Us\#1}$ is equal to 70.3 and to 68.8 MWh, respectively, $d_{May}^{Us\#1}$ and $d_{Jul}^{Us\#1}$ reduces to 7.9 and 10.4%, respectively. In particular, $d_{May}^{Us\#1}$ is the minimum value detected in 2021. Indeed, $E_{el,May}^{OSC,Us\#1}$ is equal to 5.6 MWh and

$E_{el,May}^{OSC,Us\#1}$ is equal to 7.1 MWh. In Figure 7, the stacked bars amount in total to $E_{el,i}^{Us\#1}$. The green bars keep being equal to $E_{el,i}^{OSC,Us\#1}$, whereas the blue bars equal $E_{el,i}^{PG,Us\#1}$. As shown by the orange indicators plotting the time trend of $s_i^{Us\#1}$ during 2021 with respect to the secondary axis, the maximum self-sufficiency is measured in June, being $s_{Jun}^{Us\#1}$ equal to 49.8%. As a matter of fact, $E_{el,Jun}^{Us\#1}$ and $E_{el,Jun}^{PG,Us\#1}$ are equal to 13.3 and 6.7 MWh, respectively. Conversely, $s_i^{Us\#1}$ reaches its minimum value in December, when it is equal to 18.6%, being $E_{el,Dec}^{Us\#1}$ and $E_{el,Dec}^{PG,Us\#1}$ equal to 22.1 and 4.1 MWh, respectively. In fact, December is the month characterized by the highest $E_{el,i}^{Us\#1}$ but the minimum $E_{el,i}^{PV,Us\#1}$.

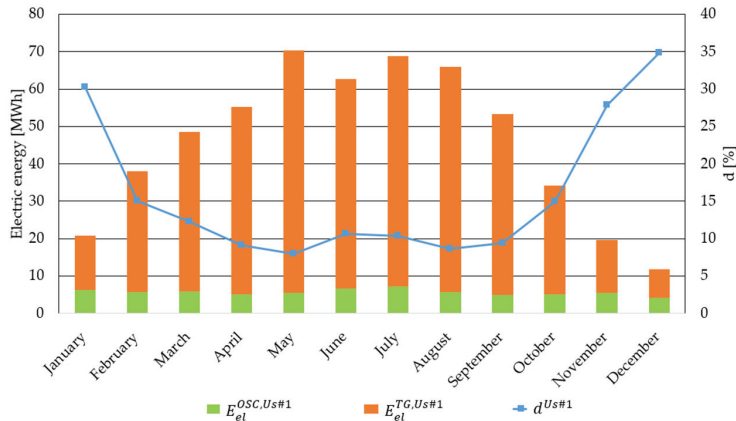


Figure 6. Producibility of the PV plant serving Us#1 in the noREC scenario. Electric energy consumed on-site and fed to the grid and self-consumption index in 2021.

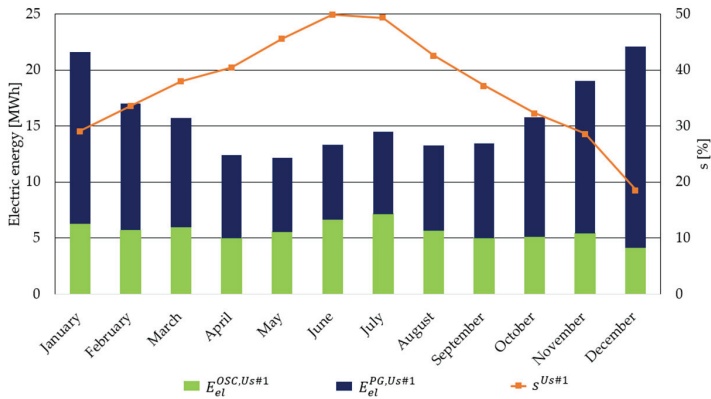


Figure 7. Load of Us#1 in the noREC scenario. Load covered by the PV plant, the grid and self-sufficiency index in 2021.

Still referring to the noREC scenario, the next Figures characterize the results obtained in regard to Us#2. The stacked bars in Figure 8 amount to $E_{el,i}^{PV,Us\#2}$, being the sum of $E_{el,i}^{OSC,Us\#2}$ and $E_{el,i}^{TG,Us\#2}$. As it can be seen, in almost all the months of 2021, the electric energy supplied by the PV plant belonging to Us#2 is fully consumed on-site. Indeed, the lowest value of $d_i^{Us\#2}$ is detected in January and is equal to 99.5%. Nevertheless, the results shown in Figure 9 highlight that the high on-site consumption rates do not imply high energy self-sufficiency. The maximum $s_i^{Us\#2}$ is measured in April, and it is equal to 16.1%

since $E_{el, Apr}^{Us\#2}$ is equal to 28.1 MWh and $E_{el, Apr}^{OSC, Us\#2}$ is equal to 4.5 MWh. By contrast, the minimum $s_i^{Us\#2}$ is measured in December when it is equal to 1.9% and $E_{el, Dec}^{Us\#2}$ and $E_{el, Dec}^{OSC, Us\#2}$ are equal to 53.5 and 1.0 MWh, respectively. The reason for the outcomes shown so far relies on the under-sizing which characterizes the portion of the PV plant serving $Us\#2$ compared to its electric load. As a matter of fact, the PV plant supplies at most 5.7 MWh in May, whereas the maximum load is equal to 100 MWh in July. On the other hand, the results regarding $Us\#1$ emphasize a significative mismatch between demand and supply. The summer months are characterized by high self-sufficiency but low self-consumption rates, as it happens in May, which is characterized by the highest supply of electric energy from the PV plant (70.3 MWh), but the load is much lower, being equal to 12.2 MWh. By contrast, the load is maximum in December (22.1 MWh), when the producibility of the PV plant reaches its minimum value (11.8 MWh). These issues are less pronounced in the REC scenario.

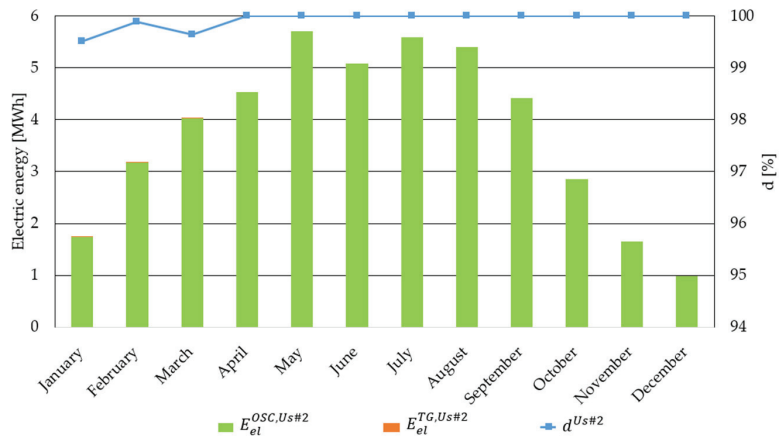


Figure 8. Producibility of the PV plant serving $Us\#2$ in the noREC scenario. Electric energy consumed on-site and fed to the grid and self-consumption index in 2021.

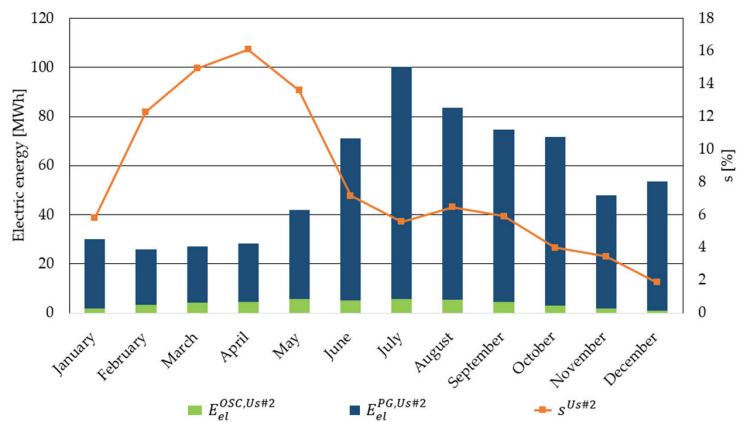


Figure 9. Load of $Us\#2$ in the noREC scenario. Load covered by the PV plant, the grid and self-sufficiency index in 2021.

By analogy with the previous cases, the stacked bars in Figure 10 amount in total to $E_{el,i}^{PV, REC}$ and represent the sum of $E_{el,i}^{OSC, REC}$ and $E_{el,i}^{TG, REC}$, whereas those in Figure 11 are equal to $E_{el,i}^{REC}$, being the sum of $E_{el,i}^{OSC, REC}$ and $E_{el,i}^{PG, REC}$. The sharing of energy between

$Us\#1$ and $Us\#2$ increases both the energy self-consumption and the self-sufficiency of users. Considering the month of May, which is the month of maximum producibility of the PV plant, $E_{el,May}^{OSC,REC}$ is equal to 26.9 MWh and is higher than the sum of $E_{el,May}^{OSC,Us\#1}$ (5.6 MWh) and $E_{el,May}^{OSC,Us\#2}$ (5.7 MWh) determined in the noREC scenario. As a result, in May s_i^{REC} is the maximum, being equal to 49.7%. The amount of electric energy in total fed to the grid reduces accordingly: $E_{el,May}^{TG,REC}$ and $E_{el,May}^{TG,Us\#1}$ are equal to 26.3 and 61.7 MWh, respectively. Similar considerations apply to July, which is the month characterized by the highest total load, being $E_{el,Jul}^{Us\#1}$ and $E_{el,Jul}^{Us\#2}$ equal to 14.5 and 100.2 MWh, respectively. In particular, $E_{el,Jul}^{OSC,REC}$ is equal to 49.1 MWh, $E_{el,Jul}^{OSC,Us\#1}$ is equal to 7.1 MWh and $E_{el,Jul}^{OSC,Us\#2}$ is equal to 5.6 MWh. As a consequence of increased self-consumption, the amount of electric energy drawn from the grid reduces compared to the noREC scenario. As a matter of fact, $E_{el,Jul}^{PG,REC}$ is equal to 66.6 MWh, whereas $E_{el,Jul}^{PG,Us\#1}$ and $E_{el,Jul}^{PG,Us\#2}$ are equal to 7.3 and 94.6 MWh, respectively. As regards the minimum value of d_i^{REC} , it is found in April and is equal to 29.9%. Hence, it is more than tripled compared to $d_{Apr}^{Us\#1}$, equal to 9.1%.

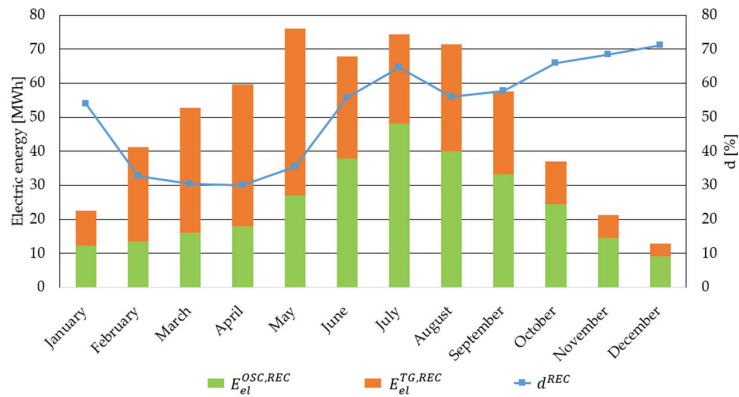


Figure 10. Producibility of the PV plant serving $Us\#1$ and $Us\#2$ in the REC scenario. Electric energy virtually shared and fed to the grid and self-consumption index in 2021.

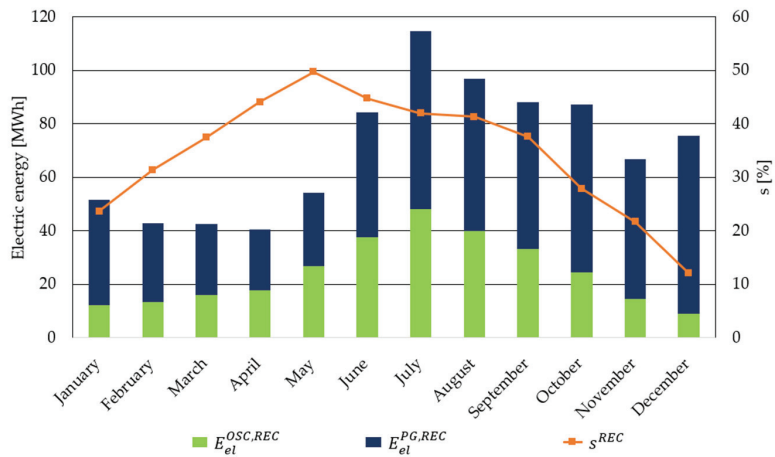


Figure 11. Load of $Us\#1$ and $Us\#2$ in the REC scenario. Load covered by the PV plant, the grid and self-sufficiency index in 2021.

The increased energy self-consumption and self-sufficiency, owing to the energy sharing and characterizing the REC scenario, results in a reduction of the primary energy demand higher than in the noREC scenario, as shown in Figure 12. Indeed, $\Delta E_{p,i}^{noREC}$ is, at most, equal to 25.0 MWh in July, whereas $\Delta E_{p,i}^{REC}$ is equal to 94.5 MWh. Overall, the primary energy demand in 2021 is equal to 1.1 GWh in the REC scenario and to 1.4 GWh in the no-REC. In the BC, the annual primary energy demand is equal to 1.7 GWh/y. The constitution of the REC allows a 34.7% primary energy saving on a yearly basis, whereas it is limited to 13.3% in the noREC scenario.

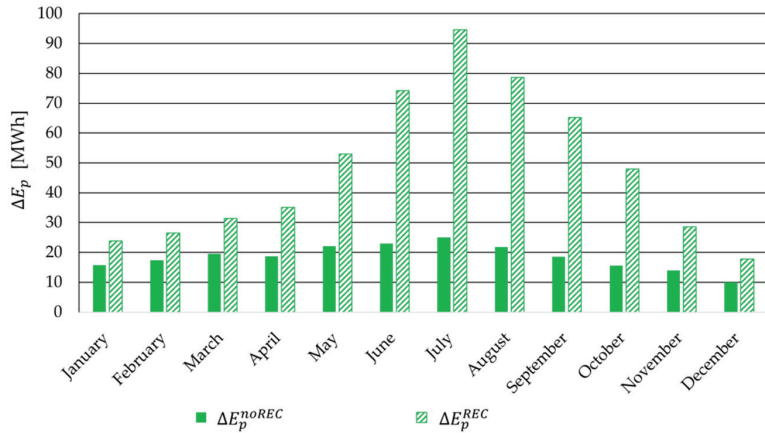


Figure 12. Primary energy saving in the noREC and REC scenario in 2021.

3.2. Environmental Analysis

Energy sharing further supports the mitigation of CO₂ emissions compared to the noREC scenario; in 2021, the emissions are equal to 242.3 tCO₂ in the BC, to 210.0 tCO₂ in the noREC scenario and to 158.2 tCO₂ in the REC scenario. Hence, the 13.3% reduction in CO₂ emissions characterizing the noREC scenario increases to 34.7% in the REC scenario. As shown in Figure 13, the best reduction on a monthly basis is found in July, and it is equal to 3.6 tCO₂ in the noREC and to 13.8 tCO₂ in the REC scenario.

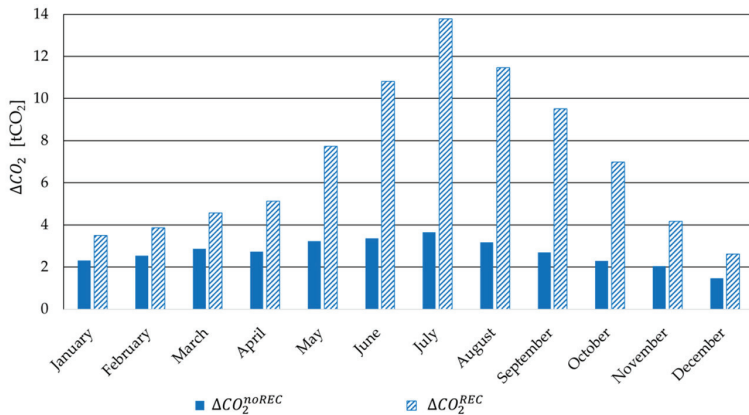


Figure 13. CO₂ emissions avoided in the noREC and REC scenarios in 2021.

3.3. Economic Analysis

In Figure 14, the operating costs relating to the first year of the investment horizon (2021) are shown. In particular, the values of OC_i^{BC} are compared with OC_i^{noREC} and OC_i^{REC} , showing that the constitution of the REC is profitable from the economic point of view since it ensures increased economic savings. As a matter of fact, OC_i^{REC} are always lower than OC_i^{noREC} . On a yearly basis, OC^{REC} are reduced by 24.6 kEUR compared to OC^{noREC} and by 100.8 kEUR compared to OC^{BC} . Instead, the annual reduction of OC^{noREC} compared to OC^{BC} is equal to 76.2 kEUR. Indeed, OC^{BC} , OC^{noREC} and OC^{REC} are equal to 238.5, 162.3 and 137.7 kEUR, respectively. Hence, the annual 31.9% economic saving characterizing the noREC scenario increases to 42.3% in the REC scenario.

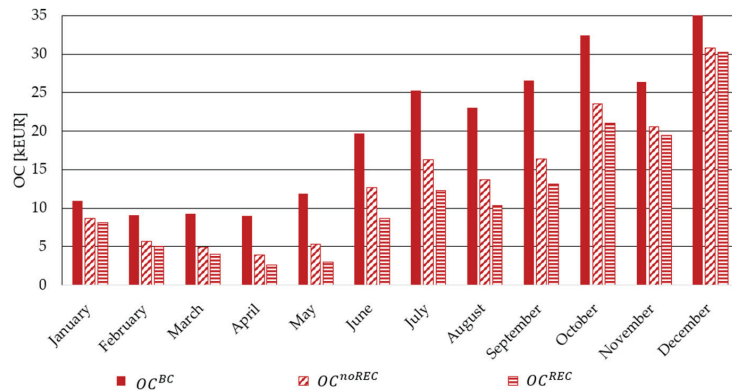


Figure 14. Operative costs in the BC, noREC and REC scenario in 2021.

Economic indexes evaluated regarding both scenarios are reported in Table 5, and further demonstrate the economic convenience of energy sharing. The value of ΔOC is referred to the first year of the investment horizon (2021) and is reported on annual basis. Although the constitution of the REC extends the *PBT* for *Us#2*, the larger increase detected in the *NPV* highlights the profitability for both users, as further shown in Figure 15, where the yearly cashflows are shown with reference to *Us#1* and *Us#2* in the noREC scenario and to the REC in the REC scenario. These results encourage the implementation of RECs in industrial parks according to the current Italian regulatory framework, which provides specific economic support mechanisms. Nevertheless, the transposition of European Directives in Italy has not yet been completed. Once the transposition has ended, the economic incentives defined by the final Italian regulation might confirm or overturn the results obtained in this work.

Table 5. Results of economic analysis.

Item		noREC		REC
		<i>Us#1</i>	<i>Us#2</i>	
<i>IC</i>	[kEUR]	431	35.0	466
	[EUR/kW _p]		1000	
ΔOC	[kEUR/y]	65.3	10.8	101
	[EUR/kW _p]	152	309	216
<i>PBT</i> [y]		7.1	4.8	4.9
<i>NPV</i> [kEUR]		695	84.1	1273

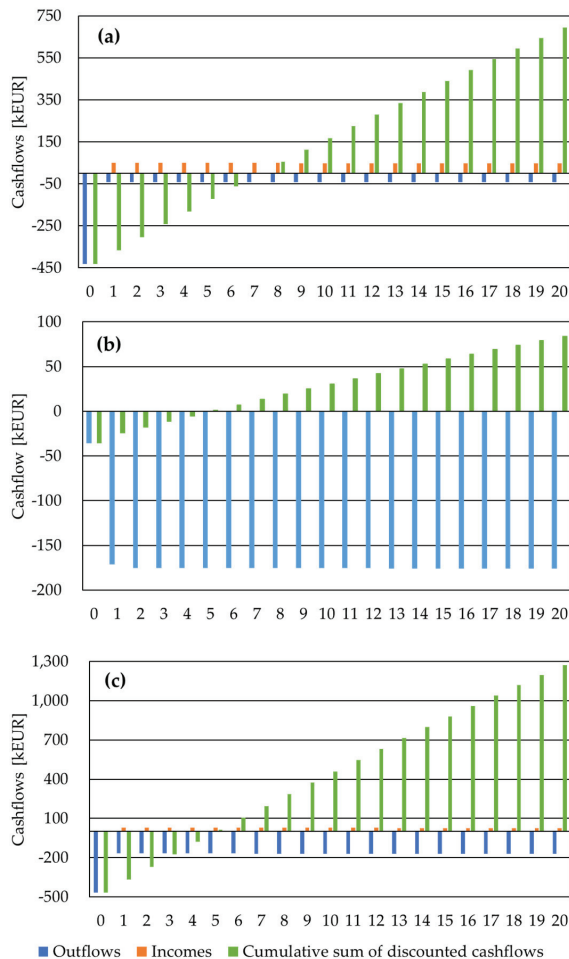


Figure 15. Yearly cashflows over the investment horizon for *Us#1* (a) and *Us#2* (b) in the noREC scenario and the REC (c) in the REC scenario.

4. Conclusions

The recast of the European Directive 2018/2001 defined in the European regulatory framework innovative configurations for energy sharing, collective production and self-consumption, known as Renewable Energy Communities. Micro, small or medium-sized enterprises have been listed as their potential members or shareholders, in addition to natural persons and local authorities. Hence, this work aims at assessing the energy, environmental and economic performance of a Renewable Energy Community, including two members located in the industrial area of Benevento (Southern Italy), namely a mixed-use building and an industrial wastewater treatment plant. This configuration has been compared with the baseline case, where the two users' electric energy demand is fully met by the power grid. Moreover, the traditional single end users' configuration has been investigated as an additional scenario in order to further emphasize the benefits owing to energy sharing. In both proposed scenarios, the users have been equipped with a 466 kW_p photovoltaic plant, which has been sized based on the surfaces available for installation. In the traditional single end users' configuration, the plant has been divided into two portions, each belonging to one user depending on its installation site. As such, each portion of the plant has been assumed to supply electric energy only to its owner, since the electric energy

sharing has been neglected, and to feed to the grid the potential surplus. By contrast, the photovoltaic plant has been treated as a whole in the Renewable Energy Community, where the virtual self-consumption scheme has been applied according to the Italian regulation for sharing energy between the community's members. In both scenarios, the plant has been modelled in HOMER Pro[®] in order to simulate its generation curve on a quarter-hour basis. As regards the users' requests, real data about their electric energy demand have been collected from their electricity bills. In addition, their electric load curves have been constructed on a quarter-hour basis when not made available by the Italian electric energy distributor. In this way, the shares of electric energy hourly supplied by the photovoltaic plant, consumed on site and fed into the grid have been evaluated, as well as the electricity withdrawn from the power grid to cover the residual load. The results obtained from the energy, environmental and economic analysis are listed as follows:

- from the energy point of view, energy sharing increases users' self-sufficiency and renewable energy on-site consumption compared to the single self-consumers' configuration. As a result, the primary energy saving owing to the constitution of the Renewable Energy Community is equal to 34.7%, and is higher than in the single end users' configuration, where it is equal to 13.3%;
- because of the reduced primary energy demand, carbon dioxide emissions are further reduced by energy sharing. In particular, carbon dioxide emissions decrease by 13.3% and 34.7% without and with the energy sharing, respectively;
- the energy sharing increases the annual operative costs' savings from 76.2 to 101 kEUR/y, reduces the pay-back time to 4.9 y and increases the net-present value to 1273 kEUR. Thus, the Renewable Energy Community scenario is characterized by higher profitability of the investment.

To sum up, the constitution of the Renewable Energy Community provides better performances than the traditional end users' configuration. In future works, it would be interesting to investigate the installation of an electric energy storage in order to further increase the users' energy self-sufficiency and renewable energy self-consumption, according to the Italian regulation on Renewable Energy Communities, which also promotes the installation of storage systems to increase the programmability of sources. Moreover, other renewable energy technologies (such as biomethane-based cogeneration plants or wind turbines) able to meet the community's loads can be investigated as solutions to reduce carbon dioxide emissions. Yet, their economic feasibility must be verified as they are less mature technologies compared to photovoltaic plants. In addition, the possibility of including other industrial members in energy sharing will be addressed, also to promote the constitution of such configurations within the industrial sector considering their many positive effects.

Author Contributions: Conceptualization, F.C., E.M., C.M., G.P., C.R. and M.S.; methodology, F.C., E.M., C.M., G.P., C.R. and M.S.; validation, F.C., E.M., C.M., G.P., C.R. and M.S.; formal analysis, F.C., E.M., C.M., G.P., C.R. and M.S.; investigation, F.C., E.M., C.M., G.P., C.R. and M.S.; resources, F.C., E.M., C.M., G.P., C.R. and M.S.; data curation, F.C., E.M., C.M., G.P., C.R. and M.S.; writing—original draft preparation, F.C., E.M., C.M., G.P., C.R. and M.S.; writing—review and editing, F.C., E.M., C.M., G.P., C.R. and M.S.; visualization, F.C., E.M., C.M., G.P., C.R. and M.S.; supervision, F.C., E.M., C.M., G.P., C.R. and M.S. All authors have read and agreed to the published version of the manuscript.

Funding: This research received no external funding.

Data Availability Statement: The data presented in this study are available on request from the corresponding author.

Conflicts of Interest: The authors declare no conflict of interest.

Nomenclature

Acronyms and abbreviations

BC	Baseline case
CO ₂	Carbon dioxide
CSC	Collective services center
GSE	<i>Gestore dei Servizi Energetici</i> (Italian energy services operator)
PG	Power grid
POD	Point of delivery
PV	Photovoltaic
REC	Renewable Energy Community
RES	Renewable energy source
Us#1	First user (collective services center building)
Us#2	Second user (consortium wastewater treatment plant)
WWTP	Wastewater treatment plant

Symbols

a	Discount rate [%]
D	Minimum spacing distance between adjacent panels' rows [m]
c_{el}	Monthly average purchase cost of electricity [EUR/kWh]
d	Self-consumption index [%]
E_{el}^{QSC}	Electric energy consumed onsite [MWh/y, MWh/m]
E_{el}^{PG}	Electric energy drawn from the grid [MWh/y, MWh/m]
E_{el}^{PV}	Electric energy supplied by the photovoltaic plant [MWh/y, MWh/m]
E_{el}^{G}	Electric energy delivered to the grid [MWh/y, MWh/m]
E_{el}^{Us}	User's electric load [MWh/y, MWh/m]
F_j	Cashflow in the j -th year of investment horizon [kEUR/y]
I_{el}^{REC}	Incentive for electric energy sharing [EUR/MWh]
IC	Investment cost [kEUR]
L	Photovoltaic panel's height [m]
MC	Maintenance costs [EUR/kW _p y, EUR/kW _p m]
N	Investment horizon [y]
NH	Number of hours [-]
NPV	Net present value [kEUR]
OC	Operative costs [kEUR/y, kEUR/m]
p_{el}	Hourly electricity selling price [EUR/MWh]
PBT	Pay-back time [y]
s	Self-sufficiency index [%]
ΔE_p	Primary energy demand saving [MWh/y, MWh/m]
ΔCO_2	Carbon dioxide emission reduction [tCO ₂ /y, tCO ₂ /m]

Superscripts, subscripts and Greek symbols

el	Electric energy
i	Month index in a year
j	Year index in the investment horizon
k	Hour index in the total number of hours in the i -th month
P	Primary energy
noREC	Scenario without the REC
OSC	Electric energy consumed on-site
PG	Electric energy drawn from the power grid
REC	Scenario with the REC
TG	Electric energy fed to the grid
Us#1	First user
Us#2	Second user
α	Sun elevation angle [°]
α_{CO_2}	Carbon dioxide emission factor [kgCO ₂ /kWh _{el}]
β	Tilt angle [°]
η_{el}^{PG}	Power grid efficiency [-]
θ	One-hour time step

References

1. European Commission. Communication from the Commission to the European Parliament, The European Council, the Council, the European Economic and Social Committee and the Committee of the Regions—A Green Deal Industrial Plan for the Net-Zero Age. Brussels. 2023. Available online: https://commission.europa.eu/system/files/2023-02/COM_2023_62_2_EN_ACT_A%20Green%20Deal%20Industrial%20Plan%20for%20the%20Net-Zero%20Age.pdf (accessed on 18 January 2023).
2. European Commission. Communication from the Commission to the European Parliament, the Council, the European Economic and Social Committee and the Committee of the Regions—Stepping up Europe’s 2030 Climate Ambition—Investing in a Climate-Neutral Future for the Benefit of Our People. Brussels. 2020. Available online: <https://eur-lex.europa.eu/legal-content/EN/TXT/PDF/?uri=CELEX:52020DC0562&from=EN> (accessed on 18 January 2023).
3. European Commission. Communication from the Commission to the European Parliament, the European Council, the Council, the European Economic and Social Committee and the Committee of the Regions—The European Green Deal. Available online: https://eur-lex.europa.eu/resource.html?uri=cellar:b828d165-1c22-11ea-8c1f-01aa75ed71a1.0002.02/DOC_1&format=PDF (accessed on 18 January 2023).
4. International Energy Agency. Industry Report. Available online: <https://www.iea.org/reports/industry> (accessed on 20 January 2023).
5. Philibert, C. Renewable Energy for Industry—From Green Energy to Green Materials and Fuels. Paris. 2017. Available online: https://iea.blob.core.windows.net/assets/48356f8e-77a7-49b8-87de-87326a862a9a/Insights_series_2017_Renewable_Energy_for_Industry.pdf (accessed on 17 January 2023).
6. ABB Accelerating Ambition—How Global Industry is speeding up Investment in Energy Efficiency. Available online: <https://www.energyefficiencymovement.com/wp-content/uploads/2022/04/ABB-Energy-Efficiency-Survey-Report-2022.pdf> (accessed on 17 January 2023).
7. International Energy Agency. Energy Efficiency 2022. Available online: <https://iea.blob.core.windows.net/assets/7741739e-8e7f-4afa-a77f-49dadd51cb52/EnergyEfficiency2022.pdf> (accessed on 16 January 2023).
8. United Nations Industrial Development Organization. Industrial Development Report 2016. Available online: https://www.unido.org/sites/default/files/2015-12/EBOOK_IDR2016_FULLREPORT_0.pdf (accessed on 11 January 2023).
9. Caballero, V.; Briones, A.; Coca-Ortegón, A.; Perez, A.; Barrios, B.; de la Mano, M. Analysis and simulation of an Urban-Industrial Sustainable Energy Community: A use case in San Juan de Mozarrifar using photovoltaic energy. *Energy Rep.* **2023**, *9*, 1589–1605. [CrossRef]
10. Butturi, M.A.; Gamberini, R. Urban-industrial symbiosis to support sustainable energy transition. *Int. J. Energy Prod. Manag.* **2020**, *5*, 355–366. [CrossRef]
11. European Commission. Clean Energy for All Europeans. 2019. Available online: <https://data.europa.eu/doi/10.2833/9937> (accessed on 19 January 2023).
12. European Union. Directive (Eu) 2018/2001 of the European Parliament and of the Council of 11 December 2018 on the Promotion of the Use of Energy from Renewable Sources (Recast). Available online: <https://eur-lex.europa.eu/legal-content/EN/TXT/PDF/?uri=CELEX:32018L2001> (accessed on 19 January 2023).
13. European Union. Directive (Eu) 2019/944 of the European Parliament and of the Council of 5 June 2019 on Common Rules for the Internal Market for Electricity and Amending Directive 2012/27/EU (Recast). Available online: <https://eur-lex.europa.eu/legal-content/EN/TXT/PDF/?uri=CELEX:32019L0944&from=EN> (accessed on 18 January 2023).
14. Ceglia, F.; Marrasso, E.; Roselli, C.; Sasso, M. Small Renewable Energy Community: The Role of Energy and Environmental Indicators for Power Grid. *Sustainability* **2021**, *13*, 2137. [CrossRef]
15. Caramizaru, A.; Uihlein, A. *Energy Communities: An Overview of Energy and Social Innovation*; Publications Office of the European Union: Luxembourg, 2020. Available online: https://publications.jrc.ec.europa.eu/repository/bitstream/JRC119433/energy_communities_report_final.pdf (accessed on 19 January 2023).
16. Ceglia, F.; Marrasso, E.; Pallotta, G.; Roselli, C.; Sasso, M. The State of the Art of Smart Energy Communities: A Systematic Review of Strengths and Limits. *Energies* **2022**, *15*, 3462. [CrossRef]
17. Angrisani, G.; Canelli, M.; Roselli, C.; Sasso, M. Microcogeneration in buildings with low energy demand in low sharing application. *Energy Convers. Manag.* **2015**, *100*, 78–79. [CrossRef]
18. Marrasso, E.; Roselli, C.; Sasso, M.; Picallo-Perez, A.; Sala Lizarra, J.M. Dynamic simulation of a microcogeneration system in a Spanish cold climate. *Energy Convers. Manag.* **2018**, *165*, 206–2018. [CrossRef]
19. Pontes Luz, G.; Amaro e Silva, R. Modeling Energy Communities with Collective Photovoltaic Self-Consumption: Synergies between a Small City and a Winery in Portugal. *Energies* **2021**, *14*, 323. [CrossRef]
20. Volpato, G.; Carraro, G.; Cont, M.; Danieli, P.; Rech, S.; Lazzaretto, A. General guidelines for the optimal economic aggregation of prosumers in energy communities. *Energy* **2022**, *258*, 124800. [CrossRef]
21. Tarpani, E.; Piselli, C.; Fabiani, C.; Pigliantile, I.; Kingma, E.J.; Pioppi, B.M.; Pisello, A.L. Energy Communities Implementation in the European Union: Case Studies from Pioneer and Laggard Countries. *Sustainability* **2022**, *14*, 12528. [CrossRef]
22. Fabrizio, E.; Branciforti, V.; Costantino, A.; Filippi, M.; Barbero, S.; Tecco, G.; Mollo, P.; Molino, A. Monitoring and managing of a micro-smart grid for renewable sources exploitation in an agro-industrial site. *Sustain. Cities Soc.* **2017**, *28*, 88–100. [CrossRef]
23. Horbach, J.; Rammer, C. Energy transition in Germany and regional spill-overs: The diffusion of renewable energy in firms. *Energy Policy* **2018**, *121*, 404–414. [CrossRef]

24. Maes, T.; Van Eetvelde, G.; De Ras, E.; Block, C.; Pisman, A.; Verhofstede, B.; Vandendriessche, F.; Vandeveldel, L. Energy management on industrial parks in Flanders. *Renew. Sustain. Energy Rev.* **2011**, *15*, 1988–2005. [CrossRef]
25. Lammers, I.; Hoppe, T. Watt rules? Assessing decision-making practices on smart energy systems in Dutch city districts. *Energy Res. Soc. Sci.* **2019**, *47*, 230–246. [CrossRef]
26. Sun, L.; Fujii, M.; Li, Z.; Dong, H.; Geng, Y.; Liu, Z.; Fujita, T.; Yu, X.; Zhang, Y. Energy-saving and carbon emission reduction effect of urban-industrial symbiosis implementation with feasibility analysis in the city. *Technol. Forecast. Soc. Chang.* **2020**, *151*, 119853. [CrossRef]
27. Anastasovski, A. What is needed for transformation of industrial parks into potential positive energy industrial parks? A review. *Energy Policy* **2023**, *173*, 113400. [CrossRef]
28. Guo, Q.; Novajan, S.; Lei, S.; Liang, X. Economic-environmental evaluation of industrial energy parks integrated with CCHP units under a hybrid IGDT-stochastic optimization approach. *J. Clean. Prod.* **2021**, *317*, 128364. [CrossRef]
29. Su, S.; Lu, H.; Zhang, L.; Alanne, K.; Yu, Z. Solar energy utilization patterns for different district typologies using multi-objective optimization: A comparative study in China. *Sol. Energy* **2017**, *155*, 246–258. [CrossRef]
30. Moreno-Camacho, C.A.; Montoya-Torres, J.R.; Jaegler, A.; Gondran, N. Sustainability metrics for real case applications of the supply chain network design problem: A systematic literature review. *J. Clean. Prod.* **2019**, *231*, 600–618. [CrossRef]
31. Simeoni, P.; Nardin, G.; Ciotti, G. Planning and design of sustainable smart multi energy systems. The case of a food industrial district in Italy. *Energy* **2018**, *163*, 443–456. [CrossRef]
32. Eslamizadeh, S.; Ghorbani, A.; Kunneke, R.; Weijnen, M. Can industries be parties in collective action? Community energy in an Iranian industrial zone. *Energy Res. Soc. Sci.* **2020**, *70*, 101763. [CrossRef]
33. Hentschel, M.; Ketter, W.; Collins, J. Renewable energy cooperatives: Facilitating the energy transition at the Port of Rotterdam. *Energy Policy* **2018**, *121*, 61–69. [CrossRef]
34. Cirone, D.; Bruno, R.; Bevilacqua, P.; Perrella, S.; Arcuri, N. Techno-Economic Analysis of an Energy Community Based on PV and Electric Storage Systems in a Small Mountain Locality of South Italy: A Case Study. *Sustainability* **2022**, *14*, 13877. [CrossRef]
35. Ancona, M.A.; Baldi, F.; Branchini, L.; De Pascale, A.; Gianaroli, F.; Melino, F.; Ricci, M. Comparative Analysis of Renewable Energy Community Designs for District Heating Networks: Case Study of Corticella (Italy). *Energies* **2022**, *15*, 5248. [CrossRef]
36. Ceglia, F.; Marrasso, E.; Samanta, S.; Sasso, M. Addressing Energy Poverty in the Energy Community: Assessment of Energy, Environmental, Economic, and Social Benefits for an Italian Residential Case Study. *Sustainability* **2022**, *14*, 15077. [CrossRef]
37. International Energy Agency. *Energy Technology Perspectives 2020: Special Report on Clean Energy Innovation*; IEA: Paris, France, 2020; Available online: <https://www.iea.org/reports/energy-technology-perspectives-2020> (accessed on 8 March 2023).
38. Rodin, V.; Moser, S. The perfect match? 100 reasons why energy cooperation is not realized in industrial parks. *Energy Res. Soc. Sci.* **2021**, *74*, 101964. [CrossRef]
39. Johannsen, R.M.; Mathiesen, B.V.; Kermeli, K.; Crijns-Graus, W.; Østergaard, P.A. Exploring pathways to 100% renewable energy in European industry. *Energy* **2023**, *268*, 126687. [CrossRef]
40. Meyers, S.; Schmitt, B.; Chester-Jones, M.; Sturm, B. Energy efficiency, carbon emissions, and measures towards their improvement in the food and beverage sector for six European countries. *Energy* **2016**, *104*, 266–283. [CrossRef]
41. Google Earth. Available online: <https://www.google.it/intl/it/earth/> (accessed on 31 January 2023).
42. E-distribuzione. Available online: <https://www.e-distribuzione.it/servizi.html> (accessed on 25 January 2023).
43. Autorità di Regolazione per Energia Reti e Ambiente, Applicazione dei prezzi per Fascia e per Mese/Raggruppamenti di Mesi per i Clienti Non Domestici del Servizio di Maggior Tutela (Diversi dall'Illuminazione Pubblica). Available online: <https://www.arera.it/it/schede/C/faq-fascenondom.htm#1> (accessed on 24 January 2023). (In Italian)
44. SunPower. Type E20-327, Series E Module Technical Datasheet. Available online: <https://sunpower.maxeon.com/it/sites/default/files/2019-09/sunpower-maxeon-serie-e-e20-327-residenziale.pdf> (accessed on 10 January 2023). (In Italian).
45. Italian Government. *Ministerial Decree 1 February 1986*; Gazzetta Ufficiale nr. 38 of 15 February 1986; Italian Government: Rome, Italy, 1986. (In Italian)
46. Tutto Norme. *Guida blu—Impianti a norme CEI 2015, Fotovoltaico*; Edizioni TNE: Torino, Italy, 2019. (In Italian)
47. HOMER Pro®. Available online: <https://www.homerenergy.com/products/pro/docs/3.13/index.html> (accessed on 31 January 2023).
48. Microsoft Corporation. Microsoft Excel. Available online: <https://office.microsoft.com/excel> (accessed on 31 January 2023).
49. Gestore dei Servizi Energetici. Gruppi di Autoconsumatori e Comunità di Energia Rinnovabile. Available online: <https://www.gse.it/servizi-per-te/autoconsumo/gruppi-di-autoconsumatori-e-comunita-di-energia-rinnovabile> (accessed on 25 January 2023). (In Italian).
50. Ceglia, F.; Marrasso, E.; Roselli, C.; Sasso, M. Time-evolution and forecasting of environmental and energy performance of electricity production system at national and at bidding zone level. *Energy Convers. Manag.* **2022**, *265*, 115772. [CrossRef]
51. Gestore dei Servizi Energetici. Ritiro Dedicato. Available online: <https://www.gse.it/servizi-per-te/fotovoltaico/ritiro-dedicato> (accessed on 18 January 2023). (In Italian)
52. International Renewable Energy Agency. Renewable Power Generation Costs in 2021. 2021. Available online: <https://irena.org/publications/2022/Jul/Renewable-Power-Generation-Costs-in-2021#:~:text=The%20global%20weighted%20average%20levelised,%25%20to%20USD%200.075%20¢/kWh> (accessed on 15 January 2023).

53. Italian Government. Decree Law 30 December 2019, n. 162. Available online: <https://www.gazzettaufficiale.it/eli/id/2020/02/29/20A01353/sg> (accessed on 16 January 2023). (In Italian).
54. Autorità di Regolazione per Energia Reti e Ambiente. Tariffe di Distribuzione. Available online: <https://www.arera.it/it/elettricita/distr.htm> (accessed on 15 January 2023). (In Italian).
55. Autorità di Regolazione per Energia Reti e Ambiente. Tariffa per il Servizio di Trasmissione. Available online: <https://www.arera.it/it/elettricitatrasmissione.htm#:~:text=La%20tariffa%20TRAS%20%C3%A8%20composta,in%20alta%20o%20altissima%20tensione> (accessed on 15 January 2023). (In Italian)
56. Gestore dei Servizi Energetici. Regole Tecniche per L'accesso al Servizio di Valorizzazione e Incentivazione dell'Energia Elettrica Condivisa. Available online: https://www.gse.it/documenti_site/Documenti%20GSE/Servizi%20per%20te/AUTOCONSUMO/Gruppi%20di%20autoconsumatori%20e%20comunita%20di%20energia%20rinnovabile/Regole%20e%20procedure/Regole%20Tecniche%20per%20accesso%20al%20servizio%20di%20valorizzazione%20e%20incentivazione%20energia%20elettrica%20condivisa.pdf (accessed on 15 January 2023). (In Italian)

Disclaimer/Publisher's Note: The statements, opinions and data contained in all publications are solely those of the individual author(s) and contributor(s) and not of MDPI and/or the editor(s). MDPI and/or the editor(s) disclaim responsibility for any injury to people or property resulting from any ideas, methods, instructions or products referred to in the content.

Article

Structural Performance of Energy Efficient Geopolymer Concrete Confined Masonry: An Approach towards Decarbonization

Muhammad Mubashir Ajmal¹, Asad Ullah Qazi¹, Ali Ahmed¹, Ubaid Ahmad Mughal¹, Safeer Abbas^{1,*}, Syed Minhaj Saleem Kazmi^{2,*} and Muhammad Junaid Munir²

¹ Department of Civil Engineering, University of Engineering and Technology, Lahore 54890, Pakistan; mmubashirajmal@gmail.com (M.M.A.); asad.qazi@uet.edu.pk (A.U.Q.); ali@uet.edu.pk (A.A.); ubaid_mughal@uet.edu.pk (U.A.M.)

² School of Engineering, RMIT University, Melbourne, VIC 3001, Australia; muhammad.munir@rmit.edu.au

* Correspondence: safeer.abbas@uet.edu.pk (S.A.); minhajkazmi17@gmail.com (S.M.S.K.)

Abstract: Geopolymer concrete is preferred over OPC due to its use of energy waste such as fly ash, making it more sustainable and energy-efficient. However, limited research has been done on its seismic characterization in confined masonry, highlighting a gap in sustainable earthquake-resistant structures. Our study compares the performance of alkali-activated fly-ash-based geopolymer concrete bare frame and confined masonry wall panels with conventional concrete. Experimental results showed that geopolymer concrete bare frame has 3.5% higher initial stiffness and 1.0% higher lateral load-bearing capacity compared to conventional concrete. Geopolymer concrete confined masonry exhibited 45.2% higher initial stiffness and 4.1% higher ultimate seismic capacity than traditional concrete. The experimental results were verified using a numerical simulation technique with ANSYS-APDL, showing good correlation. Comparison with previously tested masonry walls revealed that GPC confined masonry has similar structural behavior to cement concrete masonry. This study demonstrates that geopolymer concrete made from waste energy such as fly ash is a sustainable and low-energy substitute for OPC concrete, particularly in highly seismic-prone areas, for a cleaner environment.

Keywords: GPC confined masonry; GPC bare frame; reverse cyclic loading; ANSYS; numerical simulation

Citation: Ajmal, M.M.; Qazi, A.U.; Ahmed, A.; Mughal, U.A.; Abbas, S.; Kazmi, S.M.S.; Munir, M.J. Structural Performance of Energy Efficient Geopolymer Concrete Confined Masonry: An Approach towards Decarbonization. *Energies* **2023**, *16*, 3579. <https://doi.org/10.3390/en16083579>

Academic Editor: Izabela Hager

Received: 31 March 2023

Revised: 16 April 2023

Accepted: 19 April 2023

Published: 20 April 2023



Copyright: © 2023 by the authors. Licensee MDPI, Basel, Switzerland. This article is an open access article distributed under the terms and conditions of the Creative Commons Attribution (CC BY) license (<https://creativecommons.org/licenses/by/4.0/>).

1. Introduction

Load-bearing masonry has been the most widely used construction technology worldwide since the beginning of building construction because of its affordability, ease of implementation, and eco-friendly features [1]. However, these, non-engineered construction practices have led to a significant increase in the seismic hazard posed by masonry caused by inherent deficiencies such as low tensile strength of masonry and weak connections between elements. Therefore, poor design and detailing can result in buildings that are susceptible to earthquake damage [2,3]. Unreinforced masonry structures perform well when subjected to gravity load, due to the reasonable compressive strength of masonry units, but on the other hand, it becomes a challenge for the engineers to enhance the tension and shear capacity of masonry structures to achieve improved sustainability during seismic excitations [4,5]. Unreinforced masonry still finds broad use in existing structures across most seismic regions. The assessment of the seismic vulnerability of such buildings is of critical significance. Indeed, said buildings have exhibited poor behavior under past earthquakes resulting in massive damage, structural failure, and casualties [6]. Japan, China, Indonesia, Italy, Iran, India, and Pakistan are a few of the earthquake-prone regions, which have suffered huge losses in past ground shakes [7].

A recent earthquake (October 2005 AJK) has highlighted the vulnerability of masonry structures and resulted in substantial devastation and thousands of people losing their

lives. The same earthquake left extensive destruction, snatching the lives of more than 73,000 people, ruthlessly injuring another 70,000, and making 2.8 million people shelter-less with over 450,000 buildings fully or partially damaged [8]. The major causes of destruction encompassed the fragile interlocking bond between out-of-plane and in-plane walls, low quality of building material, and non-engineered construction practices [9].

To address these challenges, the implementation of modern seismic design codes can help assess the mechanical response of both new and existing structures, thus improving their resilience to seismic activity. Confined masonry (CM) is one of the best reinforcing masonry wall systems. It was introduced in Italy and Chile in the wake of disastrous earthquakes, namely the 1908 Messina and 1929 Talca quakes, respectively [10]. Confined masonry, which is widely used for housing in Mexico [11] and most Latin-American countries [12–15], is also a common construction technique in several European countries such as Italy, Portugal, and Slovenia [16–18], as well as Asian countries including Iran [19,20], Indonesia [21], Pakistan [22], and China [16,23]. In areas with moderate to high seismic activity, confined masonry has been used as a common building technique for low- to mid-rise structures [24,25]. Confined masonry is a structural technique that improves the load-bearing capacity of masonry walls against both vertical and lateral loads by using tie-beams and tie-columns [26,27].

Seismic performance of confined masonry has been, undoubtedly, proved to be far better than non-engineered conventional masonry structures [28–33]. At the same time, the confined masonry does consist for the most part of cement-based materials, i.e., concrete, and mortar, representing a vital ingredient in the construction industry [34,35]. The manufacturing of OPC results in significant emissions of anthropogenic carbon dioxide that contribute towards global warming [36–41]. The International Energy Agency reports that the manufacturing of OPC accounts for approximately 5–7% of global greenhouse gas emissions and lays the foundation for the onset of global warming [42–46]. The Geological Survey (2012) estimated that global OPC production is currently around 3.6 billion metric tons, and projections suggest that it will exceed 5 billion metric tons in the near future [47]. Typically, manufacturing one ton of Portland cement (PC) needs approximately 1.5 tons of raw materials, which results in the emission of approximately 0.9 tons of CO₂ [48–51].

Over the last twenty years, considerable research efforts have been focused on finding substitutes for OPC concrete. Geopolymer concrete (GPC) is one such alternative that can be made using industrial waste materials such as fly ash and slags [52–54]. Recently, geopolymer concrete has gained significant attention due to its potential to serve as a replacement for ordinary Portland cement, leading to a substantial reduction in carbon dioxide emissions [55]. GPC achieves strength through the polymerization process [56]. The reaction of aluminosilicate materials with a highly alkaline solution results in the development of geopolymeric gel [57]. Past studies show that GPC can be produced using fly ash [58], metakaolin [59], silica fume [60], ground granulated blast furnace slag [61], and rice husk ash [62], among which fly ash is the most used waste material to produce GPC due to its superior engineering and durability properties [63]. Furthermore, it is pertinent to mention that both types of concrete are heterogeneous and their physical properties at meso-scale may also impact the behavior that can be studied utilizing micro X-ray computed tomography images [64].

Geopolymer concrete has been proven to be appropriate for use in Civil engineering projects such as constructing roads, footpaths, and pipes. However, before it can be widely used in structural applications and the establishment of national codes of practice, further testing is necessary to assess its overall structural performance. Currently, most of the research on geopolymer concrete has focused on material development and mechanical behavior measurement [65–71], with relatively few studies examining the behavior of geopolymer concrete in structural elements [72–75].

Geopolymer concrete offers several environmental, structural, and economic advantages over traditional concrete, but the available literature is mostly limited to geopolymer concrete elements and very little research has been extended to reinforced geopolymer con-

crete members (beam/column/slab). However, no studies are yet reported on the seismic characterization of geopolymer concrete confined masonry using fly ash as a precursor, which highlights a huge gap in the research needed to produce a clean green environment in highly seismic-prone regions. Therefore, it is a pressing need to study the seismic resilience of geopolymer concrete at the structure level in the form of confined masonry.

This paper provides a comprehensive study on the alkali-activated fly-ash-based geopolymer concrete bare frame under reverse cyclic load and its comparison with conventional concrete. Upon successful concordance, the research has been extended to the comparison of the structural performance of GPC confined masonry with that of cement concrete. Benchmark walls tested under lateral in-plane loading are used to calibrate a finite element modeling approach for reverse cyclic analysis. For this purpose, a numerical solution based on the finite element method has been carried out to model the test results. A comparison has also been drawn among the test specimens in this study and previously tested confined and unreinforced masonry walls to estimate the difference of important seismic parameters of GPC confined masonry compared with that of cement concrete masonry. The present experimental and numerical observations and results make the basis for further testing on fly-ash-based geopolymer concrete confined masonry rooms to study different lateral and torsional behaviors to produce a green environment, especially in seismic-prone areas.

2. Methodology

2.1. Experimental Setup

2.1.1. Test Specimens and Geometric Properties

The test specimens presented in this study are bare frame and confined masonry made with alkali-activated fly-ash-based geopolymer concrete and their comparison with the conventional concrete. All the test specimens were subjected to the quasi-static reverse cyclic load. The nominal dimension of the bare frames and single wythe confined masonry walls are 1870 mm × 1850 mm × 113 mm (length × height × width). In order to prioritize shear failure over flexural failure, the aspect ratio of both bare frames and walls was kept approximately equal to 1.0. A reinforced concrete pad measuring 2470 mm × 300 mm × 300 mm (length × width × depth) was used to construct the specimen, simulating a sturdy foundation for the sample. The footing beam extended 300 mm on each side of the main structure to anchor the specimen with the testing floor, preventing any sliding or uplift at the base. Instrumentation was set up to monitor the base for sliding.

In the case of bare frames, the steel reinforcement for the columns was developed by embedding the steel cage into the footing beam before its casting. After the footing pad, columns were cast followed by the beam. The bare frame was constructed with the same dimensions of columns and beams as confining elements in the case of confined masonry to produce similarity in geometry for the purpose of comparison of both structures.

The construction of confined masonry walls was similar to the bare frames except for dowels of tie-columns embedded into the footing beam. The masonry was then assembled using common clay bricks measuring 225 mm × 113 mm × 75 mm (length × width × height) with 10 mm thick bed and head mortar joints. To improve the bond efficiency at the brick-mortar interface, all bricks were soaked as dry bricks have high water absorption. Half brick toothing was used on alternate brick courses during brickwork to ensure the masonry units were tightly packed with confining elements. The walls were built up to their full height in three stages with an English running bond, keeping the frog of bricks facing upwards to establish a strong interface. All bed and head joints between bricks were properly filled with mortar. After the masonry was constructed, tie-columns and a tie-beam measuring 225 mm × 113 mm and 113 mm × 225 mm (width × depth), respectively, were cast to fully confine the wall. All confining elements had four No. 3 deformed longitudinal steel bars and No. 2 transverse reinforcement. The thickness of the confining elements matched that of the masonry wall, which was 113 mm.

To measure the strain of longitudinal and transversal steel bars at critical sections of the columns, strain gauges were glued with cyanoacrylate adhesive. Steel strain gauges were also installed at critical sections of the beams to examine the strain of steel bars during loading before casting. The slump for the tie-columns was kept a little bit high at approximately 110 mm to allow easy flow of concrete into tooth gaps.

The OPC test specimens were water-cured for 28 days to ensure maximum shear strength, whereas GPC test specimens were subjected to ambient curing. The prototype test specimens' reinforcement details and geometric properties are shown in Figure 1.

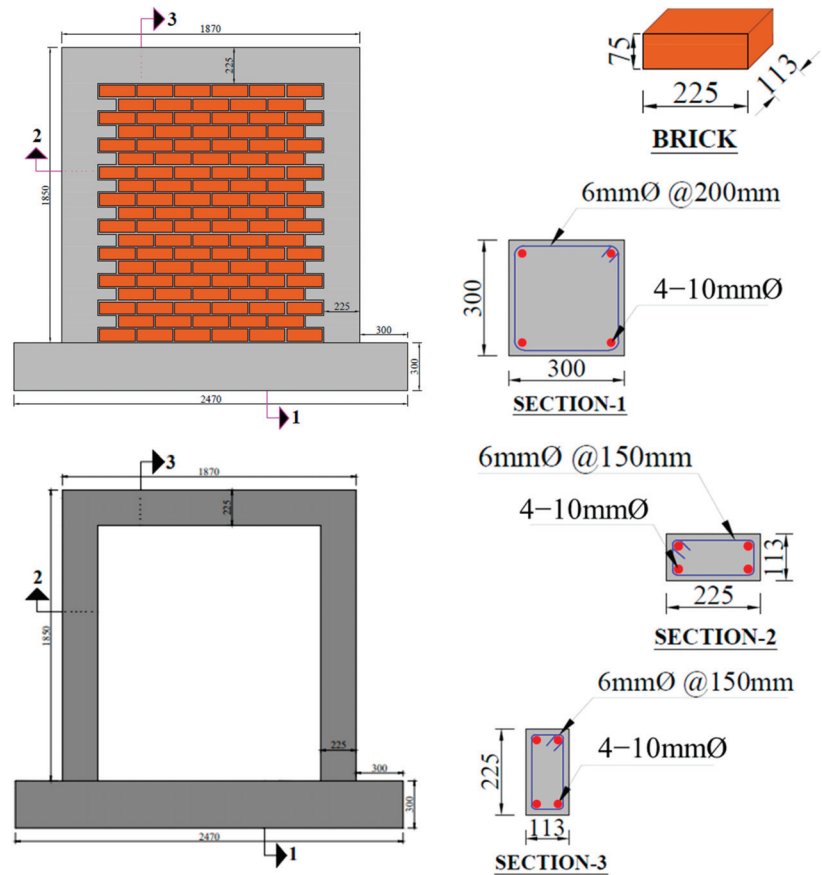


Figure 1. Schematics and reinforcement detailing of bare frame and confined masonry wall.

2.1.2. Materials and Properties

The material behavior of both types of concrete and mortar used in the construction of bare frames and confined masonry panels were determined through experimental testing according to the standards, given in Table 1. Margalla crush was used as coarse aggregate having a particle size ranging from 10 mm to 20 mm with an average size of 12.5 mm. The apparent specific gravity of coarse aggregates was determined as 2.66 g/cm³ and the water absorption was 1.34% obtained by ASTM C127 [76]. The chemical composition of fly ash is listed in Table 2. The mix proportions used for conventional concrete and cement mortar were 1:2:4 with w/c 0.45 and 1:3 (cement: sand) with w/c 0.6, respectively, whereas the mix design of fly-ash-based geopolymer concrete was taken from past studies based on the optimal mechanical performance [77] and is given in Table 3. The same mix proportion of geopolymer mortar was adopted as in the case of cement mortar, with cement

replaced by fly ash along with alkaline activator solution provided in Table 3. The chemical solution used as a composite activator consisted of liquid sodium silicate (Na_2SiO_3), and a 14-molarity solution of NaOH flakes. In both types of concrete and mortar, Lawrencepur sand was used, with a fineness modulus of 2.6, determined experimentally conforming to ASTM C136 [78]. Mortar cubes of 50 mm size were tested to obtain the compressive strength of the mortar. For the purpose of concrete, Sargodha crush was used with a particle size of 5–20 mm. The compressive strength of the masonry was determined by testing a four-brick stacked prism, whereas its modulus of elasticity was estimated by the gradient of the secant joining 5% to 33% on the compressive strength graph.

Table 1. Experimental material characteristics.

Properties	Material	Average Value (MPa)	Reference Standards
Compressive Strength, Elastic Modulus	Brick	$f_b = 19.74$ [COV 7.4%]	[79]
	Cement Mortar	$f_{jc} = 21.97$ [COV 6.5%]	[80]
	Geopolymer Mortar	$f_{jg} = 22.09$ [COV 7.1%]	
	Masonry (with cement mortar)	$f_m = 9.81$ [COV 8.5%] $E_m = 4700$	[81]
	Masonry (with geopolymer mortar)	$f_{mg} = 9.78$ [COV 4.9%] $E_{mg} = 4691$	
	OPC Concrete	$f_{c'} = 31.37$ [COV 4.4%] $E_c = 24794$	[82,83]
GPC Concrete	$f_{cg'} = 32.96$ [COV 7.2%] $E_{cg} = 25102$		
Yield Strength	Steel Rebar (6 ϕ)	$f_y = 483$ [COV 2.1%] $E = 188671$	[84]
	Steel Rebar (10 ϕ)	$f_y = 537$ [COV 1.3%] $E = 191103$	

Table 2. Chemical composition of fly ash.

Category	CaO %	MgO %	SiO ₂ %	SO ₃ %	Al ₂ O ₃ %	Fe ₂ O ₃ %	L.O.I *
FA	7.6	2.1	79.92	0.35	3.22	2.31	3.1

* Loss of ignition.

Table 3. Mix proportions of geopolymer concrete and mortar.

Material	FA (kg/m ³)	Coarse Agg. (kg/m ³)	Fine Agg. (kg/m ³)	NaOH Solution (kg/m ³)	NaOH (M)	Na ₂ SiO ₃ Solution (kg/m ³)	Na ₂ SiO ₃ /NaOH	AA/FA	Water (kg/m ³)
Concrete	368	1294	554	73.6	14	110.4	1.5	0.5	36.8
Mortar	368	-	1104	73.6	14	110.4	1.5	0.5	36.8

2.1.3. Instrumentation and Test Procedure

The experimental study was conducted in the Test Floor Laboratory of the UET Lahore. A total of two bare frames and two confined masonry walls were tested using the test set-up shown in Figure 2. Each of the bare frame and confined masonry walls was constructed with conventional concrete and geopolymer concrete on a robust RC footing beam with a cross-section of 300 mm × 300 mm, featuring an extended length of 300 mm on each side of the specimen to securely anchor it to the test floor. During the test, five LVDTs were used to record lateral, diagonal, and out-of-plane displacement as shown in Figure 2.

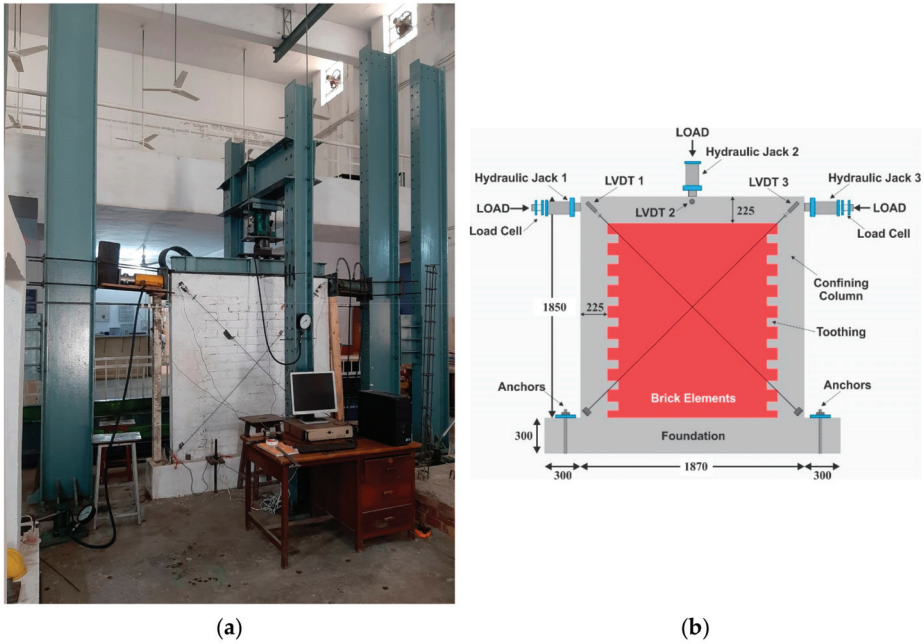


Figure 2. Experimental test setup (a) Actual, (b) Schematic.

A uniformly distributed gravity load was applied to the wall through a steel girder to simulate service roof load and was kept constant throughout the test. To allow for free lateral displacement during loading, four 50 mm diameter rollers were placed above the steel girder. Quasi-static in-plane reverse cyclic loading was then applied at the top of the beam-column joint with a low frequency of approximately 0.02 Hz, using hydraulic jacks on each side of the wall. Load cells were used to record lateral loads, and the lateral loading was increased incrementally by 5 mm after each cycle until failure, as per ACI 374.1-05 (ACI 374.1-05, 2014), as shown in Figure 3. The test was terminated when the specimens stopped taking further load and the strength degradation began together with considerable widening of bed joint cracks.

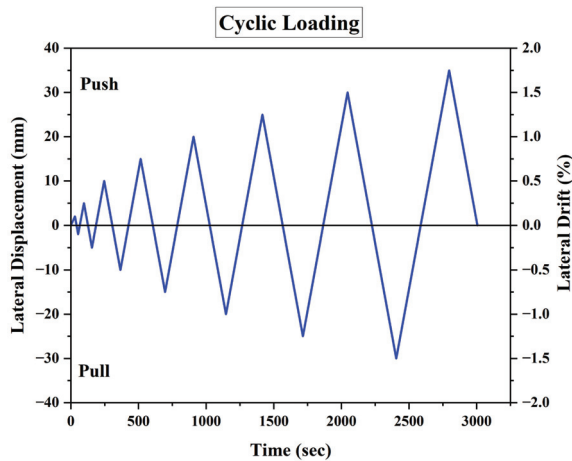


Figure 3. Quasi-static cyclic displacement time history.

2.2. Numerical Simulation

A numerical analysis was conducted to develop a three-dimensional finite element model of the confined masonry walls tested experimentally in the present study. The analysis utilized commercially available finite element software, ANSYS, which had been employed in earlier studies on masonry walls [85–89].

Based on past studies, there are various techniques utilized to analyze the structural response of masonry walls numerically. These techniques depend upon how accurately the model is capable of predicting the failure mechanisms. These techniques are categorized as detailed micro modeling, macro modeling, and simplified micro modeling.

The detailed micro modeling technique is very useful when most failure mechanisms are required to be analyzed. In this method, the mortar and bricks are considered continuum elements with defined failure criteria. The bricks and mortar interface are modeled with distinct elements representing discontinuities. Since, each part of the masonry, i.e., brick, mortar, and their interface, are modeled separately with their individual characteristics, therefore, this numerical approach takes more time to process the data. In contrast to the micro modeling technique, in the macro modeling approach the whole masonry panel is considered as a homogeneous element, where mesh size is the same as that of brick and the characteristics are assigned to a wall panel in place of mortar and brick separately. This modeling method is used due to the requirement for shorter data-processing time, but simultaneously, it is comparatively less accurate. Therefore, where more accuracy is not a big concern, this technique can be utilized, for example, for larger structures. However, in the simplified micro modeling, the general geometry of the wall including bricks is maintained, as in the detailed micro modeling, but the mortar joints and interface elements are modeled as discrete elements to represent a contact area. The compressive and shear stress properties are assigned to the mortar with the help of spring elements, and for the brick-mortar bond contact elements are used. This modeling technique requires less time for data processing as compared to the detailed micro-modeling approach. Based on the recommendations of previous research, a simplified micro-modeling technique was used in this study [90–95].

Reinforced concrete and brick units were modeled using three-dimensional hexahedron elements with eight nodes and three degrees of freedom at each node, with translational displacement along nodal x , y , and z dimensions, in ANSYS [95]. The SOLID65 element is capable of crushing in compression and cracking in tension and can incorporate reinforcement rebar that is smeared throughout the reinforced concrete element. To model the steel rebar, the LINK180 element, which is a uniaxial tension-compression element with three degrees of freedom at each node, was used. The mortar joint was modeled using two nonlinear spring elements (COMBIN39) in parallel and one contact element (CONTA178) in series with the spring elements (Figure 4).

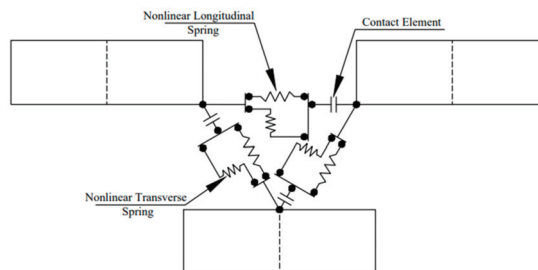


Figure 4. Brick-mortar joint detail.

The nonlinear springs represent the shear and axial response of the mortar, while the contact element represents the bond between the mortar and brick and considers friction as well. The properties of the spring and contact elements were determined directly from the

materials, with the force-deflection curve defined from the stress-strain curve. The force was defined by multiplying the stress by the tributary area over the node (Figure 5), and the deflection was expressed as the strain multiplied by the length of the spring, which was set to be 9/10 of the joint thickness, while the length of the contact element was 1/10 of the joint thickness.

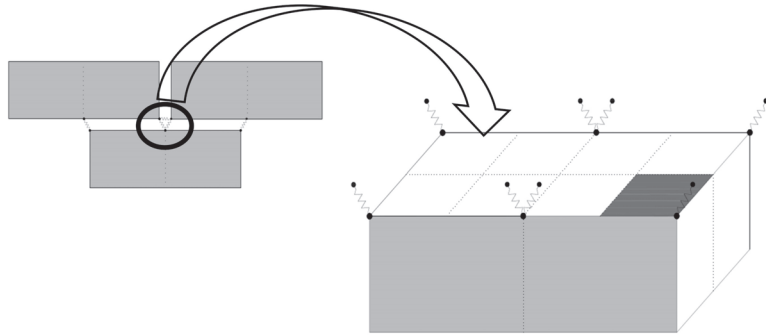


Figure 5. Tributary area on nodes for nonlinear springs.

The brick elements were meshed by dividing them vertically into two equal parts to connect them with adjacent upper and lower courses (Figure 5). The nodes of two bricks were connected with two spring elements in parallel and one contact element in series to model the mortar joint and the bond between brick and mortar, respectively. The two spring elements were assigned properties to express the longitudinal and transversal response of the mortar, while contact elements were assigned properties associated with the mortar and also friction to represent the bond between the brick and mortar. The confining elements of the wall were also modeled using SOLID65, and the steel rebar was embedded into the concrete using the LINK180 element. Before solving the analysis, all nodes of the wall were restrained along the z-direction to prevent out-of-plane movement of the panel. The lower nodes of the bottom course were restrained along all dimensions to provide fixed support at the bottom.

3. Results and Discussions

3.1. Experimental Program

3.1.1. Material Behavior

The material behavior of both types of concrete, mortar, and masonry wallets is illustrated in Table 1. Compressive strength is an important parameter to evaluate the structural performance of concrete. GPC typically has higher compressive strength compared to conventional concrete due to the strong chemical bonding between the binder and the aggregate. Additionally, geopolymer concrete often contains a higher proportion of fine aggregates, which contributes to the development of a dense and homogeneous microstructure. However, it is worth noting that the compressive strength of both kinds of concrete can be influenced by various factors such as mix design, curing conditions, water-to-binder ratio, and the size and type of aggregate. Therefore, a direct comparison of compressive strengths of two types of concrete in this study shows 4.94% more strength for geopolymer concrete. Past studies also endorse the higher compressive strength of geopolymer concrete compared to traditional concrete. For example, Neupane et al. [96] carried out a detailed study on the compressive strength of geopolymer and traditional concrete having different grades (40, 50, 65, and 80 MPa). With standard room-temperature curing of all specimens, it was observed that the compressive strength gain of geopolymer concrete was comparatively lower than conventional concrete at an early age; however, it was significantly higher at a later age. Reddy et al. conducted an experimental comparison of the compressive strengths of a novel steel-fiber-reinforced geopolymer concrete with

conventional concrete. The study found that the steel-fiber-reinforced geopolymer concrete had 13.4% higher compressive strength compared to the OPC concrete [97]. Moreover, the geopolymer mortar carries more compressive strength than OPC paste, as experimentally studied by Razak et al. [98]. It was concluded that the fly-ash-based geopolymer paste possesses more resistance to aggressive environments and compressive strength than OPC.

The second most important characteristic of a material contributing towards resistance to the applied load, Young's modulus of elasticity, also known as elastic modulus, is a measure of a material's stiffness and its resistance to deformation under load. In general, fly-ash-based geopolymer concrete has a higher Young's modulus of elasticity compared to conventional concrete. This indicates that fly-ash-based geopolymer concrete is stiffer and stronger than conventional concrete. However, the exact value of Young's modulus of elasticity of these materials can vary based on the specific mixture proportions and curing conditions used. The present study illustrates a 1.23% greater modulus of elasticity of geopolymer concrete compared to that of conventional concrete. In the literature, a large variety of experimentally-determined values of modulus of elasticity has been found for geopolymer concrete ranging from 30% lower to 20% higher than that of OPC. Bondar et al. [99] investigated the engineering properties of concrete made with alkali-activated natural pozzolan. The comparison of geopolymer concrete with traditional Portland cement concrete resulted in alkali-activated GPC possessing 5% to 20% higher modulus of elasticity after 14 days of ambient curing, making it a promising alternative to traditional concrete. However, Olivia et al. [100] experimentally evaluated a total of nine mixture variations by considering the impact of the ratio of sodium silicate to sodium hydroxide, the ratio of alkaline solution to fly ash, aggregate content, and curing method. The findings reveal that the modulus of elasticity of geopolymer concrete was 14.9–28.8% lower compared to ordinary Portland cement concrete. This suggests that a high content of silicate might enhance the elasticity of geopolymer concrete. Nath et al. [101] investigated eleven geopolymer specimens of different mix designs and two OPC cylinders to evaluate the modulus of elasticity at 28 and 90 days of ambient curing. The geopolymer concrete of similar grade to the OPC concrete achieved about 25–30% less modulus of elasticity than that of OPC at the age of 28 days, whereas at the age of 90 days' ambient curing, GPC could achieve modulus of elasticity in the range of 21.6% to 31.1% less than the value of conventional concrete. In view of the material behavior examined in the present research and previous studies, most of the findings endorse the superiority of alkali-activated fly-ash-based geopolymer concrete to ordinary concrete, which demonstrates the potential for developing and utilizing this alternative to traditional Portland cement concrete.

3.1.2. Hysteretic Response

The load-deflection hysteretic behavior of OPC-BF is given in Figure 6. During the early stages of loading and unloading, the hysteresis curves were nearly linear. As the lateral loading displacement increased, the specimen gradually entered an elastoplastic state, and its stiffness steadily declined due to the concentration of cracks at the columns and the beam-column joint. The flexural cracks initiated at the beam-column joint, at which, severe distress was noticed at increased load. In the later stages, more flexural cracks were produced at the column cross-section. The frame responded with almost symmetrical hysteresis loops by a difference of 7.8% between the peak positive and negative loads in the last cycle. The seismic resistance of the frame was discovered to escalate with each hysteresis, reaching a high of 25.39 kN and then declining to 22.81 kN during the final pushover, which corresponded to drifts of 2.30% and 3.16%, respectively. In the last cycles of load, the cracks started widening at the beam-column joint. It is important to note that the strength degradation of the bare frame was caused by plastic damage in the beam-column joints and column cross-section. A sudden decrease in seismic strength was noticed in the frame after reaching the maximum drift value, leading to the termination of the test. On the whole, the hysteretic curve of the specimen was pinched at higher drift levels. Additionally, the drift level at the peak load (δ_m) of the conventional concrete bare frame

was calculated to be 3.16% during push and 0.93% during pull cycles. The initial stiffness (K_{c0}) was recorded as 8.47 kN/mm.

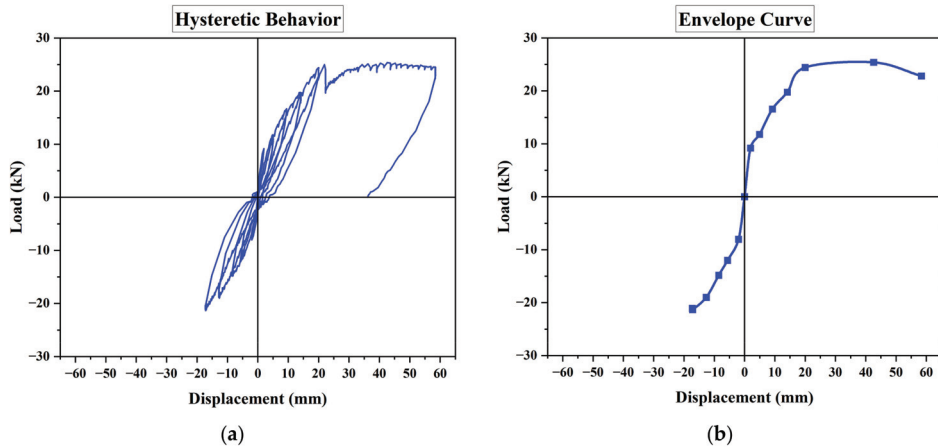


Figure 6. Experimental results of OPC-BF (a) Hysteretic response (b) Envelope curve.

The lateral load-displacement curve of GPC-BF is displayed in Figure 7. Initially, the specimen was in the elastic phase, with the load-deflection curve exhibiting a linear relationship. As lateral drift increased, cracks appeared near the beam joint, causing the hysteresis curve to slightly bend and display nonlinear behavior. This indicated that the specimen had entered the elastoplastic phase, with the enveloping area of the hysteresis loop increasing. The last push and pull load exhibiting peak positive and negative values of lateral load carrying capacity of the frame showed almost no difference. During the inelastic phase, the lateral load of the specimen gradually increased in each cyclic load, reaching a maximum value of 25.51 kN in the last pushover and gradually decreasing to 24.90 kN corresponding to 3.13% and 3.19%, respectively. Up to 58.9 mm lateral displacement, the geopolymer concrete frame resisted maximum loads. By further escalating the lateral displacements, large cracks were developed in the beam-column joint, due to which lateral load-carrying capacity decreased suddenly signaling the termination of the test. From the figure, it can be seen that the hysteresis loops are narrow at the beginning and wider at the end of the displacement cycles. This indicates that, at lower lateral displacements, crack widths were smaller, and less energy was dissipated. However, as lateral displacement increased, crack widths also increased, leading to greater energy dissipation. GPC-BF illustrated a good and stable hysteresis behavior with a slight pinching effect. The drift level at the peak load (δ_m) of the geopolymer concrete bare frame was estimated to be 3.19% during push and 1.34% during pull cycles. The initial stiffness (K_{c0}) was recorded as 8.77 kN/mm.

Approximately, all the seismic characteristics of the conventional concrete bare frame and alkali-activated fly-ash-based geopolymer concrete have shown good concordance with each other. The GPC frame has exhibited better lateral properties than the traditional concrete frame. The initial stiffness of the GPC frame has been observed 3.5% more than that of the OPC frame. However, the initial stiffness of the two frames has been found very close to the past studies [102–104]. Similarly, the ultimate positive and negative load of the GPC frame has been estimated 0.47% and 4.4%, respectively, higher than that of the cement concrete frame. The maximum lateral load strength of the OPC-BF and GPC-BF were found to be 1.37 and 1.54 times the cracking load.

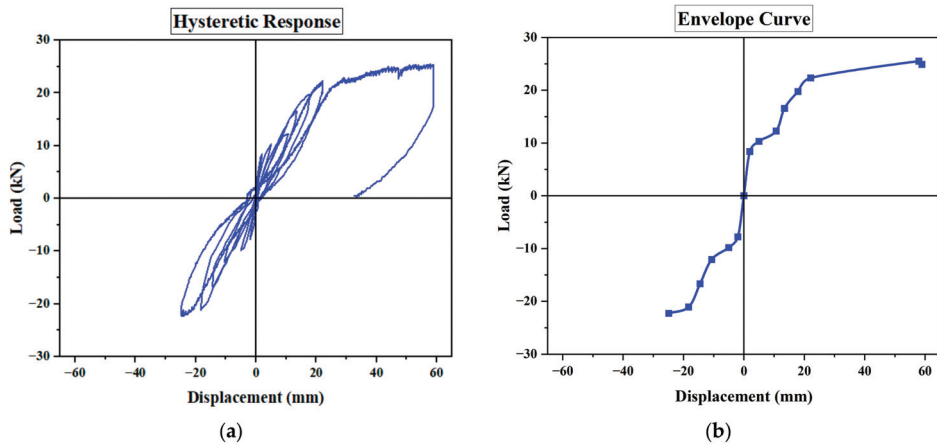


Figure 7. Experimental results of GPC-BF (a) Hysteretic response (b) Envelope curve.

The results of OPC-BF and GPC-BF show good match with the past studies. The study conducted by Sumajouw et al. [105] investigated the performance of slender columns made of fly ash concrete (measuring 175 mm × 175 mm × 1500 mm) when subjected to axial compression and uniaxial bending. The research focused on several key parameters, including compressive strength (40 MPa and 60 MPa), longitudinal reinforcement ratio (1.47 and 2.95), and load eccentricity (15, 35, and 50 mm). The study revealed that columns made of fly ash geopolymer concrete demonstrated behavior similar to that of ordinary Portland cement (OPC) concrete. Consequently, the existing design provisions contained in current standards and codes can be employed to design reinforced fly-ash-based geopolymer concrete columns.

Similarly, Rahman et al. [106] conducted a study on twelve slender columns made of fly ash concrete (measuring 175 mm × 175 mm × 1500 mm) that were subjected to axial compression and different combinations of biaxial load eccentricities. The study focused on several key parameters, including compressive strength (ranging from 37 MPa to 63 MPa), longitudinal reinforcement ratio (1.47 and 2.95), load eccentricity in the x direction (15, 30, 35, 50, and 70 mm), and load eccentricity in the y direction (15, 30, 35, 50, and 70 mm). The results of their study demonstrated the potential for fly ash geopolymer concrete to be used in structural applications instead of conventional concrete structures.

The in-plane load vs. deformation of the conventional concrete tested specimen is shown in (Figure 8). The hysteretic response of the OPC-CM wall panel illustrated almost proportional cycles in pushing and pulling directions. The seismic strength of the wall specimen was found to increase in each hysteresis reaching a maximum value of 114.3 kN and then decreasing to 109.1 kN in the last push load corresponding to 1.73% and 2.02% drifts, respectively. After the peak drift value, a sudden drop in seismic strength was observed in the wall panel, which was the main reason for the test termination. The pinching behavior was witnessed during the seismic performance of the panel at a larger drift level because of confinement. The distribution of the lateral load along the cross-section of the masonry A_w caused the development of the shear stress in the masonry panel (V_{max}/A_w), i.e., 0.67 MPa. Further, the drift level at peak load (δ_m) of the confined masonry wall was estimated as 1.73% at push and 1.35% during the pull cycles. The initial stiffness (K_{C0}) was observed as 35 kN/mm.

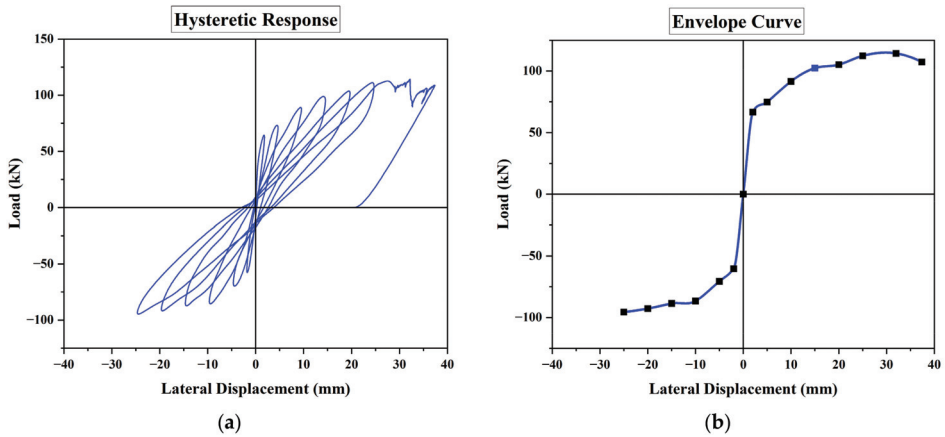


Figure 8. Experimental results of OPC-CM (a) Hysteretic response (b) Envelope curve.

The hysteretic behavior of the GPC-CM test specimen exhibited slight irregular and asymmetric loops in the push and pull cyclic loads as shown in (Figure 9). The wall specimen showed almost symmetric loops until the onset of bed joint cracks in the second loop of lateral load, after which the structural behavior of the wall shifted to an elastoplastic state and the wall stiffness steadily degenerated owing to the development and concentration of more and more cracks in the masonry pier. As with the cement concrete wall, the GPC wall also showed increasing seismic load capacity in each cycle reaching a maximum value of 119.10 kN at the drift of 2.32% in the last push load, after which the wall stopped taking further load and the lateral load carrying capacity of GPC-CM started decreasing and a sudden drop in lateral strength was observed, at which point the test was terminated to avoid any accident or damage to the equipment attached to the wall. The initial stiffness (K_{C0}) and the development of the shear stress in the masonry pier (V_{max}/A_w) were estimated as 55.45 kN/mm and 0.66 MPa, respectively.

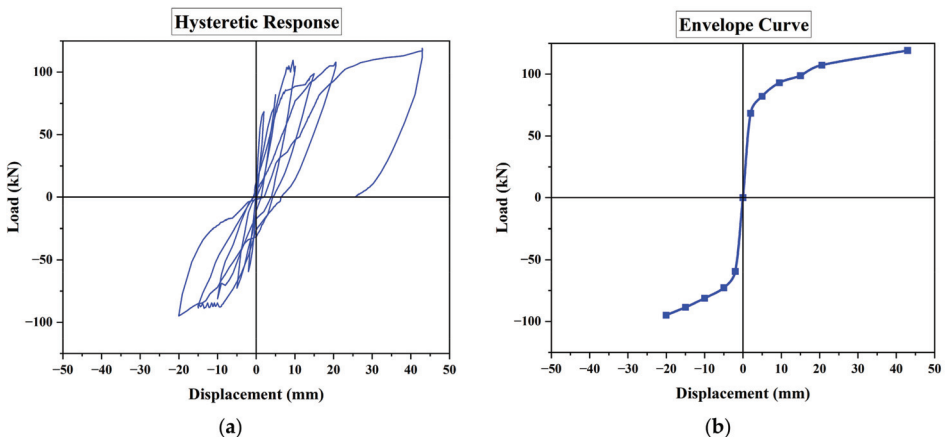


Figure 9. Experimental results of GPC-CM (a) Hysteretic response (b) Envelope curve.

As with bare frame structures, GPC confined masonry has also shown a good match of seismic characteristics with the traditional concrete wall. The initial stiffness of the GPC wall specimen was estimated 45.2% higher than that of OPC wall masonry, whereas wall shear stress was calculated as 1.5% greater in OPC-CM. As far as peak lateral load is concerned,

GPC confined masonry has exhibited a 4.11% greater peak lateral load than the OPC wall. The higher seismic capacity of alkali-activated fly-ash-based geopolymer concrete confined masonry is certainly due to more compressive strength and Young's modulus of elasticity of geopolymer concrete as determined experimentally in the present study. Approximately similar behavior is also evident from the previous research as discussed in the material behavior section. The backbone curves of both walls were plotted by joining the peak resistance of the adjacent displacement cycles (Figures 8 and 9). The maximum lateral load-bearing capacity of the OPC-CM and GPC-CM were found to be 1.52 and 1.66 times the cracking load, which are slightly more than the squat wall tested by Borah et al. [107].

The maximum seismic strength (V_{max}) of all the specimens determined experimentally and the corresponding drift (δ_m) are presented in Table 4. The cyclic stiffness (K_c) was calculated for the first hysteresis loop at every drift level as the gradient of the line connecting the maximum points of positive and negative curves. The stiffness degradation (K_c/K_{c0}) at each drift level was drawn concerning the drift δ normalized with regard to the drift level in the first loading cycle, δ_0 (Figure 10a). The strength variation factor ($C_{sv} = V/V_{max}$) obtained from the normalization of seismic loads determined against various drift points with V_{max} was plotted against δ/δ_m (Figure 10b). The plot shows that the increment in strength was found in the specimen due to confining elements in the wall.

Table 4. Hysteretic response of test walls.

Specimen	V_{cr} (kN)	V_{max} (kN)			V_{max}/A_w (MPa)	δ_m (%)			μ_d
		Push	Pull	Avg		Push	Pull	Avg	
OPC-BF	18.52	25.39	21.34	23.36	-	3.15	0.93	2.04	1.29
GPC-BF	16.56	25.51	22.30	23.90	-	3.19	1.34	2.26	1.02
OPC-CM	75.7	114.3	98.2	106.2	0.67	2.02	1.35	1.68	15.42
GPC-CM	51.14	85.10	58.25	71.67	0.44	2.32	1.08	1.70	3.27

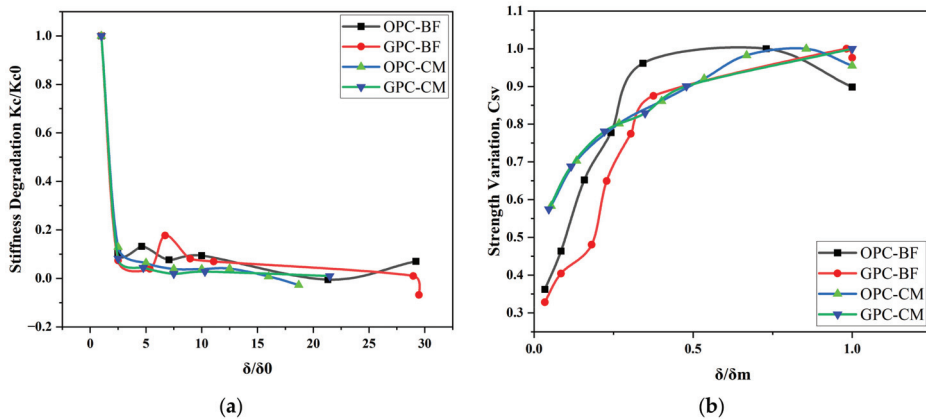


Figure 10. (a) Stiffness degradation (b) Strength variation.

3.1.3. Strain in Longitudinal Reinforcement

The strain in longitudinal reinforcement was determined at the most critical sections of the tie-columns, where plastic hinges were expected to develop, to evaluate the nonlinearity of the structures, with the help of a data logger. The strain gauges installed at the bottom of each tie-column recorded large strains related to the yielding of longitudinal reinforcement. The lowest values of the lateral drift level with respect to the yielding of the reinforcement rebars are shown in Figure 11. The drifts corresponding to the yielding of steel rebars in all test specimens were observed to be approximately comparable to each other due to the fact that the same steel was used in all specimens. It is pertinent to mention that the

yielding phenomenon in steel rebars is the same regardless of the type of concrete used in a structure, therefore the occurrence of close values of drift level related to the steel yielding is certain.

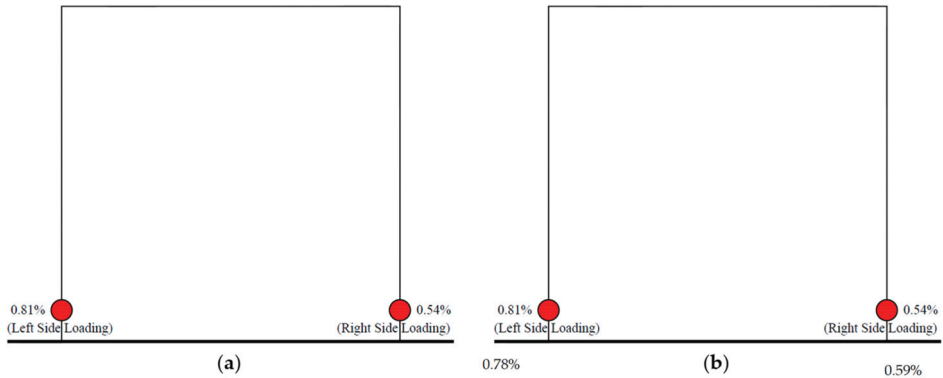


Figure 11. Locations of reinforcement yielding and corresponding drift values (a) OPC-CM (b) GPC-CM.

3.1.4. Failure Mechanism

Figure 12 displays the cracking pattern of OPC-BF, denoting the ordinary Portland cement bare frame. In the OPC-BF specimen, the initial crack appeared at the beam-column joint at 18.52 kN push load corresponding to the drift level of 0.67%. On further displacement in the pulling direction, the first flexural crack appeared at the column cross-section near the bottom, against the lateral load 19.7 kN at 0.76% drift. Few flexural cracks appeared to spread on both column cross sections at increased lateral load. At the end of the last pushover, shear cracks at the beam-column joint and a flexural crack at the bottom of the right column widened and propagated. The frame specimen achieved maximum seismic strength as 25.39 kN and 21.34 kN in the push and pull cyclic loads against the drift levels of 3.15% and 0.93% respectively. The maximum lateral displacement noted in the test specimen was 58.4 mm in the last pushover. The beam-column joint shear crack width was measured as 37 mm, whereas the maximum width of the flexural crack at the bottom of the column was recorded as 11 mm.

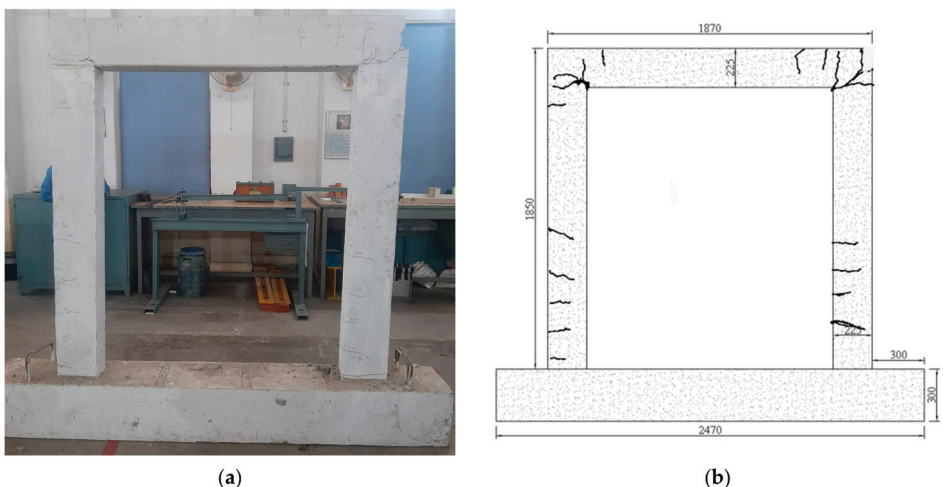


Figure 12. Crack pattern of OPC-BF (a) failure pattern of actual sample, (b) crack pattern diagram.

The fly-ash-based geopolymer concrete bare frame, denoted as GPC-BF, exhibited a ductile behavior and plastic hinges were fully produced at the beam-column joints and bottom of the columns as shown in Figure 13. The first crack appeared near the beam joint at the lateral load of 16.56 kN at 0.72% drift. Further, an increase in load to 19.75 kN against 0.97% lateral drift caused the appearance of flexural cracks in the columns. These flexural cracks were produced mostly near the bottom of columns. The most vulnerable places to failure in a bare frame are usually the bottom of columns and beam-column joints. At the lateral load of 22.32 kN push cycle corresponding to the drift level of 1.2%, the shear cracks at the beam-column joint widened significantly. The maximum lateral strength achieved by the geopolymer concrete frame specimen were 25.51 kN and 22.3 kN corresponding to the 3.18% and 1.34% drifts in the push and pull load cycle, respectively. The ultimate lateral displacement attained by the specimen was recorded as 58.9 mm in the final pushover. The maximum flexural crack width near the bottom of columns and shear crack width at the beam-column joint were measured as 10 mm and 29 mm, respectively. Both the test specimens have shown very similar failure modes and crack patterns with a slightly smaller crack width in the case of GPC-BF.

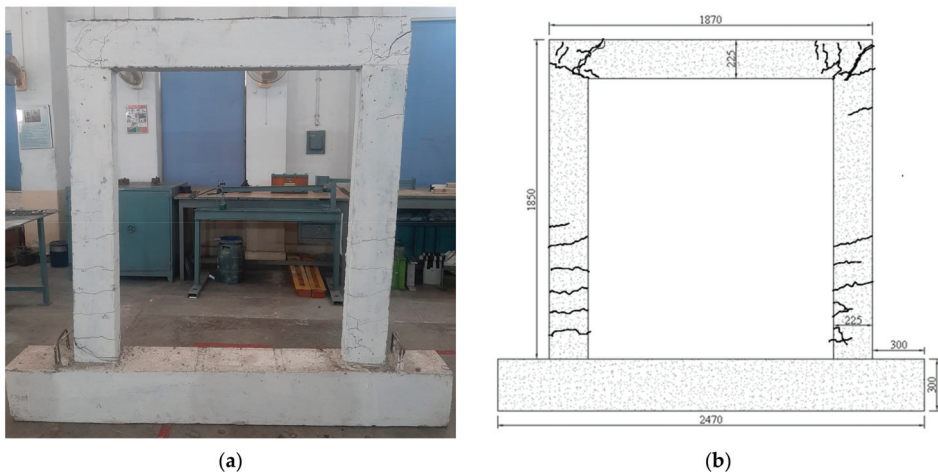


Figure 13. Crack pattern of GPC-BF (a) failure pattern of actual sample, (b) crack pattern diagram.

The specimen OPC-CM, denoting a confined masonry wall panel made of ordinary Portland cement concrete, was dominated by the shear failure of confining elements and crisscross mortar joints (Figure 14). At a drift level of 0.22%, corresponding to a lateral load of 75.74 kN for the pushing direction, the first crack initiated at the bed joint of mortar near the top. On further increasing lateral load, the cracks started propagating downward through the bricks-mortar joints at 0.54% drift against 89.85 kN. Diagonal stair-stepped cracks spread from the column-beam joint to the bottom of the other column through the bricks interface at 1.08% drift and a lateral load of 103.21 kN. On increasing further lateral drift, flexural cracks appeared in one tie-column. The possible reason for flexural cracks is the rocking of the masonry panel after the reinforced tie-column approaches the maximum tension capacity at the base. Most of the diagonal cracks developed passed through the mortar joints and only a few went through the bricks. The wall specimen achieved maximum lateral load-bearing capacity in pushing and pulling direction as 114.29 kN and 108.48 kN against drift levels of 1.73% and 1.35%, respectively. The peak lateral displacement recorded in the test specimen was approximately 37.4 mm in the last pushing direction. The diagonal crack width was measured as 24 mm, whereas the largest width of flexural cracks in tie-column was noted as 9.0 mm. The damage in the specimen was mostly concentrated in the top one-third part.

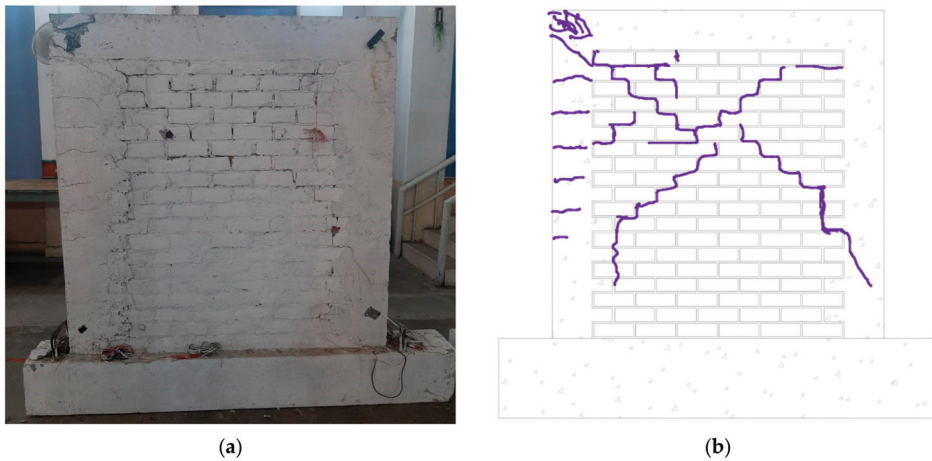


Figure 14. Crack pattern of OPC-CM (a) failure pattern of actual sample, (b) crack pattern diagram.

The failure mode in the GPC-CM wall, designating GPC confined masonry, may be characterized by the shear failure of masonry as well as confining elements including the tie-beam (Figure 15). The very first crack developed at the bed joint of bricks near the top left of the masonry close to the tie-column at 0.25% drift and 71.73 kN lateral load in the pushing direction. On increase in load, until 86.50 kN corresponding to 0.49% drift, the cracks' dissemination started downward along the bed and head joints. The first crack developed, spread upward, and entered the tie-column against 0.81% drift and 98.75 kN lateral load. The diagonal crisscross cracks produced propagated upward into the tie-column and downward into masonry. At 1.08% drift and 94.95 kN seismic load in the pulling direction, the right column-beam joint failed badly with considerable crack size. Further increase in lateral displacement led to shear cracks in the tie-beam and flexural cracks in the left tie-column at 1.11% drift and 107.98 kN lateral load in the sixth cycle of load. At the same load, the mortar spalled off at the center of the masonry wall. Almost all the cracks passed through the brick interface due to weak brick-mortar joints. The crack distribution was observed uniformly across the test wall. The wall specimen exhibited peak load carrying capacity of 119.1 kN and 95.0 kN in pushing and pulling directions at 2.32% and 1.08% drifts, respectively. The ultimate lateral displacement noted was 42.97 mm in the last push. The maximum shear crack width measured in the test specimen was around 28 mm and the width of flexural cracks in the tie-column and shear cracks in the tie-beam were recorded as 8.0 mm and 4.0 mm, respectively.

In both walls, the failure mode may be considered as the shear failure in form of diagonal cracks in the masonry panel propagated in slanted directions. The failure mechanism and the damage pattern were very similar to the research conducted by El-Diasity et al. on confined masonry under cyclic load [108]. The existence of the confining elements prolonged the occurrence of shear cracks in the masonry panel [109]. It is pertinent to mention that no separation was noticed at the toothed interface between confining columns and the masonry panel, clearly illustrating a significant advantage of confined masonry over infilled masonry structures [110]. The test experiments were terminated at the stage when the collapse prevention (CP) level of wall performance was attained as mentioned in ASCE/SEI 41-06 [111].

The cracking load of OPC-CM was observed to be 5.44% greater than that of GPC-CM. In GPC-CM, almost all the cracks propagated through the masonry joints separating the mortar from the brick interface instead of the crack passing through the geopolymer mortar.

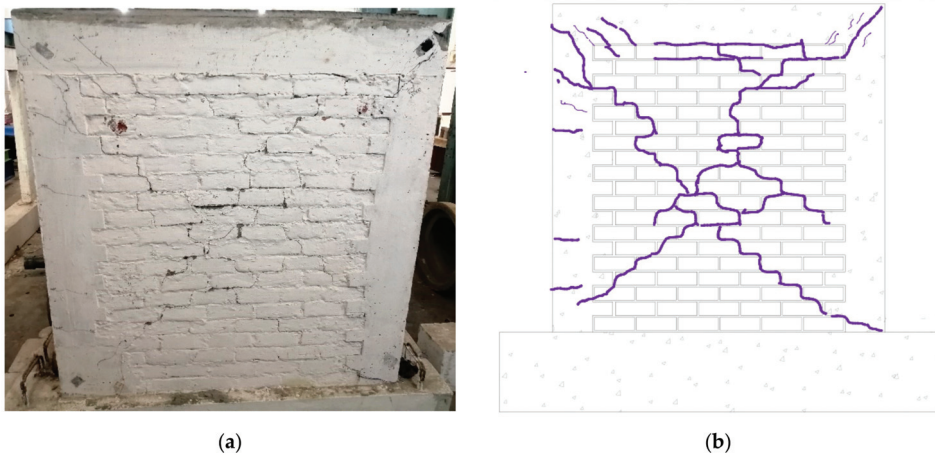


Figure 15. Crack pattern of GPC-CM (a) failure pattern of actual sample, (b) crack pattern diagram.

3.2. Numerical Modeling

The validation of the numerical model through experimental testing is considered a crucial aspect of FEA-based research to determine the accuracy of simulated parameters. Two confined masonry walls were tested experimentally to validate the numerical models used in this study. The wall panels built with confining elements of 225 mm depth and longitudinal reinforcement of No. 10 were tested under reverse cyclic loading. The seismic behavior of the test specimens was compared with that of the numerical models, which showed good agreement.

The comparison of the numerical model and experimental results of OPC-CM showed a difference of 10.81% in seismic capacity (V_{num}) as shown in (Figure 16a). The numerical validation also revealed very similar hysteretic behavior in initial cycles, with increased energy dissipation at higher drift level. It is clear from the envelope curves that the numerical model demonstrated an increase in lateral strength with an increase in lateral drift, just as in the experimental results. The initial stiffness found from the numerical analysis was closely comparable with the experimental result by a difference of 5.4%.

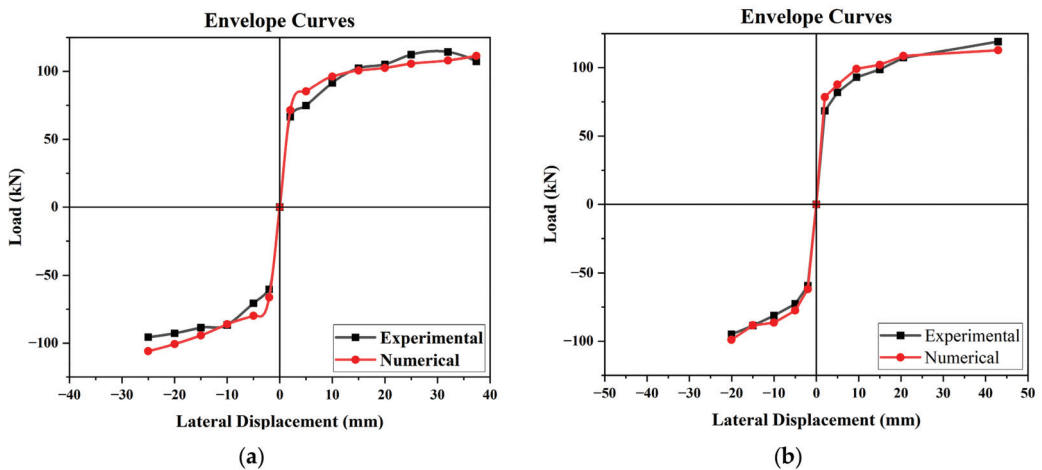


Figure 16. Comparison of experimental and numerical results (a) OPC-CM (b) GPC-CM.

Figure 16b illustrates the validation of the numerical model of GPC-CM by experimental results with a difference of 5.39% in peak lateral load. Similar to the OPC masonry case, FE analysis of the GPC wall also depicted an increasing trend of lateral load capacity with an increase in drift level as compared to the experimental results, evident from the backbone curves. The initial stiffness calculated from the numerical analysis was almost matchable to the experimental result by a difference of 6.1%.

Figure 17 displays the contour plot of both wall panels at the stage of failure. The diagonal contours that appeared on the damaged shape, clearly indicate that two panels failed in shear which matched with the failure mode of the tested walls. The FE model of conventional concrete confined masonry reached its maximum compressive strength and failed at the toe of the confining column, whereas the GPC model failed at the point of load application after reaching the peak compressive strength. The principal stresses varied as a result of loading and unloading during push and pull. The FE model, despite limitations in showing bed joint cracks, provided an approximate agreement with experimental damage as represented by stress contours in ANSYS (Figure 17).

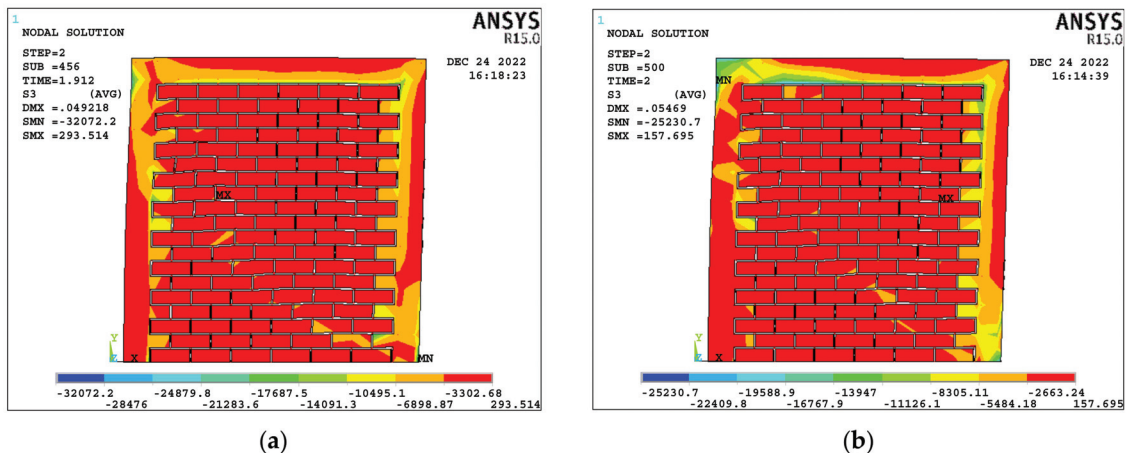


Figure 17. Contour plots of damaged shape (a) OPC-CM (b) GPC-CM.

4. Comparison of Seismic Parameters

Geopolymer concrete confined masonry has shown considerable resistance to seismic load in this study. The lateral load strength of the GPC masonry wall has presented a good concordance not only with the conventional concrete confined masonry in this study. It is pertinent to mention that the lateral load-carrying capacity of confined masonry walls with an even higher reinforcement ratio has been observed to be less than that of a GPC wall. From Table 5, it is observed that GPC confined masonry has proved to be a seismically resistant structure in comparison to non-engineered masonry walls. The results exhibited comparable seismic resistance to other confined masonry tested in the past as given in Table 6. A comparison has also been drawn between the present study, especially regarding GPC confined masonry, and the past studies on infill masonry and bare frame in Tables 7 and 8, illustrating the significant advantages of GPC masonry over cement concrete infill masonry and bare frame.

Table 5. Comparison of the present study with past studies on unconfined masonry.

Sr. No	Study	Aspect Ratio (H/L)	ρ (%)	Cracking Load V_{cr} (kN)	Maximum Load V_{max} (kN)	V_{max}/V_{cr}	Failure Mode
1	Ashraf [112]	1.08	-	-	77.8	-	Rocking
		1.08	-	-	103.1	-	Rocking
		1.08	-	47.0	120.3	2.55	Shear
		1.08	-	39.5	131.7	3.33	Shear
2	Nadège et al. [113]	1.22	-	-	12.0	-	Shear-Flexure
3	A Hasnat et al. [114]	0.75	-	4.42	13.1	2.96	Rocking
4	Konthesingha et al. [115]	1.0	-	-	257	-	Shear
		0.5	-	-	345	-	Rocking
5	Mojsilovic et al. [116]	1.0	-	-	89.17	-	Compression (Toe Crushing)
		1.0	-	-	145.89	-	Compression (Toe Crushing)
		1.0	-	-	53.37	-	Rocking
6	OPC-BF	0.99	1.08	18.52	25.39	1.37	Ductile
7	GPC-BF	0.99	1.08	16.56	25.51	1.54	Ductile
8	OPC-CM	0.99	1.08	75.7	114.3	1.51	Shear
9	GPC-CM	0.99	1.08	51.1	85.1	1.66	Shear

Table 6. Comparison of the present study with past studies on confined masonry.

Sr. No	Study	Aspect Ratio (H/L)	ρ (%)	Cracking Load V_{cr} (kN)	Maximum Load V_{max} (kN)	V_{max}/V_{cr}	Failure Mode
1	Aguilar et al. [117]	1	1.51	103.1	140.6	1.36	Shear
2	Yáñez et al. [118]	0.61	1.12	68.5	127	1.85	Shear
		0.61	1.12	128.5	185.5	1.44	Shear
3	Marinili et al. [119]	0.77	2.25	142.2	205.9	1.45	Shear
4	Zabala et al. [120]	0.97	0.79	82.6	118	1.42	Shear
		0.97	2.01	140.76	207	1.47	Shear
5	Bourzam et al. [121]	1.62	2.01	70	81.4	1.16	Shear
6	Gavilan et al. [122]	1.52	2.82	71.3	75.8	1.06	Shear
		0.98	2.82	100.5	157.0	1.56	Shear
		0.67	2.82	250.2	320.8	1.28	Shear
7	Colunga et al. [123]	1.00	1.18	49.0	80.4	1.64	Shear
8	Borah et al. [107]	1.63	0.72	34.1	47.5	1.39	Shear
		1.30	0.72	38.2	55.8	1.46	Shear
		0.93	0.72	60.7	81.2	1.34	Shear
9	OPC-BF	0.99	1.08	18.52	25.39	1.37	Ductile
10	GPC-BF	0.99	1.08	16.56	25.51	1.54	Ductile
11	OPC-CM	0.99	1.08	75.7	114.3	1.51	Shear
12	GPC-CM	0.99	1.08	51.1	85.1	1.66	Shear

Table 7. Comparison of the present study with past studies on infill masonry.

Sr. No	Study	Aspect Ratio (H/L)	ρ (%)	Cracking Load V_{cr} (kN)	Maximum Load V_{max} (kN)	V_{max}/V_{cr}	Failure Mode
1	Kuang et al. [124]	0.60	2.57	248	432	1.74	Shear
2	Ozkaynak et al. [125]	0.75	1.00	48.5	89.7	1.85	Shear
3	Van et al. [126]	0.61	1.57	13.7	36.6	2.67	Shear
		1.01	1.57	11.4	43.5	3.80	Shear
4	Li et al. [127]	0.74	1.09	-	261.1	-	Shear
		0.74	1.09	-	390	-	Shear
5	Durrani et al. [128]	0.97	1.76	33.3	49.7	1.49	Shear
6	OPC-BF	0.99	1.08	18.52	25.39	1.37	Ductile
7	GPC-BF	0.99	1.08	16.56	25.51	1.54	Ductile
8	OPC-CM	0.99	1.08	75.7	114.3	1.51	Shear
9	GPC-CM	0.99	1.08	51.1	85.1	1.66	Shear

Table 8. Comparison of the present study with past studies on bare frame.

Sr. No	Study	Aspect Ratio (H/L)	ρ (%)	Cracking Load V_{cr} (kN)	Maximum Load V_{max} (kN)	V_{max}/V_{cr}	Failure Mode
1	Jiang et al. [129]	0.49	1.57	129.7	379.3	2.92	ductile
2	Peng et al. [130]	0.57	1.03	-	334.7	-	ductile
3	Ozkaynak et al. [125]	0.75	1.00	20.6	41.6	2.02	ductile
4	Van et al. [126]	1.01	1.57	7.8	22.7	2.9	ductile
5	Penava et al. [131]	0.68	2.35	61.2	106.4	1.74	ductile
6	OPC-BF	0.99	1.08	18.52	25.39	1.37	Ductile
7	GPC-BF	0.99	1.08	16.56	25.51	1.54	Ductile
8	OPC-CM	0.99	1.08	75.7	114.3	1.51	Shear
9	GPC-CM	0.99	1.08	51.1	85.1	1.66	Shear

5. Viability of Geopolymer Concrete

Geopolymer concrete is a type of concrete that is made using industrial waste materials such as fly ash, blast furnace slag, and other mineral admixtures instead of traditional cement. The resulting material is known to have several advantages over conventional concrete, including improved mechanical properties, increased durability, and reduced carbon emissions.

Recently, sustainable, strong and durable concrete has become an important aspect of the construction industry [132–135]. Geopolymer concrete is considered to be more environmentally friendly than conventional concrete because it reduces the need for Portland cement, which is a major contributor to carbon dioxide emissions during its manufacturing process. By using industrial waste materials such as fly ash in geopolymer concrete, it is possible to reduce the amount of waste that is sent to landfills while simultaneously producing a material that is strong and durable.

One of the key benefits of geopolymer concrete is its strength and durability. In this study, geopolymer concrete has shown higher compressive strength (3.89%) and Young's modulus of elasticity (1.23%) than traditional concrete, and the similar mechanical behavior of geopolymer concrete is evident from past studies [96–101]. These attributes make it a

promising material for a wide range of applications, including infrastructure projects such as bridges, highways, and buildings [105,106,132].

In this paper, the research to investigate the structural performance of geopolymer concrete bare frames against the seismic load has demonstrated 3.5% and 0.93% higher values of initial stiffness and maximum lateral load carrying capacity, respectively, of the GPC frame as compared to the OPC frame. The investigation was extended to the experimental and numerical study of confined masonry with comparable results. The findings highlight that GPC confined masonry has displayed 45.2% and 4.11% more initial stiffness and peak seismic strength, respectively, than traditional concrete walls.

The topmost benefit of geopolymer concrete is its low carbon footprint. The production of traditional Portland cement is responsible for a significant amount of carbon dioxide emissions, and the use of geopolymer concrete can significantly reduce these emissions. In addition, the use of industrial waste materials in geopolymer concrete can reduce the amount of waste that is sent to landfills, which can help to reduce environmental pollution.

Overall, geopolymer concrete shows promise as a viable and green substitute for conventional concrete. Its strength, durability, and low carbon footprint make it a promising material for a wide range of infrastructure projects. However, more research and development are needed to improve the production process and address the challenges associated with its use.

6. Conclusions

The aim of the research was to compare the performance of fly-ash-based geopolymer concrete bare frames and confined masonry wall panels with conventional OPC concrete. The study aimed to provide valuable insights into the design and evaluation of GPC confined masonry structures, especially in high seismic regions, to encourage cost-effective, eco-friendly, sustainable, and earthquake-resistant construction. The experimental and numerical program evaluated the seismic behavior of bare frames and single-wythe confined masonry walls made with geopolymer and conventional concrete, with an aspect ratio close to 1.0, subjected to displacement-controlled pseudo-static reverse cyclic loading. The response of the test specimens was analyzed based on seismic parameters, such as lateral load strength, initial stiffness and stiffness degradation, maximum drift level, failure mode, and damage pattern. Finite Element models of confined masonry walls were established using a simplified micro-modeling technique and validated based on the test results. The study compared the significant structural parameters of the walls tested in this study with those of unconfined masonry, confined masonry, infill masonry, and bare frame tested in previous research.

The research yielded several inferences drawn from both experimental and numerical analyses. Firstly, the mechanical strength parameters of the GPC and OPC concrete mixtures were compared. The compressive strength and Young's modulus of elasticity of cylindrical specimens were 4.94% and 1.23% higher, respectively, in GPC compared to OPC concrete. Afterwards, the wall panels were tested incorporating each of the materials. The seismic characteristics of conventional concrete bare frame and geopolymer concrete bare frame showed good concordance with each other. The GPC frame exhibited better lateral properties than the traditional concrete frame. This initial stiffness calculated in the case of the GPC frame was 8.77 kN/mm which was 3.5% higher than the corresponding value of the OPC frame, 8.47 kN/mm. The maximum lateral load borne by both types was very similar, i.e., 25.51 kN by GPC-BF and 25.39 kN by OPC-BF. Similarly, the GPC confined masonry wall showed improved seismic properties compared to the cement concrete wall. The ultimate load capacity of the GPC-CM wall was 1.66 times the cracking load, whereas the OPC-CM wall was 1.52 times the cracking load, indicating that the GPC-CM wall bears more percentage load from the initiation of cracks until failure. The GPC wall resisted up to 119.1 kN load while the OPC wall resisted up to 114.3 kN of lateral load. Although the difference of 4.2% is small, it might be considered enough to offer GPC confinement as an environmentally-friendly alternative to conventional concrete. The failure mode was

identified as shear failure in both walls with no separation at the toothed interface between the tie-column and the masonry panel, demonstrating the superiority of the confined masonry compared to the infill masonry structures. The numerical models of the two confined masonry walls were well-validated by the experimental results.

The research suggests that alkali-activated fly-ash-based geopolymer concrete is a good substitute for OPC concrete and should be preferred in various applications to reduce the global usage of OPC and mitigate its detrimental environmental effects. The structural response of geopolymer concrete confined masonry made from fly ash is comparable to that of OPC concrete, indicating that the current engineered masonry design can be comfortably adopted, especially in highly seismic-prone areas, to produce a green environment. However, additional research is necessary to develop well-grounded seismic design criteria to predict the lateral in-plane load strength for GPC confined masonry structures with multiple stories.

Author Contributions: Conceptualization, M.M.A. and A.U.Q.; Methodology, M.M.A., A.U.Q., A.A. and S.A.; Software, M.M.A.; Validation, M.M.A., A.U.Q. and M.J.M.; Formal analysis, M.M.A., S.M.S.K. and A.A.; Investigation, A.U.Q. and A.A.; Data curation, A.A.; Writing—review and editing, M.M.A., U.A.M. and S.A.; Supervision, A.U.Q. and A.A. All authors have read and agreed to the published version of the manuscript.

Funding: This research received no external funding.

Data Availability Statement: Complete data has not been shared due to on-going PhD research work.

Acknowledgments: The authors would like to thank Asif Hameed, Test Floor Laboratory and Burhan Shareef, Concrete Laboratory at UET Lahore for the successful completion of experimental work from casting to testing. The authors also wish to express their gratitude to Rashid Hameed for his cooperation regarding equipment. Special thanks to the laboratory staff including Afzaal, Umer, Hamza, Touseef, Shahid, Faisal, Nadeem, Zahoor, Mahmood, who have helped in undertaking the necessary arrangements for the test setups.

Conflicts of Interest: The authors declare no conflict of interest.

References

1. Almssad, A.; Almusaed, A.; Homod, R.Z. Masonry in the Context of Sustainable Buildings: A Review of the Brick Role in Architecture. *Sustainability* **2022**, *14*, 14734. [CrossRef]
2. Borah, B.; Kaushik, H.B.; Singhal, V. Lateral load-deformation models for seismic analysis and performance-based design of confined masonry walls. *J. Build. Eng.* **2022**, *48*, 103978. [CrossRef]
3. Macabuag, J.; Guragain, R.; Bhattacharya, S. Seismic retrofitting of non-engineered masonry in rural Nepal. *Proc. Inst. Civ. Eng. Build.* **2012**, *165*, 273–286. [CrossRef]
4. Bhattacharya, S.; Nayak, S.; Dutta, S.C. A critical review of retrofitting methods for unreinforced masonry structures. *Int. J. Disaster Risk Reduct.* **2014**, *7*, 51–67. [CrossRef]
5. Varela-Rivera, J.; Fernandez-Baqueiro, L.; Gamboa-Villegas, J.; Prieto-Coyoc, A.; Moreno-Herrera, J. Flexural behavior of confined masonry walls subjected to in-plane lateral loads. *Earthq. Spectra* **2019**, *35*, 405–422. [CrossRef]
6. Bruneau, M. State-of-the-art report on seismic performance of unreinforced masonry buildings. *J. Struct. Eng.* **1994**, *120*, 230–251. [CrossRef]
7. So, E.K.M.; Pomonis, A. Derivation of globally applicable casualty rates for use in earthquake loss estimation models. In Proceedings of the 15th World Conference on Earthquake Engineering, USB, Lisbon, Portugal, 24–28 September 2012.
8. Asian Development Bank and World Bank (ADB-WB). *Preliminary Damage and Needs Assessment-Pakistan 2005 Earthquake*; Asian Development Bank and World Bank: Islamabad, Pakistan, 2005.
9. Naseer, A.; Khan, A.N.; Hussain, Z.; Ali, Q. Observed seismic behavior of buildings in northern Pakistan during the 2005 Kashmir earthquake. *Earthq. Spectra* **2010**, *26*, 425–449. [CrossRef]
10. Marques, R.; Lourenço, P.B. A model for pushover analysis of confined masonry structures: Implementation and validation. *Bull. Earthq. Eng.* **2013**, *11*, 2133–2150. [CrossRef]
11. Meli, R. Structural design of masonry buildings: The Mexican practice. *Spec. Publ.* **1994**, *147*, 239–262.
12. Gallegos, H. Masonry in Peru. *Spec. Publ.* **1994**, *147*, 307–332.
13. Alcocer, S.M.; Klingner, R.E. Masonry research in the Americas. *Spec. Publ.* **1994**, *147*, 127–170.
14. Hidalgo, P.A. Seismic behavior and earthquake-resistant design of masonry buildings in Chile. *Spec. Publ.* **1994**, *147*, 333–356.
15. Garcia, L.E.; Yamin, L.E. Review of Masonry Construction in Columbia. *Spec. Publ.* **1994**, *147*, 283–306.

16. ElGawady, M.; Lestuzzi, P.; Badoux, M. A review of conventional seismic retrofitting techniques for URM. In Proceedings of the 13th International Brick and Block Masonry Conference, Amsterdam, The Netherlands, 4–7 July 2004; pp. 1–10.
17. Tomazevic, M. *Earthquake-Resistant Design of Masonry Buildings*; World Scientific: Singapore, 1999; Volume 1.
18. Brzev, S.; Meli, R. International guideline for seismic design of low-rise confined masonry buildings in regions of high seismic risk. In Proceedings of the 15th World Conference Earthquake Engineering, Lisbon, Portugal, 24–28 September 2012.
19. Yekrangnia, M.; Bakhshi, A.; Ghannad, M.A. Force-displacement model for solid confined masonry walls with shear-dominated failure mode. *Earthq. Eng. Struct. Dyn.* **2017**, *46*, 2209–2234. [CrossRef]
20. Najafgholipour, M.A.; Maheri, M.R.; Khajepour, M. Performance of confined masonry buildings in November 2017, Sarpole Zahab earthquake (Mw = 7.3), Iran. *Bull. Earthq. Eng.* **2022**, *20*, 4065–4095. [CrossRef]
21. Boen, T.; Pribadi, K.S. Engineering the non-engineered houses for better earthquake resistance in Indonesia. In Proceedings of the DRH Contents Meeting-EDMNIED 2007, Kobe, Japan, 12–13 March 2007; Volume 7.
22. Qazi, A.U.; Rasool, A.M.; Ibrahim, Y.E.; Hameed, A.; Ali, M.F. Behavior of Scaled Infilled Masonry, Confined Masonry & Reinforced Concrete Structures under Dynamic Excitations. *Buildings* **2022**, *12*, 774.
23. Hori, N.; Inoue, N.; Purushotam, D.; Nishida, T.; Kobayashi, J. Experimental and analytical studies on earthquake resisting behaviour of confined concrete block masonry structures. *Earthq. Eng. Struct. Dyn.* **2006**, *35*, 1699–1719. [CrossRef]
24. Marques, R.; Lourenço, P.B. Structural behaviour and design rules of confined masonry walls: Review and proposals. *Constr. Build. Mater.* **2019**, *217*, 137–155. [CrossRef]
25. Huang, L.; Lu, Y.; Yan, L.; Kasal, B.; Wang, L.; Zhang, T. Seismic performance of mortarless reinforced masonry walls. *J. Build. Eng.* **2020**, *31*, 101368. [CrossRef]
26. Jain, S.K.; Basu, D.; Ghosh, I.; Rai, D.C.; Brzev, S.; Bhargava, L.K. Application of confined masonry in a major project in India. In Proceedings of the NCEE 2014–10th U.S. National Conference on Earthquake Engineering Frontiers of Earthquake Engineering, Anchorage, AK, USA, 21–25 July 2014. [CrossRef]
27. Zhou, Y.; Zheng, S.; Chen, L.; Long, L.; Dong, L. Mechanical properties and seismic behavior of confined masonry walls in freeze-thaw environment. *Structures* **2021**, *31*, 647–659. [CrossRef]
28. Yoshimura, K.; Kikuchi, K.; Kuroki, M.; Nonaka, H.; Kim, K.T.; Wangdi, R.; Oshikata, A. Experimental study for developing higher seismic performance of brick masonry walls. In Proceedings of the 13th World Conference on Earthquake Engineering, Vancouver, BC, Canada, 1–6 August 2004. Paper, 1597.
29. Tomaževič, M.; Klemenc, I. Seismic behaviour of confined masonry walls. *Earthq. Eng. Struct. Dyn.* **1997**, *26*, 1059–1071. [CrossRef]
30. Borah, B.; Singhal, V.; Kaushik, H.B. Sustainable housing using confined masonry buildings. *SN Appl. Sci.* **2019**, *1*, 983. [CrossRef]
31. Erberik, M.A.; Citiloglu, C.; Erkoşeoğlu, G. Seismic performance assessment of confined masonry construction at component and structure levels. *Bull. Earthq. Eng.* **2019**, *17*, 867–889. [CrossRef]
32. Gouveia, J.P.; Lourenço, P.B. Masonry shear walls subjected to cyclic loading: Influence of confinement and horizontal reinforcement. In Proceedings of the North American Masonry Conference, St. Luis, MI, USA, 3–5 June 2007.
33. Brzev, S. *Earthquake-Resistant Confined Masonry Construction*; NICEE, National Information Center of Earthquake Engineering, IIT Kanpur: Kanpur, India, 2007.
34. Sharma, P.; Verma, M.; Sharma, N. Examine the mechanical properties of recycled coarse aggregate with MK GGBS. In Proceedings of the IOP Conference Series: Materials Science and Engineering, Sanya, China, 2–14 November 2021; Volume 1116, p. 12152.
35. Verma, M.; Sharma, N.; Sharma, P.; Singh, P. Evaluate the Effect in Terms of Setting Time and Compressive Strength of Oleic Acid as an Admixture in Cement. *Test Eng. Manag.* **2020**, *12422*, 12422–12427.
36. Nagar, P.A.; Gupta, N.; Kishore, K.; Parashar, A.K. Coupled effect of B. Sphaericus bacteria and calcined clay mineral on OPC concrete. *Mater. Today Proc.* **2021**, *44*, 113–117. [CrossRef]
37. Kishore, K.; Gupta, N. Application of domestic & industrial waste materials in concrete: A review. *Mater. Today Proc.* **2020**, *26*, 2926–2931.
38. Sharma, P.; Sharma, N.; Singh, P.; Verma, M.; Parihar, H.S. Examine the effect of setting time and compressive strength of cement mortar paste using iminodiacetic acid. *Mater. Today Proc.* **2020**, *32*, 878–881. [CrossRef]
39. Gupta, N.; Gupta, A.; Saxena, K.K.; Shukla, A.; Goyal, S.K. Mechanical and durability properties of geopolymer concrete composite at varying superplasticizer dosage. *Mater. Today Proc.* **2021**, *44*, 12–16. [CrossRef]
40. Barcelo, L.; Kline, J.; Walenta, G.; Gartner, E. Cement and carbon emissions. *Mater. Struct.* **2014**, *47*, 1055–1065. [CrossRef]
41. Bosoaga, A.; Masek, O.; Oakey, J.E. CO₂ capture technologies for cement industry. *Energy Procedia* **2009**, *1*, 133–140. [CrossRef]
42. Malhotra, V.M. Introduction: Sustainable development and concrete technology. *Concr. Int.* **2002**, *24*, 7.
43. Yıldırım, G.; Kul, A.; Özçelicki, E.; Şahmaran, M.; Aldemir, A.; Figueira, D.; Ashour, A. Development of alkali-activated binders from recycled mixed masonry-originated waste. *J. Build. Eng.* **2021**, *33*, 101690. [CrossRef]
44. Aprianti, E.; Shafiqh, P.; Bahri, S.; Farahani, J.N. Supplementary cementitious materials origin from agricultural wastes—A review. *Constr. Build. Mater.* **2015**, *74*, 176–187. [CrossRef]
45. Kishore, K.; Gupta, N. Mechanical characterization and assessment of composite geopolymer concrete. *Mater. Today Proc.* **2021**, *44*, 58–62. [CrossRef]
46. Parashar, A.K.; Gupta, A. Investigation of the effect of bagasse ash, hooked steel fibers and glass fibers on the mechanical properties of concrete. *Mater. Today Proc.* **2021**, *44*, 801–807. [CrossRef]

47. Parashar, A.K.; Gupta, A. Experimental study of the effect of bacillus megaterium bacteria on cement concrete. *IOP Conf. Ser. Mater. Sci. Eng.* **2021**, *1116*, 12168. [CrossRef]
48. Mehta, P.K. *Concrete Technology for a Sustainable Development in the 21st Century*; CRC Press: Boca Raton, FL, USA, 1999; Volume 83.
49. Van Oss, H.G.; Padovani, A.C. Cement manufacture and the environment part II: Environmental challenges and opportunities. *J. Ind. Ecol.* **2003**, *7*, 93–126.
50. Li, C.; Gong, X.Z.; Cui, S.P.; Wang, Z.H.; Zheng, Y.; Chi, B.C. CO₂ emissions due to cement manufacture. *Mater. Sci. Forum* **2011**, *685*, 181–187. [CrossRef]
51. De Brito, J.; Saikia, N. *Recycled Aggregate in Concrete: Use of Industrial, Construction and Demolition Waste*; Springer Science & Business Media: Berlin/Heidelberg, Germany, 2012.
52. Diaz-Loya, E.I.; Allouche, E.N.; Vaidya, S. Mechanical properties of fly-ash-based geopolymer concrete. *ACI Mater. J.* **2011**, *108*, 300.
53. Yildirim, H.; Sümer, M.; Akyüncü, V.; Gürbüz, E. Comparison on efficiency factors of F and C types of fly ashes. *Constr. Build. Mater.* **2011**, *25*, 2939–2947. [CrossRef]
54. Duxson, P.; Provis, J.L.; Lukey, G.C.; Van Deventer, J.S.J. The role of inorganic polymer technology in the development of ‘green concrete’. *Cem. Concr. Res.* **2007**, *37*, 1590–1597. [CrossRef]
55. Albitar, M.; Ali, M.S.M.; Visintin, P. Experimental study on fly ash and lead smelter slag-based geopolymer concrete columns. *Constr. Build. Mater.* **2017**, *141*, 104–112. [CrossRef]
56. Kaya, M.; Koksall, F.; Gencil, O.; Munir, M.J.; Kazmi, S.M.S. Influence of micro Fe₂O₃ and MgO on the physical and mechanical properties of the zeolite and kaolin based geopolymer mortar. *J. Build. Eng.* **2022**, *52*, 104443. [CrossRef]
57. Panagiotopoulou, C.; Kontori, E.; Perraki, T.; Kakali, G. Dissolution of aluminosilicate minerals and by-products in alkaline media. *J. Mater. Sci.* **2007**, *42*, 2967–2973. [CrossRef]
58. Rangan, B.V. *Fly Ash-Based Geopolymer Concrete*; Curtin University of Technology: Perth, WA, Australia, 2008.
59. Marín-López, C.; Araiza, J.L.R.; Manzano-Ramírez, A.; Avalos, J.C.R.; Perez-Bueno, J.J.; Muñoz-Villareal, M.S.; Ventura-Ramos, E.; Vorobiev, Y. Synthesis and characterization of a concrete based on metakaolin geopolymer. *Inorg. Mater.* **2009**, *45*, 1429–1432. [CrossRef]
60. Okoye, F.N.; Durgaprasad, J.; Singh, N.B. Effect of silica fume on the mechanical properties of fly ash based-geopolymer concrete. *Ceram. Int.* **2016**, *42*, 3000–3006. [CrossRef]
61. Mathew, B.J.; Sudhakar, M.; Natarajan, C. Strength, economic and sustainability characteristics of coal ash–GGBS based geopolymer concrete. *Int. J. Comput. Eng. Res.* **2013**, *3*, 207–212.
62. Detphan, S.; Chindaprasirt, P. Preparation of fly ash and rice husk ash geopolymer. *Int. J. Miner. Metall. Mater.* **2009**, *16*, 720–726.
63. Ojha, A.; Aggarwal, P. Fly ash based geopolymer concrete: A comprehensive review. *Silicon* **2022**, *14*, 2453–2472. [CrossRef]
64. Huang, Y.-J.; Guo, F.; Zhang, H.; Yang, Z. An Efficient Computational Framework for Generating Realistic 3D Mesoscale Concrete Models Using Micro X-Ray Computed Tomography Images and Dynamic Physics Engine. *Cem. Concr. Compos.* **2022**, *126*, 104347. [CrossRef]
65. Albitar, M.; Visintin, P.; Ali, M.S.M.; Lavigne, O.; Gamboa, E. Bond slip models for uncorroded and corroded steel reinforcement in class-F fly ash geopolymer concrete. *J. Mater. Civ. Eng.* **2017**, *29*, 4016186. [CrossRef]
66. Yu, R.; Spiesz, P.; Brouwers, H.J.H. Development of an eco-friendly Ultra-High Performance Concrete (UHPC) with efficient cement and mineral admixtures uses. *Cem. Concr. Compos.* **2015**, *55*, 383–394. [CrossRef]
67. Sugama, T.; Pyatina, T. Effect of sodium carboxymethyl celluloses on water-catalyzed self-degradation of 200 °C-heated alkali-activated cement. *Cem. Concr. Compos.* **2015**, *55*, 281–289. [CrossRef]
68. Ioannou, S.; Paine, K.; Reig, L.; Quillin, K. Performance characteristics of concrete based on a ternary calcium sulfoaluminate–anhydrite–fly ash cement. *Cem. Concr. Compos.* **2015**, *55*, 196–204. [CrossRef]
69. Albitar, M.; Visintin, P.; Ali, M.S.M.; Drechsler, M. Assessing behaviour of fresh and hardened geopolymer concrete mixed with class-F fly ash. *KSCE J. Civ. Eng.* **2015**, *19*, 1445–1455. [CrossRef]
70. Laskar, A.I.; Bhattacharjee, R. Effect of Plasticizer and Superplasticizer on Rheology of Fly-Ash-Based Geopolymer Concrete. *ACI Mater. J.* **2013**, *110*, 5.
71. Albitar, M.; Ali, M.S.M.; Visintin, P.; Drechsler, M. Effect of granulated lead smelter slag on strength of fly ash-based geopolymer concrete. *Constr. Build. Mater.* **2015**, *83*, 128–135. [CrossRef]
72. Fan, X.; Zhang, M. Experimental study on flexural behaviour of inorganic polymer concrete beams reinforced with basalt rebar. *Compos. Part B Eng.* **2016**, *93*, 174–183. [CrossRef]
73. Kathirvel, P.; Kaliyaperumal, S.R.M. Influence of recycled concrete aggregates on the flexural properties of reinforced alkali activated slag concrete. *Constr. Build. Mater.* **2016**, *102*, 51–58. [CrossRef]
74. Maranan, G.B.; Manalo, A.C.; Benmokrane, B.; Karunasena, W.; Mendis, P. Behavior of concentrically loaded geopolymer-concrete circular columns reinforced longitudinally and transversely with GFRP bars. *Eng. Struct.* **2016**, *117*, 422–436. [CrossRef]
75. Yost, J.R.; Radlińska, A.; Ernst, S.; Salera, M. Structural behavior of alkali activated fly ash concrete. Part 1: Mixture design, material properties and sample fabrication. *Mater. Struct.* **2013**, *46*, 435–447. [CrossRef]
76. *ASTM C127-88(2001)*; Standard Test Method for Specific Gravity and Absorption of Coarse Aggregate 1; no. Reapproved. ASTM: West Conshohocken: PA, USA, 2001; Volume 4, pp. 1–5.

77. Ghafoor, M.T.; Khan, Q.S.; Qazi, A.U.; Sheikh, M.N.; Hadi, M.N.S. Influence of alkaline activators on the mechanical properties of fly ash based geopolymer concrete cured at ambient temperature. *Constr. Build. Mater.* **2021**, *273*, 121752. [CrossRef]
78. *ASTM C 136-06*; Standard Test Method for Sieve Analysis of Fine and Coarse Aggregates. ASTM: West Conshohocken, PA, USA, 2006; pp. 1–5. [CrossRef]
79. *ASTM C67-07*; Standard Test Methods for Sampling and Testing Brick and Structural Clay Tile. ASTM International: West Conshohocken, PA, USA, 2007; Volume i, pp. 1–12. Available online: www.astm.org (accessed on 15 September 2022).
80. *ASTM C109*; ASTM C109/C109M-20b: Standard Test Method for Compressive Strength of Hydraulic Cement Mortars (Using 2-inor [50 mm] Cube Specimens). Annual Book of ASTM Standards; ASTM: West Conshohocken, PA, USA, 2020; Volume 4, p. 9.
81. Masonry Standards Joint Committee (MSJC) of the Masonry Society. *Building Code Requirements for Masonry Structures (TMS 402-11/ACI 530-11/ASCE 6-11) and Specification for Masonry Structures (TMS 602-11/ACI 530.1-11/ASCE 5-11) and Companion Commentaries*; American Concrete Institute: Farmington Hills, MI, USA, 2011.
82. *ASTM C39/C39M*; Standard Test Method for Compressive Strength of Cylindrical Concrete Specimens 1. ASTM Stand. B; ASTM: West Conshohocken: PA, USA, 2003; Volume i, no. March. pp. 1–5.
83. *ASTM C469/C469M-10*; Standard Test Method for Static Modulus of Elasticity and Poisson's Ratio of Concrete in Compression. ASTM Stand. C; ASTM: West Conshohocken, PA, USA, 2010; Volume 469.
84. *IS 1608-2005*; Metallic Materials-Tensile Testing at Ambient Temperature. Bur. Indian Stand.; Instron: Norwood, MA, USA, 2005.
85. Lourenço, P.B. Computational Strategies for Masonry Structures. Doctoral Thesis, Delft University of Technology, Delft, The Netherlands, 1996.
86. Kömürçü, S.; Gedikli, A. Macro and Micro Modelling of the Unreinforced Masonry Shear Walls. *Eur. J. Eng. Nat. Sci.* **2019**, *3*, 116–123. Available online: <https://dergipark.org.tr/en/pub/ejens/issue/49410/369461> (accessed on 15 September 2022).
87. Mynarz, M.; Mynarzova, L. Non-linear approaches to the response of brick masonry wall to lateral loading. *Int. J. GEOMATE* **2018**, *14*, 76–82. [CrossRef]
88. Dhanasekar, M.; Elsalakawy, T. IJERT-Numerical Simulation of Masonry Prism Test Using ANSYS and ABAQUS Related Papers Review of Modelling of Masonry Shear Numerical Simulation of Masonry Prism Test Using ANSYS and ABAQUS. *IJERT J. Int. J. Eng. Res. Technol.* **2015**, *4*. Available online: www.ijert.org (accessed on 15 September 2022).
89. Kanit, R.; Döndüren, M.S. Investigation of Using Ansys Software in the Determination of Stress Behaviours of Masonry Walls under out of Plane Cycling Load. *Int. J. Phys. Sci.* **2010**, *5*, 97–108. Available online: <http://www.academicjournals.org/IJPS> (accessed on 15 September 2022).
90. Magenes, G.; Della Fontana, A. Simplified non-linear seismic analysis of masonry buildings. *Proc. Br. Masonry Soc.* **1998**, *8*, 190–195.
91. Vanin, A.; Foraboschi, P. Journal-Modelling of Masonry Panels by Truss Analogy–Part 1. *Mason. Int.* **2009**, *22*, 1.
92. Tomažević, M.; Gams, M. Shaking table study and modelling of seismic behaviour of confined AAC masonry buildings. *Bull. Earthq. Eng.* **2012**, *10*, 863–893. [CrossRef]
93. Lagomarsino, S.; Penna, A.; Galasco, A.; Cattari, S. TREMURI program: An equivalent frame model for the nonlinear seismic analysis of masonry buildings. *Eng. Struct.* **2013**, *56*, 1787–1799. [CrossRef]
94. Caliò, L.; Marletta, M.; Pantò, B. A new discrete element model for the evaluation of the seismic behaviour of unreinforced masonry buildings. *Eng. Struct.* **2012**, *40*, 327–338. [CrossRef]
95. Ansys Inc. “Element Reference,” Volume 15317, No. November, p. 9, 2010. Available online: https://www.mm.bme.hu/~gyebro/files/fea/ansys/ansys_13_element_reference.pdf (accessed on 25 September 2022).
96. Neupane, K.; Kidd, P.; Chalmers, D.; Baweja, D.; Shrestha, R. Investigation on compressive strength development and drying shrinkage of ambient cured powder-activated geopolymer concretes. *Aust. J. Civ. Eng.* **2016**, *14*, 72–83. [CrossRef]
97. Reddy, P.C.; Ganesan, R. Comparative study of compressive strength of novel steel fiber reinforced geopolymer concrete and conventional concrete. *Mater. Today Proc.* **2023**, *77*, 504–508. [CrossRef]
98. Razak, S.; Zainal, F.F.; Shamsudin, S.R. Effect of porosity and water absorption on compressive strength of fly ash based geopolymer and OPC Paste. *IOP Conf. Ser. Mater. Sci. Eng.* **2020**, *957*, 12035. [CrossRef]
99. Bondar, D.; Lynsdale, C.J.; Milestone, N.B.; Hassani, N.; Ramezaniapour, A.A. Engineering properties of alkali-activated natural pozzolan concrete. *ACI Mater. J.* **2011**, *108*, 64–72.
100. Olivia, M.; Nikraz, H. Properties of fly ash geopolymer concrete designed by Taguchi method. *Mater. Des.* **2012**, *36*, 191–198. [CrossRef]
101. Nath, P.; Sarker, P.K. Flexural strength and elastic modulus of ambient-cured blended low-calcium fly ash geopolymer concrete. *Constr. Build. Mater.* **2017**, *130*, 22–31. [CrossRef]
102. Ganesan, N.; Indira, P.V.; Irshad, P. Effect of ferrocement infill on the strength and behavior of RCC frames under reverse cyclic loading. *Eng. Struct.* **2017**, *151*, 273–281. [CrossRef]
103. Li, B.; Wang, J.; Duan, M.; Guo, L.; Wang, B. Cyclic experimental and numerical analytical investigation of precast concrete frames with buckling-restrained braces considering various assembling connections. *Structures* **2021**, *34*, 1135–1153. [CrossRef]
104. Lyu, H.; Deng, M.; Ma, Y.; Yang, S.; Cheng, Y. In-plane cyclic tests on strengthening of full-scale autoclaved aerated concrete blocks infilled RC frames using highly ductile concrete (HDC). *J. Build. Eng.* **2022**, *49*, 104083. [CrossRef]
105. Sumajouw, D.M.J.; Hardjito, D.; Wallah, S.E.; Rangan, B.V. Fly ash-based geopolymer concrete: Study of slender reinforced columns. *J. Mater. Sci.* **2007**, *42*, 3124–3130. [CrossRef]

106. Rahman, M.; Sarker, P. Geopolymer concrete columns under combined axial load and biaxial bending. In Proceedings of the Concrete 2011 Conference, Perth, WA, Australia, 12 October 2011.
107. Borah, B.; Singhal, V.; Kaushik, H.B. Assessment of seismic design provisions for confined masonry using experimental and numerical approaches. *Eng. Struct.* **2021**, *245*, 112864. [CrossRef]
108. El-Diasity, M.; Okail, H.; Kamal, O.; Said, M. Structural performance of confined masonry walls retrofitted using ferrocement and GFRP under in-plane cyclic loading. *Eng. Struct.* **2015**, *94*, 54–69. [CrossRef]
109. Ahmed, A.; Ahmad, I.; Shahzada, K.; Naqash, M.T.; Alam, B.; Fahad, M.; Khan, S.W. Seismic Capacity Assessment of Confined Brick Masonry Building: An Experimental Approach. *Shock. Vib.* **2018**, *2018*, 4756352. [CrossRef]
110. Gioffrè, M.; Cavalagli, N.; Gusella, V.; Pepi, C. Confined vs. unreinforced masonry: Construction and shaking table tests of two-storey buildings. *Constr. Build. Mater.* **2022**, *333*, 126961. [CrossRef]
111. ASCE/SEI 41-06; Supplement to Seismic Rehabilitation of Existing Buildings. ASCE: Reston, VA, USA, 2007.
112. Ashraf, M. Development of Low-Cost and Efficient Retrofitting Technique for Unreinforced Masonry Buildings. Ph.D. Dissertation, University of Engineering and Technology, Peshawar, Pakistan, 2010.
113. Reboul, N.; Mesticou, Z.; Larbi, A.S.; Ferrier, E. Experimental study of the in-plane cyclic behaviour of masonry walls strengthened by composite materials. *Constr. Build. Mater.* **2018**, *164*, 70–83. [CrossRef]
114. Hasnat, A.; Ahsan, R.; Yashin, S.M. Quasi-static in-plane behavior of full-scale unreinforced masonry walls retrofitted using ferro-cement overlay. *Asian J. Civ. Eng.* **2022**, *23*, 649–664. [CrossRef]
115. Konthesingha, K.M.C.; Masia, M.J.; Petersen, R.B.; Page, A.W. Experimental evaluation of static cyclic in-plane shear behavior of unreinforced masonry walls strengthened with NSM FRP strips. *J. Compos. Constr.* **2015**, *19*, 4014055. [CrossRef]
116. Mojsilović, N.; Simundic, G.; Page, A. Masonry wallettes with damp-proof course membrane subjected to cyclic shear: An experimental study. *Constr. Build. Mater.* **2010**, *24*, 2135–2144. [CrossRef]
117. Aguilar, G.; Meli, R.; Diaz, R.; Vázquez-del-Mercado, R. Influence of horizontal reinforcement on the behavior of confined masonry walls. In Proceedings of the Eleventh World Conference on Earthquake Engineering, Acapulco, Mexico, 23–28 June 1996.
118. Yáñez, F.; Astroza, M.; Holmberg, A.; Ogaz, O. Behavior of confined masonry shear walls with large openings. In Proceedings of the 13th World Conference on Earthquake Engineering, Vancouver, BC, Canada, 1–6 August 2004; Volume 3438.
119. Marinilli, A.; Castilla, E. Experimental evaluation of confined masonry walls with several confining-columns. In Proceedings of the 13th World Conference on Earthquake Engineering, Vancouver, BC, Canada, 1–6 August 2004.
120. Zabala, F.; Bustos, J.L.; Masanet, A.; Santalucia, J. Experimental behaviour of masonry structural walls used in Argentina. In Proceedings of the 13th World Conference on Earthquake Engineering, Vancouver, BC, Canada, 1–6 August 2004.
121. Bourzam, A.; Goto, T.; Miyajima, M. Shear capacity prediction of confined masonry walls subjected to cyclic lateral loading. *Doboku Gakkai Ronbunshuu A* **2008**, *64*, 692–704. [CrossRef]
122. Gavilan, J.J.P.; Flores, L.E.; Alcocer, S.M. An experimental study of confined masonry walls with varying aspect ratios. *Earthq. Spectra* **2015**, *31*, 945–968. [CrossRef]
123. Tena-Colunga, A.; Juárez-Ángeles, A.; Salinas-Vallejo, V.H. Cyclic behavior of combined and confined masonry walls. *Eng. Struct.* **2009**, *31*, 240–259. [CrossRef]
124. Kuang, J.S.; Wang, Z. Cyclic load tests of rc frame with column-isolated masonry infills. In Proceedings of the Second European Conference on Earthquake Engineering and Seismology, Istanbul, Turkey, 25–29 August 2014; pp. 25–29.
125. Ozkaynak, H.; Yuksel, E.; Buyukozturk, O.; Yalcin, C.; Dindar, A.A. Quasi-static and pseudo-dynamic testing of infilled RC frames retrofitted with CFRP material. *Compos. Part B Eng.* **2011**, *42*, 238–263. [CrossRef]
126. Van, T.C.; Lau, T.L. Experimental evaluation of reinforced concrete frames with unreinforced masonry infills under monotonic and cyclic loadings. *Int. J. Civ. Eng.* **2021**, *19*, 401–419. [CrossRef]
127. Li, Y.; Zhu, J.; Wang, Z. Investigation on mechanical properties of masonry infill wall strengthened with ECC. *KSCE J. Civ. Eng.* **2019**, *23*, 295–306. [CrossRef]
128. Durrani, A.J.; Haider, S. Seismic response of R/C frames with unreinforced masonry infills. In Proceedings of the 11th World Conference on Earthquake Engineering, Acapulco, Mexico, 23–28 June 1996.
129. Jiang, H.; Liu, X.; Mao, J. Full-scale experimental study on masonry infilled RC moment-resisting frames under cyclic loads. *Eng. Struct.* **2015**, *91*, 70–84. [CrossRef]
130. Peng, Q.; Zhou, X.; Yang, C. Influence of connection and constructional details on masonry-infilled RC frames under cyclic loading. *Soil Dyn. Earthq. Eng.* **2018**, *108*, 96–110. [CrossRef]
131. Penava, D.; Sarhosis, V.; Kožar, I.; Guljaš, I. Contribution of RC columns and masonry wall to the shear resistance of masonry infilled RC frames containing different in size window and door openings. *Eng. Struct.* **2018**, *172*, 105–130. [CrossRef]
132. Aldred, J.; Day, J. Is geopolymer concrete a suitable alternative to traditional concrete. In Proceedings of the 37th Conference on Our World in Concrete & Structures, Singapore, 29–31 August 2012; pp. 29–31.
133. Munir, M.J.; Kazmi, S.M.S.; Khitab, A.; Hassan, M. Utilization of rice husk ash to mitigate alkali silica reaction in concrete. In Proceedings of the 2nd International Multi-Disciplinary Conference (IMDC 2016), University of Lahore (Gujrat Campus), Gujrat, Pakistan, 19–20 December 2016; pp. 1–3.

134. Munir, M.J.; Abbas, S.; Qazi, A.U.; Nehdi, M.L.; Kazmi, S.M.S. Role of test method in detection of alkali–silica reactivity of concrete aggregates. *Proc. Inst. Civ. Eng.—Constr. Mater.* **2018**, *171*, 203–221. [CrossRef]
135. Munir, M.J.; Kazmi, S.M.S.; Wu, Y.F.; Lin, X. Axial stress-strain performance of steel spiral confined acetic acid immersed and mechanically rubbed recycled aggregate concrete. *J. Build. Eng.* **2021**, *34*, 101891. [CrossRef]

Disclaimer/Publisher’s Note: The statements, opinions and data contained in all publications are solely those of the individual author(s) and contributor(s) and not of MDPI and/or the editor(s). MDPI and/or the editor(s) disclaim responsibility for any injury to people or property resulting from any ideas, methods, instructions or products referred to in the content.

Surrogate Models for Efficient Multi-Objective Optimization of Building Performance

Gonçalo Roque Araújo ^{1,2}, Ricardo Gomes ¹, Maria Glória Gomes ^{2,*}, Manuel Correia Guedes ³ and Paulo Ferrão ¹

¹ Center for Innovation, Technology and Policy Research, Mechanical Engineering Department, Instituto Superior Técnico, Universidade de Lisboa, Av. Rovisco Pais, 1049-001 Lisbon, Portugal

² Civil Engineering Research and Innovation for Sustainability, Civil Engineering Department, Instituto Superior Técnico, Universidade de Lisboa, Av. Rovisco Pais, 1049-001 Lisbon, Portugal

³ Center for Innovation in Territory, Urbanism, and Architecture, Civil Engineering Department, Instituto Superior Técnico, Universidade de Lisboa, Av. Rovisco Pais, 1049-001 Lisbon, Portugal

* Correspondence: maria.gloria.gomes@tecnico.ulisboa.pt

Abstract: Nowadays, the large set of available simulation tools brings numerous benefits to urban and architectural practices. However, simulations often take a considerable amount of time to yield significant results, particularly when performing many simulations and with large models, as is typical in complex urban and architectural endeavors. Additionally, multiple objective optimizations with metaheuristic algorithms have been widely used to solve building optimization problems. However, most of these optimization processes exponentially increase the computational time to correctly produce outputs and require extensive knowledge to interpret results. Thus, building optimization with time-consuming simulation tools is often rendered unfeasible and requires a specific methodology to overcome these barriers. This work integrates a baseline multi-objective optimization process with a widely used, validated building energy simulation tool. The goal is to minimize the energy use and cost of the construction of a residential building complex. Afterward, machine learning and optimization techniques are used to create a surrogate model capable of accurately predicting the simulation results. Finally, different metaheuristics with their tuned hyperparameters are compared. Results show significant improvements in optimization results with a decrease of up to 22% in the total cost while having similar performance results and execution times up to 100 times faster.

Keywords: building optimization; building simulation; surrogate models; multi-objective optimization

Citation: Araújo, G.R.; Gomes, R.; Gomes, M.G.; Guedes, M.C.; Ferrão, P. Surrogate Models for Efficient Multi-Objective Optimization of Building Performance. *Energies* **2023**, *16*, 4030. <https://doi.org/10.3390/en16104030>

Academic Editors: Ala Hasan and Hassam Ur Rehman

Received: 24 April 2023

Revised: 7 May 2023

Accepted: 9 May 2023

Published: 11 May 2023



Copyright: © 2023 by the authors. Licensee MDPI, Basel, Switzerland. This article is an open access article distributed under the terms and conditions of the Creative Commons Attribution (CC BY) license (<https://creativecommons.org/licenses/by/4.0/>).

1. Introduction

One of the largest shares of energy consumption is associated with the building stock (in Europe, it is responsible for 40% of the total energy consumption). In this context, the European Parliament established the “Energy Performance of Buildings Directive”, which promotes policies to help to achieve the energy efficiency and decarbonization of buildings by 2050 [1,2]. This directive highlights the need to improve the existing building stock and establishes guidelines and frameworks to achieve this. Since a building’s lifetime can exceed 100 years, it is important to improve regulations and specific instruments that promote energy efficiency and the reduction of greenhouse gas emissions while improving the thermal comfort and quality of life of occupants [3].

To obtain information regarding the building stock and define strategies to improve it via these directives, Building Performance Simulation (BPS) tools can help to predict building design and rehabilitation impacts in multiple aspects of a building’s performance [4]. BPS tools predict these results through models described by specific inputs that yield the desired outputs. With these simulations, it is possible to integrate iterative Building Performance Optimization (BPO) into building design, planning, and rehabilitation processes [5].

Unfortunately, the use of BPS tools with BPO is still out of reach for most practitioners and presents several limitations:

1. BPS tools are not portable and require different model formats and descriptions. This forces practitioners to develop models with different descriptions and inputs for each simulation, which is error-prone [6,7].
2. Most BPS is time-consuming and still requires a considerable amount of time to perform the calculations for multiple or large models. This constitutes a significant limitation, particularly for BPO that requires testing of multiple iterations of a project [8,9].
3. The use of BPS tools requires extensive knowledge regarding building physics and performed calculations to understand and process the inputs and results [10,11].

BPO typically entails multiple objectives, which are often conflicting [5]. Additionally, most building performance indicators are outputs of BPS or extensive calculations performed by field experts [12]. Because of this, optimization problems that are focused outside the practitioner's realm of knowledge are usually treated as multi-objective optimization (MOO) problems with derivative-free functions [5,13–15]. Metaheuristics, a class of optimization algorithms, have been widely used in the field of optimization for the built environment with positive results. These algorithms guide the search based on biological heuristics such as evolutionary ones and swarms of different kinds, among others [16]. Furthermore, Wolpert and Macready state with the "No Free Lunch" theorem that no algorithm outperforms all others for all problems. This means that one has to either know from experience which algorithms yield better performance for each BPO problem or test multiple metaheuristics to find the best one [17]. Moreover, these algorithms have variables that define how they search for the optimal space, called hyperparameters. These need to be fine-tuned to provide optimum results [18]. To fine-tune optimization algorithms, one must optimize the combination of hyperparameters that yield the best indicators of their performance. The most commonly used evaluation metric for multi-objective optimization algorithms is the hypervolume [19–21].

Pereira et al. [13] evaluated multiple optimization algorithms and benchmarked their hypervolumes for a daylighting and a structural optimization problem. This study established that algorithms that performed worse in one problem performed best in the other. This highlights the need to benchmark multiple algorithms according to their hypervolumes for different building optimization problems.

BPO functions that are outputs of BPS are significantly time-consuming [10,11,22], and when integrating them with the above-mentioned pipeline of activities for a derivative-free MOO problem, it usually renders the process unfeasible. Thus, emerging research in this field has been studying alternatives and approaches that allow us to overcome these barriers.

Algorithmic Design (AD) emerged as a way to solve the portability issue of BPS tools. AD allows practitioners to describe a design project with a single algorithm. With this design process, it is possible to swiftly change parameters or design heuristics and obtain the respective model without effort. Additionally, some AD tools are either capable of supporting BPS tools or exporting models that are able to be read by them. Consequently, with AD, it is possible to integrate BPO to automatically explore a design space, a process often referred to as Algorithmic Design and Analysis (ADA) [23].

The use of ADA constitutes a trade-off, since it allows practitioners to obtain higher portability between their projects' design, performance analysis, and optimization, at the cost of having to learn programming languages that have a high learning curve [23]. Moreover, ADA does not address the remaining limitations of BPS processes, which still require significant computation time, expertise, and testing to be successfully applied [9,13].

Coincidentally, recent advances in research have been demonstrating the advantages of surrogate models (SM) developed with machine learning (ML) techniques to help

practitioners to execute their projects that integrate BPO [24]. SM are capable of predicting a target output after being trained with a database that illustrates its variation according to specific training features. In particular, SM developed with a building database can help to reduce the number of required inputs and features while significantly improving BPS and BPO's computational times [12,25,26].

The resulting research is intended to support practitioners and stakeholders to make better-informed project decisions in the following ways.

1. Tackling portability issues by deploying the developed SM for a widely used BPS tool and a common BPO problem.
2. Significantly improving the required computational time to use BPS and BPO.
3. Providing SM that are easier to grasp than the respective BPS inputs and do not require as much knowledge and expertise.
4. Providing workflows capable of addressing the current limitations regarding the use of BPS tools and BPO.

In this sense, this work documents the processes required to perform a standard pipeline of activities for a BPO of time-consuming functions. Initially, an ADA approach is used to integrate a baseline MOO problem with a metaheuristic and a widely used BPS tool. The obtained results are coupled with machine learning techniques and regression algorithms to generate a surrogate model capable of yielding significantly faster simulation results based on the BPO decision variables. With this surrogate model, it is then feasible to fine-tune the metaheuristics hyperparameters, compare their performance for a specific BPO problem, and benchmark their results. This process is applied to a case study of a residential complex construction composed of six buildings in Lisbon, Portugal.

2. Materials and Methods

The methodology for this work can be further subdivided into four sections: baseline optimization, surrogate model, hyperparameter tuning, and results and discussion (Figure 1). In the baseline optimization section, the optimization objectives and decision variables are described, and a simulation-based optimization with EnergyPlus [27] in a Python environment [28] is integrated to compile a training database. This database is used in the surrogate model section to train a convolutional neural network (CNN) with the Keras and TensorFlow packages [29], capable of predicting the total energy use of the 6 buildings and their standard deviations. The CNN layers' nodes are optimized with a Bayesian optimization using Gaussian processes [30]. In the hyperparameter tuning section, four metaheuristics are selected to be compared. Each algorithm's hyperparameters are fine-tuned with a Bayesian optimization as well. Finally, the metaheuristics are compared regarding their performance indicators, and optimization results are discussed for this particular class of BPO problems.

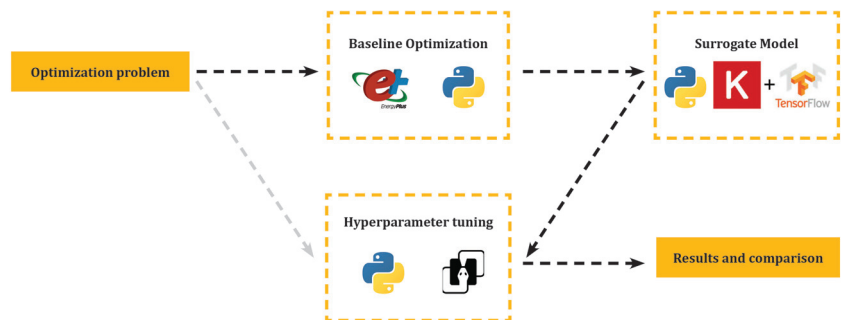


Figure 1. Methodology diagram.

2.1. Baseline Optimization

Our BPO problem is to find the best combination of constructions for each building's surface type that minimizes the construction cost and total energy use. The case study comprises a standard midrise apartment program from LadybugTools for building operation, usage, and schedules [31] applied to a geometric model of 6 buildings in Lisbon, Portugal, illustrated in Figure 2. LadybugTools integrates the Rhino3D tool with EnergyPlus by translating geometrical representations and weather files into a file folder and format that is readable by EnergyPlus. In this case study, a simulation of each building's total heating and cooling energy (J) is performed with an ideal air load system for one year with residential occupation schedules (Table 1).

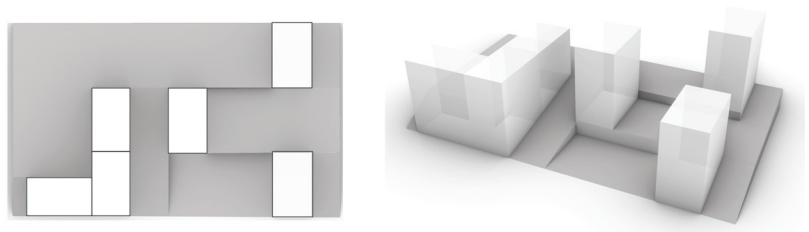


Figure 2. Plan (left) and 3D model (right) of the studied residential building complex.

Table 1. Simulation setting values for the proposed case study.

Simulation Setting	Value
Period	1 year
Timestep	1 timestep per hour
Program and schedules	Midrise apartment
Window-to-wall ratio	0.2
Outputs	Zone Ideal Load Supply Air Total Heating Energy (J) Zone Ideal Load Supply Air Total Cooling Energy (J)

Each building can have one out of three different constructions for each surface type: exterior walls, interior floors, roofs, and windows. Thus, our optimization problem comprises the walls, roofs, floors, and windows of 6 buildings, with a total of 24 variables with 3 possible constructions each (Table 2). The opaque materials' properties are represented from their outermost layer to their innermost, and the window materials are defined using a simple glazing system definition with the window U-value, solar (τ_{sol}), and visible transmittance (τ_{vis}). Each simulation takes ≈ 25 (s).

The optimization variables and goals are described in Equations (1) to (4). E_n (Equation (1)) represents the total energy use of building n , f_1 (Equation (2)) is the total energy use of all buildings, f_2 (3) is the standard deviation of the building sample, and f_3 (4) is the total cost of construction. The BPO problem objectives are to minimize these functions to guarantee the minimum total energy use (f_1), the best fairness of performance among buildings (f_2), and minimum costs (f_3). The Non-Dominated Sorting Genetic Algorithm II (NSGAI) [32] was the chosen algorithm to run for 1000 iterations.

$$E_n(x_0, \dots, x_{n \times 4}) = Heating_n + Cooling_n \text{ kWh/m}^2 \quad (1)$$

$$f_1(x_0, \dots, x_{n \times 4}) = \sum E_n(x_0, \dots, x_{n \times 4}) \text{ kWh/m}^2 \quad (2)$$

$$f_2(x_0, \dots, x_{n \times 4}) = \sigma(E_n(x_0, \dots, x_{n \times 4})) \text{ kWh/m}^2 \quad (3)$$

$$f_3(x_0, \dots, x_{n \times 4}) = Cost(x_0, \dots, x_{n \times 4}) \text{ €} \quad (4)$$

$$x \in \{0, 1, 2\} \text{—Number of construction types}$$

$$n = \text{Number of buildings}$$

Table 2. Materials for each surface type construction solution.

Construction Type	Total Area m ²	x	Cost [€/m ²]	Materials		
Walls	8699.94	0	20	Plaster—2 cm Bored brick—11 cm Air gap—6 cm Bored brick—11 cm Stucco—1.5 cm		
		1	25	Plaster—2 cm Bored brick—15 cm Air gap—6 cm Bored brick—11 cm Stucco—1.5 cm		
		2	35	Plaster—2 cm Bored brick—11 cm Air gap—6 cm XPS—4 cm Bored brick—11 cm Stucco—1.5 cm		
Interior floors	9327.27	0	10	Wood panels—12 cm Stucco—1.5 cm		
		1	25	Ceramics—1 cm Screed—8 cm Lightweight slab—15 cm Stucco—1.5 cm		
		2	30	Ceramics—1 cm Screed—8 cm Concrete slab—15 cm Stucco—1.5 cm		
Roofs	1216.67	0	20	Screed—8 cm Waterproofing—0.2 cm Screed—8 cm Lightweight slab—15 cm Stucco—1.5 cm		
		1	30	Screed—8 cm Waterproofing—0.2 cm XPS—4 cm Screed—8 cm Lightweight slab—15 cm Stucco—1.5 cm		
		2	35	Screed—8 cm Waterproofing—0.2 cm XPS—4 cm Screed—8 cm Concrete slab—15 cm Stucco—1.5 cm		
Windows	2174.98	0	50	U[W/m ² K]	τ_{sol}	τ_{vis}
		1	80	2.69	0.75	0.80
		2	100	1.70	0.38	0.70
				1.25	0.20	0.70

2.2. Surrogate Model

The SM was developed using the simulation-based optimization data as a training set. Afterward, the data were split into a train and test set with a ratio of 67/33, and the variables were used to train a sequential neural network with 1 dense layer, 4 convolutional layers, and 1 dense output layer. To optimize the layers' filters (number of nodes), a Bayesian optimization using Gaussian processes with 100 iterations was integrated to maximize the CNN coefficient of variation (R^2 score) between the test set results and the model predictions (Equation (5)). Finally, this process was employed to train two CNN models that predicted f_1 and f_2 (Equations (2) and (3)), with an early stopping callback to avoid over-fitting. The optimized CNN structure's final R^2 score and Root Mean Squared Error (RMSE) are documented in Tables 3 and 4. The SM obtained an R^2 score of 0.96 and 0.97, and an RMSE of 0.54 and 0.01, for f_1 and f_2 , respectively. Additionally, the SM prediction execution time was ≈ 0.25 (s) for each iteration, which is 100 times faster than the simulation computation time.

$$f_4(i_0, \dots, i_n) = R^2(\text{test}, \text{predictions}) \quad (5)$$

$$i \in [6, 300] \text{—Number of filters}$$

$$n = \text{Number of layers}$$

Table 3. Optimum convolutional neural network structure and performance for surrogate model of Equation (2).

Layer (Type)	Filters	Kernel Size
Dense	300	1
1D-Convolutional	157	2
1D-Convolutional	6	2
1D-Convolutional	290	2
1D-Convolutional	70	1
Dense	1	1
R² score		0.96
RMSE (kWh/m²)		0.54

Table 4. Optimum convolutional neural network structure and performance for a surrogate model of Equation (3).

Layer (Type)	Filters	Kernel Size
Dense	300	1
1D-Convolutional	300	2
1D-Convolutional	300	2
1D-Convolutional	6	2
1D-Convolutional	100	1
Dense	1	1
R² score		0.97
RMSE (kWh/m²)		0.01

2.3. Hyperparameter Tuning

This section describes the selected metaheuristics and the optimization problem that fine-tunes each algorithm's hyperparameters. Two evolutionary (EA) and two particle swarm optimization (PSO) algorithms were selected. From the EA class of algorithms, we selected NSGAI and the Indicator-Based Evolutionary Algorithm (IBEA) [33]. From the PSO class, the Speed-Constrained Multi-Objective PSO (SMPSO) [34] and the OMOPSO [35] were selected. The algorithms were run for 500 iterations and, besides each one's default hyperparameters, a polynomial mutation and an SBX crossover were added [36]. Table 5 documents each algorithm's considered hyperparameters.

Table 5. Considered hyperparameters and their ranges for all the optimization algorithms.

Algorithm	Iterations	Hyperparameters	Range
NSGAI	500	Population size P_s	[30 .. 200]
		SBX crossover S	[0, 1]
IBEA	500	Polynomial mutation P_m	[0, 1]
		P_s	[30 .. 200]
		S	[0, 1]
SMPSO	500	P_m	[0, 1]
		Swarm size S_s	[30 .. 200]
		Leader size L_s	[30 .. 200]
		Max iterations i	[30 .. 200]
OMOPSO	500	S	[0, 1]
		P_m	[0, 1]
		S_s	[30 .. 200]
		L_s	[30 .. 200]
		i	[30 .. 200]
		S	[0, 1]
		P_m	[0, 1]
Epsilon ϵ	[0.0001, 1]		

To evaluate an optimization model's performance for MOO, most performance metrics are calculated regarding the optimum solutions found by the algorithm. These solutions are called non-dominated solutions. They represent solutions that cannot improve more in one objective, without harming the other/s [37]. In this case study, the problem's non-dominated solutions illustrate the trade-offs between the total energy use of the buildings (f_1), the fairness of performance among buildings (f_2), and the cost of construction (f_3) (Equations (2) to (4)). Thus, an algorithm that explores the largest solution space tends to perform better for this particular problem. To measure this, the hypervolume of each algorithm's non-dominated solutions is calculated as a means of describing the area/volume of the solutions obtained in a ratio of a specific boundary domain [19,20]. In this case, our boundary domain represents the highest and lowest possible thresholds for the minimum total energy use (f_1), standard deviation (f_2), and costs of construction (f_3).

The fine-tuning of the algorithms' hyperparameters can be described as a single objective optimization problem to find the combination of parameters that yields the maximum hypervolume in f_{NSGAI} , f_{IBEA} , f_{SMPSO} , and f_{OMOPSO} (Equations (6) to (9)). Thus, a Bayesian optimization with 100 iterations is integrated to find the best combination of hyperparameters for each algorithm's settings.

$$f_{NSGAI}(P_s, S, P_m) = H(f_1, f_2, f_3) \quad (6)$$

$$f_{IBEA}(P_s, S, P_m) = H(f_1, f_2, f_3) \quad (7)$$

$$f_{SMPSO}(S_s, L_s, i, S, P_m) = H(f_1, f_2, f_3) \quad (8)$$

$$f_{OMOPSO}(S_s, L_s, i, S, P_m, \epsilon) = H(f_1, f_2, f_3) \quad (9)$$

H —Hypervolume;

Boundaries for H calculation :

$$f_1 \in [30, 60] \text{ - kWh/m}^2$$

$$f_2 \in [0.25, 0.50] \text{ - kWh/m}^2$$

$$f_3 \in [400,000, 900,000] \text{ - €}$$

3. Results and Discussion

After the optimizations with the fine-tuned metaheuristics, the algorithms' non-dominated solutions are calculated and plotted according to the results of each objective.

Afterward, the algorithms' hypervolumes are compared and the best-performing algorithm is selected for the final optimization process. Results are presented and discussed.

3.1. Results

The solution space explored by each algorithm is illustrated in Figure 3. It is visible that the algorithms obtained different results regarding the exploration of the objective space. SMPSO and OMOPSO explored a wider range of values, while IBEA focused more on one area of the solution space. NSGAI explored an acceptable area but failed to find solutions with higher total energy use (f_1 , Equation (2)), a lower standard deviation (f_2 , Equation (3)), and lower construction costs (f_3 , Equation (4)), in contrast to the PSO algorithms. In total, the algorithms explored a solution space with values of f_1 between ≈ 45 and ≈ 55 kWh/m², f_2 between ≈ 0.30 and ≈ 0.40 kWh/m², and f_3 between $\approx 400,000$ and $\approx 600,000$ €.

Table 6 documents the algorithms' hypervolumes for the optimum values of their hyperparameters. The IBEA algorithm (f_{IBEA} , Equation (7)) obtained the best hypervolume of 0.54, followed by NSGAI, with 0.53 (f_{NSGAI} , Equation (6)), and SMPSO and OMOPSO, with 0.52 (f_{SMPSO} and f_{OMOPSO} Equations (8) and (9)). Additionally, it is visible in Figure 3 that IBEA obtained the higher hypervolume because it focused on a specific area, not because it explored the largest solution space. Thus, IBEA successfully found better optimum solutions but ultimately failed in the exploration of the solution space and its inherent trade-offs between the buildings' energy usage, standard deviation, and cost of construction. For these reasons, the NSGAI algorithm, which obtained the highest hypervolume and explored a balanced solution space, was chosen to perform the final optimization.

Table 6. Optimum metaheuristics hyperparameters and respective hypervolumes.

	Hyperparameter	Value	Hypervolume
NSGAI	P_s	30	0.53
	S	1	
	P_m	0.59	
IBEA	P_s	32	0.54
	S	0.66	
	P_m	1	
SMPSO	S_s	68	0.52
	L_s	59	
	i	67	
	S	0.43	
	P_m	0.35	
OMOPSO	S_s	30	0.52
	L_s	200	
	i	200	
	S	1	
	P_m	0	
	ϵ	0.001	

The NSGAI algorithm was run with the optimum hyperparameters found for 10,000 iterations and the non-dominated solutions found were simulated to validate the surrogate model predictions. Results show a hypervolume of 0.60, which is significantly larger when compared with the values obtained for the 500 iterations in Table 6. Additionally, Figure 4 shows that the algorithm explored values between 40 and 60 kWh/m², 0.2 and 0.5 kWh/m², and 400,000 and 900,000 €. With these results, it is possible to discern the existing trade-offs between energy consumption, fairness of performance among buildings, and the total cost of construction. Moreover, assuming that this construction has a fixed budget, it is possible to find the best available solution with a minimum f_1 and f_2 . Finally, Figure 4 also shows how a solution with the most expensive construction for all surfaces is not necessarily the best solution, with the algorithm finding a significant number of cheaper solutions with lower f_1 and f_2 , which can allow savings of up to 22% (200,000 €) on the total cost of construction while maintaining the same performance (f_1) and fairness of performance among buildings (f_2).

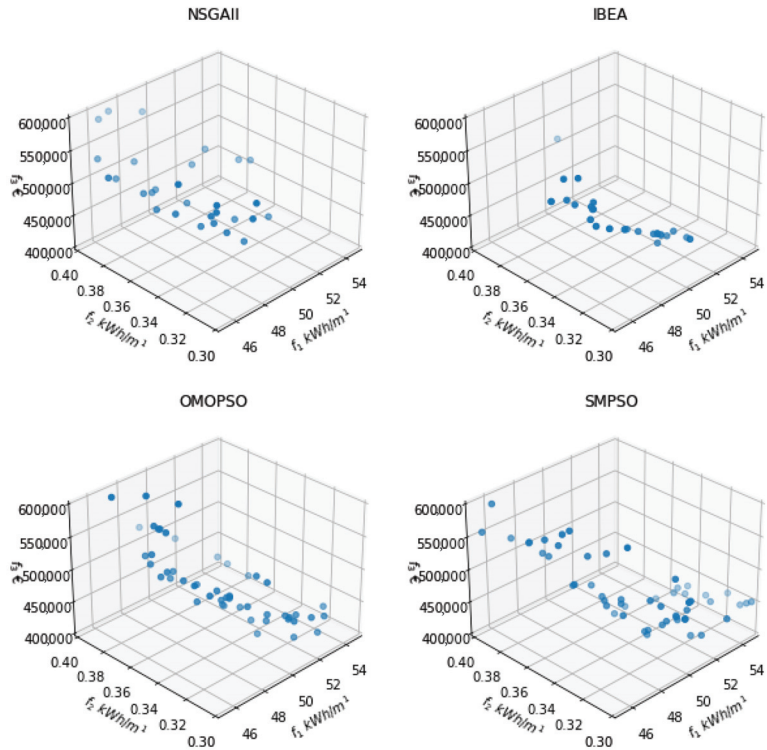


Figure 3. Plotted non-dominated solutions of optimized metaheuristics.

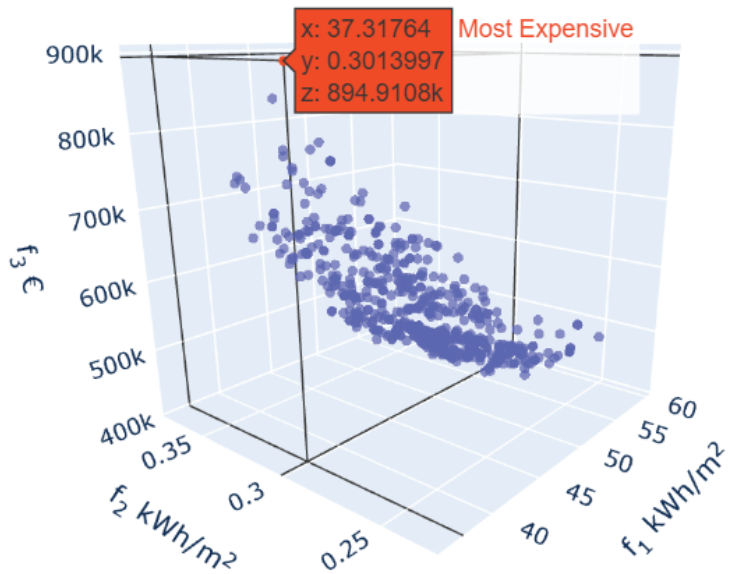


Figure 4. NSGAI non-dominated solutions for 10,000 iterations—the most expensive solution is represented in red.

3.2. Discussion

The use of SM to estimate building energy use speeds up a building simulation process exponentially. Additionally, SM can be deployed in a single platform (e.g., web applications, programming environments, mobile applications, among others), and because they use only optimization problem variables as inputs, they reduce the simulation complexity and provide a more accessible analysis to users with any expertise level. As an example, the optimization process performed in this study can be integrated into a web application where the user specifies variables and costs and performs the optimization with the selected algorithm. Afterward, the algorithm's hypervolume is calculated and a figure illustrates the obtained optimum solutions.

The comparison of the optimization algorithms shows that, for this particular BPO problem, different algorithms explored different solution spaces. These can be more or less suitable for the practitioner's decision-making goals. Additionally, they show that the algorithm with the highest hypervolume obtained the best solutions, but did not explore the desired solution space. In particular, the PSO algorithms excelled in exploring a wide solution space, the IBEA algorithm obtained the highest hypervolume and best solution, and NSGAIII showed an even balance between the hypervolume and solution space.

The comparison of the four MOO algorithms' hypervolumes (Table 6) and solution spaces (Figure 3) provided a confident selection of the most suitable algorithm for the proposed optimization problem, with results that allowed us to save up to 22% of the total construction cost while maintaining acceptable energy performance. In the future, an extensive comparison of optimization algorithms for different aspects of building performance can provide a comprehensive foundation regarding the algorithms' performance for different building performance optimization problems.

4. Conclusions

Most building and urban optimization problems typically have objectives that are outputs of analysis and simulation tools. These tools are prone to errors, take significant time to yield results, and lack model portability among tools (different building models must be developed for each tool). Because of this, it is often unfeasible to perform a correct optimization process. This work integrates a surrogate model approach in the optimization structure that allows us to perform a standard pipeline of activities for the optimization of a time-consuming function in an acceptable timeframe. This approach is illustrated with the optimization of a six-building residential complex in Lisbon, Portugal.

The optimization problem is described as the best combination of construction materials that yield the minimum annual total energy use, construction cost, and standard deviation (to guarantee the fairness of performance among buildings). Four different optimization algorithms were compared and NSGAIII was selected to perform the optimization. Results of this case study show that adjusting building materials with this approach can result in savings of up to 22% in the construction cost, while showing the minimum energy use and standard deviation. The processes required for the optimization are integrated with a surrogate model developed with a convolutional neural network, with R^2 scores of ≈ 0.96 in the prediction of the simulation results, and being 100 times faster than a simulation.

Surrogate models are efficient in not only reducing the time taken for simulations to run but also in reducing the number of input features required to obtain results. Additionally, they are portable and can be deployed easily within a single platform. In spite of this methodology focusing on a particular problem, research shows that these approaches are efficient and can be applicable transversely to other time-consuming optimization problems within the building performance realm, such as computational fluid dynamics, agent-based modeling, daylighting, and structural analysis, among others. By developing and deploying multiple surrogate models that predict aspects of building performance, it is possible to obtain a broader understanding of a building's performance and tackle portability issues associated with the use of multiple simulation tools.

Future work must focus on (1) the benchmarking of specific algorithms for optimization problems, and (2) the development of end-user interfaces with automated optimization and surrogate model development. In (1), multiple algorithms must be extensively compared regarding their hypervolumes and solution spaces for optimization problems that encompass different building performance aspects. In (2), the surrogate model development and optimization must be automated according to the benchmarked algorithms and problems, while a user defines the variables and objectives. These studies are extremely relevant in order to bridge the existing gap between practitioners and building performance analysis and optimization processes such as the one portrayed in this study.

Author Contributions: Conceptualization, G.R.A., R.G., P.F., M.C.G. and M.G.G.; methodology, G.R.A., R.G., P.F. and M.G.G.; software, G.R.A.; formal analysis, P.F., M.G.G. and M.C.G.; investigation, G.R.A., R.G., M.G.G. and P.F.; data curation, G.R.A.; writing—original draft preparation, G.R.A.; writing—review and editing, R.G., M.G.G., M.C.G. and P.F.; supervision, R.G., M.G.G., M.C.G. and P.F. All authors have read and agreed to the published version of the manuscript.

Funding: This research was funded by Fundação para a Ciência e Tecnologia (FCT) through IN+UIDP/EEA/50009/2020—IST-ID and CERIS UIDB/04625/2020, and a Ph.D. grant under the contract of FCT 2021.04849.BD. This research was also funded by Project C-TECH—Climate Driven Technologies for Low Carbon Cities, grant number POCI-01-0247-FEDER-045919, LISBOA-01-0247-FEDER-045919, co-financed by the ERDF—European Regional Development Fund—through the Operational Program for Competitiveness and Internationalization—COMPETE 2020, the Lisbon Portugal Regional Operational Program—LISBOA 2020, and the FCT under the MIT Portugal Program.

Data Availability Statement: Data supporting the reported research can be found via the GitHub private repository at <https://github.com/goncalo-araujo/OSE>, accessed on 22 April 2023.

Conflicts of Interest: The authors declare no conflict of interest. The funders had no role in the design of the study; in the collection, analyses, or interpretation of data; in the writing of the manuscript; or in the decision to publish the results.

Abbreviations

The following abbreviations are used in this manuscript:

BPS	Building Performance Simulation
BPO	Building Performance Optimization
MOO	Multi-Objective Optimization
AD	Algorithm Design
ADA	Algorithm Design and Analysis
SM	Surrogate Models
CNN	Convolutional Neural Network
EA	Evolutionary Algorithms
PSO	Particle Swarm Optimization
NSGAI	Non-Dominated Sorting Genetic Algorithm II
IBEA	Indicator-Based Genetic Algorithm
SMP	Speed-Constrained Multi-Objective PSO
OMOPSO	MOPSO Algorithm

References

1. European Parliament. *Directiva 2010/31/UE do Parlamento Europeu e do Conselho, de 19 de Maio de 2010, Relativa ao Eesempenho Energético dos Edifícios*; Jornal Oficial n° L 153; European Parliament: Strasbourg, France, 2010; pp. 13–35.
2. European Parliament. *Directiva 2018/844 do parlamento europeu e do conselho de 30 de maio de 2018 que altera a Diretiva 2010/31/UE relativa ao desempenho energético dos edifícios e a Diretiva 2012/27/UE sobre a eficiência energética*. *J. União Eur.* **2018**, *L156*, 75–91.
3. Mourão, J.; Gomes, R.; Matias, L.; Niza, S. Combining embodied and operational energy in buildings refurbishment assessment. *Energy Build.* **2019**, *197*, 34–46. [CrossRef]
4. Lomas, K.J.; Eppel, H. Sensitivity analysis techniques for building thermal simulation programs. *Energy Build.* **1992**, *19*, 21–44. [CrossRef]

5. Nguyen, A.T.; Reiter, S.; Rigo, P. A review on simulation-based optimization methods applied to building performance analysis. *Appl. Energy* **2014**, *113*, 1043–1058. [CrossRef]
6. Crawley, D.B.; Hand, J.W.; Kummert, M.; Griffith, B.T. Contrasting the capabilities of building energy performance simulation programs. *Build. Environ.* **2008**, *43*, 661–673. [CrossRef]
7. Reinhart, C.F.; Dogan, T.; Jakubiec, A.J.; Rakha, T.; Sang, A. UMI—An Urban Simulation Environment For Building Energy Use, Daylighting and Walkability. In Proceedings of the 13th Conference of International Building Performance Simulation Association, Chambéry, France, 26–28 August 2013; pp. 476–483.
8. Wei, T. A review of sensitivity analysis methods in building energy analysis. *Renew. Sustain. Energy Rev.* **2013**, *20*, 411–419. [CrossRef]
9. Araújo, G.; Pereira, I.; Leitão, A.; Correia Guedes, M. Conflicts in passive building performance: Retrofit and regulation of informal neighbourhoods. *Front. Archit. Res.* **2021**, *10*, 625–638. [CrossRef]
10. Hopfe, C.J.; Hensen, J.L. Uncertainty analysis in building performance simulation for design support. *Energy Build.* **2011**, *43*, 2798–2805. [CrossRef]
11. Ruiz, G.R.; Bandera, C.F. Validation of calibrated energy models: Common errors. *Energies* **2017**, *10*, 1587. [CrossRef]
12. Wortmann, T.; Costa, A.; Nannicini, G.; Schroepfer, T. Advantages of surrogate models for architectural design optimization. *Artif. Intell. Eng. Des. Anal. Manuf.* **2015**, *29*, 471–481. [CrossRef]
13. Pereira, I.; Belém, C.; Leitão, A. Escaping evolution. In Proceedings of the 25th International Conference of the Association for Computer-Aided Architectural Design Research in Asia (CAADRIA) 2020, Bangkok, Thailand, 5–6 August 2020; Volume 1, pp. 295–304.
14. Pereira, I.; Leitão, A. More is more: The no free lunch theorem in architecture. In Proceedings of the International Conference of Architectural Science Association 2020, Lisbon, Portugal, 27–29 October 2020; pp. 765–774.
15. Waibel, C.; Wortmann, T.; Evins, R.; Carmeliet, J. Building energy optimization: An extensive benchmark of global search algorithms. *Energy Build.* **2019**, *187*, 218–240. [CrossRef]
16. Yang, X.S. *Nature-Inspired Metaheuristic Algorithms*; Luniver Press: UK, 2010. Available online: https://books.google.pt/books?id=iVB_ETlh4ogC&dq=Nature-Inspired+Metaheuristic+Algorithms+Yang+2010&lr=&source=gbs_navlinks_s (accessed on 20 January 2023)
17. Wolpert, D.H.; Macready, W.G. No free lunch theorems for optimization. *IEEE Trans. Evol. Comput.* **1997**, *1*, 67–82. [CrossRef]
18. Bengio, Y. Gradient-Based Optimization of Hyperparameters. *Neural Comput.* **2000**, *12*, 1889–1900. [CrossRef] [PubMed]
19. Bradstreet, L.; While, L.; Barone, L. Maximising hypervolume for selection in multi-objective evolutionary algorithms. In Proceedings of the 2007 IEEE Congress on Evolutionary Computation, CEC 2006, Vancouver, BC, Canada, 16–21 July 2006; pp. 1744–1751. [CrossRef]
20. Bradstreet, L. The Hypervolume Indicator for Multi-Objective Optimisation: Calculation and Use. Ph.D. Thesis, University of Western Australia, Perth, Australia, 2011.
21. Guerreiro, A.P.; Fonseca, C.M.; Paquete, L. The hypervolume indicator: Computational problems and algorithms. *ACM Comput. Surv. (CSUR)* **2021**, *54*, 1–42. [CrossRef]
22. Reinhart, C.F.; Cerezo Davila, C. Urban building energy modeling—A review of a nascent field. *Build. Environ.* **2016**, *97*, 196–202. [CrossRef]
23. Aguiar, R.; Cardoso, C.; Leitão, A. Algorithmic design and analysis fusing disciplines. In *Disciplines and Disruption, Proceedings Catalog of the 37th Annual Conference of the Association for Computer Aided Design in Architecture, ACADIA 2017, Cambridge, MA, USA, 2–4 November 2017*; MIT: Cambridge, MA, USA, 2017; pp. 28–37.
24. Alizadeh, R.; Allen, J.K.; Mistree, F. Managing computational complexity using surrogate models: A critical review. *Res. Eng. Des.* **2020**, *31*, 275–298. [CrossRef]
25. Araujo, G.; Santos, L.; Leitão, A.; Gomes, R. Ad based surrogate models for simulation and optimization of large urban areas. In Proceedings of the 27th International Conference of the Association for Computer-Aided Architectural Design Research in Asia (CAADRIA 2022), Sydney, Australia, 9–15 April 2022.
26. Østergård, T.; Jensen, R.L.; Maagaard, S.E. A comparison of six metamodeling techniques applied to building performance simulations. *Appl. Energy* **2018**, *211*, 89–103. [CrossRef]
27. Drury, B.; Curtis, O.; Linda, K.; Frederick, C. EnergyPlus: Energy simulation program. *ASHRAE J.* **2000**, *42*, 49–56.
28. Philip, S. eppy Documentation. 2019. Available online: <https://buildmedia.readthedocs.org/media/pdf/eppy/latest/eppy.pdf> (accessed on 12 December 2022).
29. Géron, A. *Hands-On Machine Learning with Scikit-Learn, Keras, and TensorFlow: Concepts, Tools, and Techniques to Build Intelligent Systems*; O’Reilly Media, Inc.: Sebastopol, CA, USA, 2019.
30. Shahriari, B.; Swersky, K.; Wang, Z.; Adams, R.P.; De Freitas, N. Taking the human out of the loop: A review of Bayesian optimization. *Proc. IEEE* **2016**, *104*, 148–175. [CrossRef]
31. Roudsari, M.S.; Pak, M. Ladybug: A Parametric Environmental Plugin for Grasshopper to Help Designers Create an Environmentally-Conscious Design. In Proceedings of the 13th Conference of International Building Performance Simulation Association, Chambéry, France, 26–28 August 2013; pp. 3128–3135.
32. Deb, K.; Pratap, A.; Agarwal, S.; Meyarivan, T. A fast and elitist multiobjective genetic algorithm: NSGA-II. *IEEE Trans. Evol. Comput.* **2002**, *6*, 182–197. [CrossRef]

33. Eckart, Z.; Künzli, S. Indicator-based selection in multiobjective search. In Proceedings of the International Conference on Parallel Problem Solving from Nature, Birmingham, UK, 18–22 September 2004; pp. 832–842.
34. Nebro, A.J.; Durillo, J.J.; Nieto, G.; Coello, C.A.; Luna, F.; Alba, E. SMPSO: A new pso-based metaheuristic for multi-objective optimization. In Proceedings of the 2009 IEEE Symposium on Computational Intelligence in Multi-Criteria Decision-Making, MCDM 2009, Nashville, TN, USA, 30 March–2 April 2009; Volume 2, pp. 66–73. [CrossRef]
35. Sierra, M.R.; Coello Coello, C.A. Improving PSO-based Multi-Objective optimization using crowding, mutation and ϵ -dominance. In Proceedings of the Third International Conference, EMO 2005, Guanajuato, Mexico, 9–11 March 2005; Volume 3410, pp. 505–519. [CrossRef]
36. Deb, K.; Agrawal, R.B. Simulated Binary Crossover for Continuous Search Space The crossover operator is believed to be the main search operator in the working of a genetic. *Complex Syst.* **1994**, *9*, 115–148.
37. Censor, Y. Pareto optimality in multiobjective problems. *Appl. Math. I Optim.* **1977**, *4*, 41–59. [CrossRef]

Disclaimer/Publisher’s Note: The statements, opinions and data contained in all publications are solely those of the individual author(s) and contributor(s) and not of MDPI and/or the editor(s). MDPI and/or the editor(s) disclaim responsibility for any injury to people or property resulting from any ideas, methods, instructions or products referred to in the content.

Article

The Sense and Non-Sense of PEDs—Feeding Back Practical Experiences of Positive Energy District Demonstrators into the European PED Framework Definition Development Process

Han Vandevyvere^{1,2,*}, Dirk Ahlers¹ and Annemie Wyckmans¹

¹ Department of Architecture and Planning, NTNU—Norwegian University of Science and Technology, 7491 Trondheim, Norway; dirk.ahlers@ntnu.no (D.A.); annemie.wyckmans@ntnu.no (A.W.)

² VITO/EnergyVille, 3600 Genk, Belgium; han.vandevyvere@vito.be

* Correspondence: han.h.b.vandevyvere@ntnu.no

Abstract: This article discusses early developments of the Positive Energy District (PED) concept, both in terms of its definition and of its implementation in real world demonstrators. Based on the specific challenges for creating an operational definition for the European +CityxChange project, the feasibility of creating a PED was practically explored by identifying 4 possible subtypes that respond to varying constraints regarding the energy balance of the PED. This article provides the context and describes these 4 ambitions levels: PED_{autonomous}, PED_{dynamic}, PED_{virtual}, and PrePED; and the 3 boundary modes: geographical, functional, and virtual. The work thus expands on the first general PED definitions as they were put forward in the SET-plan and by the European Commission, while allowing a better response to the specific boundary conditions of PEDs' physical context. As such, it provides an operational, city-focused, bottom-up PED definition. The present study analyses how these efforts connect to current work being performed on the development of a European PED Framework Definition. In the latter, new elements such as context factors are introduced in order to account for the varying boundary conditions that PEDs must address, and in particular the difficulties of realising PEDs in existing and densely built-up urban areas. Hereby it can be argued that the approach with 4 subtypes is a bottom-up method of addressing the same challenges as a context factor based approach operating in a top-down manner, this time starting from the regional or national renewable energy potentials. Both approaches indeed strive towards an optimum setup of PEDs both within their geographical boundaries and in their interactions with the surrounding energy infrastructures and cities. These efforts are instrumental in helping to prevent that a PED is being regarded as a goal in se, functionally disconnected from its surroundings. There are strong arguments in favour of handling PEDs as building blocks for the broader realisation of carbon neutral cities and regions, thus contributing to the systemic change that is needed to futureproof the built environment as a whole. Without applying this integrating perspective, PEDs risk creating a sub-optimal lock-in within their sites and thus remain one-off experiments, lacking connection to the wider urban sustainability strategies that are needed to properly address today's energy and climate emergencies. This holds even more when considering the quality-related requirements that come with sustainable urban design and governance. Therefore, this study further explores how PEDs can fully support such a deep urban sustainability transition, and what could consequently be the next steps towards successful and upscaled PED deployment.

Citation: Vandevyvere, H.; Ahlers, D.; Wyckmans, A. The Sense and Non-Sense of PEDs—Feeding Back Practical Experiences of Positive Energy District Demonstrators into the European PED Framework Definition Development Process. *Energies* **2022**, *15*, 4491. <https://doi.org/10.3390/en15124491>

Academic Editors: Ala Hasan and Hassam Ur Rehman

Received: 18 April 2022

Accepted: 31 May 2022

Published: 20 June 2022

Publisher's Note: MDPI stays neutral with regard to jurisdictional claims in published maps and institutional affiliations.



Copyright: © 2022 by the authors. Licensee MDPI, Basel, Switzerland. This article is an open access article distributed under the terms and conditions of the Creative Commons Attribution (CC BY) license (<https://creativecommons.org/licenses/by/4.0/>).

Keywords: positive energy districts; positive energy blocks; PED concept; energy transition; climate neutrality; smart sustainable cities; Smart Cities and Communities; European energy transition; energy planning; urban planning; sustainable urban design, advanced energy systems

1. Problem Statement

In the context of achieving climate neutrality for cities, the concept of Positive Energy Districts (PEDs) has recently gained widespread attention [1–4]. One contributing factor to

this success certainly is the scale level at which a PED operates, transcending the individual building level intervention and thus opening up more and better possibilities of both advanced technical energy system integration and the upscaled contribution of many societal actors to sustainable urban (re)development. At the same time, PEDs remain an enterprise at a scale which is manageable in terms of straightforward planning and execution. PEDs thus can help to divide the enormous challenge of making cities climate-neutral into more practicable projects.

An important reason for targeting energy and climate strategies at the district level is that such an approach can deliver benefits over a building-by-building approach, both in terms of energy system design and integration and in terms of striving towards optimized urban morphology. Specific opportunities emerge regarding technical and economical scale advantages of setting up district energy systems compared to the mere juxtaposition of individual building installations, facilitating local exchanges of energy between different building programmes and mobility applications, and providing district scale energy storage systems. Integrated sector coupling, involving exchanges between electrical and thermal systems, completes the palette of such strategies. This shows that PEDs are not only advanced energy systems from the technological point of view, but also from the integration view and regarding innovative larger-scale urban deployments. At the same time, PEDs are not an entirely new concept and have predecessors such as Net Zero Energy Districts (NZEDs) [5], while district scale approaches for energy systems and the effects of urban morphology and programming on energy use have since long been studied in the research literature [5–11].

When the term ‘positive energy district’ was coined, there was an intention to use the word ‘positive’ rather than the terms (net) ‘zero’ (energy or emission) or climate ‘neutral’, thus leveraging on the positive connotation it entails. Whether such naming effectively helped the uptake of the concept would however require a specific study.

The PED concept has now been taken up beyond the original scope of the European Commission and is under study by organisations such as the European Energy Research Alliance (EERA) [12], the Urban Europe Research Alliance (UERA), the Joint Programming Initiative Urban Europe (JPI UE) [13], and the International Energy Agency (IEA) [14] for further development and roll-out. Within this, specific actors have also proposed to interpret the term ‘positive’ as a ‘positive impact on the wider energy systems’ of a city or a region, rather than just an internal positive yearly energy balance [15].

The practical realisation of the concept, in the way it was initially conceived, does however come with significant difficulties, as can be illustrated by experiences gained in recent Horizon 2020 Smart Cities and Communities Lighthouse projects (including +CityxChange). For example, it appears to be particularly challenging to realise a PED in the context of an urban district renovation project when the building density in the district is high or when many heritage buildings are present. In such a context, it becomes difficult to generate sufficient renewable energy onsite while regulatory and organisational constraints, both in the energy domain and beyond, tend to complicate matters even more. These difficulties seem, at least, to jeopardise the possibilities of implementing a narrow interpretation of the PED concept. At the same time, it can be questioned if such a narrow approach is desirable at all. Indeed, PEDs do not constitute a goal of their own but must rather be considered as building blocks of the climate neutral cities and regions of the future, whether that is expressed in the technical terms of renewable energy system integration or through the wider requirements of achieving integrated urban sustainability through high quality district design and governance.

The main research questions addressed in this article are therefore: How to improve the qualities of the PED concept and its applicability in practice? What recommendations can be drawn from experiences with past and ongoing PED pilots, in particular regarding the way these pilots translate general PED requirements into an operational working definition? How can this feed back into the ongoing research for the formulation of an EU-wide PED framework definition? These questions shall not only be addressed from a

technical viewpoint, but also from the broader perspective of realising integrated urban sustainability, entailing both quantitative and qualitative considerations.

2. Materials and Methods

The research materials supporting the analysis and conclusions of the present article stem from three main sources:

1. the implementation of PED pilots in the Horizon 2020 SCC Lighthouse project +CityxChange [16,17]. These pilots are situated in Trondheim (NO) and Limerick (IE). In Trondheim, three pilot areas distributed across the city test positive energy blocks (PEBs, see further for the relation with PEDs) and local flexibility markets for exchanging and trading energy, both heat and electricity. In Limerick, one pilot area is situated in the historical Georgian city centre while a turbine in the Shannon river completes the pilot's energy infrastructure. Realising PEBs and exchanging and trading energy are also the main goals. In Limerick the pilot project includes the energy retrofit of heritage buildings. Two challenges needed to be addressed: translating the general PED definition of the H2020 call into an operational framework on the ground, and subsequently realizing the operational requirements in practice. This included substantial challenges, especially with regard to effectively building the PED pilots under the present regulatory, economic and societal circumstances. In addition, realising PEDs in existing urban districts is considered more difficult than through newbuilt areas, but the city and PED ambitions include the transformation of existing areas;
2. the editing of a PED 'solution booklet' [3] for the Smart Cities Information System (SCIS), now integrated in the Smart Cities Marketplace. The booklet was a co-production between SCIS and four H2020 SCC Lighthouse projects focusing on the realization of PED pilots: Atelier, SPARCS, MakingCity and +CityxChange. The resulting guidance document is based on a systematic analysis of the barriers and opportunities encountered in the different PED pilots;
3. participation in the Alignment Core Group for a PED definition and integrated approach (see Section 6), led by JPI Urban Europe. Participating organisations include EERA JPSC PED modules, SET Plan Action 3.2 PED Programme/DUT PED pillar, COST Action PED-EU-NET, IEA EBC Annex 83, UERA PED WG, PED-related H2020 SCC projects, H2020 SCC Task Group Replication, Scalable Cities (EU SCC Lighthouse Project group) and the Smart Cities Marketplace. The working group is thus composed of members from academia, research & technology organisations (RTOs) and the field of practice, and aims to formulate a PED framework definition that can be used throughout the EU by combining a scientifically sound approach with requirements of accessibility and ease of use by all concerned stakeholders. It operates through regular working meetings of the core expert group while broader consultations of PED stakeholders (e.g., JPI Urban Europe member state representations) provide for feedback from the field of practice.

In this way the research method for this article confronts applied case study analysis (points 1 and 2) with the ongoing transdisciplinary research for formulating a PED framework definition (points 3 and 2). The main underlying methodological framework for making analyses and recommendations in the present article is based on multimodal system analysis, a knowledge theory originally formulated by the Dutch philosopher of law Herman Dooyeweerd and subsequently elaborated in, among others, systems science and urban planning theory [9,18–21]. This knowledge theory also structures the content of the SCIS solution booklets. It has proven to be both methodologically robust and operationally performant for dealing with complex, interdisciplinary research questions.

3. Background: The Emergence of PEB and PED Concepts from 2015 Onwards

The concept of a *Positive Energy Block* (PEB) can be understood in the context of increasing European ambitions in the topics of *energy in buildings* [22] and the *energy transition* [23]. It initially emerged out of a European project demonstrator, *Hikari*, a housing

complex at the Confluence district in Lyon (FR), as part of the EU FP7 EeB-generation project Next-Buildings [24], completed in 2015 [25]. It was estimated that the demonstrator displayed some performances and qualities that merited to be replicated. As Hikari had been defined as an *îlot à énergie positive* (energy positive islet), it was chosen to adapt a translation to English as ‘Positive Energy Block’. That idea was subsequently presented at an EU conference in December 2015 for uptake by the EIP SCC Marketplace (European Innovation Partnership on Smart Cities and Communities) in a new Action Cluster initiative on PEBs [2,26].

Subsequently the concept was promoted through the EIP SCC Marketplace as a way forward in scaling up zero or positive energy concepts from the building level to groups of buildings and, eventually, districts. At this stage, the PEB concept requested “*at least three connected neighbouring buildings producing on a yearly basis more primary energy than what they use.*” [27] Initially, realising a functional mix (and thus also enabling useful energy exchanges between different building programmes and buildings’ energy profiles) in a PEB was judged to be paramount as well, but would not yet be included in the definition. However, realising integrated sustainability would come back in later definitions. The initiators of the concept were also sensitive to a positive connotation of the wording in the definition, which is rather hard to find in terms such as ‘zero emissions’, ‘carbon neutral’ or ‘zero energy’ [28].

The 2018 Implementation Plan of SET-plan Action 3.2 [1] (Strategic Energy Technology Plan), developed by JPI UE [13] (Joint Programming Initiative Urban Europe) in cooperation with EERA JPSC [12] (Joint Programme on Smart Cities of the European Energy Research Alliance), EU Member States and Associated Countries and other European initiatives, set out the goal of realising 100 PEDs by 2025. In this instance, the requirement for a PED was stated as:

“Positive Energy Districts (PED) are energy efficient districts that have net zero carbon dioxide (CO₂) emissions and work towards an annual local surplus production of renewable energy (RES). Such districts help raise the quality of life in European cities, while reaching the COP21 targets and making Europe a global role model. An open innovation framework with cities, industry, investors, research institutes and citizens’ organisations all working together will help develop PEDs and the necessary R&I Activities. The approach integrates the technological, spatial, regulatory, financial, legal, environmental, social and economic perspectives.” [29] (pp. 28–29).

Equally starting in 2018, the European Commission formally introduced PEB & PED related requirements in the Horizon 2020 project calls on Smart Cities and Communities Lighthouse projects (LC-SC3-SCC-1-2018 call) [30] (The PEB/PED requirement is included in the calls as of 2018, [31,32]). The 2018-2020 H2020 Work Programme for these calls defined a PEB/PED as an implementation goal for the innovation projects as follows:

“Positive Energy Blocks/Districts consist of several buildings (new, retro-fitted or a combination of both) that actively manage their energy consumption and the energy flow between them and the wider energy system. Positive Energy Blocks/Districts have an annual positive energy balance. They make optimal use of elements such as advanced materials (e.g., bio-based materials), local RES, local storage, smart energy grids, demand-response, cutting edge energy management (electricity, heating and cooling), user interaction/involvement and ICT.

Positive Energy Blocks/Districts are designed to be an integral part of the district/city energy system and have a positive impact on it (also from the circular economy point of view). Their design is intrinsically scalable and they are well embedded in the spatial, economic, technical, environmental and social context of the project site.” [31], (p. 117, [33]).

The calls featured for the first time, a requirement for PEBs/PEDs to fit into an overall Bold City Vision of city-level climate neutrality strategies. This is a step change because they do not just include more positive energy buildings, but highlight the opportunities of

using a complete urban block/district and its multi-faceted characteristics. They also had an additional section on expected focus areas, which highlight further expectations and clarify ambitions and motivations:

- *“Focus on mixed use urban districts and positively contribute to the overall city goals;*
- *Develop solutions that can be replicated/gradually scaled up to city level. The technical, financial, social, and legal feasibility of the proposed solutions should be demonstrated in the actual proposal.*
- *Make local communities and local governments (particularly city planning departments) an active and integral part of the solution, increase their energy awareness and ensure their sense of ownership of the smart solutions. This should ensure sustainability of Positive Energy Blocks/Districts;*
- *Promote decarbonisation, while improving air quality.*
- *[...]” [31]*

JPI UE and EERA JPSC meanwhile set out to further develop a PED framework definition that could be used EU-wide. JPI UE held a workshop, partially based on a request for input by JPI UE for a collection of potential PED projects [34] (Positive Energy Districts and Neighbourhoods Programme—Cities Workshop and Site Visit, 3–4 April 2019, Nordbahnhof, Vienna [35]). The event was combined with, amongst others, a +CityxChange Learning Workshop on 2 April 2019 addressing related challenges and gathering project requirements and insights [36]. A joint outcome was an initial PED definition [37] with the main characteristics as presented later in this article.

This led to the following formulation, consulted among national delegations in and beyond the EU and published in a white paper in 2020:

“Positive Energy Districts are energy-efficient and energy-flexible urban areas or groups of connected buildings which produce net zero greenhouse gas emissions and actively manage an annual local or regional surplus production of renewable energy. They require integration of different systems and infrastructures and interaction between buildings, the users and the regional energy, mobility and ICT systems, while securing the energy supply and a good life for all in line with social, economic and environmental sustainability.” [38]

This definition forms the basis for further analysis through the present article. Note that the definition leaves space for ‘local or regional’ energy production, thus hinting at solutions for the problem of realising self-sufficiency on the basis of on-site energy production alone. Note also the inclusion of mobility, which can be interpreted as a PED providing a share towards mobility energy use, and also optimises other mobility impacts.

Meanwhile, experiences from the field of practice such as the Horizon 2020 Smart Cities and Communities Lighthouse Projects (H2020 SCC LH) and their practical implementations were being made, testing and implementing the concept in practise. These experiences show that major challenges occur in turning existing urban districts into PEDs on the one hand from the technical and energy view and need for local generation, and on the other hand from the needed long term strategies involving multiple actors in complex stakeholder networks. One of the early outcomes was the SCIS PED solution booklet [3]. This solution booklet was co-created with participants from the H2020 SCC Lighthouse Projects +CityxChange (including authors of the present article), MakingCity, SPARCS and Atelier and thus directly translates the practical experience gained from PED pilots. It included the insight that a PED is not a product, but rather a process.

Building further on these initiatives and experiences, the COST Action PED-EU-NET [4] (European Cooperation in Science and Technology - Positive Energy Districts European Network) and the Annex 83 on Positive Energy Districts by the International Energy Agency’s Energy in Buildings and Communities Programme (IEA EBC Annex 83) [14] were created to perform more in-depth collaborative research on the PED concept and its potentials, and to publish their findings.

4. An Operational PED Definition with 4 Subtypes: Addressing the Practical Implementation Challenges from a Bottom-Up Perspective

The SET implementation plan was publicly issued in 2018, and the EU H2020 work programme in 2017 for the 2018 calls, with their initial definitions as described above in Section 3. The same year, at the end of 2018, the first SCC projects granted from that call started their PEB demonstrators.

4.1. Process

These projects had a strong need for a concrete and operational working definition of PEBs that could be used in practice with cities and solution providers. An operational definition was initiated from the +CityxChange project in cooperation with EERA JPSC. The +CityxChange project [17] includes 32 partners among which 7 cities: 2 Lighthouse cities with detailed plans and immediate deployment activities in the project, and 5 Fellow Cities, which refine their plans within the project towards setting up PEBs. It was important to build an operational PEB definition that included the contexts and requirements of the different PEBs in all the cities, as a first requirement. It also became even clearer that an inclusive definition was needed. City representatives pointed out that cities each follow different development paths, which need to be possible to align with the definition. More generally, it was considered very important to not be too restrictive, as not to reduce or prevent any innovation potential towards PEBs and local development [36,39].

The process included a number of workshops such as an initial +CityxChange Learning Workshop, 2 April 2019, Vienna [36]; the SET-plan PED definition and boundaries work group meeting, 6 May 2019, Brussels ('PED definition development v3') [39]; and a PED workshop at the 3rd International Conference on Smart and Sustainable Planning for Cities and Regions SSPCR 2019, Bolzano, 11 December 2019 ('PED definition development v4'). At the Brussels meeting, some reflections on the Horizon Europe Mission Area on "Climate-Neutral and Smart Cities" were included in the programme, and as such cities obviously can be considered as an upscaling from PEBs and PEDs towards PECs or PERs (Positive Energy Cities or Regions, currently not established terms) as steps towards the EU goal of Climate-Neutrality by 2050. Such strategic alignment and city-level scaling ambitions were present early for example in +CityxChange [40] and definition work [41]. Results were summarised in multiple project reports and presentations [36,39].

The workshops collaboratively developed insights in a wide range of technical and governance challenges:

- economic feasibility and cost efficiency: in particular, energetic retrofitting of existing buildings remains costly with long payback periods—often going far beyond the range of a 30 years investment horizon [42]. In the European context, most PEDs are expected to be urban retrofit PEDs. Business models that turn the PED opportunities into benefits are being developed, but many secondary benefits cannot be captured in financials while being invaluable for cities;
- optimum renewable and sustainable energy provision: in many cases, the amount of renewable or sustainable energy needed for the district could possibly be produced in a cheaper and more efficient way outside the district or the city, but such a setup would at least partly go against the PED ambition. Nevertheless this can be balanced against the reduced needs for grid upgrades or other 'hidden' costs;
- the stated need of PEDs to flexibly interact with their hinterland in terms of exchanging energy flows and helping to balance energy grids [38]: whereas the theoretical need for this faculty is commonly recognized, its practical implementation through operational schemes such as Energy Communities (in line with the recast EU directives in this field) is yet at the experimentation phase—see also below;
- the share of mobility energy to be provided by a PED: none of the current definitions have managed to define a desired performance level. It can be argued that mobility can only be partially included in PEDs as transport tends to act at a different scale.

Examples of emission accounting models for mobility can also be widely varying in different regions;

- regulatory barriers: beneficial local cost sharing models are not yet possible in the electrical grid and markets. Examples include no opportunity for local exchange of energy through the grid while extra wires would break the system, or feeding back energy for prosumers not being viable under present regulations and technicalities, or no feed-in tariff for surplus energy from prosumers being available, meaning they could not receive any payment [43]. Currently the implementation of the Clean Energy for All Europeans Package [44], including the facilitation of Energy Communities and peer-to-peer trading, is not yet finished in several Member States (like Belgium [45] or the Netherlands [46] to name just a few), thus prolonging the stated difficulties;
- cultural factors such as landscape and heritage value: rarely the full technical potential of onsite renewable energy generation can be realised. For example, neither shall all building roofs and façades be clad with PV panels nor shall urban wind turbines be installed wherever possible throughout the urban texture.
- organisational and governance factors: PEDs are not a status, but a process. Taking this further, PEDs are also not a single product. They are a multi-stakeholder undertaking, addressing the full complexity of urban (re)development.

4.2. Supporting Evidence from Cases

The above stated technical and governance challenges can be illustrated by examples from +CityxChange's PED pilots in Limerick and Trondheim [17]. In Limerick, the PED pilot is situated in the city's central Georgian heritage district. It is characterised by mixed use (residential and non-residential building programmes), varying urban densities in a typical range of 20 to 50 dwellings per hectare, and a strong presence of heritage buildings [3,16]. The district is in need of urban renewal. Given the urban density and the heritage character, the possibilities of both increasing energy efficiency by insulating building envelopes and producing sufficient renewable energy on-site, mainly through PV, are limited. A choice was therefore made to complement on-site renewable energy production with energy supply from a water turbine to be placed in the Shannon river, about 1–2 km upstream from the district. This implied that the turbine should be considered as a virtual asset of the PED neighbourhood, as it is not situated within the strict geographical boundaries of the PED. A number of challenges need to be addressed. First, it remains difficult to convince individual building owners to step into the PED pilot and perform substantial investments on their properties. This makes setting high retrofit standards for the housing stock more difficult. Second, current regulations do not allow for implementing the flexibility and peer-to-peer trading mechanisms needed for the operation of the PED, and special dispensation is hard to achieve, even if the EU Clean Energy Package's electricity directives have meanwhile been (partially) transposed to Member State legislation. Third, and linked, permitting procedures to allow for the placement of the turbine in the Shannon river are challenging, not the least because this regulatory case is virtually unseen in Ireland. In this way the Limerick pilot demonstrates all of the above-mentioned challenges. If all these challenges receive a proper address and the PED can be realised, another challenge immediately comes forward. While this first PED could profit from the opportunity of placing a turbine in the Shannon river—first come, first serve—more areas of the city with PED ambitions would meet increasing difficulties for realising their goals as the pool of virtual assets such as the turbine will continue to decrease. This brings forward a question of fairness and balancing: how much external energy may be reserved for a given district while not jeopardising the possibilities of other districts to become PEDs as well. This situation is a major argument to support the use of context factors and national or regional 'energy envelopes' with wider integration and balancing potential as discussed further below.

In the Trondheim case, multiple PEDs were planned in the city. As part of the deployment, work is underway to connect these and allow interaction, exchange, and trading of energy between PEDs [47]. In addition, local renewables may not be sufficient in all

cases. Integration of dedicated external renewable sources is being considered, in line with the PED_{virtual} concept. Challenges include as above the willingness to invest and finding suitable risk/benefit sharing models. Financing of PEDs and of overall decarbonisation efforts thus remain challenging, though PEDs can contribute with additional unlocked business models.

4.3. Outcome: PED Definition, 3 System Boundary Modes, 4 Ambition Levels

The resulting operational PED definition includes a working definition, 4 ambition levels, and 3 system boundaries [39]. The agreed working definition states:

“Positive Energy Districts (PED) are mixed-use energy-efficient districts that have net zero carbon dioxide (CO₂) emissions and actively manage an annual local surplus production of renewable energy (RES). They require interaction and integration between buildings, the users and the regional energy, mobility and ICT system, while ensuring social, economic and environmental sustainability for current and future generations.” [39]

For the question of system boundaries, a distinction was proposed (as early as 3 April 2019 [37]) [36] and consolidated [39] between 3 modes:

- **Geographical boundary:** Spatial-physical limits of the PED in terms of delineated buildings, sites and (energy) infrastructures—these may be contiguous or in a configuration of detached patches;
- **Functional boundary:** Limits of the PED in terms of energy grids, e.g., the electricity grid behind a substation that can be considered as an independent functional entity serving the PED; a district heating system that can be considered as a functional part of the PED even if the former’s service area is substantially larger than the heating sector of the PED in question; or a gas network in the same sense;
- **Virtual boundary:** Limits of the PED in terms of contractual boundaries, e.g., including an energy production infrastructure owned by the PED occupants but situated outside the normal geographical PED boundaries (for example an offshore wind turbine owned through shares by the PED occupant community).

Based on these boundary conditions, 4 possible types of PEDs were proposed according to the realisable ambition levels. (These were initially named as Diamond, Platinum, Gold, and Silver, used in April 2019 mainly in internal documents [36], and quickly changed from May 2019 onwards into the more descriptive terms.) The ambition levels are: *Autonomous PED*, *Dynamic PED*, *Virtual PED* and *Pre-PED*, having definitions as follows [37,39,41]:

- PED_{autonomous}: ‘plus-autarkic’, net positive yearly energy balance within the geographical boundaries of the PED and internal energy balance at any moment in time (no imports from the hinterland) or even helping to balance the wider grid outside, not expected as a common case (see Figure 1);
- PED_{dynamic}: net positive yearly energy balance within the geographical boundaries of the PED but dynamic exchanges with the hinterland to compensate for momentary surpluses and shortages (see Figure 2);
- PED_{virtual}: net positive yearly energy balance within the virtual boundaries of the PED but dynamic exchanges with the hinterland to compensate for momentary surpluses and shortages (see Figure 3);
- PED_{pre}: candidate PED, no net positive yearly energy balance within the geographical boundaries of the PED but energy difference acquired on the market by importing certified green energy (i.e., realizing a zero carbon district).

These levels were carefully chosen and developed to correspond to both a group of set points of ambition and technical potential, and to form a clear pathway of development, thus allowing for growing achievements towards high synergistical ambitions with clear milestones:

A Pre PED does not yet achieve a positive annual energy balance by itself, but achieves it through buying green energy through outside general markets, while developing the PED. A $PED_{virtual}$ achieves a net positive annual energy balance within the virtual boundaries of the PED, allowing for adaptation of local generation sites. This situation is found in many on-the-ground cases. It reflects the challenges of direct local generation in urban areas and on any type of buildings, and allows flexibility in planning boundaries and implementation paths to include generation sites that are not building-integrated or outside the core geographical boundary. A $PED_{dynamic}$ has a net positive annual energy balance within the geographical boundaries of the PED. It exchanges energy with the wider grid, into which it is integrated. This is a type of PED that can be implemented in geographical/urban conditions that have better pre-conditions for local renewables. $PED_{dynamic}$ and $PED_{virtual}$ will be the most common types in regenerated European urban environments, allowing the built environment to act as a kind of battery for the broader energy grid. Finally, a $PED_{autonomous}$ is autonomous from the grid on the demand side—it will have a positive energy balance not on average, but at any point in time—possibly turning it into a pure energy producer from the grid view—though usually not fully a virtual power plant. Only few areas will be able to become $PED_{autonomous}$, however, in particular when other co-benefits and potential negative externalities such as urban quality of life, spatial quality, nature-based solutions are taken into account.

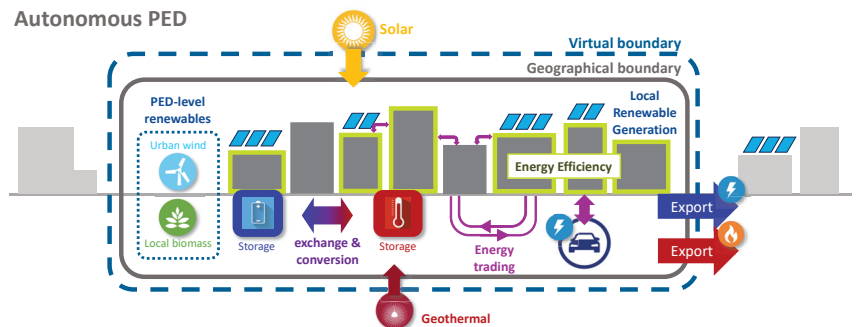


Figure 1. Autonomous PED, principle and system boundaries. Only exports to the surrounding system. Including energy efficiency measures, renewables (solar, PV, wind, biomass, geothermal, small hydropower), waste heat recovery, electric and thermal storage, integration of mobility energy needs (and EVs as batteries), sector coupling between electric and thermal.

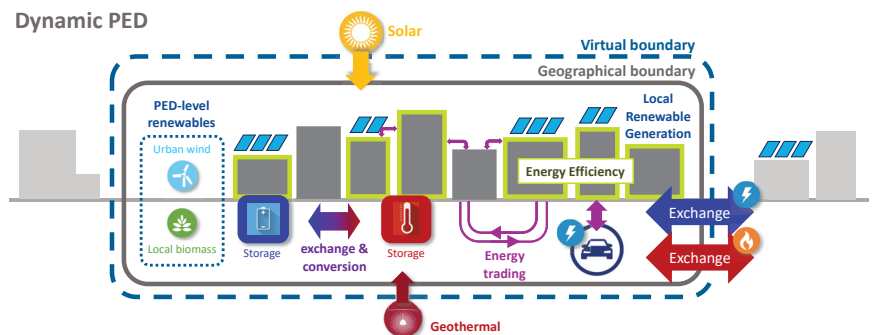


Figure 2. Dynamic PED, principle and system boundaries. Including energy efficiency measures, renewables (solar, PV, wind, biomass, geothermal, small hydropower), waste heat recovery, electric and thermal storage, integration of mobility energy needs (and EVs as batteries), sector coupling between electric and thermal, and exchange with the surrounding systems.

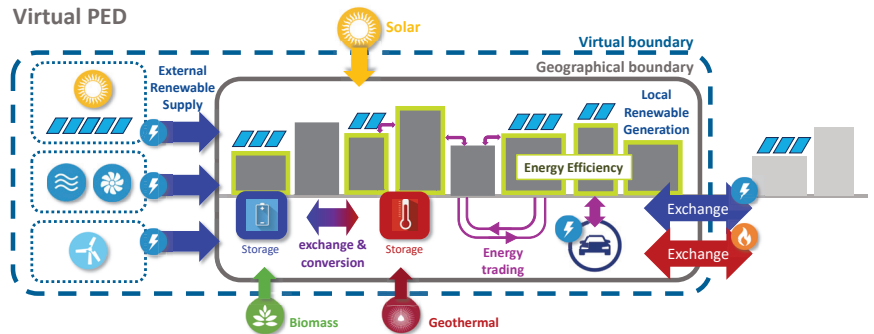


Figure 3. Virtual PED, principle and system boundaries. Including virtual integration of external renewables and exchange with the surrounding systems. Including energy efficiency measures, renewables (solar, PV, wind, biomass, geothermal, small hydropower), waste heat recovery, electric and thermal storage, integration of mobility energy needs (and EVs as batteries), sector coupling between electric and thermal, and exchange with the surrounding systems.

In summary, identifying PEDs from such differentiated perspectives would allow sufficient flexibility for adaptations to a range of different city conditions from existing projects, while keeping a certain standardisation and commonality, all within the H2020 SCC programme, the SET Plan, and future refinements. It would for example allow PEDs to import energy from outside the strict district boundaries, in situations where it is not feasible to generate all needed renewable resources onsite. This setup also interprets and translates the aspect of ‘local or regional’ energy production, as put forward in the JPI UE framework definition, into precise operating conditions.

The differentiation into 4 subtypes was subsequently picked up in the PED definitions of, for example, SCC Lighthouse Projects such as +CityxChange [17] (including the authors of the present article) [16,39,48] or SPARCs [49] and other projects such as syn.ikia [50].

5. From Technical Solutions to Urban Transition Governance for Systemic Change: Addressing the Contribution of PEDs towards Realising Climate Neutral Cities and Regions

The four PED types identified in the previous section are intended to also be able to tackle the second major implementation barrier for PEDs. This second barrier is strongly related to the challenge of overhauling the energy paradigm that underlies the current modus operandi of cities: decentralised fossil fuel based energy supply. In order to achieve this, deep structural change is required in all strata of society: technical infrastructures, economic setups, value chains and business models, types of collaboration between the different concerned urban actors, social rules, policies and cultural habits, up to the behavioural routines of citizens and enterprises and the (often hidden) value systems that ultimately steer all of these strata. Hereby the questions regarding energy cannot be disconnected from those regarding the adopted economic models, social justice and respect of the earth’s ecological carrying capacity. In other words, effectively solving this puzzle simultaneously requires realising overall integrated sustainable functioning at the level of the district or the city [20].

The four types of PEDs are created to be able to support the following main transition challenges.

From the simple, individual short term solution to complex, collective long term formats: it becomes increasingly obvious that many preferable set-ups for PEDs and, at the higher scale level, climate neutral cities, require different configurations and business models than current standard practice. The four types of PEDs, in particular the PED_{virtual} and PED_{dynamic}, will be able to support a shift in preferred assets from individual ones such as the individual heat pump, the individual PV installation on the individually energy-

retrofitted home or the individual electric car, towards collective and integrated assets such as micro district heating and cooling networks, shared renewable energy generation installations managed by local energy communities, sustainable collective- or co-housing, and shared or collective mobility solutions including mobility-as-a-service (MaaS).

Aligning interests and agendas of the different urban stakeholders: in order to achieve these solutions, the interests, agendas and investment horizons of a multitude of urban actors in complex stakeholder networks must become sufficiently aligned in order to arrive at a shared development process. This requires new organisational set-ups and business models, new collaboration formats with new types of legitimacy and an overall strong co-creation and governance process that facilitates all of the former. The integrated set-up of the PED_{dynamic} and PED_{virtual}, with intensive interaction between building, grid, mobility, ICT and citizen experts and end users, will favour cooperative financial and partnership models to optimise economic sustainability. It is to be noted that also established PED definitions such as the ones formulated by the SET-Plan, the European Commission and JPI UE refer to quantitative (energy and carbon related) aspects as much as qualitative (sustainable development related) aspects. This implies that those definitions recognise the fact that both challenges, stated in the context of the present analysis, need to receive a full address. Studying the full spectrum of deep systemic change in cities is however beyond the scope of the present article. It is nevertheless necessary and sufficient to indicate that PED challenges must be linked to the wider issues at stake for sustainable urban development, of which reaching climate neutrality is one important pillar. Taking into account the two main challenges as stated above will hereby provide for a good starting point. It assures that PED strategies and agendas can be fully integrated in urban (climate) action planning.

6. Current Work on an EU-Wide PED Framework Definition: From PED Types to Context Factors—Situating PEDs in Their Wider Energy Generation Landscape

Through the PED definition work undertaken under the umbrella of JPI UE, an alternative approach has emerged to accommodate for the different contexts in which PEDs operate. These developments have been documented and shared for consultation through a working paper [51]. This reviewed draft version processes feedback from dedicated stakeholder workshops on 17 and 20 September 2021 (EERA Joint Programme Smart Cities, Nordic Edge conference) as well as main comments from an IEA workshop on 22 October 2021 (IEA Annex 83 on Positive Energy Districts).

Instead of addressing these boundary conditions by distinguishing 4 subtypes with increasing degrees of self-sufficiency, the approach is reversed. Whereas the subtypes start from a bottom-up vision, analysing how much ‘exterior help’ a PED needs given its starting condition, a top-down manner of addressing the same constraint consists of situating the PED in its wider energy landscape and deriving a proportional contribution of the PED to the total renewable and sustainable energy generation capacity of the considered region or country. In this way, a fair ‘*effort sharing*’ mechanism can be established between the PED and the other areas of the region, whether they be urban or rural. Hereby, ‘*context factors*’ define the specific characteristics of the PED, allowing to propose a justified amount of effort sharing that can be assigned to the PED. The basis of this mechanism is derived from work on system boundaries in the energy system [52,53].

More precisely, these context factors will account for:

- **Urban density:** the higher the urban density, the more difficult it becomes to generate all needed energy on-site. Therefore a reversely proportional context factor can be applied, allowing the district to self-generate lower shares of its operating energy with increasing urban densities;
- **Heritage:** the more heritage buildings or protected views are present in a district, the more restrictions there will appear on building envelope interventions and the installation of renewable energy generation capacity such as PV panels. Therefore,

another reversely proportional context factor will allow to reduce the self-generation share of the district with increasing heritage value.

- **Mobility:** it should be pointed out how much of the mobility energy for the users of the PED shall be generated onsite. This is a discussion that remains far from established, even for PEDs that can be considered as having the potential of generating 100% of their own energy needs. As mobility strongly relates to higher functional scale levels than the district itself, it may be expected that the mobility energy produced in a PED will always remain a share of the total mobility energy needed by its users, be they inhabitants, commuters or visitors;
- **Climate** and embedding in the regional or national energy system: each region has its own challenges to address in terms of generating sufficient renewable and sustainable energy. In this way, the regional energy equation may be more difficult to solve in a context of cold and dark winters with high heating demand and little available resources to supply heat pumps, versus warm and sunny summers with dominant cooling demand and ample potential for PV-input. The complete energy balance for the region will thus influence the share of energy production that is assigned to a PED.

Such an approach implies that national or regional effort sharing mechanisms must be established and quantified, which lifts the needed level of solution building to a higher scale. From an overall viewpoint of reaching climate-neutral functioning in the most ecologically efficient and cost effective manner, this is indeed a logical step to take. Heat and cold balances will to a large degree be addressed by a regional approach, while for electricity an EU and beyond approach remains preferable. It is to be noted that sector coupling may further change the working parameters. For example, the future import of green hydrogen may become an important factor in the overall energy equation.

Whereas current PED definitions hint at integrated sustainable urban development, the above method with context factors goes even further by situating cities in their regional or national energy hinterland – and beyond. This leads to an approach of full-scale subsidiarity, whereby the integration of macro-, meso- and micro-scale energy generation is being realised at the methodological optimum [9].

7. Conclusions and Outlook

The present article discusses PED development from a practical implementation viewpoint, reflecting on the evolving definition framework and suggesting approaches that may help to make PED development more feasible while at the same time integrating PEDs meaningfully in their surrounding (energy) systems and living environments. This is considered both at the technical level of a positive yearly energy balance and zero greenhouse gas emissions, and at the level of PEDs supporting integrated urban sustainable development, thus becoming an effective building block towards creating climate neutral and smart cities. Specific indicators related to PEDs, including energy, carbon, LCA, economic and qualitative indicators, are not in scope for this article and will be addressed in future developments of the wider European framework definition.

The use of an operational PED definition with 4 subtypes helps to address a PED's practical implementation challenges from a bottom-up perspective. The 3 system boundary modes and 4 ambition levels provide a practical framework for projects, cities, and developers to work with. The 4 PED subtypes, and the Dynamic PED and the Virtual PED in particular, also allow to effectively address qualitative requirements for PEDs as well as to enhance their embedding in the surrounding environment both from the technical and the integrated sustainable development point of view. We discuss this with selected case studies and examples to show how it can help support project implementation. Further case studies will be part of future work.

Meanwhile a top-down approach for PEDs is also under development, whereby the same implementation challenges are being tackled by considering the total renewable energy potential of a region or country as the starting point for setting the PED's specific energy requirements. Thereby context factors account for the different starting positions

for PED development, for example when a PED project regards urban retrofit, includes high-density urban fabric, or contains many heritage buildings.

Both approaches serve the same goal: providing an operational and practical approach towards building PEDs, while allowing for flexibility in the PED definition requirements.

In terms of the formulated research questions, we conclude that the case-based bottom-up approach and the research-based top-down approach do meet each other regarding practical solutions for the technical energy balancing of PEDs. However, three differences can be noted. First, the top-down method accounts of the sustainable energy potential of the wider region or state, thus assuring ‘fair share’ access to this overall potential by different PEDs. Such an approach prevents a ‘first come first serve’ strategy that could be the consequence of using the bottom-up definition in a case-by-case fashion, without considering its impacts on the wider energy system. Such risk occurs foremost in the case of virtual PEDs, and with limited outside potential for renewable generation. Second, although an approach based on context factors would therefore be preferable, the latter method requires that the total energy potential of a region or country is first established and that proper allocation keys are identified before any individual PED can be built. However, this would only become relevant if PEDs would become a significant fraction of the energy transition. The current state rather shows that we are too slow, and any fast deployment is preferable from our view. Third, the bottom-up approach allows qualitative requirements for PEDs to be addressed in a flexible and context-sensitive way that allows for fast deployment. Addressing qualitative aspects of PEDs in the top-down work organised by JPI Urban Europe is still in its early phases.

Next recommended development steps therefore include:

- Further mapping on-the-ground experiences in creating and managing PEDs, to extract viable technical, social and economic pathways to PEDs for use by cities, real estate developers and other urban decision makers. In particular, further elaborating context factors to account of the wider sustainable energy potentials and inquiring practical feasibility of this method;
- In this way, developing a definition framework that is at the same time sufficiently precise to allow PED benchmarking, sufficiently flexible to accommodate for the many contexts in which PEDs will be developed, and sufficiently simple not to repel urban actors such as city administrators, project developers or building owners in using the definition framework;
- Further investigating the quality-related factors, co-benefits and potential negative externalities of PED applications better, and identifying how these may contribute to generating willingness to invest in PEDs (public, private and citizen funding);
- Analysing which efforts are best fit at district or at city level, to see PEDs as important stepping stones towards climate-neutral cities and regions. This makes PEDs not only targets in themselves, but establishes them as growth and transition enablers.

Overall, this continued work on framework definitions and real-life demonstrators will contribute to successful and upscaled PED deployment within the urban sustainability transition.

Author Contributions: Conceptualization, H.V., D.A. and A.W.; methodology, H.V., D.A. and A.W.; writing—original draft preparation, review and editing, H.V., D.A. and A.W. All authors have read and agreed to the published version of the manuscript.

Funding: Parts of the work have been performed within the +CityxChange (Positive City Exchange) [17] project funded by EU H2020 under Grant Agreement No. 824260 under the Smart Cities and Communities (SCC) topic; parts have been performed under EERA Smart Cities [12], which acknowledges funding from the Research Council of Norway under project number 296176.

Institutional Review Board Statement: Not applicable.

Informed Consent Statement: Not applicable.

Data Availability Statement: Not applicable.

Acknowledgments: We thank Jens Bartholmes (European Commission) and Paul Cartuyvels (Bouygues Europe and Smart Cities Marketplace) for their insights and support in clarifying initial steps and initiatives with us regarding the early development of the PED concept, in which they were primarily involved. We thank Simon Schneider for insights and a review of relevant aspects of this manuscript. We further thank Christoph Gollner, Vicky Albert-Seifried, Gerhard Stryi-Hipp and the other members of the JPI Urban Europe PED Framework Definition working group for insights and discussion around the PED definition development. For the Vienna workshop, 3 April 2019, we thank the participants, especially Terence Connolly, Jiří Tencar, Ricardo Bandli, Lorenz Leppin, Ömer Akyürek, and Dudley Stewart. For the EERA workshop in Brussels, 6 May 2019, we thank the +CityxChange municipalities of Limerick and Pisek, participants from JPI, from H2020 SCC projects MAKING-CITY and GrowSmarter, and members of the EERA JPSC. We further thank the cities and partners of the +CityxChange project for ongoing discussions and insights on PED demonstrator development and deployment. We finally thank the numerous participants and colleagues from various projects, cities, institutions, and initiatives that we could discuss this topic with.

Conflicts of Interest: The authors declare no conflict of interest. The authors hold leading or contributing roles in the +CityxChange project or in EERA JPSC.

References

1. European Strategic Energy Technology Plan (SET Plan), Action n°3.2—Implementation Plan on Positive Energy Districts. Available online: https://setis.ec.europa.eu/implementing-actions/set-plan-documents_en (accessed on 15 April 2022).
2. Smart Cities Marketplace Initiative on Positive Energy Blocks. Available online: <https://smart-cities-marketplace.ec.europa.eu/action-clusters-and-initiatives/action-clusters/sustainable-built-environment/positive-energy> (accessed on 15 April 2022).
3. Vandevyvere, H.; Ahlers, D.; Alpagut, B.; Cerna, V.; Cimini, V.; Haxhija, S.; Hukkalainen, M.; Kuzmic, M.; Livik, K.; Padilla, M.; et al. Positive Energy Districts Solution Booklet. Technical Report, EU SCIS Smart Cities Information System. 2020. Available online: <https://smart-cities-marketplace.ec.europa.eu/insights/solutions/solution-booklet-positive-energy-districts> (accessed on 15 April 2022).
4. PED-EU-NET | Cost Action CA19126—Positive Energy Districts European Network. Available online: <https://pedeu.net/> (accessed on 15 April 2022).
5. Polly, B.; Kutscher, C.; Macumber, D.; Schott, M.; Pless, S.; Livingood, B.; Van Geet, O. From zero energy buildings to zero energy districts. In Proceedings of the 2016 ACEEE Summer Study on Energy Efficiency in Buildings, Pacific Grove, CA, USA, 21–26 August 2016; pp. 21–26.
6. Ratti, C.; Baker, N.; Steemers, K. Energy consumption and urban texture. *Energy Build.* **2005**, *37*, 762–776. [CrossRef]
7. Salat, S. Energy loads, CO₂ emissions and building stocks: Morphologies, typologies, energy systems and behaviour. *Build. Res. Inf.* **2009**, *37*, 598–609. [CrossRef]
8. Salat, S.; Nowacki, C. De l'importance de la morphologie dans l'efficience énergétique des villes. *Liaison Energ. Francoph.* **2010**, 141–146.
9. Vandevyvere, H.; Stremke, S. Urban Planning for a Renewable Energy Future: Methodological Challenges and Opportunities from a Design Perspective. *Sustainability* **2012**, *4*, 1309–1328. [CrossRef]
10. Conci, M.; Schneider, J. A District Approach to Building Renovation for the Integral Energy Redevelopment of Existing Residential Areas. *Sustainability* **2017**, *9*, 747. [CrossRef]
11. Perera, A.; Javanroodi, K.; Wang, Y.; Hong, T. Urban cells: Extending the energy hub concept to facilitate sector and spatial coupling. *Adv. Appl. Energy* **2021**, *3*, 100046. [CrossRef]
12. EERA Joint Programme Smart Cities. Available online: <https://www.eera-sc.eu/> (accessed on 15 April 2022).
13. JPI Urban Europe—Positive Energy Districts (PED). Available online: <https://jpi-urbaneurope.eu/ped/> (accessed on 15 April 2022).
14. IEA EBC—Annex 83—Positive Energy Districts. Available online: <https://annex83.iea-ebc.org/> (accessed on 15 April 2022).
15. Stryi-Hipp, G.; Albert-Seifried, V. Unpublished Work; Fraunhofer Institute for Solar Energy Systems (ISE): Freiburg, Baden-Württemberg, Germany, 2021.
16. Ahlers, D.; Driscoll, P.; Wibe, H.; Wyckmans, A. Co-Creation of Positive Energy Blocks. In Proceedings of the 1st Nordic conference on Zero Emission and Plus Energy Buildings, Trondheim, Norway, 6–7 November 2019; IOP Conference Series: Earth and Environmental Science; Volume 352. [CrossRef]
17. +CityxChange Project. Available online: <https://cityxchange.eu/> (accessed on 15 April 2022).
18. Lombardi, P.; Brandon, P. The multimodal system approach to sustainability planning evaluation. In *Sustainable Urban Development Volume 2: The Environmental Assessment Methods*; Deakin, M., Mitchell, G., Nijkamp, P., Vreeker, R., Eds.; Routledge: London, UK, 2007.
19. Basden, A. The critical theory of Herman Dooyeweerd? *J. Inf. Technol.* **2002**, *17*, 257–269. [CrossRef]
20. Vandevyvere, H. How to cut across the catch-all? A philosophical-cultural framework for assessing sustainability. *Int. J. Innov. Sustain. Dev.* **2011**, *5*, 403–424. [CrossRef]
21. Vandevyvere, H. Evaluating the Sustainable Performance of an Urban District: Measured Score or Reflexive Governance? *Int. J. Sustain. Dev. Plan.* **2013**, *8*, 36–58. [CrossRef]

22. European Commission. Energy Performance of Buildings Directive. Available online: https://energy.ec.europa.eu/topics/energy-efficiency/energy-efficient-buildings/energy-performance-buildings-directive_en (accessed on 15 April 2022).
23. Investing in a Sustainable Energy Future for Europe. Available online: https://european-union.europa.eu/priorities-and-actions/actions-topic/energy_en (accessed on 15 April 2022).
24. CORDIS: NEXT-BUILDINGS Project. Available online: <https://cordis.europa.eu/project/id/284533> (accessed on 15 April 2022).
25. Hikari, Premier ilot à Énergie Positive, Lyon Confluence. Available online: <https://www.lyon-confluence.fr/en/node/4736> (accessed on 15 April 2022).
26. Cartuyvels, P. (Smart Cities Marketplace Action Cluster on Sustainable Built Environment, Brussels, Belgium). Personal communication, 2021.
27. EIP SCC, Sustainable Districts and Built Environment: Positive Energy Blocks, Infosheet. Available online: <https://smart-cities-marketplace.ec.europa.eu/sites/default/files/PostiveEB.pdf> (accessed on 15 April 2022).
28. Cartuyvels, P. (Smart Cities Marketplace Action Cluster on Sustainable Built Environment, Brussels, Belgium); Bartholmes, J. (European Commission—DG Energy, Brussels, Belgium). Personal communication, 2021.
29. European Commission and Directorate-General for Energy and Joint Research Centre. SET Plan Delivering Results: The Implementation Plans: Research & Innovation Enabling the EU's Energy Transition. Publications Office. 2018. Available online: https://www.google.com.hk/url?sa=t&rct=j&q=&esrc=s&source=web&cd=&cad=rja&uact=8&ved=2ahUKewjulojhbv4AhXHnFYBHXCfCs4QFnoECAGQAQ&url=https%3A%2F%2Fwww.ccus-setplan.eu%2Fwp-content%2Fuploads%2F2019%2F10%2Fsetplan_delivering_results_2018.pdf&usg=AOvVaw0gAIWwG4HSC3NiY_NQHDAL (accessed on 15 April 2022).
30. INEA, Smart Cities & Communities. Available online: <https://ec.europa.eu/inea/en/horizon-2020/smart-cities-communities> (accessed on 15 April 2022).
31. European Commission. Funding and Tenders: Smart Cities and Communities, TOPIC ID: LC-SC3-SCC-1-2018-2019-2020. Available online: <https://ec.europa.eu/info/funding-tenders/opportunities/portal/screen/opportunities/topic-details/lc-sc3-scc-1-2018-2019-2020> (accessed on 15 April 2022).
32. European Commission. FAQ—Frequently Asked Questions, Work Programme (WP) 2018 for Horizon 2020, Smart Cities and Communities—Lighthouse Projects, Topic Identifier: LC-SC3-SCC-1-2018-2019-2020. Available online: https://ec.europa.eu/research/participants/portal4/doc/call/h2020/lc-sc3-scc-1-2018-2019-2020/1800106-faq_ssc1_2018_v07_en.pdf (accessed on 15 April 2022).
33. European Commission. EU Horizon 2020 Work Programme 2018-2020–10. Secure, Clean and Efficient Energy. Available online: https://ec.europa.eu/research/participants/data/ref/h2020/wp/2018-2020/main/h2020-wp1820-energy_en.pdf (accessed on 15 April 2022).
34. JPI Urban Europe. Europe towards Positive Energy Districts. A Compilation of Projects towards Sustainable Urbanization and the Energy Transition. Available online: https://jpi-urbaneurope.eu/wp-content/uploads/2020/06/PED-Booklet-Update-Feb-2020_2.pdf (accessed on 15 April 2022).
35. JPI Urban Europe—PED Programme Cities Workshop: Towards a European Positive Energy Cities Network. Available online: <https://jpi-urbaneurope.eu/news/short-review-ped-programme-cities-workshop-towards-a-european-positive-energy-cities-network/> (accessed on 15 April 2022).
36. Wyckmans, A.; Ahlers, D. D9.2: Report on Intra-Project Collaboration, Including Study Visits and Peer to Peer Workshops. Technical Report +CityxChange Project Deliverable 9.2, +CityxChange Project. 2019. Available online: <https://cityxchange.eu/knowledge-base/report-on-intra-project-collaboration-including-study-visits-and-peer-to-peer-workshops/> (accessed on 15 April 2022).
37. Vandevyvere, H.; Connolly, T.; Tencar, J.; Bandli, R.; Leppin, L.; Akyürek, Ö.; Stewart, D. PED Definition Development, 2019. In Proceedings of the JPI UE workshop, Vienna, Austria, 3 April 2019.
38. JPI Urban Europe / SET Plan Action 3.2. White Paper on Reference Framework for Positive Energy Districts and Neighbourhoods. Key lessons from national consultations. Available online: <https://jpi-urbaneurope.eu/app/uploads/2020/04/White-Paper-PED-Framework-Definition-2020323-final.pdf> (accessed on 15 April 2022).
39. Wyckmans, A.; Karatzoudi, K.; Brigg, D.; Ahlers, D. D9.5: Report on Attendance at Events Held by Other SCC-01 Co-ordinators 2. Technical Report +CityxChange Project Deliverable 9.5, +CityxChange Project. 2019. Available online: <https://cityxchange.eu/knowledge-base/report-on-attendance-at-events-held-by-other-scc-01-co-ordinators-2/>, (accessed on 15 April 2022).
40. +CityxChange/European Commission. Positive City ExChange | CityxChange Project | Fact Sheet | H2020 | CORDIS. Available online: <https://cordis.europa.eu/project/id/824260> (accessed on 15 April 2022).
41. Vandevyvere, H. PED Definitions and approaches: An overview. Presented at SCIS Webinar 'Actions & Recommendations: Creating a Joint Vision for PEDs', Moderated by Jelle Jaubin; EUSEW 2020; 30.06.2020, online. Available online: <https://smart-cities-marketplace.ec.europa.eu/news-and-events/news/2020/eusew-2020-webinar-creating-joint-vision-peds-recap> (accessed on 15 April 2022).

42. Vandevyvere, H.; Reynders, G.; Baeten, R.; De Jaeger, I.; Ma, Y. The Trade-Off between Urban Building Stock Retrofit, Local Renewable Energy Production and the Roll-Out of 4G District Heating Networks. Case Study Modelling for 9 Urban Districts in Flanders, Belgium. Position Paper. EnergyVille. Available online: <https://www.energyville.be/en/press/trade-between-urban-building-stock-retrofit-local-renewable-energy-production-and-roll-out-4g> (accessed on 15 April 2022).
43. Bertelsen, S.; Livik, K.; Myrstad, M. D2.1 Report on Enabling Regulatory Mechanism to Trial Innovation in Cities. Technical Report +CityxChange Project Deliverable 2.1, +CityxChange Project. 2019. Available online: <https://cityxchange.eu/knowledge-base/report-on-enabling-regulatory-mechanism-to-trial-innovation-in-cities/> (accessed on 15 April 2022).
44. European Commission. Clean Energy for All Europeans Package. Available online: https://energy.ec.europa.eu/topics/energy-strategy/clean-energy-all-europeans-package_en (accessed on 15 April 2022).
45. Energiedelen en Persoon-aan-Persoonverkoop | VREG. Available online: <https://www.vreg.be/nl/energiedelen-en-persoon-aan-persoonverkoop> (accessed on 15 April 2022).
46. Wetsvoorstel Energiewet (UHT) | Publicatie | Rijksoverheid.nl. Available online: <https://www.rijksoverheid.nl/documenten/publicaties/2021/11/26/wetsvoorstel-energiewet-uhf> (accessed on 15 April 2022).
47. Gulbrandsøy, E.N.; Granado, P.C.D.; Pedrero, R.A.; Backe, S.; Pinel, D.; Lauvland, M.; Rosales, M.G.; Danielsen, S.; Sizov, G. D5.3 Campus Microgrid Model Prototype. Technical Report +CityxChange Project Deliverable 5.3, +CityxChange Project. 2022. Available online: <https://cityxchange.eu/knowledge-base/d5-3-campus-microgrid-model-prototype/> (accessed on 15 April 2022).
48. Gall, T.; Carbonari, G.; Wyckmans, A.; Ahlers, D. Co-Creating Local Energy Transitions Through Smart Cities: Piloting a Prosumer-Oriented Approach. In *Review of World Planning Practice Volume 16: Post-Oil Urbanism*; ISOCARP Review; Hanzl, M., Reilly, J., Agrawal, M., Eds.; ISOCARP: The Hague, The Netherlands, 2020; Volume 16, Chapter 7, pp. 108–123. Available online: <https://cityxchange.eu/wp-content/uploads/2020/11/Co-Creating-Local-Energy-Transitions-Through-Smart-Cities.pdf> (accessed on 15 April 2022).
49. Lindholm, O.; Rehman, H.u.; Reda, F. Positioning Positive Energy Districts in European Cities. *Buildings* **2021**, *11*, 19. [CrossRef]
50. Brozovsky, J.; Gustavsen, A.; Gaitani, N. Zero emission neighbourhoods and positive energy districts—A state-of-the-art review. *Sustain. Cities Soc.* **2021**, *72*, 103013. [CrossRef]
51. Gollner, C.; Vandevyvere, H. *Towards a European PED Definition*; Version 26.10.2021; Working Paper for consultation; 2021, unpublished.
52. Schneider, S.; Zelger, T.; Leibold, J.; Schöfmann, P. PED Definition and Methodology—Preliminary results from 3 years and 5 projects of PED research. In *Presentation for the PED Framework Definition Alignment Group*; Internal Presentation; 2021, unpublished.
53. Schneider, S.; Bartlmä, N.; Leibold, J.; Schöfman, P.; Tabakovic, M.; Zelger, T. New Assessment Method for Buildings and Districts towards Net Zero Energy Buildings Compatible with the Energy Scenario 2050. 2019. In Proceedings of the REAL CORP 2019, Karlsruhe, Germany, 2–4 April 2019.

Article

Technical–Financial Feasibility Study of a Micro-Cogeneration System in the Buildings in Italy

Gabriele Battista ^{1,*}, Emanuele de Lieto Vollaro ², Andrea Vallati ³ and Roberto de Lieto Vollaro ¹

¹ Department of Industrial, Electronic and Mechanical Engineering, Roma TRE University, Via Vito Volterra 62, 00146 Rome, Italy; roberto.delietovollaro@uniroma3.it

² Department of Architecture, Roma TRE University, Largo Giovanni Battista Marzi 10, 00154 Rome, Italy; emanuele.delietovollaro@uniroma3.it

³ Department of Ingegneria Astronautica, Elettrica ed Energetica, Sapienza University of Rome, Via Eudossiana 18, 00184 Rome, Italy; andrea.vallati@uniroma1.it

* Correspondence: gabriele.battista@uniroma3.it

Abstract: The current global context, marked by crises such as climate change, the pandemic, and the depletion of fossil fuel resources, underscores the urgent need to minimize waste. Cogeneration technology, which enables simultaneous production of electricity and thermal energy from electricity generation waste, offers a promising solution to enhance energy efficiency. Its widespread adoption, particularly in the European Union, where several cogeneration systems are in place, demonstrates its growing popularity. Italy alone has 1865 high-efficiency cogeneration units, contributing significantly to total cogeneration energy generation. Micro-cogeneration, specifically, has attracted attention for its potential to reduce energy waste and environmental impact. This study focuses on assessing the technical and financial feasibility of a micro-cogeneration plant using natural gas-fuelled internal combustion engines, considering different scenarios of plant operating strategies in order to optimize energy production, minimize waste, and mitigate environmental footprints associated with conventional methods. Additionally, it provides valuable guidance for policymakers, industry stakeholders, and decision-makers invested in sustainable energy solutions. By advancing micro-cogeneration technology, this study aims to promote a more sustainable and environmentally conscious approach to energy production. The methodology applied is based on the development of a numerical model via RETScreen Expert 8 and it was calibrated with one-year energy bills. The study was performed by focusing on the analysis of the annual energy savings, greenhouse gas emission savings, tonnes of oil equivalents savings, and financial parameters such as Net Present Value (NPV), Internal Rate of Return (IRR), Profitability Index (PI) and Payback time (PBT). The results show, using a micro-cogeneration system in a big complex of buildings, that the financial parameters can continually increase with the plant's capacity with the electrical load following, but with a loss of the recovered heat from the cogenerator because it may reach values that are not necessary for the users. When the thermal load variation is much more significant than the electrical load variation, it will be useful to design the plant to follow the thermal load variation which allows the full utilization of the thermal and energy production from the plant without any waste energy and choosing a system capacity that can optimize the energy, emissions and financial aspects.

Keywords: climate change; cogeneration technology; energy efficiency measures; energy retrofit; micro-cogeneration; feasibility; RETScreen

Citation: Battista, G.; Vollaro, E.d.L.; Vallati, A.; Vollaro, R.d.L.

Technical–Financial Feasibility Study of a Micro-Cogeneration System in the Buildings in Italy. *Energies* **2023**, *16*, 5512. <https://doi.org/10.3390/en16145512>

Academic Editors: Ala Hasan and Hassam Ur Rehman

Received: 18 June 2023

Revised: 17 July 2023

Accepted: 18 July 2023

Published: 20 July 2023



Copyright: © 2023 by the authors. Licensee MDPI, Basel, Switzerland. This article is an open access article distributed under the terms and conditions of the Creative Commons Attribution (CC BY) license (<https://creativecommons.org/licenses/by/4.0/>).

1. Introduction

The historical context we are living in, with an ongoing climate crisis caused by global warming, a pandemic, and the gradual depletion of traditional energy sources such as fossil fuels, along with tensions in the relationship between Europe and Russia, has brought the need to minimize waste back to the forefront of human attention.

One-third of total greenhouse gas emissions worldwide are produced by the sector involved in building and infrastructure development, making it a significant contributor to the phenomenon of global warming [1]. In order to contrast the climate change caused by greenhouse gas emissions, global initiatives have been undertaken to create innovative net-zero energy buildings (nZEBs) [2,3] and to improve the energy efficiency of existing buildings [4–6]. The expansion of urban areas has led to the emergence of the urban heat island phenomenon [7,8], which describes the unique microclimate of cities [9]. This phenomenon is characterized by an increase in temperatures in urban areas compared to rural areas. The effects of urban heat islands can negatively impact human well-being, leading to various adverse consequences [10]. Additionally, it can lead to a surge in the utilization of air conditioning plants in buildings to combat the heat [11,12]. This, in turn, results in higher electricity consumption [13,14] and increased levels of pollutants emitted in urban environments [15,16]. Recent attention has been given to studying strategies to reduce the impacts of urban heat islands, such as the use of green roofs [17,18], cool materials [19,20], vegetation [21,22], and water sources [23,24]. The adoption of these mitigation techniques is crucial not only for large urban areas but also for smaller, localized areas such as urban canyons [25–27].

Retrofitting existing buildings offers significant potential for energy efficiency improvements, in contrast to newly built nZEBs, given that existing buildings constitute the majority of structure stocks and have an absence of essential energy efficiency components [28]. A multitude of studies on recommendations and approaches for retrofitting energy performance for single buildings [29,30] and building stocks [31] can be sourced in the existing literature and are frequently driven by efforts undertaken by many nations to attain carbon neutrality in their economies. Nevertheless, energy-saving initiatives typically exclude historical buildings to safeguard their architectural heritage. Retrofitting historic buildings was previously perceived as a potential risk to their cultural value, but this perception is gradually evolving [32]. Moreover, multiple studies have indicated notable improvements in energy efficiency for rehabilitated historic buildings in Europe, with Italy leading the way, followed by the United Kingdom, Spain [33,34], and China [35,36]. Striking a balance between energy efficiency, thermal comfort, and the preservation of cultural heritage is vital when renovating historic buildings. For instance, external wall insulation, which can compromise the aesthetic character, may not be a suitable choice. However, updating internal energy systems such as lighting fixtures and appliances is fully compatible with heritage conservation. Additionally, the installation of building-integrated solar photovoltaic systems is often feasible and merits careful consideration [37]. Previous studies have proposed systemic methods [38] and evaluated various retrofit alternatives, encompassing energy efficiency strategies concerning building envelopes [39], heating, ventilation, and air conditioning (HVAC) systems [40], a combination of envelope and HVAC systems [41], as well as occupant behaviour [42]. For instance, Ascione et al. [43] conducted experimental and numerical assessments on an administrative building in Italy to develop a multi-criteria approach for energy retrofits of historic buildings. The study evaluated several energy efficiency measures, such as wall thermal insulation, air leakage, setpoint management, window glazing, and heating systems. The results indicated that energy retrofits could reduce the building's primary energy consumption by 20%. In a protected residential complex in London, Ben and Steemers [42] examined the advantages of energy retrofits through both physical and behavioural interventions. The study presented three potential levels of retrofitting, considering capital costs and payback periods for enhancing energy efficiency in HVAC and envelope systems. The investigation revealed that behavioural changes presented significant opportunities for energy savings (ranging from 62% to 86%), sometimes surpassing the energy efficiency improvements achieved through physical enhancements.

Energy retrofitting has emerged as an essential strategy for enhancing the energy efficiency and environmental impact of existing buildings [44]. However, the implementation of retrofit measures in institutional buildings is often constrained by budget limitations

and the need for profitability [45,46]. Therefore, it is crucial to assess the financial feasibility of retrofitting projects during the process of decision-making. According to Menassa [47], inaccurate financial assessment in 57% of renovation projects resulted in unexpectedly long payback periods. To address this issue, various evaluation tools have been developed over the years to identify the most economical measures. The two predominant methods for financial evaluation in energy retrofitting are life-cycle cost (LCC) analysis and cost-benefit analysis (CBA) [48,49]. Both approaches take into account the time value of money (TVM) and offer trustworthy ways to select economically optimal retrofitting measures [50]. LCC centres on the complete capital investment and forthcoming operating expenses, encompassing management and maintenance costs. It has been widely used in numerous studies to determine cost-optimal retrofitting measures for residential and non-residential buildings [51], including various building types such as residential, commercial, and educational buildings [52–57]. On the other hand, CBA is explicitly recommended by Sartori et al. [58] as a necessary procedure for financial decision-making. Some studies have applied CBA to assess optimal retrofitting measures for residential buildings [59,60], and a few have examined its economic assessment for non-residential buildings [61,62]. However, LCC has been more commonly employed in previous research. Nevertheless, Gabay et al. [63] investigated the advantage of CBA over the LCC approach in selecting optimal energy retrofitting measures. The study indicated that CBA favours the choice of higher-performance measures, even if they entail higher life-cycle costs, which remains preferable to stakeholders. The European Commission also recommends the application of CBA incorporating risk analysis into investment assessment [58]. However, it is generally considered that the potential of CBA in financial retrofitting measures evaluation is underestimated. Consequently, in this study, we utilized CBA as the primary financial evaluation approach to demonstrate its effectiveness in evaluating the actual profitability of retrofitting measures.

During the process of producing electricity, a significant amount of energy is dissipated, and therefore lost, in terms of heat. Therefore, one of the most promising ways to make energy production more efficient is to simultaneously produce electricity and thermal energy, using the remaining energy content in the waste products generated by the production of the former. Cogeneration is based on this principle and offers an effective and efficient way to use fossil fuels, ensuring sustainable management of natural and financial resources, and minimizing environmental impact [64].

Several companies have dedicated themselves to the development of this technology, and with a greater variety of solutions and greater availability on the market, there has been a significant increase in the global adoption of this technology, also due to the practicality it presents from a technical point of view.

In recent years, in the United Kingdom there has been a steady growth in installed cogeneration capacity from 3 to 6 GWe, where 68% of plants operate on natural gas [65]. The total capacity of cogeneration systems installed in European Union countries in 2010 exceeded 105 GW, with Germany ranking first with 22% of the total capacity, followed by Poland and Denmark with 9%. In Denmark, more than 50% of electricity production is provided by cogeneration systems, with 40% in Finland and 30% in Latvia and the Netherlands [66].

Finally, in Italy, according to the Ministry of Economic Development's 2020 report [67], there are 1865 High-Efficiency Cogeneration units, with a total installed capacity of 13.4 GW, electricity production of 57.7 TWh (of which 28.6 TWh are in high-efficiency mode) and 35.6 TWh of useful heat. It is estimated that these data related to HEC represent about half of the total energy generation from cogeneration. The majority of these plants (about 90% of the total) are of the internal combustion type, with an average size of 1 MW: these are the typical installations in an industrial context [68].

Micro-cogeneration is an increasingly popular technology that enables the simultaneous production of electricity and heat. This technology has gained significant attention in recent years due to its potential to reduce energy waste and decrease the environmental

impact of energy production. However, the COVID-19 pandemic and the Ukraine War has had a significant impact on the global and, in particular, European economy, and it is unclear how this will affect the feasibility and financial viability of energy retrofit strategies. Therefore, it is crucial to conduct a comprehensive analysis of the energy financial feasibility and this study aims to perform an analysis of a micro-cogeneration plant based on internal combustion engines fuelled by natural gas, considering different scenarios of plant operating strategies.

2. Materials and Methods

2.1. Methodology

The objective of this study is to focus on analysing the technical and financial feasibility of installing a new plant. In particular, in the present paper we analysed the use of a micro-cogeneration system.

The methodology is shown in Figure 1 and starts with the development of a numerical model to evaluate various types of energy used in the building. The RETScreen Expert 8 tool [69] was used to implement the numerical model. This tool allows for the comparison of various system setups from an energy, environmental, and financial perspective. It analyses investment, operation, and maintenance costs to determine the economic benefit of intervention. RETScreen Expert 8 is a proper tool for pre-feasibility and feasibility studies [70], and it is used for both electrical and thermal system design.

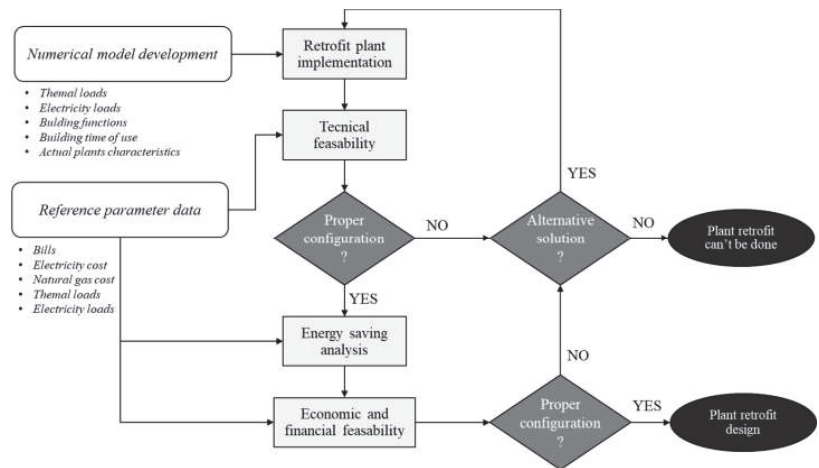


Figure 1. Flowchart of the methodology.

RETScreen Expert 8 can conduct a thorough feasibility analysis, encompassing technical, economic, risk, sensitivity, and environmental aspects of retrofit solutions for buildings. It enables the simulation, optimization, and evaluation of the performance of both traditional energy-saving measures and renewable energy systems. This comprehensive analysis aids in the decision-making process by providing insights into technical, economic, and environmental factors. RETScreen Expert 8 can immediately evaluate the effects of a retrofit solution separately or aggregated, significantly reducing the time-cost of energy retrofit decision-making.

The RETScreen Expert 8 tool was selected for its user-friendly interface compared to other commercially available software options. It offers comprehensive analysis of energy, financial, and environmental aspects, aiding in identifying the most suitable retrofit strategy. RETScreen Expert 8, the Clean Energy Project Analysis Software, enables the assessment of energy efficiency and feasibility of various energy models, including renewable energy systems and high-performance models.

The software facilitates the modelling of power plants for real estate, providing valuable output data for technical, economic, and environmental analysis related to investments in clean energy projects or cogeneration, as applicable in this case. The Canadian Government developed the calculation model with extensive support from industry, institutions, and academic experts.

The energy model is calibrated based on a one-year analysis of energy bills. Subsequently, multiple energy retrofit measures can be explored to reduce the building's energy consumption.

This study starts with an analysis of the energy consumption of the building, both in terms of methane gas and electricity, correlating them with the expenses incurred in the various years. Therefore, the average cost of energy per year was calculated, which is necessary for calculating the annual savings.

Once average thermal and electrical loads have been identified, simulations are carried out to evaluate the coverage of the building's thermal and electrical consumption by varying the power of the system to be installed. The simulations also consider energy savings, economic benefits, reduction in polluting emissions, and financial impact.

2.2. Case Study

The case study concerns a complex of buildings located in Rome, used for tertiary sector activities, served by several boilers for winter heating and by the national power grid for supplying various uses and summer cooling. The building complex covers over 100,000 square meters of useful space, divided into ten buildings. They mainly host offices and production spaces. The predominant working hours are 12 h a day, from Monday to Saturday, throughout the year for some spaces, while others are used 24 h a day, every day of the week. In addition, there are no prolonged periods of work suspension, as may occur, for example, during the summer in other typical types of work functions in Italy. The buildings present significant energy issues, such as the presence of low-efficiency plant technologies for the distribution of hot and cold fluids, and the production of hot and cold water.

The external building envelope is mainly composed of concrete and has walls with a thickness of 25 cm that correspond to an average calculated transmittance of $1.95 \text{ W/m}^2\text{K}$, while the roof and the pavement has a calculated transmittance of $0.42 \text{ W/m}^2\text{K}$ and $0.55 \text{ W/m}^2\text{K}$, respectively. The current windows in place are of the 4/9/4 type, featuring a 9 mm air gap sandwiched between two 4 mm glass layers. The calculated thermal transmittance for these windows is approximately $3.07 \text{ W/m}^2\text{K}$, accompanied by a g-value of 0.6.

The climate of the case study zone, considering the average monthly data that were used in the numerical model, is shown in Figure 2. It is characterised with an air temperature from 7°C in January to 24.8°C in July, an air humidity from 66.8% in July to 83.8% in November.

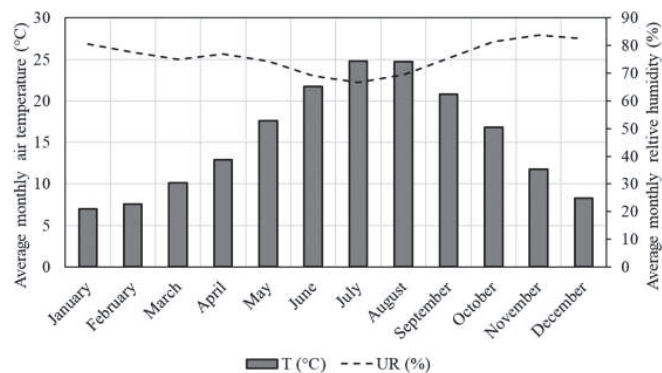


Figure 2. Monthly average air temperature and relative humidity of the case study zone.

2.3. Boundary Conditions

The annual average cost of energy, in terms of methane gas and electrical energy, for the 2022 year was, respectively, 0.40 €/kWh and 1.03 €/Nm³. For this study, the annual average costs of electrical energy and natural gas were extracted from the utility bills. In Table 1 are shown the conversion factors used to calculate the tonne of oil equivalent (TOE) and the tonne of CO₂ emissions (tCO₂), while in Table 2 are shown the main parameters used to simulate the building and plant characteristics.

Table 1. Conversion factor parameters used in the analysis.

Parameter	Value
Conversion factor TOE-electricity (toe/MWh) [71]	0.187
Conversion factor TOE-natural gas (toe/MWh) [72]	0.086
Conversion factor tCO ₂ -electricity (tCO ₂ /MWh) [73]	0.483
Conversion factor tCO ₂ -natural gas (tCO ₂ /MWh) [73]	0.202

Table 2. Parameter used for the case study.

Parameter	Value
Seasonal efficiency of existing boiler system (%)	93.7
Thermal load (W/m ²)	75.27
Hot water demand (%)	21.5
Annual availability of the cogeneration system (h)	8000
Minimum operating power of the cogenerator (%)	60
Useful life of the cogenerator plant (years)	20
Discount rate referred to the 1 December 2022 (%)	3.04

The discount rate of 3.04% is the nominal discount rate and was considered the last value in the period of the analysis in the present study because the paper aims to perform an analysis in the situation where it is necessary to model the investment decision process of an investor in the proposed energy solution.

The investment and maintenance costs were calculated starting from the data obtained from a commercial investigation. Specifically, cost is a function of size or capacity raised to a scaling exponent or scale factor [74]. The applicable equation is as follows:

$$C_2 = C_1 \cdot \left(\frac{P_2}{P_1} \right)^a \quad (1)$$

where C_2 is the cost to be estimated that has a capacity of P_2 , C_1 which is the known cost of the facility that has a capacity of P_1 , while a is a scale factor that depends on the facility technology. The scaling exponent quantifies the non-linear relationship and economies of scale, indicating that the incremental cost decreases as the facility's capacity increases.

In the present paper, after a commercial investigation, it was possible to set the investment and maintenance cost of a micro-cogenerator plant of 330 kWe at €330,000 and 62,750 €/year, respectively.

2.4. Energy Plant Retrofit

The cogenerators chosen to propose various solutions for this case study are "high power" cogenerators. These consists of internal combustion engines powered by natural gas with capacity varying from 240 to 1500 kWe (kW electricity power).

The tested configurations were chosen to cover any value of the thermal load, starting from the minimum value up to the maximum, first by using all the available cogenerators individually, then gradually coupling them in parallel until the desired load was met. The remaining thermal energy necessary for the building's uses comes from the current thermal power station made up of condensing boilers. Instead, the electricity needed is taken from the national grid.

Finally, the results were extrapolated, and the financial part of the analysis was carried out. The annual energy savings were calculated, and together with the costs for purchasing and maintaining the system, the investment's goodness was analysed through various economic factors such as Net Present Value (NPV), Internal Rate of Return (IRR), Profitability Index (PI), Payback time (PBT), and normalized Net Present Value (nNPV) with the plant capacity (NPV/kW).

3. Results

3.1. Model Calibration

The RETScreen Expert 8 tool was used for conducting the simulation analysis, which was then calibrated using readings obtained from the thermal and electricity energy consumption bills. The numerical model incorporated the building envelope's characteristics, as well as the heating, cooling, lighting, and electrical equipment used within the building. Additionally, the occupancy profile information was taken into account to determine the power requirements of the systems and consider the thermal internal gains.

The calibration process involved comparing the simulated annual heating, cooling, and electrical demand from the numerical model with the actual data obtained from the utility bills. To reduce any discrepancies between the observed and simulated data, we adjusted the gains within the numerical model. Regarding the calibration of the electrical demand, since it is often challenging to accurately quantify the number of electrical devices, we introduced varying amounts of electrical equipment into the numerical model. As for the heating and cooling demand, the calibration pays attention to adjusting the thermal gains. It is important to note that introducing thermal gains can affect the cooling demand, which in turn impacts the electricity demand due to the use of chillers that rely on this energy source. Hence, the calibration method employed a step-by-step process to minimize differences in the numerical, thermal, and electrical demand compared to the readings from the bills.

In the case study, calibration was performed to address a discrepancy in the annual thermal and electricity consumption, resulting in respective deviations of +1.7% and +1.8%.

3.2. Analysis of the Actual Electrical and Thermal Consumption

In Figures 3 and 4 are shown the thermal and electrical energy consumption taken from the bill of the building complex in the year 2022. From the graphs, there is a much more significant variation in power during the annual time frame for the thermal load (Figure 3), which has a minimum in August of 313 MWht and a maximum in January of 2433 MWht, compared to the electrical load, which has a minimum in February of 1889 mWhe and a maximum in August of 2654 mWhe. For this reason, with the introduction of a cogenerator it will be useful to design the plant to follow the thermal load variation because the electrical energy produced will be fully utilized. Otherwise, by following the electrical load, part of the thermal energy would have been lost unnecessarily.

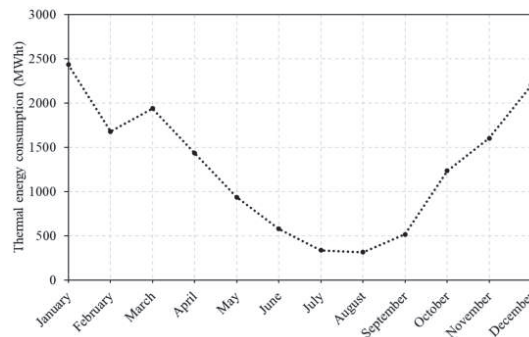


Figure 3. Thermal energy consumption in 2022 taken from the bills.

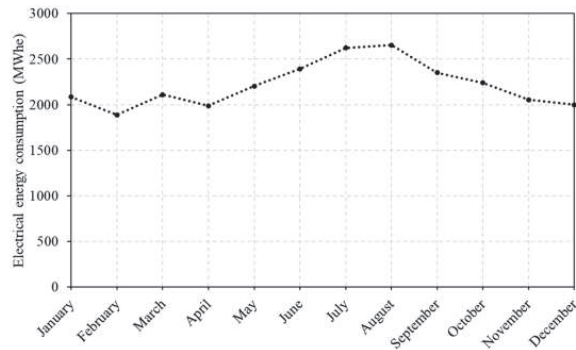


Figure 4. Electrical energy consumption in 2022 taken from the bills.

Analysing the trend of the thermal and electrical loads, it is possible to notice that the thermal load has a positive value during the summer, denoting the use of the thermal energy for the domestic hot water or for the air handling units' use. The electrical load has, indeed, a quite high base load during all the years, denoting a high electrical use in the building.

Finally, the total annual consumption of electricity was approximately 26,592 mWhe, with a billing cost of €10,691,117.58, and a natural gas consumption of 15,995 MWht with a billing cost of €1,560,840.85.

3.3. Analysis of the Cogenerator Performances

After identifying the average thermal and electrical loads of the buildings, the analysis focused on following the thermal load, so that all the heat and electricity produced would be fully utilized, with the electrical load increasing more than the thermal load. Based on this, energy production, consumption, and emissions were analysed using RETScreen software for each configuration.

Figures 5–7 show the cogenerator performance in terms of electricity production, gas consumption for cogeneration, and the gas that needs to be drawn from the network to satisfy other thermal uses. The results are shown as a function of the cogenerator plant capacity obtained with the use of different types of systems or by coupling cogenerators of different sizes. This analysis was carried out by adopting both the thermal load following strategy and the electric load following strategy. In the first case, the cogenerator is used primarily to meet thermal demands and the resulting electricity is used for electrical applications. In the second case, the cogenerator is used primarily to meet electricity demands and the resulting thermal energy is recovered to meet thermal needs.

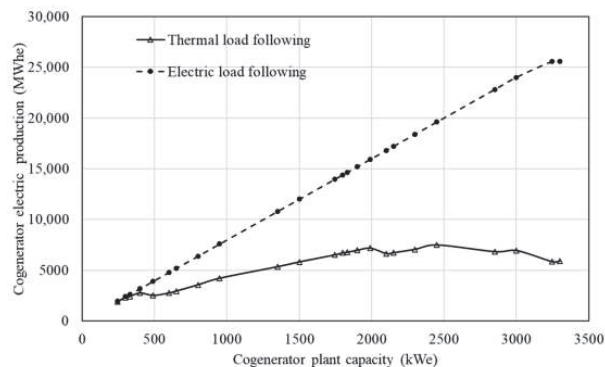


Figure 5. Cogenerator electricity production for different plant capacities and different types of operation: thermal or electric load following.

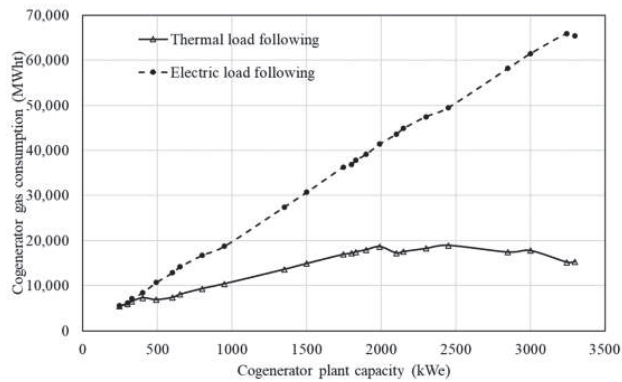


Figure 6. Cogenerator gas consumption for different plant capacities and different types of operation: thermal or electric load following.

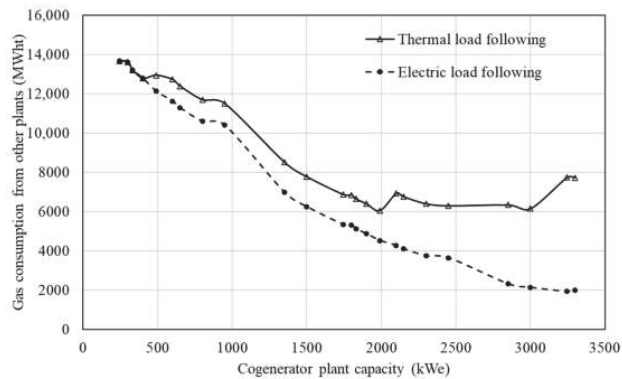


Figure 7. Gas consumption of the other plants for the different types of cogenerator operation: thermal or electric load following.

3.4. Analysis of the Cost, Energy, Toe and tCO₂ Savings

Figure 8 shows the annual savings in terms of cost, energy, tCO₂ emissions, and TOE (tonnes of oil equivalent). The results are shown as the function of the cogenerator plant capacity obtained with the use of different types of systems or by coupling cogenerators of different sizes. This analysis was carried out by adopting both the thermal load following strategy and the electric load following strategy.

It is very evident that the annual cost and percentage energy saving has the same trend shown in Figures 5 and 6, while different results are obtained for the savings in tCO₂ and TOE.

Regarding the thermal load following, the annual cost varies from about 446 k€ to 2049 k€ and the annual percentage energy savings vary from 3.6% to 16.7%, considering the increase in the cogenerator plant capacity with a peak at 2450 kWe. The annual TOE saving varies from 90.98 toe to 616.72 toe with a peak at 3000 kWe and the annual tCO₂ savings vary from 297.77 tCO₂ to 1754.87 tCO₂ with a peak at 2450 kWe.

Regarding the electric load following, the annual cost varies from about 450 k€ to 4891 k€ and the annual percentage energy savings vary from 3.7% to 39.9%, considering that the values increase with the increase in the cogenerator plant capacity. The annual TOE saving varies from 88.94 toe to 441.66 toe with a peak at 1800 kWe and the annual tCO₂ savings vary from 294.53 tCO₂ to 2024.22 tCO₂ with a peak at 2850 kWe.

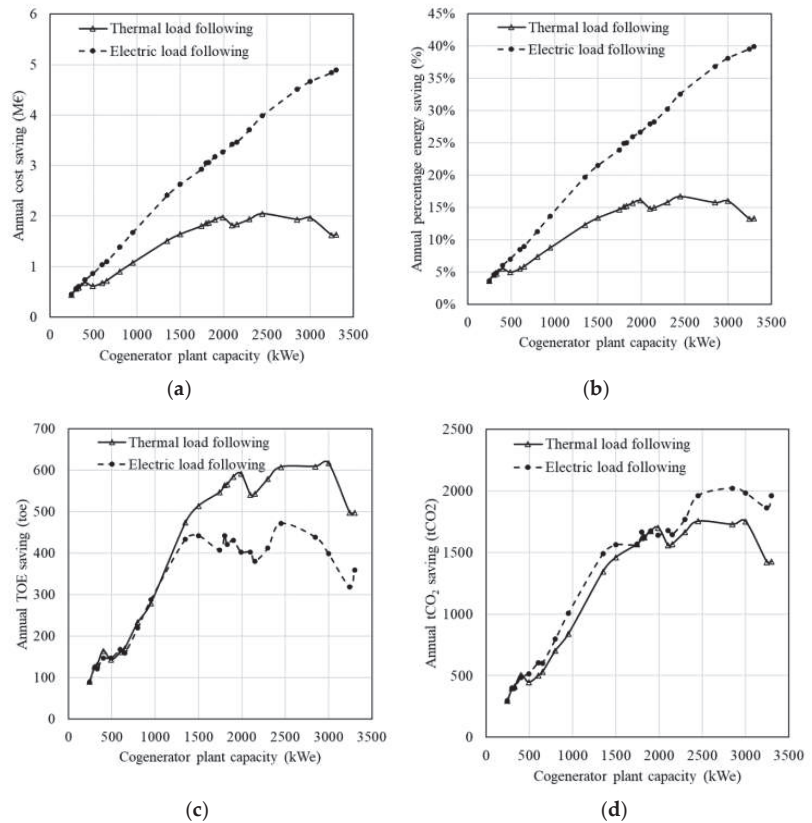


Figure 8. Results for the different types of cogenerator operation (thermal or electric load following) and size in terms of annual cost savings (a), annual percentage energy saving (b), annual TOE saving (c) and annual tCO₂ saving (d).

3.5. Analysis of the Finances

In Tables 3 and 4, the results of financial parameters considered to evaluate the economic feasibility of the investment are indicated, in order to find the most advantageous configuration from an economic point of view. The financial parameters used as a reference are: Net Present Value (NPV), normalized NPV (nNPV) with the plant capacity (NPV/kW), Internal Rate of Return (IRR), Profitability Index (PI), and Payback time (PBT).

The analysis was performed by evaluating the financial parameters for both the thermal and electrical load following and comparing them.

Regarding the results for the thermal load following, it can be noted that the maximum NPV values are obtained for configurations of 1990 and 2450 kWe, while the maximum nNPV value is obtained for a low power configuration, specifically 300 kW. As for IRR and PI, the results are consistent, as the highest values, which are 182% and 25.96, respectively, correspond to the configuration composed of a single cogenerator of 1500 kWe. Regarding PBT, it is 1 year for most cases.

Regarding the results for the electrical load following, it can be noted that the maximum NPV values are obtained for the last configuration of 3300 kWe and it can be higher with higher plant capacity. The nNPV values had a low variation which depends on the plant capacity, while IRR and PI have the highest values of 302% and 43.84, respectively, with the configuration composed of a single cogenerator of 1500 kWe, as the thermal load following case. Regarding PBT, it is 1 year for all the cases.

Table 3. Net Present Value (NPV), normalized NPV with the plant capacity, Internal Rate of Return (IRR), Profitability Index (PI) and Payback time (PBT) for the different types of cogenerator plant capacities with the operating function of thermal load following.

Plant Capacity	NPV	nNPV	IRR	PI	PBT
245	€5,566,976.31	€22,722.35	143%	20.17	1
300	€7,154,401.55	€23,848.01	162%	22.96	1
330	€7,376,916.47	€21,076.90	158%	22.35	1
400	€8,705,759.20	€21,764.40	165%	23.51	1
490	€7,507,681.27	€15,321.80	128%	17.95	1
600	€8,260,047.20	€13,766.75	125%	17.49	1
650	€8,842,052.39	€13,603.16	127%	17.84	1
800	€11,311,468.74	€14,139.34	143%	20.15	1
950	€13,584,974.03	€14,299.97	154%	21.83	1
1350	€19,493,752.00	€14,439.82	178%	25.37	1
1500	€21,247,350.49	€14,164.90	182%	25.96	1
1745	€22,569,546.41	€12,933.84	146%	20.62	1
1800	€23,259,027.79	€12,921.68	146%	20.58	1
1830	€23,371,687.32	€12,771.41	144%	20.35	1
1900	€24,061,363.64	€12,663.88	143%	20.24	1
1990	€24,542,433.23	€12,332.88	141%	19.84	1
2100	€22,014,212.60	€10,482.96	122%	17.05	1
2150	€22,215,128.59	€10,332.62	121%	16.90	1
2300	€23,482,913.53	€10,209.96	122%	17.02	1
2450	€24,874,818.16	€10,152.99	123%	17.26	1
2850	€22,637,673.38	€7943.04	103%	14.26	2
3000	€22,859,717.60	€7619.91	101%	13.96	2
3245	€16,815,002.93	€5181.82	66%	8.79	2
3300	€16,806,605.07	€5047.03	65%	8.62	2

Table 4. Net Present Value (NPV), normalized NPV with the plant capacity, Internal Rate of Return (IRR), Profitability Index (PI) and Payback time (PBT) for the different types of cogenerator plant capacities with the operating function of electrical load following.

Plant Capacity	NPV	nNPV	IRR	PI	PBT
245	€5,622,120.40	€22,947.43	144%	20.37	1
300	€7,271,290.50	€24,237.64	164%	23.33	1
330	€7,755,099.59	€22,157.43	165%	23.50	1
400	€9,521,708.27	€23,804.27	180%	25.71	1
490	€11,190,561.73	€22,837.88	187%	26.75	1
600	€13,638,818.32	€22,731.36	202%	28.87	1
650	€14,436,134.03	€22,209.44	203%	29.13	1
800	€18,379,397.78	€22,974.25	228%	32.74	1
950	€22,469,412.78	€23,652.01	250%	36.10	1
1350	€32,828,788.13	€24,317.62	295%	42.72	1
1500	€35,883,170.92	€23,922.11	302%	43.84	1
1745	€39,265,264.43	€22,501.58	249%	35.87	1
1800	€40,886,064.65	€22,714.48	251%	36.17	1
1830	€41,055,220.56	€22,434.55	248%	35.74	1
1900	€42,539,676.68	€22,389.30	248%	35.78	1
1990	€43,698,785.56	€21,959.19	245%	35.33	1
2100	€45,764,754.19	€21,792.74	246%	35.45	1
2150	€46,306,026.38	€21,537.69	244%	35.24	1
2300	€49,722,535.89	€21,618.49	250%	36.03	1
2450	€53,661,901.44	€21,902.82	258%	37.24	1
2850	€60,761,329.20	€21,319.76	265%	38.29	1
3000	€62,953,078.18	€20,984.36	266%	38.45	1
3245	€64,438,082.38	€19,857.65	234%	33.68	1
3300	€65,056,159.47	€19,536.38	232%	33.38	1

4. Discussion

Analysing the case of thermal load following, it is possible to observe how the energy production curve flattens out after a certain power onwards since the total thermal energy demand of the system is reached, thus stabilizing the production of electricity. This consideration does not apply in the case of electric load following, which has a continuously increasing electricity production with the increase in cogenerator capacity. However, in this case, it is possible that the recovered heat from the cogenerator may reach values that are not necessary for the users and would be lost, making the system less efficient.

Analysing the strategies of following the thermal load and the electrical load, contrasting results are obtained. As a matter of fact, following the thermal load leads to lower savings in terms of costs and energy, and higher savings in terms of TOE, while following the electrical load leads to the opposite. Regarding the savings on tCO₂ emissions, it is possible to notice more advantages in the following electricity load case than in the other case. However, in most of the cases of cogenerator plant capacity, the tCO₂ emissions are quite similar. Finally, it is evident how much greater the savings are for the configuration that best satisfies the thermal load since, in these cases, the cogeneration system completely replaces traditional boilers, while simultaneously producing electrical energy.

Regarding the financial analysis, it can be observed that, for configurations with powers greater than 1500 kWe, there is a decrease in financial indices, from that point onwards, parallel configurations require the purchase of an additional machine, which significantly increases the initial expense, and has an impact on the performance indicators of the investment.

As previously mentioned, the eventual high electrical energy produced by electrical load following systems leads to configurations with much higher power, resulting in unnecessary thermal energy production, which would be lost, with a corresponding increase in tCO₂ emissions. Therefore, from an energy perspective, the choice of a thermal load following configuration is preferable.

5. Conclusions

This study focused on analysing the technical and financial feasibility of installing a micro-cogeneration system for a building's energy needs. The methodology involved developing a numerical model using the RETScreen Expert 8 tool to evaluate various plant setups from energy, environmental, and financial perspectives. The energy model was calibrated using one year of bills' analysis to identify average thermal and electrical loads.

Simulations were carried out to evaluate the coverage of the building's thermal and electrical consumption by varying the power of the micro-cogeneration system. The simulations considered energy savings, economic benefits, reduction in polluting emissions, and financial impact. The results showed that installing a micro-cogeneration system can lead to significant cost savings and reduction in polluting emissions, making it a viable option for meeting the building's energy demands.

The results showed that the thermal load variation was much more significant than the electrical load variation, making it useful to design the plant to follow the thermal load variation. It was found that it would be useful to design the cogenerator plant to follow the thermal load variation, as the electrical energy produced would be fully utilized. The analysis of the cogenerator performance showed that following the thermal load would lead to stable electricity production, while following the electrical load would have continuously increasing electricity production, but the recovered heat may reach values that are not necessary for the users and would be lost, making the system less efficient. Following the thermal load led to lower savings in terms of costs and energy but higher savings in terms of TOE. On the other hand, following the electrical load led to the opposite. The analysis also showed that the cogeneration system could replace traditional boilers and produce electrical energy simultaneously, resulting in significant savings. The financial analysis indicated that the maximum NPV values were obtained for configurations of 1990 and 2450 kWe for thermal load following and for the last configuration of 3300 kWe for electrical

load following. In both cases, the IRR and PI were highest for the configuration composed of a single cogenerator of higher capacity.

Overall, this study demonstrates the usefulness of using a numerical model such as RETScreen to evaluate the technical and financial feasibility of energy retrofit strategies. The findings suggest that micro-cogeneration can be an effective solution for reducing energy waste and decreasing the environmental impact of energy production, while also providing cost savings. However, further research is needed to optimize the micro-cogeneration system's performance and to investigate the long-term economic and environmental benefits of energy retrofit strategies.

Author Contributions: Conceptualization, G.B. and E.d.L.V.; methodology, G.B. and E.d.L.V.; software, G.B.; validation, G.B.; investigation, G.B.; resources, G.B., E.d.L.V. and R.d.L.V.; writing—original draft preparation, G.B., E.d.L.V., A.V. and R.d.L.V.; writing—review and editing, G.B., E.d.L.V., A.V. and R.d.L.V.; supervision, A.V. and R.d.L.V. All authors have read and agreed to the published version of the manuscript.

Funding: This research received no external funding.

Data Availability Statement: Not applicable.

Conflicts of Interest: The authors declare no conflict of interest.

References

- Dehwah, A.H.A.; Asif, M.; Rahman, M.T. Prospects of PV application in unregulated building rooftops in developing countries: A perspective from Saudi Arabia. *Energy Build.* **2018**, *171*, 76–87. [CrossRef]
- Congedo, P.M.; Baglivo, C.; D'Agostino, D.; Zacà, I. Cost-optimal design for nearly zero energy office buildings located in warm climates. *Energy* **2015**, *91*, 967–982. [CrossRef]
- D'Agostino, D.; Parker, D. A Framework for the cost-optimal design of nearly zero energy buildings (NZEBs) in representative climates across Europe. *Energy* **2018**, *149*, 814–829. [CrossRef]
- Rabani, M.; Bayera Madessa, H.; Mohseni, O.; Nord, N. Minimizing delivered energy and life cycle cost using graphical script: An Office building retrofitting case. *Appl. Energy* **2020**, *268*, 114929. [CrossRef]
- Nematchoua, M.K.; Marie-Reine Nishimwe, A.; Reiter, S. Towards nearly zero-energy residential neighbourhoods in the European Union: A case study. *Renew. Sustain. Energy Rev.* **2021**, *135*, 110198. [CrossRef]
- Mauri, L.; Vallati, A.; Ocoñ, P. Low impact energy saving strategies for individual heating systems in a modern residential building: A case study in Rome. *J. Clean. Prod.* **2019**, *214*, 791–802. [CrossRef]
- Mohammad Harmay, N.S.; Kim, D.; Choi, M. Urban heat island associated with land use/land cover and climate variations in Melbourne, Australia. *Sustain. Cities Soc.* **2021**, *69*, 102861. [CrossRef]
- Vallati, A.; Mauri, L.; Colucci, C. Impact of shortwave multiple reflections in an urban street canyon on building thermal energy demands. *Energy Build.* **2018**, *174*, 77–84. [CrossRef]
- Memon, R.A.; Leung, D.Y.C.; Liu, C.H. An investigation of urban heat island intensity (UHII) as an indicator of urban heating. *Atmos. Res.* **2009**, *94*, 491–500. [CrossRef]
- Battista, G.; Evangelisti, L.; Guattari, C.; de Lieto Vollaro, E.; de Lieto Vollaro, R.; Asdrubali, F. Urban heat island mitigation strategies: Experimental and numerical analysis of a university campus in Rome (Italy). *Sustainability* **2020**, *12*, 7971. [CrossRef]
- Li, X.; Zhou, Y.; Yu, S.; Jia, G.; Li, H.; Li, W. Urban heat island impacts on building energy consumption: A review of approaches and findings. *Energy* **2019**, *174*, 407–419. [CrossRef]
- Yang, X.; Peng, L.L.H.; Jiang, Z.; Chen, Y.; Yao, L.; He, Y.; Xu, T. Impact of urban heat island on energy demand in buildings: Local climate zones in Nanjing. *Appl. Energy* **2020**, *260*, 114279. [CrossRef]
- Kaloustian, N.; Aouad, D.; Battista, G.; Zinzi, M. Leftover spaces for the mitigation of urban overheating in Municipal Beirut. *Climate* **2018**, *6*, 68. [CrossRef]
- Larsen, M.A.D.; Petrović, S.; Radoszynski, A.M.; McKenna, R.; Balyk, O. Climate change impacts on trends and extremes in future heating and cooling demands over Europe. *Energy Build.* **2020**, *226*, 110397. [CrossRef]
- Abbassi, Y.; Ahmadikia, H.; Baniasadi, E. Prediction of pollution dispersion under urban heat island circulation for different atmospheric stratification. *Build. Environ.* **2020**, *168*, 106374. [CrossRef]
- Battista, G. Analysis of the air pollution sources in the city of Rome (Italy). *Energy Procedia* **2017**, *126*, 392–397. [CrossRef]
- Iaria, J.; Susca, T. Analytic hierarchy processes (AHP) evaluation of green roof- and green wall- based UHI mitigation strategies via ENVI-Met simulations. *Urban Clim.* **2022**, *46*, 101293. [CrossRef]
- Battista, G.; Pastore, E.M.; Mauri, L.; Basilicata, C. Green roof effects in a case study of Rome (Italy). *Energy Procedia* **2016**, *101*, 1058–1063. [CrossRef]
- Battista, G.; de Lieto Vollaro, E.; de Lieto Vollaro, R. How cool pavements and green roof affect building energy performances. *Heat Transf. Eng.* **2021**, *43*, 326–336. [CrossRef]

20. Battista, G.; Pastore, E.M. Using cool pavements to mitigate urban temperatures in a case study of Rome (Italy). *Energy Procedia* **2017**, *113*, 98–103. [CrossRef]
21. Diz-Mellado, E.; López-Cabeza, V.P.; Rivera-Gómez, C.; Roa-Fernández, J.; Galán-Marín, C. Improving school transition spaces microclimate to make them liveable in warm climates. *Appl. Sci.* **2020**, *10*, 7648. [CrossRef]
22. Aboelata, A. Vegetation in different street orientations of aspect ratio (H/W 1:1) to mitigate UHI and reduce buildings' energy in arid climate. *Build. Environ.* **2020**, *172*, 106712. [CrossRef]
23. Theeuwes, N.E.; Solcerová, A.; Steeneveld, G.J. Modeling the influence of open water surfaces on the summertime temperature and thermal comfort in the city. *J. Geophys. Res. Atmos.* **2013**, *118*, 8881–8896. [CrossRef]
24. Fahed, J.; Kinab, E.; Ginestet, S.; Adolphe, L. Impact of Urban heat island mitigation measures on microclimate and pedestrian comfort in a dense urban district of Lebanon. *Sustain. Cities Soc.* **2020**, *61*, 102375. [CrossRef]
25. Battista, G.; de Lieto Vollaro, E.; Grignaffini, S.; Ocloñ, P.; Vallati, A. Experimental investigation about the adoption of high reflectance materials on the envelope cladding on a scaled street canyon. *Energy* **2021**, *230*, 120801. [CrossRef]
26. Vollaro, A.D.L.; Galli, G.; Vallati, A.; Romagnoli, R. Analysis of Thermal field within an urban canyon with variable thermophysical characteristics of the building's walls. *J. Phys. Conf. Ser.* **2015**, *655*, 012056. [CrossRef]
27. Battista, G.; Mauri, L. Numerical study of buoyant flows in street canyon caused by ground and building heating. *Energy Procedia* **2016**, *101*, 1018–1025. [CrossRef]
28. Cornaro, C.; Puggioni, V.A.; Strollo, R.M. Dynamic simulation and on-site measurements for energy retrofit of complex historic buildings: Villa mondragone case study. *J. Build. Eng.* **2016**, *6*, 17–28. [CrossRef]
29. Rabani, M.; Bayera Madessa, H.; Nord, N. Achieving zero-energy building performance with thermal and visual comfort enhancement through optimization of fenestration, envelope, shading device, and energy supply system. *Sustain. Energy Technol. Assess.* **2021**, *44*, 101020. [CrossRef]
30. Vallati, A.; Grignaffini, S.; Romagna, M.; Mauri, L. Effects of different building automation systems on the energy consumption for three thermal insulation values of the building envelope. In Proceedings of the 2016 IEEE 16th International Conference on Environment and Electrical Engineering (EEEIC), Florence, Italy, 7–10 June 2016. [CrossRef]
31. Ali, U.; Shamsi, M.H.; Bohacek, M.; Hoare, C.; Purcell, K.; Mangina, E.; O'Donnell, J. A data-driven approach to optimize urban scale energy retrofit decisions for residential buildings. *Appl. Energy* **2020**, *267*, 114861. [CrossRef]
32. Battista, G.; de Lieto Vollaro, E.; Ocloñ, P.; de Lieto Vollaro, R. Retrofit analysis of a historical building in an architectural constrained area: A case study in Rome, Italy. *Appl. Sci.* **2022**, *12*, 12305. [CrossRef]
33. Martínez-Molina, A.; Tort-Ausina, I.; Cho, S.; Vivancos, J.L. Energy efficiency and thermal comfort in historic buildings: A review. *Renew. Sustain. Energy Rev.* **2016**, *61*, 70–85. [CrossRef]
34. Bottero, M.; D'Alpaos, C.; Oppio, A. Ranking of adaptive reuse strategies for abandoned industrial heritage in vulnerable contexts: A multiple criteria decision aiding approach. *Sustainability* **2019**, *11*, 785. [CrossRef]
35. Wu, Z.; Xu, J. Predicting and optimization of energy consumption using system dynamics-fuzzy multiple objective programming in world heritage areas. *Energy* **2013**, *49*, 19–31. [CrossRef]
36. Langston, C.; Wong, F.K.W.; Hui, E.C.M.; Shen, L.Y. Strategic assessment of building adaptive reuse opportunities in Hong Kong. *Build Environ.* **2008**, *43*, 1709–1718. [CrossRef]
37. Polo López, C.S.; Frontini, F. Energy efficiency and renewable solar energy integration in heritage historic buildings. *Energy Procedia* **2014**, *48*, 1493–1502. [CrossRef]
38. De Berardinis, P.; Rotilio, M.; Marchionni, C.; Friedman, A. Improving the energy-efficiency of historic masonry buildings. A case study: A minor centre in the Abruzzo Region, Italy. *Energy Build.* **2014**, *80*, 415–423. [CrossRef]
39. Ascione, F.; Bianco, N.; De Masi, R.F.; De' Rossi, F.; Vanoli, G.P. Energy retrofit of an educational building in the ancient center of Benevento. Feasibility study of energy savings and respect of the historical value. *Energy Build.* **2015**, *95*, 172–183. [CrossRef]
40. Alongi, A.; Scoccia, R.; Motta, M.; Mazzarella, L. Numerical investigation of the Castle of Zena energy needs and a feasibility study for the implementation of electric and gas driven heat pump. *Energy Build.* **2015**, *95*, 32–38. [CrossRef]
41. Franco, G.; Magrini, A.; Cartesegna, M.; Guerrini, M. Towards a systematic approach for energy refurbishment of historical buildings. The case study of Albergo Dei Poveri in Genoa, Italy. *Energy Build.* **2015**, *95*, 153–159. [CrossRef]
42. Ben, H.; Steemers, K. Energy retrofit and occupant behaviour in protected housing: A case study of the Brunswick Centre in London. *Energy Build.* **2014**, *80*, 120–130. [CrossRef]
43. Ascione, F.; De Rossi, F.; Vanoli, G.P. Energy retrofit of historical buildings: Theoretical and experimental investigations for the modelling of reliable performance scenarios. *Energy Build.* **2011**, *43*, 1925–1936. [CrossRef]
44. Kumbarglu, G.; Madlener, R. Evaluation of economically optimal retrofit investment options for energy savings in buildings. *Energy Build.* **2012**, *49*, 327–334. [CrossRef]
45. Amini Toosi, H.; Lavagna, M.; Leonforte, F.; Del Pero, C.; Aste, N. Life cycle sustainability assessment in building energy retrofitting: A review. *Sustain. Cities Soc.* **2020**, *60*, 102248. [CrossRef]
46. Vogel, J.A.; Lundqvist, P.; Arias, J. Categorizing barriers to energy efficiency in buildings. *Energy Procedia* **2015**, *75*, 2839–2845. [CrossRef]
47. Menassa, C.C. Evaluating sustainable retrofits in existing buildings under uncertainty. *Energy Build.* **2011**, *43*, 3576–3583. [CrossRef]

48. Jenkins, G.P.; Kuo, C.-Y.; Harberger, A.C. Cost-Benefit Analysis for Investment Decisions, Chapter 8: The Economic Opportunity Cost of Capital. JDI Executive Programs. 2011. Available online: <https://ideas.repec.org/p/qed/dpaper/201.html> (accessed on 14 June 2023).
49. Wyatt, P. *Property Evaluation in an Economic Context*; John Wiley & Sons: Hoboken, NJ, USA, 2007; p. 411.
50. Remer, D.S.; Nieto, A.P. A compendium and comparison of 25 project evaluation techniques. Part 1: Net present value and rate of return methods. *Int. J. Prod. Econ.* **1995**, *42*, 79–96. [CrossRef]
51. Gabrielli, L.; Ruggeri, A.G. Developing a model for energy retrofit in large building portfolios: Energy assessment, optimization and uncertainty. *Energy Build.* **2019**, *202*, 109356. [CrossRef]
52. De Angelis, E.; Pansa, G.; Serra, E. Research of economic sustainability of different energy refurbishment strategies for an apartment block building. *Energy Procedia* **2014**, *48*, 1449–1458. [CrossRef]
53. Copiello, S.; Gabrielli, L.; Bonifaci, P. Evaluation of energy retrofit in buildings under conditions of uncertainty: The prominence of the discount rate. *Energy* **2017**, *137*, 104–117. [CrossRef]
54. Tadeu, S.; Rodrigues, C.; Tadeu, A.; Freire, F.; Simões, N. Energy retrofit of historic buildings: Environmental assessment of cost-optimal solutions. *J. Build. Eng.* **2015**, *4*, 167–176. [CrossRef]
55. Kneifel, J. Life-cycle carbon and cost analysis of energy efficiency measures in new commercial buildings. *Energy Build.* **2010**, *42*, 333–340. [CrossRef]
56. Fregonara, E.; Lo Verso, V.R.M.; Lisa, M.; Callegari, G. Retrofit scenarios and economic sustainability. A case-study in the Italian context. *Energy Procedia* **2017**, *111*, 245–255. [CrossRef]
57. Sharif, S.A.; Hammad, A. Simulation-based multi-objective optimization of institutional building renovation considering energy consumption, life-cycle cost and life-cycle assessment. *J. Build. Eng.* **2019**, *21*, 429–445. [CrossRef]
58. Sartori, D.; Gelsomina, C.; Genco, M.; Pancotti, C.; Sirtori, E.; Vignetti, S.; Del Bo, C. *Guide to Cost-Benefit Analysis of Investment Projects*; European Union: Luxembourg, 2014. [CrossRef]
59. Liu, Y.; Liu, T.; Ye, S.; Liu, Y. Cost-benefit analysis for energy efficiency retrofit of existing buildings: A case study in China. *J. Clean. Prod.* **2018**, *177*, 493–506. [CrossRef]
60. Zavadskas, E.K.; Kaklauskas, A.; Raslanas, S. Evaluation of investments into housing renovation. *Int. J. Strateg. Prop. Manag.* **2004**, *8*, 177–190. [CrossRef]
61. Friedman, C.; Becker, N.; Erell, E. Energy retrofit of residential building envelopes in Israel: A cost-benefit analysis. *Energy* **2014**, *77*, 183–193. [CrossRef]
62. Zhao, S.; Feng, W.; Zhang, S.; Hou, J.; Zhou, N.; Levine, M. Energy savings and cost-benefit analysis of the new commercial building standard in China. *Procedia Eng.* **2015**, *121*, 317–324. [CrossRef]
63. Gabay, H.; Meir, I.A.; Schwartz, M.; Werzberger, E. Cost-benefit analysis of green buildings: An Israeli office buildings case study. *Energy Build.* **2014**, *76*, 558–564. [CrossRef]
64. Memon, A.G.; Memon, R.A. Parametric based economic analysis of a trigeneration system proposed for residential buildings. *Sustain. Cities Soc.* **2017**, *34*, 144–158. [CrossRef]
65. Jradi, M.; Riffat, S. Tri-generation systems: Energy policies, prime movers, cooling technologies, configurations and operation strategies. *Renew. Sustain. Energy Rev.* **2014**, *32*, 396–415. [CrossRef]
66. Kerr, T. *Combined Heat and Power: Evaluating the Benefits of Greater Global Investment*; International Energy Agency: Washington, DC, USA, 2008.
67. Relazione Annuale sulla Cogenerazione in Italia. Available online: https://www.mimit.gov.it/images/stories/documenti/IT_-_Relazione_annuale_CAR_2020.pdf (accessed on 14 June 2023).
68. Il Presente e Il Futuro della Cogenerazione in Italia. Available online: <https://industriale.viessmann.it/blog/presente-e-futuro-cogenerazione-italia> (accessed on 4 December 2022).
69. RETScreen. Available online: <https://www.nrcan.gc.ca/maps-tools-and-publications/tools/modelling-tools/retscreen/7465> (accessed on 19 June 2022).
70. Lee, K.H.; Lee, D.W.; Baek, N.C.; Kwon, H.M.; Lee, C.J. Preliminary determination of optimal size for renewable energy resources in buildings using RETScreen. *Energy* **2012**, *47*, 83–96. [CrossRef]
71. ARERA—Aggiornamento del Fattore di Conversione dei KWh in Tonnellate Equivalenti di Petrolio Connesso al Meccanismo dei Titoli di Efficienza Energetica. Available online: <https://www.arera.it/it/docs/08/003-08een.htm> (accessed on 14 June 2023).
72. Gazzetta Ufficiale. Available online: https://www.gazzettaufficiale.it/atto/serie_generale/caricaDettaglioAtto/originario?atto.dataPubblicazioneGazzetta=2014-04-07&atto.codiceRedazionale=14G00069&elenco30giorni=false (accessed on 14 June 2023).
73. Indicatori Di Efficienza e Decarbonizzazione Del Sistema Energetico Nazionale e Del Settore Elettrico—Italiano. Available online: <https://www.isprambiente.gov.it/it/pubblicazioni/rapporti/indicatori-di-efficienza-e-decarbonizzazione-del-sistema-energetico-nazionale-e-del-settore-elettrico> (accessed on 14 June 2023).
74. Kenneth, K.H. *Jelen's Cost and Optimization Engineering*; McGraw-Hill: New York, NY, USA, 1991; Volume 386.

Disclaimer/Publisher's Note: The statements, opinions and data contained in all publications are solely those of the individual author(s) and contributor(s) and not of MDPI and/or the editor(s). MDPI and/or the editor(s) disclaim responsibility for any injury to people or property resulting from any ideas, methods, instructions or products referred to in the content.

Article

Evaluation of Building Mass Characterization for Energy Flexibility through Rule- and Schedule-Based Control: A Statistical Approach

Joscha Reber *, Xenia Kirschstein and Nadja Bishara

Institute of Structural Mechanics and Design, Department of Civil and Environmental Engineering, Technical University of Darmstadt, 64287 Darmstadt, Germany

* Correspondence: reber@ismd.tu-darmstadt.de

Abstract: As renewables become more established in the electricity grid, the focus, and therefore adaptability, will need to shift from the generation side to the demand side. Since the building sector accounts for a large share of the energy demand, it will be strongly affected by this development. One possibility for adaptation is so-called demand side management (DSM). To assess the contribution of the building sector to energy flexibility, some key performance indicators (KPIs) have already been developed in previous work. In this study, we investigate and statistically compare two control strategies for temporarily raising the room temperature—one rule-based and one schedule-based—with regard to their influence on the characterization of the building mass as a type of thermal energy storage. In each case, we determine the thermal energy demand of a residential district based on a dynamic simulation that occurred for a period of one year. The rule-based control assigns in the median approximately 60% (mean: 41%) less capacity to the building mass than the schedule-based control for the same boundary conditions. The calculation of the time-independent heating load results in a median difference of 34% (mean: 36%). In addition, the establishment of energy-flexible control in the evening hours just before a night-time reduction in the room temperature has a negative impact on the efficiency of the thermal storage.

Keywords: energy flexibility; active demand response; thermal storage; buildings labeling

Citation: Reber, J.; Kirschstein, X.; Bishara, N. Evaluation of Building Mass Characterization for Energy Flexibility through Rule- and Schedule-Based Control: A Statistical Approach. *Energies* **2023**, *16*, 6878. <https://doi.org/10.3390/en16196878>

Academic Editors: Ala Hasan and Hassam Ur Rehman

Received: 28 August 2023

Revised: 21 September 2023

Accepted: 25 September 2023

Published: 29 September 2023



Copyright: © 2023 by the authors. Licensee MDPI, Basel, Switzerland. This article is an open access article distributed under the terms and conditions of the Creative Commons Attribution (CC BY) license (<https://creativecommons.org/licenses/by/4.0/>).

1. Introduction

As part of the energy transition, the German government has committed itself to achieving greenhouse gas neutrality by 2045 [1]. This also applies to the national electricity grid, which means that an accelerated expansion of renewable energies is being promoted. Weather-dependent and therefore fluctuating power sources such as wind and solar power require a trend reversal in energy systems [2,3]. Storage technologies can already be used to transfer energy surpluses in times of energy shortages and thus partially cover demand and stabilize the electrical grid [4]. However, the focus and adaptability will have to shift from electricity generation to the demand side to avoid grid overloads. It will be necessary to adjust the energy demand to compensate for surpluses and shortages in energy supply [5,6]. Given that the building sector accounts for 40% of total energy consumption worldwide [7], there is significant potential for future energy systems to achieve a higher share of renewability and energy flexibility on the demand-side [8]. The implementation of energy flexibility in buildings has also already found its way into EU directives. The 2018 revision of the energy performance of buildings directive (EPBD) highlights the importance of energy flexibility in buildings and introduces the Smart Readiness Indicator (SRI) to assess a building's ability to adapt its operation to the needs of the occupants and the requirements of the grid, and goes beyond a mere energy label [9]. The International Energy Agency's (IEA) Energy in Buildings and Communities Program (EBC) Annex 67 has focused more generally on defining energy flexibility in buildings [10]. This includes

the effective management of both demand and generation to match local climate conditions, user preferences, and energy grid requirements.

Within this domain, demand side management (DSM) offers a wide range of methods to influence electricity demand patterns. These methods include reduction (peak shaving, conservation), increases (valley filling, load growth), and rescheduling (load shifting) in electrical loads [11,12]. The term demand response (DR) includes all of the measures that are not categorized within energy efficiency [13], as shown in Figure 1. In practice, DR strategies can be implemented through active demand response (ADR), which employs short-term load management tactics [14]. The goal of ADR is to meet day-ahead load curve constraints by adjusting the daily schedule based on factors such as user behavior, weather conditions, and energy market prices.

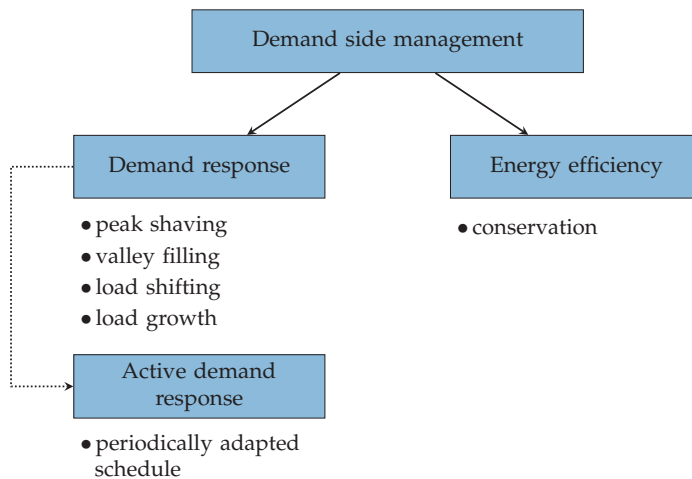


Figure 1. Classification of demand side management, adapted from [11,13,14].

To create a financial incentive for consumers to participate in ADR measures on DSM, a control signal can be implemented through a dynamic price tariff, which may be based on the electricity market price or locally generated energy as described by Lauro et al. [14], Arteconi et al. [15], Arteconi and Polonara [16], de Coninck and Helsen [17] and Luc et al. [18]. In Germany, the Act to Restart the Digitization of the Energy Transition came into force in May 2023, obliging electricity providers to include dynamic electricity prices in their portfolios by 2025, paving the way for energy-flexible applications [19]. Examples of common household electrical appliances suitable for ADR include time-controlled appliances such as washing machines and dishwashers, and thermostatically controlled appliances such as heat pumps or boilers [20], which are essential for space heating and domestic hot water production. In particular, the inherent thermal inertia of the building mass [21], which is often present anyway, and/or additional thermal energy storage (TES) [22] can contribute to load shifting in combination with heat pumps: the thermal storage systems allow short- to medium-term changes in the load pattern without compromising indoor comfort. The floor heating system used at low supply temperatures contributes to active thermal storage systems and thus represents a possibility for the implementation of thermally activated building structures (TABS) [15].

Developing a methodology to assess and quantify the energy flexibility of buildings is a crucial challenge when it comes to recognizing their active role in future energy networks [23]. Several approaches have already been introduced in the literature and presented in the form of key performance indicators (KPIs), considering different aspects. According to Li et al. [24] the top five popular energy flexibility metrics are Peak Power reduction [25], the Flexibility Factor [26], Self-Sufficiency and Self-Consumption [27], the Ca-

capacity and the Efficiency of ADR [28] and the Flexibility Index [29]. The method presented by Reynders et al. [28] does not directly consider monetary savings from an optimized DSM, but is dedicated to quantifying the building mass as a storage option during an ADR. For this purpose, the setpoint temperature in the heated spaces is increased for a certain time and the thermal energy stored in the activated building mass is evaluated [18,26,30]. The increase in the setpoint temperature can be controlled by a fixed schedule or according to certain rules via an external signal, such as the electricity market price [16,18,31,32]. The factors influencing thermal capacity and efficiency in terms of ADR have been studied several times, e.g., by Vivian et al. [33], comparing different building ages and insulation thicknesses. Foteinaki et al. [32] further developed different signal scenarios and investigated flexible peak load and cost reduction in residential buildings. However, we are not aware of any research that statistically quantifies the storage capacity and storage efficiency of building mass over the term of one year, comparing the different results for control strategies, namely rule-based and schedule-based strategies.

In this study, we determine the storage capacity and efficiency of ADR of a newly planned residential district in Darmstadt, Germany, by means of a dynamic building simulation including energy flexible control, according to Reynders et al. [28]. The novelty lies in the statistical comparison of two different energy flexible control signals, namely rule-based and schedule-based signals, and their effect on the characterization of the building mass in terms of its ability to provide an electrical grid serving behavior.

In Section 2, the method used to quantify the building mass, the control options, the statistical evaluation, and the building simulation model is presented. In Section 3 the duration, the additional heat demand and the additional heating load of the two control strategies, both rule-based and schedule-based, are calculated with the building simulation. First, an analysis without night-time reduction in the room temperature is carried out, followed by the more realistic case that includes night-time reduction. In Section 4, we discuss the results of the different control strategies and the main conclusions are drawn.

2. Materials and Methods

2.1. Energy Flexibility Event

In this study, the active demand response (ADR) strategy for the inherent thermal inertia of the building mass is achieved by temporarily raising the setpoint room temperature to the upper limit of a temperature comfort band. The permitted range is defined from $T_{low} = 20.5 \text{ }^\circ\text{C}$ to $T_{up} = 22 \text{ }^\circ\text{C}$, in accordance with other publications such as Arteconi et al. [31]. This enables an additional heat input into the building mass, which is activated by the floor heating system. The resulting upward process of the room temperature compared to a reference control that maintains the lower limit T_{low} of the comfort band is defined below as an up event and can usually be divided into three phases, as shown in Figure 2, and is used by several other authors [32,34]:

- Charge: compared to the lower limit of the comfort temperature T_{low} , the increase in the setpoint temperature to T_{up} leads to an increased heating load and, accordingly, the building mass is charged with thermal energy.
- Steady state: the raised setpoint temperature T_{up} is reached and only the increased transmission heat losses are additionally compensated compared to the reference state with the continuous lower setpoint temperature T_{low} .
- Discharge: the reset of the setpoint temperature to T_{low} leads to a decreased heating load compared to the reference state and, accordingly, the building mass is discharged

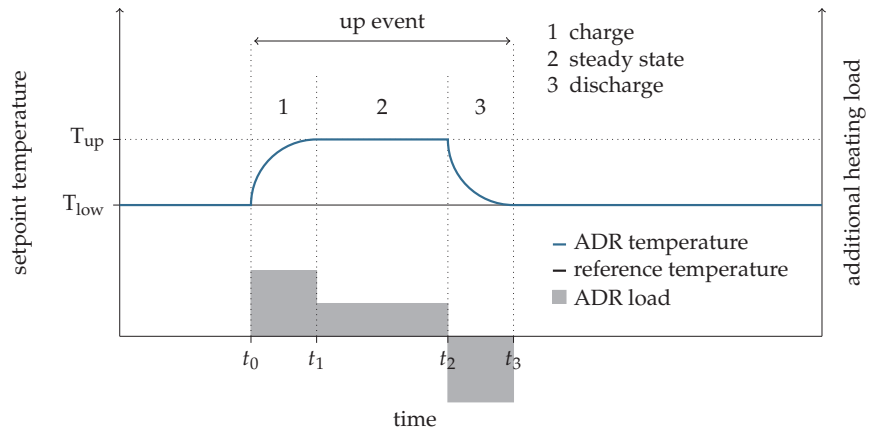


Figure 2. Concept of an up event as an active demand response strategy, including the three defining phases (charge, steady state, discharge).

A temporary decrease in the setpoint temperature, referred to as a downward event, is also possible for energy flexibility purposes, but is not investigated further in this work. The properties of the respective phases, such as duration t , amount of added heat Q and heating load P , can be derived from the following equations, where “up” denotes the case with and “ref” the case without ADR:

$$t_{\text{charge}} = t_1 - t_0 \tag{1}$$

$$t_{\text{steady state}} = t_2 - t_1 \tag{2}$$

$$t_{\text{discharge}} = t_3 - t_2 \tag{3}$$

$$Q_{\text{charge}} = \int_{t_0}^{t_1} (P_{\text{up}} - P_{\text{ref}}) dt \tag{4}$$

$$Q_{\text{steady state}} = \int_{t_1}^{t_2} (P_{\text{up}} - P_{\text{ref}}) dt \tag{5}$$

$$Q_{\text{discharge}} = \int_{t_2}^{t_3} (P_{\text{up}} - P_{\text{ref}}) dt \tag{6}$$

$$P_{\text{charge}} = \frac{Q_{\text{charge}}}{t_{\text{charge}}} \tag{7}$$

$$P_{\text{steady state}} = \frac{Q_{\text{steady state}}}{t_{\text{steady state}}} \tag{8}$$

$$P_{\text{discharge}} = \frac{Q_{\text{discharge}}}{t_{\text{discharge}}} \tag{9}$$

2.2. Capacity and Efficiency of ADR through Up Events

According to Reynders et al. [28], the characteristics of the activated building mass can be derived from the three phases of an up event. The amount of additional heat required in the charge phase represents the storage capacity C_{ADR} in an energy flexibility event enabled by ADR (Equation (10)). In addition to the actual building mass, the control-related setpoint temperatures (T_{low} and T_{up}) also have a significant influence. It is therefore important to ensure that the same boundary conditions are used in all studies. Furthermore, the charge

phase must be clearly distinguished from the steady state phase to avoid incorrectly assigning the increased transmission heat losses to the storage capacity. Reynders et al. [28] did not make this distinction due to relatively short steady state phases.

$$C_{ADR} = Q_{\text{charge}} \quad (10)$$

$$\eta_{\text{charge/discharge}} = \frac{|Q_{\text{discharge}}|}{Q_{\text{charge}}} \quad (11)$$

$$\eta_{\text{up}} = \frac{|Q_{\text{discharge}}|}{Q_{\text{charge}} + Q_{\text{steady state}}} \quad (12)$$

The efficiency of the up event or thermal storage in the energy-flexible control can also be determined from the three phases. This allows a comparison with conventional storage technologies and represents the basis for an economic evaluation; for example, with dynamic electricity prices. To identify the influence of the higher transmission heat losses when maintaining the increased setpoint temperature, the storage efficiency η is calculated in this study both with (Equation (11)) and without (Equation (12)) the steady state phase.

2.3. Implementation of Control Strategies

The energy flexible control is implemented in two ways: rule-based and schedule-based, as shown in Figure 3. The rule-based control uses a signal that increases the setpoint temperature from $T_{\text{low}} = 20.5 \text{ }^{\circ}\text{C}$ to $T_{\text{up}} = 22 \text{ }^{\circ}\text{C}$ when prices are favorable, depending on the electricity market. For this purpose, spot market electricity prices from 2021 in Germany are selected at an hourly resolution and the lower quantile is calculated monthly as described by Foteinaki et al. [32]. If the price falls below the quantile, the setpoint temperature is increased. Accordingly, there are shorter and longer energy flexibility events. The schedule-based variant is characterized by a fixed period per day in which the setpoint temperature is increased from $20.5 \text{ }^{\circ}\text{C}$ to $22 \text{ }^{\circ}\text{C}$, as described in many publications [30,31]. In this study, the approximate mean duration of the rule-based control events of 2.5 h, taking into account a night-time reduction in the temperature, is used to set the duration of the schedule-based control and to ensure comparability. The afternoon from 2 pm to 4.30 pm is the time period chosen to precondition the building mass for the evening hours, as it means that tenants do not need to turn on the heating system when coming home from work.

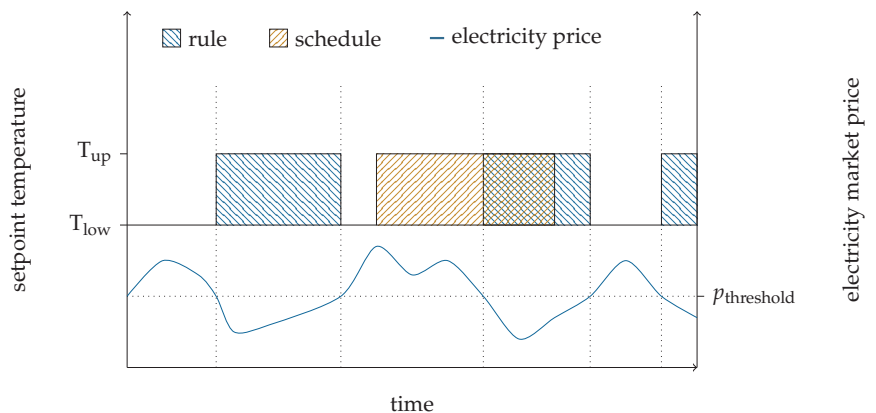


Figure 3. Concept of rule- and schedule-based control for the implementation of up events.

2.4. Identification of Phases in Up Events

To separate the phases of all up events from one another, rules are required that identify each of them properly. However, fluctuations in room temperature due to external influences complicate this process and lead to misidentification of some energy flows. For example, a room temperature fluctuating around the increased setpoint temperature due to a hysteresis control should be assigned to a single steady state phase and not to many shorter charge and discharge phases. The rules for determining the current phase i in each time step are implemented as follows, where T_{air} represents the simulated room temperature with and $T_{\text{air,ref}}$ without energy flexible control:

$$i_{\text{charge}}(T_{\text{set}}, T_{\text{air}}) = \begin{cases} 1, & \text{if } (T_{\text{set}} = T_{\text{up}} \wedge T_{\text{air}} < T_{\text{up}} - 0.25) \\ 0, & \text{otherwise} \end{cases} \quad (13)$$

$$i_{\text{steady state}}(T_{\text{set}}, T_{\text{air}}) = \begin{cases} 1, & \text{if } (T_{\text{set}} = T_{\text{up}} \wedge T_{\text{air}} \geq T_{\text{up}} - 0.25 \wedge T_{\text{air}} < T_{\text{up}} + 0.1) \\ 0, & \text{otherwise} \end{cases} \quad (14)$$

$$i_{\text{discharge}}(T_{\text{set}}, T_{\text{air}}, T_{\text{air,ref}}) = \begin{cases} 1, & \text{if } (T_{\text{set}} \leq T_{\text{low}} \wedge T_{\text{air}} < T_{\text{up}} - 0.25 \wedge T_{\text{air}} > T_{\text{air,ref}} + 0.055) \\ & \vee (T_{\text{set}} = T_{\text{low}} \wedge T_{\text{air}} \leq T_{\text{low}} \wedge T_{\text{air}} > T_{\text{air,ref}} + 0.055) \\ 0, & \text{otherwise} \end{cases} \quad (15)$$

The identification of the discharge phase $i_{\text{discharge}}$ refers to the temperature decrease to the lower comfort temperature T_{low} , as well as to the heating up in the morning after a night-time reduction. If the discharge phase occurs during the night-time reduction, no energy can be saved compared to the reference state, but a higher initial temperature can be assumed in the morning. The discharge phase can therefore also take place during active heating. To verify the correct identification of the individual phases using the method described above, the overall efficiency $\eta_{\text{up,tot}}$ of all up events (Equation (16)) is alternatively calculated by simply comparing the simulation with up events to the reference simulation without up events (Equation (17)).

$$\eta_{\text{up,tot}} = \frac{|\sum_{j=1}^n Q_{\text{discharge},j}|}{\sum_{j=1}^m Q_{\text{charge},j} + \sum_{j=1}^p Q_{\text{steady state},j}} \quad (16)$$

$$\eta_{\text{up,alt}} = \frac{|\int_0^{t=1a} (P_{\text{up}} - P_{\text{ref}})^- dt|}{\int_0^{t=1a} (P_{\text{up}} - P_{\text{ref}})^+ dt} \quad (17)$$

2.5. Statistical Evaluation

Depending on the type of energy flexible control, e.g., rule-based or schedule-based, up events will always occur at the same time or be distributed throughout the day. External boundary conditions such as solar radiation, ambient temperature and internal heat gains ensure that every up event is unique. In order to obtain a representative capacity and efficiency for the characterization of the building mass by the rule-based and schedule-based control, we perform a simulation over a whole year and statistically evaluate the up events in the heating period. As the generated data are not necessarily normally distributed, the median is calculated in addition to the mean to compare the control strategies. However, since the size of the data sets (rule-based and schedule-based) is limited by the simulation duration and the time steps, it must also be determined whether they are statistically suitable for comparison at all.

The Brunner–Munzel test [35] can be used for non-normally distributed data sets to test whether there is a stochastic difference between two sets. The null hypothesis, which is the statement being tested, is that there is no significant difference (in terms of central tendency) between the two sets of data, rule-based and schedule-based. A probability of

$p \leq 0.05$ is considered significant and means that it is safe to assume that there is indeed a difference between the two sets and, therefore, a valid comparison of the means and medians is possible. However, a p -value greater than 0.05 does not mean that the two sets are stochastically equal. The data quality is simply not good enough to interpret the observed direction. In the box plots, the following annotation is selected to indicate a significant difference that allows comparability:

- $p > 0.05$: ns (not significant)
- $p \leq 0.05$: * (significant)
- $p \leq 0.01$: ** (significant)
- $p \leq 0.001$: *** (significant)
- $p \leq 0.0001$: **** (significant)

2.6. Building Energy Simulation and Boundary Conditions

The subject of the study is a new high-energy-standard residential district planned in Darmstadt, Germany, consisting of eight multi-family buildings with a total of 140 residential units, to be completed in 2025. Three decentralized water-to-water heat pumps connected to a central borehole heat exchanger field provide the heat supply. We implemented a detailed model of the building energy system using the simulation software Trnsys18. Trnsys is a graphical software environment used to simulate the behaviour of transient systems [36], based on the Fortran programming language. There are other tools for dynamic building simulations available, such as EnergyPlus [37], IDA ICE [38] or Modelica [39]. Despite different levels of detail and focus, the simulation tools show good agreement in the results for the calculation of energy demand [40]. In this study, the energy supply system is not considered; instead, a constant supply temperature of the floor heating system of 40 °C is assumed, as only the building mass is to be evaluated. To reduce complexity, the individual apartments were grouped floor by floor into one thermal zone each, which proved to be a good compromise between simulation speed and accuracy [41,42]. The statistical investigation of the individual phases as well as the storage capacity is carried out as an example on the second floor of the northeastern building, as shown in Figure 4, to limit the scope within this study, while the storage efficiency is calculated for all floors of all buildings due to the reasons mentioned in Section 2.4. The building simulation also contains the basements, which are not actively heated and are therefore not part of the energy-flexible control.

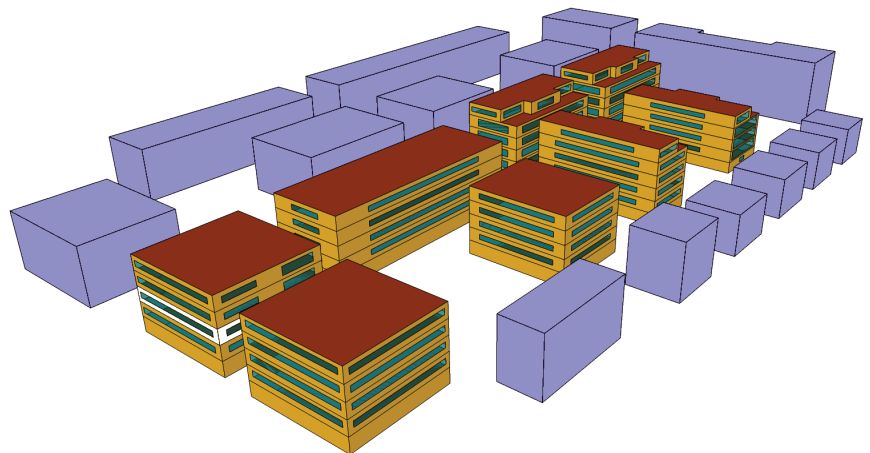


Figure 4. Building model of the district. The white marked floor is used for a detailed investigation of the storage capacity (NW view).

The boundary conditions of the simulation model are defined to correspond to the aforementioned district in Darmstadt, Germany. For the weather data, the test reference year 2015 of dwd is chosen, which also considers solar radiation. The internal heat sources and the minimum air exchange rate are selected according to the user boundary conditions of DIN V 18599 [43]. All boundary conditions are listed in Table 1. The annual space heating demand, determined using the dynamic simulation with time steps of one minute, is $23.22 \text{ kWh}\cdot\text{m}^{-2}\cdot\text{a}^{-1}$ for the described district section.

Table 1. Boundary conditions and properties for the building simulation.

Category	Property	Attribute
Building	Location	64285 Darmstadt, Germany
	Number of buildings	8
	Floor area	9827 m ²
	U-value wall	0.118–0.151 W·m ⁻² ·K ⁻¹
	U-value roof	0.078–0.104 W·m ⁻² ·K ⁻¹
	U-value ground floor	0.157–0.193 W·m ⁻² ·K ⁻¹
	U-value window	0.78 W·m ⁻² ·K ⁻¹
	Thermal bridges	0.03 W·m ⁻² ·K ⁻¹
	Screed thickness	0.065 m
Relative heated floor area	≈75%	
Simulation	Simulation time	8760 h
	Time step	1 min
	Heating set temperature	20.5 °C
	Night-time reduction	11 pm–6 am
	Night-time	18.5 °C
	Weather data	TRY 2015 for Darmstadt
	Heating season	30 September–30 April
	Air exchange rate	0.44 h ⁻¹
	Internal gains	90 Wh·m ⁻² ·d ⁻¹
	Supply temperature	40 °C
Heat demand	23.22 kWh·m ⁻² ·a ⁻¹	
Energy flexibility	Up event set temperature	22 °C
	Electricity price data	Spot market Germany 2021
	Schedule-based control	2 pm–4.30 pm
	Rule-based control	External price signal

3. Results

In this section, we evaluate and compare the properties of the up events, i.e., raising the setpoint temperature from 20.5 °C to 22 °C in schedule-based and rule-based control. The thermal simulation is carried out once with and once without night-time reduction in the room temperature. The focus is on the statistical distribution of the individual phases in the up events in terms of their duration and stored thermal energy over a whole year. Subsequently, we calculate the storage capacity and the storage efficiency for both control strategies according to Reynders et al. [34]. The methodology for the statistical study of the phases is performed for a selected zone to limit the scope within this study. The comparison of annual efficiencies includes all floors of all buildings.

3.1. Statistical Evaluation of Up Events with Schedule-Based and Rule-Based Control without Night-Time Reduction

Over a simulation period of one year, a total of 163 triggered up events are identified in the heating season using the rule-based control and 116 up events are identified in the schedule-based control. However, a triggered up event does not necessarily lead to the occurrence of all phases: charge, steady state and discharge. These depend in particular on the duration and the prevailing room temperature. For example, if the room temperature is in the upper range of the comfort band due to solar gain or prior up events,

the probability of the occurrence of steady state phases increases. In addition, the phase identification algorithm is designed so that there is a difference in the heating load compared to the reference control. This prevents phases from being incorrectly assigned based on solar gains.

The temporal distribution of the charge, steady state and discharge phases in the rule-based and schedule-based controls over one year is shown in Figure 5a. The notation ns stands for “not significant” and therefore no statement about the stochastic differences between the two data sets is possible. If not specified otherwise, the value of the rule-based control is always given first when listing medians or means. The median of the duration of the charge events in the rule-based control is 1.88 h (mean: 2.20 h). The median of the duration in the schedule-based control is 2.47 h (mean: 2.01 h), which corresponds to 2.5 h due to the predefined increase in setpoint temperature. However, when using the Brunner–Munzel test, no significant difference is found between the two sets of data, so the difference in duration cannot be statistically confirmed. The discharge phases of the rule-based control (median: 5.04 h) are also shorter than those of the schedule-based control (median: 6.06 h), as charge phases are repeatedly inserted due to volatile electricity prices. In general, the discharge times are about 2.5 times longer than the charge times, which can be explained by the high insulation standard. This has a positive effect on the potential to avoid periods of high electricity prices. The steady state phase, i.e., reaching and maintaining the increased setpoint temperature, is only maintained for a short time in the rule-based and schedule-based control strategy (median: 1.02/0.69 h).

The statistical distribution of charged and discharged heat per event is shown in Figure 5b. The median of the additional heat transferred per charge phase is $0.023 \text{ kWh}\cdot\text{m}^{-2}$ (mean: $0.029 \text{ kWh}\cdot\text{m}^{-2}$) in the rule-based control and $0.058 \text{ kWh}\cdot\text{m}^{-2}$ (mean: $0.049 \text{ kWh}\cdot\text{m}^{-2}$) in the schedule-based control. In comparison, the medians of the heat saved in the discharge phases are $-0.022 \text{ kWh}\cdot\text{m}^{-2}$ and $-0.043 \text{ kWh}\cdot\text{m}^{-2}$ (not significant according to Brunner–Munzel).

The heating load per phase in the up events is derived from the duration of the events and the transferred heat, which is shown in Figure 5c. The rule-based control has lower additional heating loads in the charge phase than the schedule-based control (median: $16.53/25.11 \text{ W}\cdot\text{m}^{-2}$), but reduces the heating load more in the discharge phase (median: $-6.34/-5.33 \text{ W}\cdot\text{m}^{-2}$). In the steady state phase, both control strategies require an additional heating load to compensate for the higher transmission heat losses (median: $4.29/6.39 \text{ W}\cdot\text{m}^{-2}$).

According to Reynders’ approach [28], the charged heat of an event corresponds to the flexible storage capacity of the building mass. This is largely dependent on the setpoint temperature or the temperature achieved per event. In contrast to Reynders, we considered the charge phase independently from the steady state phase. In the rule-based control, the median of the additional heat demand is only 39.7% of the median in the schedule-based variant. This implies that $0.023 \text{ kWh}\cdot\text{m}^{-2}$ (mean: $0.029 \text{ kWh}\cdot\text{m}^{-2}$) or $0.058 \text{ kWh}\cdot\text{m}^{-2}$ (mean: $0.049 \text{ kWh}\cdot\text{m}^{-2}$) of energy per flexibility event can be stored in the activated building mass.

Similarly, the efficiency of the building mass as a thermal storage site can also be calculated from the ratio of the respective heat transfer in the charge and discharge phases, as shown in Section 2.2. The storage efficiencies with and without consideration of the steady state phases in the rule-based and schedule-based control of all floors and houses are shown in Figure 5d. The storage efficiency without consideration of the steady state phases achieves similarly high values in both control strategies (median: 0.92/0.94, mean: 0.93/0.92). According to the Brunner–Munzel test, there is no statistically significant difference between the efficiency distributions. When the steady state phases and the associated higher transmission heat losses are included, it is noticeable that the overall storage efficiency decreases, especially for the rule-based control (median: 0.78/0.91, mean: 0.77/0.89). The steady state phase, as described above, does not contribute to the stored energy, and therefore cannot achieve higher savings in the discharge phase.

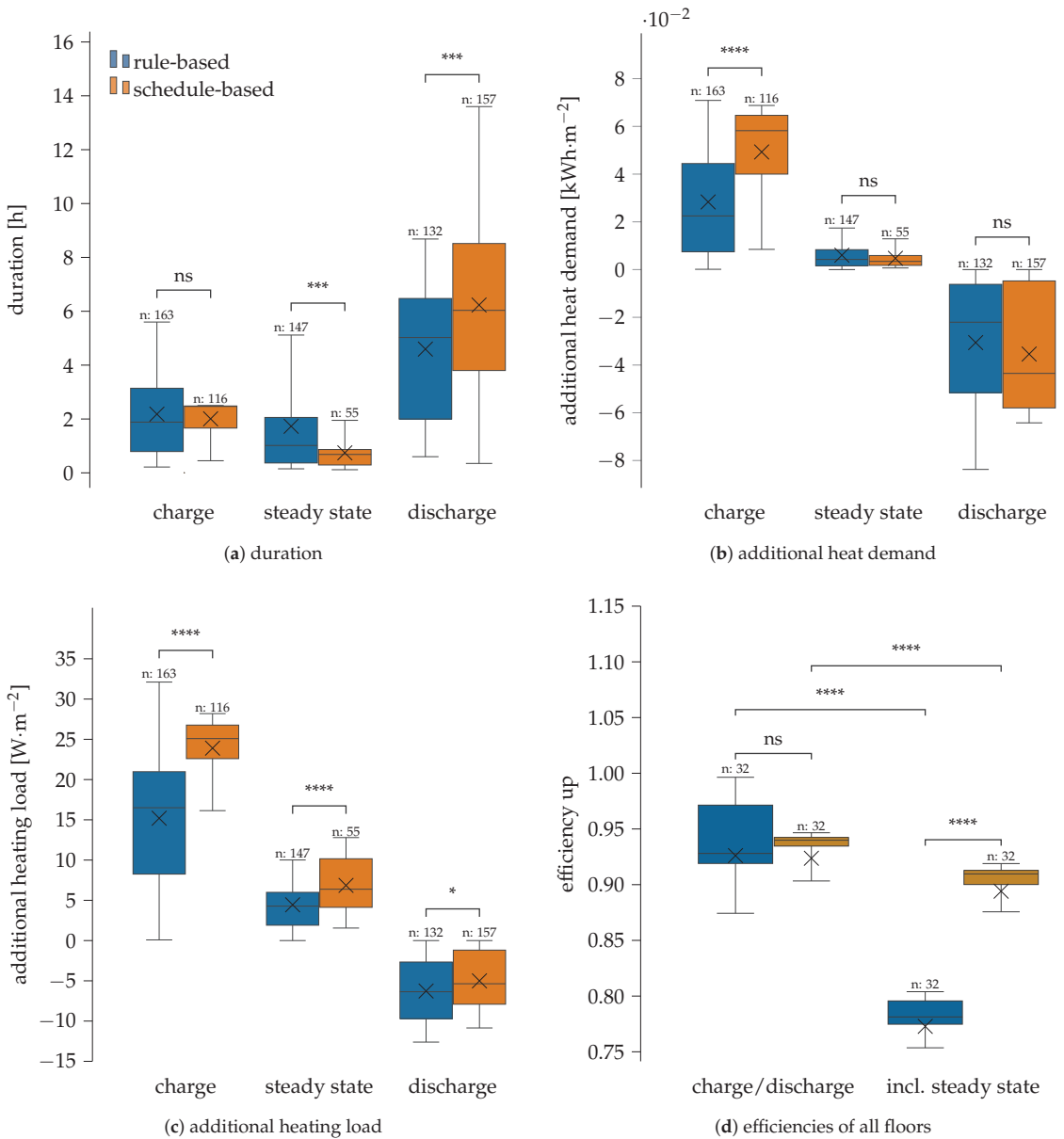


Figure 5. Statistical evaluation of charge, steady state and discharge phases over one year. Brunner-Munzel test p -values indicate statistical significance (* $p \leq 0.05$, *** $p \leq 0.001$, **** $p \leq 0.0001$), ns: no significance.

3.2. Statistical Evaluation of Up Events with Schedule-Based and Rule-Based Control with Night-Time Reduction

The following results for rule-based and schedule-based control refer to a simulation period of one year and, accordingly, one heating period as well, but now consider the more realistic night-time reduction in the setpoint temperature in the heating period to 18.5 °C. In addition to the total annual energy demand, the night-time reduction has an

influence on the previously listed characteristics of the up events. As stated previously, the schedule-based control includes a daily increase in the setpoint temperature for 2.5 h from 2 pm to 4.30 pm.

The duration of all charge, steady state and discharge phases in the rule-based and schedule-based control is shown in Figure 6a. Compared to the temperature control without night-time reduction (Figure 5a), the charge (median: 1.99/2.47 h, mean: 2.32/2.04 h—ns) and steady state phases (median: 1.10 / 0.60 h, mean: 1.75/0.69 h) with night-time reduction have similar values. The slight increase during the regulated charge phase can be explained by the lower average room temperatures due to the night-time reduction. In the discharge phase, the rule-based control results in higher values (median: 6.03 h), as the events just before the night-time reduction can be extended.

For the determination of the additional heat demand (Figure 6b), the rule-based control again shows differences compared to the investigation without night-time reduction, especially in the charge (median: $0.007 \text{ kWh}\cdot\text{m}^{-2}$, mean: $0.014 \text{ kWh}\cdot\text{m}^{-2}$) and discharge phase (median: $\approx 0 \text{ kWh}\cdot\text{m}^{-2}$, mean: $-0.010 \text{ kWh}\cdot\text{m}^{-2}$). As the night-time reduction creates natural discharge phases in the reference control, there are several discharge phases in the rule-based control that show little or no energy savings compared to the reference. The schedule-based control has similar values in the charge phase (median: $0.052 \text{ kWh}\cdot\text{m}^{-2}$, mean: $0.046 \text{ kWh}\cdot\text{m}^{-2}$) and discharge phase (median: $-0.035 \text{ kWh}\cdot\text{m}^{-2}$, mean: $-0.029 \text{ kWh}\cdot\text{m}^{-2}$) to the control without night-time reduction due to the up events in the midday to afternoon period.

The differences to the control without night-time reduction can also be seen in the additional heating load (Figure 6c), especially in the rule-based control in the charge phase (median: $4.42 \text{ W}\cdot\text{m}^{-2}$) and the discharge phase (median: $\approx 0 \text{ W}\cdot\text{m}^{-2}$, mean: $-2.27 \text{ W}\cdot\text{m}^{-2}$). Schedule-based control is less affected and results in $23.83 \text{ W}\cdot\text{m}^{-2}$ in the charge phase and $-3.28 \text{ W}\cdot\text{m}^{-2}$ in the discharge phase. As described above, the storage capacity of the building mass for flexibility events can be derived from the additional heat demand (Figure 6b) according to Reynders' approach. For the rule-based control, the median capacity is given as $0.007 \text{ kWh}\cdot\text{m}^{-2}$ (mean: $0.014 \text{ kWh}\cdot\text{m}^{-2}$), while the schedule-based control, largely unaffected by the night-time reduction, has a capacity of $0.052 \text{ kWh}\cdot\text{m}^{-2}$ (mean: $0.046 \text{ kWh}\cdot\text{m}^{-2}$).

Figure 6d shows the storage efficiencies for all buildings and floors studied as a ratio of the sum of the discharged energy to the sum of the charged energy. The night-time reduction in the room temperature leads to lower efficiencies, especially in the rule-based control (median: 0.72/0.93, mean: 0.73/0.91), since discharge phases can partly not be used. By including the steady state phase, the median of the total efficiency decreases to 0.54 (mean: 0.54) in the rule-based control and to 0.90 (mean: 0.88) in the schedule-based control, since the steady state phase is associated with higher transmission heat losses and does not store any further energy in the building mass.

3.3. Verification of Phase Identification Via Efficiencies of Up Events

As described in Section 2.4 it is possible to verify the correct identification of the phases using the efficiencies of the up events. For this purpose, in addition to calculating the efficiencies $\eta_{\text{up,tot}}$ from the identified phases, we calculated the efficiency $\eta_{\text{up,alt}}$ alternatively simply by comparing the simulation with energy flexible control and the reference simulation, without assigning energy differences to a specific event. The two ways of calculating the rule-based control efficiencies for all simulated floors are shown in Figure 7. The high agreement of the efficiencies (maximum deviation less than 4%) indicates the mostly correct identification of the events.

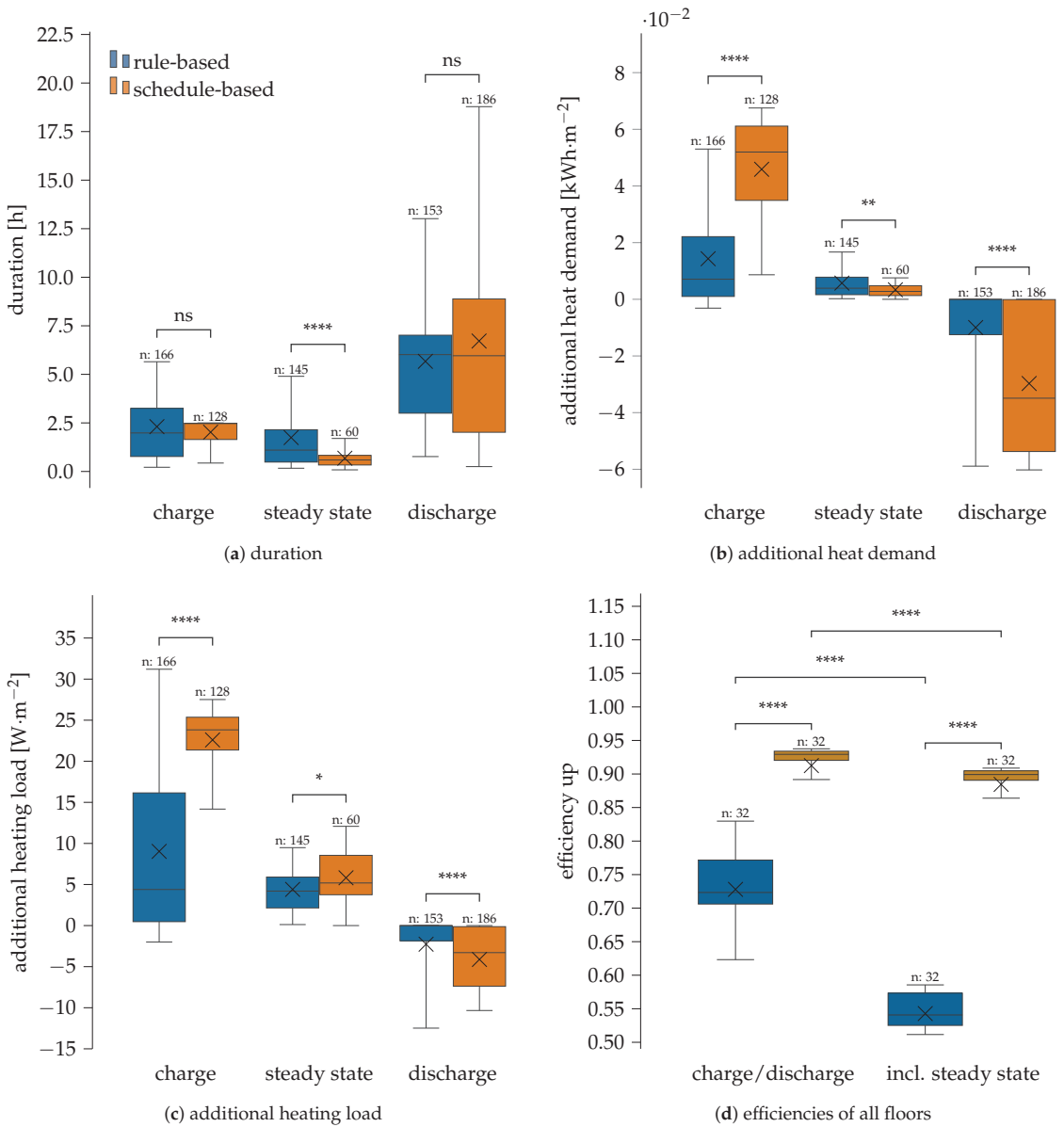


Figure 6. Statistical evaluation of charge, steady state and discharge phases over one year with night-time reduction. Brunner-Munzel test p -values indicate statistical significance (* $p \leq 0.05$, ** $p \leq 0.01$, **** $p \leq 0.0001$), ns: no significance.

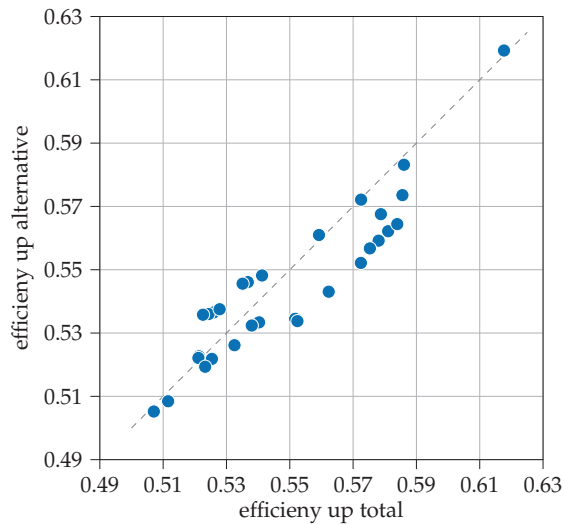


Figure 7. Verification of the phase identification by comparing the efficiencies calculated according to Section 2.4 of all floors.

4. Discussion

In this study, we focus on characterizing the storage capacity of the building mass for energy flexible control. For this purpose, we make a comparison between two control strategies: rule-based and schedule-based. It should be noted, however, that the strategies used represent only a subset of each category. The rule we use is based on the electricity price market, but could also be based on electricity greenhouse gas emissions, for example. Thus, further research is needed to quantify the impact of other rule-based controls. In addition, the building simulation has not yet been validated with real data, so absolute values in the comparison of the two control strategies should be treated with caution.

4.1. Comparability of the Data Sets

Some data sets in our study do not show statistical differences according to the Brunner–Munzel test, which is due to the distribution and quantity of the data. The observed differences, e.g., in charge duration for the different strategies, are quite possible, but should be interpreted with caution due to the limited data available. In some cases, larger data sets are needed to increase statistical confidence. To address this, future investigations could include additional heating periods in the simulations.

4.2. Differences in the Rule- and Schedule-Based Control without Night-Time Reduction

To minimize external influences, we run the first simulation without night-time reduction in the room temperature. Since the duration of the charge phase for up events in schedule-based control must be defined in advance, a duration of 2.5 h is chosen, which corresponds to the average duration of rule-based control with night-time reduction (≈ 2.3 h). As the distribution of events over a year in both control strategies cannot be described by a common probability distribution, a clear characterization is not possible. However, for the purpose of comparison, we utilize both the mean values and the more robust median, which is less affected by outliers. This results in a median value of 1.88 h for rule-based control and 2.47 h for schedule-based control (mean: 2.20/2.01 h). The differences in duration are also reflected in the additional heat transferred per charge phase in each control strategy, but cannot be explained by this alone (median: 0.023/0.058 kWh·m⁻², mean: 0.029/0.049 kWh·m⁻²). The time-independent representation using the additional heating load emphasizes the control-related discrepancy (median: 16.53/25.11 W·m⁻²,

mean: 15.30/23.91 $W \cdot m^{-2}$). Accordingly, the rule-based control for characterizing the storage mass in this study leads to a 60% smaller storage capacity in the median (mean: 41%) and a 34% (mean: 36%) smaller heating load (time-independent) than characterization by schedule-based control.

4.3. Challenges in the Phase Identification

To make a statement about the efficiency of the energy flexible control, it is necessary to determine the energy saved compared to the reference control in the discharge phase. As there is no fixed time between two up events in rule-based control, it is possible for a new charge phase to occur before the previous discharge phase is complete. As a result, there is no clear assignment of the discharge phases, and therefore no efficiency per single up event can be determined. In addition, due to the ambiguous assignment of energy to phases and temperature fluctuations caused by the heating control, energy is sometimes assigned to the wrong phases or not assigned at all, which leads to the discrepancy in the verification of efficiency. To evaluate the overall efficiency, we calculate the sum of all phase-related energies over one year individually, as described in Section 2.4. Hence, the characterization of storage capacity and storage efficiency using rule-based control requires a more detailed examination and verification of the assigned phases and is therefore more time-consuming than characterization using schedule-based control.

4.4. Difficulties in the Rule-Based Control with Night-Time Reduction

The introduction of the more realistic scenario with night-time reduction in the room temperature to 18.5 °C has an impact on the rule-based control and the resulting characterization of the storage capacity (median: 0.007/0.052 $kWh \cdot m^{-2}$, mean: 0.014/0.046 $kWh \cdot m^{-2}$) and storage efficiency (median: 0.72/0.93, mean: 0.73/0.91) of the building mass. This is due to up events just before the night-time reduction. The discharge phase occurs during the temperature-reduced operation, which is also present in the reference variant, and therefore cannot compensate for the previously increased heating load. With rule-based control only according to the electricity market price without time restrictions, the median of the total storage efficiency drops from 0.78 to 0.54. The characterization of the building mass by means of rule-based control therefore requires further boundary conditions to ensure reasonable operation. This includes measures such as evening curfews and weather forecasting to take into account solar gains, which would allow the room temperature to be raised without additional heating.

5. Conclusions

In this study, we use dynamic simulations over one year, including flexible control, to calculate both the storage capacity and storage efficiency for the building mass. We show that the type of flexible control (rule-based versus schedule-based) has a significant impact on the characterization. Since rule-based control is likely to be implemented in the future, this result should be considered when characterizing the building mass. Based on this study, we can make the following statements about the implemented rule-based control:

- The characterization of the building mass using the rule-based control without a night-time reduction leads to a 60% smaller median in the storage capacity (mean: 41%) than using schedule-based control under comparable boundary conditions. The calculation of the time-independent heating load results in a median difference of 34% (mean: 36%).
- By establishing a night-time reduction in the setpoint temperature, the median of the storage efficiency using rule-based control drops from 0.92 to 0.72 (mean: 0.93/0.73).
- The evaluation of the storage capacity and the storage efficiency with the help of the rule-based control requires a more detailed examination and verification of the assigned phases and is accordingly more time-consuming than the characterization by means of the schedule-based control.

- The characterization of the building mass with the help of rule-based control requires, in addition to the simple use of electricity market prices, further boundary conditions that ensure reasonable operation. These include, for example, evening curfews and weather forecasting.

Further research will optimize the characterization of the building mass by the rule-based control and make the phase detection algorithm for up events more robust. Based on this, the up events will be complemented by down events in times of high electricity prices. In addition, the properties assigned to the building mass will be validated using real measured data.

Author Contributions: Conceptualization, J.R.; methodology, J.R.; software, J.R. and X.K.; validation, J.R. and X.K.; formal analysis, J.R.; investigation, J.R.; resources, N.B.; data curation, J.R.; writing—original draft preparation, J.R.; writing—review and editing, X.K., N.B. and J.R.; visualization, J.R.; supervision, N.B.; project administration, N.B.; funding acquisition, N.B. All authors have read and agreed to the published version of the manuscript.

Funding: The authors gratefully acknowledge the financial support of the project Living Lab: DELTA (grant agreement No. 03EWR002A) which is funded by the Federal Ministry for Economic Affairs and Climate Action (BMWK) and the NextGenerationEU and is managed by the management agency Project Management Jülich (PtJ).

Data Availability Statement: Not applicable.

Acknowledgments: The authors would like to thank Anja Schaffarczyk, Bernadette Lang-Eurisch and Yang Xue for their support.

Conflicts of Interest: The authors declare no conflicts of interest. The funders had no role in the design of the study; in the collection, analyses, or interpretation of data; in the writing of the manuscript; or in the decision to publish the results.

Abbreviations

The following abbreviations are used in this manuscript:

DSM	Demand side management.
DR	Demand response.
ADR	Active demand response.
KPI	Key performance indicator.
TABS	Thermally activated building structures.
TES	Thermal energy storage.
ns	Not significant.

References

1. Die Bundesregierung Informiert. Startseite. Klimaschutzgesetz: Klimaneutralität bis 2045 | Bundesregierung. Available online: <https://www.bundesregierung.de/breg-de/schwerpunkte/klimaschutz/klimaschutzgesetz-2021-1913672> (accessed on 10 July 2023).
2. Denholm, P.; Hand, M. Grid flexibility and storage required to achieve very high penetration of variable renewable electricity. *Energy Policy* **2011**, *39*, 1817–1830. [CrossRef]
3. Morales, J.M.; Conejo, A.J.; Madsen, H.; Pinson, P.; Zugno, M. *Integrating Renewables in Electricity Markets*; Springer: New York, NY, USA, 2014. [CrossRef]
4. Hu, X.; Zou, C.; Zhang, C.; Li, Y. Technological Developments in Batteries: A Survey of Principal Roles, Types, and Management Needs. *IEEE Power Energy Mag.* **2017**, *15*, 20–31. [CrossRef]
5. Lund, H.; Münster, E. Integrated energy systems and local energy markets. *Energy Policy* **2006**, *34*, 1152–1160. [CrossRef]
6. O'Malley, M.; Kroposki, B.; Hannegan, B.; Madsen, H.; Andersson, M.; D'haeseleer, W.; McGranaghan, M.F.; Dent, C.; Strbac, G.; Baskaran, S.; et al. *Energy Systems Integration. Defining and Describing the Value Proposition*; Office of Scientific and Technical Information (OSTI): Oak Ridge, TN, USA, 2016.
7. Nejat, P.; Jomehzadeh, F.; Taheri, M.M.; Gohari, M.; Abd. Majid, M.Z. A global review of energy consumption, CO₂ emissions and policy in the residential sector (with an overview of the top ten CO₂ emitting countries). *Renew. Sustain. Energy Rev.* **2015**, *43*, 843–862. [CrossRef]

8. Zafar, R.; Mahmood, A.; Razzaq, S.; Ali, W.; Naeem, U.; Shehzad, K. Prosumer based energy management and sharing in smart grid. *Renew. Sustain. Energy Rev.* **2018**, *82*, 1675–1684. [CrossRef]
9. European Parliament. *Directive (EU) 2018/844 of the European Parliament and of the Council of 30 May 2018 Amending Directive 2010/31/EU on the Energy Performance of Buildings and Directive 2012/27/EU on Energy Efficiency (Text with EEA Relevance)*; European Parliament: Brussels, Belgium, 2018.
10. Jensen, S.Ø.; Marszal-Pomianowska, A.; Lollini, R.; Pasut, W.; Knotzer, A.; Engelmann, P.; Stafford, A.; Reynders, G. IEA EBC Annex 67 Energy Flexible Buildings. *Energy Build.* **2017**, *155*, 25–34. [CrossRef]
11. Lund, P.D.; Lindgren, J.; Mikkola, J.; Salpakari, J. Review of energy system flexibility measures to enable high levels of variable renewable electricity. *Renew. Sustain. Energy Rev.* **2015**, *45*, 785–807. [CrossRef]
12. Gellings, C.W.; Smith, W.M. Integrating demand-side management into utility planning. *Proc. IEEE* **1989**, *77*, 908–918. [CrossRef]
13. Morales-España, G.; Martínez-Gordón, R.; Sijm, J. Classifying and modelling demand response in power systems. *Energy* **2022**, *242*, 122544. [CrossRef]
14. Lauro, F.; Moretti, F.; Capozzoli, A.; Panzieri, S. Model Predictive Control for Building Active Demand Response Systems. In Proceedings of the 7th International Conference (Energy Procedia) SEB-15, Lisbon, Portugal, 1–3 July 2015; Volume 83, pp. 494–503. [CrossRef]
15. Arteconi, A.; Costola, D.; Hoes, P.; Hensen, J. Analysis of control strategies for thermally activated building systems under demand side management mechanisms. *Energy Build.* **2014**, *80*, 384–393. [CrossRef]
16. Arteconi, A.; Polonara, F. Assessing the Demand Side Management Potential and the Energy Flexibility of Heat Pumps in Buildings. *Energies* **2018**, *11*, 1846. [CrossRef]
17. de Coninck, R.; Helsen, L. Quantification of flexibility in buildings by cost curves— Methodology and application. *Appl. Energy* **2016**, *162*, 653–665. [CrossRef]
18. Luc, K.M.; Li, R.; Xu, L.; Nielsen, T.R.; Hensen, J.L. Energy flexibility potential of a small district connected to a district heating system. *Energy Build.* **2020**, *225*, 110074. [CrossRef]
19. Bundesministerium der Justiz. Gesetz zum Neustart der Digitalisierung der Energiewende *Bundesgesetzblatt*. **2023**, Teil I Nr. 133. Bonn, Germany, 2023. <https://www.recht.bund.de/bgbl/1/2023/133/VO.html> (accessed on 28 August 2023).
20. Callaway, D.S.; Hiskens, I.A. Achieving Controllability of Electric Loads. *Proc. IEEE* **2011**, *99*, 184–199. [CrossRef]
21. Reynders, G.; Nuytten, T.; Saelens, D. Potential of structural thermal mass for demand-side management in dwellings. *Build. Environ.* **2013**, *64*, 187–199. [CrossRef]
22. Arteconi, A.; Hewitt, N.J.; Polonara, F. State of the art of thermal storage for demand-side management. *Appl. Energy* **2012**, *93*, 371–389. [CrossRef]
23. Airò Farulla, G.; Tumminia, G.; Sergi, F.; Aloisio, D.; Cellura, M.; Antonucci, V.; Ferraro, M. A Review of Key Performance Indicators for Building Flexibility Quantification to Support the Clean Energy Transition. *Energies* **2021**, *14*, 5676. [CrossRef]
24. Li, H.; Wang, Z.; Hong, T.; Piette, M.A. Energy flexibility of residential buildings: A systematic review of characterization and quantification methods and applications. *Adv. Appl. Energy* **2021**, *3*, 100054. [CrossRef]
25. Cetin, K.S. Characterizing large residential appliance peak load reduction potential utilizing a probabilistic approach. *Sci. Technol. Build Environ.* **2016**, *22*, 720–732. [CrossRef]
26. Le Dréau, J.; Heiselberg, P. Energy flexibility of residential buildings using short term heat storage in the thermal mass. *Energy* **2016**, *111*, 991–1002. [CrossRef]
27. Vanhoudt, D.; Geysen, D.; Claessens, B.; Leemans, F.; Jespers, L.; van Bael, J. An actively controlled residential heat pump: Potential on peak shaving and maximization of self-consumption of renewable energy. *Renew. Energy* **2014**, *63*, 531–543. [CrossRef]
28. Reynders, G.; Saelens, D.; Diriken, J. A generic quantification method for the active demand response potential of structural storage in buildings. In Proceedings of the 14th Conference of International Building Performance Simulation Association, Hyderabad, India, 7–9 December 2015; pp. 1986–1993. [CrossRef]
29. Vigna, I.; de Jaeger, I.; Saelens, D.; Lovati, M.; Lollini, R.; Perneti, R. Evaluating Energy and Flexibility Performance of Building Clusters. In Proceedings of the 16th IBPSA International Conference and Exhibition, Rome, Italy, 2–4 September 2019; pp. 3326–3333. [CrossRef]
30. Foteinaki, K.; Li, R.; Heller, A.; Rode, C. Heating system energy flexibility of low-energy residential buildings. *Energy Build.* **2018**, *180*, 95–108. [CrossRef]
31. Arteconi, A.; Mugnini, A.; Polonara, F. Energy flexible buildings: A methodology for rating the flexibility performance of buildings with electric heating and cooling systems. *Appl. Energy* **2019**, *251*, 113387. [CrossRef]
32. Foteinaki, K.; Li, R.; Péan, T.; Rode, C.; Salom, J. Evaluation of energy flexibility of low-energy residential buildings connected to district heating. *Energy Build.* **2020**, *213*, 109804. [CrossRef]
33. Vivian, J.; Chiodarelli, U.; Emmi, G.; Zarrella, A. A sensitivity analysis on the heating and cooling energy flexibility of residential buildings. *Sustain. Cities Soc.* **2020**, *52*, 101815. [CrossRef]
34. Reynders, G.; Diriken, J.; Saelens, D. Generic characterization method for energy flexibility: Applied to structural thermal storage in residential buildings. *Appl. Energy* **2017**, *198*, 192–202. [CrossRef]
35. Brunner, E.; Munzel, U. The Nonparametric Behrens-Fisher Problem: Asymptotic Theory and a Small-Sample Approximation. *Biom. J.* **2000**, *42*, 17–25. [CrossRef]

36. Welcome. TRNSYS : Transient System Simulation Tool. Available online: <https://www.trnsys.com/> (accessed on 28 July 2023).
37. EnergyPlus. Available online: <https://energyplus.net/> (accessed on 26 July 2023).
38. IDA ICE—Simulation Software. EQUA. Available online: <https://www.equa.se/de/ida-ice> (accessed on 28 July 2023).
39. Dymola—Dassault Systèmes®. Available online: <https://www.3ds.com/de/produkte-und-services/catia/produkte/dymola/> (accessed on 26 July 2023).
40. Magni, M.; Ochs, F.; de Vries, S.; Maccarini, A.; Sigg, F. Detailed cross comparison of building energy simulation tools results using a reference office building as a case study. *Energy Build.* **2021**, *250*, 111260. [CrossRef]
41. David Bewersdorff. *HYGGiency : Room Hygiene and Comfort through Energetic Refurbishment in District*; Volume 61 , *Mechanik, Werkstoffe und Konstruktion im Bauwesen*, Springer: Wiesbaden, Germany, 2021.
42. Kirschstein, X.; Reber, J.; Zeus, R.; Schuster, M.; Bishara, N. Modelling of Floor Heating and Cooling in Residential Districts. *Energies* **2023**, *16*, 5850. [CrossRef]
43. DIN V 18599-10. Energetische Bewertung von Gebäuden – Berechnung des Nutz-, End- und Primärenergiebedarfs für Heizung, Kühlung, Lüftung, Trinkwarmwasser und Beleuchtung – Teil 10: Nutzungsrandbedingungen. Deutsches Institut für Normung e. V.: Berlin Germany, 2018. Available online: <https://dx.doi.org/10.31030/2874436> (accessed on 20 July 2023).

Disclaimer/Publisher’s Note: The statements, opinions and data contained in all publications are solely those of the individual author(s) and contributor(s) and not of MDPI and/or the editor(s). MDPI and/or the editor(s) disclaim responsibility for any injury to people or property resulting from any ideas, methods, instructions or products referred to in the content.

Article

Optimal Sizing of Renewable Energy Communities: A Multiple Swarms Multi-Objective Particle Swarm Optimization Approach

João Faria ^{1,2}, Carlos Marques ², José Pombo ^{1,2,*}, Sílvio Mariano ^{1,2,*} and Maria do Rosário Calado ^{1,2}

¹ IT—Instituto de Telecomunicações, Faculty of Engineering, Calçada Fonte do Lameiro, 6201-001 Covilhã, Portugal

² Department of Electromechanical Engineering, Faculty of Engineering, University of Beira Interior, Calçada Fonte do Lameiro, 6201-001 Covilhã, Portugal

* Correspondence: sm@ubi.pt

Abstract: Renewable energy communities have gained popularity as a means of reducing carbon emissions and enhancing energy independence. However, determining the optimal sizing for each production and storage unit within these communities poses challenges due to conflicting objectives, such as minimizing costs while maximizing energy production. To address this issue, this paper employs a Multi-Objective Particle Swarm Optimization (MOPSO) algorithm with multiple swarms. This approach aims to foster a broader diversity of solutions while concurrently ensuring a good plurality of nondominant solutions that define a Pareto frontier. To evaluate the effectiveness and reliability of this approach, four case studies with different energy management strategies focused on real-world operations were evaluated, aiming to replicate the practical challenges encountered in actual renewable energy communities. The results demonstrate the effectiveness of the proposed approach in determining the optimal size of production and storage units within renewable energy communities, while simultaneously addressing multiple conflicting objectives, including economic viability and flexibility, specifically Levelized Cost of Energy (LCOE), Self-Consumption Ratio (SCR) and Self-Sufficiency Ratio (SSR). The findings also provide valuable insights that clarify which energy management strategies are most suitable for this type of community.

Keywords: renewable energy community (REC); energy management strategies; multi-objective optimization algorithm; multi-swarm MOPSO; energy storage systems; energy storage sharing

Citation: Faria, J.; Marques, C.; Pombo, J.; Mariano, S.; Calado, M.d.R. Optimal Sizing of Renewable Energy Communities: A Multiple Swarms Multi-Objective Particle Swarm Optimization Approach. *Energies* **2023**, *16*, 7227. <https://doi.org/10.3390/en16217227>

Academic Editors: Ala Hasan and Hassam Ur Rehman

Received: 20 September 2023

Revised: 17 October 2023

Accepted: 20 October 2023

Published: 24 October 2023



Copyright: © 2023 by the authors. Licensee MDPI, Basel, Switzerland. This article is an open access article distributed under the terms and conditions of the Creative Commons Attribution (CC BY) license (<https://creativecommons.org/licenses/by/4.0/>).

1. Introduction

The centralized production of electric energy from fossil fuels is still a significant component of the global energy matrix [1]. However, to decrease the reliance on these non-renewable sources, there has been a growing trend towards renewable energy sources [2]. Furthermore, the increasing economical accessibility of renewable energy production technologies, combined with recent government policies aimed at promoting renewable production, has encouraged more consumers to become prosumers. By assuming the role of both consumers and producers, they contribute to a decentralization of electrical energy production [3,4]. Although beneficial for the environment, the integration of distributed energy resources into the electrical grid poses new challenges due to the variability of endogenous resources and the changes to the paradigm for which distribution networks were designed (i.e., distributing energy from upstream to downstream) [5]. Currently, one of the most popular solutions to this problem is Renewable Energy Communities (RECs) [6]. RECs can be defined as groups of individuals and/or organizations that combine decentralized production resources, forming prosumer communities that share renewable energy production with one another [7]. On one hand, these communities promote the decentralization of energy production, increase energy efficiency, enhance energy security, and ensure

greater independence of participants from conventional energy sources. On the other hand, these communities face significant variability and unpredictability due to renewable energy production [8]. Nonetheless, this variability and unpredictability can be mitigated by the complementarity of resources (such as wind and solar) to balance the variability in energy production, or by the introduction of energy storage systems [9]. Energy storage systems can store surplus energy produced during times of high production and discharge it during times of low production, enabling RECs to become more self-sufficient and reducing their reliance on the electrical grid. Additionally, the introduction of energy storage systems in RECs also enables new energy-sharing concepts (such as storage sharing) that enable the sharing of the same energy storage system by different community participants [10]. However, minimizing the reliance on the electrical grid and enabling this type of operation (energy and storage sharing) requires an energy management system (EMS) to optimize the energy flow and manage the different energy sources within the RECs [11]. EMS strategies can be divided into three categories: (i) classical strategies, (ii) metaheuristic strategies, and (iii) intelligent strategies [12].

Classical EMS strategies refer to straightforward mathematical programming and classical programming approaches, which can be further categorized into constrained and unconstrained strategies. Constrained strategies are used to optimize the power flow while adhering to specific constraints and include linear programming [13], nonlinear programming [14], mixed-integer nonlinear programming [15] and mixed-integer linear programming [16]. On the other hand, unconstrained strategies involve decision theory (rule-based and deterministic-based) that uses technical, economic, or environmental constraints to optimize, control, schedule, and manage the different energy sources (production and storage units) [17–19]. Classical EMS strategies are a common method to obtain energy-efficient systems in a secure and reliable way. In [20], a linear programming optimization model was employed to investigate the impact on distribution grids of the different energy community configurations, different operating strategies, and different battery placements. In [21], an individual peer energy trading price model is proposed for the diversified community to allocate an individual peer trading price to each building group according to its intrinsic energy characteristic and grid import price. However, despite their capabilities and the availability of versatile classical EMS strategies, they present some disadvantages, especially in large-scale systems (with high number of decision variables). To overcome this limitation, some authors choose to divide the optimization problem into subproblems (decentralization). In [22], a decentralized demand response in energy communities is proposed, incorporating flexible loads and energy storage systems. A multi-block alternating direction method of multipliers (ADMM) approach is used to decompose the large scheduling problem into a set of home optimization subproblems.

Metaheuristic strategies rely on optimization algorithms to achieve efficient power flow optimization while ensuring compliance with specific REC constraints. These algorithms can explore the search space using multiple variables and constraints, thus achieving high-quality solutions. Some of the most popular metaheuristic algorithms are Particle Swarm Optimization (PSO) [23], Genetic Algorithms [24], Cuckoo Search Algorithm [25], Whale Optimization Algorithm (WOA) [26], Tabu Search Algorithm [27], Grey Wolf Optimizer [28], Black Widow Optimization (BWO) [29], Self-Adaptive Elephant Herd Optimization (SA-EHO) [30], Mixed Integer Distributed Ant Colony Optimization (MIDACO) [31] and Grasshopper Optimization Algorithm (GHA) [32]. Intelligent EMS strategies are nonlinear computational algorithms generally based on Artificial Neural Networks (ANNs) and Fuzzy Logic (FL) [12,33,34].

Artificial Neural Networks (ANNs) are a type of machine learning algorithm inspired by the structure and function of the human brain. They were developed in the 1940s and have since become an important tool for solving complex problems even when working with incomplete data. Recent advancements have led to an increased adoption of ANNs in EMS for forecasting and control applications. ANNs provide an effective means for analyzing complex and nonlinear relationships within RECs because of their ability to

recognize patterns in data and make accurate predictions for future load demand and renewable energy production.

Game theory is a type of strategy that studies how individuals and entities make strategic decisions in interactive situations, examining the choices and behaviors that arise from these interactions. In this context, innovative approaches like the Vickrey–Clark–Groves (VCG) and optimization techniques are used to create decentralized, peer-to-peer (P2P) energy trading solutions within microgrids. These methods help optimize prices and trade quantities between energy producers and consumers. In [35], the Vickrey–Clarke–Groves (VCG) mechanism and the particle swarm optimization (PSO) are applied to optimize P2P energy trading in a microgrid. The objective of the optimization problem is to identify the ideal prices and the amounts of energy traded between producers and consumers in a decentralized way.

One of the fundamental aspects that contribute to the efficient operation of an REC is the optimal sizing of each participant's production and storage units. This is especially important to complement the variability of natural resources used for energy production; ensure system reliability; manage the initial investment effectively; and account for the diverse profiles of each participant, whether residential or industrial. Thus, the optimal sizing of energy communities has been the subject of great interest by the scientific community due to the growing maturity of renewable technologies (mainly with the reduction of their cost) and the increase and enormous volatility in electricity prices [36–39].

To increase efficiency and spread the adoption of RECs, this article determines the optimal sizing of all renewable energy production and storage units within an REC, regardless of the number of participants. Through the optimal sizing of the various energy production and storage units, participants can produce, consume, share, store, and sell the energy produced by RECs, actively contributing to decarbonization and energy transition.

Another distinguishing aspect of this study lies in the dimensioning methodology, which is based on the Multi-Objective Particle Swarm Optimization (MOPSO) algorithm with multiple swarms. This approach aims to enhance solution diversity and ensure a wide range of nondominant solutions, creating a Pareto frontier. Furthermore, to ensure greater independence in the exploration of the multidimensional search space and mitigate the problem of premature convergence, the implemented optimization technique decomposes the multidimensional search space into smaller subspaces [40,41]. Thus, the various swarms act in their corresponding multidimensional subspace, allowing a cooperative and collaborative way of sizing the various energy production and storage units inherent to each REC participant. The sizing of the various units was carried out considering economic and technical criteria, namely the levelized cost of energy (LCOE), the self-consumption ratio (SCR), and the self-sufficiency ratio (SSR).

Furthermore, to assess the performance and sustainability of various energy management strategies within the REC, four distinct approaches were implemented. These strategies encompass different levels of cooperation, participation, and collaboration among the various production and storage units of electric energy. By employing these management strategies, the study aims to comprehensively analyze and compare their effectiveness in the REC operations.

The structure of this paper is as follows: Section 2 offers an overview of the system modeling; Section 3 presents the energy management strategies, problem formulation, and the optimization approach; Section 4 discusses the results; and finally, Section 5 presents the study's conclusion.

2. System Modeling

Before sizing the system's individual technologies, the models must be defined to simulate the system realistically and accurately. However, simulating any REC as close to reality as possible can be very complex, given the numerous variables and constraints that need to be considered [42].

In this section, we present the mathematical models of the system components. The simulated community consists of different energy sources (namely solar and wind power) that directly supply the existing electrical load. Additionally, the community includes an energy storage system (specifically batteries) that plays a crucial role in storing excess renewable energy for later use. These models are essential for a comprehensive understanding of the renewable energy community’s dynamics and for devising effective energy management strategies.

2.1. Batteries

In the existing literature, many different models can be found to simulate and describe, in a feasible and detailed way, the behavior of different types of batteries under different operating conditions [43]. They can be divided into four different groups: Electrochemical, Stochastic, Electrical, and Analytical models [44].

The Kinetic Battery Model (KiBaM) is a popular analytical model developed by Maxwell and McGowan [45] that is widely used in energy storage system simulations. As illustrated in Figure 1, this mathematical model represents a battery with two reservoirs (available charge and bound charge) separated by a conductance. The available charge reservoir contains the available energy of the battery (q_1) that can be immediately supplied to the load, and the bound charge reservoir contains the battery’s remaining energy (q_2) that cannot be immediately converted into electrical energy since it is only responsible for supplying energy to the available charge reservoir. The battery’s capacity ratio of available energy to total energy is defined by c [46]. The energy flow exchange between reservoirs depends on the conductance (k) that represents how quickly the energy from the bound charge reservoir is converted to the available charge reservoir or vice-versa, depending on the operating condition, and on their height difference ($h_1 - h_2$), where $h_1 = q_1/c$ and $h_2 = q_2/(1 - c)$. The battery’s capacity is the sum of both reservoirs’ capacity, $q_{bat} = q_1 + q_2$.

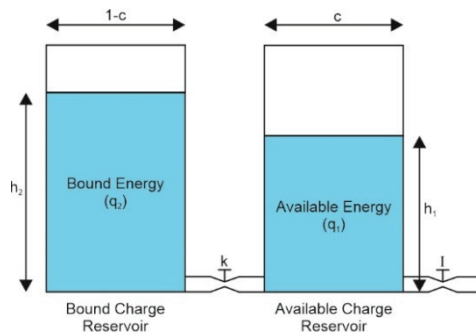


Figure 1. Kinetic Battery Model (KiBaM).

When the battery is discharging, the available charge reservoir supplies its energy to the connected load, while the bound charge reservoir supplies its energy to the available charge reservoir at a slower rate, causing the height difference of both reservoirs to increase. When the battery is charging, the available charge reservoir charges at a faster rate than the bound charge reservoir. When the battery is not being used, a flow of energy occurs between both reservoirs, causing the reservoirs to balance each other until both reservoirs’ heights are equal ($h_1 = h_2$). The amount of energy contained in each reservoir, in each time step, is represented by the following equations [46]:

$$q'_1 = q_1 e^{-k\Delta t} + \frac{(q_{bat}kc - P_{cd}) (1 - e^{-k\Delta t})}{k} - \frac{P_{cd}c (k\Delta t - 1 + e^{-k\Delta t})}{k} \tag{1}$$

$$q'_2 = q_2 e^{-k\Delta t} + q_{bat}(1-c)(1-e^{-k\Delta t}) - \frac{P_{cd}(1-c)(k\Delta t - 1 + e^{-k\Delta t})}{k} \quad (2)$$

where q'_1, q'_2 and q_1, q_2 are the available charge and bound energy at the end and beginning of each time step, respectively, in [kWh] [46]; Δt is the time step; and P_{cd} is the charge or discharge power of each time step [kW], depending on the operating conditions.

The maximum discharging and charging power of the battery in kW, in each time step, is given by the following Equations (3) and (4):

$$P_d = \frac{kq_1 e^{-k\Delta t} + q_{bat}kc(1-e^{-k\Delta t})}{1-e^{-k\Delta t} + c(k\Delta t - 1 + e^{-k\Delta t})} \quad (3)$$

$$P_c = \frac{-kcq_{bat} + kq_1 e^{-k\Delta t} + q_{bat}kc(1-e^{-k\Delta t})}{1-e^{-k\Delta t} + c(k\Delta t - 1 + e^{-k\Delta t})} \quad (4)$$

This mathematical model is computationally efficient and allows for the description of electrochemical processes occurring within the battery using a reduced set of parameters: the total charge ratio stored in the available charge reservoir (c), the conductance (charge flow rate) between both reservoirs (k), and the maximum capacity of the battery (q_{bat}). These parameters can be estimated through a series of experimental measurements with constant discharge currents or by using the battery datasheet (at least three discharge curves). Furthermore, it can capture nonlinear effects during charging and discharging, such as recovery effects and capacity rate. However, it does not account for the effects of temperature and battery aging [47].

2.2. Photovoltaic System

The Photovoltaic system (PV) is a crucial and impactful component of an REC, although it provides intermittent production with large variability and unpredictability. Therefore, carefully selecting a model that best suits each specific application is essential. Various models in the literature are used to simulate the behavior of Photovoltaic (PV) modules under different operating conditions, including factors such as dust, cell temperature, partial shading, irradiance, and others. [43]. Various models with one, two, or even three or more diodes are commonly used in literature. However, these models imply a considerable amount of computational time and effort, unnecessary for this type of simulation. In this paper, to reduce the computation effort, a synthesized model is used to determine the output power of the PV modules, defined as a function of the PV cell temperature and solar irradiance (G). The power output of the PV system in each time step, with N_s modules connected in series and N_p modules connected in parallel, is given by Equation (5) [48,49].

$$P_{PV} = \mu_{mppt} \left(P_{STC} \frac{G}{G_{STC}} (1 + \alpha_{VOC}(T_{cell} - T_{STC})) \right) N_s N_p \quad (5)$$

where μ_{mppt} is the photovoltaic system efficiency of the maximum power point tracking method (MPPT) [%]; P_{STC} is the maximum power under Standard Test Conditions (STC) [W], i.e., a solar irradiance of 1000 W/m² and a temperature of 25 °C; G is the given solar irradiance in each time step [Wm⁻²]; G_{STC} is the irradiance under STC [Wm⁻²]; α_{VOC} is the temperature coefficient of the open-circuit voltage under STC [V°C⁻¹]; T_{STC} is the cell temperature under STC conditions [°C]; and T_{cell} is the cell temperature in each time step [°C] given by Equation (6) [50,51].

$$T_{cell} = T_{amb} + \frac{G}{G_{NOCT}} \times (NOCT - T_{NOCT}) \quad (6)$$

where T_{amb} is the ambient temperature in each time step [$^{\circ}\text{C}$]; $NOCT$ is the Nominal Operating Cell Temperature [$^{\circ}\text{C}$], measured with 800 W/m^2 irradiance, $20\text{ }^{\circ}\text{C}$ ambient temperature and wind speed of 1 m/s ; G_{NOCT} is the irradiance under $NOCT$ [Wm^{-2}]; and T_{NOCT} is the temperature under $NOCT$ conditions [$^{\circ}\text{C}$].

2.3. Wind Turbine Generator

The power output of a wind turbine generator is influenced by both the site characteristics and the technical features of the wind turbine. The most significant factors are the wind speed at the turbine hub height and the power output curve.

The wind speed measured by an anemometer is not directly at the turbine hub height. Therefore, it must be converted to that height to accurately estimate the true wind speed. This conversion is essential to ensure precise calculations and effective evaluation of the wind turbine's power generation [52,53]. A widely used conversion approach employs the power law expressed by Equation (7).

$$V_h = V_a \left(\frac{h_h}{h_a} \right)^{\alpha} \quad (7)$$

where V_h [ms^{-1}] is the wind speed at hub height h_h [m]; V_a [ms^{-1}] is the wind speed at the anemometer height h_a [m]; and α is the power law exponent or friction coefficient.

Many different models are used in the literature to simulate and obtain the power curve of a wind turbine regarding the wind speed and hub height, such as physical, linear, and nonlinear models. Although these methods are straightforward to implement in any REC simulation, they are not always accurate when simulating stall-controlled wind turbines. In this type of wind turbine, the pitch angle is fixed, so when the wind speed is above the rated wind speed the turbine power output cannot be held constant and decreases because of aerodynamic losses between the blades and the wind. Thus, in this paper, the authors used the power output curve provided by the manufacturer to accurately simulate the wind power system.

3. Problem Formulation and Energy Management Strategies

In this section, we present the employed energy management strategies, the optimization strategy, and the problem formulation for determining the optimal sizes of the system components within the REC. The management strategies were designed with a focus on real-world operations, aiming to replicate the practical challenges encountered in actual RECs, thus enhancing the approach's realism and applicability. The problem formulation defines the objective function and constraints that describe the purpose/goals of the optimization problem.

3.1. Energy Management Strategies

To test the performance of the REC in different operating conditions, four energy management scenarios proposed in [54] were implemented. A summarized description of these scenarios can be found in Table 1.

Table 1. Renewable Energy Community Scenarios.

Scenarios	Description
Scenario 1	Independent microgrid participants.
Scenario 2	Sharing renewable energy after charging individual batteries.
Scenario 3	Sharing renewable energy before charging individual batteries.
Scenario 4	Sharing distributed renewable energy and battery storage systems among participants before charging individual batteries.

In Scenario 1 (S1), an individualist position is assumed by all the community participants, mimicking a conventional microgrid with no energy transactions between them. In Scenario 2 (S2), the surplus energy from distributed renewable systems is shared within the community after fully charging the individual batteries. In this scenario, the community participants prioritize charging or discharging their own batteries when they have an energy surplus or shortage. If the battery reaches the upper limit of its state of charge (SOC_{max}), any remaining excess energy is shared within the community before being exported to the electrical grid. Inversely, if the battery reaches its lower limit (SOC_{min}), any remaining required energy is supplied by available energy from other prosumers before importing from the grid. In contrast, in Scenario 3 (S3), the surplus renewable energy is shared directly to cover other community participants' load demand before being dispatched to the individual batteries. This scenario considers the efficiency losses associated with battery operations and ensures that the excess renewable energy is efficiently utilized to meet the REC's energy needs. In Scenario 4 (S4), all the batteries and renewable energy sources are shared to enhance renewable penetration and minimize grid dependence. The operation in this scenario follows a specific rule: when one participant has surplus power, it can be utilized to meet the load demand of other peers. The participants first charge their own batteries to SOC_{max} and then proceed to charge other peers' batteries sequentially. Conversely, when a participant faces an energy deficiency, they can purchase redundant generation from other peers, then discharge their own battery to SOC_{min} , and finally discharge other peers' batteries if needed. This collaborative approach allows for improved renewable integration and effective utilization of distributed energy resources within the community.

3.2. Problem Formulation

The optimal sizing of the studied REC is evaluated based on two different system evaluation criteria: economic and flexibility criteria. The economic criteria involve analyzing cost-related factors, while flexibility criteria assess the system's ability to adapt to varying demand and supply conditions, ensuring an efficient and reliable energy management.

3.2.1. Economic Criteria

The Levelized Cost of Energy (LCOE) is widely recognized as a crucial economic factor in the optimal planning and design of Hybrid Energy Systems (HES) [55]. Its prominence attracts investors, policymakers, and consumers, making it a pivotal consideration in the design of the REC [56].

LCOE can be defined as the effective cost of energy generated by the REC, in \$/kWh [57]. It is calculated by the ratio of the sum of the total annualized cost (C_{annual}) and the annual electrical energy served by the system (E_{served}), as expressed in Equation (8).

$$LCOE = \frac{C_{annual}}{E_{served}} \quad (8)$$

where C_{annual} is the product of the net present cost (NPC) and the capital recovery factor (CRF), as expressed by Equation (9):

$$C_{annual} = NPC \cdot CRF(i, N) \quad (9)$$

The Net Present Cost (NPC) of a system, representing its life-cycle cost, is determined by Equation (10) [51], where i denotes the nominal interest rate and N represents the project's lifetime:

$$NPC = C_{O\&M} + C_{cap} \quad (10)$$

$$C_{cap} = E_{bat} \cdot C_{bat} + N_{PV} \cdot C_{PV} + N_{WT} \cdot C_{WT} \quad (11)$$

In Equation (11), C_{cap} is the initial capital cost, where $C_{O\&M}$ is the maintenance and operation cost; E_{bat} is the sum of the participants' battery-rated capacities; N_{PV} and N_{WT}

are the sum of the PV modules and wind turbines of the participants, respectively; and C_{bat} , C_{PV} and C_{WT} define the cost per kWh of the batteries, the cost of each PV module, and the cost of each wind turbine, respectively. The capital recovery factor (CRF) is calculated with Equation (12).

$$CRF(i, N) = \frac{i(1+i)^N}{(1+i)^N - 1} \quad (12)$$

The economic parameters are shown in Table 2.

Table 2. Economic parameters.

Parameter	Value
Nominal interest rate (i) [%]	0.05
Project lifetime (N) [years]	20

3.2.2. Flexibility Criteria

The flexibility criteria are crucial parameters for optimizing both energy consumption and production [58]. The Self-Consumption Ratio (SCR) and Self-Sufficiency Ratio (SSR) are two well-known parameters that enhance the flexibility of energy systems. These criteria play a significant role in achieving an efficient and resilient renewable energy community.

SCR can be defined as the quantity of energy produced internally by the system's renewable energy sources, which is also used internally for consumption [58]. This includes both the energy directly used by the load, as well as the batteries' charging energy (acting like an additional load) [59]. Figure 2 shows a typical power profile of an REC with this type of renewable energy production system. In this Figure, Area B represents the surplus energy produced during that day, Area C represents the renewable energy directly consumed or stored by the REC, while Area A shows the energy deficit that must be imported to satisfy the load demand.

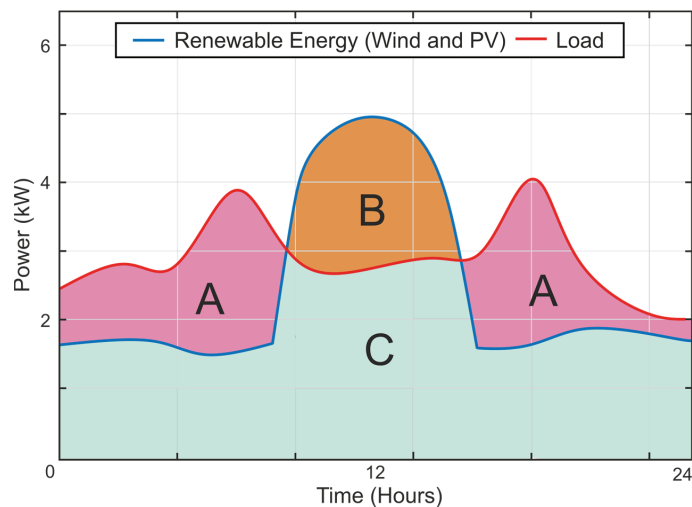


Figure 2. Typical load and production profile.

Using the nomenclature in Figure 2, SCR can be defined by Equation (13):

$$SCR = \frac{C}{B + C} \quad (13)$$

Although SCR is a valuable and viable parameter for designing an REC, if the optimization problem were solely formulated to maximize SCR, the resulting configuration

would always be the smallest possible in terms of produced energy. This limitation underscores the need to use SCR in combination with other criteria when formulating an REC optimization problem. By incorporating multiple criteria, the solution can achieve a more comprehensive and balanced configuration that optimizes both energy production and consumption, ensuring the REC's effectiveness and practicality [58]. SSR is also considered to minimize energy community transactions with the electrical grid. SSR represents the proportion of energy consumption supplied by internally produced energy. Using the nomenclature depicted in Figure 2, SSR can be defined by the following equation:

$$SSR = \frac{C}{A + C} \quad (14)$$

3.2.3. Variables and Constraints

For each participant p , the design variables considered for the optimal sizing and design of the REC are the battery-rated capacity (C_{bat_p}) [kWh]; the number of PV modules (N_{PV_p}); and the number of wind turbines (N_{WT_p}), each subject to upper and lower bounds, as enumerated in Equation (15). These bounds were designed based on a typical renewable energy installation in residential areas.

$$\begin{cases} 0 \leq C_{bat_p} \leq 25 \\ 0 \leq N_{PV_p} \leq 50 \\ 0 \leq N_{WT_p} \leq 10 \end{cases} \quad (15)$$

The primary goal of any REC is to minimize its exchanges with the electrical grid by enabling the exchange of surplus energy consumed or produced among participants. To achieve this objective in the simulated REC discussed in this article, two additional design restrictions were implemented in the simulation parameters to further optimize the results. To significantly increase independence from the grid, the energy interactions with the electrical grid were limited to 25% of the total energy transacted in the REC, as specified by Equation (16). This limitation was implemented to foster a greater reliance on intra-community energy exchanges and storage, leading to reduced reliance on the grid and enhancing the overall self-sufficiency of the renewable energy community.

$$\sum_{t=1}^{8760} E_{Imp}^p(t) + E_{Exp}^p(t) < 0.25 \cdot E_{Total}^p(t) \quad (16)$$

where E_{Imp}^p and E_{Exp}^p are the imported and exported energy exchanged by the REC with the electrical grid by each participant p , respectively, in each hour t . Furthermore, E_{Total}^p is the total energy transacted by the participant p , as given by Equation (17):

$$E_{Total}^p = \sum_{p=1}^n \left(\sum_{t=1}^{8760} E_{PV}^p(t) + E_{Wind}^p(t) + E_{BatCharge}^p(t) + E_{BatDischarge}^p(t) + E_{ImpCom.}^p(t) + E_{ExpCom.}^p(t) + E_{Imp}^p(t) + E_{Exp}^p(t) \right) \quad (17)$$

where E_{PV}^p and E_{Wind}^p are the PV and wind energy produced by each participant p , respectively; $E_{BatCharge}^p$ and $E_{BatDischarge}^p$ are the charging and discharging energy used to charge and discharge the batteries, respectively; and $E_{ImpCom.}^p$ and $E_{ExpCom.}^p$ represent the intra-community transactions of each participant: $E_{ImpCom.}^p$ defines the intra-community energy importations, while $E_{ExpCom.}^p$ defines the intra-community energy exportation by each participant p .

The other optimizing restriction promotes intra-community energy interactions, encouraging participants to exchange surplus or required energy among themselves, as shown in Equation (18). This equation sets a lower limit for the intra-community energy value traded between participants, ensuring that it remains above 30% of the total energy imported by the REC. By encouraging such interactions, the renewable energy community

fosters a collaborative approach, optimizing energy utilization and minimizing dependency on external sources.

$$\sum_{p=1}^n \left(\sum_{t=1}^{8760} E_{ImpCom.}(t) + \sum_{t=1}^{8760} E_{ExpCom.}(t) \right) > 0.3 \cdot \sum_{t=1}^{8760} E_{Imp}(t) \quad (18)$$

where E_{ImpCom} and E_{ExpCom} defines the sum of all the REC participant's intra-community energy importations and exportations, respectively.

3.3. Optimization Strategy

The optimization technique implemented in this paper combines the specificities of the Multi-Objective Particle Swarm Optimization (MOPSO) algorithm with the use of multiple swarms that cooperate and share information and lived experiences (history) to achieve a set of high-quality solutions. The use of multiple swarms constructs a greater diversity of new solutions and explores the multidimensional search space with greater independence and efficiency. Moreover, the optimization technique used divides the multidimensional search space into smaller subspaces, providing greater independence in the construction of new solutions (exploration of the search space) and minimizing the problem of premature convergence. The number of subspaces and the number of swarms depend on the number of participants in the REC. Each swarm acts in its corresponding subspace, optimizing the sizing of the various energy production and energy storage units inherent to each participant of the REC (N_{PV_p} , N_{WT_p} , C_{bat_p}) cooperatively and collaboratively. The multiple swarms use the broadcast strategy to share information and lived experiences (history) with each other, i.e., the social component of each swarm ($gbest$) is transmitted and shared with all the other swarms.

3.3.1. Multi-Objective Particle Swarm Optimization (MOPSO)

Multi-Objective Particle Swarm Optimization (MOPSO) is a population-based, stochastic metaheuristic algorithm that is very effective in solving multi-objective optimization problems, i.e., optimization problems involving two or more objective, typically antagonistic, functions [60]. It is a metaheuristic algorithm inspired by the foraging behavior of certain animal species involving a population of particles that represent possible solutions. The particles can communicate and cooperate with each other to determine a set of promising solutions, i.e., a set of solutions with a good trade-off between the different objective functions (nondominated solutions). The particles are randomly positioned within the multidimensional search space (d) and evaluated using the objective functions inherent to the optimization problem (with or without constraints). Particles move based on their current velocities and positions, the individual experience of each particle (cognitive factor), and the collective experience of the population's particles (social factor). Thus, during the optimization process, the velocity and position vector are updated according to Equations (19) and (20), respectively:

$$v_{i,d}^{k+1} = \omega \cdot v_{i,d}^k + c_1 \cdot r_1 \cdot (pbest_{i,d}^k - x_{i,d}^k) + c_2 \cdot r_2 \cdot (gbest_d^k - x_{i,d}^k) \quad (19)$$

$$x_{i,d}^{k+1} = x_{i,d}^k + v_{i,d}^{k+1} \quad (20)$$

where $v_{i,d}^k$ represents the velocity of each particle i in iteration k ; $x_{i,d}^k$ is the position of particle i in iteration k ; ω is the inertia factor; c_1 e c_2 are the acceleration coefficients used to adjust the cognitive and social contributions when updating the velocities, respectively; and r_1 e r_2 define the stochastic characteristic given by two random numbers evenly distributed in the interval [0, 1].

For single-objective optimization problems, $gbest$ and $pbest$ represent the global and personal best positions, respectively. However, for multi-objective optimization problems, there is more than one global optimal solution, requiring the determination of a set of

nondominated solutions (nondominated front, Pareto optimal front, or simply Pareto front). The concept of dominance is a relationship between two possible solutions within the multidimensional search space. A nondominated solution is one that is better than other solutions in at least one objective function, yet not the worst solution in any of the remaining functions. In each iteration, this set of nondominated solutions is determined, registered in a given hypercube, and stored in a repository with limited capacity.

For the collective experiment (*gbest*), in the MOPSO algorithm, each particle selects a solution from the repository associated with a given hypercube through the roulette wheel selection method that selects a nondominated solution from the repository based on a probability. This probability is calculated using the ratio between the individual fitness of the solutions (objective function value) and the quality of the solutions that compose the repository, i.e., the sum of all the individual fitness of the solutions. Furthermore, for its individual experience (*pbest*), each particle considers the current/recent nondominated solution produced by the particle itself in the iterative process. These selection procedures of *gbest* and *pbest* promote a good diversification in the construction of new solutions (population) and, simultaneously, maximize convergence to the real Pareto optimal front, ensuring a good diversity in the solutions that constitute it.

As aforementioned, the movement of each particle belonging to the population, i.e., its new velocity and position, is calculated through Equations (19) and (20), respectively. However, it is essential to prevent particles from “traveling” outside the multidimensional search space during the iterative process. This constraint is expressed mathematically by Equation (21):

$$\begin{cases} \text{if } x_{i,d}^{k+1} > ub_d \text{ then } x_{i,d}^{k+1} = ub_d \\ \text{if } x_{i,d}^{k+1} < lb_d \text{ then } x_{i,d}^{k+1} = lb_d \end{cases} \quad (21)$$

Through this procedure, if any of the lower (*lb*) or upper (*ub*) limits are exceeded, the movement of the particle is modified to ensure that the new position is within the search space.

The iterative process ends when the stopping criterion is reached. The stopping criterion may reflect several aspects inherent to the optimization problem: simulation time; maximum number of iterations; the maximum number of objective function evaluations; and population stagnation, i.e., if there is no significant improvement of the solutions during a certain number of iterations; among others.

3.3.2. Proposed Optimization Procedure

Figure 3 presents the flowchart of the implemented optimization procedure in this article for an REC with *n* participants. Initially, all the variables relative to the optimization problem and all the required variables for the correct use of the MOPSO optimization algorithm are initialized, such as the number of participants in the REC (*n*); the meteorological variables (temperature, irradiance, wind speed); the load profiles of each participant of the REC; the dimension of the optimization problem (*d*), the lower (*lb*) and upper (*ub*) bounds; the number of particles in the population (*np*); the maximum capacity of the repository of nondominant solutions; and the number of maximum iterations allowed (*tmax*), among others. After these initializations, the initial positioning of the particles is determined with the following structure:

$$x_i = \overbrace{\underbrace{N_{PV_1}, N_{WT_1}, C_{bat_1}}_{\text{swarm 1}}, \underbrace{N_{PV_2}, N_{WT_2}, C_{bat_2}}_{\text{swarm 2}}, \underbrace{N_{PV_3}, N_{WT_3}, C_{bat_3}}, \dots, \underbrace{N_{PV_n}, N_{WT_n}, C_{bat_n}}_{\text{swarm n}}}_{\text{Multidimensional Search Space}} \quad (22)$$

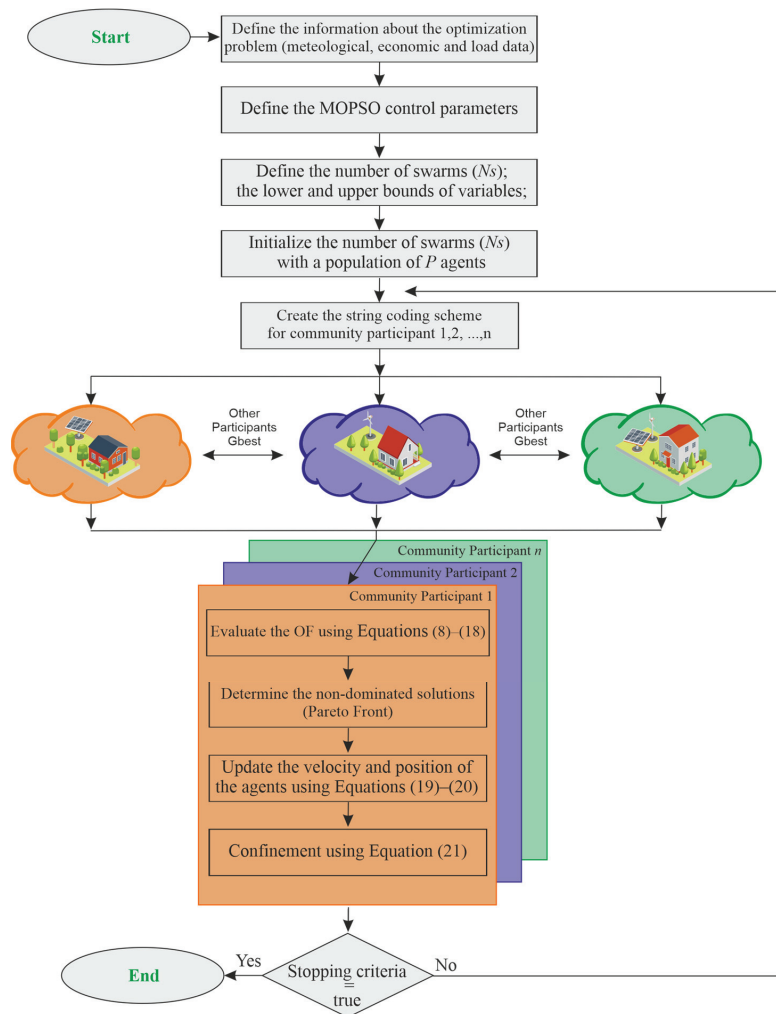


Figure 3. Optimization Strategy Diagram.

A random initial position is determined within the multidimensional search space (defined in Equation (15)), considering a population of 15 individuals per dimension and a maximum number of allowed interactions (100 iterations per dimension). The population of particles is divided into several swarms with a star topology, i.e., in each swarm, all particles communicate with each other. The various swarms evolve and move independently, while maintaining their own repository of nondominated solutions.

In each iteration, the performance of each particle regarding each swarm was determined using the economic and technical criteria detailed in Section 4.1 (Equations (8)–(18)). However, to evaluate the performance of each particle, a string code scheme was constructed by broadcasting the social component of each swarm ($gbest_{1,2,3,\dots,n}$), where n is the number of participants in the REC, as described in Equation (23):

$$x_i = \overbrace{N_{PV_1}, N_{WT_1}, C_{bat_1}, gbest_2, gbest_3, \dots, gbest_n}^{\text{Particle Position for swarm}_1} \quad (23)$$

Subsequently, a repository control mechanism evaluated the individual and collective performance of each particle and, consequently, determined the nondominant solutions inherent to each swarm. As aforementioned, the movement of each particle was determined by Equations (19) and (20). However, to prevent a new position of the particles outside the multidimensional search space, during the successive iterations, the confinement strategy described by Equation (21) was implemented. In this strategy, if any of the limits (lower or upper limit) were exceeded, the particle movement was modified ensuring that the new position was within the search space.

The execution of the various swarms, i.e., the various MOPSO optimization algorithms, ended when the established stopping criterion was reached. The established stopping criterion was within the maximum number of allowed interactions (100 iterations per dimension). Once the optimization process was completed, i.e., when the stopping criterion was reached, an external repository was created with all the nondominated solutions determined by the various swarms. Through this external repository, a nondominated solution (Final Trade-Off Solution) was selected based on the fuzzy set membership function [61,62].

4. Results Discussion and Analysis

In this section, an evaluation and performance analysis is conducted based on the results obtained from the implemented multi-objective optimization algorithm for each scenario. Firstly, the characteristics of the simulated renewable energy community and the corresponding data profiles will be presented and analyzed. Lastly, all the optimized scenarios obtained from the application of the implemented multi-objective optimization algorithm will be evaluated and discussed.

4.1. Renewable Energy Community

The community under study represents a microcosm of sustainable energy production and consumption, comprising three participants, denoted as (a), (b), and (c) in Figure 4. This configuration enables a comprehensive analysis of the interactions and dynamics among participants utilizing different energy sources. Each of the three participants in the community can produce, consume, and potentially store renewable energy under the four energy management scenarios described in Section 3.1.

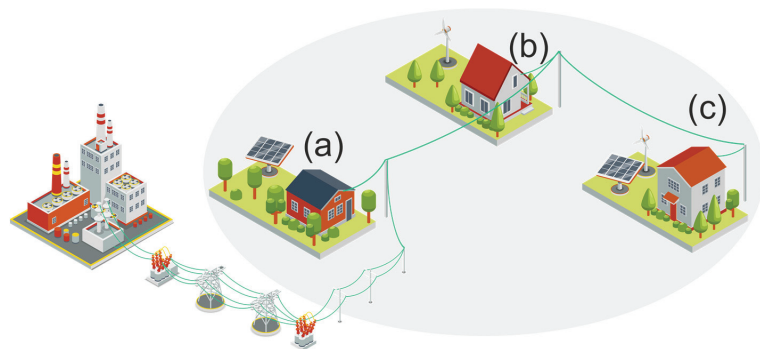


Figure 4. Renewable Energy Community Architecture.

Additionally, when the community's load demand exceeded the local renewable energy production capacity, participants could import additional energy from the electrical grid. This interaction with the grid provides several advantages for the renewable energy community. First, it ensures a reliable power supply, particularly during periods of low renewable energy production or high load demand. Second, it allows for the integration of intermittent renewable energy sources with the grid's baseload power, ensuring a continuous and stable energy supply. Third, the grid connection enables the community to

participate in feed-in tariff programs, incentivizing the production and export of excess renewable energy.

4.1.1. Mathematical Models Parameters

This subsection presents a comprehensive overview of the key mathematical model's parameters used in the simulations. These parameters encompass the characteristics of the batteries, PV, and wind turbine models.

Batteries Model Parameters

To accurately replicate the dynamic behavior of a battery within an energy community, it is necessary to adjust certain model parameters values. These parameters enable the model to mimic nuances and interactions that batteries exhibit when integrated into the energy systems of real-world communities, allowing for a more precise representation of their performance [45,57]. Table 3 presents the battery model parameters values used in the simulation.

Table 3. Batteries Model Parameters Values.

Battery Model Parameter	Value
k	0.38
c	0.271

Photovoltaic Model Parameters

The photovoltaic module selected for simulation purposes was the Sharp ND-R250A5, characterized by 60 polycrystalline silicon cells (with 156.5 mm × 156.5 mm) connected in series, divided into three strings, with each string protected by a bypass diode, i.e., a bypass diode for every 20 cells in the PV module [63]. The specifications of the selected PV module are displayed in Table 4.

Table 4. Photovoltaic Model Parameters.

PV Model Parameter	Value
μ_{mppt}	95%
P_{STC}	250 W
G_{STC}	1000 Wm ⁻²
α_{VOC}	-0.0044 V°C ⁻¹
T_{STC}	25 °C
G_{NOCT}	800 Wm ⁻²
$NOCT$	47.5 °C
T_{NOCT}	20 °C

Wind Turbine Generator

The selected wind turbine generator was the Bergey BWC XL-1, a 1 kW three-bladed wind turbine, with horizontal axis and a 2.5 m rotor diameter. It shows remarkable low-wind-speed performances, with intended applications for charging batteries and supply electrical loads in remote power systems or rural electrification programs. The corresponding power curve is displayed in Figure 5, and the corresponding parameters provided by the manufacturer are displayed in Table 5.

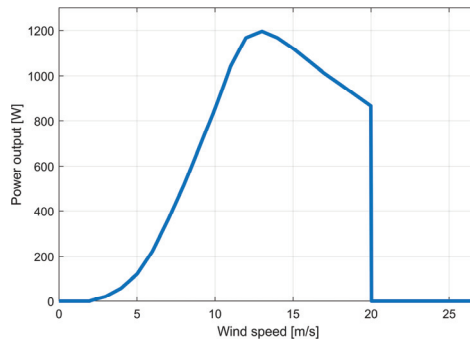


Figure 5. Power curve of the Bergey BWC XL-1 Wind Turbine.

Table 5. Wind Turbine parameters.

Wind Turbine Model Parameter	Value
Rated Power	1.000 W
Maximum output power	1.200 W
Rated wind speed	11.0 m/s
Cut-in wind speed	2.5 m/s
Furling wind speed	13.0 m/s
Cut-out wind speed	20.0 m/s
h_h	20 m
h_a	10 m
α	0.4

To complete the wind component modeling, the power law exponent (α) must be addressed for the simulation site characteristics. The power law exponent or friction coefficient value depends on numerous factors like terrain roughness, altitude, exposed site level, temperature, and season of site [64].

The value normally used for this parameter in open land areas is 0.142 [65]. However, this value does not take into consideration various terrain roughness characteristics and atmospheric stability classes, leading to large discrepancies in wind speed value prediction and huge errors in energy estimation [66]. Given this fact, the value chosen for this parameter was 0.4, a fair value considering a location with high surface roughness, with a high stability atmosphere [66–68].

4.2. Data Profiles

The data profiles used in this article were obtained from the U.S. Department of Energy's (DOE) Open Energy Data Initiative (OEDI) [69], a large and centralized repository of datasets containing weather data of all the Typical Meteorological Year version 3 (TMY3) locations, as well as dataset simulations of the residential and commercial prototype model load profiles for these locations. TMY3 is the most recent version of the TMY, a group of selected weather data measured in more than a thousand different locations across the US for at least 15 years [70], fused and shortened into a single year, representing hypothetically typical weather data in each different location, with one year of values with one-hour resolution (8760 h time series data) based on real-life values.

Load data: Three different location datasets were selected from the TMY3 residential load datasets with different time-series statistical values and shape profiles. *Weather data:* The weather data profiles were made by scaling the TMY3 weather data of one of the locations (base location), proportionally to the other two locations, including a $\pm 20\%$ deviation to induce additional variability [71]. These weather datasets contain multiple parameters, three of which are required to simulate the energy community using

the mathematical models described in Section 2: air temperature, solar irradiance, and wind speed.

Box and whisker diagrams were used to visualize and understand in greater detail the dataset profiles used to simulate the REC. The dataset profiles for each REC participant are presented with two different resolutions: hourly and monthly. Thus, one can visualize the behavior and evolution of each dataset profile during the 24 h of the day, but also visualize throughout the 12 months of the year. Figure 6 shows the hourly resolution box and whisker diagrams of the three load data profiles: Load 1 in diagram (a), Load 2 in diagram (b), and Load 3 in diagram (c); and the three weather data variables of the base location (simulation location of load 2): air temperature in diagram (d), irradiance in diagram (e), and wind speed in diagram (f). Figure 7 shows the same datasets but in a monthly resolution box and whisker diagrams, with the same disposition and identification.

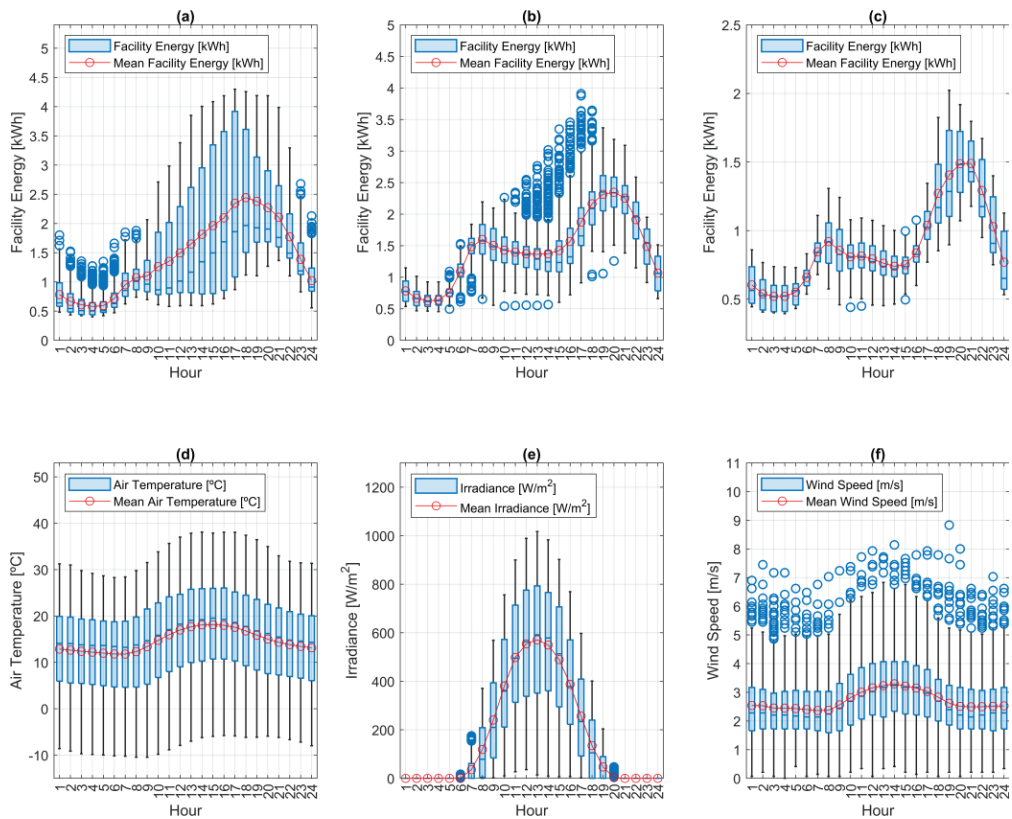


Figure 6. Box-and-whisker diagrams with an hourly resolution for each dataset profile. (a) Participant (a). (b) Participant (b). (c) Participant (c). (d) Air temperature. (e) Solar Irradiance. (f) Wind speed.

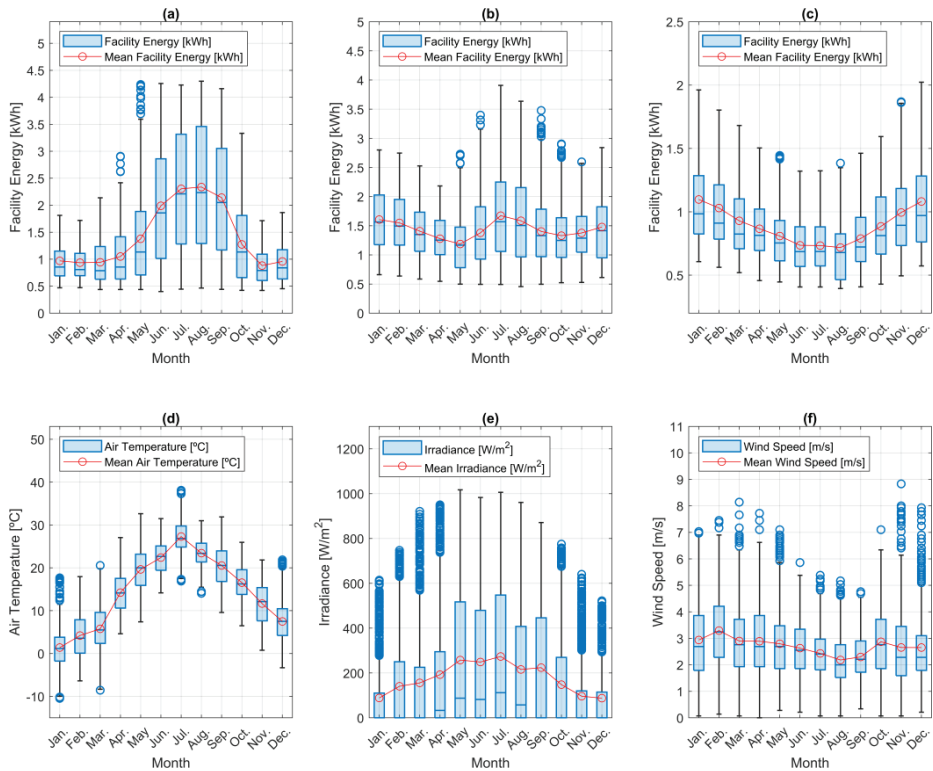


Figure 7. Box-and-whisker diagrams with a monthly resolution for each dataset profile. (a) Participant (a). (b) Participant (b). (c) Participant (c). (d) Air temperature. (e) Solar Irradiance. (f) Wind speed.

Table 6 presents the time-series statistical analysis for each dataset profile, including the mean, median, standard deviation, and statistics related to the shape of the dataset profiles, such as skewness and kurtosis. As can be seen, load profiles 1 and 2 exhibited very similar mean values. However, they differed significantly in terms of their standard deviation: Load Profile 1 had a high standard deviation of 66%, while Load Profile 2 had a standard deviation of only 42%. Moreover, these two load profiles displayed distinct skewness values: Load Profile 1 had a positively skewed distribution, while Load Profile 2 showed an approximately symmetric distribution. On the other hand, Load Profile 3 featured a lower mean and median values, with a lower standard deviation compared to the other two loads, as intended. However, its shape metrics were similar to Load Profile 1. The air temperature revealed a very symmetric shape distribution, also demonstrated by the proximity between the mean and median values, despite a high standard deviation value. Inevitably, the irradiance showed very dispersed values, demonstrated by the high value of standard deviation in contrast with the null median value.

Table 6. Time-Series Analysis of Dataset Profiles: Statistical Values.

Parameter	Mean	Median	St. Dev.	Skewness	Kurtosis
Load 1 [kWh]	1.4347	1.0874	0.95063	1.2517	3.6939
Load 2 [kWh]	1.4373	1.3567	0.60812	0.56598	2.849
Load 3 [kWh]	0.88781	0.80909	0.33569	0.99622	3.5528
Air Temperature [°C]	14.6192	15.4	9.306	−0.20139	2.1832
Irradiance [Wm^{-2}]	177.8128	0	261.7154	1.3709	3.6711
Wind Speed [ms^{-1}]	2.7075	2.48	1.2744	0.80935	3.7417

Table 7 provides detailed information on the maximum and minimum values of each dataset profile, including the corresponding month, day, and hour when these values occurred. As expected, the maximum energy demand of the load profiles occurred during the evening, and the minimum energy demand of the load profiles happened during the night. Similarly, the air temperature showed expected results, registering the highest temperature during the afternoon of summer times, in harmony with the irradiance, and reaching the minimum air temperature value in the winter.

Table 7. Time-Series Analysis of Dataset Profiles: Maximum and Minimum Values and Corresponding Dates.

Parameter	Max.	Hour of the Day	Month of the Year	Min.	Hour of the Day	Month of the Year
Load 1 [kWh]	4.2977	17	8 (Aug.)	0.40097	4	6 (Jun.)
Load 2 [kWh]	3.9086	17	7 (Jul.)	0.45593	4	8 (Aug.)
Load 3 [kWh]	2.0233	19	12 (Dec.)	0.39432	4	8 (Aug.)
Air Temperature [°C]	38.09	14	7 (Jul.)	−10.46	9	1 (Jan.)
Irradiance [Wm^{-2}]	1017	13	5 (May)	0	*	*
Wind Speed [ms^{-1}]	8.83	19	11 (Nov.)	0	*	*

* Multiple results.

Finally, Table 8 details the highest and lowest mean dataset values of each profile, with the respective hour and month they occurred. In the hour resolution diagrams, all load profiles show a similar shape with a slight peak during early morning hours and reaching daily peaks during the end of the evening/beginning of the night. Monthly, all the load profiles have completely different behaviors: Load Profile 1 had a substantial increase in values during the summer months, while Load Profile 3 displayed the opposite scenario, and Load Profile 2 had no significant changes during the months of the year. Relative to the air temperature data profile, as expected, the temperature rose with sun exposure, but with very little variation, increasing hourly after sunrise and dropping during the evening, and throughout the night. Monthly, the temperature increased gradually until the summer months and decreased substantially during the autumn and winter months. The hour of the day with the highest mean air temperature was the 15th hour (18.1138 °C), while the hour with the lowest mean air temperature (11.787 °C) was the 7th hour. The month of July had the highest mean air temperature (27.3003 °C), while January had the lowest mean air temperature (1.3899 °C).

Table 8. Time-Series Analysis of Dataset Profiles: Mean value details of each dataset profile.

Parameter	Evaluation	Hourly Resolution Profiles		Monthly Resolution Profiles	
		Value	Hour	Value	Month
Load 1 [kWh]	Highest mean value	2.4427	18	2.3372	8 (Aug.)
	Lowest mean value	0.58	4	0.88195	11 (Nov.)
Load 2 [kWh]	Highest mean value	2.3471	20	1.6732	7 (Jul.)
	Lowest mean value	0.6279	3	1.1867	5 (May)
Load 3 [kWh]	Highest mean value	1.4899	21	1.0971	1 (Jan.)
	Lowest mean value	0.51981	3	0.7179	8 (Aug.)
Air Temperature [°C]	Highest mean value	18.1138	15	27.3003	7 (Jul.)
	Lowest mean value	11.787	7	1.3899	1 (Jan.)
Irradiance [Wm^{-2}]	Highest mean value	570.8571	13	273.5148	7 (Jul.)
	Lowest mean value	0	*	87.5972	12 (Dec.)
Wind Speed [ms^{-1}]	Highest mean value	3.2959	14	3.2932	2 (Feb.)
	Lowest mean value	2.3648	7	2.1831	8 (Aug.)

* Multiple results.

Regarding solar irradiance, the location was not very privileged, reaching the monthly highest mean value (273.5148 Wm^{-2}) in the month of June and the lowest monthly mean irradiance (87.5972 Wm^{-2}) in December. The hour with the highest mean irradiance (570.8571 Wm^{-2}) was the 13th hour of the day.

The wind speed at the location was relatively slow and revealed consistent wind speeds throughout the day and the year, with the highest monthly mean value (3.2932 ms^{-1}) in February, approximately the same as the highest hourly mean value, while the lowest monthly mean value (2.1831 ms^{-1}) was in August.

4.3. Performance Evaluation and Results Discussion

This section presents and analyzes the results obtained with the implemented multi-objective optimization algorithm discussed in the previous sections. To ensure the reliability of the results, the implemented optimization algorithm underwent 15 simulations. Figure 8 provides a representation of the statistical distribution and variability of the objective functions' fitness values.

As can be seen, Scenario 1 presents a low standard deviation for LCOE, indicating relatively consistent operational costs. The mean LCOE value is 0.0609, while the median LCOE is slightly lower at 0.0604. The SSR and SCR present relatively high mean values, with 0.8154 and 0.6676 respectively. In Scenario 2, the LCOE exhibits a higher mean value of 0.0435 and a slightly higher median value of 0.0429. The SSR and SCR values are also valuable, with SSR at 0.6805 and SCR at 0.6451. This suggests that, despite higher operational costs, the community maintains a high degree of self-sufficiency and self-consumption. Scenario 3 presents the highest LCOE among the scenarios, with a mean value of 0.0523 and a median of 0.0468. The SSR and SCR values are lower in this scenario, indicating a focus on community independence over cost-efficiency. Lastly, Scenario 4 demonstrates a lower mean LCOE of 0.0371 and a median of 0.0468, making it the most cost-effective scenario. The SSR and SCR values are also advantageous, with SSR at 0.5082 and SCR at 0.5524, suggesting a balanced approach between cost efficiency and community independence.

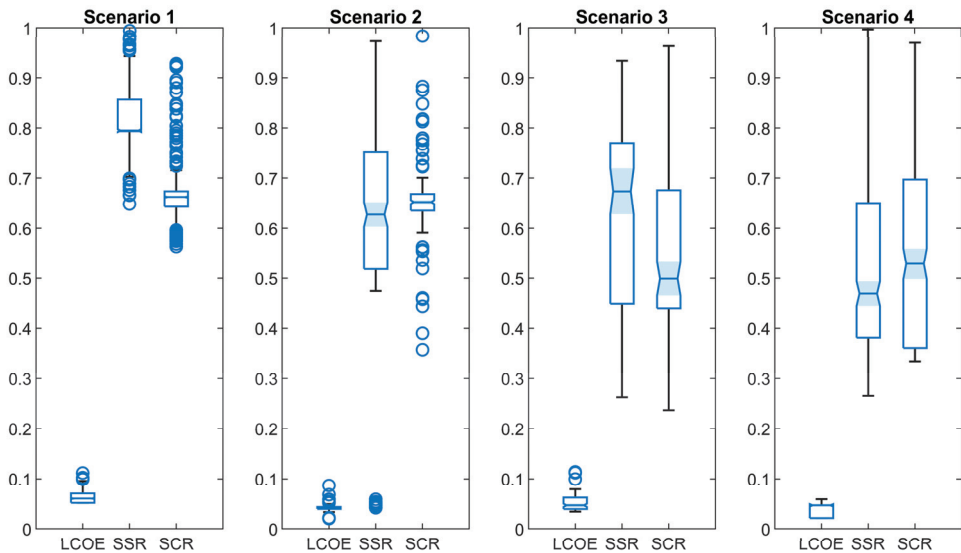


Figure 8. Statistical distribution of the objective functions’ fitness values.

Table 9 displays the sizing ratio for each participant’s optimal battery capacity and the optimal installed renewable capacity in each scenario. This ratio is calculated by dividing the installed capacity of the storage systems or the renewable energy sources for each participant by their load’s maximum value. This ratio ensures a more reliable assessment of each element’s optimal sizing within the renewable energy community.

Table 9. Sizing Ratio for Renewable Energy Community Scenarios.

Scenarios	Participant 1		Participant 2		Participant 3	
	Storage Systems Ratio	Renewable Energy Systems Ratio	Storage Systems Ratio	Renewable Energy Systems Ratio	Storage Systems Ratio	Renewable Energy Systems Ratio
Scenario 1	7.9079	2.5955	4.8611	1.9828	3.7229	2.1523
Scenario 2	6.4251	1.4827	1.7909	2.6864	2.3268	2.0941
Scenario 3	2.4712	0.7426	2.0468	2.3666	2.3268	2.0941
Scenario 4	0.9885	2.2241	0.7675	2.0468	2.5595	2.9085

In the following subsections, we discuss a performance analysis of each scenario, considering the optimal sizing of each element within the renewable energy community. This analysis provides a comprehensive understanding of the strengths and weaknesses of each scenario, aiding in the selection of the most suitable approach for a sustainable and efficient renewable energy community.

4.3.1. Scenario 1

This scenario provides a baseline comparison for the other scenarios where each participant adopts an individualist position within the community. Scenario 1 resembles a conventional microgrid where there are no energy transactions between the participants. Participants rely on their own individual renewable production and batteries to meet their load demand, exchanging required or surplus energy only with the electrical grid. Figure 9 shows the hourly average values of PV production, battery discharge and charge, imported and exported energy from/to the grid, and the average load of each participant. These diagrams offer a concise visual representation of the energy dynamics and transactions of the community, allowing for a comprehensive understanding of the participants’ renewable

production, battery usage, grid interaction, and overall energy flow throughout the course of a typical day.

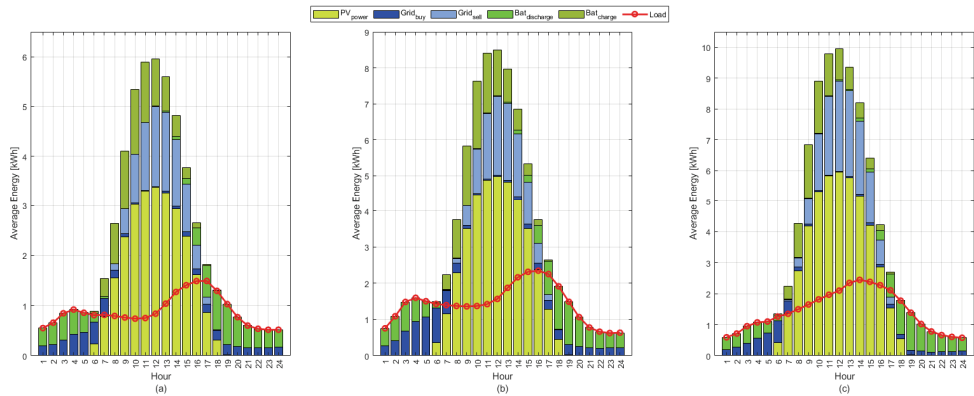


Figure 9. Scenario 1: hourly energy contributions. (a) Participant (a). (b) Participant (b). (c). Participant (c).

In this scenario, the energy storage systems are exclusively used for individual energy storage, with no coordination or collaboration among community participants to maximize the community's energy independence. As indicated in Table 9, all participants exhibit a similar renewable production ratio of approximately two. However, they present considerable differences in their Storage Systems Ratio.

As Figure 9 illustrates, this lack of energy-sharing mechanisms within the community result in surplus energy being exported to the electrical grid without benefiting other REC members. Consequently, most of the available renewable energy in the RECs is exported to the main grid.

Importantly, all participants rely solely on solar energy production systems, with each participant achieving their maximum PV production at 12:00 PM: Participant (a) achieved a maximum PV production of 5.82 kWh, Participant (b) reached 8.34 kWh, and Participant (c) achieved 10.26 kWh. Therefore, during periods of low solar irradiation, the community becomes dependent on the electrical grid to supply its load demand. Similarly, when renewable energy production is insufficient to satisfy the participant's load demand and the energy storage systems present a reduced SOC, the community relies exclusively on the electrical grid for energy supply. On average, each participant imports 0.19 kWh of energy from the electrical grid per hour to satisfy their demand. This reliance is evident in the increased energy importation from the grid throughout the night hours. As a result, the use of the energy storage systems during these hours decreases in correlation with the respective SOC levels.

To perform a broader analysis of the community operation in Scenario 1, Figure 10 depicts a diagram that illustrates the monthly cumulative energy values of PV production, energy storage systems, imported and exported energy from/to the grid, and the load for all the community's participants. This diagram provides a comprehensive overview of the community's energy dynamics over the course of a year. By showcasing the cumulative values, this analysis allows a macro-level understanding of the participants' renewable energy production, storage, grid interaction, and overall energy consumption patterns over the year.

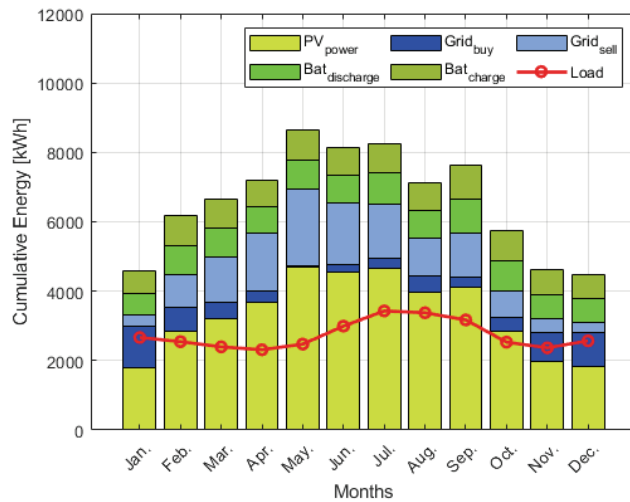


Figure 10. Scenario 1: monthly energy contributions.

As seen in Figure 10, the community's overall PV production varies in solar energy production throughout the year, reaching maximum production in May and a mean monthly production of 4677.43 kWh.

During the summer months, there is a significant rise in load demand, which decreases during the spring and autumn months. However, there is a slight increase in load demand during the peak winter months (November, December, and January). Notably, during these months, the total renewable production cannot satisfy the REC's total load demand. As a result, there is a substantial increase in energy importation from the electrical grid, surpassing the amount of exported energy. Conversely, in other months, particularly during the spring and summer, renewable production greatly exceeds the load demand. This creates an evident disparity in energy flow, with higher energy exportation to the grid.

The energy storage systems usage remains relatively consistent throughout the year, which indicates a consistent reliance on the energy storage systems to meet the community's load demand regardless of seasonal variations in load demand and renewable production.

4.3.2. Scenario 2

In contrast to the individualist position in Scenario 1, where participants rely solely on their renewable production and batteries, Scenario 2 promotes a collaborative approach. In this scenario, participants prioritize meeting their load demand, and any surplus or deficit power is exchanged among other participants within the community. This enables efficient utilization of available energy resources within the community and reduces reliance on the electrical grid. As Table 9 suggests, in this scenario, participant (a) has a storage system ratio much higher than the other participants but, however, presents a lower renewable production ratio. As for participants (b) and (c), they present very similar ratios in terms of production and storage. Figure 11 presents the hourly average values for each participant in Scenario 2.

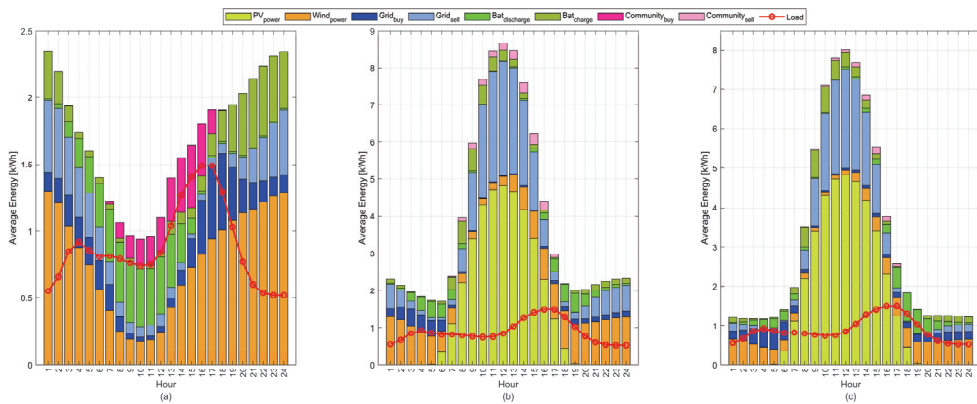


Figure 11. Scenario 2: hourly energy contributions. (a) Participant (a). (b) Participant (b). (c). Participant (c).

As depicted in Figure 11, Participant (a) exhibits a notable load demand during the day. To meet this demand, Participant (a) relies on the electrical grid, individual energy storage systems, or intra-community energy transactions with other participants, especially during the afternoon. These transactions become necessary during hours of low wind energy production, when the capacity of the individual storage systems is insufficient to meet the load demand and other participants have surplus energy due to high PV production. Although only two participants had solar production systems, this type of production significantly contributed to the community's renewable energy supply, producing, on average, approximately 1.03 kWh of electricity per hour. Conversely, Participant (a) benefits from significant surplus energy during the night due to the wind energy production systems. This surplus energy facilitates the charging of Participant (a)'s energy storage systems, thereby reducing the reliance on other transactions. In contrast, Participant (b) experiences significant energy surpluses during hours of high solar irradiation, due to the PV production systems. This surplus energy is mainly used to charge the energy storage systems and fulfill the load demand of other participants. Additionally, Participant (b) typically experiences an energy production surplus throughout the entire day, benefiting from the advantageous complementarity between PV and wind production. Consequently, Participant (b) became the community's top exporter, with an hourly average intra-community transaction of 0.081 kWh and an average energy sale to the electrical grid of 0.96 kWh per hour. Figure 12 depicts the monthly cumulative energy contributions that resume the RES operation in Scenario 2.

As shown in Figure 12, grid interactions exhibit a significant pattern throughout the year. Initially, during the early months, grid interactions are primarily characterized by energy exportation to the electrical grid, indicating a surplus of energy within the community. However, as we transition into the summer months, the balance shifts and grid interactions predominantly involve energy importations. This shift can be attributed to the reduced production of wind power during this period, resulting in a deficit of renewable production to meet the total load demand.

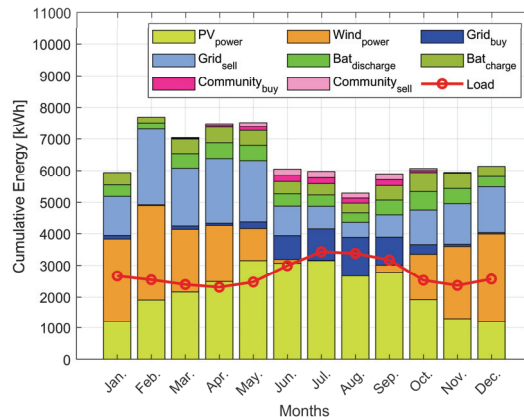


Figure 12. Scenario 2: monthly energy contributions.

4.3.3. Scenario 3

In Scenario 3, community participants share their surplus renewable energy directly to fulfill the load demand of other participants before relying on their batteries for charging. This collaborative approach ensures an efficient utilization of excess renewable energy to effectively supply the energy needs of the community, reducing the utilization of the individual storage systems and, therefore, improving their lifespan. As can be seen in Table 9, both participants have similar installed capacity ratio, but, on the other hand, participant (a) present a distinct renewable production ratio when compared to the other participants. Figure 13 illustrates the hourly average energy for each participant in Scenario 3.

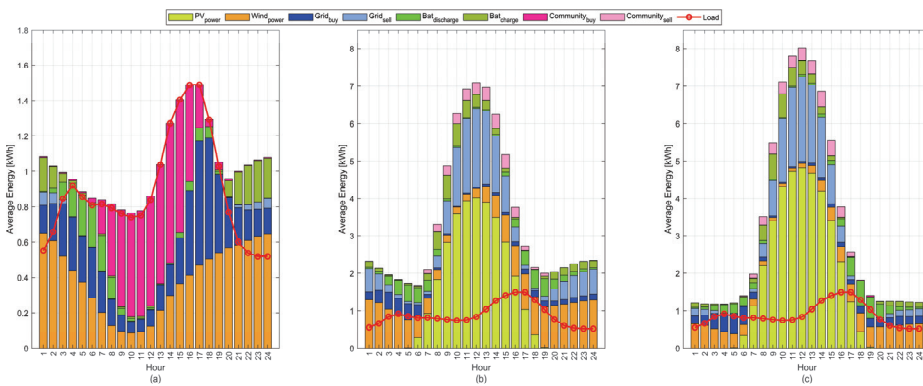


Figure 13. Scenario 3: hourly energy contributions. (a) Participant (a). (b) Participant (b). (c) Participant (c).

As can be observed in Figure 13, Participant (a) exhibits a distinct load demand pattern, particularly during daylight hours, when there is a decrease in energy consumption. To supply its energy needs during daylight hours, Participant (a) mostly relies on intra-community energy exchanges and grid importation. On average, Participant (a) imports 0.255 kWh of electricity per hour from the community and 0.253 kWh from the grid, reflecting its low renewable energy production during daylight hours. In contrast, Participants (b) and (c) demonstrate significant surplus renewable generation, primarily due to their PV generation systems. During the night hours, both Participant (a) and Participant (b) experience a substantial surplus in wind energy production. Figure 14 illustrates a monthly cumulative energy diagram for Scenario 3.

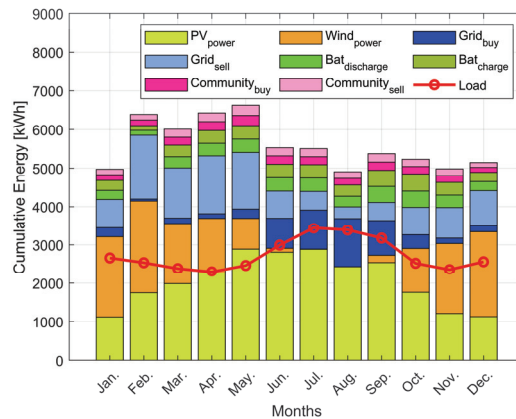


Figure 14. Scenario 3: monthly energy contributions.

Figure 14 exhibits a similar behavior to Scenario 2 but with a notable increase in inner-community transactions. During the early months, the renewable energy production matrix is largely dominated by wind energy and, as the peak summer months approach, gradually decreases and is partially replaced by PV production. However, during these peak months, renewable energy production becomes insufficient to meet the high load demand, mainly due to the decrease in wind energy production. As a result, the grid interactions, which were predominantly energy exportation, shift towards energy importation to satisfy the load demand. Moreover, community transactions account for a significant portion of the energy flow, reaching an average of 191 kWh per month.

4.3.4. Scenario 4

In Scenario 4, all renewable energy sources and storage systems are shared among the participants. When one participant has surplus energy, it can be used to meet the load demand of others. Firstly, they charge their own batteries to SOC_{max} and then proceed to charge other peers' batteries sequentially. Conversely, if a participant faces an energy deficit, they can use the energy surplus from others, discharge their battery to the lower limit of SOC_{min} , and even discharge other peers' batteries if necessary. As can be seen in Table 9, both participants present similar renewable production ratio, but with a diversified production mix. Specifically, participant (a) presents a production mix consisting only of wind production, participant (b) a mix of photovoltaic and wind production and, on the other hand, participant (c) only has photovoltaic production.

Figure 15 presents the hourly average energy for each participant in Scenario 4. As shown, Participant (a) experiences frequent energy deficits during the day, relying on intra-community energy exchanges, occasional grid transactions, and even energy exchanges with other participants to fulfill its energy needs. These deficits are primarily due to the limited wind energy production, while the other participants have significant surplus energy, especially during peak PV production in the afternoon. However, during the night, Participant (a) benefits from excessive energy production, enabling the charge of their individual batteries. In contrast, Participant (b) has substantial surplus energy during the day, due to their PV production, complemented by considerable wind energy production during the night. On the other hand, Participant (c) consistently faces energy deficits during the first and last hours of the day, as no renewable energy production is available in that period. Nevertheless, Participant (c) has substantial surplus energy from PV sources during daylight hours. Like Participant (b), Participant (c) also capitalizes on the high PV production during energy deficit hours to charge its storage systems. Figure 16 presents a monthly cumulative energy diagram that summarizes the RES operation in Scenario 4.

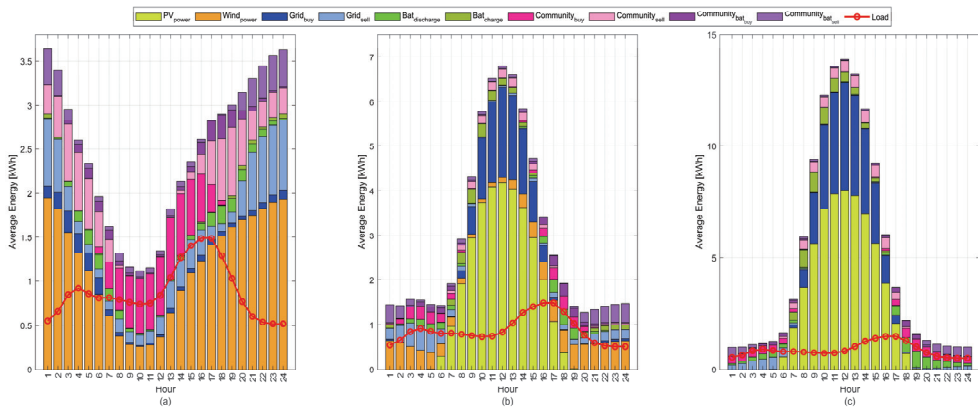


Figure 15. Scenario 4: hourly energy contributions. (a) Participant (a). (b) Participant (b). (c). Participant (c).

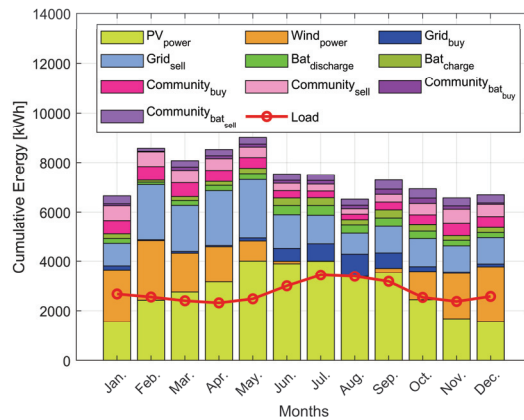


Figure 16. Scenario 4: monthly energy contributions.

Unlike the previous scenarios, in Scenario 4, the total renewable energy production consistently exceeds the total load demand every month of the year, even during peak summer months when wind production is negligible. This indicates a more efficient and optimized energy system. In the winter and autumn period, grid transactions are primarily energy exportations, and the community heavily relies on inner-community exchanges and battery exchanges. However, individual battery reserves are not frequently needed. On the other hand, in the spring and summer periods, grid transactions gradually shift towards grid importation. Moreover, energy storage system reserves increase in this period, while community and battery exchanges have a relatively lower impact on the overall community operation.

4.4. Overall Results and Analysis of Renewable Energy Scenarios

The following section presents and discusses the overall results of each scenario, including an analysis of the energy dynamics, performance metrics, and the impact of collaborative approaches on renewable energy integration. Examining the outcomes of each scenario one can evaluate the effectiveness of different energy management strategies and their implications for achieving greater energy independence, optimizing renewable resource utilization, and minimizing reliance on the electrical grid within the renewable energy community.

As seen in Figure 17, Scenario 1 exhibits a high percentage of grid exchanges (33%), which can be attributed to the individualist approach adopted by the community participants. With no energy transactions among participants, the participants' surplus energy is exported to the grid, resulting in a higher percentage of exportations (22.4%) compared to importations (10.4%). In this scenario, all the renewable energy generation (67%) comes exclusively from PV production, with no wind power production.

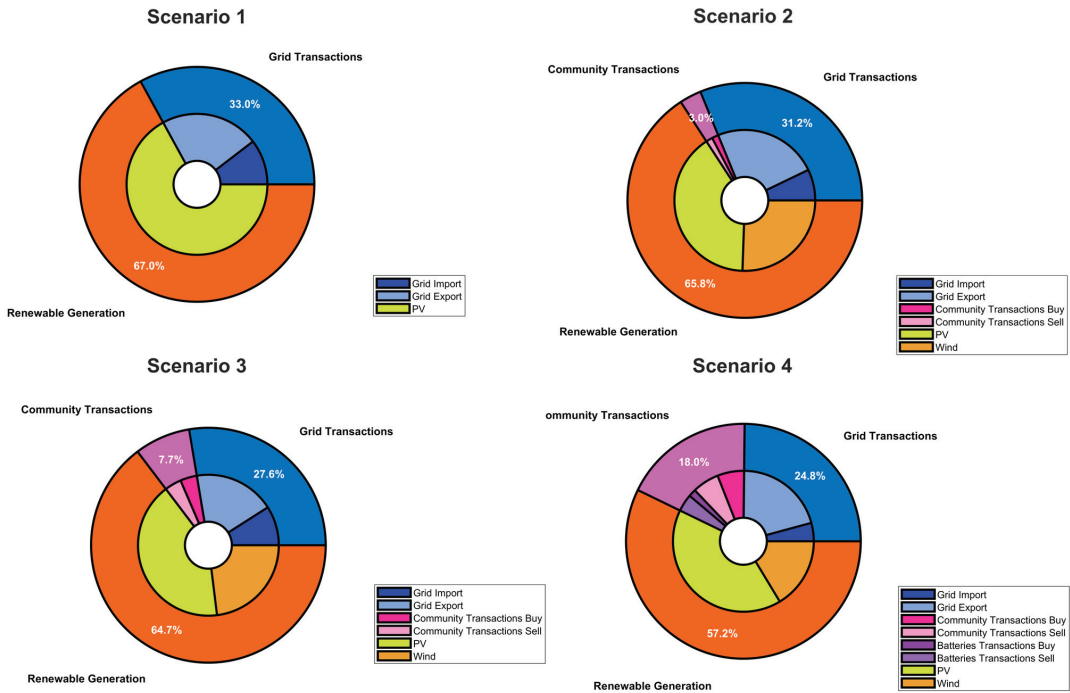


Figure 17. Percentage of transacted energy in each scenario.

In Scenario 2, grid transactions constitute 31.2% of the total energy usage, where 24.0% are grid exportations and 7.2% are grid importations. Community transactions accounted for 3% of the energy usage, while renewable energy sources (RES) contributed 65.8% of the energy supply. Within the renewable energy generation category, PV generation accounts for 40.3%, and wind power generation contributes 25.5%.

In Scenario 3, grid transactions represent 27.6% of the total energy in the renewable energy community (where grid importations represent 9% and exportations 18.6%). By prioritizing the use of excess energy to meet the load demand of other participants before charging their individual batteries, the need for grid interactions is reduced. This balanced distribution between exports and imports from the grid reflects a more efficient use of renewable energy resources, which reached a percentage of 64.7%, of which 41.6% resulted from solar origin and the remaining 23.1% from wind production.

In Scenario 4, the decrease in overall grid interactions (24.8%, where 20.6% were grid exportations and 4.2% were importations) can be attributed to the collaborative approach adopted by the community participants. By sharing batteries and renewable energy sources, surplus energy can be used to meet the load demand of other community participants, resulting in a higher percentage of community transactions (12.3%). Notably, most of the battery transactions were selling transactions (70%), indicating the community's proactive use of surplus energy to reduce dependence on external sources.

Overall, the variations in the percentage of grid transactions and community transactions in each scenario reflect the different energy management strategies employed. The collaboration and sharing of resources within the community leads to a more efficient utilization of renewable energy and a reduction in dependence on the electrical grid.

Table 10 presents several performance metrics that summarize the renewable energy community's operations in each scenario. The Initial Investment column represents the amount of money required to initially implement each scenario. This parameter is calculated based on the initial investment required to build each CER, assuming costs of 170 Euros per solar panel, 3500 Euros per wind turbine, and 800 Euros per kW of battery. The Annual Cost of Energy indicates the annual energy cost associated with the community's operation under each scenario. This parameter is calculated based on the total energy imported and exported by the CER during the simulated year, assuming a cost of 0.22 Euros per kWh for importing and 0.06 Euros per kWh for exporting to the grid.

Table 10. Performance Metrics for Renewable Energy Community Scenarios.

Scenario	Initial Investment Cost (Euro)	Annual Energy Cost (Euro)	Annual Exported Energy (kWh)	Annual Imported Energy (kWh)	Annual Community Transactions (kWh)	Annual Community Battery Transactions (kWh)	Annual Greenhouse Gas (kgCO ₂)
Scenario 1	55,930	1371.3	13,536	6233	0	0	72,908
Scenario 2	51,700	1054.7	16,176	4794	2021.3	0	73,750
Scenario 3	41,750	1185.5	11,090	5388.6	4584.7	0	57,879
Scenario 4	39,720	777.53	17,329	3534.2	10,318	4793	72,037

The Annual Exported Energy and Annual Imported Energy columns show the amount of energy exported to and imported from the electrical grid, respectively. The Annual Intra-Community Transactions and Annual Community Battery Transactions columns represent the amount of energy exchanged within the community and through battery transactions, respectively. Lastly, Annual Greenhouse Gas Emissions quantifies the amount of greenhouse gases emitted during the year under each scenario. The reference values used for the calculations was 0.373 kg CO₂ per kWh, which corresponds to the United States electrical grid average Greenhouse Gas Emissions in 2021. Additionally, the specific values for greenhouse gas emissions factors were as follows: 0.028 kg CO₂ per kWh for the energy storage system, 0.225 kg CO₂ per kWh for the PV modules and 0.008 kg CO₂ per kWh for the Wind Turbine [72].

As shown in Table 10, Scenario 4 emerges as the most favorable option in terms of economic factors, with a relatively lower Initial Investment compared to other scenarios, indicating a more cost-effective implementation. Additionally, this scenario demonstrates a significantly lower Annual Energy Cost, highlighting its efficiency and cost-effectiveness in long-term operations. Scenarios 2 and 3 show a balanced Initial Investment Cost with a relatively low Annual Energy Cost. In contrast, Scenario 1 exhibits a higher Initial Investment Cost and Annual Energy Costs.

In terms of energy independence and grid interaction, Scenarios 2 and 4 exhibit the highest Annual Exported Energy, suggesting a higher surplus of energy. Additionally, Scenario 4 has a relatively lower Annual Imported Energy, indicating reduced reliance on the electrical grid. This scenario also shows the highest Annual Community Transactions and Annual Community Battery Transactions, highlighting active collaboration and battery energy sharing among community participants. In terms of environmental impact, Scenario 2 has the lowest Annual Greenhouse Gas Emissions, indicating a more sustainable energy operation.

Based on these performance metrics, Scenario 4 stands out as the most favorable option, offering a lower Initial Investment, which contributes to cost savings in the implementation phase. Additionally, it demonstrates reduced energy costs, ensuring long-term

affordability and sustainability. Scenario 4 also presents higher energy independence, with a significant amount of exported energy and a lower reliance on imports from the grid. Moreover, this scenario exhibits a reasonably low rate of greenhouse gas emissions, reflecting its environmentally friendly approach. Nonetheless, Scenarios 2 and 3 also display promising characteristics, demonstrating active community engagement and a well-balanced energy operation. While they do not outperform Scenario 4 in all aspects, they present valuable alternatives that foster collaboration and contribute to the community's energy sustainability.

4.5. Future Works

The research presented in this study provides valuable insights into the optimization of renewable energy communities. However, several avenues for future research and exploration can further enhance our understanding and practical implementation of collaborative energy sharing and optimization strategies:

Scalability Assessment: Exploring the scalability of the proposed optimization approach is crucial. Investigating its applicability to larger and more complex renewable energy community settings can help determine its robustness and efficiency in a broader range of scenarios [73].

Geographical Variability: Examining how different geographical locations and climates impact the effectiveness of energy management strategies is important. Understanding how environmental factors influence energy sharing and distribution can lead to region-specific optimization models [74].

Regulatory and Policy Implications: Research into potential regulatory and policy implications for the successful implementation of collaborative renewable energy sharing in communities. This includes exploring legal frameworks and policy changes necessary to support and incentivize energy sharing initiatives at various levels [9].

Practical Case Studies: Implement pilot RES or collaborate with real-world stakeholders and implement the proposed optimization strategies in pilot projects to validate theoretical models and provide practical insights [75].

Integration of Emerging Technologies: Evaluate the integration of emerging renewable energy technologies, including blockchain, into the optimization framework. Assess the efficiency gains, economic benefits, and potential for enhancing trust and transparency in energy sharing and management [76,77].

5. Conclusions

In conclusion, this article presented a comprehensive analysis of a renewable energy community, examining four different scenarios with varying degrees of collaboration and energy management strategies. The sizing of the various energy production and storage units inherent to each participant was carried out using a multi-swarm MOPSO considering economical and technical criteria, namely the leveled cost of energy (LCOE), self-consumption ratio (SCR) and self-sufficiency ratio (SSR).

The results revealed valuable insights into the performance and effectiveness of each scenario. Scenario 4 emerged as the most beneficial option, showing a lower initial investment, reduced energy costs, higher energy independence, and a reasonable greenhouse gas emission. This collaborative approach, where surplus power is shared among participants and individual storage systems are utilized as a last resort, demonstrated improved renewable energy integration and a decreased reliance on the electrical grid. Additionally, Scenarios 2 and 3 also displayed promising characteristics, emphasizing active community engagement and balanced energy operations.

The study further demonstrated the effectiveness of using a multi-swarm and multi-objective optimization approach to find the optimal solutions that balance various aspects of community energy dynamics. Overall, the findings from this research contribute to advancing our understanding of renewable energy integration in community settings and offer valuable guidance for enhancing the resilience and sustainability of future energy

systems. As renewable energy adoption continues to grow, collaborative approaches like those explored in these scenarios will play a vital role in building more sustainable and self-reliant communities.

Author Contributions: Conceptualization, J.F., C.M., J.P., M.d.R.C. and S.M.; methodology, J.F., C.M. and J.P.; software, J.F., C.M. and J.P.; investigation, J.F., C.M., J.P., M.d.R.C. and S.M.; formal analysis, M.d.R.C. and S.M.; writing—original draft preparation, J.F., C.M. and J.P.; writing—review and editing, M.d.R.C. and S.M.; visualization, J.F., C.M. and J.P.; supervision, M.d.R.C., J.P. and S.M. All authors have read and agreed to the published version of the manuscript.

Funding: J.P.D. Faria was supported by the doctoral Grant SFRH/BD/151349/2021 financed by the Portuguese Foundation for Science and Technology (FCT), and with funds from MPP2030, under MIT Portugal Program.

Conflicts of Interest: The authors declare no conflict of interest.

References

1. Lowe, R.J.; Drummond, P. Solar, Wind and Logistic Substitution in Global Energy Supply to 2050—Barriers and Implications. *Renew. Sustain. Energy Rev.* **2022**, *153*, 111720. [CrossRef]
2. Overland, I.; Juraev, J.; Vakulchuk, R. Are Renewable Energy Sources More Evenly Distributed than Fossil Fuels? *Renew. Energy* **2022**, *200*, 379–386. [CrossRef]
3. Gržanić, M.; Capuder, T.; Zhang, N.; Huang, W. Prosumers as Active Market Participants: A Systematic Review of Evolution of Opportunities, Models and Challenges. *Renew. Sustain. Energy Rev.* **2022**, *154*, 111859. [CrossRef]
4. 2030 Climate & Energy Framework. Available online: https://climate.ec.europa.eu/eu-action/climate-strategies-targets/2030-climate-energy-framework_en (accessed on 23 March 2023).
5. Buraimoh, E.; Aluko, A.O.; Oni, O.E.; Davidson, I.E. Decentralized Virtual Impedance- Conventional Droop Control for Power Sharing for Inverter-Based Distributed Energy Resources of a Microgrid. *Energies* **2022**, *15*, 4439. [CrossRef]
6. Ourahou, M.; Ayrir, W.; EL Hassouni, B.; Haddi, A. Review on Smart Grid Control and Reliability in Presence of Renewable Energies: Challenges and Prospects. *Math Comput. Simul.* **2020**, *167*, 19–31. [CrossRef]
7. Martirano, L.; Rotondo, S.; Kermani, M.; Massarella, F.; Gravina, R. Power Sharing Model for Energy Communities of Buildings. *IEEE Trans. Ind. Appl.* **2021**, *57*, 170–178. [CrossRef]
8. Ahmadifar, A.; Ginocchi, M.; Golla, M.S.; Ponci, F.; Monti, A. Development of an Energy Management System for a Renewable Energy Community and Performance Analysis via Global Sensitivity Analysis. *IEEE Access* **2023**, *11*, 4131–4154. [CrossRef]
9. Lowitzsch, J.; Hoicka, C.E.; van Tulder, F.J. Renewable Energy Communities under the 2019 European Clean Energy Package—Governance Model for the Energy Clusters of the Future? *Renew. Sustain. Energy Rev.* **2020**, *122*, 109489. [CrossRef]
10. Li, Y.; Qian, F.; Gao, W.; Fukuda, H.; Wang, Y. Techno-Economic Performance of Battery Energy Storage System in an Energy Sharing Community. *J. Energy Storage* **2022**, *50*, 104247. [CrossRef]
11. Salehi, N.; Martinez-Garcia, H.; Velasco-Quesada, G.; Guerrero, J.M. A Comprehensive Review of Control Strategies and Optimization Methods for Individual and Community Microgrids. *IEEE Access* **2022**, *10*, 15935–15955. [CrossRef]
12. Amrutha Raju, B.; Vuddanti, S.; Salkuti, S.R. Review of Energy Management System Approaches in Microgrids. *Energies* **2021**, *14*, 5459. [CrossRef]
13. Dolara, A.; Grimaccia, F.; Magistrati, G.; Marchegiani, G. Optimization Models for Islanded Micro-Grids: A Comparative Analysis between Linear Programming and Mixed Integer Programming. *Energies* **2017**, *10*, 241. [CrossRef]
14. Panwar, L.K.; Konda, S.R.; Verma, A.; Panigrahi, B.K.; Kumar, R. Operation Window Constrained Strategic Energy Management of Microgrid with Electric Vehicle and Distributed Resources. *IET Gener. Transm. Distrib.* **2017**, *11*, 615–626. [CrossRef]
15. Helal, S.A.; Najee, R.J.; Hanna, M.O.; Shaaban, M.F.; Osman, A.H.; Hassan, M.S. An Energy Management System for Hybrid Microgrids in Remote Communities. In Proceedings of the 2017 IEEE 30th Canadian Conference on Electrical and Computer Engineering (CCECE), Windsor, ON, Canada, 30 April–3 May 2017. [CrossRef]
16. Murty, V.V.S.N.; Kumar, A. Multi-Objective Energy Management in Microgrids with Hybrid Energy Sources and Battery Energy Storage Systems. *Prot. Control Mod. Power Syst.* **2020**, *5*, 1–20. [CrossRef]
17. Huo, Y.; Bouffard, F.; Joós, G. Decision Tree-Based Optimization for Flexibility Management for Sustainable Energy Microgrids. *Appl. Energy* **2021**, *290*, 116772. [CrossRef]
18. Byrne, R.H.; Nguyen, T.A.; Copp, D.A.; Chalamala, B.R.; Gyuk, I. Energy Management and Optimization Methods for Grid Energy Storage Systems. *IEEE Access* **2017**, *6*, 13231–13260. [CrossRef]
19. Liu, Y.; Li, Z.; Lin, Z.; Zhao, K.; Zhu, Y. Multi-Objective Optimization of Energy Management Strategy on Hybrid Energy Storage System Based on Radau Pseudospectral Method. *IEEE Access* **2019**, *7*, 112483–112493. [CrossRef]
20. Weckesser, T.; Dominković, D.F.; Blomgren, E.M.V.; Schledorn, A.; Madsen, H. Renewable Energy Communities: Optimal Sizing and Distribution Grid Impact of Photo-Voltaics and Battery Storage. *Appl. Energy* **2021**, *301*, 117408. [CrossRef]
21. Liu, J.; Yang, H.; Zhou, Y. Peer-to-Peer Energy Trading of Net-Zero Energy Communities with Renewable Energy Systems Integrating Hydrogen Vehicle Storage. *Appl. Energy* **2021**, *298*, 117206. [CrossRef]

22. Mohsen Hosseini, S.; Carli, R.; Jantzen, J.; Dotoli, M. Multi-Block ADMM Approach for Decentralized Demand Response of Energy Communities with Flexible Loads and Shared Energy Storage System. In Proceedings of the 2022 30th Mediterranean Conference on Control and Automation, MED 2022, Vouliagmeni, Greece, 28 June–1 July 2022; pp. 67–72. [CrossRef]
23. Kennedy, J.; Eberhart, R. Particle Swarm Optimization. In Proceedings of the ICNN'95—International Conference on Neural Networks 4, Perth, WA, Australia, 27 November–1 December 1995; pp. 1942–1948. [CrossRef]
24. Rehman, A.U.; Wadud, Z.; Elavarasan, R.M.; Hafeez, G.; Khan, I.; Shafiq, Z.; Alhelou, H.H. An Optimal Power Usage Scheduling in Smart Grid Integrated with Renewable Energy Sources for Energy Management. *IEEE Access* **2021**, *9*, 84619–84638. [CrossRef]
25. Faria, J.; Pombo, J.; Calado, M.R.; Mariano, S. Current control optimization for grid-tied inverters using cuckoo search algorithm. In Proceedings of the International Congress on Engineering University da Beira Interior—“Engineering for Evolution”, Covilhã, Portugal, 28 November 2019.
26. Jayalakshmi, N.S.; Jadoun, V.K.; Gaonkar, D.N.; Shrivastava, A.; Kanwar, N.; Nandini, K.K. Optimal Operation of Multi-Source Electric Vehicle Connected Microgrid Using Metaheuristic Algorithm. *J. Energy Storage* **2022**, *52*, 105067. [CrossRef]
27. Laayati, O.; Elmaghraoui, A.; El Hadraoui, H.; Ledmaoui, Y.; Bouzi, M.; Chebak, A. Tabu search optimization for energy management in microgrids: A solution to grid-connected and standalone operation modes. In Proceedings of the 2023 IEEE 5th Global Power, Energy and Communication Conference (GPECOM), Nevsehir, Turkiye, 14–16 June 2023; pp. 401–406. [CrossRef]
28. Faria, J.; FERMEIRO, J.; Pombo, J.; Calado, M.; Mariano, S. Proportional Resonant Current Control and Output-Filter Design Optimization for Grid-Tied Inverters Using Grey Wolf Optimizer. *Energies* **2020**, *13*, 1923. [CrossRef]
29. Singh, A.R.; Ding, L.; Raju, D.K.; Kumar, R.S.; Raghav, L.P. Demand Response of Grid-Connected Microgrid Based on Metaheuristic Optimization Algorithm. *Energy Sources Part A Recovery Util. Environ. Eff.* **2021**. [CrossRef]
30. Somakumar, R.; Kasinathan, P.; Monicka, G.; Rajagopalan, A.; Ramchandaramurthy, V.K.; Subramaniam, U. Optimization of Emission Cost and Economic Analysis for Microgrid by Considering a Metaheuristic Algorithm-Assisted Dispatch Model. *Int. J. Numer. Model. Electron. Netw. Devices Fields* **2022**, *35*, e2993. [CrossRef]
31. Suresh, V.; Janik, P.; Jasinski, M.; Guerrero, J.M.; Leonowicz, Z. Microgrid Energy Management Using Metaheuristic Optimization Algorithms. *Appl. Soft Comput.* **2023**, *134*, 109981. [CrossRef]
32. Rizvi, M.; Pratap, B.; Singh, S.B. Demand-Side Management in Microgrid Using Novel Hybrid Metaheuristic Algorithm. *Electr. Eng.* **2023**, *105*, 1867–1881. [CrossRef]
33. Kang, K.M.; Choi, B.Y.; Lee, H.; An, C.G.; Kim, T.G.; Lee, Y.S.; Kim, M.; Yi, J.; Won, C.Y. Energy Management Method of Hybrid AC/DC Microgrid Using Artificial Neural Network. *Electronics* **2021**, *10*, 1939. [CrossRef]
34. Faria, J.; Pombo, J.; Calado, M.; Mariano, S. Power Management Control Strategy Based on Artificial Neural Networks for Standalone PV Applications with a Hybrid Energy Storage System. *Energies* **2019**, *12*, 902. [CrossRef]
35. Laayati, O.; El Hadraoui, H.; Bouzi, M.; Elmaghraoui, A.; Mousaid, I.; Chebak, A. A game theory approach (VCG-PSO) for optimal P2P energy trading in blockchain-enabled microgrids. In Proceedings of the IEEE EUROCON 2023—20th International Conference on Smart Technologies, Torino, Italy, 6–8 July 2023; pp. 210–215. [CrossRef]
36. Park, S.H.; Jang, Y.S.; Kim, E.J. Multi-Objective Optimization for Sizing Multi-Source Renewable Energy Systems in the Community Center of a Residential Apartment Complex. *Energy Convers. Manag.* **2021**, *244*, 114446. [CrossRef]
37. Duchaud, J.L.; Notton, G.; Darras, C.; Voyant, C. Multi-Objective Particle Swarm Optimal Sizing of a Renewable Hybrid Power Plant with Storage. *Renew. Energy* **2019**, *131*, 1156–1167. [CrossRef]
38. Sadeghi, D.; Hesami Naghshbandy, A.; Bahramara, S. Optimal Sizing of Hybrid Renewable Energy Systems in Presence of Electric Vehicles Using Multi-Objective Particle Swarm Optimization. *Energy* **2020**, *209*, 118471. [CrossRef]
39. Ang, Y.Q.; Polly, A.; Kulkarni, A.; Chambi, G.B.; Hernandez, M.; Haji, M.N. Multi-Objective Optimization of Hybrid Renewable Energy Systems with Urban Building Energy Modeling for a Prototypical Coastal Community. *Renew. Energy* **2022**, *201*, 72–84. [CrossRef]
40. Vakhnin, A.; Sopov, E.; Semenkin, E. On Improving Adaptive Problem Decomposition Using Differential Evolution for Large-Scale Optimization Problems. *Mathematics* **2022**, *10*, 4297. [CrossRef]
41. de Campos, A.; Pozo, A.T.R.; Duarte, E.P. Parallel Multi-Swarm PSO Strategies for Solving Many Objective Optimization Problems. *J. Parallel Distrib. Comput.* **2019**, *126*, 13–33. [CrossRef]
42. Bhandari, B.; Lee, K.-T.; Lee, G.-Y.; Cho, Y.-M.; Ahn, S.-H. Optimization of Hybrid Renewable Energy Power Systems: A Review. *Int. J. Precis. Eng. Manuf.-Green Technol.* **2015**, *2*, 99. [CrossRef]
43. Ridha, H.M.; Gomes, C.; Hizam, H.; Ahmadipour, M.; Heidari, A.A.; Chen, H. Multi-Objective Optimization and Multi-Criteria Decision-Making Methods for Optimal Design of Standalone Photovoltaic System: A Comprehensive Review. *Renew. Sustain. Energy Rev.* **2021**, *135*, 110202. [CrossRef]
44. Bento, P.; Nunes, H.; Pombo, J.; do Rosário Calado, M.; Mariano, S. Daily Operation Optimization of a Hybrid Energy System Considering a Short-Term Electricity Price Forecast Scheme. *Energies* **2019**, *12*, 924. [CrossRef]
45. Manwell, J.F.; McGowan, J.G. Lead Acid Battery Storage Model for Hybrid Energy Systems. *Sol. Energy* **1993**, *50*, 399–405. [CrossRef]
46. Mahesh, A.; Sandhu, K.S. Optimal Sizing of a Grid-Connected PV/Wind/Battery System Using Particle Swarm Optimization. *Iran. J. Sci. Technol.-Trans. Electr. Eng.* **2019**, *43*, 107–121. [CrossRef]
47. Rodrigues, L.M.; Bitencourt, N.L.; Rech, L.; Montez, C.; Moraes, R. An Analytical Model to Estimate the State of Charge and Lifetime for Batteries with Energy Harvesting Capabilities. *Int. J. Energy Res.* **2020**, *44*, 5243–5258. [CrossRef]

48. Mandelli, S.; Brivio, C.; Colombo, E.; Merlo, M. A Sizing Methodology Based on Levelized Cost of Supplied and Lost Energy for Off-Grid Rural Electrification Systems. *Renew. Energy* **2016**, *89*, 475–488. [CrossRef]
49. Yousri, D.; Farag, H.E.Z.; Zeineldin, H.; El-Saadany, E.F. Integrated Model for Optimal Energy Management and Demand Response of Microgrids Considering Hybrid Hydrogen-Battery Storage Systems. *Energy Convers. Manag.* **2023**, *280*, 116809. [CrossRef]
50. Mahesh, A.; Sandhu, K.S. A Genetic Algorithm Based Improved Optimal Sizing Strategy for Solar-Wind-Battery Hybrid System Using Energy Filter Algorithm. *Front. Energy* **2020**, *14*, 139–151. [CrossRef]
51. Okoye, C.O.; Solyali, O. Optimal Sizing of Stand-Alone Photovoltaic Systems in Residential Buildings. *Energy* **2017**, *126*, 573–584. [CrossRef]
52. Justus, C.G. Wind Energy Statistics for Large Arrays of Wind Turbines (New England and Central U.S. Regions). *Sol. Energy* **1978**, *20*, 379–386. [CrossRef]
53. Hamanah, W.M.; Abido, M.A.; Alhems, L.M. Optimum Sizing of Hybrid PV, Wind, Battery and Diesel System Using Lightning Search Algorithm. *Arab. J. Sci. Eng.* **2020**, *45*, 1871–1883. [CrossRef]
54. Zheng, S.; Huang, G.; Lai, A.C. Techno-Economic Performance Analysis of Synergistic Energy Sharing Strategies for Grid-Connected Prosumers with Distributed Battery Storages. *Renew. Energy* **2021**, *178*, 1261–1278. [CrossRef]
55. Aziz, A.S.; Tajuddin, M.F.N.; Zidane, T.E.K.; Su, C.L.; Alrubaie, A.J.K.; Alwazzan, M.J. Techno-Economic and Environmental Evaluation of PV/Diesel/Battery Hybrid Energy System Using Improved Dispatch Strategy. *Energy Rep.* **2022**, *8*, 6794–6814. [CrossRef]
56. Das, B.K.; Hassan, R.; Islam, M.S.; Rezaei, M. Influence of Energy Management Strategies and Storage Devices on the Techno-Enviro-Economic Optimization of Hybrid Energy Systems: A Case Study in Western Australia. *J. Energy Storage* **2022**, *51*, 104239. [CrossRef]
57. Mandal, S.; Das, B.K.; Hoque, N. Optimum Sizing of a Stand-Alone Hybrid Energy System for Rural Electrification in Bangladesh. *J. Clean. Prod.* **2018**, *200*, 12–27. [CrossRef]
58. Simoiu, M.S.; Fagarasan, I.; Ploix, S.; Calofir, V. Sizing and Management of an Energy System for a Metropolitan Station with Storage and Related District Energy Community. *Energies* **2021**, *14*, 5997. [CrossRef]
59. Venet, P.; Zaghib, K.; Song, S.-W.; Wu, X.; Tang, Z.; Stroe, D.-I.; Kerekes, T. Overview and Comparative Study of Energy Management Strategies for Residential PV Systems with Battery Storage. *Batteries* **2022**, *8*, 279. [CrossRef]
60. Coello Coello, C.A.; Lechuga, M.S. MOPSO: A Proposal for multiple objective particle swarm optimization. In Proceedings of the 2002 Congress on Evolutionary Computation, CEC, Honolulu, HI, USA, 12–17 May 2002; Volume 2, pp. 1051–1056. [CrossRef]
61. Zhang, Q.; Ding, J.; Shen, W.; Ma, J.; Li, G. Multiobjective Particle Swarm Optimization for Microgrids Pareto Optimization Dispatch. *Math Probl. Eng.* **2020**, *2020*, 5695917. [CrossRef]
62. Chen, G.; Liu, L.; Song, P.; Du, Y. Chaotic Improved PSO-Based Multi-Objective Optimization for Minimization of Power Losses and L Index in Power Systems. *Energy Convers. Manag.* **2014**, *86*, 548–560. [CrossRef]
63. Nunes, H.G.G.; Morais, F.A.L.; Pombo, J.A.N.; Mariano, S.J.P.S.; Calado, M.R.A. Bypass Diode Effect and Photovoltaic Parameter Estimation under Partial Shading Using a Hill Climbing Neural Network Algorithm. *Front. Energy Res.* **2022**, *10*, 837540. [CrossRef]
64. Ma, T.; Javed, M.S. Integrated Sizing of Hybrid PV-Wind-Battery System for Remote Island Considering the Saturation of Each Renewable Energy Resource. *Energy Convers. Manag.* **2019**, *182*, 178–190. [CrossRef]
65. Bansal, R.C.; Bhatti, T.S.; Kothari, D.P. On Some of the Design Aspects of Wind Energy Conversion Systems. *Energy Convers. Manag.* **2002**, *43*, 2175–2187. [CrossRef]
66. Albani, A.; Ibrahim, M.Z. Wind Energy Potential and Power Law Indexes Assessment for Selected Near-Coastal Sites in Malaysia. *Energies* **2017**, *10*, 307. [CrossRef]
67. Touma, J.S. Dependence of the Wind Profile Power Law on Stability for Various Locations. *J. Air Pollut. Control Assoc.* **1977**, *27*, 863–866. [CrossRef]
68. Ikhwan, M. *Investigation of Flow and Pressure Characteristics around Pyramidal Buildings*; Institut für Hydromechanik (IFH), Universitätsverlag Karlsruhe: Karlsruhe, Germany, 2005. [CrossRef]
69. Ong, S.; Clark, N. Commercial and Residential Hourly Load Profiles for All TMY3 Locations in the United States. 2014. Available online: <https://data.openei.org/submissions/153> (accessed on 7 August 2023).
70. Wilcox, S.; Marion, W. Users Manual for TMY3 Data Sets (Revised). 2008. Available online: <https://www.osti.gov/biblio/928611> (accessed on 7 August 2023).
71. Lin, J.; Pipattanasomporn, M.; Rahman, S. Comparative Analysis of Auction Mechanisms and Bidding Strategies for P2P Solar Transactive Energy Markets. *Appl. Energy* **2019**, *255*, 113687. [CrossRef]
72. National Inventory Submissions 2021 | UNFCCC. Available online: <https://unfccc.int/ghg-inventories-annex-i-parties/2021> (accessed on 9 August 2023).
73. Aklilu, Y.T.; Ding, J. Survey on Blockchain for Smart Grid Management, Control, and Operation. *Energies* **2021**, *15*, 193. [CrossRef]
74. Kamal, M.M.; Ashraf, I.; Fernandez, E. Planning and Optimization of Microgrid for Rural Electrification with Integration of Renewable Energy Resources. *J. Energy Storage* **2022**, *52*, 104782. [CrossRef]
75. Sperling, K. How Does a Pioneer Community Energy Project Succeed in Practice? The Case of the Samsø Renewable Energy Island. *Renew. Sustain. Energy Rev.* **2017**, *71*, 884–897. [CrossRef]

76. Mololoth, V.K.; Saguna, S.; Åhlund, C. Blockchain and Machine Learning for Future Smart Grids: A Review. *Energies* **2023**, *16*, 528. [CrossRef]
77. Mureddu, M.; Ghiani, E.; Pilo, F. Smart grid optimization with blockchain based decentralized genetic algorithm. In Proceedings of the 2020 IEEE Power & Energy Society General Meeting, Montreal, QC, Canada, 2–6 August 2020. [CrossRef]

Disclaimer/Publisher’s Note: The statements, opinions and data contained in all publications are solely those of the individual author(s) and contributor(s) and not of MDPI and/or the editor(s). MDPI and/or the editor(s) disclaim responsibility for any injury to people or property resulting from any ideas, methods, instructions or products referred to in the content.

Article

Evaluating Reinforcement Learning Algorithms in Residential Energy Saving and Comfort Management

Charalampos Rafail Lazaridis ^{1,2,†}, Iakovos Michailidis ^{1,*}, Georgios Karatzinis ^{1,2,†}, Panagiotis Michailidis ^{1,2,†} and Elias Kosmatopoulos ^{1,2,†}

¹ Department of Electrical and Computer Engineering, Democritus University of Thrace, 67100 Xanthi, Greece; gkaratzis@iti.gr (G.K.); panosmih@iti.gr (P.M.); kosmatop@iti.gr (E.K.)

² Information Technologies Institute (I.T.I.), Centre for Research & Technology—Hellas (C.E.R.T.H.), 57001 Thessaloniki, Greece

* Correspondence: michaild@iti.gr; Tel.: +30-2310-464160

† These authors contributed equally to this work.

Abstract: The challenge of maintaining optimal comfort in residents while minimizing energy consumption has long been a focal point for researchers and practitioners. As technology advances, reinforcement learning (RL)—a branch of machine learning where algorithms learn by interacting with the environment—has emerged as a prominent solution to this challenge. However, the modern literature exhibits a plethora of RL methodologies, rendering the selection of the most suitable one a significant challenge. This work focuses on evaluating various RL methodologies for saving energy while maintaining adequate comfort levels in a residential setting. Five prominent RL algorithms—Proximal Policy Optimization (PPO), Deep Deterministic Policy Gradient (DDPG), Deep Q-Network (DQN), Advantage Actor-Critic (A2C), and Soft Actor-Critic (SAC)—are being thoroughly compared towards a baseline conventional control approach, exhibiting their potential to improve energy use while ensuring a comfortable living environment. The integrated comparison between the different RL methodologies emphasizes the subtle strengths and weaknesses of each algorithm, indicating that the best selection relies heavily on particular energy and comfort objectives.

Keywords: reinforcement learning; energy efficiency; thermal comfort; buildings; residents; Energym

Citation: Lazaridis, C.R.; Michailidis, I.; Karatzinis, G.; Michailidis, P.; Kosmatopoulos, E. Evaluating Reinforcement Learning Algorithms in Residential Energy Saving and Comfort Management. *Energies* **2024**, *17*, 581. <https://doi.org/10.3390/en17030581>

Academic Editors: Ala Hasan and Hassam Ur Rehman

Received: 29 November 2023

Revised: 18 January 2024

Accepted: 21 January 2024

Published: 25 January 2024



Copyright: © 2024 by the authors. Licensee MDPI, Basel, Switzerland. This article is an open access article distributed under the terms and conditions of the Creative Commons Attribution (CC BY) license (<https://creativecommons.org/licenses/by/4.0/>).

1. Introduction

1.1. Motivation

Contrary to the outdated standpoint considering residents as static constructions, the modern perspective identifies them as multifunctional cyber-physical entities able to provide efficient thermal comfort and promote occupants' quality of life [1–5]. However, to provide adequate comfort to residents—using the potential integrated heating, ventilation, and air conditioning (HVAC) equipment—a specific amount of energy needs to be consumed. Such an amount portrays a significant portion of the overall energy consumption, rendering residential buildings as energy-intensive consumers and a significant contributor to the surge in greenhouse gas (GHG) emissions [6–8]. To this end, to maintain residential comfort in a viable way, the need to harmonize energy conservation while maintaining comfort levels has become an essential objective [9–12].

For many years, residents relied on manual approaches to control HVAC by adjusting thermostats, opening windows, or turning on fans based on their immediate comfort needs. While these actions provided quick adjustments to the indoor environment, the lack of real-time adaptability often resulted in energy wastage during unoccupied or temperate periods [12,13]. Recognizing this gap, scheduling devices emerged, facilitating pre-configured temperature preferences and timed functions, granting a level of autonomous management while ensuring a stable comfortable environment. However, their static configurations often

resulted in energy wastage during, e.g., vacant periods or unforeseen climatic changes, highlighting the necessity of a more sophisticated control mechanism [14].

Following the initial steps in automation, Rule-Based Control (RBC) emerged as the dominant strategy to strike a balance between energy saving and comfort. The utilized rules derived from hands-on observations and expert recommendations, setting actions for specific conditions, like reducing temperatures during off-hours or adjusting ventilation according to occupancy [15]. RBC, however, illustrated numerous limitations, struggling to adapt in real-time to varying factors such as changing weather, fluctuating occupancy, or equipment variations [16]. Additionally, RBC was primarily centered on upholding comfort standards, neglecting energy conservation or financial efficiency. The absence of a holistic understanding of the interplay between various HVAC elements also resulted in less ideal outcomes [16–18].

The complexity and unpredictability of managing HVAC led to the rise of algorithm-based control methods, such as RL [19–23]. At its core, RL algorithms learn from interactions with the environment, allowing decisions based on real-time data. Instead of relying on predefined rules such as RBC, RL methodologies continuously refine their strategy, ensuring optimal energy use without compromising comfort. Since residential environments are dynamic—with changing occupancies and external conditions—RL frameworks were adequate to anticipate and respond to different scenarios, whether it is a sudden weather change or varying resident preferences [23,24]. This continuous learning and adaptability mean that RL is sufficient to achieve long-term energy efficiency while always prioritizing the comfort of inhabitants [25–27].

However, choosing the optimal RL approach for enhancing energy efficiency in HVAC systems presents a significant challenge [28,29]. Given the dynamic nature of HVAC environments, influenced by fluctuating weather conditions, varying building occupancy, and equipment performance, no single RL algorithm stands out as a universal solution [29]. The plethora of RL algorithms, each tailored to specific scenarios and action spaces, further complicated the selection. The lack of a one-size-fits-all RL solution for HVAC systems suggests that evaluating numerous RL approaches is pivotal in identifying the best-suited strategy for specific applications, such as HVAC systems. Different RL algorithms operate uniquely when controlling residential HVAC due to their varied underlying principles, learning mechanisms, and optimization strategies [23]. Each algorithm is designed with certain assumptions and priorities, which means they respond differently to the dynamic nature of HVAC environments, influenced by fluctuating weather conditions, varying building occupancy, and equipment performance. Some might excel in rapidly changing conditions, while others might be more stable and consistent over longer periods [29]. By comparing different algorithms under consistent conditions, researchers may gain clarity on their respective performances, ensuring evaluations are both fair and insightful [30]. This process highlights the strengths and weaknesses of each algorithm, aiding in making informed decisions. Furthermore, it is not just about finding the best algorithm but understanding how each can be optimized or tailored for specific scenarios.

Motivated by the plethora of RL approaches, current work integrates a comparison between different RL control algorithms towards a conventional RBC approach for exhibiting their adequacy to support an efficient optimal control scheme for balancing energy saving and comfort. To this end, PPO, DDPG, DQN, A2C, and SAC methodologies are thoroughly assessed in a simulative environment for their ability to control the operation of HVAC and thus reduce energy consumption while ensuring indoor comfort. By testing their energy-saving capabilities in a standard residential apartment setting, the research reveals which algorithm stands out as the most suitable.

These algorithms have demonstrated superior performance in similar tasks in previous research, indicating their potential effectiveness for the specific application of HVAC control. Their ability to handle the complexities of an environment like a residential apartment requires balancing between energy saving and comfort. Defining which RL approach balances exploration and exploitation more efficiently is beneficial in finding the optimal

control strategies for HVAC and portrays a key factor for the current study. Each of these algorithms has unique strengths and characteristics which render them suitable for the problem of HVAC control for energy saving and comfort. For instance, PPO is known for its stability and reliability in different environments, making it a good choice for applications where safety and consistency are important. DDPG and SAC, being off-policy algorithms, are effective in environments with continuous action spaces, like HVAC control. Another key factor for the selection of the specific set of algorithms was influenced by their practicality in terms of implementation and the availability of support. Algorithms like PPO, DDPG, DQN, A2C, and SAC are often well-documented and supported by popular machine learning frameworks. This makes them more accessible for integration into existing systems, particularly in HVAC applications, fostering potential future real-life deployment.

It should be mentioned, that the concerned RL algorithms are meticulously evaluated against established criteria and user preferences, offering valuable insights into their performance trends. This approach adopts a user-centric perspective, aligning algorithmic control with individual comfort needs and energy efficiency goals, thereby providing customized solutions for various thermal comfort categories. Additionally, by emphasizing the distinct features of each algorithm, the study underscores the significance of choosing the appropriate algorithm based on the specific requirements of the application.

1.2. Related Literature Work

The literature exhibits numerous RL applications in residential buildings for the efficient control of different HVAC equipment. RL approaches such as PPO, DDPG, DQN, A2C, and SAC are commonly utilized to balance energy saving and comfort, reducing costs and the environmental impact on residents. More specifically, in [31], a comparison of the DQN methodology towards a thermostat controller was assessed. The findings indicate that the DQN-enabled intelligent controller surpassed the baseline controller. In the simulated setting, this advanced controller enhanced thermal comfort by approximately 15% to 30% while concurrently achieving a reduction in energy expenses ranging from 5% to 12%. The DQN algorithm in residents was also evaluated in [32], where a data-driven approach was aimed at managing split-type inverter HVACs, factoring in uncertainties. Data from similar AC units and homes were merged to balance out data disparities, and Bayesian convolutional neural networks (BCNNs) were employed to estimate both the ACs' performance and the associated uncertainties. Subsequently, the Q-learning RL mechanism was established to perform informed decisions about setpoints, using insights derived from the BCNN models. According to the outcome, the novel approach achieved slightly lower energy consumption (19.89 kWh) and discomfort (1.44 °C/h) compared to the rule-based controller [32].

In [33], a DDPG framework was tailored to regulate HVAC and energy storage systems without relying on a building's thermal dynamics model. This approach took into account a desired temperature bracket and various uncertain parameters. Comprehensive simulations grounded in real-world data attest to the potency and resilience of the suggested algorithm in comparison to the baseline ON/OFF control policy. According to the results, the proposed energy management algorithm was able to reduce the mean value of total energy cost by 15.21% compared to the baseline controller while also achieving a lower mean value of total temperature deviation, indicating improved thermal comfort. Similarly, in [34], researchers employed a dual-focused control strategy for HVAC systems that balanced energy costs with user comfort. By addressing such objectives simultaneously, an optimization model was structured toward energy cost predictions, past usage trends, and external temperatures. Utilizing the DDPG method, an optimal control strategy was achieved that was able to harmonize cost and comfort. According to the results, different weighting factor prices balancing energy cost saving and comfort provided different results. For instance, when the weighting factor reached 0.5, 38.5% energy cost saving was achieved. Increasing the weighting factor to 0.55, energy cost savings reached a 50% improvement in comparison to a predefined temperature schedule control approach. Thermal

Comfort Improvement Factor ranged from 42.75% to −28.7% across different weighting factor values.

A comparative analysis between DQN and DDPG methodologies was also carried out to control multi-zone residential HVAC systems in [35]. The concerned optimization objective was twofold: cut down energy expenses and ensure occupant comfort. By using the DDPG method, they effectively learned from continuous interactions in a simulated building setting, even without prior model insights. Their findings reveal that this DDPG-guided HVAC management surpassed the leading DQN, slashing energy costs by 15% and decreasing comfort breaches by 79%. Impressively, when pitted against a conventional RBC method, the DDPG approach reduced comfort infractions by a staggering 98%.

The PPO approach was evaluated in [36] to fine-tune the operation of a building's HVAC system, aiming to enhance energy efficiency, uphold thermal comfort, and meet set demand response targets. Simulated results showcased that leveraging RL for standard HVAC management was sufficient to achieve energy savings of nearly 22% in weekly energy consumption in comparison to a conventional baseline controller. Furthermore, during periods requiring demand response, employing a controller attuned to demand response with RL can lead to power fluctuations of about 50% over a week, in comparison to a conventional RL controller, all the while ensuring the thermal comfort of the inhabitants.

To assess the effectiveness of deep reinforcement learning (DRL)-based control systems, the researchers conducted evaluations of both PPO and A2C controllers. This evaluation focused on summer cooling performance over one month, followed by a test in the subsequent month using the pre-trained models [37]. Findings indicated that A2C generally outperformed the PPO methodology, particularly with medium-sized network estimation models, except in cool and humid climates, where a PPO control proved more effective. According to the outcome, the A2C control methodology delivered 4% and 22% lower energy consumption concerning the RBC methodology in cooling mode, all while ensuring thermal comfort.

The SAC methodology was evaluated in [38], where the combination of an RL with Long Short-Term Memory (LSTM) neural networks was aimed to steer heat pumps and storage systems across four buildings. Their simulation framework incorporates LSTM models, trained on an artificial dataset from EnergyPlus, to gauge indoor temperature dynamics. The engineered controller effectively sustained comfortable indoor conditions across various buildings, achieving a cost reduction of approximately 3% against the baseline RBC approach. Furthermore, this DRL controller facilitated a peak demand reduction by 23% and decreased the Peak-to-Average Ratio (PAR) by 20%. Additionally, the DRL controller successfully harnessed interactions among diverse sources of flexibility, enhancing the flexibility factor by 4%. Moreover, in [39], the SAC approach was also utilized to efficiently control the thermal storage of a four-building cluster with unique energy profiles. The goal was to optimize individual building energy usage while leveling the overall energy load. When compared to a traditionally set RBC, the novel methodology achieved 4% cost savings, reduced peak demand by up to 12%, and led to a 10% drop in daily average peak, showcasing the benefits of SAC in energy management.

1.3. Novelty

Current work stands out for its comprehensive analysis, exploration of energy and comfort trade-offs, performance evaluation against international standards, user-centric algorithm selection, and detailed characterization of each algorithm. These facets collectively contribute to the novelty and value of our research in advancing the field of residential energy management.

Grounded in a comprehensive analysis of several prominent RL algorithms, namely SAC, PPO, A2C, DDPG, and DQN, within the context of residential energy management, current research evaluates each algorithm's ability to balance energy efficiency and occupant comfort—a critical consideration in modern living spaces. A key aspect of the current effort lies in exploring the intricate trade-offs between energy reduction and thermal comfort.

Such attributes have been achieved by implementing specific weighting parameters—a novel approach that allows us to gauge each algorithm’s performance meticulously. Such attributes not only assess the algorithms based on established criteria, but also factor in user preferences in line with international standards. This approach yields valuable insights into the general trends and performance nuances of the five algorithms under scrutiny, especially regarding how alterations in weight factors and user preferences impact their effectiveness. Moreover, additional emphasis has been given to the scalability and adaptability of these algorithms in different residential settings. Contrary to the majority of the literature, current efforts explore how these RL schemes may be effectively scaled up or down, catering to a wide range of residential environments, from small apartments to large houses, thus broadening the applicability and impact of findings.

Another interesting attribute highlighted in this study concerns the fact that some particular algorithmic schemes, like DQN, may not be directly comparable with others due to their intrinsic mechanisms. Conversely, it is observed that the PPO algorithm consistently maintains lower Predicted Percentage of Dissatisfied (PPD) values, illustrating its adaptability in shifting priorities between objectives. Such observations highlight the necessity of understanding the unique characteristics of each RL algorithm, underscoring the importance of selecting the most appropriate one for specific applications. To this end, contrary to the majority of existing literature approaches, current research does not merely provide a comparative analysis of these algorithms but also delves deep into their traits and suitability for varied applications in residential energy management.

Moreover, current effort enables a user-centric selection of algorithms to empower users to customize algorithmic control and align with their specific comfort needs and energy efficiency objectives. Such attributes pave the way for choosing the most suitable algorithm for each category of thermal comfort, thereby offering personalized solutions. The integration of dynamic user feedback into algorithm performance evaluation is a significant advancement. Unlike traditional static assessments, this approach allows for a more realistic and adaptable evaluation, considering how user preferences can evolve. To this end, current work reflects real-world scenarios accurately, where occupant preferences and comfort levels are not constant but change in response to various factors.

The environmental impact of the current research also concerns a critical aspect. By focusing on energy efficiency and sustainable living, the current study directly contributes to the broader goals of reducing carbon footprints and promoting eco-friendly practices in residential settings. This aligns with global environmental objectives and demonstrates the societal relevance of your work. Last but not least, the potential for real-world implementation and commercialization of these algorithms portrays a fruitful prospect. Current research efforts pave the way for developing new products or services that integrate these advanced algorithms into smart home systems, offering tangible benefits to consumers and industry stakeholders.

1.4. Paper Structure

The paper is structured as follows. In Section 1: Introduction, the motivation of the current work is assessed and the related previous work and the novelty of the current work are elaborated. Section 2: Joint Materials and Methods delivers the general mathematical overview of the RL methodology while providing the conceptual background of the algorithms concerned—PPO, DDPG, DQN, A2C, and SAC—regarding the implementation in HVAC. Section 3: Testbed Description elaborates on the aspects of the concerned simulative testbed description, while Section 4: Results and Discussion illustrates a thorough comparative analysis of RL algorithms’ performance in energy saving and comfort measures. Last but not least, Section 5: Conclusions and Future Work concludes the outcomes of the current study and describes the future work generated by the current research effort.

2. Joint Materials and Methods

This section provides the mathematical description as well as the particularities of RL applications in HVAC control applications. Providing the generalized concept of the RL approach as well as the concept of the individual RL algorithms, the current work aims to establish the landscape of the concerned RL concepts, familiarizing the reader with the current state of the art and highlighting the relevance of the study at hand.

The General Reinforcement Learning Conceptual Background

In RL, an agent interacts with an environment over discrete time steps to achieve a certain objective. At each time step, the agent observes the current state of the environment, which provides a snapshot of all pertinent information about the environment at that moment. Based on this state, the agent selects an action according to its policy. The policy is essentially the strategy or behavior that the agent follows, and it can be deterministic (always giving the same action for a given state) or stochastic (providing a distribution over possible actions) [23,40].

Once the action is taken, the environment transitions to a new state and provides feedback to the agent as a reward (Figure 1). This reward offers a numerical value indicating how good or bad the action was in achieving the agent's objective. Over time, the agent aims to learn a policy that maximizes its expected cumulative reward, often referred to as the return. To aid in this learning, the agent often estimates a value function, which predicts the expected return from a given state when following a particular policy. This value function helps the agent to judge the long-term consequences of its actions, enabling it to favor actions that lead to higher cumulative rewards in the future [23,40].

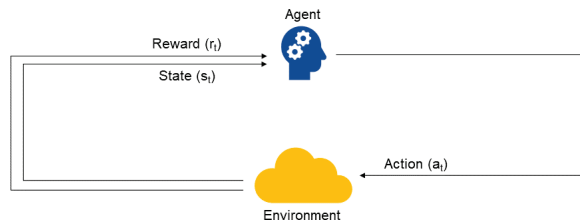


Figure 1. The general reinforcement learning framework, with an autonomous agent acting in an environment.

More specifically:

- **State:** The state, denoted as s , encapsulates the current environmental and system-specific conditions that are pertinent to the decision-making process of HVAC control. In the context of HVAC control, the state can be formally represented as [23]:

$$s = [T_{\text{room}}, T_{\text{setpoint}}, T_{\text{external}}, n_{\text{occupants}}, t, \dots] \quad (1)$$

where T_{room} is the current room temperature; T_{setpoint} is the desired temperature; T_{external} denotes the external temperature; $n_{\text{occupants}}$ is the number of occupants; t represents the current time or time of day.

- **Action:** The action space encompasses the set of all feasible actions that the HVAC system can take at any given state. Let a denote an action taken by the RL agent. In the HVAC context, this is represented as:

$$a \in \{\text{ON}, \text{OFF}, \Delta T_{\text{setpoint}}, \Delta \text{airflow}\} \quad (2)$$

where ON and OFF denote the operational status of the HVAC; $\Delta T_{\text{setpoint}}$ represents the adjustment to the temperature setpoint; $\Delta \text{airflow}$ signifies changes in the airflow rate.

- **Reward:** The reward function provides a quantitative measure of the quality of an action taken by the agent in a particular state. For HVAC systems, the reward function

aims to strike a balance between energy efficiency and occupant comfort. Formally, the reward $r(s, a)$ can be defined as:

$$r(s, a) = -\alpha E_{\text{consumed}} + \beta C_{\text{comfort}} - \delta |T_{\text{room}} - T_{\text{setpoint}}| \quad (3)$$

where α , β , and δ are weighting parameters; E_{consumed} is the energy consumed by the HVAC system; C_{comfort} quantifies the comfort level of occupants.

- **Policy:** The policy, denoted as π , provides a mapping from states to actions. It represents the strategy that the RL agent employs to act in the environment. Depending on the RL approach, this policy can be deterministic or stochastic. In deep RL contexts, this policy is often parameterized by a neural network, leading to a functional representation:

$$a = \pi_{\theta}(s) \quad (4)$$

where θ represents the parameters of the neural network.

- **Value Function:** The value function offers a prediction of the expected cumulative reward from a given state when following a particular policy. For a policy π , the value function $V^{\pi}(s)$ is defined as:

$$V^{\pi}(s) = \mathbb{E}_{\pi} \left[\sum_{t=0}^{\infty} \gamma^t r(s_t, a_t) | s_0 = s \right] \quad (5)$$

Here, γ is a discount factor that ensures future rewards are discounted to reflect their temporal delay.

In the context of HVAC control, the goal is twofold: achieve energy saving while maintaining occupant comfort. The state typically captures variables that influence HVAC decisions, such as current room temperature, desired temperature setpoint, external temperature, and the number of occupants. This comprehensive state representation ensures that the RL agent has enough information to make informed decisions. The reward function is designed to balance energy efficiency and comfort. For instance, the agent could receive a positive reward for keeping room temperatures within a comfortable range and a negative reward proportional to the energy consumed. This way, the agent is encouraged to maintain comfort while using as little energy as possible [23,41].

The policy in this scenario maps from the rich state information to HVAC control actions, such as turning the system on/off or adjusting temperature setpoints. As the agent interacts with the environment (the residence and its HVAC system), it refines this policy to better achieve the dual objectives. The value function in the HVAC context provides insights into the long-term benefits of current actions. For instance, turning off the HVAC system might save energy now but could lead to discomfort later, resulting in a lower value. By considering such long-term consequences, the agent is adequate to provide decisions that balance immediate energy savings against future comfort levels [41].

3. Testbed Description

In this study, the simulative testbed concerned a four-floor residential building in Tarragona, Spain, with diverse equipment like thermostats and a central geothermal heat pump, which was integrated into the Energym open-source building simulation library. The setup employed the *Stable Baselines3* Python library, creating an environment where the RL agent interacts with the building model, and adjusts thermostat setpoints, while other settings are fixed. The agent's actions influence the building's thermal zones, with the environment providing feedback in terms of temperature, humidity, and energy consumption data. A multi-objective reward function guides the agent, balancing energy efficiency and thermal comfort, modifiable by adjusting weight parameters. The setup was benchmarked against a classic temperature control system, fostering a sufficient evaluation of the RL algorithms' effectiveness in optimizing residential energy management while maintaining occupant comfort.

3.1. *Energym Framework*

Energym [42] is a Python-based open-source library that is based on both *Energy-Plus* and *Modelica*, providing different benchmark building models that are interfaced using the Functional Mockup Interface (FMI) standard. This building framework consists of 11 simulation models providing diverse equipment installments (thermostat, heat pump, battery, air handling unit, electric vehicle, photovoltaic), distinct building usages (apartments, houses, offices, seminar center, and mixed-use), and different methods in the control settings (controlling thermostat setpoints and controlling the equipment directly). In this work, the *ApartmentsGrid-v0* case is adopted. This is a residential building located in Tarragona, Spain, consisting of four floors, each of them being an apartment, and there are eight thermal zones (two per floor). The thermal system of the building has a central geothermal heat pump (HP) directly connected to hot water tanks (one per apartment) used only for domestic hot water (DHW) consumption, and to a heating loop providing heat to the entire building. Therefore, regarding the equipment that is present in the building, there are four controllable thermostats (one per floor), a non-controllable heat pump, one battery, and one electric vehicle (EV). The simulation inputs (11 in total) involve thermostat setpoints for the four floors ($P1_T_Thermostat_sp, \dots, P4_T_Thermostat_sp$), heat pump temperature setpoint ($Bd_T_HP_sp$), temperature setpoints for each tank ($P1_T_Tank_sp, \dots, P4_T_Tank_sp$), battery charging/discharging setpoint rate ($Bd_Pw_Bat_sp$), and EV battery charging setpoint rate ($Bd_Ch_EVBat_sp$). The output part consists of an extensive set (69 in total) of measurements with respect to the behavior of the building for a given input vector. These simulation outputs provide temperature ($Z01_T \dots Z08_T$), humidity, and appliance energy measurements in different zones of the building, supply and return temperature for the heat pump, total energy consumption and HVAC energy consumption (Fa_E_HVAC), outdoor temperature (Ext_T), and other outputs related to the batteries. For more information about the building *ApartmentsGrid-v0*, including its thermal zones, components, inputs, and outputs, please refer to the *Energym* documentation <https://bsl546.github.io/energym-pages/sources/apg.html> (accessed on 28 November 2023).

3.2. *Building Simulative Testbed*

The overall workflow contains two gym-based environments which work in conjunction with the well-known Python library, *Stable Baselines3* [43]. The chosen model from the *Energym* framework, i.e., the *ApartmentsGrid-v0*, serves as a building model that responds with 69 output measurements for a given set of 11 input signals each time, whereas the second gym-based environment, named *IntermediateEnv*, establishes the interaction between the *ApartmentsGrid-v0* and the RL agent implementations of *Stable Baselines3*. Sections 3.3 and 3.4 describe the encapsulated operation within *IntermediateEnv*. Thus, the RL agent is encountered with *IntermediateEnv* with a Markov property interacting constantly. The overall workflow is depicted in Figure 2. More specifically, the *Energym* simulation model operates at a fine granularity, running for 480 time steps per day, with each step representing a 3 min interval. This detailed time scale allows for a nuanced simulation of the building environment's dynamic responses. In contrast, the *IntermediateEnv*, which facilitates the interaction between the RL agent and the *Energym* simulation, operates on a coarser time scale. It runs for 48 time steps per day, with each step corresponding to a 30 min interval. This difference in time step granularity is critical for the application of RL actions. Actions determined by the RL agent in the *IntermediateEnv* are applied to the *Energym* simulation model and held constant (clamped) for a duration of 10 *Energym* time steps, cumulatively amounting to 30 min. This approach ensures that each action has a sustained impact on the building environment, allowing the system enough time to reach a more stable state in response to the action. Also, it ensures that the system's response is not merely a transient reaction to the changes but rather a reflection of a more settled state. Such a setup is important in evaluating the effectiveness of the RL algorithms over a

realistically significant duration, accurately capturing the implications of each action on energy consumption and thermal comfort in the simulated building.

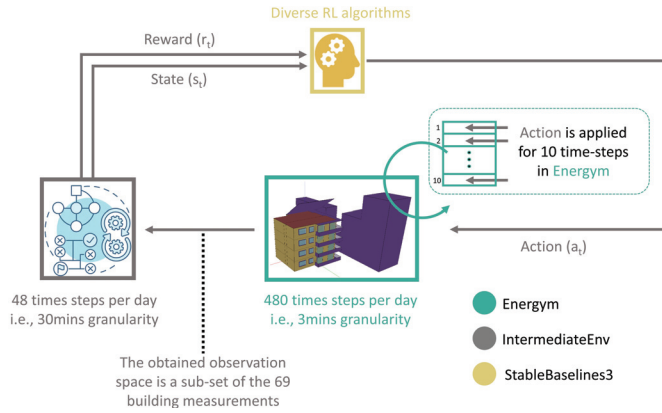


Figure 2. Operational scheme for the residential energy saving and comfort management application, coupling *Energy*, *IntermediateEnv*, and *Stable Baselines3* library.

As mentioned, *Energy* includes a wide set of input and output measurements on this specific building. The utilized input and output signals are depicted in Tables 1 and 2, respectively. Note that we change the notation of these measurements. To enhance the comprehensibility of the actions and states within our experimental setup, we have opted to use descriptive names that differ from the original *Energy* nomenclature. This decision was made to ensure clarity and ease of understanding for readers not familiar with the specific terminologies of the *Energy* platform.

Table 1. Action signals of the RL agent.

Parameter Description	Parameter Description	Symbol in Energy	Symbol in This Work
Thermostat setpoints for floors 1 to 4 (°C)	[16, 26]	$P\{X\}_T_{Thermostat_sp}$	$Thermostat_{\{X\}}$
Heat pump temperature setpoint (°C)	[35, 55]	$Bd_T_HP_sp$	$Heatpump$
Temperature setpoints for tanks 1 to 4 (°C)	[30, 70]	$P\{X\}_T_{Tank_sp}$	$Tank_{\{X\}}$
Battery charging/discharging setpoint rate	[-1, 1]	$Bd_Pw_Bat_sp$	$Batteryrate$
EV battery charging setpoint rate	[0, 1]	$Bd_Ch_EVBat_sp$	$EVBatteryrate$

Table 2. Subset of output measurements (state signals) from the building model that are inserted in the *IntermediateEnv*.

Parameter Description	Parameter Description	Symbol in Energy	Symbol in This Work
Zone temperatures for zones 1 to 8 (°C)	$Z0\{X\}_T$	[10, 40]	$Temp_{zone\{X\}}$
Outdoor temperature	Ext_T	[-10, 40]	$Temp_{ext}$
HVAC energy consumption (Wh)	Fa_E_HVAC	[0, 2000]	E^{cons}

3.3. Actions and State

The ongoing interaction between the agent and the environment involves the agent selecting actions, to which the environment responds by providing rewards and introducing new states for the agent to consider. The action is of the following form:

$$action = \{(Thermostat_1 \dots Thermostat_4), Heatpump, \dots, \dots, (Tank_1 \dots Tank_4), Battery_{rate}, EVBattery_{rate}\} \quad (6)$$

where $(Thermostat_1 \dots Thermostat_4)$ represent the thermostat setpoints for each floor, $Heatpump$ is the heat pump temperature setpoint that constantly takes a mean value in its operating bounds, $(Tank_1 \dots Tank_4)$ are the tank temperature setpoints for each floor constantly taking a mean value of their operating bounds, $Battery_{rate}$ stands for the battery charging/discharging setpoint rate that is constantly zero, and $EVBattery_{rate}$ is the EV battery charging setpoint rate that is also zero every time. The action variables that are left free to be adjusted/trained by the agent are the four thermostats, while the remaining setpoints for the tanks and the heat pump constantly take a mean operating value. In this work, we leave aside the electrical parts of the battery and EV battery, so these values will constantly be zero throughout the interaction with the building model. Thus, the action space is completely aligned with the input space of the *ApartmentsGrid-v0* building model. As mentioned, the building model returns 69 measurements for a given action vector. The observation space is a subset of those building responses. The state variables are defined as follows:

$$state = \{(Temp_{zone1} \dots Temp_{zone8}), Temp_{ext}, E^{cons}\} \quad (7)$$

where $(Temp_{zone1} \dots Temp_{zone8})$ and $Temp_{ext}$ represent the temperature measurements in degrees Celsius for the eight different building zones and outdoor conditions, respectively, and E^{cons} stands for the HVAC energy consumption, which is also measured continuously.

3.4. Reward Function

The objective here is to reduce energy consumption while sustaining thermal comfort for occupants controlling solely the thermostats of the building. Indeed, two contradictory factors together formulate the multi-objective reward function. Thus, the reward function is defined as:

$$reward = \{\alpha[E^{cons}(t)] - \beta[Th^{com}(t)]\} \quad (8)$$

where $E^{cons}(t)$ is the HVAC energy consumption that is straightforwardly measured from the building at each time instance, while $Th^{com}(t)$ is directly connected with the thermal comfort index. The emerging trade-off between HVAC energy consumption and thermal comfort is shifted into the tuning process of parameters α and β in reducing the first factor as much as possible while sustaining acceptable levels of comfort with minimum penalty. Different weights between the two tuning parameters present different results in favoring either the first or the second reward sub-term. In this work, we keep $\beta = (1 - \alpha)$, considering three weight sets $\{0.1, 0.5, 0.9\}$ towards testing three different operational modes. The intermediate scenario (weight = 0.5) induces a balance between the two reward factors, while the other two cases maintain slightly extreme cases that focus on either reducing electricity bills with a large thermal comfort penalty or increasing high levels of thermal comfort regardless of energy consumption.

3.5. Baseline Classic Controller Description

To evaluate the effectiveness of the adopted RL controllers, it is essential to compare their performance against a traditional, established control system. For this purpose, we utilize a classic controller, as implemented in the Energym framework, to serve as our baseline. This controller operates on a simple yet effective principle; it maintains a specified indoor temperature within a defined tolerance range. The operational mechanism of this classic controller is straightforward. It requires a set temperature and a tolerance limit.

Whenever the indoor temperature deviates from the set value by more than the tolerance (in absolute terms), the controller activates to restore the temperature to the predetermined level. For our comparative analysis, we have set the average indoor temperature to 20.375 °C. This setpoint is coupled with a tolerance of 0.3 °C to allow for minor fluctuations without triggering the control mechanism unnecessarily.

During the operation of the classic controller, we observed an average PPD index of 5.9%. This metric provides insight into the level of thermal comfort experienced by occupants and is crucial for assessing the practicality of the control strategy from a human-centric perspective. In terms of energy efficiency, the classic controller showed an average energy consumption of 430.183 Wh per time step. This consumption rate is a critical benchmark for evaluating the energy performance of our RL controllers under identical conditions. By comparing the performance of the RL controllers with this classic controller, we aim to ascertain not only their relative energy efficiency but also their ability to maintain occupant comfort, thereby determining their viability for practical applications in building energy management.

3.6. Thermal Comfort Metrics

The energy consumption of buildings is significantly influenced by various factors, such as indoor environmental conditions (including temperature, ventilation, and lighting) and the design and operation of the building and its systems. Simultaneously, these indoor conditions have a profound impact on the well-being, performance, and overall satisfaction of occupants within the built environment. It has been established that maintaining high-quality indoor environmental conditions can enhance work and learning performance, reduce absenteeism, and increase overall comfort. In addition, occupants who experience discomfort are more inclined to take actions to enhance their comfort, which might have implications for energy usage. Consequently, there is an increasing demand for well-defined criteria to guide building design and energy assessments [44]. To address these concerns, a series of indices have been developed, rigorously tested, and implemented to evaluate and optimize the indoor thermal environment. The wide set of international standards in this area include (i) ASHRAE 55 [45]—thermal environment conditions for human occupancy; (ii) ISO 7730 [46]—ergonomics of the thermal environment and analytical determination and interpretation of thermal comfort using calculation of the Predicted Mean Vote (PMV) and Predicted Percentage of Dissatisfied (PPD) and local thermal comfort effects; (iii) EN 16798 [47]—specification of criteria for measurements and methods for long-term evaluation of the indoor environment obtained as a result of calculations or measurements.

Thermal comfort assessment is a multifaceted process that takes into account several critical factors and aims to predict how a group of individuals perceives their thermal environment. This involves considering environmental parameters, including relative humidity (RH) and dry-bulb air temperature (tdb), and individual variables such as total clothing insulation (I_{cl}) and metabolic rate (M). The PMV is the established reference for assessing thermal comfort in mechanically conditioned buildings, serving as a tool to anticipate individuals' perceptions of their thermal environment. For naturally conditioned buildings, the adaptive models of EN and ASHRAE are utilized. The PPD index provides insight into the percentage of people likely to feel too warm or too cool. Figure 3 illustrates the thermal sensation scale and the representation of PPD as a function of PMV [48,49]. The PMV values correlate with the PPD index, highlighting the balance between thermal comfort and dissatisfaction.

The application of these comfort models in practical scenarios is detailed in Table 3. The table categorizes levels of thermal comfort expectation, delineating the acceptable PMV ranges and corresponding PPD percentages, which formulate the assessment metrics for building thermal comfort. These categories range from Category I, which signifies a high level of thermal comfort expectation suitable for sensitive groups (expectation with less than 6% predicted dissatisfaction), to Category IV, indicating a lower expectation that is considered acceptable for only part of the year.

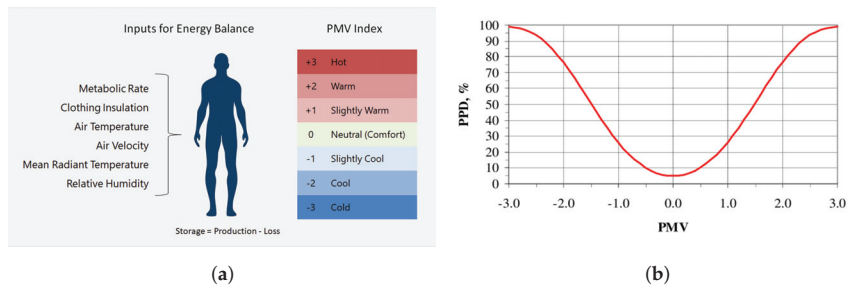


Figure 3. Thermal sensation scale and representation of PPD as function of PMV. (a) Thermal comfort variables and PMV range: <https://www.dexma.com/wp-content/uploads/2022/10/Predicted-Mean-Vote-index-Dexma.png> (accessed on 28 November 2023). (b) Correlation between PMV and PPD indices.

Table 3. Different levels of criteria regarding thermal comfort based on EN 16798-2 standard [47].

Category	PPD %	PMV	Description
I	<6	$-0.2 < PMV < +0.2$	High level of expectation and also recommended for spaces occupied by very sensitive and fragile persons with special requirements like some disabilities, sick, very young children, and elderly persons, to increase accessibility.
II	<10	$-0.5 < PMV < +0.5$	Normal level of expectation.
III	<15	$-0.7 < PMV < +0.7$	An acceptable, moderate level of expectation.
IV	<25	$-1.0 < PMV < +1.0$	Low level of expectation. This category should only be accepted for a limited part of the year.

4. Results and Discussion

This section delves deeper into the comparative performance of various RL algorithms in the context of a multi-objective reward function focusing on energy consumption and thermal comfort. In the context of the classic controller, with an average energy consumption of 430.183 Wh per time step and an average PPD of 5.9%, these RL algorithms demonstrate a range of performances. This comparative analysis highlights the strengths and limitations of each RL algorithm in balancing energy efficiency and occupant comfort. Such insights are vital for selecting the most suitable algorithm for specific building environments and occupant needs, ultimately contributing to more intelligent and sustainable building management systems. The performance of these algorithms, as shown in Table 4, is evaluated under different weight scenarios ($w = 0.1$, $w = 0.5$, and $w = 0.9$) that prioritize either energy reduction or thermal comfort to varying degrees. The average values for each algorithm presented in Table 4 are derived from five distinct evaluation runs for generalization purposes. For metrics such as Predicted Percentage Dissatisfied (PPD), the average is computed across the building's eight zones, providing a comprehensive view of the occupant's comfort throughout the entire building. This methodical approach to averaging ensures that the reported values accurately reflect the overall performance of the algorithms in varying spatial contexts within the simulated environment. Note that the architecture and hyper-parameter configuration of the utilized RL algorithms are presented in Appendix B, i.e., Tables A1–A5.

In Appendix C, we provide a comprehensive collection of supplementary results (see Figures A1–A15) that encapsulate the extensive simulations conducted across various algorithmic cases. For each RL algorithm examined, we present detailed visual data under different weight scenarios, including (a) the Predicted Percentage Dissatisfied (PPD) for each thermal zone within the building, offering insights into the thermal comfort levels achieved; (b) the measured temperature for each building zone, which illustrates the algorithms' performance in maintaining the desired thermal conditions; (c) the HVAC energy consumption throughout the day, providing a quantitative measure of the algorithms'

energy efficiency. This ensemble of 45 images serves to augment the empirical findings discussed in the main text, allowing for a granular assessment of each RL algorithm's ability to navigate the trade-offs between thermal comfort and energy consumption. By presenting these data visually, we aim to facilitate a deeper understanding of the nuanced performance characteristics of each algorithm within a residential building energy management context.

Table 4. Performance comparison after 5 distinct runs for each algorithm.

Weight Case	RL Algorithm	Average HVAC Energy Consumption (Wh)	Average PPD (%)	Average Power Diff (%)
w = 0.1	SAC	119.0829	25.11	72.32
	PPO	307.7933	6.54	28.45
	A2C	82.4841	34.91	80.83
	DDPG	191.3231	24.40	55.53
	DQN	318.9417	7.78	25.86
w = 0.5	SAC	258.8230	9.63	39.83
	PPO	297.7426	6.8	30.79
	A2C	320.5797	7.04	25.48
	DDPG	214.5196	25.15	50.13
	DQN	507.4004	7.27	−17.95
w = 0.9	SAC	258.6270	8.68	39.88
	PPO	314.7583	6.50	26.83
	A2C	301.9630	6.92	29.81
	DDPG	199.7418	25.08	53.57
	DQN	467.2232	6.30	−8.61

4.1. Weight Implications on Performance

The weight factor in the reward function plays a crucial role in balancing between reducing energy consumption and maintaining thermal comfort, specifically:

Weight 0.1: This weight setting places a higher emphasis on energy reduction. Algorithms operating under this weight are expected to minimize energy usage, potentially at the expense of occupant comfort.

Weight 0.5: Represents a balanced approach, giving equal importance to both energy savings and maintaining a satisfactory PPD level.

Weight 0.9: Prioritizes thermal comfort, aiming to achieve a PPD level close to 6%, akin to the performance of the classic controller, and aligning with the standards of Category I, which represents a high level of thermal comfort expectation.

4.2. Analysis of RL Algorithms

Each RL algorithm demonstrates unique characteristics under the aforementioned weight settings:

Soft Actor-Critic (SAC): Under weight 0.1, SAC significantly reduces energy consumption but with a higher PPD, indicating a compromise in comfort. As the weight shifts towards thermal comfort (w = 0.9), SAC shows a balance, maintaining lower energy consumption while keeping the PPD close to the desired 6%. This performance makes SAC particularly suitable for environments that require normal levels of thermal comfort. Its ability to achieve a relatively low PPD while also providing substantial energy savings exemplifies its applicability in scenarios where both comfort and energy efficiency are important, but a perfect balance is not critical (like Category II).

Proximal Policy Optimization: PPO demonstrates moderate energy consumption across all weight settings, with consistently lower PPD values, indicating a steady performance in balancing energy efficiency and comfort. One of PPO's strengths is its ability to achieve lower PPD values, which is indicative of higher occupant thermal comfort. This is particularly significant in settings where maintaining a comfortable indoor environment is as important as energy efficiency. PPO shows a commendable adaptability to varying

weights in the reward function. Whether the focus is on energy efficiency or thermal comfort, PPO adjusts its strategy accordingly, showcasing its flexibility. Perhaps the most notable aspect of PPO is its balanced approach to energy efficiency and occupant comfort. Unlike some algorithms that may excel in one aspect but fall short in the other, PPO provides a harmonious balance, making it a versatile choice for a wide range of applications. Another aspect is related to the reliability it offers. In terms of operational predictability and reliability, PPO presents fewer fluctuations in performance metrics, which is beneficial for long-term planning and consistent building management operations. However, it is crucial to recognize that due to its intrinsic algorithmic design, PPO inherently lacks the granularity to precisely adjust the equilibrium between energy saving and thermal comfort objectives in this formulated problem. PPO is influenced by the reward function's design, neural network architecture, and entropy term. Adjustments to these factors can help fine-tune the algorithm's policy, potentially improving adherence to desired comfort levels. This limitation subtly guides its performance to align more closely with scenarios characteristic of Category I, irrespective of the weight variations in the reward function. PPO's operational framework, therefore, inherently favors occupant comfort optimization, a trait that becomes increasingly apparent under diverse reward function conditions. This inclination towards maintaining lower PPD values, despite shifts in prioritization, highlights PPO's aptness for environments where thermal comfort is paramount, yet also underscores a potential limitation in settings where a distinct emphasis on energy efficiency, with a more flexible balance, is essential.

Advantage Actor-Critic: At a weight of 0.1, A2C demonstrates the lowest energy usage among all tested algorithms, highlighting its strong inclination towards energy conservation, but with the highest PPD, suggesting a strong bias towards energy saving over comfort. As the weight shifts towards prioritizing thermal comfort (such as at weight 0.9), A2C shows a slight improvement in maintaining comfort levels. However, this improvement is marginal, suggesting that while A2C can adapt to different priorities, its strength lies predominantly in energy saving with a small fraction of penalty in thermal comfort. A2C's performance profile makes it a decent candidate for energy-critical applications, especially in scenarios where energy budgets are tight, and slight compromises in comfort can be tolerated. One of A2C's advantages is its predictability in energy-saving outcomes, making it a reliable option for long-term energy management strategies where consistent low energy usage is paramount.

Deep Deterministic Policy Gradient: DDPG's performance in terms of PPD and energy consumption remains relatively consistent across different weight settings, as indicated by its PPD values ranging from 24.4% to 25.15%. However, it is important to note that these PPD values, hovering around 25%, signify a lower level of occupant thermal comfort, aligning more with Category IV standards (Low Expectation, $PPD < 25\%$). While DDPG demonstrates a certain level of stability in its performance, it does so at a relatively lower standard of thermal comfort. This aspect is crucial for applications where higher thermal comfort is a priority.

Deep Q-Network: The performance of the DQN algorithm across different weights suggests a tendency towards higher energy consumption without proportionate gains in thermal comfort with an exception to $w = 0.1$, where it provides an adequate energy reduction with a small penalty on thermal comfort. Even at a weight of 0.9, where the focus is more on comfort, DQN consumes considerably more energy compared to the classic controller (-8.61%), while achieving only marginally better PPD values (6.3%). This trend is more pronounced at weights 0.5 and 0.9, where DQN's energy consumption far exceeds the baseline set by the classic controller, indicating inefficiency. This suggests that DQN, despite its potential to achieve lower PPD values, does so at a significant energy cost, making it less suitable for applications where energy efficiency is a priority or where a balance between energy consumption and thermal comfort is desired. The inherent design of DQN, particularly its approach to discretizing the action space, might be a contributing factor to its performance characteristics. Non-continuous discretization can limit the algorithm's

ability to fine-tune its actions for optimal performance, potentially leading to higher energy consumption and only marginal improvements in thermal comfort.

4.3. Overall Comparison and Implications

The analysis reveals a diverse range of responses from each RL algorithm to the prioritization of energy reduction versus thermal comfort. PPO and A2C exhibit a more balanced approach across different weights, suggesting their suitability for scenarios where both energy efficiency and comfort are equally prioritized. SAC and A2C are the most energy-efficient but they heavily compromise comfort in the $w = 0.1$ scenario. On the other hand, these two algorithms produce the desired performance on the other two weighting scenarios in both objective metrics. DDPG and DQN appear more inclined towards optimizing comfort, especially at higher weights, leading to degraded models.

However, it is essential to identify the best-performing algorithm for each thermal comfort category based on the results to provide clear guidance on which RL algorithms are most suitable for different levels of thermal comfort expectations, from the most strict (Category I) to the least (Category IV). Thus, the best-performing RL algorithms for each thermal comfort category, considering both energy consumption and PPD values, as follows:

Category I (High Expectation, $PPD < 6\%$): For this category, where a high level of thermal comfort is expected, the algorithm that maintains PPD closest to 6% with the lowest energy consumption is ideal. In our results, PPO and A2C stand out as the most suitable choices, balancing energy efficiency while maintaining a high level of comfort. More specifically, the lowest achieved PPD values are 6.5% and 6.92% for PPO and A2C, respectively, under weight case $w = 0.9$, providing energy reduction of 26.83% and 29.81%. Both PPO and A2C demonstrate their capability to operate effectively in scenarios demanding stringent comfort requirements, as defined by Category I. Their performances suggest that they can achieve near-optimal thermal comfort levels while also contributing to energy savings, making them well-suited for applications where occupant comfort is a paramount concern, but energy efficiency cannot be overlooked.

Category II (Normal Expectation, $PPD < 10\%$): Here, the acceptable level of discomfort is slightly higher but still lies within the normal level of expectation. Thus, algorithms that can maintain PPD below 10% while optimizing energy consumption are preferred. SAC demonstrates a commendable balance between energy efficiency and thermal comfort. In our results, under the weight case $w = 0.9$, SAC achieved a PPD of 8.68%, which is within the acceptable range for Category II. Moreover, it managed to reduce energy consumption by nearly 40% (39.88%), indicating its effectiveness in optimizing energy usage while maintaining a reasonable level of occupant comfort. This performance makes SAC particularly suitable for environments that require normal levels of thermal comfort. Its ability to achieve a relatively low PPD while also providing substantial energy savings exemplifies its applicability in scenarios where both comfort and energy efficiency are important, but a perfect balance is not critical.

Category III (Moderate Expectation, $PPD < 15\%$): Based on the produced results, no case lies within the PPD range of [10%, 15%), so the selected algorithm would still be SAC. We should select an algorithm that keeps the PPD within this threshold while optimizing energy consumption. Looking at the data, SAC with weight 0.9 could be a better fit for Category III, as it has a PPD of 8.68%, which is within the threshold, and offers a reasonable energy reduction of 39.88%.

Category IV (Low Expectation, $PPD < 25\%$): This category allows for a higher level of discomfort in favor of energy savings, but the PPD still needs to be below 25%. DDPG with weight 0.1 might be a suitable option for Category IV, as it has a PPD of 24.4%, which is within the threshold, and an average HVAC power of 191.3231 Wh, indicating high energy efficiency (55.53% consumption reduction with respect to classic controller).

Figure 4 provides a visualized representation of Table 4 to easily compare the trade-offs between energy savings and thermal comfort provided by each algorithm under different preference weightings, giving a clear picture of which algorithms are more suitable for

certain comfort categories and energy efficiency objectives. The data points are color-coded and shape-coded for each RL algorithm across three different weight conditions ($w = 0.1$, $w = 0.5$, and $w = 0.9$). The lines with arrows are intended to depict the trajectory from energy reduction towards thermal comfort for each RL algorithm as the weighting factor changes from $w = 0.1$ to $w = 0.9$. This way, the arrows represent the direction of increasing weight on the PPD in the reward function, moving from right to left on the graph.

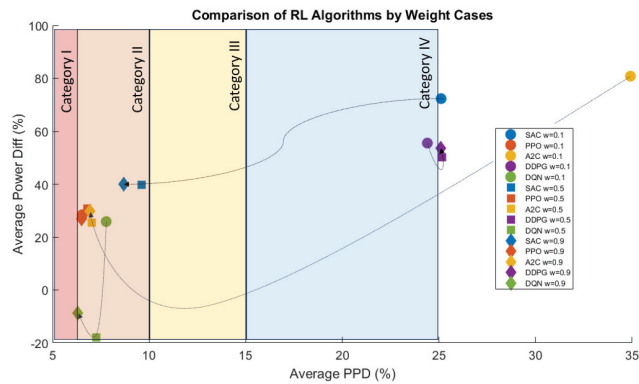


Figure 4. Visualized version of Table 4 incorporating thermal comfort categories. Dotted lines with arrows show the direction of each algorithm from energy saving to thermal comfort case based on reward function weights.

This categorization approach allows for a targeted selection of RL algorithms based on specific thermal comfort requirements and energy efficiency goals. It enables the implementation of more nuanced and effective building management strategies, catering to the varying needs of building occupants and operational efficiency mandates. In the broader context of multi-objective optimization in building management, these insights are critical. They not only inform the selection of appropriate algorithms for specific building environments but also highlight the inherent trade-offs between energy efficiency and occupant comfort. This understanding is pivotal for developing intelligent and sustainable building management systems that align with various occupant needs and environmental sustainability goals.

5. Conclusions and Future Work

The current study presents a comprehensive analysis of five prominent RL algorithms—PPO, DDPG, DQN, A2C, and SAC—in the context of residential energy management, with a focus on balancing energy efficiency and occupant comfort. The research stands out for its in-depth evaluation of these algorithms' performance in maintaining energy efficiency while ensuring thermal comfort, taking into account different occupant comfort expectations and energy efficiency goals. It should be noted that the study does not merely advance the perception of different RL applications in residential energy and comfort management but also serves as a guide for implementing RL algorithms in real-world scenarios. It underscores the potential of these algorithms to create more energy-efficient and comfortable living environments, while also emphasizing the importance of aligning algorithm selection with specific user preferences and comfort requirements.

The current study quantified thermal comfort using the PPD, aligned with international standards, categorizing levels of thermal comfort expectations into four categories based on the PMV range. The results demonstrated that SAC and A2C are particularly effective in scenarios emphasizing energy savings, presenting minimal deviations in thermal comfort from the ideal thermal comfort category. PPO maintained a balanced performance in energy efficiency and thermal comfort irrespective of the weighting factors in the reward function. DDPG provided a lower level of occupant thermal comfort, leading to a

degraded performance, whereas DQN offered an adequate energy reduction with a small penalty on thermal comfort. However, DQN's tendency to increase energy consumption when prioritizing thermal comfort was evident. This analysis underscored the nuanced capabilities and limitations of each algorithm, suggesting that the optimal choice is highly dependent on specific energy and comfort goals. To this end, the study highlighted the importance of tailored algorithm selection in intelligent building management systems and offered insights for future applications aimed at harmonizing energy conservation with occupant comfort.

The future work generated from the current study is primarily focused on the real-life implementation of RL algorithms in residential energy management. This will provide invaluable data on their performance and robustness in diverse real-world environments, where variables such as varying weather conditions, different architectural designs, and fluctuating occupant behaviors play significant roles. Additionally, integrating user feedback mechanisms to refine the algorithms' responsiveness to dynamic comfort preferences portrays another essential aspect for the continuation of the work. Moreover, the integration of renewable energy sources (RESs) and the algorithms' adaptability to smart grid technologies may also significantly enhance their applicability and efficiency, aligning with broader sustainability goals. Such real-world application and continuous refinement will validate the research findings in real life, while also contributing to the evolution of more intelligent, adaptive, and user-centric home energy management systems (BEMS).

Author Contributions: Conceptualization, all authors; methodology, C.R.L. and I.M.; software, C.R.L., I.M. and G.K.; validation, all authors; formal analysis, P.M.; investigation, P.M.; resources, all authors; writing—original draft preparation, C.R.L., G.K., and P.M.; writing—review and editing, G.K. and P.M.; visualization, P.M.; supervision, I.M. and E.K. All authors have read and agreed to the published version of the manuscript.

Funding: This work was partially supported by MASTERPIECE project funded by the European Union's Horizon Europe programme, Grant Agreement ID. 101096836 (<https://masterpiece-horizon.eu/>) and also financed through SMART2B Horizon 2020 programme of the European Union, Grant Agreement ID. 101023666 (<https://smart2b-project.eu/>).

Data Availability Statement: Data are contained within the article.

Conflicts of Interest: The authors declare no conflicts of interest.

Abbreviations

A2C	Advantage Actor-Critic
A3C	Asynchronous Advantage Actor-Critic
BCNN	Bayesian Convolutional Neural Network
DDPG	Deep Deterministic Policy Gradients
DQN	Deep Q-Network
HVAC	Heating, Ventilation, and Air Conditioning
LSTM	Long Short-Term Memory Neural Networks
PAR	Peak-to-Average Ratio
PMV	Predicted Mean Vote
PPD	Predicted Percentage of Dissatisfied
PPO	Proximal Policy Optimization
RBC	Rule-Based Control
SAC	Soft-actor-critic

Appendix A. Reinforcement Learning Algorithm Background

Appendix A.1. DQN Conceptual Background

The DQN methodology [50] was introduced in 2015, igniting the field of deep RL and replacing the need for a table to store the Q-values. Deep neural networks are used to approximate the Q-function for each state–action pair in a given environment, by minimizing the mean squared error between actual and predicted Q-values. The contributions of DQN

are as follows. (i) Policies can be learned directly utilizing a design of an end-to-end RL approach. (ii) The training of action value function approximation is stabilized with the adoption of deep neural networks that use the core ideas of experience replay (removes the correlations in the observation sequence and smoothes over changes in the data distribution) and target network. (iii) It has an iterative update that adjusts the action values (Q) towards target values that are only periodically updated, thereby reducing correlations with the target. (iv) A flexible network is trained using the same algorithm, architecture, and hyperparameters, performing well in diverse applications. The pseudo-code of DQN is presented in Algorithm A1.

Algorithm A1 DQN [50]

```

Initialize replay memory  $D$ 
Initialize action-value function  $Q$  with random weights  $\theta$ 
Initialize target action-value function  $\hat{Q}$  with weights  $\theta^- = \theta$ 
1: for  $episode = 1$  to  $M$  do
2:   Initialize sequence  $s_1 = \{x_1\}$  and preprocessed sequence  $\phi_1 = \phi(s_1)$ 
3:   for  $t = 1$  to  $T$  do
4:     Following  $\epsilon$ -greedy policy, select  $a_t = \begin{cases} \text{a random action,} & \text{with probability } \epsilon \\ \arg \max_a Q(\phi(s_t), a; \theta), & \text{otherwise} \end{cases}$ 
5:     Execute action  $a_t$  in emulator and observe reward  $r_t$  and image  $x_{t+1}$ 
6:     Set  $s_{t+1} = s_t, a_t, x_{t+1}$  and preprocess  $\phi_{t+1} = \phi(s_{t+1})$ 
7:     Store transition  $(\phi_t, a_t, r_t, \phi_{t+1})$  in  $D$  ▷ Store the experience in replay buffer
8:     Sample random minibatch of transitions  $(\phi_j, a_j, r_j, \phi_{j+1})$  from  $D$ 
9:     Set  $y_j = \begin{cases} r_j, & \text{if episode terminates at step } j + 1 \\ r_j + \gamma \max_{a'} \hat{Q}(\phi_{j+1}, a'; \theta^-), & \text{otherwise} \end{cases}$ 
10:    Perform a gradient descent step on  $(y_j - Q(\phi_j, a_j; \theta))^2$  with respect to the network parameters  $\theta$  ▷ Update the Q-network by minimizing the loss
11:    Every  $C$  steps reset  $\hat{Q} = Q$ , i.e., set  $\theta^- = \theta$  ▷ Periodic update of target Q-network
12:  end for
13: end for

```

Appendix A.2. DDPG Conceptual Background

Deep Deterministic Policy Gradient (DDPG) [51] provides a combination of DQN and deterministic policy gradient (DPG) [52] in an actor-critic and model-free approach for continuous action spaces. In contrast with DQN, which tries to predict the Q-values for each state–action pair at every time step, obtaining a greedy policy, DDPG is an actor-critic method. DDPG adopts the ideas of experience replay (store past transitions and off-policy learning) and separate target network (stabilize learning) from DQN. Another issue for DDPG is that it seldom performs exploration for actions. Additionally, in the DDPG implementation, the update frequency of the target networks is modified, keeping a slower track of the trained networks compared with DQN. Thus, the updates in the target network weight parameters are being updated after each update of the trained network using a sliding average for both the actor and the critic; thus, $\theta : \theta' \leftarrow \tau\theta + (1-\tau)\theta'$ with $\tau \ll 1$. Using this update rule, the target networks are always “late” concerning the trained networks, providing more stability to the learning of Q-values. The next-state Q-values are calculated with the target value network and target policy network. The key idea borrowed from DPG is the policy gradient for the actor. The critic is learned using regular Q-learning and target networks minimizing the mean squared loss between the updated Q-value and the original Q-value (the original Q-value is calculated with the value network, not the target value network). For the actor, to calculate the policy loss, the derivative of the objective function concerning the policy parameter is taken. The actor network in DDPG simply uses the negative average Q-value generated by the critic model as the loss for it.

This way, the actor network learns to generate actions to maximize the Q-value in each state. The general pseudo-code of the DDPG algorithm is represented in Algorithm A2.

Algorithm A2 DDPG [51]

Randomly initialize critic network $Q(s, a | \theta^Q)$ and actor $\mu(s | \theta^\mu)$ with weights θ^Q and θ^μ

Initialize target network Q' and μ' with weights $\theta^{Q'} \leftarrow \theta^Q, \theta^{\mu'} \leftarrow \theta^\mu$

Initialize replay buffer R

1: **for** $episode = 1$ to M **do**

2: Initialize a random process N for action exploration sequence

3: Receive initial observation state s_1

4: **for** $t = 1$ to T **do**

5: Select action $a_t = \mu(s_t | \theta^\mu) + N_t$ according to the current policy and exploration noise

6: Execute action a_t and observe reward r_t and observe new state s_{t+1}

7: Store transition (s_t, a_t, r_t, s_{t+1}) in R ▷ Store the experience in replay buffer

8: Sample a random minibatch of N transitions (s_i, a_i, r_i, s_{i+1}) from R

9: Set $y_i = r_i + \gamma Q'(s_{i+1}, \mu'(s_{i+1} | \theta^{\mu'})) | \theta^{Q'}$

10: Update critic by minimizing the loss: $L = \frac{1}{N} \sum_i (y_i - Q(s_i, a_i | \theta^Q))^2$

11: Update the actor policy using the sampled policy gradient:

$$\nabla_{\theta^\mu} J(\theta) \approx \frac{1}{N} \sum_i [\nabla_a Q(s, a | \theta^Q) |_{s=s_i, a=\mu(s_i)} \nabla_{\theta^\mu} \mu(s | \theta^\mu) |_{s=s_i}]$$

12: Update the target networks:

$$\theta^{Q'} \leftarrow \tau \theta^Q + (1 - \tau) \theta^{Q'}$$

$$\theta^{\mu'} \leftarrow \tau \theta^\mu + (1 - \tau) \theta^{\mu'}$$

13: **end for**

14: **end for**

Appendix A.3. PPO Conceptual Background

The PPO methodology [53] has gained prominence for its stability and efficiency in training agents to perform tasks within diverse environments. PPO is classified as a policy optimization method and operates as an on-policy algorithm. The algorithm's distinguishing feature is its utilization of a trust region approach, which constrains policy changes to avoid large deviations from the existing policy. This trust region is enforced through a clipped objective function, which curbs excessive policy adjustments. PPO often combines value function estimation to reduce variance, performs multiple optimization epochs, and employs exploration strategies for efficient learning. With its versatility and proven track record, PPO has been widely applied to tackle complex tasks across a variety of domains, making it a valuable tool in the field of RL. The PPO consists of two neural networks belonging to the actor-critic family of approaches. The policy network is represented by the actor determining the policy function $\pi_\theta(s, a)$. The critic part provides the evaluation of the selected policy utilizing the estimation of state value function $\hat{V}_\phi^\pi(s)$ or \hat{R}_t . The parameters of the actor (θ) and critic (ϕ) are optimized in a separate way using mini-batch stochastic gradient descent. The critic parameters are updated utilizing a value loss function, while the policies from the policy network side are clipped using a hyperparameter ϵ , so that the probability ratio $r(\theta) = \frac{\pi_\theta(a|s)}{\pi_{\theta_{old}}(a|s)}$ is constrained within the interval $(1 - \epsilon, 1 + \epsilon)$. The latter means that the policy function is restricted from potentially large policy updates, providing enhanced stability during the training phase. The pseudo-code of PPO is given in Algorithm A3.

Algorithm A3 PPO [53]

-
- Initialize policy parameters θ_0 and value function parameters ϕ_0
- 1: **for** $k = 0, 1, 2, \dots$ **do**
 - 2: Collect set of trajectories $D_k = \{\tau_i\}$ by running policy $\pi_k = \pi(\theta_k)$ in the environment
 - 3: Compute rewards-to-go \hat{R}_t
 - 4: Compute advantage estimates, \hat{A}_t based on the current value function V_{ϕ_k}
 - 5: Update the policy by maximizing the PPO-Clip objective:

$$\theta_{k+1} = \arg \max_{\theta} \frac{1}{|D_k|T} \sum_{\tau \in D_k} \sum_{t=0}^T \min \left(\frac{\pi_{\theta}(a_t | s_t)}{\pi_{\theta_k}(a_t | s_t)} A^{\pi_{\theta_k}}(s_t, a_t), g(\epsilon, A^{\pi_{\theta_k}}(s_t, a_t)) \right)$$

- 6: Fit value function by regression on mean squared error:

$$\phi_{k+1} = \arg \min_{\phi} \frac{1}{|D_k|T} \sum_{\tau \in D_k} \sum_{t=0}^T (V_{\phi}(s_t) - \hat{R}_t)^2$$

- 7: **end for**
-

Appendix A.4. SAC Conceptual Background

Soft Actor-Critic (SAC) [54] is an off-policy maximum entropy actor-critic algorithm known for its effectiveness in training agents to perform tasks in challenging and continuous-action environments. SAC is capable of reusing collected data efficiently for training. It leverages an entropy-regularized objective function to encourage exploration while optimizing the policy. One notable feature of SAC is its ability to balance between maximizing expected cumulative rewards and maximizing entropy, promoting both efficiency and exploration. SAC also incorporates a critic network to estimate the value function, reducing variance in policy updates and enhancing stability. The algorithm typically involves a target value network, and it employs a form of the soft Bellman backup, which helps maintain smooth policy updates. SAC is highly regarded for its robust performance and adaptability across a wide range of tasks, making it a valuable asset in the field of RL.

Soft Actor-Critic (SAC) distinguishes itself from conventional actor-critic methods by emphasizing the maximization of information entropy in addition to cumulative rewards. SAC favors stochastic policies, achieved by augmenting the objective function with an extra component representing the expected entropy of the policy. An adaptive temperature parameter (α) is introduced to regulate the trade-off between entropy and expected return. This parameter allows the agent to automatically adjust exploration based on the task's difficulty. More specifically, the temperature or trade-off coefficient is tuned automatically through minimizing the $J(\alpha)$ throughout the training (in every step), with $J(\alpha) = \mathbb{E}_{a_t \sim \pi_t} [-\alpha \ln(\pi_t(a_t | s_t)) - \alpha H_0]$ leading to $\alpha \leftarrow \alpha - \lambda \hat{\nabla}_{\alpha} J(\alpha)$, where H_0 equals $-\dim(A_1)$ and A_1 is the dimensions of action. The significance of entropy maximization in SAC is rooted in its ability to promote policies that exhibit substantial exploration, thereby capturing multiple modes of near-optimal strategies. Furthermore, the augmentation of entropy acts as a protective measure against the premature convergence of policies to undesirable local minima. The Q-function parameters are updated using $\phi_i \leftarrow \phi_i - \lambda_Q \hat{\nabla}_{\phi_i} J_Q(\phi_i)$ for $i \in \{1, 2\}$ while for the policy weights as $\theta \leftarrow \theta - \lambda_{\pi} \hat{\nabla}_{\theta} J_{\pi}(\theta)$ and finally the target network parameters are updated using $\phi'_i \leftarrow \tau \phi_i + (1 - \tau) \phi'_i$ for $i \in \{1, 2\}$. The pseudo-code of the SAC algorithm is presented in Algorithm A4.

Algorithm A4 Soft-Actor-Critic (SAC) [54]

Initialize policy parameters θ , Q-function parameters ϕ_1, ϕ_2 and empty replay buffer D
 Set target parameters equal to main parameters $\phi'_1 \leftarrow \phi_1, \phi'_2 \leftarrow \phi_2$

- 1: **repeat**
- 2: Observe state s and select action $a \sim \pi_\theta(\cdot | s)$
- 3: Execute a in the environment
- 4: Observe next state s' , reward r , and done signal d to indicate whether s' is terminal
- 5: Store (s, a, r, s', d) in replay buffer D
- 6: **if** it is time to update **then**
- 7: **for** j in range (however many updates) **do**
- 8: Randomly sample a batch of transitions, $B = \{(s, a, r, s', d)\}$ from D
- 9: Compute targets for the Q functions:

$$y(r, s', d) = r + \gamma(1 - d) \left(\min_{i=1,2} Q_{\phi'_i}(s', \tilde{a}') - \alpha \log \pi_\theta(\tilde{a}' | s') \right), \tilde{a}' \sim \pi_\theta(\cdot | s')$$

- 10: Update Q-functions by one step of gradient descent using

$$\nabla_{\phi_i} \frac{1}{|B|} \sum_{(s,a,r,s',d) \in B} \left(Q_{\phi_i}(s, a) - y(r, s', d) \right)^2 \text{ for } i = 1, 2$$

- 11: Update policy by one step of gradient ascent using:

$$\nabla_{\theta} \frac{1}{|B|} \sum_{s \in B} \left(\min_{i=1,2} Q_{\phi_i}(s, \tilde{a}_\theta(s)) - \alpha \log \pi_\theta(\tilde{a}_\theta(s) | s) \right)$$

- 12: where $\tilde{a}_\theta(s)$ is a sample from $\pi_\theta(\cdot | s)$ which is differentiable wrt θ via the reparametrization trick
- 13: Update target networks with:

$$\phi'_i \leftarrow \tau \phi_i + (1 - \tau) \phi'_i \text{ for } i = 1, 2$$

- 14: **end for**
- 15: **end if**
- 16: **until** convergence

Appendix A.5. A2C Conceptual Background

The A2C method is a derivative of the more general actor-critic methods, which have been studied for several decades in RL. The specific formulation of A2C, especially in the context of DRL, was popularized by its asynchronous version, the Asynchronous Advantage Actor-Critic (A3C) [55]. Such techniques utilize two neural networks: the actor, which proposes actions based on the current environment state, and the critic, which evaluates these actions. To this end, while traditional Q-learning focuses on learning the Q-values directly, in the A2C method, the critic is trained to learn the advantage values instead of the Q-values. By emphasizing the advantage, the algorithm assesses actions not just by their intrinsic value, but also by their superiority relative to other possible actions. As a consequence, the algorithm reduces the high variance often seen in policy networks, leading to a more stable model.

In the HVAC framework, A2C illustrates a promising approach to curb energy wastage. Balancing energy efficiency with occupant comfort is a challenging problem, making it an ideal candidate for sophisticated RL techniques like A2C. By continuously learning and adapting to changing conditions, A2C is adequate to dynamically adjust HVAC parameters, such as temperature setpoints or airflow rates, aiming for an optimal trade-off between energy conservation and user comfort. Algorithm A5 illustrates the pseudo-code of A2C.

Algorithm A5 Advantage Actor-Critic

```

1: Initialize Actor network with random weights  $\theta$ 
2: Initialize Critic network with random weights  $\phi$ 
3: Initialize empty experience buffer  $D$ 
4: for  $episode = 1$  to  $M$  do
5:   Initialize sequence  $s_1$ 
6:   for  $t = 1$  to  $T$  do
7:     Use Actor to get policy  $\pi(a|s_t; \theta)$ 
8:     Sample action  $a_t$  from  $\pi$ 
9:     Execute action  $a_t$  in environment and observe reward  $r_t$  and next state  $s_{t+1}$ 
10:    Store transition  $(s_t, a_t, r_t, s_{t+1})$  in  $D$ 
11:    Sample random minibatch of transitions  $(s_j, a_j, r_j, s_{j+1})$  from  $D$ 
12:    Use Critic to get value estimates  $V(s_j; \phi)$  and  $V(s_{j+1}; \phi)$ 
13:    Compute advantage  $A(s_j, a_j) = r_j + \gamma V(s_{j+1}; \phi) - V(s_j; \phi)$ 
14:    Update Actor using gradient ascent on  $\log \pi(a_j|s_j; \theta) \times A(s_j, a_j)$ 
15:    Update Critic by minimizing  $(r_j + \gamma V(s_{j+1}; \phi) - V(s_j; \phi))^2$ 
16:   end for
17: end for

```

Appendix B. Architecture and Hyperparameter Configuration of RL Algorithms

This appendix is dedicated to ensuring the reproducibility of the results presented in this study. It details the specific hyperparameter configurations for each RL algorithm evaluated. Providing this information is essential for transparency and allows other researchers and practitioners to replicate the experiments, verify the findings, and extend the work if desired. For each RL algorithm—A2C, DDPG, DQN, SAC, and PPO—we include tables that list the parameters utilized along with their default values. These parameters encompass learning rates, neural network architectures, discount factors, and other key settings that significantly influence algorithm performance (see Tables A1–A5).

Table A1. A2C hyperparameter configuration.

Parameter	Default Value
Learning Rate	7×10^{-4}
Number of Steps per Rollout	5
Discount Factor (γ)	0.99
Neural Network Architecture	2 layers, 64 neurons each
Entropy Coefficient	0.01

Table A2. DDPG hyperparameter configuration.

Parameter	Default Value
Learning Rate	1×10^{-3}
Batch Size	100
Discount Factor (γ)	0.99
Neural Network Architecture	2 layers (400, 300 neurons)
Replay Buffer Size	1,000,000
Polyak Coefficient (Tau)	0.005
Exploration Noise (Std Dev)	0.2
Noise Clip	0.5

Table A3. DQN hyperparameter configuration.

Parameter	Default Value
Learning Rate	1×10^{-4}
Batch Size	32
Discount Factor (γ)	0.99
Neural Network Architecture	2 layers, 64 neurons each
Replay Buffer Size	1,000,000
Exploration Strategy (Epsilon)	Start: 1.0, End: 0.05
Target Network Update Frequency	1000 steps
Learning Starts	5000 steps

Table A4. SAC hyperparameter configuration.

Parameter	Default Value
Learning Rate	3×10^{-4}
Batch Size	256
Discount Factor (γ)	0.99
Neural Network Architecture	2 layers, 256 neurons each
Polyak Coefficient (Tau)	0.005

Table A5. PPO hyperparameter configuration.

Parameter	Default Value
Learning Rate	3×10^{-4}
Batch Size	64
Discount Factor (γ)	0.99
Neural Network Architecture	2 layers, 64 neurons each
Number of Epochs	10
Clip Range	0.2
GAE Lambda	0.95
Value Function Coefficient	0.5
Entropy Coefficient	0.01
Number of Steps per Rollout	2048

Appendix C. Analytical Results for Each RL Algorithm

This appendix provides a visual compendium of the simulation results for various RL algorithms applied within the scope of residential building energy management (see Figures A1–A15). The following visual data are presented for each algorithm under multiple weight scenarios:

- *Predicted Percentage of Dissatisfied Measurements:* Illustrations of the PPD across different building zones, reflecting the occupant comfort levels attained during the simulations.
- *Zone Temperature Measurements:* Temperature readings for each building zone, demonstrating the algorithms' effectiveness in maintaining thermal conditions.
- *HVAC Energy Consumption Profiles:* Graphs depicting the energy consumed by the HVAC system throughout the day, showcasing the algorithms' energy performance.

Each of the 45 images within this appendix is integral to the comprehensive evaluation of the algorithms' performance, providing an empirical basis for the analysis discussed in the main body of the paper. These images offer readers an opportunity to visually assess the impact of RL-driven control on both the micro-scale (zone-specific comfort and temperature) and macro-scale (overall energy consumption) aspects of building management.

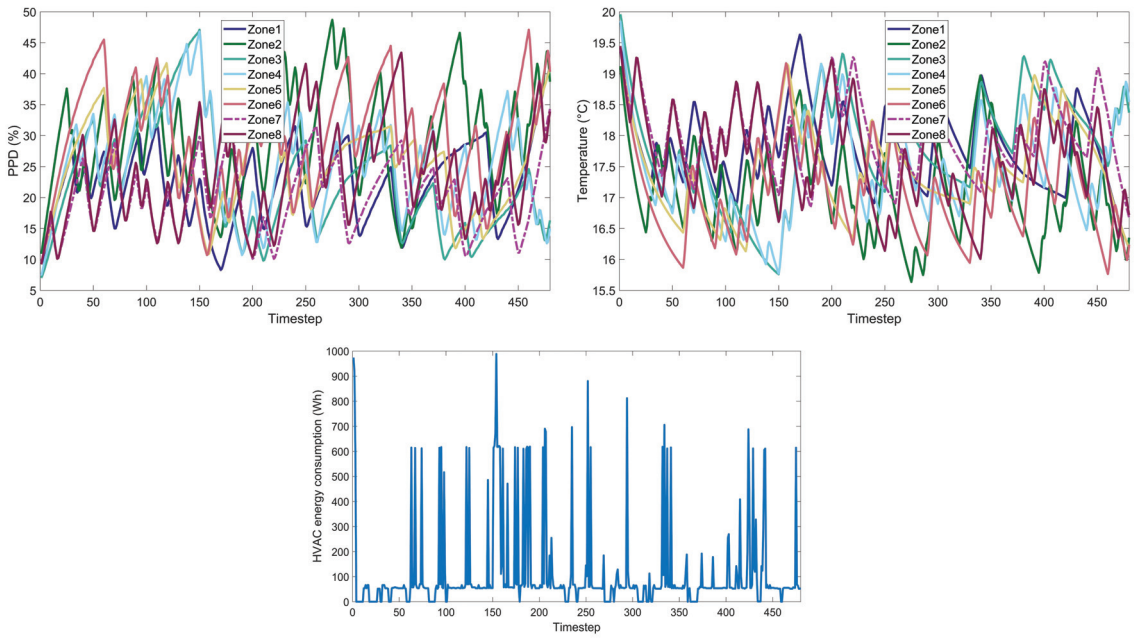


Figure A1. SAC under weight case $w = 0.1$. (Upper left): PPD for each building zone; (Upper right): Temperature for each building zone; (Lower): HVAC energy consumption within day.

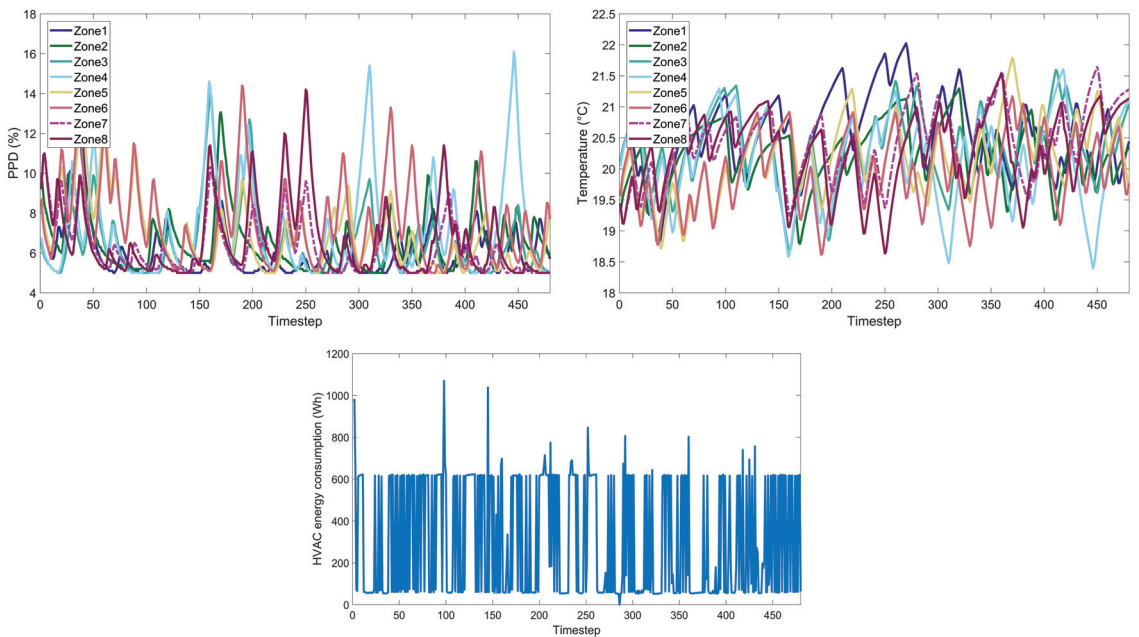


Figure A2. PPO under weight case $w = 0.1$. (Upper left): PPD for each building zone; (Upper right): Temperature for each building zone; (Lower): HVAC energy consumption within day.

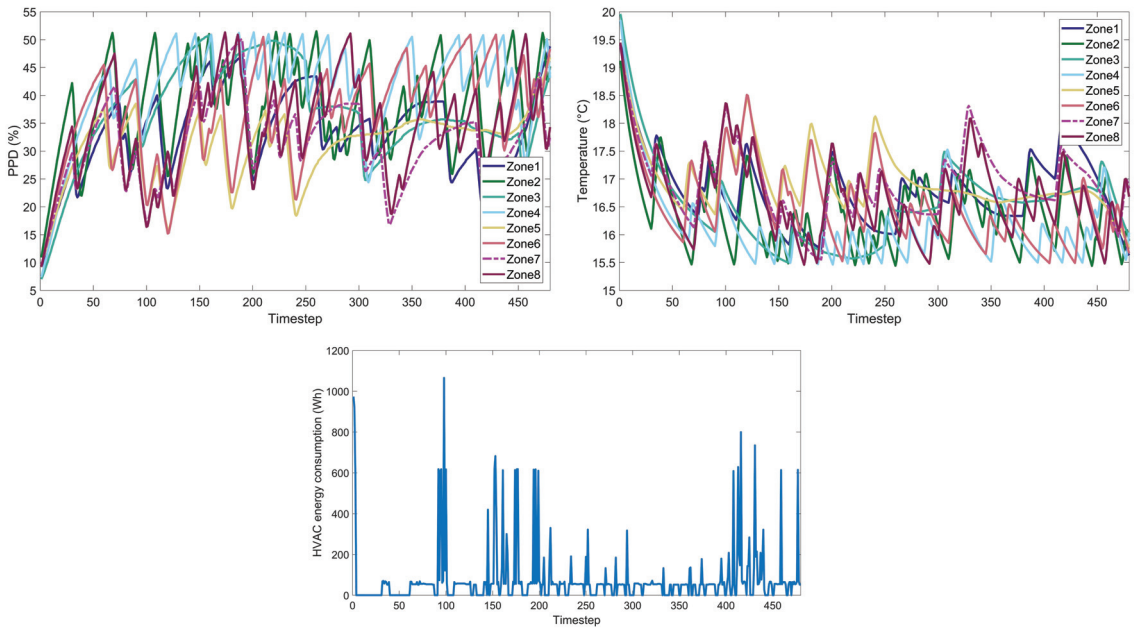


Figure A3. A2C under weight case $w = 0.1$. (Upper left): PPD for each building zone; (Upper right): Temperature for each building zone; (Lower): HVAC energy consumption within day.

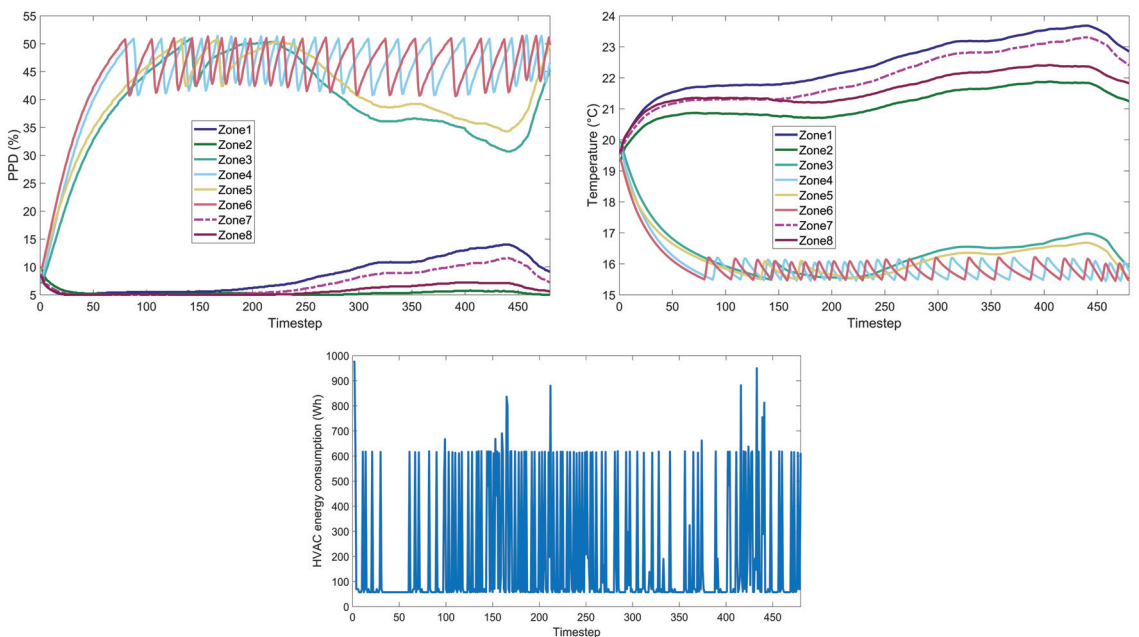


Figure A4. DDPG under weight case $w = 0.1$. (Upper left): PPD for each building zone; (Upper right): Temperature for each building zone; (Lower): HVAC energy consumption within day.

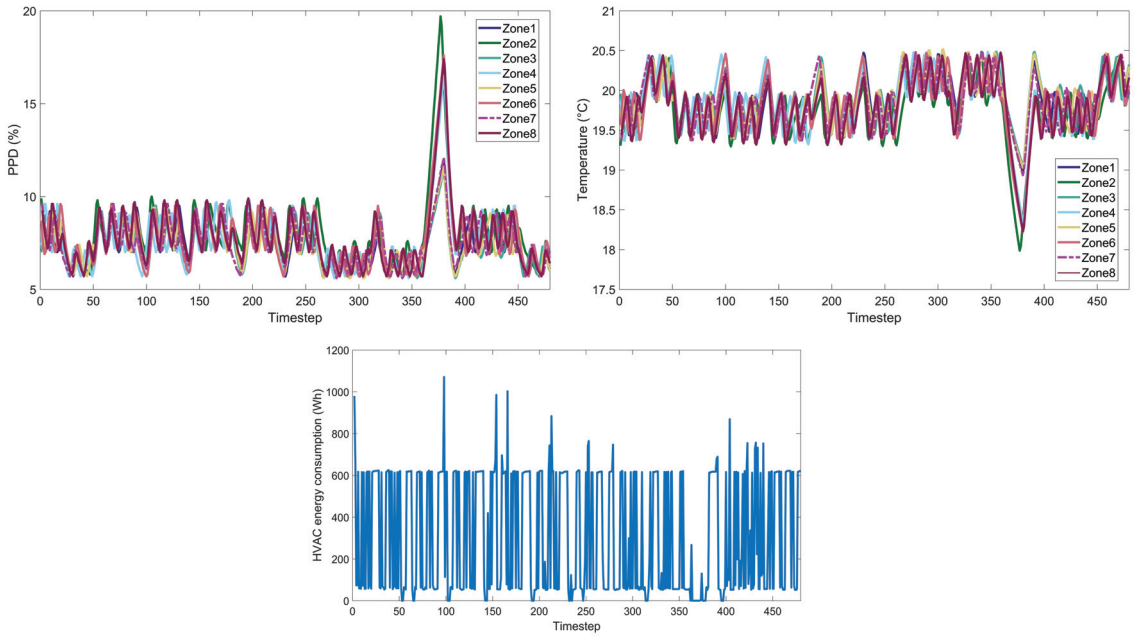


Figure A5. DQN under weight case $w = 0.1$. (Upper left): PPD for each building zone; (Upper right): Temperature for each building zone; (Lower): HVAC energy consumption within day.

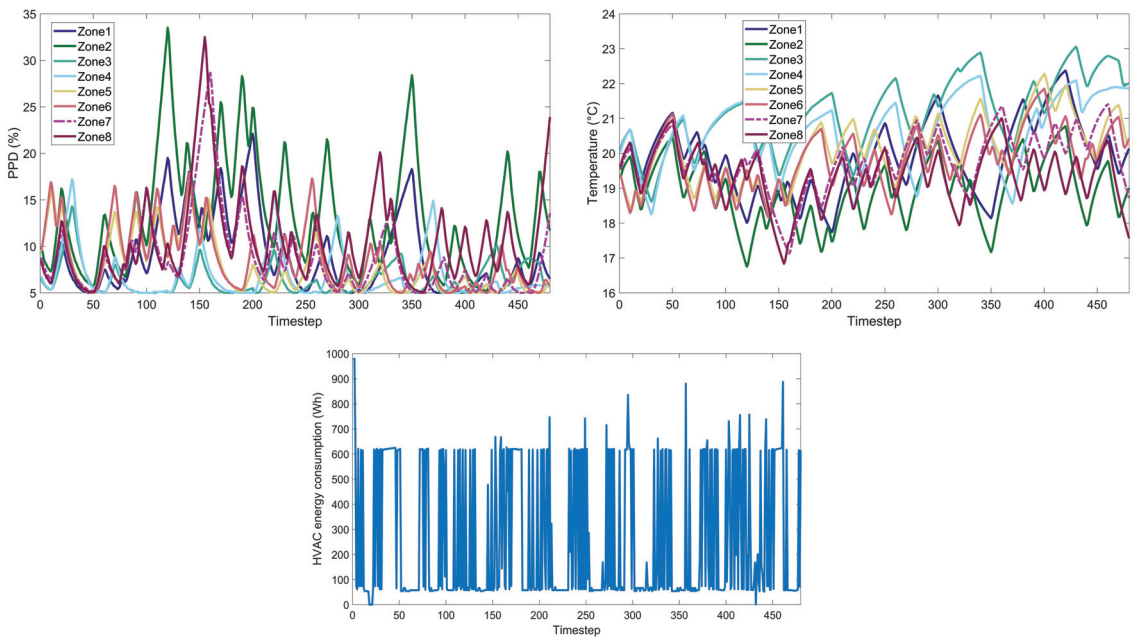


Figure A6. SAC under weight case $w = 0.5$. (Upper left): PPD for each building zone; (Upper right): Temperature for each building zone; (Lower): HVAC energy consumption within day.

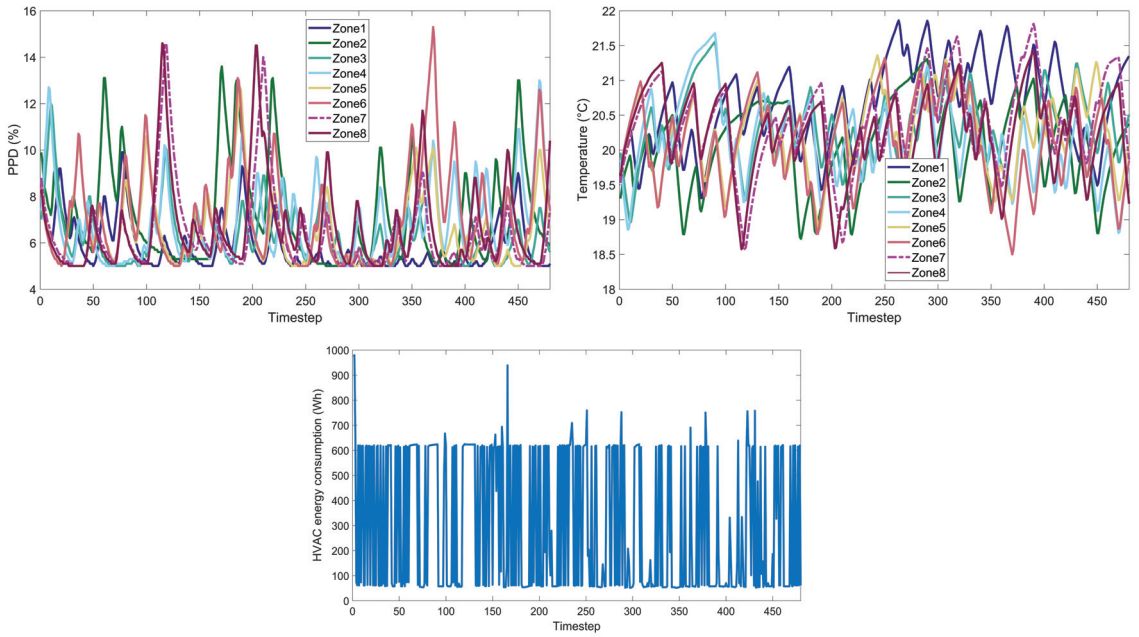


Figure A7. PPO under weight case $w = 0.5$. (Upper left): PPD for each building zone; (Upper right): Temperature for each building zone; (Lower): HVAC energy consumption within day.

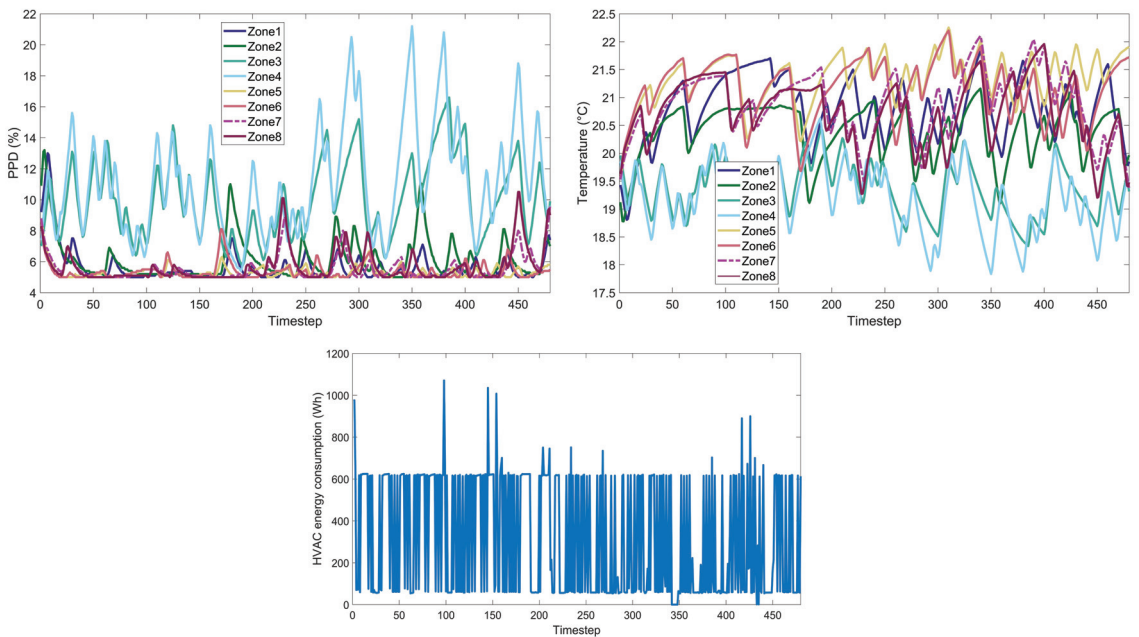


Figure A8. A2C under weight case $w = 0.5$. (Upper left): PPD for each building zone; (Upper right): Temperature for each building zone; (Lower): HVAC energy consumption within day.

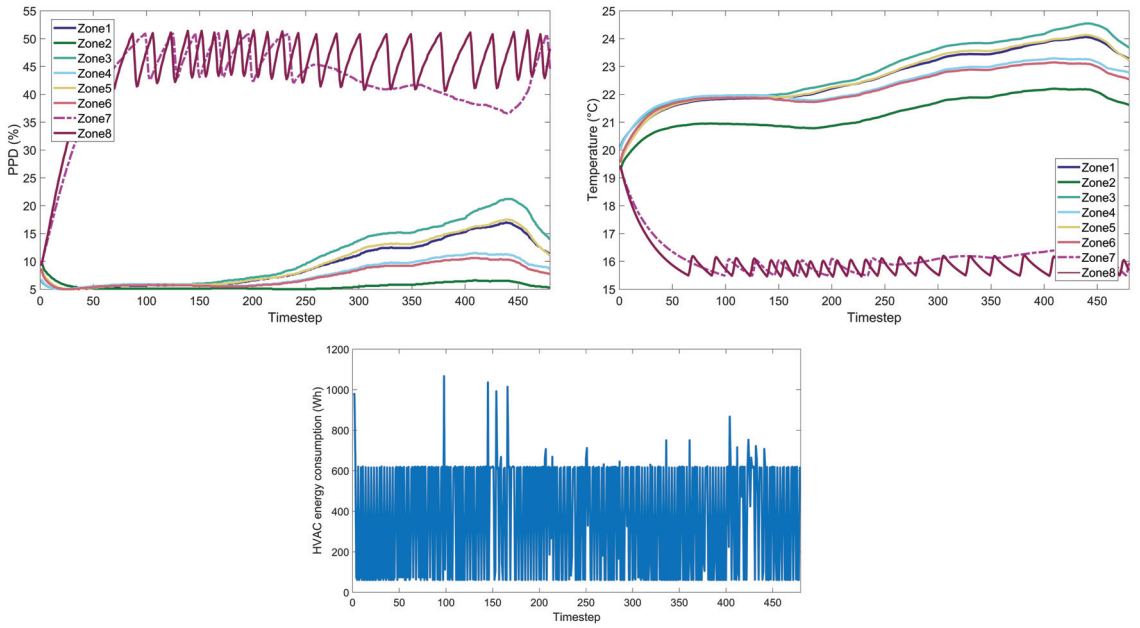


Figure A9. DDPG under weight case $w = 0.5$. (Upper left): PPD for each building zone; (Upper right): Temperature for each building zone; (Lower): HVAC energy consumption within day.

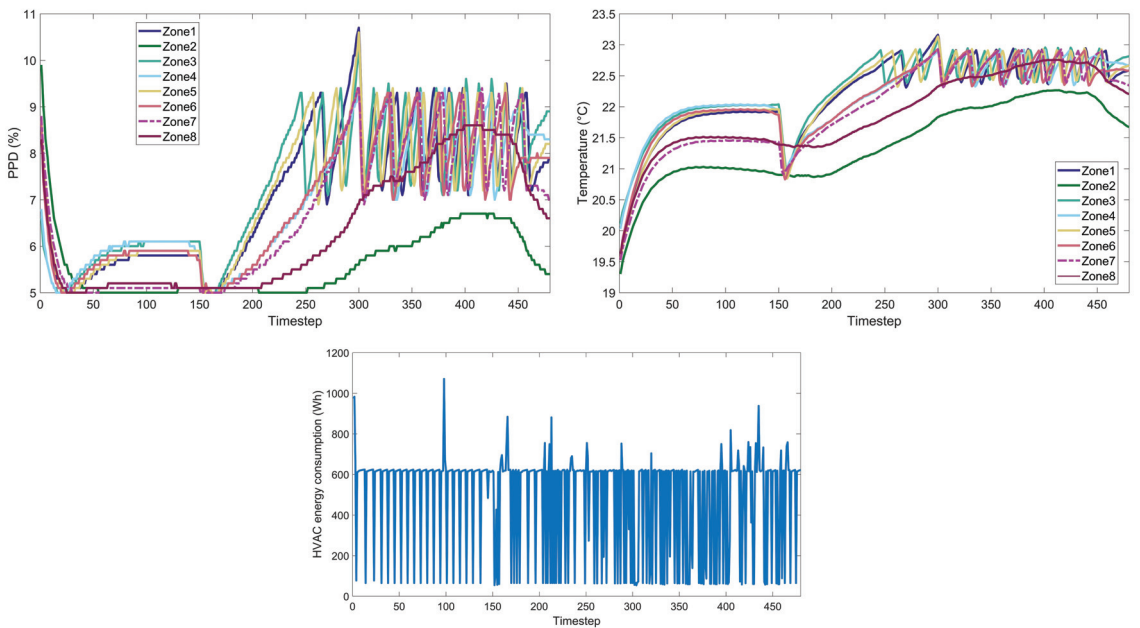


Figure A10. DQN under weight case $w = 0.5$. (Upper left): PPD for each building zone; (Upper right): Temperature for each building zone; (Lower): HVAC energy consumption within day.

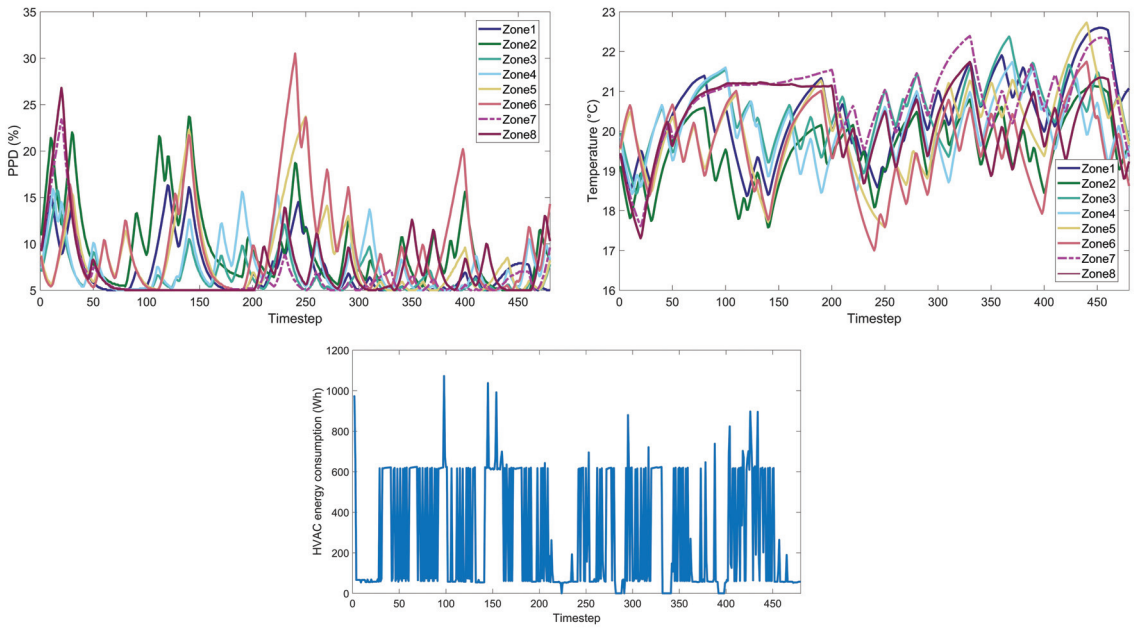


Figure A11. SAC under weight case $w = 0.9$. (Upper left): PPD for each building zone; (Upper right): Temperature for each building zone; (Lower): HVAC energy consumption within day.

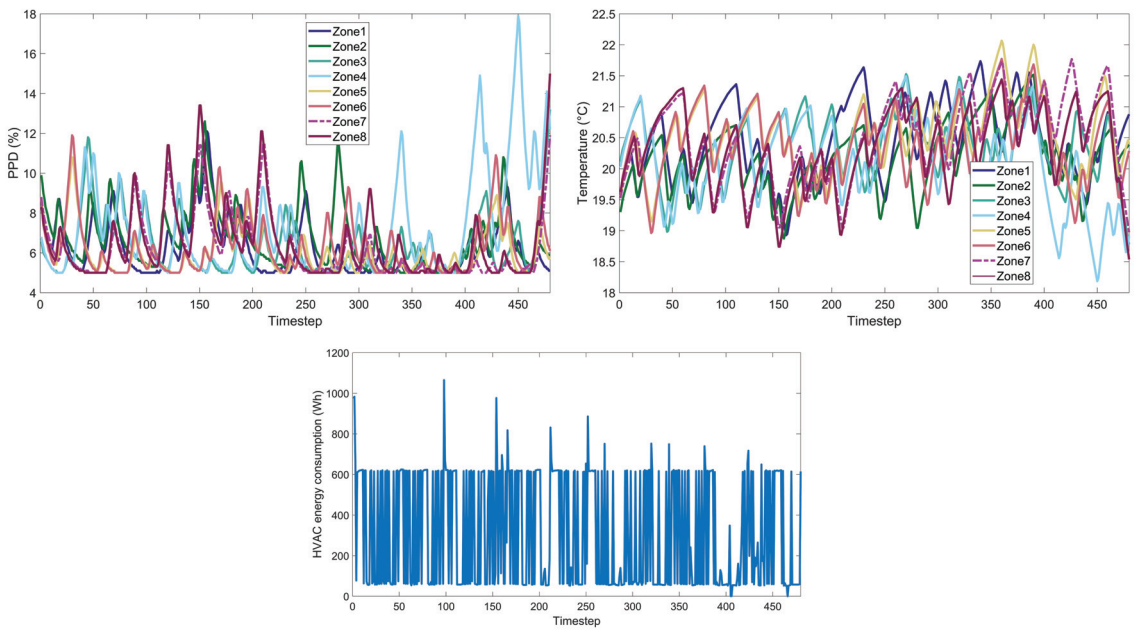


Figure A12. PPO under weight case $w = 0.9$. (Upper left): PPD for each building zone; (Upper right): Temperature for each building zone; (Lower): HVAC energy consumption within day.

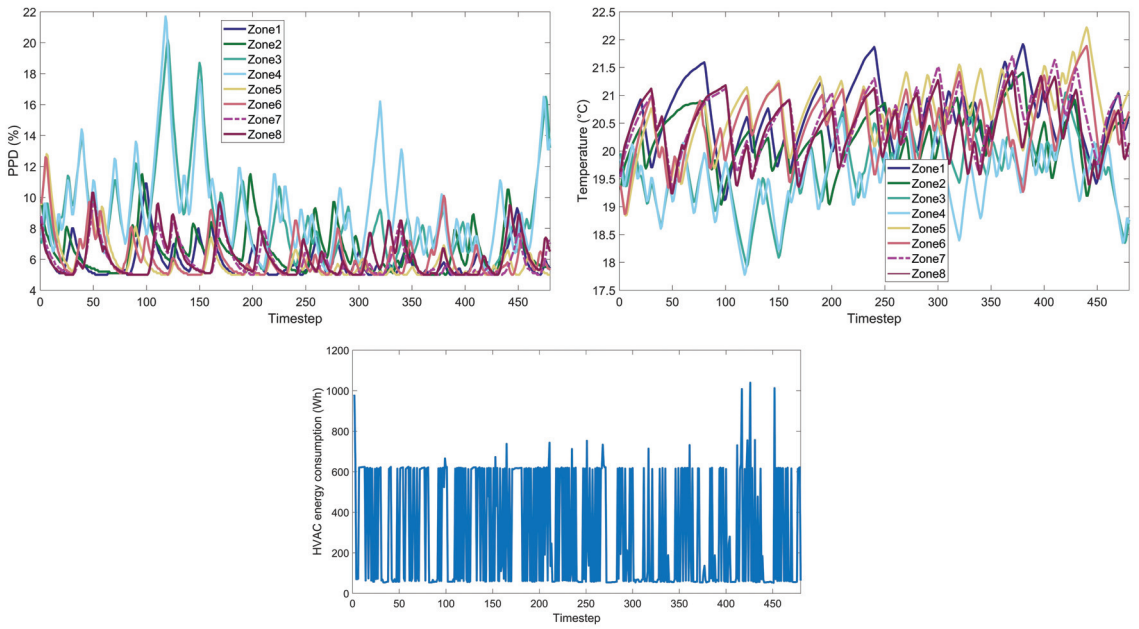


Figure A13. A2C under weight case $w = 0.9$. (Upper left): PPD for each building zone; (Upper right): Temperature for each building zone; (Lower): HVAC energy consumption within day.

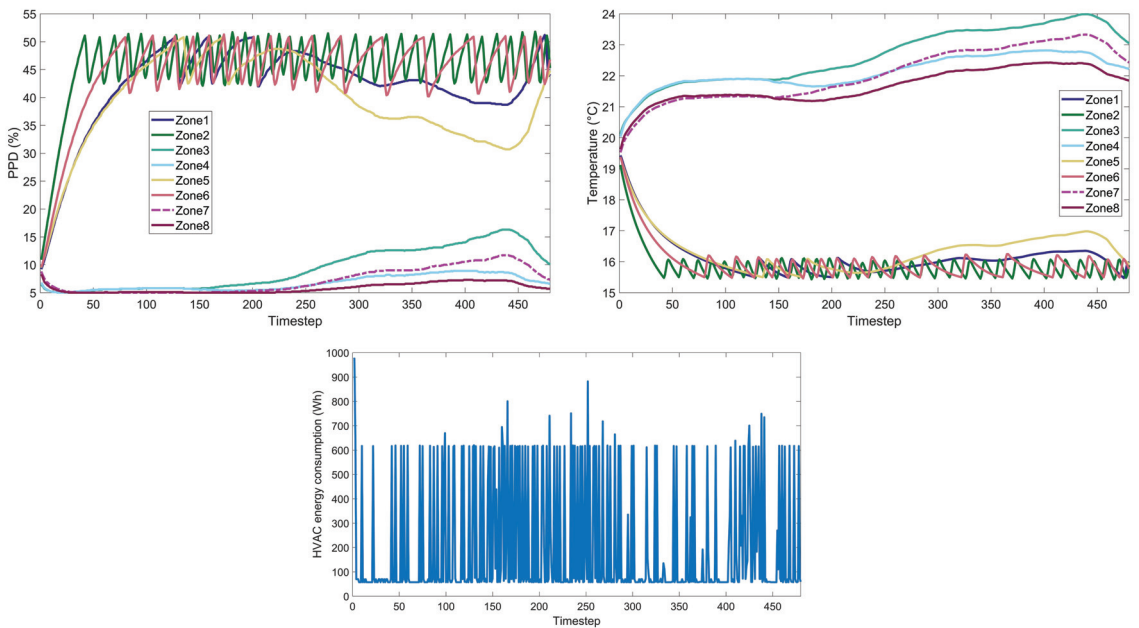


Figure A14. DDPG under weight case $w = 0.9$. (Upper left): PPD for each building zone; (Upper right): Temperature for each building zone; (Lower): HVAC energy consumption within day.

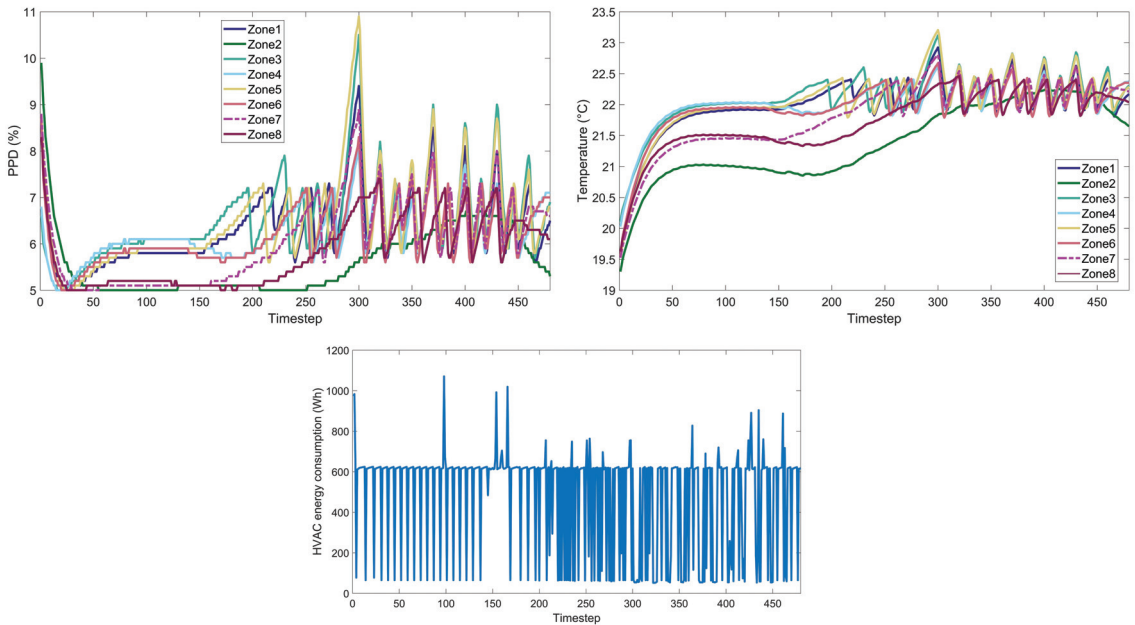


Figure A15. DQN under weight case $w = 0.9$. (**Upper left**): PPD for each building zone; (**Upper right**): Temperature for each building zone; (**Lower**): HVAC energy consumption within day.

References

1. Marikyan, D.; Papagiannidis, S.; Alamanos, E. A systematic review of the smart home literature: A user perspective. *Technol. Forecast. Soc. Chang.* **2019**, *138*, 139–154. [CrossRef]
2. Dimara, A.; Anagnostopoulos, C.N.; Kotis, K.; Krinidis, S.; Tzovaras, D. BEMS in the Era of Internet of Energy: A Review. In *Proceedings of the Artificial Intelligence Applications and Innovations, Proceedings of the 17th IFIP WG 12.5 International Conference, AIAI 2021, Hersonissos, Crete, Greece, 25–27 June 2021*; Proceedings 17; Springer: Berlin/Heidelberg, Germany, 2021; pp. 465–476.
3. Alaa, M.; Zaidan, A.A.; Zaidan, B.B.; Talal, M.; Kiah, M.L.M. A review of smart home applications based on Internet of Things. *J. Netw. Comput. Appl.* **2017**, *97*, 48–65. [CrossRef]
4. Michailidis, P.; Michailidis, I.; Vamvakas, D.; Kosmatopoulos, E. Model-Free HVAC Control in Buildings: A Review. *Energies* **2023**, *16*, 7124. [CrossRef]
5. Keroglou, C.; Kansizoglou, I.; Michailidis, P.; Oikonomou, K.M.; Papapetros, I.T.; Dragkola, P.; Michailidis, I.T.; Gasteratos, A.; Kosmatopoulos, E.B.; Sirakoulis, G.C. A Survey on Technical Challenges of Assistive Robotics for Elder People in Domestic Environments: The ASPiDA Concept. *IEEE Trans. Med. Robot. Bionics* **2023**, *5*, 196–205. [CrossRef]
6. Miko, R.; Thompson, S. The Environmental Impact of Housing: Local and Global Ecological Footprint of a House. In *Future as Fairness*; Brill: New York, NY, USA, 2004.
7. Goldstein, B.; Gounaridis, D.; Newell, J.P. The carbon footprint of household energy use in the United States. *Proc. Natl. Acad. Sci. USA* **2020**, *117*, 19122–19130. [CrossRef]
8. Lettenmeier, M.; Laakso, S.; Toivio, V. Future Households: Smaller Footprint, Better Life. In *Boosting Resource Productivity by Adopting the Circular Economy*; Paul Scherrer Institute: Villigen, Switzerland, 2017; pp. 293–297.
9. Xue, F.; Zhao, J. Building thermal comfort research based on energy-saving concept. *Adv. Mater. Sci. Eng.* **2021**, *2021*, 7132437. [CrossRef]
10. Ma, Z.; Zhao, D.; She, C.; Yang, Y.; Yang, R. Personal thermal management techniques for thermal comfort and building energy saving. *Mater. Today Phys.* **2021**, *20*, 100465. [CrossRef]
11. Cottafava, D.; Magariello, S.; Ariano, R.; Arrobio, O.; Baricco, M.; Barthelmes, V.; Baruzzo, G.; Bonansone, M.; Console, L.; Contin, L.; et al. Crowdsensing for a sustainable comfort and for energy saving. *Energy Build.* **2019**, *186*, 208–220. [CrossRef]
12. Michailidis, I.T.; Sangi, R.; Michailidis, P.; Schild, T.; Fuetterer, J.; Mueller, D.; Kosmatopoulos, E.B. Balancing energy efficiency with indoor comfort using smart control agents: A simulative case study. *Energies* **2020**, *13*, 6228. [CrossRef]
13. Xu, Y.; Peet, Y.T. Effect of an on/off HVAC control on indoor temperature distribution and cycle variability in a single-floor residential building. *Energy Build.* **2021**, *251*, 111289. [CrossRef]

14. Chinnakani, K.; Krishnamurthy, A.; Moyne, J.; Gu, F. Comparison of energy consumption in HVAC systems using simple ON-OFF, intelligent ON-OFF and optimal controllers. In Proceedings of the 2011 IEEE Power and Energy Society General Meeting, Detroit, MI, USA, 24–28 July 2011; pp. 1–6.
15. Oldewurtel, F.; Sturzenegger, D.; Morari, M. Importance of occupancy information for building climate control. *Appl. Energy* **2013**, *101*, 521–532. [CrossRef]
16. Michailidis, P.; Pelitaris, P.; Korkas, C.; Michailidis, I.; Baldi, S.; Kosmatopoulos, E. Enabling optimal energy management with minimal IoT requirements: A legacy A/C case study. *Energies* **2021**, *14*, 7910. [CrossRef]
17. Michailidis, I.T.; Schild, T.; Sangi, R.; Michailidis, P.; Korkas, C.; Fütterer, J.; Müller, D.; Kosmatopoulos, E.B. Energy-efficient HVAC management using cooperative, self-trained, control agents: A real-life German building case study. *Appl. Energy* **2018**, *211*, 113–125. [CrossRef]
18. Lu, X.; Fu, Y.; O'Neill, Z. Benchmarking high performance HVAC Rule-Based controls with advanced intelligent Controllers: A case study in a Multi-Zone system in Modelica. *Energy Build.* **2023**, *284*, 112854. [CrossRef]
19. Merabet, G.H.; Essaaidi, M.; Haddou, M.B.; Qolomany, B.; Qadir, J.; Anan, M.; Al-Fuqaha, A.; Abid, M.R.; Benhaddou, D. Intelligent building control systems for thermal comfort and energy-efficiency: A systematic review of artificial intelligence-assisted techniques. *Renew. Sustain. Energy Rev.* **2021**, *144*, 110969. [CrossRef]
20. Shaikh, P.H.; Nor, N.B.M.; Nallagownden, P.; Elamvazuthi, I.; Ibrahim, T. A review on optimized control systems for building energy and comfort management of smart sustainable buildings. *Renew. Sustain. Energy Rev.* **2014**, *34*, 409–429. [CrossRef]
21. Khajenasiri, I.; Estebesari, A.; Verhelst, M.; Gielen, G. A review on Internet of Things solutions for intelligent energy control in buildings for smart city applications. *Energy Procedia* **2017**, *111*, 770–779. [CrossRef]
22. Panchalingam, R.; Chan, K.C. A state-of-the-art review on artificial intelligence for Smart Buildings. *Intell. Build. Int.* **2021**, *13*, 203–226. [CrossRef]
23. Vamvakas, D.; Michailidis, P.; Korkas, C.; Kosmatopoulos, E. Review and Evaluation of Reinforcement Learning Frameworks on Smart Grid Applications. *Energies* **2023**, *16*, 5326. [CrossRef]
24. Fu, Q.; Han, Z.; Chen, J.; Lu, Y.; Wu, H.; Wang, Y. Applications of reinforcement learning for building energy efficiency control: A review. *J. Build. Eng.* **2022**, *50*, 104165. [CrossRef]
25. Fang, X.; Gong, G.; Li, G.; Chun, L.; Peng, P.; Li, W.; Shi, X.; Chen, X. Deep reinforcement learning optimal control strategy for temperature setpoint real-time reset in multi-zone building HVAC system. *Appl. Therm. Eng.* **2022**, *212*, 118552. [CrossRef]
26. Blad, C.; Bøgh, S.; Kallešøe, C.S. Data-driven offline reinforcement learning for HVAC-systems. *Energy* **2022**, *261*, 125290. [CrossRef]
27. Lissa, P.; Schukat, M.; Barrett, E. Transfer learning applied to reinforcement learning-based hvac control. *SN Comput. Sci.* **2020**, *1*, 127. [CrossRef]
28. Du, G.; Zou, Y.; Zhang, X.; Liu, T.; Wu, J.; He, D. Deep reinforcement learning based energy management for a hybrid electric vehicle. *Energy* **2020**, *201*, 117591. [CrossRef]
29. Zhang, S.; Nandakumar, S.; Pan, Q.; Yang, E.; Migne, R.; Subramanian, L. Benchmarking Reinforcement Learning Algorithms on Island Microgrid Energy Management. In Proceedings of the 2021 IEEE PES Innovative Smart Grid Technologies-Asia (ISGT Asia), Brisbane, Australia, 5–8 December 2021; pp. 1–5.
30. Zhou, Y.; Ma, Z.; Zhang, J.; Zou, S. Data-driven stochastic energy management of multi energy system using deep reinforcement learning. *Energy* **2022**, *261*, 125187. [CrossRef]
31. Gupta, A.; Badr, Y.; Negahban, A.; Qiu, R.G. Energy-efficient heating control for smart buildings with deep reinforcement learning. *J. Build. Eng.* **2021**, *34*, 101739. [CrossRef]
32. Lork, C.; Li, W.T.; Qin, Y.; Zhou, Y.; Yuen, C.; Tushar, W.; Saha, T.K. An uncertainty-aware deep reinforcement learning framework for residential air conditioning energy management. *Appl. Energy* **2020**, *276*, 115426. [CrossRef]
33. Yu, L.; Xie, W.; Xie, D.; Zou, Y.; Zhang, D.; Sun, Z.; Zhang, L.; Zhang, Y.; Jiang, T. Deep reinforcement learning for smart home energy management. *IEEE Internet Things J.* **2019**, *7*, 2751–2762. [CrossRef]
34. Liu, B.; Akcakaya, M.; McDermott, T.E. Automated control of transactive hvacs in energy distribution systems. *IEEE Trans. Smart Grid* **2020**, *12*, 2462–2471. [CrossRef]
35. Du, Y.; Zandi, H.; Kotevska, O.; Kurte, K.; Munk, J.; Amasyali, K.; Mckee, E.; Li, F. Intelligent multi-zone residential HVAC control strategy based on deep reinforcement learning. *Appl. Energy* **2021**, *281*, 116117. [CrossRef]
36. Azuatalam, D.; Lee, W.L.; de Nijs, F.; Liebman, A. Reinforcement learning for whole-building HVAC control and demand response. *Energy AI* **2020**, *2*, 100020. [CrossRef]
37. Lee, J.Y.; Rahman, A.; Huang, S.; Smith, A.D.; Katipamula, S. On-policy learning-based deep reinforcement learning assessment for building control efficiency and stability. *Sci. Technol. Built Environ.* **2022**, *28*, 1150–1165. [CrossRef]
38. Pinto, G.; Deltetto, D.; Capozzoli, A. Data-driven district energy management with surrogate models and deep reinforcement learning. *Appl. Energy* **2021**, *304*, 117642. [CrossRef]
39. Pinto, G.; Piscitelli, M.S.; Vázquez-Canteli, J.R.; Nagy, Z.; Capozzoli, A. Coordinated energy management for a cluster of buildings through deep reinforcement learning. *Energy* **2021**, *229*, 120725. [CrossRef]
40. Zhou, S.; Shah, A.; Leung, P.; Zhu, X.; Liao, Q. A Comprehensive Review of the Applications of Machine Learning for HVAC. *DeCarbon* **2023**, 100023. [CrossRef]

41. Jia, R.; Jin, M.; Sun, K.; Hong, T.; Spanos, C. Advanced building control via deep reinforcement learning. *Energy Procedia* **2019**, *158*, 6158–6163. [CrossRef]
42. Scharnhorst, P.; Schubnel, B.; Fernández Bandera, C.; Salom, J.; Taddeo, P.; Boegli, M.; Gorecki, T.; Stauffer, Y.; Peppas, A.; Politi, C. Energym: A building model library for controller benchmarking. *Appl. Sci.* **2021**, *11*, 3518. [CrossRef]
43. Raffin, A.; Hill, A.; Ernestus, M.; Gleave, A.; Kanervisto, A.; Dormann, N. Stable-baselines3: Reliable reinforcement learning implementations. *J. Mach. Learn. Res.* **2021**, *22*, 12348–12355.
44. Taleghani, M.; Tenpierik, M.; Kurvers, S.; Van Den Dobbelsteen, A. A review into thermal comfort in buildings. *Renew. Sustain. Energy Rev.* **2013**, *26*, 201–215. [CrossRef]
45. ASHRAE 55; Thermal Environmental Conditions for Human Occupancy. ASHRAE Standards: Peachtree Corners, GA, USA, 2004.
46. ISO 7730; Ergonomics of the Thermal Environment—Analytical Determination and Interpretation of Thermal Comfort Using Calculation of the Pmv and Ppd Indices and Local Thermal Comfort Criteria. ISO (International Organization for Standardization): Geneva, Switzerland, 2005.
47. EN 16798; Ventilation for Non-Residential Buildings—Performance Requirements for Ventilation and Room-Conditioning Systems. European Committee for Standardization Brussels: Brussels, Belgium, 2007.
48. Nicol, J.F.; Humphreys, M.A. A stochastic approach to thermal comfort-occupant behavior and energy use in buildings/discussion. *ASHRAE Trans.* **2004**, *110*, 554.
49. Markov, D. Practical evaluation of the thermal comfort parameters. In *Annual International Course: Ventilation and Indoor Climate, Avangard, Sofia*; Technical University of Sofia: Sofia, Bulgaria, 2002; pp. 158–170.
50. Mnih, V.; Kavukcuoglu, K.; Silver, D.; Rusu, A.A.; Veness, J.; Bellemare, M.G.; Graves, A.; Riedmiller, M.; Fidjeland, A.K.; Ostrovski, G.; et al. Human-level control through deep reinforcement learning. *Nature* **2015**, *518*, 529–533. [CrossRef] [PubMed]
51. Lillicrap, T.P.; Hunt, J.J.; Pritzel, A.; Heess, N.; Erez, T.; Tassa, Y.; Silver, D.; Wierstra, D. Continuous control with deep reinforcement learning. *arXiv* **2015**, arXiv:1509.02971.
52. Silver, D.; Lever, G.; Heess, N.; Degris, T.; Wierstra, D.; Riedmiller, M. Deterministic policy gradient algorithms. In Proceedings of the 31st International Conference on Machine Learning, Beijing, China, 21–26 June 2014; pp. 387–395.
53. Schulman, J.; Wolski, F.; Dhariwal, P.; Radford, A.; Klimov, O. Proximal policy optimization algorithms. *arXiv* **2017**, arXiv:1707.06347.
54. Haarnoja, T.; Zhou, A.; Abbeel, P.; Levine, S. Soft actor-critic: Off-policy maximum entropy deep reinforcement learning with a stochastic actor. In Proceedings of the 35th International Conference on Machine Learning, Stockholm, Sweden, 10–15 July 2018; pp. 1861–1870.
55. Mnih, V.; Badia, A.P.; Mirza, M.; Graves, A.; Lillicrap, T.; Harley, T.; Silver, D.; Kavukcuoglu, K. Asynchronous methods for deep reinforcement learning. In Proceedings of the 33rd International Conference on Machine Learning, New York, NY, USA, 19–24 June 2016; pp. 1928–1937.

Disclaimer/Publisher’s Note: The statements, opinions and data contained in all publications are solely those of the individual author(s) and contributor(s) and not of MDPI and/or the editor(s). MDPI and/or the editor(s) disclaim responsibility for any injury to people or property resulting from any ideas, methods, instructions or products referred to in the content.

MDPI
St. Alban-Anlage 66
4052 Basel
Switzerland
www.mdpi.com

Energies Editorial Office
E-mail: energies@mdpi.com
www.mdpi.com/journal/energies



Disclaimer/Publisher's Note: The statements, opinions and data contained in all publications are solely those of the individual author(s) and contributor(s) and not of MDPI and/or the editor(s). MDPI and/or the editor(s) disclaim responsibility for any injury to people or property resulting from any ideas, methods, instructions or products referred to in the content.



Academic Open
Access Publishing

[mdpi.com](https://www.mdpi.com)

ISBN 978-3-7258-0706-2